

BULETINUL INSTITUTULUI POLITEHNIC DIN IAȘI

**Publicat de
UNIVERSITATEA TEHNICĂ "GH.ASACHI", IAȘI**

Tomul LI (LV)

Fasc. 1

**Secția
ȘTIINȚA ȘI INGINERIA MATERIALELOR**

2005

President of the Editorial Board of Bulletin of the Polytechnic Institute

Prof. univ. dr. eng Nicolae Badea, Technical University “Gh. Asachi” Iași, Romania
Rector of Technical University “Gh. Asachi” of Iasi

Editor-in-Chief of Bulletin of the Polytechnic Institute

Prof. univ. dr. eng Ion Giurma, Technical University “Gh. Asachi” Iași, Romania
Vice-Rector of Technical University “Gh. Asachi” of Iasi

Managing Editor of Bulletin of the Polytechnic Institute

Prof. univ. dr. eng. Dan Gălușcă, Technical University “Gh. Asachi” Iași, Romania
Dean of the Faculty of Materials Science and Engineering

Managing Editor of the *MATERIALS SCIENCE AND ENGINEERING*

Assoc. prof. dr. eng. Iulian Ioniță, Technical University “Gh. Asachi” Iași, Romania
Scientific secretary of the Faculty of Materials Science and Engineering

Editorial Board of the Section *MATERIALS SCIENCE AND ENGINEERING*

Prof.univ.dr.eng. Yuri A. Burennikov, Vinnitsia State Technical University, Ukraine

**Prof.univ.dr.eng. Borivoje Miškovič, Yugoslav Association of Metallurgical Engineers,
Belgrad, Serbia-Montenegro**

Prof.univ.dr.eng. Paolo Nanni, Universita degli Studi da Genova, Italy

Prof.univ.dr.eng. Strul Moisa, Ben-Gurion University of the Negev, Beer-Sheva, Israel

**Prof.univ.dr.eng. Corneliu Munteanu, Technical University “Gh. Asachi” Iași,
Romania**

**Prof.univ.dr.eng. Vasile Cojocaru-Filipiuc, Technical University “Gh. Asachi” Iași,
Romania**

Prof.univ.dr.eng. Constantin Baciu, Technical University “Gh. Asachi” Iași, Romania

Prof.univ.dr.eng. Luchian Zaharia, Technical University “Gh. Asachi” Iași, Romania

Prof.univ.dr.eng. Ioan Carcea, Technical University “Gh. Asachi” Iași, Romania

Prof.univ.dr.eng. Adrian Dima, Technical University “Gh. Asachi” Iași, Romania

Prof.univ.dr.eng. Ioan Alexandru, Technical University “Gh. Asachi” Iași, Romania

**Assoc.prof.dr.eng. Leandru Gheorghe Bujoreanu, Technical University “Gh. Asachi”
Iași, Romania**

Assoc. prof.dr. eng. Ioan Rusu, Technical University “Gh. Asachi” Iași, Romania

**Assoc. prof.dr. eng. Gheorghe Bădărău, Technical University “Gh. Asachi” Iași,
Romania**

**Assoc. prof.dr. eng. Petrică Vizureanu, Technical University “Gh. Asachi” Iași,
Romania**

Editorial Secretary of the *MATERIALS SCIENCE AND ENGINEERING*

**Assoc.prof.dr.eng. Gheorghe Bădărău, Technical University “Gh. Asachi” Iași,
Romania**

MATERIALS SCIENCE AND ENGINEERING

| CONTENTS | |
|--|----|
| COJOCARU-FILIPCIUC, V., IMPROVEMENT OF OBTAINING OF SPHEROIDAL GRAPHITE CAST IRON BY INOCULATING LADLES (TWO CHAMBERS AND TWO STOPPERS LADLE) | 1 |
| PRISACARIU, C., CARACULACU, A., THE INFLUENCE OF AGEING CONDITIONS AND CHEMICAL STRUCTURE ON THE STRESS-STRAIN DATA OF DIBENZYL BASED POLYURETHANE FILMS | 9 |
| AMARIEI, N., COMANDAR, C., LEON, D., DUMITRACHE, C., THE INFLUENCE OF THE RESIDUAL STRESS PRODUCED DURING THE NITRIDING PROCESS ON THE FATIGUE STRENGTH AT HIGH TEMPERATURES | 17 |
| MUSTAȚĂ, F., BICU, I., NARCIS, A., FORMALDEHYDE RESINS FROM RENOVABLE RESOURCES | 25 |
| BORDEASU, I., BALASOIU, V., BADARAU, R., POPOVICIU, M.O., DOBANDA, E., ON THE STRUCTURAL TRANSFORMATIONS PRODUCED BY CAVITATIONAL STRESSES | 31 |
| BADARAU, R., BORDEASU, I., BALASOIU, V., SPOREA, I., NICOARA, M., CONSIDERATIONS CONCERNING THE CAVITATIONAL DISTRUCTION OF THE COMPOSITE MATERIAL ARMURED WITH 20% CERAMIC PARTICLES | 39 |
| HULUBEI, C., MORARIU, S., STRUCTURE – THERMAL AND VISCOMETRIC PROPERTIES RELATIONSHIP FOR SOME POLY(N-SUBSTITUTED MALEIMIDE-co-N-VINYL-2-PYRROLIDONE)S | 47 |
| VRAPCEA, M., STOIAN, P., PREDĂ, N., STUDIES AND RESERCH AS REGARDS SPECTRAL REFERENCE MATERIALS FOR NI-CR ALLOYS | 55 |
| VRAPCEA, M., STOIAN, P., THE INTERELEMENT EFFECT STUDY IN SPECTRAL ANALYSIS ON THE SPECTRAL REFERENCE MATERIALS FOR cR-nI STAINLESS STEELS | 61 |
| BELOIU, M., ALEXANDRU, I., CHELARIU, R., ROMAN, C., CARCEA, I., THE INFLUENCE OF MODIFICATION ON THE PHYSICO-MECHANICAL PROPERTIES OF SOME TIN BRONZES | 69 |
| BELOIU, M., ALEXANDRU, I., ROMAN, C., CHELARIU, R., CARCEA, I., WEAR BEHAVIOUR OF SOME BRONZES | 77 |
| BADARAU, GH., BADARAU, V., IONITA, I., STEFAN, M., DIAGNOSIS METHOD AND EVALUATION OF THE METALIC MATERIALS CHOICE | 83 |
| MIREA, C., THE WEAR OF THE METALIC SURFACES IN ABRASIVE TRIBOSYSTEMS I: WEAR TYPES AND MODIFICATIONS OF THE ABRADED SURFACES | 89 |

| | |
|--|-----|
| MIREA, C., THE WEAR OF THE METALIC SURFACES IN ABRASIVE TRIBOSYSTEMS II: WEAR TYPES AND MODIFICATIONS OF THE ABRADED SURFACES | 97 |
| MIREA, C., THE WEAR OF THE METALIC SURFACES IN ABRASIVE TRIBOSYSTEMS III: WEAR TYPES AND MODIFICATIONS OF THE ABRADED SURFACES | 105 |
| GORDIN, D.M., GLORIAN, T., CHELARIU, R., NEMTOI, GH., AELENEI, N., MICROSTRUCTURAL CHARACTERISATION AND ELECTROCHEMICAL BEHAVIOUR OF THE NEW BETA Ti-12Mo-5Ta ALLOY FOR BIOMEDICAL APPLICATIONS | 115 |
| CIUBOTARIU, C.I., MARIN, C., CIUBOTARIU, C., CIUBOTARIU, C., A NEW NANOMATERIAL FOR QUANTUM COMPUTING PROCESSORS AND QUANTUM CELLULAR AUTOMATA. I. INTUITIVE MODELS | 123 |
| SCANTEIANU, N., THE CONFIGURATION OF THE REUSABLE MATERIALS' RECYCLATION PROGRAMMES INSIDE THE EUROPEAN UNION | 131 |
| MINEA, A.A., MECHANICAL PROPERTIES OPTIMISATION OF AN AlCu4Mg1 ALLOY | 139 |
| CARJA, G., FRUNZA, M., POPA, M.I., POPESCU, C., NEW HYBRID NANOCOMPOSITES OF MgAlHT ANIONIC CLAYS INCORPORATED WITH ACETAMIPRID | 145 |
| BERCEA, M., LUBRICANT PERFORMANCES AND ENVIRONMENTAL PROBLEMS | 151 |
| BERCEA, M., MORARIU, S., EFECT OF ADSORPTION ON THE VISCOSITY OF POLYMER SOLUTION AT VERY LOW CONCENTRATIONS | 159 |
| MARECI, D., AELENEI, D.M., NEMTOI, GH, UNGUREANU, G., METALLURGICAL TREATMENT AND SURFACE INFLUENCE ON THE CORROSION RESISTANCE OF NICROMALSOFT ALLOY | 167 |
| SUTIMAN, D., NECHITA, M.T., CĂILEAN, A., MARECI, D., STABILITY OF IRON IN THE SYSTEM METHANOL – ADIPIC ACID – WATER | 175 |
| GHERGHISOR, G., COSMELEATA, G., MIRON, V., GEORGESCU, I., STRUCTURAL CHARACTERISTICS AND MAGNETICAL PROPERTIES OF SILICON STEEL SHEETS | 181 |
| GHIBAN, B., COSMELEATA, G., ALUMINUM DEPOSITION BY CVD METHOD ON NICKEL- BASED SUPERALLOY SUPPORTS | 189 |
| HOTEA, V., IEPURE, GH., POP, E., TALPOȘ, E., IUHAZS, J., POP, A., KINETIC CONSIDERATION OF COPPER REFINING PROCESS | 195 |
| BÂRSĂNESCU, P.D., BÎTCĂ, C., MIHĂLCUȚ, M., CREEP OF SOME POLYURETHANIC ELASTOMERS | 203 |
| BÂRSĂNESCU, P.D., BÎTCĂ, C., BEJENARIU, C., COMPARATIV STUDY ON THE BEHAVIOR OF THE RUBBER AND SOME POLYURETHANS UNDER CREEP CONDITIONS | 209 |
| GHERGHESCU, I., CIUCĂ, S., STRUCTURAL ASPECTS OF A Ni ₅₀ Ti ₄₈ Nb ₂ SHAPE MEMORY ALLOY REVEALED BY SCANNING AND TRANSMISSION ELECTRON MICROSCOPY | 213 |
| BÎTCĂ, C., MIHALCUT, M., BÂRSĂNESCU, P.D., CONSIDERATIONS ON MECHANICAL PROPERTIES OF THE HUMAN BONES | 221 |
| COMANDAR, C., AMARIEI, N., LEON, D., DUMITRACHE, C., SOME ASPECTS REGARDING THE DESIGN OF NAIMOV SAMPLES FOR STRESS RELAXATION BENDING TESTS | 227 |

| | |
|--|-----|
| MARECI, D., SUTIMAN, D., FOCA, N., CARJA, G., BOCANU, C., THE ALLOYING ELEMENTS INFLUENCE OVER CORROSION RESISTANCE OF SOME BIOMATERIALS NICKEL BASED | 233 |
| BÂRSĂNESU, P.D., BÎTCĂ, C., STOIAN, A., INFLUENCES OF ENVIRONMENT ON DEFORMATION AND CRACK OF ESTANE ELASTOMERS | 241 |
| LEONTIE, L., DRUTA, I., DANILOAIA, T., RUSU, G.I., ON THE D.C. CONDUCTION MECHANISM OF N-(p-R-PHENACYL)-1,7-PHENANTHROLINIUM BROMIDES IN THIN FILMS | 247 |
| SUTEU, D., GORDUZA, V.M., TOFAN, L., FUNCTIONALIZED MATERIALS IN MONITORING AND REMEDIATION OF ENVIRONMENT | 255 |
| DOBREA, V., CHIRIAC, H., CRAUS, M.L., STRUCTURAL PROPERTIES AND TRANSITION TEMPERATURES OF POLYCRYSTALLINE NiMnGa SHAPE MEMORY ALLOYS | 263 |
| CANTEMIR, D., VALENTINI, R., PAGLIARO, M., INFLUENCE OF TEMPERATURE AND STRAIN RATE ON MECHANICAL PROPERTIES OF A BORON STEEL | 269 |
| VLADESCU, A., BRAIC, V., BALACEANU, M., BRAIC, M., KISS, A., COTRUT, C.M., CHARACTERIZATION OF LUBRICANT COATINGS | 277 |
| VLADESCU, A., BALACEANU, M., BRAIC, V., BRAIC, M., ZAMFIR, R., CORROSION OF TIN COATINGS DEPOSITED ON COCR ALLOY SUBSTRATES | 283 |
| FOCA, N., MARECI, D., BOCANU, C., TOFAN, A., CHARACTERIZATION OF PHOSPHOGYPSUM BY PHYSICAL AND CHEMICAL METHODS | 289 |
| HULUBEI, C., HAMCIUC, E., POLYESTERS BASED ON EPICLON | 295 |
| CATANGIU, A., NONLINEAR BEHAVIOR IN CROSS-PLY GLASS/EPOXY COMPOSITE LAMINATES | 303 |
| BATIN, G., POPA, C., VIDA-SIMITI, I., TITANIUM/HYDROXYAPATITE GRADED MATERIALS FOR ENDOSSEUS IMPLANTS | 311 |

ȘTIINȚA ȘI INGINERIA MATERIALELOR

| CUPRINS | |
|--|----|
| COJOCARU FILIPIUC, V., ÎMBUNĂȚĂȚIREA OBȚINERII FONTEI CU GRAFIT NODULAR PRIN MODIFICARE ÎN OALA DE TURNARE (CU DOUĂ CAMERE DE REACȚIE ȘI BARE PORT-DOP) | 1 |
| PRISACARIU, C., CARACULACU, A., INFLUENȚA CONDIȚIILOR DE ÎMBĂTRÂNIRE ȘI A STRUCTURII CHIMICE ASUPRA CURBELOR DE ÎNTINDERE-DEFORMARE LA FILMELE POLIURETANICE CU STRUCTURI DIBENZILICE | 9 |
| AMARIEI, N., COMANDAR, C., LEON, D., DUMITRACHE, C., INFLUENȚA TENSIUNILOR REMANENTE REZULTATE DIN PROCESUL DE NITRURARE ASUPRA REZISTENȚEI LA OBOSEALA LA TEMPERATURI RIDICATE | 17 |
| MUSTAȚĂ, F., BICU, I., NARCIS, A., RAȘINI FORMALDEHIDICE DIN RESURSE NATURALE | 25 |
| BORDEASU, I., BALASOIU, V., BADARAU, R., POPOVICIU, M., DOBANDA, E., ASUPRA TRANSFORMĂRIILOR STRUCTURALE PRODUSE DE SOLICITĂRILE CAVITAȚIONALE | 31 |
| BADARAU, R., BORDEASU, I., BALASOIU, V., SPOREA, I., NICOARA, M., CONSIDERATII PRIVIND DISTRUGEREA PRIN CAVITAȚIE A MATERIALULUI COMPOZIT ARMAT CU 20% PARTICOLE CERAMICE | 39 |
| HULUBEI, C., MORARIU, S., RELAȚIA STRUCTURĂ-PROPRIETĂȚI TERMICE ȘI VÂSCOZIMETRICE PENTRU POLY(MALEIMIDĂ N-SUBSTITUITĂ-co-N-VINILPIROLIDONĂ) | 47 |
| VRAPCEA, M., STOIAN, P., PREDĂ, N., STUDII SI CERCETARI PRIVIND MATERIALELE DE REFERINȚA SPECTRALE PENTRU ALIAJE NI-CR | 55 |
| VRAPCEA, M., PETRE STOIAN, P., STUDIUL EFECTULUI INTERELEMENT IN ANALIZA SPECTRALA PE MATERIALE DE REFERINȚA SPECTRALE PENTRU OTELURI INOXIDABILE CR-NI | 61 |
| BELOIU, M., ALEXANDRU, I., CHELARIU, R., ROMAN, C., CARCEA, I., INFLUENȚA MODIFICĂRII ASUPRA UNOR PROPRIETĂȚI FIZICO-MECANICE ALE UNOR BRONZURI CU STANIU | 69 |
| BELOIU, M., ALEXANDRU, I., ROMAN, C., CHELARIU, R., CARCEA, I., COMPORTAREA LA UZARE A UNOR BRONZURI | 77 |
| BADARAU, GH., BADARAU, V., IONITA, I., STEFAN, M., METODA DE DIAGNOSTICARE SI EVALUARE A ALEGERII MATERIALELOR METALIC | 83 |
| MIREA, C., UZAREA SUPRAFETELOR METALICE ÎN TRIBOSISTEME | 89 |

| | |
|---|-----|
| ABRAZIVE, I: TIPURI DE UZARE ȘI MODIFICĂRI ALE SUPRAFETELOR UZATE PRIN ABRAZIUNE | |
| MIREA, C., UZAREA SUPRAFETELOR METALICE ÎN TRIBOSISTEME ABRAZIVE, II: TIPURI DE UZARE ȘI MODIFICĂRI ALE SUPRAFETELOR UZATE PRIN ABRAZIUNE | 97 |
| MIREA, C., UZAREA SUPRAFETELOR METALICE ÎN TRIBOSISTEME ABRAZIVE, III: TIPURI DE UZARE ȘI MODIFICĂRI ALE SUPRAFETELOR UZATE PRIN ABRAZIUNE | 105 |
| GORDIN, D.M., GLORANT, T., CHELARIU, R., NEMTOI, GH., AELENEI, N., CARACTERIZAREA MICROSTRUCUTRALA SI COMPORTAREA ELECTROCHIMICA A NOULUI ALIAJ Ti-12Mo-5Ta PENTRU APLICATII BIOMEDICALE | 115 |
| CIUBOTARIU, C.I., MARIN, C., CIUBOTARIU, C., CIUBOTARIU, C., UN NOU NANOMATERIAL PENTRU PROCESOARELE DE CALCUL CUANTIC SI AUTOMATELE CELULARE CUANTICE. I. MODELE INTUITIVE | 123 |
| SCANTEIANU, N., CONFIGURAREA PROGRAMELOR DE RECICLARE A MATERIALELOR REFOLOSIBILE IN UNIUNEA EUROPEANA | 131 |
| MINEA, A.A., OPTIMIZAREA PROPRIETATILOR MECANICE ALE UNUI ALIAJ AlCu4Mg1 | 139 |
| CARJA, G., FRUNZA, M., POPA, M.I., POPESCU, C., NOI NANOCOMPOSITE HIBRIDE A ARGILELOR ANIONICE DE TIP MgAlHT INCORPORATE CU ACETAMIPRID | 145 |
| BERCEA, M., PERFORMANTE ALE LUBRIFIANTILOR SI PROBLEME LEGATE DE MEDIUL INCONJURATOR | 151 |
| BERCEA, M., MORARIU, S., EFECTUL ADSORBTIEI ASUPRA VISCOZITATII SOLUTIILOR DE POLIMERI LA CONCENTRATII FOARTE MICI | 159 |
| MARECI, D., AELENEI, D.M., NEMTOI, GH, UNGUREANU, G., INFLUENTA TRATAMENTULUI METALURGIC SI SUPRAFETEI ASUPRA REZISTENTEI LA COROZIUNE A ALIAJULUI NICROMALSOFT | 167 |
| SUTIMAN, D., NECHITA, M.T., CĂILEAN, A., MARECI, D., STABILITATEA FIERULUI ÎN SISTEMUL METANOL-ACID ADIPIC-APĂ | 175 |
| GHERGHISOR, G., COSMELEATA, G., MIRON, V., GEORGESCU, I., CARACTERISTICILE STRUCTURALE ȘI PROPRIETĂȚILE MAGNETICE ALE BENZILOR DIN OȚEL SILICIOS | 181 |
| GHIBAN, B., COSMELEATA, G., DEPUNEREA ALUMINIULUI PRIN METODE CVD PE SUPPORT DIN SUPERALIAJE PE BAZA DE NICHEL | 189 |
| HOTEA, V., IEPURE, GH., POP, E., TALPOȘ, E., IUHAZS, J., POP, A., CONSIDERAȚII CINETICE PRIVIND PROCESUL DE RAFINARE TERMICĂ A CUPRULUI | 195 |
| BĂRSĂNESCU, P.D., BÎTCĂ, C., MIHĂLCUȚ, M., STUDIUL LA FLUAJ A UNOR ELASTOMERI POLIURETANICI LA TRACȚIUNE | 203 |
| BĂRSĂNESCU, P.D., BÎTCĂ, C., BEJENARIU, C., STUDIUL COMPARATIV ASUPRA COMPORTĂRII LA FLUAJ A CAUCIUCULUI ȘI A UNOR POLIURETANI | 209 |
| GHERGHESCU, I., CIUCĂ, S., ASPECTE STRUCTURALE ALE UNUI ALIAJ CU MEMORIA FORMEI Ni ₅₀ Ti ₄₈ Nb ₂ RELEVATE PRIN MICROSCOPIE ELECTRONICĂ PRIN BALEIAJ ȘI TRANSMISIE | 213 |
| BÎTCĂ, C., MIHALCUT, M., BĂRSĂNESCU, P.D., CONSIDERAȚII ASUPRA | 221 |

| | |
|--|-----|
| PROPRIETĂȚILOR MECANICE ALE OASELOR UMANE | |
| COMANDAR, C., AMARIEI, N., LEON, D., DUMITRACHE, C., CÂTEVA ASPECTE PRIVIND PROIECTAREA EPRUVETELOR NAIMOV PENTRU ÎNCERCĂRI DE RELAXARE A TENSIUNILOR PRIN ÎNCOVOIERE | 227 |
| MARECI, D., SUTIMAN, D., FOCA, N., CARJA, G., BOCANU, C., INFLUENȚA ELEMENTELOR DE ALIERE ASUPRA COROZIUNII UNOR BIOMATERIALE PE BAZĂ DE NICHEL | 233 |
| BĂRSĂNESU, P. D., BÎTCĂ, C., STOIAN, A., INFLUENȚA MEDIULUI ASUPRA DEFORMĂRII ȘI RUPERII ELASTOMERILOR ESTANE | 241 |
| LEONTIE, L., DRUTA, I., DANILOAIA, T., RUSU, G.I., ASUPRA MECANISMULUI DE CONDUCTIE ELECTRICA IN STRATURI SUBTIRI DE BROMURI DE N-(PARA-R-FENACIL)-1,7-FENANTROLINIU | 247 |
| SUTEU, D., GORDUZA, V.M., TOFAN, L., MATERIALE FUNCȚIONALIZATE ÎN MONITORIZAREA ȘI REMEDIEREA MEDIULUI | 255 |
| DOBREA, V., CHIRIAC, H., CRAUS, M.L., PROPRIETĂȚI STRUCTURALE ȘI TEMPERATURI DE TRANSFORMARE PENTRU UNELE ALIAJE NiMnGa POLICRISTALINE CU MEMORIA FORMEI | 263 |
| CANTEMIR, D, VALENTINI, R., PAGLIARO, M., INFLUENTA TEMPERATURII SI A VITEZEI DE DEFORMARE ASUPRA PROPRIETILOR MECANICE ALE UNUI OTEL ALIAT CU BOR | 269 |
| VLADESCU, A., BRAIC, V., BALACEANU, M., BRAIC, M., KISS, A., COTRUT, C.M., CARACTERIZAREA ACOPERIRILOR LUBRIFIANTE | 277 |
| VLADESCU, A., BALACEANU, M., BRAIC, M., BRAIC, M., ZAMFIR, R., COROZIUNEA STRATURILOR TiN DEPUSE PE SUBSTRATURI DE ALIAJ CoCr | 283 |
| FOCA, N., MARECI, D., BOCANU, C., TOFAN, A., CARACTERIZAREA FOSFOGIPSULUI PRIN METODE FIZICE ȘI CHIMICE | 289 |
| HULUBEI, C., HAMCIUC, E., POLIESTERI PE BAZA DE EPICLON | 295 |
| CATANGIU, A., COMPORTAREA NELINIARA A COMPOZITELOR STRATIFICATE STICLĂ-EPOXI [0/90]_s | 303 |
| BATIN, G., POPA, C., VIDA-SIMITI, I., MATERIALE CU GRADIENT PE BAZA DE TITAN SI HIDROXIAPATITA PENTRU IMPLANTE ENDOOSOASE | 311 |

IMPROVEMENT OF OBTAINING OF SPHEROIDAL GRAPHITE CAST IRON BY INOCULATING LADLES (TWO CHAMBERS AND TWO STOPPERS LADLE)

BY

VASILE COJOCARU-FILIPCIUC

Abstract: The inoculating ladle has two chambers limited by a vertical separating plate and two horizontal separating plates. The horizontal separating plates are furnished each with an orifice. These orifices are blocked and unblocked by the stoppers which are operated by two mechanisms. The magnesium from the chambers evaporates itself when iron penetrates into them. The magnesium vapours leave the chambers and they are distributed in all molten metal when they touch the heads of the stoppers.

This paper presents two new methods of improvement of the iron inoculating regularity degree.

The first improvement method consists in equidistant placing of the stoppers and the second one consists in sketching of a new shape of the stoppers heads. Thus, the degree of graphite spheroidizing and the degree of uniformity of iron inoculation are better.

Keywords: inoculating, magnesium vapours, distribution in liquid iron

1. General considerations

Spheroidal graphite cast iron is obtained usually by ladle inoculation. There is a lot of introduction methods of the inoculant in the molten metal. Every introduction method assures a certain assimilation efficiency of inoculant in iron, / 1, 2, 3 ... 7/.

Obtained inoculated iron must have a big degree of regularity of iron inoculating, a big degree of graphite spheroidizing, a better size of spheroidal graphite inclusions and a good matrix of the metallographic microstructure.

[1] presents an inoculating procedure what consist in a ladle, which has a inoculant chamber, a horizontal plate with an orifice and a stopper which is placed in the center of the ladle cavity. The stopper obturates and unobturates orifice from the horizontal plate where liquid iron penetrates into inoculant chamber and the magnesium vapours are evacuated – Fig. 1 ([1] shows that the stopper has ceramics ribs and is turned by an electric motor). Because the stopper is placed central in the ladle cavity, the magnesium vapours are distributed uniform, in all directions in the metallic bath.

1. Inoculating ladle with two chambers and two stoppers

The conceived and projected inoculating ladle is presented in Fig. 2, [2].

The achieved inoculated ladle is an adaptation of a steel stopper ladle. So, an operating mechanism of stopper is become attached supplementary to the ladle (the bottom orifice of the steel stopper ladle was annulled).

The capacity of inoculating ladle is 2 t.

The conceiving of the inoculating ladle had taken into consideration that the maximum inoculant consumption (FeSiCaMg) is about 3%.

The horizontal separating plates have been dimensioned with PLOBA 02 program, [3].

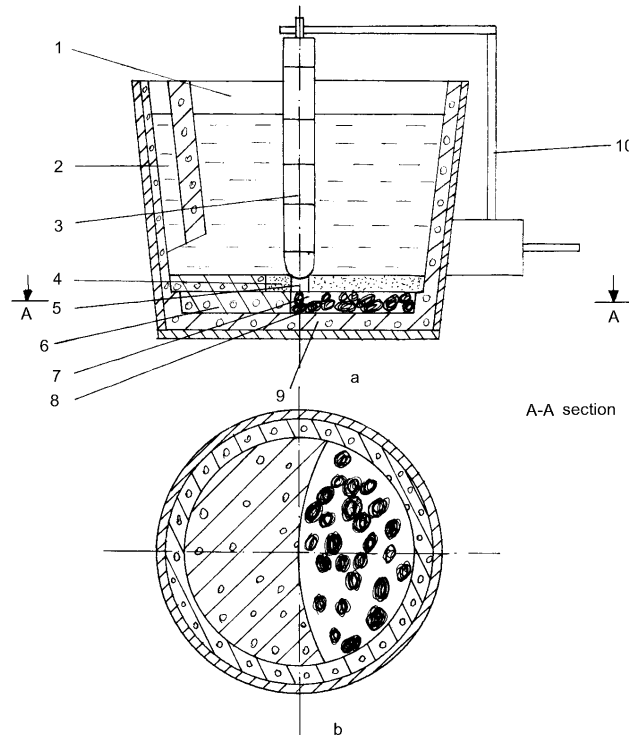


Fig.1. The ladle with an stopper and a inoculant chamber. a – longitudinal section; b – cross section A-A; 1 – ladle cavity; 2 – up-hill casting channel; 3 – stopper; 4 – horizontal plate; 5 – orifice; 6 – propping up refractory lining; 7 – inoculant chamber; 8 – inoculant; 9 – refractory lining; 10 – training mechanism.

Corresponding to Fig. 2 and [2], the stoppers are not placed equidistantly between the walls and between themselves.

The Fig. 3 presents a new variant of the ladle with two stoppers and two inoculant chambers. This one has the stoppers placed equidistantly given the walls and themselves. So, diffusion distances of the magnesium particles become less, the magnesium vapours are distributed more uniform, iron is inoculated more uniform, inoculating degree is bigger etc.

The inoculating ladle is prepared corresponding to Fig. 1. The stopper rods and the stoppers are the same of stopper ladles which mainly serve for pouring molten steel.

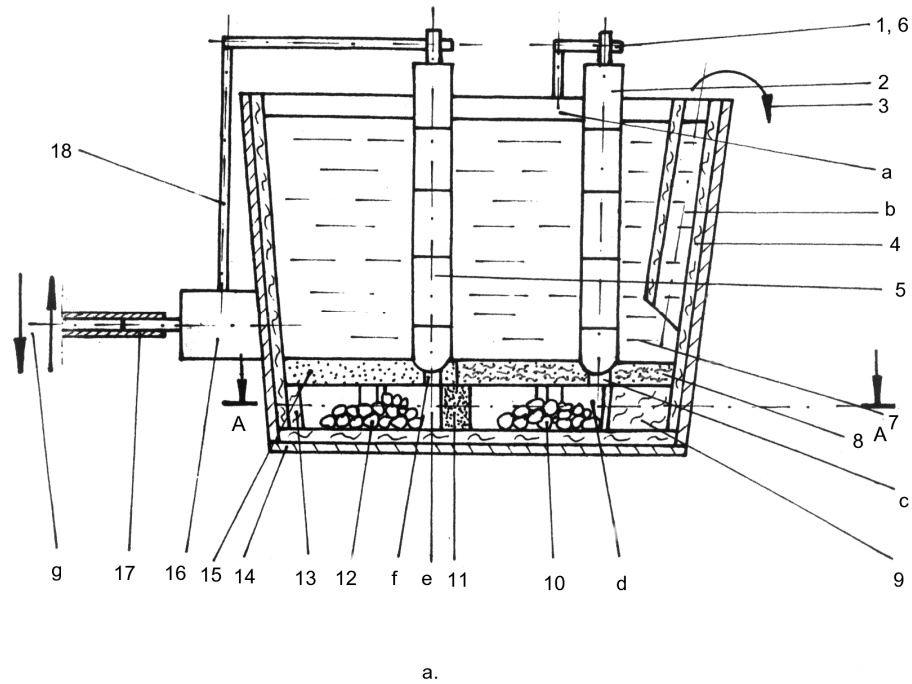
Fig. 4 presents the ladle with two stoppers and two inoculant chambers, the stoppers being placed equidistant – the capacity of 2 t. This inoculating ladle was used for experiments.

For experiments the same inoculant (FeSiCaMg) was used in those inoculant chambers.

2. Inoculating technology

The vertical separating plate is assembled as in Fig. 2. The possible leakiness between the vertical separating plate and the vertical wall of the bottom of the

inoculating ladle are packed with core mixture with soda water glass (or others bindings). Then, the inoculant (or inoculants) is located in chambers I and II. Afterwards the horizontal separating plates are assembled and then the possible leakiness between the horizontal separating plates and the vertical wall or between the horizontal separating plates are packed with core mixture, too. The stoppers are assembled perpendicular on the horizontal separating plates, these obturating the orifices I and II.



A-A section

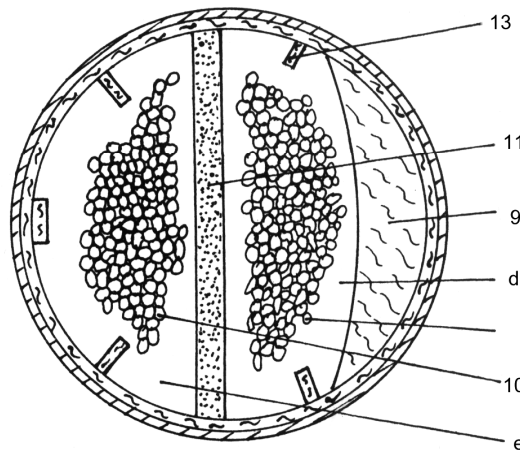


Fig. 2. The ladle with two chambers and two stoppers: a – longitudinal section; b – cross section A-A; 1 – operating mechanism I; 2 – stopper I; 3 – tilting way with a view to the eviction of iron from the ladle; 4 – refractory lining; 5 – stopper II; 6 – training mechanism I; 7 – uninoculated molten iron; 8 – horizontal separating plate I; 9 – propping up refractory lining; 10 – inoculant I; 11 – vertical separating plate; 12 – inoculant II; 13 – propping up refractory brick; 14 – ladle shell; 15 – horizontal separating plate II; 16 – training mechanism II; 17 – operating pipe; 18 – operating mechanism II; a – ladle cavity; b – up-hill casting channel; c – orifice I; d – chamber I; e – chamber II; f – orifice II; g – operating way of the pipe 17.

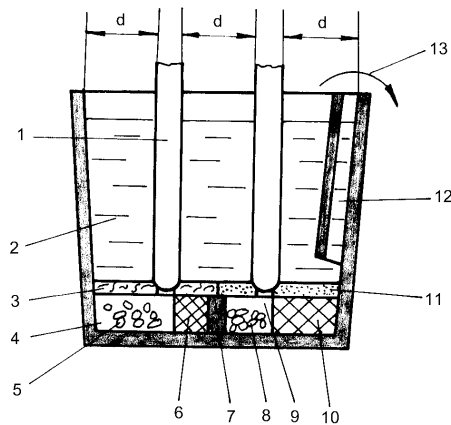


Fig.3. Sketch of the ladle with two stoppers and two inoculant chambers, the stoppers being placed equidistant. 1 – stoppers; 2 – uninoculant molten iron; 3 – horizontal separating plate I; 4 – inoculant chamber I; 5 – inoculant I; 6 – propping up refractory lining I; 7 – vertical separating plate; 8 – inoculant II; 9 – inoculant chamber II; 10 – propping up refractory lining II; 11 – horizontal separating plate II; 12 – up-hill casting channel; 13 – tilting way with a view to the eviction of iron from the ladle; d – distance.



Fig. 4. The inoculant ladle achieved and used for experiments (with two stoppers placed equidistantly and two inoculant chambers).

The inoculating ladle is preheated, then, with a mobile gas burner.

The inoculating ladle is displaced to the pouring platform where the molten cast iron is casted in it (without the slag). Iron can be cast in inoculating ladle from the melting aggregate, too, this case being normal one.

The next stage is the first inoculation phase which consists in operating of the pipe (17) downward until a click is heard and felt. This click comes from a blocking-unblocking mechanism of the stopper operating. The second race is for the case when the inoculation is not achieved.

Orifice I is open by the operating mechanism and iron penetrates into the chamber I where touches the inoculant. Magnesium is evaporated and magnesium vapours leave the chamber I, evacuating through the molten metal. First, magnesium vapours touch the stopper head and they are distributed in a lot of directions, thus the area of contact between inoculant and iron enlarging itself. The second inoculating phase begins after the finishing of first of the inoculating phase (when light signals of magnesium oxidizing and the barbotage of the molten metal are stopped). The second inoculating phase starts and goes on similarly

as the first inoculating phase.

The size of vertical separating plate is 674x80x100 mm, for the horizontal one the height is 100 mm, and the orifices diameter is 50 mm.

4. Characteristics of inoculating technology

The moment of the inoculating beginning is under control. So, the inoculating ladle with iron is displaced to the pouring platform, the inoculated being achieved when all is ready. Thus, time between inoculation and solidification is minimum.

The inoculating ladles with big capacities can have one, three or more chambers. So, the inoculant can be more sorts for the same inoculation. The inoculation by two phases or more, determines a superior efficiency (a smaller inoculant consumption, too).

In all cases of inoculating classical ladle, the magnesium vapours do not touch an obstacle when they evacuate themselves through the molten metal. In the case of this new technology, magnesium vapours touch the head of the stopper, thus, the magnesium vapours being scattered in a big molten metal volume. So, diffusing distances of magnesium are shorted.

The head of the stopper determines the division of the magnesium vapours when they touch it. Thus, the rate of evacuating of magnesium vapours through the molten metal is smaller thanks to the smaller size of the vapours. The smaller size determines a bigger area of contact between the inoculant and the molten metal. So, the inoculating efficiency is higher.

The ascension force of magnesium vapours is small near the head of the stopper because there is a shearing force between the magnesium vapours and the head of the stopper. So, the contact time between magnesium vapours and the molten metal increases – inoculation efficiency increases, too.

4. Experiments and results

Table 1 presents chemical the composition of the metallographic specimens, before the inoculation/after the inoculation.

Table 1 Chemical composition, before the inoculation/after the inoculation

| Number of the charge | Composition, % by mass | | | | | |
|----------------------|------------------------|-----------|-----------|-------------|-------------|---------|
| | C | Mn | Si | S | P | Mg |
| 0 | 1 | 2 | 3 | 4 | 5 | 6 |
| 1 | 3.08/2.80 | 0.72/1.08 | 1.50/2.02 | 0.040/0.030 | 0.150/0.098 | -/0.050 |
| 2 | 3.52/3.46 | 0.98/1.05 | 1.54/2.28 | 0.034/0,026 | 0.130/0.100 | -/0.050 |
| 3 | 3.12/3.40 | 0.93/1.30 | 1.61/2.52 | 0.032/0.030 | 0.040/0.098 | -/0.057 |
| 4 | 3.28/3.04 | 0.56/0.68 | 1.36/2.42 | 0.023/0.029 | 0.125/0.087 | -/0.038 |
| 5 | 3.52/3.40 | 0.52/0.99 | 1.57/2.39 | 0.055/0.030 | 0.100/0.092 | -/0.050 |
| 6 | 3.80/3.28 | 0.72/0.63 | 1.43/2.80 | 0.036/0.030 | 0.160/0.090 | -/0.023 |

Table 1 – continuation

| 0 | 1 | 2 | 3 | 4 | 5 | 6 |
|----|-----------|-----------|-----------|-------------|-------------|---------|
| 7 | 4.00/3.48 | 0.72/1.22 | 1.52/2.48 | 0.028/0.029 | 0.150/0.080 | -/0.021 |
| 8 | 3.16/3.60 | 0.34/0.25 | 0.84/1.85 | 0.012/0.060 | 0.020/0.100 | -/0.040 |
| 9 | 3.20/2.28 | 0.15/0.80 | 0.86/2.02 | 0.027/0.031 | 0.080/0.050 | -/0.039 |
| 10 | 4.00/2.86 | 0.34/1.15 | 0.41/1.88 | 0.035/0.038 | 0.175/0.061 | -/0.043 |
| 11 | 3.40/3.43 | 0.38/1.01 | 1.27/2.76 | 0.049/0.023 | 0.100/0.120 | -/0.053 |
| 12 | 3.80/3.32 | 0.32/1.32 | 2.60/2.82 | 0.033/0.028 | 0.125/0.100 | -/0.050 |
| 13 | 3.66/3.30 | 0.36/1.08 | 0.72/2.60 | 0.042/0.020 | 0.120/0.100 | -/0.055 |

Table 2 presents the area of the spheroidal graphite inclusions in the metallographic structure, the diameters of the spheroidal graphite inclusions and the area of perlite in the metallic matrix.

The charges of the furnace has been constituted of pig iron.

Table 2 Areas of graphite and perlite and diameters of the spheroidal graphite inclusions

| Number of the charge | Area of graphite, % | The diameters of graphite, μm | Area of perlite, % |
|----------------------|---------------------|--|--------------------|
| 1 | 8...12 | 60...100 | 90...98 |
| 2 | 8...12 | 60...100 | 90...98 |
| 3 | 8...12 | 60...100 | 90...98 |
| 4 | 8...12 | min.100 | 70...90 |
| 5 | 5...8 | 6...40 | 70...90 |
| 6 | 5...8 | 60...100 | 70...90 |
| 7 | 5...8 | 60...100 | 70...90 |
| 8 | 5...8 | 60...100 | 90...98 |
| 9 | max. 3 | 25...40 | 70...90 |
| 10 | 5...8 | 60...100 | 70...90 |
| 11 | 8...12 | 60...100 | 70...90 |
| 12 | 8...12 | 40...60 | 70...90 |
| 13 | 8...12 | 40...60 | 70...90 |

All the charges have been inoculated with 2.1% FeSiCaMg (5.5% Mg). The big addition of inoculant is on account of the big sulphur content.

Ultimate tensile strenght varied among 600-690 N/mm², elongation at fracture among 1.0...4.3% and resilience (for U notched specimen) among 0.3...0.9 daJ/cm². The small elongation at fracture is on account of the big manganese content.

The small resilience is on account of the big phosphorus content.

This inoculating technology has been useful for antifriction cast iron making. For 76 charges, the chemical composition was the next: C = 2.64... 4.24%; Mn = 0.17... 1.29%; Si = 1.00... 3.19%; P = 0.05... 0.2%; S = 0.01... 0.08%; Mg = 0.04 ...0.06 (the maximum frequency was C = 3.540%; Mn = 0.660%; Si = 1.950%; P = 0.140%, S = 0.033%; Mg = 0.050%).

All the graphite inclusions are nodulized for iron charges whose chemical composition are presented in the Table 3.

The magnesim content has been analysed for the charges in table 3 (the

variation of the magnesium content depending on the time), obtaining the equation $Mg = 0.0001455 \tau + 0.03346$, τ being the time. The coefficient of the τ is very small and thus the magnesium content is relative constant (the time was maximum 27 minutes and the mass of the charge has been 1,500 Kg). The time τ can be replaced with the distance because the specimens are sampled during emptying of the inoculating ladle. The inoculation of cast iron is very uniform because the magnesium content has been relative constant.

Table 3 Chemical composition of charges with all the graphite nodulized

| Number of the charge | Chemical composition, % by mass | | | | |
|----------------------|---------------------------------|------|------|------|------|
| | C | Mn | Si | P | Mg |
| 1 | 3.40 | 0.31 | 2.40 | 0.08 | 0.04 |
| 2 | 3.38 | 0.34 | 2.40 | 0.08 | 0.04 |
| 3 | 3.40 | 0.32 | 2.41 | 0.08 | 0.04 |
| 4 | 3.37 | 0.36 | 2.32 | 0.08 | 0.04 |

6. Proposal for improvement of the stoppers heads

Fig. 5 shows a new variant for the stopper head. So, the stopper head has a distribution chamber of the magnesium vapours (4) in ladle cavity by the evacuating channels (1).

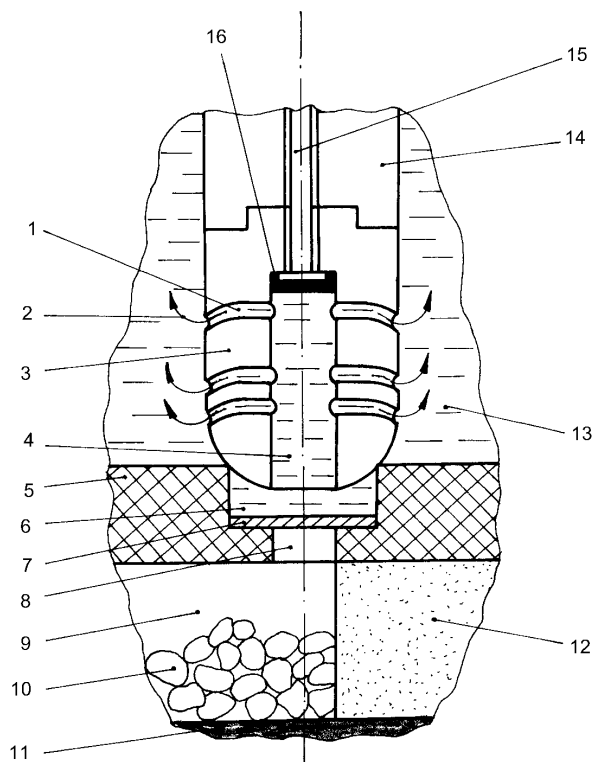


Fig. 5. Sketch of the new variant of the stopper head: 1 – evacuating channels of the magnesium vapours; 2 – evacuating trajectories of the magnesium vapours; 3 – stopper head; 4 – distribution chamber; 5 – horizontal separating plate; 6 – metal plate chamber; 7 – metal plate; 8 – orifice; 9 – inoculant chamber; 10 – inoculant; 11 – refractory lining; 12 – propping up refractory lining; 13 – uninoculated liquid iron; 14 – stopper circular brick; 15 – metallic rod; 16 – tightness refractory material

The horizontal separating plate (5) has an orifice (8) and a metal plate chamber where a metallic plate is placed.

Inoculating technology consists in penetrating of liquid iron into evacuating channels, then into distribution chamber and then into metal plate chamber. In metal plate chamber, liquid iron dissolves the metallic plate and, so, finally, liquid iron penetrates into inoculant chamber where meets the inoculant. Then, the magnesium vapours are evacuated through orifice, distribution chamber, evacuating channels and, finally, through liquid iron from the ladle cavity.

The big number of evacuating channels involves a very good distribution of the magnesium vapours in all metallic bath.

Received May 10 2005

The "Gh.Asachi" Technical University Iași

References

1. Cojocaru, V., Barbu, G. and Oprinca, S. *Oală de turnare*. **Romania patent**. No. 101223, 1992 ;
2. Cojocaru, V. *Tehnologie de elaborare a fontei cu grafit nodular*. **Romania patent**, No 93 691, 1987 ;
3. Cojocaru-Filipiuc, V. *Designing of the semicircular cores of the pouring-modification ladle by the theories of finite elements and dimensioning of the continuous plates*. **Buletinul Institutului Politehnic Iași**. Tomul XL IX (L III), Fasc. 1-4, 2003. Secția Știința și Ingineria Materialelor, p. 65...74 ;
4. *** *Traitement de la fonte a graphite spheroidal*. **Fonderie. Fondeur d'aujourd'hui**, No.5, page 26, 1981;
5. *** **New concepts in nodularisation and inoculation**. **Foundry Trade Journal**, nr. 3217, page 105-107, 1981;
6. Bylund, G. *Holding Nodular Iron in a Channel Induction Furnace*. **Trans. Amer. Foundrymen' s Soc.** vol.83, Des Plaines, 11, page 385...392, 1975;
7. Friederich, R. and Stoian, V. *Ploba program. Calculul și dimensionarea plăcilor plane din beton armat*. **Pachet D.I.M.**, Timișoara, 1984;
8. Georges Fischer-Société Anonyme Schaffhause. *La fonte á graphite spheroidal á Mg pure et know-how*. **Fonderie. Fondeur d'aujourd'hui**, No. 28, page 16, 1983;
9. Jeingwirth, K.H. *Treating Process a New Variant of Magnesium Treatment for the Production of Ductile Iron*. **Giesserei-Praxis**, No. 7, page 93...100, 1983;
10. Tahako, K. *Method for adding alloying elements to molten metals*. **U.S. Patent**, 3,729,309, Apr. 24, 1973;

Vasile Cojocaru-Filipiuc, D.Sc.Prof. Technical University "Gh. Asachi", Bv. Mangeron, no. 61, Iași, România

ÎMBUNĂȚIREA OBȚINERII FONTEI CU GRAFIT NODULAR PRIN MODIFICARE ÎN OALA DE TURNARE (CU DOUĂ CAMERE DE REACȚIE ȘI BARE PORT-DOP)

Rezumat: Oala de turnare-modificare este prevăzută cu două camere de reacție separate de cavitatea oalei de turnare prin intermediul a câte unui orificiu ce este obturat și dezobturat de câte o bară port-dop.

Barele port-dop, conform acestei lucrări, sunt amplasate echidistant față de peretele oalei și între ele, ceea ce determină o micșorare a distanțelor de difuzie, o distribuire mai bună a vaporilor de magneziu și, în final, o îmbunătățire a randamentului de modificare.

Se sugerează o nouă geometrie a capului barelor port-dop, acesta având o cameră de distribuție și niște canale de evacuare a vaporilor de magneziu. Bara port-dop obturează tot timpul orificiul din placa separatoare orizontală în care se află amplasată o placă metalică. Fonta lichidă pătrunde prin canalele de evacuare și camera de distribuție în locașul plăcii metalice din placa separatoare orizontală, dizolvă placa metalică, astfel, fonta lichidă ajungând în locașul modificadorului, la modificador. Vaporii de magneziu se vor evacua prin orificiu, camera de distribuție și canalele de evacuare în fonta lichidă din cavitatea oalei, modificând-o în mod uniform.

THE INFLUENCE OF AGEING CONDITIONS AND CHEMICAL STRUCTURE ON THE STRESS-STRAIN DATA OF DIBENZYL BASED POLYURETHANE FILMS

BY

CRISTINA PRISACARIU and ADRIAN CARACULACU

Abstract: Two series of thin polyurethanic (PU) films derived from 4,4'-methylene bis(phenyl isocyanate) (MDI) and 4,4'-dibenzyl diisocyanate (DBDI) respectively were achieved: (a) casted humidity post cured PU films; (b) PU urea films with three-dimensional structures which were synthesized on employing constant quantities of solutions of polyol. In the case of dibenzyl PU films, rotation around the central $-\text{CH}_2-\text{CH}_2-$ bridge allows alignment of aromatic rings. The effect of $-\text{CH}_2\text{CH}_2-$ vs. CH_2 spacers between the aromatic rings was followed. The soft segment macrodiol (MD) was polytetrahydrofuran (PTHF) or poly(ethylene adipate) (PEA) of molar mass 2000 ± 50 . The influence of the soft segment nature on the PU films mechanical performance in time was undertaken under different ageing conditions and hostile environments. The influence of the geometry of isocyanate on the modification of PU films properties in time was studied and the stress-strain data were determined to enable monitoring of evolution of PU strength stress, elongation at break and residual elongation. The determination of the optimum mixture proportion of components in PU films was made by means of a multiple regression calculus to follow the way in which the excess of isocyanate and the quantity of catalyst influence the mechanical performance of PU urea films with three-dimensional structures.

Keywords: dibenzyl disocyanate, polyurethane films, ageing, mechanical performance.

1. Introduction

Polyurethane (PU) films form a class of materials with a unique versatility. PU films are characterized by presence of the urethane link $-\text{CO}-\text{NH}-\text{O}-$ in the macromolecular backbone, and formed by reaction between isocyanates and polyols, but materials with wide variations in physical properties are possible, by varying the choice of these ingredients. In the segmented polyurethane films, molecules consist of alternating flexible (soft) and relatively rigid (hard) segments [1], (Figs.1 and 2).

Two series of thin polyurethanic (PU) films derived from 4,4'-methylene bis(phenyl isocyanate) (MDI) [1] and 4,4'-dibenzyl diisocyanate (DBDI) [2] respectively were achieved: (a) casted humidity post cured PU films; (b) tridimensional PU urea films which were synthesized on employing constant quantities of solutions of polyol. In the case of dibenzyl PU films, rotation around the central $-\text{CH}_2-\text{CH}_2-$ bridge allows alignment of aromatic rings. and hence crystallization within the PU hard phase,[2,3]. The soft segment macrodiol (MD) was polytetrahydrofuran (PTHF) or poly(ethylene adipate) (PEA) of molar mass 2000 ± 50 . The influence of the soft segment nature on the PU films mechanical performance in time was followed. The influence of the geometry of isocyanate on the modification of PU films properties in time was studied and the stress-strain data were approached to monitor the evolution of PU strength stress, elongation at break and residual elongation for casting PU of

variable isocyanic index. Postcuring phenomena in DBDI based PU films were previously undertaken [3,4].

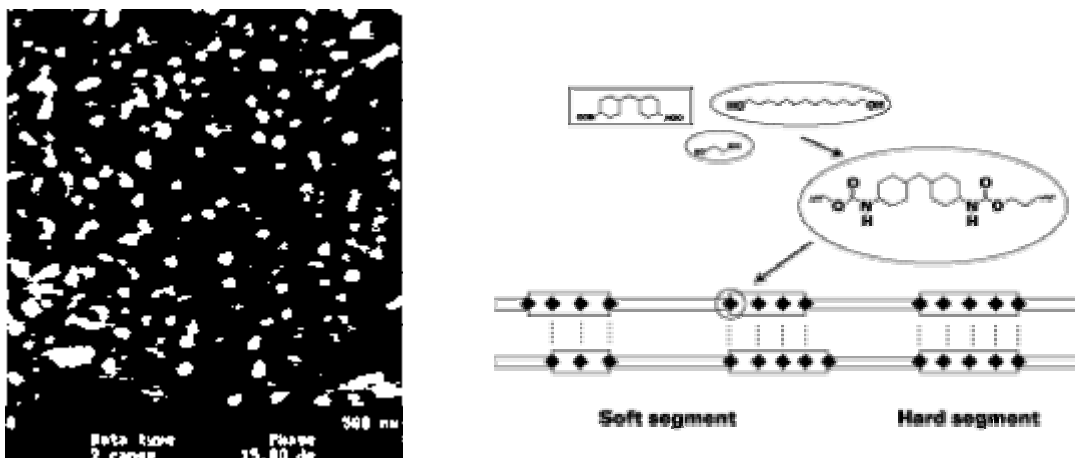


Fig. 1. PU hard and soft domains.

Fig. 2. PU structure. After Christoph Irle and Rolf Roschu / Bayer Hispania S.A.

2. Experimental procedure

2.1. Casted humidity post cured PU films

2.1.1. *Materials.* Hydroxy terminated macrodiols ($M=2000 \pm 50$) i.e. polyethylene adipate (PEA) produced by CIFIC –Savinesti, Romania, and polytetrahydrofuran (PTHF), (BASF Germany) were used without other purification. Commercial available components i.e. 4,4'-dibenzyl diisocyanate (DBDI) (CIFIC-Savinesti) as well as 4,4'-methylene bis(phenyl isocyanate) (MDI) [3] and diethylene glycol (DEG) were purified and anhydrided by vacuum distillation or other appropriate techniques as that of crystallization. More than 99% purity has been established.

2.1.2. *Polyaddition Porcedure.* The polyaddition in two steps by the prepolymer route was approached. 100 g (0.05 moles) of macrodiol was dehydrated under mixing at 115°C and vacuum, (1mm Hg) for 2 hours. Then, 400 g (1.5151 mol) of DBDI crystals (in the case of PU derived from dybenzyl structures) were added under intense mixing to the anhydrous macrodiol and the vacuum was restored. After 30 minutes of mixing under vacuum at 100°C , the temperature was reduced at 90°C , and the vacuum was removed, then 93.1 g (0.877 mol) anhydrous diethylene glycol (DEG) were added at once under very rapid stirring. The mixing was continued for a maximum of 40 seconds. The seconds “pot life” of this nature is about 5 minutes; during this time the liquid mixture was cast onto closed teflonated moldings pre-heated at 90°C so as to avoid the interference of air humidity during the cure process. In the case of open molding the presence of air usually leads to some perturbing uncontrolled and unhomogeneous enhancement of the mechanical properties. About 20μ thin PU films of different thickness and were obtained [3]. For the cure process after casting, the closed moldings were maintained at 110°C for 24 hours. After an additional 24 hours at room temperature, PU sheets were demolded.

2.2. PU urea films with tridimensional structures

PU urea films were synthesized on approaching a special technique which has consisted of three stages involving the achievement of: (a) the solution of polyol; (b) the solution of diisocyanate with rigid (MDI) or flexible (DBDI) structures; (c) the solution of catalyst. The solution of polyol has consisted of a macrodiol (MD) e.g. polyethylene adipate (PEA) or polytetrahydrofuran (PTHF), diethylene glycol (DEG) as a chain extender and small variable quantities of trifunctional agents (tryols). Other details regarding the synthesis of tridimensional PU urea films are given elsewhere [5,6].

3. Results and Discussion

3.1. Stress-strain data of casted humidity post cured PU films

As observed, of the 100 % (σ^{100}) and 300% (σ^{300}) tensile stress PU values and those regarding the PU tensile strength values (σ_r), σ^{300} and σ were found to be higher in thin 0.5 to 1 mm thick PU films than in 2 mm thicker PU sheets as casted after synthesis, (Table 1). This is due to the fact that in the case of PU thinner films, the more polar urea group formation is favored to the prejudice of allophanate groups appearance [3]. The relatively similar σ^{100} values can be explained by the fact that till to this level of stretching the main energy in the PU macromolecule network is consumed for the loosening of the soft segments tangle.

Table 1. Influence of Thickness on the Stress-Strain Data of Casting Postcured PU^a

| Thickness, Δ (mm) | Hardness, (Sh ⁰ A) | σ^{100} , (MPa) | σ^{300} , (MPa) | σ_r , (MPa) | Elongation at break, (%) | Residual elongation, (%) |
|--------------------------|-------------------------------|------------------------|------------------------|--------------------|--------------------------|--------------------------|
| 0.5 | 90 | 7.1 | 16.7 | 77.4 | 665 | 5 |
| 0.75 | 90 | 7.0 | 16.3 | 76.0 | 650 | 5 |
| 1.0 | 90 | 6.4 | 15.1 | 74.2 | 600 | 5 |
| 2.0 | 90 | 5.8 | 13.6 | 71.4 | 550 | 10 |

^a PU were synthesized with an isocyanic index $I = 110$ – e.g. when employing an excess of 10% isocyanic groups (NCO) against the hydroxyl (OH) sum proceeded from the polyol and chain extender. $I = \{[\text{NCO}] / ([\text{OH}]_{\text{Macrodiol}} + [\text{OH}]_{\text{CE}})\} \cdot 100$.

As shown by the IR dichroic studies [3], the influence of the hydrogen bonding becomes decisive at elongations over 300% when all the hard segments achieve a parallel orientation towards the stress direction.

3.2. Stress-strain data of PU urea films with three-dimensional structures.

Influence of the geometry of isocyanate on the modification of PU films mechanical properties in time

The study of the lifetime extension and ageing of three-dimensional structure PU urea films towards environmental and hostile condition was undertaken. The influence of the geometry of isocyanate on the modification of PU films properties in time was studied and the stress-strain data were approached to monitor the evolution of PU. Polyurethanic urea films based on 4,4'-dibenzyl diisocyanate as an isocyanate of conformational mobility were compared to classical PU urea films derived from an isocyanate with a rigid geometry, 4,4'-methylene bis(phenyl isocyanate (MDI). The modification in time of the mechanical properties of PU films exposed to solar

radiation and weather or when the PU urea films were immersed in salt, river and stagnant water was followed, (Figs.3 and 4).

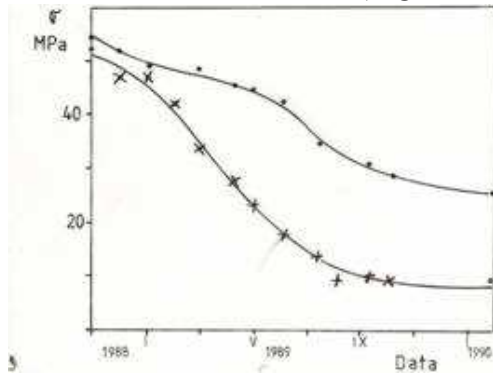


Fig. 3

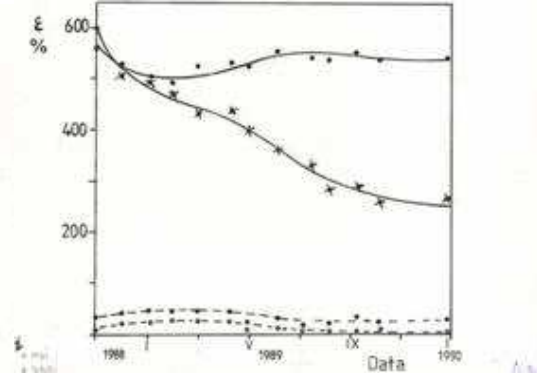


Fig. 4

Fig. 3. PU films exposed to solar radiation and weather. Influence of the geometry of isocyanate on the PU strength stress (σ); (•) – DBDI; (x) – MDI..

Fig. 4. PU films exposed to solar radiation and weather. Influence of the geometry of isocyanate on the PU residual elongation ($\epsilon\%$); (•) – DBDI; (x) – MDI..

3.3. Influence of the soft segment nature on the modification in time of the stress-strain data of PU urea films with three-dimensional structures

Previous studies had shown that when immersed in salt, river or stagnant water or oil for six months to three years, the best mechanical properties were found for the DBDI based urea films with PEA and PTHF [3]. There remain many details in the present results that still require further investigation, so part of these issues remain as targets for further work. The influence of the nature of the soft segment on the stability of PU films mechanical properties in time was followed, (Figs. 5,6 and 7). The best mechanical behaviour when exposing the films within average temperatures was found as corresponding to PU urea films based on macrodiol PTHF, when using the isocyanate DBDI. The study was performed on employing two types of macrodiols, i.e. a polyesteric hydroxy terminated poly(ethylene adipate) $M = 2000$ (PEA₂₀₀₀) or a polyetheric hydroxy terminated polytetrahydrofuran $M = 2000$ (PTHF₂₀₀₀) macrodiol.

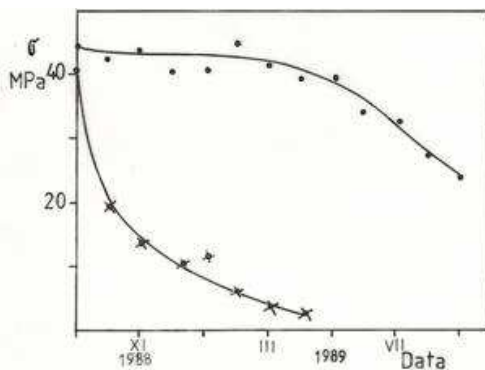


Fig. 5

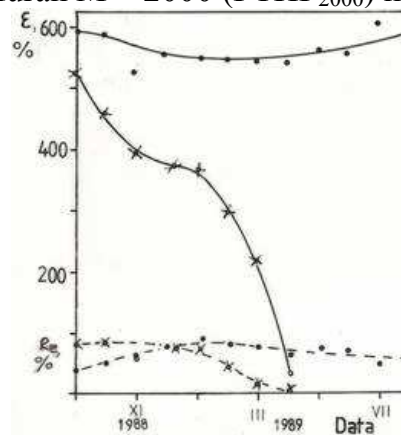


Fig. 6

Fig. 5. PU films exposed to solar radiation and weather. Influence of the nature of the soft segment on the PU strength stress (σ); (•) – PTHF; (x) – PEA.

Fig. 6. PU films immersed in salt water. Influence of the geometry of the nature of the soft segment on the PU elongation at break ($\epsilon\%$) and on the Residual elongation ($R_E\%$); (•) – PTHF; (x) – PEA.

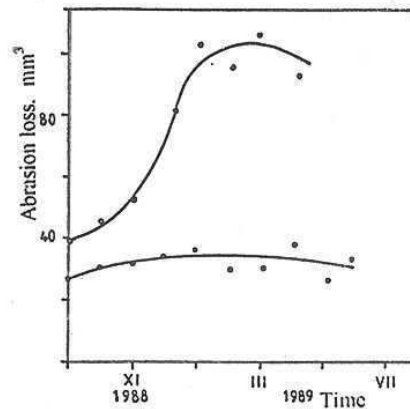


Fig.7. Variation of the abrasion loss for DBDI and PEA or PTHF based three-dimensional structure PU urea films subjected to solar radiation and weather; (o) –PTHF (the upper slope curve); (•)- PEA.

When following the abrasion loss in two PU urea films with DBDI derived from either PEA or PTHF, it was seen that smaller values of the abrasion loss were characteristic to films with macrodiol PEA, (Fig.7).

3.4. The determination of optimum mixture proportion of components in three-dimensional structure PU urea films derived from DBDI, by means of the multiple regression calculus.

The determination of the optimum mixture proportion of components in PU films was made by means of a multiple regression calculus. To follow the way in which the excess of isocyanate and the quantity of catalyst influence the PU films mechanical performance, it was achieved an experimental program and PU films were synthesized on employing constant quantities of solutions of polyol. PU films mechanical behaviour was followed by means of 100% and 300% tensile stress, strength stress, elongation at break and residual elongation.

The values of these mechanical properties were processed on employing a multiple regression program and it obtained the curves of level as a function of the X_1 and X_2 parameters.

Two examples are given in Figs. 8 and 9 where there are depicted the curves of level corresponding to the variation of the elongation at break (Fig 8) and strength stress (Fig.9), as a function of isocyanate excess (X_1) and catalyst (X_2) [3].

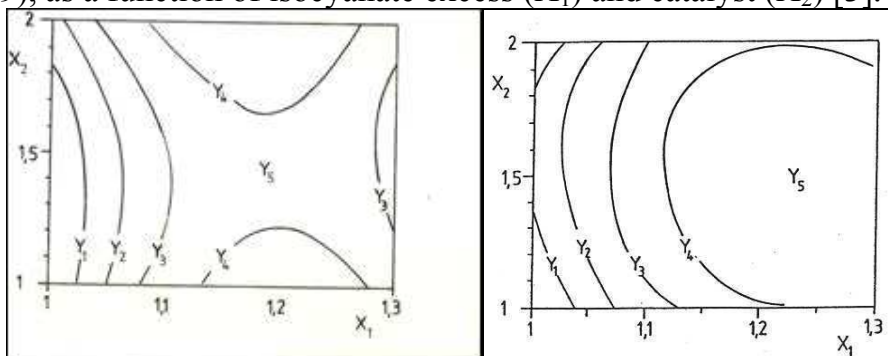


Fig. 8. DBDI based PU urea film curves of level corresponding to the variation of the elongation at break as a function of isocyanate excess (X_1) and catalyst (X_2);

$$Y_1 = 304.6\%; Y_2 = 414.5\%; Y_3 = 525\%; Y_4 = 635.2\%; Y_5 = 745.9\%.$$

Fig. 9. DBDI based PU urea film strength stress curves of level as a function of isocyanate excess (X_1) and catalyst (X_2); $Y_1 = 19.4\%$; $Y_2 = 28.5\%$; $Y_3 = 37.5\%$; $Y_4 = 46.7\%$; $Y_5 = 55.7\%$.

Similar curves of level have been obtained when considering the variation of the 100% and 300% tensile stress [3].

Table 2. Optimization of three-dimensional structure PU urea films mechanical properties by means of multiple regression calculus

| PU | X ₁ | X ₂ | 100% Tensile Stress, [MPa] | 300% Tensile stress, [MPa] | Elongation at break, [%] | Tensile strength stress, [MPa] | Residual elongation, [%] |
|----|----------------|----------------|----------------------------|----------------------------|--------------------------|--------------------------------|--------------------------|
| 1 | 1.044 | 1.15 | 2.0 | 2.3 | 868.3 | 4.0 | 156.6 |
| 2 | 1.044 | 1.85 | 2.3 | 3.5 | 821.6 | 23.7 | 86.7 |
| 3 | 1.256 | 1.15 | 3.7 | 8.0 | 545.0 | 16.7 | 9.5 |
| 4 | 1.256 | 1.85 | 3.5 | 8.3 | 518.3 | 51.2 | 12.5 |
| 5 | 1.000 | 1.50 | 2.6 | - | 150.0 | 2.75 | 16.6 |
| 6 | 1.300 | 1.50 | 3.8 | 8.1 | 330.0 | 47.4 | 11.7 |
| 7 | 1.150 | 1.00 | 3.2 | 3.3 | 641.7 | 38.4 | 28.3 |
| 8 | 1.150 | 2.00 | 2.7 | 3.9 | 733.3 | 30.5 | 50.0 |
| 9 | 1.150 | 1.50 | 3.5 | 6.2 | 566.7 | 49.7 | 10.0 |
| 10 | 1.150 | 1.50 | 3.4 | 6.2 | 590.0 | 48.6 | 15.0 |
| 11 | 1.400 | 1.50 | 5.3 | 10.8 | 436.7 | 42.3 | 15.0 |

With the aid of the data processed by means of the multiple regression program it obtained the curves of level as a function of parameters X₁ and X₂, as shown in Figs.8 and 9 from above, but when considering in addition also the variation of the 100% and 300% tensile stress as other parameters[3].

Considering these factors, from the curves of level it resulted that: (a) the maximum film strength stress value of 56 MPa is reached at X₁ = 1.23 and X₂ = 1.5; (b) the maximum film elongation at break of 746% is for X₁ = 1.19 and X₂ = 1.45; (c) the minimum film residual elongation corresponds to X₁ = 1.26 and X₂ = 1.45. The optimized values of the PU urea films with three-dimensional structures are given in Table 3.

Table 3. Stress-strain data of three-dimensional structure PU urea films, by means of optimization calculus

| PU | 100% Tensile stress, [MPa] | 300% Tensile stress, [MPa] | Elongation at break, [%] | Tensile strength stress, [MPa] | Residual elongation, [%] |
|-----------|----------------------------|----------------------------|--------------------------|--------------------------------|--------------------------|
| Optimized | 3.8 | 9.0 | 550 | 52 | 25 |

3.5. Stiffness properties of PU urea films as a function of temperature

The investigation of three-dimensional structure PU films stiffness properties as a function of temperature was made also. As described elsewhere [3,7], PU films behaviour in the field of low temperatures ranging among +20⁰C to -70⁰C was undertaken. As shown, PU films based on DBDI and PTHF maintain their elastic character with decreasing of temperature. For specific adopted PU structures [3,7] the Shear Modulus has shown only small variations till - 70⁰ C.

3. Conclusions

The mechanical performance of casted humidity post cured PU films depend on the polymer thickness and are somewhat higher in thinner films when the more polar

urea group formation is favored to the prejudice of the appearance of the allophanate groups.

In comparison to classical PU films based on hard segments with a rigid geometry, the three-dimensional structure PU urea films derived from DBDI display a better stability of the mechanical properties in time (up to three years). When immersed in salt, river or stagnant water the best mechanical behaviour was found as corresponding to the DBDI series of three-dimensional structure PU urea films with PTHF. Same conclusions were obtained when these films were subjected to accelerated hydrolysis [3,6] and when they were subjected to low temperatures.

4. REFERENCES

1. G. Oertel G, Polyurethane Handbook, Ed. Hanser Publishers, Munich, Viena, N.Y. (1985).
2. A. Caraculacu, G. Caraculacu, **J. Macromol. Sci.-Chem**, A22 (5-7) (1985), **631-651**.
3. C. Prisacariu, Doctorate Thesis, Technical University "Gh. Asachi", Iasi, Romania, (1998).
4. C. Prisăcariu, I. Agherghinei, **J.M.S.-Pure Appl. Chem.**, **A37 (7)**, (2000), **785-806**.
5. C. Prisacariu, A. Caraculacu, - *Novel polyurethane films with a coplanar packing in the hard segments: from synthesis to optimisation of mechanical performance* - 8th International Seminar on Elastomers, 9-11 May, 2001, Le Mans, France, **281-283**.
6. A. Caraculacu G. Caraculacu, C. Prisacariu, C. Gaina, **Raport de cercetare** - "Lac Poliuretanic Carapren H – Determinarea Condițiilor de Exploatare sub Acțiunea Factorilor de mediu" – contract nr. S / 360 / 29.XI.1990
7. D. Horbaniuc, C. Prisacariu, V. Baușic și A. Caraculacu, **Rev. Materiale Plastice**, 33, Nr.3., (1996), **168 – 176**.

CRISTINA PRISACARIU and ADRIAN CARACULACU

The Romanian Academy, Institute of Macromolecular Chemistry „Petru Poni” Iasi, Aleea Grigore Ghica Voda, Nr.41 A, 700487, Iasi, Romania

INFLUENȚA CONDIȚIILOR DE ÎMBĂTRÂNIRE ȘI A STRUCTURII CHIMICE ASUPRA CURBELOR DE ÎNTINDERE-DEFORMARE LA FILMELE POLIURETANICE CU STRUCTURI DIBENZILICE

Au fost realizate două familii de filme poliuretanică (PU) având la bază 4,4'- metilen bis(fenil izocianat) (MDI) și respectiv 4,4'- dibenzil diizocianat (DBDI), după cum urmează: (a) filme poliuretanică de turnare post maturate în prezența umidității atmosferice: (b) filme poliuretanică ureice cu structuri tridimensionale sintetizate prin utilizarea unor cantități constante de soluții de polioliol. În cazul filmelor cu structuri dibenzilice, rotația în jurul punții etilenice $-\text{CH}_2\text{CH}_2-$ permite alinierea nucleelor aromatice. A fost urmărit efectul introducerii grupelor $-\text{CH}_2\text{CH}_2-$ vs. CH_2 între nucleele aromatice. Segmentul moale (MD) adoptat a fost politetrahidrofură (PTHF) sau poli(etilen adipat) (PEA) cu masa moleculară 2000 ± 50 . Influența naturii segmentului moale asupra performanței mecanice a PU în timp a fost urmărită sub diferite condiții de îmbătrânire și medii ostile. A fost studiată influența geometriei izocianatului asupra modificării în timp a proprietăților filmelor poliuretanică și au fost determinate curbele specifice de tensiune-deformare care să permită monitorizarea evoluției valorilor rezistențelor la rupere, ale alungirii la rupere și ale deformațiilor reziduale ale filmelor. Determinarea proporției optime de amestec a componentelor în filmele poliuretanică a fost realizată prin intermediul unui program de calcul de regresie multiplă, pentru a urmări modul în care excesul de izocianat și cantitatea de calatizator influențează performanța mecanică a filmelor poliuretanică ureice cu structură tridimensională.

THE INFLUENCE OF THE RESIDUAL STRESS PRODUCED DURING THE NITRIDING PROCESS ON THE FATIGUE STRENGTH AT HIGH TEMPERATURES

BY

NICUȘOR AMARIEI¹, CORNELIU COMANDAR¹, DOREL LEON¹ and CONSTANTIN
DUMITRACHE²

Abstract: The paper presents the general causes of the residual stress generated during the production of the pieces, in particular the thermochemical nitriding treatment. It is explained the beneficial effect of the nitriding process on the fatigue behaviour and it is proposed a variant for the testing programme at high temperatures.

Keywords: residual stress, steel, nitriding, fatigue, high temperatures

1. Introduction

The nitriding is a thermo-chemical treatment generally used to improve the fatigue life of the steel pieces. Subjected to nitriding are a large category of mechanical pieces like gears, shafts, etc that require a very high superficial hardness, wear resistance, fatigue and impact strength. The treatment consists in nitrogen enrichment of the superficial layer of the steel and cast iron pieces at temperatures within 400 ... 580°C range, in gaseous environment, in salts or plasma nitration bathes. The minimum nitration temperature is determined by the diffusion coefficient of the nitrogen and can go no lower than 580°C. The maximum temperature is generally chosen to be 50-60 °C lower than the recovery temperature in order to minimise the the structural modification during the nitriding treatment. The treatment duration may vary from tens of minutes to tens of hours, according to the selected process, the type of material and the depth of the nitrided layer desired [1, 2].

The numerous thermal, thermo-mechanical and mechanical treatment processes [3] generate I order residual stress (macroscopic). Generally, the residual stress may appear when the material is subjected to thermal loads, to changes in composition and/or structure and to mechanical loads. These causes of the residual stress of thermal, metallurgical and mechanical nature can act alone or in the case of numerous processes may interact.

So, each thermal, chemical, mechanical treatment and any possible combination determine stresses within the material. If these stresses generate inhomogeneous plastic strains that exist still at the end of the treatment than the treated piece will present residual stress. The temperature variations within the piece lead to stresses of thermal nature and to phase transition. The phase transition also originates stresses, due to the strains (changes in volume, the transition plasticity) and the variation of the mechanical properties they cause. On the other hand, the structural modifications

affect the temperature fields (the transition latent heat and the thermophysical properties depending on the material microstructure), while the stresses/strains affect the phase transition. The strain heat is negligible in the case of the thermal treatment due to the low plastic strains. Furthermore, the variation in the chemical composition of the piece material (determined by the thermochemical treatments, such as nitriding) affects also the evolution of the structure, microstructure, strains and stresses. These aspects explain the complexity of the residual stress generating phenomenon in the case of material treatments and the difficulty of modelling their generation.

In the case of the nitriding process, the main causes that generate and influence the residual stress are of metallurgical (structural) and thermal nature. So, during the material is kept at the nitriding temperature, there are two important phenomenon:

- a) The strains incompatibility due to the difference between the specific volume of the formed phases and the one of the material;
- b) The decrease of these stresses as a consequence of the thermal relaxation phenomenon.

During the cooling period, the strain incompatibility determined by the difference between the thermal expansion coefficients of the formed phases and of the material is the main cause of the residual stress appearance [4-18].

During the nitrogen diffusion, the precipitation phenomenon causes nitrides that increase the superficial hardness of the pieces and generates significant compression residual stress within the superficial layer, with positive effects on the fatigue strength. The profile of the generated residual stress depends on the nitriding conditions (time, temperature, the nitrogen activity, etc), the chemical composition of the steel and also on piece geometry.

2. The influence of the nitriding process on the fatigue strength

The superficial treatment produces a double effect. First, the strength of the superficial layer increases, while maintaining the inner layers tenacity. Second, compression residual stress appears in the superficial layer, preventing the crack formation [19, 20].

The possibility of obtaining favourable and controllable residual stress is more important considering that there is no mechanical processing (exceptionally finishing) after the nitriding treatment.

The great interest shown for the nitrided layers is based on the substantial increase in life duration mostly due to the improvement in fatigue strength and superficial hardness. Barrallier, Barralis și Castex [14] explain this aspect using the multiaxial fatigue Crossland criterium (see Figure 1).

The schematisation presented in Figure 1 considers the octahedral tangential stress as the x-axis, while the maximum hydrostatic pressure is considered for the y-axis.

The (compression) residual stress having negative values for the nitriding treatment, the hydrostatic pressure decreases. The point corresponding to the strain translates from A (the absence of residual stress) to A' (the presence of residual stress)

with an amplitude of $\frac{2}{3}\sigma_{11}^r$.

The hardness effect that moves the Crossland limit lines adds to the positive effect of the compression residual stress produced during the nitriding treatment. Actually, in the case of steels the endurance limit σ_D generally increases with the material strength, itself depending on hardness. In this conditions the Crossland limit lines (D_1) are displaced toward position (D_2) from Figure 1.

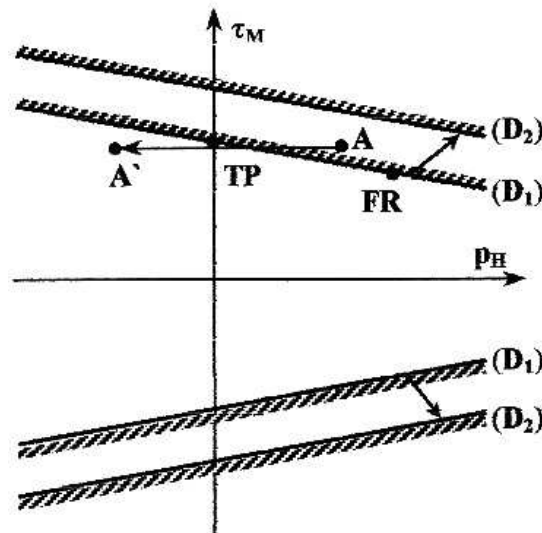


Fig.1 Schematisation of the effect of the compression residual stress and the hardness of the superficial layer on the Crossland diagram

As an example, in the case of 20 HN 3 MF steel, the superficial hardening and the formation of compression residual stress within the nitrided layer increase the fatigue strength with 20-30% for the finished test pieces and with 100% for the notched specimens. The influence of the nitriding treatment on the fatigue strength increases with the decrease of the cross section and the increase of the constructive or technological stress concentrations [1, 19-20].

The experimental trials shown that the higher the nitriding temperature the lower the fatigue strength. This situation is caused by the core hardness (the transformations taking place within the core) and by the decrease of the compression residual stress. The fatigue limit of the nitrided pieces can rise up to 15-20% through rolling. The straightening of the nitrided pieces reduces the fatigue limit.

A special problem considered by the researchers is the taking into consideration of the residual stress when the prediction of the fatigue strength of the piece is wanted. A set of multi-axial fatigue criteria was proposed for this problem [22], such as the Sines, Crossland, Dang Van, Findley-Matake [24] criteria. The use of these criteria is conditioned by the mechanical and thermal relaxation process of the residual stress generated through nitriding.

Generally, the selection of an efficient surface treatment must consider the influence of the mechanical and thermal loads on the evolution of the material initial metallurgical and mechanical characteristics. The knowledge about the evolution of the stress distribution due to the relaxation phenomenon is indispensable to the applications that require an improvement in life time for the pieces subjected to fatigue strain.

3. High temperatures fatigue behaviour of the nitrided pieces

The fatigue behaviour can be influenced significantly by a set of factors. The most important factors that determine the values of the fatigue strength are grouped in three categories:

- ◆ constructive factors (the stress concentrations, the piece dimensions);
- ◆ technological factors (material structure, processing technology, residual stress, surface quality);
- ◆ exploitation factors (the nature of the load, the cycle assymetry, the over and underloads, the action of corosive agents, the temperature).

In high temperature conditions, the effects of variable loads combine with the effects of the creep, the fatigue behaviour being determined mostly by the plastic strains that appear at a cyclic load. At high temperatures the steel present no endurance limit, the fatigue curve becoming a line [25].

With regard to the positive effect of the compression residual stress on the fatigue behaviour, one must consider also the problem of the mechanical and thermal stability of these stresses.

In the case of variable loads, the residual stress have the same effect as the average dynamic stress, observing that the residual stress can be diminished or even annuled when the load goes over a certain value, diminishing or completely cutting off the favavourable effect for which the pieces were produced. The decrease of the residual stress takes place when the sum of stresses in one point goes over the yield stress. Because of this, the compression residual stress is better used in the case of pieces made of steels and alloys with a high yield stress. The mechanical stress relaxation of nitrided pieces is negligible in the domain of fatigue load with a high number of cycles (more than 10^5 cycles) [14]. The mechanical stability of the residual stress generated through nitriding is important in comparison to shot peening where a stress relaxation appears during the first cycles as a consequence of the adaptation phenomenon [26].

Metallurgical modifications that lead to the diminishing of the mechanical characteristics generally appear if the working temperature of a mechanical system goes over a certain value. In the case of steels, depending also on their initial metallurgical structure, these critical temperatures are placed between 200 ... 400 °C. A consequence generally observed is the modification of the distribution of the residual stress.

For mechanical surface treatments, such as pre-tensioning shot peening and the rolling the reduction of the residual stress is produced due to the diminishing of the initial plastic strain that are in fact the cause of these stresses in the superficial layers of the pieces. In the case of nitriding, the origin of the residual stress is different and there is no modification of its distribution until over 400 °C. These evolutions can be explained taking into consideration the different physical phenomenon that occur in the two situations. In the case of surface mechanical treatments, the stress relaxation is connected to the dislocation displacement that have a low activation energy, in the range of some tens of kilojoules. In the case of nitriding, the evolution of the stress distribution concordes with the nitrogen diffusion in the ferritic matrix [16].

Therefore it is obligatory that the nitrided pieces working at high temperatures be tested in order to obtain data referring to the fatigue behaviour in this conditions. In the following part of the paper a programme variant for the fatigue testing at high temperature is presented.

Two types of pieces are tested in order to study the influence of the residual stress generated during the nitriding treatment on the high temperatures fatigue behaviour of a material. Half of the pieces were nitrided and are characterised by compression residual stress while the second half were not.

Before the fatigue testing the steel is subjected to following analysis and tests:

- ◆ Chemical and metallographical analysis;
- ◆ The structural analysis of the nitrided layer;
- ◆ Tensile tests at environment temperature, according to SR EN 10002-1:95;
- ◆ Tensile tests at high temperature (basically at the temperatures used for the fatigue tests), according to SR EN 10002-2:95;
- ◆ Creep tests at the temperatures and with the stresses characterising the fatigue testing that, in certain conditions are useful to the design of the fatigue testing programme and to the data interpretation.

The fatigue testing at a certain temperature requires 6-8 sets of test pieces nitrided respectively not subjected to the nitriding treatment. These pieces are made of the same material, with the same technological process and with same shape and dimensions, including for the stress concentrations (different shapes for the stress concentrations can be studied). The thermochemical nitriding treatment will be done for all pieces at one time, recording the process parameters.

The tests are performed on the same machine in the same conditions and maintaining the same asymmetry coefficient R . Based on the machine type and/or the requirements the fatigue tests can be performed using rotational bending or plane bending.

In the case of fatigue tests through rotational bending the test pieces have a circular cross section, the calibrated part having a toroid shape or any other shape specific to the stress concentration. In the case of fatigue tests through plane flexure the test pieces are flat with a rectangular cross section and a low width for the calibrated part with different stress concentration.

The testing temperatures and the stress steps complete the testing programme, as presented in Table 1.

Based on the real testing conditions and taking into consideration that the high temperatures testing technique is influenced by the material warming behaviour the testing temperatures, the stress steps, the test duration and the number of pieces can be modified accordingly.

For each test there are recorded the values of the maximum stress $\sigma_{\max i}$ and the number of cycles corresponding to breaking N_i . A comparative study and the interpretation of the experimental data are performed in the end.

The machines used for the fatigue testing at high temperatures are specially adapted for this purpose [27]. An original testing machine for variable loads at high temperatures (pattern no. 113596/2000 [28]) is presented in the followings. The machine is found at the "Gh. Asachi" Technical University, Strength of Materials Department (see Figure 2).

Table 1 Programming variant for high temperature fatigue testing, for the influence study of the residual stress generated during nitriding

| Programme | Temperature [°C] | Test pieces | Maximum testing load $\sigma_{\max i}$ |
|-----------|------------------|------------------------|--|
| A | $T_A = T_1$ | No nitriding treatment | $\sigma_{\max 1} = (0,5 - 0,6)R_m^{T_A}$ $\sigma_{\max i} = \sigma_{\max i-1} - \Delta\sigma_i, i \geq 2$ |
| | | Nitriding treatment | $\Delta\sigma_i = 30-60$ MPa, for the first pieces; $\Delta\sigma_i = 10-20$ MPa, for the next pieces |
| B | $T_B = T_2$ | No nitriding treatment | $\sigma_{\max 1} = (0,5 - 0,6)R_m^{T_B}$ $\sigma_{\max i} = \sigma_{\max i-1} - \Delta\sigma_i, i \geq 2$ |
| | | Nitriding treatment | $\Delta\sigma_i = 30-60$ MPa, for the first pieces; $\Delta\sigma_i = 10-20$ MPa, for the next pieces |

The testing equipment works with a fixed specimen and rotational load P , placed at a R distance from piece axis and allows to obtain a alternating-symmetrical bending cycle. The piece is placed vertically and fixed rigidly at its lower head and it is subjected to rotational bending by a centrifugal force produced through a weight on a rotational rod.

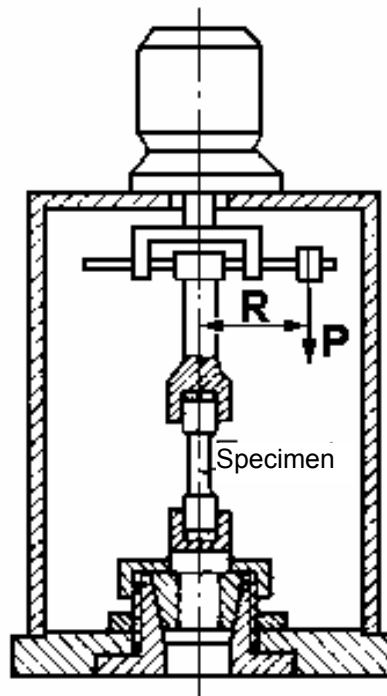


Fig. 2 The testing machine used for rotational bending fatigue tests

The vertical position of the specimen has the advantage to eliminate the influence of its own weight on the test results. The superior piece head is introduced in a self-aligning ball bearing on the weight rod. The threaded rod can move freely in a driving fork and is guided by some ball bearings. The driving fork is placed on the axis of a electric motor at the superior part of the machine.

The heating of the specimen is obtained in an electric oven that constitutes the vertical walls of the working medium. The temperature is measured using a Pt-PtRh type thermocouple. The maintenance and the adjustment of the temperature is done with a electronic controller. The different stress values in the specimen are obtained varying the weight P and the radius R .

The partial results of the rotational bending fatigue tests performed at 500 °C on Al-Cr-Mo alloyed steel test pieces, plasma nitrided and non-nitrided with circular cross section and a toroid shaped calibrated part it is concluded that the thermochemical treatment has a beneficial influence determining an increase of the fatigue strength. The positive effect of the compression residual stress is more enhanced in the domain of long time or intermediate time loads.

4. Conclusions

The thermochemical nitriding treatment generates high-level compression residual stress in the superficial layers of the pieces. The great interest shown for the nitrided layers comes from the significant increase of the fatigue life of the treated pieces mostly due to the improvement of the fatigue strength and the rise in superficial hardness. The beneficial effect of the residual stress generated during the nitriding process is also present to a lesser level at high temperatures. The existing data in literature are still insufficient and further investigations into this problem are required.

Acknowledgements

The present investigation was conducted with the financiar support of the National University Research Council (CNCSIS), the main Romanian funding organisation for university and postgraduate research programmes, Grant A cod CNCSIS 759.

Received April 25, 2005

¹The "Gh.Asachi" Technical University Iași

²The Maritime University Constanța

REFERENCES

1. Vermeșan, G., Deac, V. – **Bazele tehnologice ale nitrurării ionice**, Editura Universității din Sibiu, 1992, ISBN 973-95604-0-7
2. Gălușcă, D.G., Dima, A., Comaneci, R. – **Nitrurarea ionică**, Editura Sedcom Libris, Iași, 1997, ISBN 973-98187-0-6
3. Vermeșan, G., Vermeșan, E., Jichișan-Matieșan, D., Crețu, A., Negrea, G., Vermeșan, H., Vlad, M. – **Introducere în ingineria suprafețelor**, Editura Dacia, Cluj-Napoca, 1999, ISBN 973-35-0922-1
4. Amariei, N. et Bârsănescu, P.D. (coordonateurs) – **Tensiuni remanente**, Editura "Gh. Asachi", Iași, 2003, ISBN 973-8292-91-3
5. Amariei, N. – **Tensiuni remanente generate în procesul de nitrurare**, Editura "Gh. Asachi", Iași, 2001, ISBN 973-8050-88-X
6. Amariei, N. – **Contribuții la studiul și determinarea tensiunilor remanente**, Teză de doctorat, Universitatea Tehnică "Gh. Asachi" Iași, 1997
7. Amariei, N., Leon, D., Comandar, C. – *Stresses Generated During the Nitriding Process as a Result of the Difference of Specific Volume Between the Basic Material and the Formed Constituents*, **Buletinul I.P. Iași**, Tomul XLII, Secț. V., Fasc. 3-4, 1996, ISSN 0304-5188, **47-53**
8. Amariei, N., Leon, D., Comandar, C. – *Stresses Generated During the Nitriding Process as a Result of the Difference of Specific Volume Between the Basic Material and the Formed Constituents*,

Buletinul I.P. Iași, Tomul XLII, Secț. V., Fasc. 3-4, 1996, ISSN 0304-5188, **47-53**

9. Amariei, N., Leon, D., Comandar, C. – *Influences of the Specific Volume and of the Creep Phenomenon on the Residual Stresses Generated During Plasma Nitriding*, **Buletinul I.P. Iași**, Tomul XLV (XLIX), Fasc. 1-2, Secția Construcții de mașini, 1999, ISSN 0304-5188, **75-87**

10. Amariei, N., Leon, D., Comandar, C. – *A Mathematical Model for the Study of Residual Stresses Using the Displacements Measured During Plasma Nitriding*, **Proc. of the 35th International Conference on Experimental Stress Analysis, EAN '97** (Hrabovský, M., editor), Olomouc, Czech Republic, 4-6 June 1997, **9-14**

11. Amariei, N., Leon, D., Comandar, C. – *On the Monitoring of Residual Stresses Generation During Plasma or Gas Nitriding by in situ Deflection Measurements*, **Proc. of the Symposium "Danubia-Adria" on Experimental Methods in Solid Mechanics**, Bertinoro, Italy, Sept. 30-Oct. 3, 1998, **13-14**

12. Barrallier, L. – **Génese des contraintes résiduelles de nitruration. Modélisation et experimentation**, Thèse, Centre d'Enseignement et de Recherche de l'École Nationale Supérieure d'Arts et de Métiers d'Aix-en-Provence, France, 1992

13. Barrallier, L. – **Génese des contraintes résiduelles de nitruration. Modélisation et experimentation**, Thèse, Centre d'Enseignement et de Recherche de l'École Nationale Supérieure d'Arts et de Métiers d'Aix-en-Provence, France, 1992

14. Barrallier, L., Barralis, J., Castex, L. – *Caractéristique mécaniques des couches nitrurées. Cas des pièces en acier*, **Traitement Thermique**, **276**, 1994, ISSN 0041 0950, **49-53**

15. Barrallier, L., Barreau, G., Barralis, J. – *Influence de l'origine des contraintes résiduelles sur leur relaxation thermique dans le cas d'aciers alliés*, **La Revue de Métallurgie-CIT/Science et Génie des Matériaux**, **5**, 1993, **637-649**

16. Barrallier, L., Barreau, G., Barralis, J. – *Influence de l'origine des contraintes résiduelles sur leur relaxation thermique dans le cas d'aciers alliés*, **La Revue de Métallurgie-CIT/Science et Génie des Matériaux**, **5**, 1993, **637-649**

17. Darbinjan, W., Oettel, H., Schreiber, G. – *Comparison of Mechanical Methods and X-ray Methods for Measurement of Residual Stresses on Nitrided Steels*, **Residual Stresses** (Hauk, V., Hougardy, H.P., Macherauch, E., Tietz, H.D., editors), DGM Informationsgesellschaft VERLAG, 1993, **565-574**

18. Vermeșan, G., Amariei, N., Lieurade, H.P., Duchateau, D., Ghiglione, D., Leon, D., Comandar, C. – *Mesure in situ des déformations d'une éprouvette durant une nitruration assistée par plasma*, **Traitement Thermique**, **311**, 1998, ISSN 0041 0950, **78-83**

19. Feodosiev, V.I. – **Rezistența materialelor** (traducere din limba rusa de Hagioglo, A.), Editura Lumina, Chișinău, 1992, ISBN 5-372-01188-2

20. Pisarenko, Gh., Agarev, V., Kvitka, A., Popkov, V., Umanski, E. **Rezistența materialelor** (traducere din limba rusă de Hagioglo, A.), Editura Lumina, Chișinău, 1993, ISBN 5-372-01383-4

21. Bannantine, J.A., Comer, J.J., Handrock, J.L. – **Fundamentals of Metal Fatigue Analysis**, Prentice-Hall, 1990

22. Suresh, S. – **Fatigue of materials**, Cambridge University Press, 1991

23. Șomotecan, M. – **Comportarea la solicitări variabile a oțelurilor aliate 42MoCr11 și 39MoAlCr15 nitrurate ionic**, Teză de doctorat, Universitatea Tehnică din Cluj-Napoca, 1996

24. Skalli, N., Flavenot, J.F. – *Prise en compte des contraintes résiduelles dans un calcul prévisionnel de tenue en fatigue*, **CETIM-Informations**, **90**, 1985, ISSN 0399-0001, **35-47**

25. Rusu, O., Teodorescu, M., Lașcu-Simion, N. **Oboseala metalelor**, vol.1,2, Editura Tehnică, București, 1992, ISBN 973-31-0350-0, ISBN 973-31-0351-9

26. Rusu, O. – *Shake-Down. Adaptare*, **Mecanica Ruperii**, **8**, 2000, ISSN 1453-8148, **23-28**

27. Okrajni, J. – *Fatigue of High Temperature Components*, **Zeszyty Naukowe Politechniki Opolskiej**, Seria: Mechanika z.67, Nr kol. 269/2001, **219-238**

28. Palihovici, V., Miros, I., Leon, D. – *Instalație pentru încercări la solicitări variabile la temperaturi ridicate și scăzute*, Brevet de invenție RO 113596 C1, 2000

INFLUENȚA TENSIUNILOR REMANENTE REZULTATE DIN PROCESUL DE NITRURARE ASUPRA REZISTENȚEI LA OBOSEALA LA TEMPERATURI RIDICATE

Rezumat: Se prezintă cauzele generale ale apariției tensiunilor remanente generate în procesele de fabricație ale pieselor, în particular, în cazul tratamentului termochimic de nitrurare, se explică efectul benefic al nitrurării asupra comportării la oboseală și se propune o variantă de program de încercări la temperaturi ridicate.

FORMALDEHYDE RESINS FROM RENOVABLE RESOURCES

BY

FĂNICĂ MUSTAȚĂ, IOAN BICU, and ANGHEL NARCIS

Abstract: *Starting from epoxy resins (ER), resin acids (RA) and formaldehyde (FA), novel formaldehyde resins bearing hydrophenanthrene moieties in its structures were synthesized under acid catalysis (hydrochloric acid). The resins thus obtained were characterized from the spectral (IR, ¹H-NMR), chemical composition and thermal analyses. These products (slightly brown colour) have low molecular weights and are soluble in a large majority of organic solvents, because of their chemical structure (posed OH groups and hydrophenanthrene fragments). The presence of these formaldehyde resins in the structure of pressure sensitive adhesive compositions allows them to have a high adhesiveness and acceptable cohesive strength*

Keywords: resin acids, epoxy resins, formaldehyde resins, pressure-sensitive adhesives.

1. Introduction

Formaldehyde resins represent an important class of resins which exhibit of outstanding properties, such as chemical resistance, high thermal and mechanical behaviours, as well as excellent electrical properties and are used in many field of industrial applications as electrical and electronic industry, car industry, aerospace and hydrospace etc. These resins are used as structural adhesives or resin matrix in composite materials or as encapsulation materials for semiconductor devices, or as tackifiers for adhesive formulation as a consequence of his good adherence to many substrates. A large variety of monomers were such as phenols and substituted phenols, aromatic amines, melamine, urea, and so on was used as in preparation of these polymers. [1-11].

In the last decades, as consequence of oil crisis, the renewable raw materials become important resources for chemical industry. Resin acids, the main components of rosin offer attractive high chemical reactivity at carboxylic group and at the double bonds, and are used as raw material in synthesis of new polymers. The presence of the hydrophenanthrene moieties in the chemical structure of these polymers confer them, high solubility in common organic solvents, high adhesiveness, hydrophobicity and water resistance [12-20].

In this work, a hydrophenanthrene compound with hydroxyl groups were first synthesized. These compounds were obtained through a simple addition reaction between the oxirane ring of epoxy resins and carboxylic group from resin acids. The resulting hydroxyetheresters of resin acids were reacted with formaldehyde in the acid catalysis to obtain the formaldehyde resin. The synthesis characterization and the adhesivity properties of these products were investigated.

2. Experimental procedure

Measurements

The average epoxy equivalent weights were obtained using literature method and were expressed as geq^{-1} [22]. Nitrogen content was determined in accordance with Kjeldahl method [23]. Acid number (a.n.) was obtained (from acetone solution of RA) by direct titration with 0.1N alcoholic KOH, in the presence of phenolphthalein as indicator. Average molecular weights were determined by cryoscopic method using DMSO as solvent [24]. The softening points were registered by means of a Mettler DSC 12E Toledo apparatus at heating rate of $10^{\circ}\text{C}\text{min}^{-1}$.

FTIR spectra were taken on a Bio-Rad Digi Lab Division (Portmann Instruments) using KBr pellets. ^1H -NMR spectra were recorded on an JEOL-JNMC 60HL (Japan) spectrometer. Samples were runned at 50°C , using tetramethylsilane as internal standard and DMSO- d_6 as solvents. Thermogravimetric analyses (TGA) was performed in air by a MOM-Budapest of Paulik, Paulik-Erdey type derivatograph at heating rate of $10^{\circ}\text{C}\text{min}^{-1}$, in the temperature range from 25 to 700°C . The activation energies of decomposition reaction (E_a) for the obtained resins were calculated from TGA curves using Coats, and Redfern and Swaminathan, and Modhavan equations [25,26]. The adhesiveness behaviours were estimated using the standard adhesion test (0° peel adhesion) (ASTM D-1000), the cumulative test of adhesion and cohesion strength (0° hold time), and Williams plasticity [27].

3. Experimental results and discussion

Synthesis of formaldehyde resins

The raw material used in these syntheses was epoxy resins, RA and p-FA. The chemical reactions were conducted in two steps: synthesis of hydroxyetheresters of RA and synthesis of formaldehyde resins.

Synthesis of hydroxyetheresters of RA

A typical synthesis of synthesis of hydroxyetheresters of RA is presented as follows (Sample 1, Table 1): A 500-mL four-necked round-bottomed flask, equipped with mechanical stirrer, temperature controller, water reflux condenser, oil bath and nitrogen inlet was charged with 0.1 mol of epoxy resin (DGEBA) and 0.2 mol of RA. The reaction mixture was heated at 110°C while stirring for 15 minutes. Then the 0.05 mol (15.5g) of catalyst (TEBAC) was added. The reaction mass was maintained at this level of temperature under stirring for 4 h (until the acid number is 30 or less) and a viscous melt was obtained. The crude reaction mass was cooled at room temperature and divided as fine grain and extracted twice under stirring at room temperature. After filtration, the cake was dried under vacuum at 80°C overnight. Resulted a pale brown resin (yield 94 %, melting point: 72°C).

Synthesis of formaldehyde resins

Synthesis of formaldehyde resins was conducted in acid catalysis (HCl 35 %) at molar ratio 1/0.95 (hydroxyetheresters/formaldehyde). Reaction conditions are presented in Table 1. In a representative experiment, a 500- mL four-necked round-bottomed flask equipped as above, was added 0.1 mol of hydroxyetheresters of RA and 0.095 mol (2.85 g) of p-FA and 50 ml of toluene. After heating at 70°C (15 min), 9ml of

catalyst (HCl 35%)(3 % based on the weight of reactants) were added. A weak exothermic effect (5°C) was observed, and the mixture becomes transparent. Then the reaction mass was heated at reflux and maintained at this level under stirring 1.5 h with the purpose to obtain CH_2OH groups. Then, a Dean-Stark trap was attached to the water condenser and the water was extracted azeotropically with toluene under a slowly vacuum. As a consequence of water extraction, the temperature was increased at 140°C , and methylene bridges appeared. The total reaction time was 3h. Finally, the formaldehyde resins are cooled, broken as fine grain size, extracted twice with petroleum ether and dried under vacuum at 80°C 16 hours. A pale brown or pale red brown colour resins (as function of chemical structures) were obtained.

Preparation of pressure sensitive composition and pressure sensitive tapes

Acrylic copolymer was obtained as in a previous paper at molar ratio 2-EHA/Ac 0.5/0.05 as 50 wt-% solutions in toluene [17]. The pressure sensitive composition was obtained by mixing the solution of formaldehyde resins with solution of acrylic copolymer at weight ratio presented in Table 2. The final concentration of the mixtures was corrected at 20 wt-% with toluene. Pressure sensitive tapes were obtained by application of pressure sensitive composition (using a conventional draw bar procedure) on the both side of non-woven polyester fabrics to obtain a final dry coating weight of $50 \text{ g}\cdot\text{m}^{-2}$. Then the adhesive tapes were covered with silicon paper and cutting in samples with 25 mm width and 200 mm long.

The formaldehyde resins were obtained in two steps (Table 1).

Table 1. Reaction condition and some physical-chemical characteristics of resulted formaldehyde resins

| Sample | Monomer ratio (molar ratio) | Number average molecular weight a) | Softening point ($^{\circ}\text{C}$) | Catalyst (HCl) (%) | Yield (%) | Colour | Nitrogen content (%) |
|--------|--------------------------------|--|--|------------------------------|--------------|--------------------------|--------------------------------|
| 1 | DGEBA/RA/p-FA (1/2/1) | 6400 | 72 | 3 | 93 | Pale brown | - |
| 2 | DGEHQ/RA/p-FA (1/2/1) | 5100 | 70 | 3 | 95 | Pale brown | - |
| 3 | DGAN/RA/p-FA (1/2/1) | 5800 | 50 | 3 | 91 | Pale reddish brown | 1.69 |

First, RA in presence of TEBAC as catalyst reacts with epoxy rings and hydroxyetheresters appears. In the second step, in presence of HCl as catalyst, formaldehyde react with catalyst protons and form a carbonyl component which react at double bonds of methylene groups (with increased reactivity produced by the neighborhood of ester groups) and form methylol groups. By rising of the temperature, the water was eliminated and the methylol groups were rapid transformed into methylene bridges between hydrophenanthrene rings, resulting formaldehyde resins. The resulting resins are solid, brittle, with colour varying from

pale brown (for resin with DGEBA and DGEHQ) to reddish brown colour (for resin with DGAN) as a consequence of their chemical structure.

The possible structure of the synthesized products was confirmed by FT-IR, $^1\text{H-NMR}$ spectroscopy and as well as by elemental analysis of nitrogen. The fact that the obtained value of nitrogen content is in good agreement with the calculated value evidenced the proposal structure of the synthesized polymers.

IR spectra show an intense unresolved band in the range of $3450\text{-}3500\text{ cm}^{-1}$ which is specific to tertiary OH groups resulted from the reaction between epoxy ring and COOH groups. The peaks specific to symmetric and asymmetric vibration of CH, CH_2 , CH_3 , groups presented in the hydrophenanthrene and in the glycerol moieties appear in the range of $2280\text{-}2960\text{ cm}^{-1}$. The peaks specific to ester groups are placed at 1725 cm^{-1} (CO group) and in the range of $1280\text{-}1160\text{ cm}^{-1}$ (C-O-C). The multiple peaks located in the range of $680\text{-}840\text{ cm}^{-1}$, indicated the presence of aromatic ring of p-substituted benzene introduced by the epoxy resins. The $^1\text{H-NMR}$ spectra also confirm the structure of obtained polymers. The major signals are located in the range of $0.9\text{-}2.15$ ppm chemical shift represent the vibration of CH, CH_2 , CH_3 , groups presented in the hydrophenanthrene and DGEBA moieties. The CH, CH_2 , protons of the glycerol groups and methylene bridges are situated in the range of $2.8\text{-}3.8$ ppm chemical shift, the newly formed OH protons appear in the range of $3.9\text{-}4.6$ ppm chemical shift and the aromatic protons in the range of $6.8\text{-}7.6$ ppm chemical shift. The thermal properties of obtained formaldehyde resins were evaluated using their thermal degradation curves. The main parameters and the values of activation energies of degradation processes are summarized in Table 2. The relative thermal stability, using TG parameters were quantitatively determined. Accepting T_{10} , T_{50} , WL_{500} parameters as criteria of thermal stability it can be concluded that the formaldehyde resins with DGEBA in structure are more stable in comparison with the polymers with DGEHQ and DGAN. The activation energy of degradation process has values between 123 to 150 kJ/mol.

Table 2. Thermal parameters of formaldehyde resins

| Epoxy resin | Molar ratio (epoxy resin/ RA/p-FA) (mol/mol) | Temperature corresponding to 10 % (T_{10}) and 50% (T_{50}) weight loss ($^{\circ}\text{C}$) | | Weight loss at 500°C (WL_{500}) (%) | Decomposition activation energy (kJ/mol) | | Pre-exponential factor ($\ln A_{SM}$) ^{c)} (min^{-1}) |
|-------------|--|--|----------|---|--|-------------------------|---|
| | | T_{10} | T_{50} | | E_{aC} ^{a)} | E_{aSM} ^{b)} | |
| DGEBA | 1/2/1 | 290 | 351 | 25 | 123.56 | 127.17 | 24.63 |
| DGEHQ | 1/2/1 | 285 | 350 | 18 | 150.65 | 142.53 | 27.18 |
| DGAN | 1/2/1 | 250 | 350 | 15 | 133.09 | 128.64 | 16.31 |

a) evaluated by Coats and Redfern equation

b),c) evaluated by Swaminathan and Modhavan equation

The formaldehyde resins with hydrophenanthrene in structure were used as tacky materials in pressure sensitive composition used in fabrication of double stick tapes. The various formulae of adhesive composite and the behaviours of obtained pressure sensitive of double stick tapes were shown in the Table 3. The 0° peel adhesion test, the cumulative test of adhesion and cohesion strength (0° hold time) and Williams

plasticity were used to characterize the cumulative information about tapes behaviours. From the Table 3 appears that the pressure sensitive tapes obtained only acrylic adhesive have the smallest value for the cohesive strength. The tapes obtained from the composition with formaldehyde resins in structure (up to 10 wt-% referred to the adhesive composition) confer to them a high increase of the cohesive strength without affecting the adhesive strength. When the formaldehyde resin exceeding 10 wt-%, the cohesive strength increase very much, but the adhesive strength lead to a dramatically decreases of it.

The formaldehyde resins with hydrophenanthrene in structure were used as tacky materials in pressure sensitive composition used in fabrication of double stick tapes. The various formulae of adhesive composite and the behaviours of obtained pressure sensitive of double stick tapes were shown in the Table 3.

Table 3 Pressure sensitive adhesive formulations and some characteristics of the realized pressure sensitive tapes.

| Sample | Adhesive formulae (^a formaldehyde resin/ acrylic adhesives) (w/w) | William plasticity (mm) | Tape substrate | Adhesive tape characteristics | |
|--------|--|-----------------------------------|-----------------------------|-------------------------------|-------------------------|
| | | | | 0° hold test (hours) | 180° peel test(g/cm) |
| 1 | 0/100 | 1.65 | Polyester nonowen fabric | 0.25 | 740 |
| 2 | 10(sample 1)/90 | | Polyester nonowen fabric | | 1050 |
| 3 | 20 (sample 1)/80 | | Polyester nonowen fabric | | 710 |
| 4 | 10(sample 2)/90 | | Polyester nonowen fabric | | 610 |
| 5 | 20 (sample 2)/80 | | Polyester nonowen fabric | | 540 |
| 6 | 10(sample 3)/90 | | Polyester nonowen fabric | | 510 |
| 7 | 20 (sample 3)/80 | | Polyester nonowen fabric | | 550 |

a) sample cf. Table 1

The 0° peel adhesion test, the cumulative test of adhesion and cohesion strength (0° hold time) and Williams plasticity were used to characterize the cumulative information about tapes behaviours. From the Table 3 appears that the pressure sensitive tapes obtained only acrylic adhesive have the smallest value for the cohesive strength. The tapes obtained from the composition with formaldehyde resins in structure (up to 10 wt-% referred to the adhesive composition) confer to them a high increase of the cohesive strength without affecting the adhesive strength. When the formaldehyde resin exceeding 10 wt-%, the cohesive strength increase very much, but the adhesive strength lead to a dramatically decreases of it.

4. Conclusions

New formaldehyde resin with hydrophenanthrene moieties in its structures were obtained and characterized. These solid, brittle resins with pale brown colour,

soluble in a large variety of organic solvents and can be used as tackifier in pressure sensitive composition and of fabrication of adhesive tapes. The presence of hydrophenanthrene moieties (up to 10 wt-% referred to the adhesive composition) confer them high increase of cohesive strength without affecting the adhesive strength.

REFERENCES

1. Knoph P.W., Little A.D. Encyclopedia of Polymer Science and Technology, H.F.Mark Ed, vol.11, John Willey & Sons, New York 1988.
2. Pat. USA 3,887,539 (1975).
3. Pat. USA 4,021,391 (1977).
4. Pat. WO 02064655 (2002).
5. Rosu D., Cascaval C.N., **Mater. Plast.**, 1991, **28**, **92** Knoph P.W., Little A.D. Encyclopedia of Polymer Science and Technology, H.F.Mark Ed, vol.11, John Willey & Sons, New York 1988.
6. EP0859374 JP (1998)
7. Knop A., Pilato L.A, Phenolic Resins: Chemistry, Applications and Performance, Future Directions, Springer Verlag Heidelberg, Germany, 1985.
8. Mustata F., Bicu I., **J.Polym.Eng.** 2002,**22**, **369**
9. EP0220133, CH (1987).
10. Pizzi A., *Phenolic Resin Adhesives* - Handbook of Adhesive Thechnology , A.Pizzi , K.I.Mittal Ed., Marcel Dekker Inc., New York, 1994.
11. Barth B.P., *Phenolic Resins Adhesives* "Hand-book of Adhesives" I.Skeist ed. Nostrand Reinhold Comp., New York, 1977.
12. Stonecipher W.D., Turner R.W.:Encyclopedia of Polymer Science and Technology Interscience Publishers, vol.12, John Wiley & Sons, New York 1970.
13. Pat. Jap. 7615004 (1976), cf. CA 1976, **85**, 34916
14. Pat. U.R.S.S. 519435 (1976), cf. CA 1976, **85**, 144853.
15. Pat. U.R.S.S. 489765(1975), cf. CA 1976, **84**, 75895.
16. Jpn Kokai Tokkyo Koho **JP** 35,655 (2004), cf. CA 2004, **140**, 129841p
17. Mustata F., Bicu I.: **Desing. Monom. Polym.** 2000, **3**, **489**
18. Mustata F., Bicu I.: **Polimery** 2001, **46**, **534**
20. Mustata F., Bicu I.: **Polimery** 2000, **45**, **258**.
21. Mustata F., Bicu I.: **Polym. Test.** 2001, **20**, **533**.
22. C.N.Cascaval, F.Mustata, D. Rosu, **Angew. Makromol. Chem.** 1993, **209**, **157**.
23. Cheronis, N.D., Ma, T.S., Organic Functional Group Analysis by Micro and Semimicro Methods, Interscience Publishers, Wiley & Son, New York, 1964
24. R.U.Bonnar, M.Dimbat and F.Stross, Number Average Molecular Weight, Interscience Publishers, Inc. New York, 1958.
25. Sawiminthan V., Modhavan N.S., **J.Anal. Appl. Pyrolysis**, , 1981, **3**, **131**.
26. Coats A.W, Redfern J.R., **Nature**, 1964, **201**, **68**.
27. Bemmels, C.W. Handbook of Adhesives, I.Skeist (Ed.), Van Nostrand Reinhold Company, N.York, 1977.

*"P.Poni" Institute of Macromolecular Chemistry,
Aeea Gr.Ghica Vodă nr.41 A, Iasi-700487, Romania*

RAȘINI FORMALDEHIDICE DIN RESURSE NATURALE

Rezumat: Pomind de la rășini epoxidice, de la acizi rezinici din colofoniu și formaldehidă s-au sintetizat în cataliză acidă, rășini formaldehidice cu nuclee hidrogenantrenice în structură. Acestea au fost caracterizate prin metode spectrale (IR, ¹H-NMR), analiză elementală și din punct de vedere al comportării termice. Folosind aceste rășini ca agenți de conferire de adezivitate în structura unor compoziții adezive sensibile la presiune se poate observa că ele induc o creștere substanțială a forței de coeziune fără a afecta semnificativ adezivitatea.

ON THE STRUCTURAL TRANSFORMATIONS PRODUCED BY CAVITATIONAL STRESSES

By

**ILARE BORDEASU, VICTOR BALASOIU, RODICA BADARAU, MIRCEA OCTAVIAN
POPOVICIU and EUGEN DOBANDA**

***Abstract:** The paper deals with some aspects concerning the behavior of the micro-structure of various types of materials submitted to cavitation erosion. For this, a grouping of the results obtained by different laboratories, including the Laboratory of Hydraulic Machines from Timisoara, is done. The results are presented in the literature, shown with different occasions at symposiums, conferences, congresses and they are subject to the material structure response at cavitation attack as well as at the micro-structural transformations during this kind of attack.*

the purpose of the paper is to understand the cavitation erosion phenomenon and constructing a global, clearer image on the ways in what the material is being destroyed by cavitation.

***Keywords:** cavitation, structural transformations*

1. Introduction

The cavitation erosion is an unwanted effect of the cavitation no matter the place where it actions. Because it develops in different ways from a material to another, as a function of the material resistance to cavitation attack, one of the preoccupations of the scientists is to establish the causes that determines this particular resistance.

As this resistance is not constant during the attack, the aim of the researchers is also to find out the elements that determine this phenomenon.

This is why, a great number of scientists are involved in the analysing of the microstructure of the materials eroded by cavitation, feature considered as the characteristic that influences the cavitation resistance to erosion.

So, the micro-structure of the materials submitted to cavitation erosion become a problem very well studied in great universities and laboratories all over the world as: Grenoble (France), Gdansk (Poland), Hanover (Germany), Milano (Italy), Hiroshima, (Japan), Timisoara (Romania), Montreal (Canada) etc.

Among the researchers having results in this field one can mention names like: R. Simoneau, P. Lambert [16] from Canada, P. Franc [6] and A. Karini [11] from France, A.J. Graham [10], from the USA, S. Fujikawa and t Akamatsu [7] from Japan. The results published by the above mentioned attract more and more scientists in the studying of the microstructure of the cavitation eroded material together with the analysis of its resistance on the basis of cavitation characteristics curves and parameters.

The method of the approach is at the beginning and it is based on the use of the most effective optical and electronic microscopes.

In the paper we group the results obtained in various laboratories including the Laboratory of Hydraulic Machines from Timisoara and published or communicated at various scientific events, congresses, conferences, symposiums in respect to the answer of the structure of the materials at the cavitation attack as well as at the microstructural transformations that take place during the attack.

2. Structural factors having influence on the material erosion

During the cavitation attack the surface of the material is submitted to a cyclic stress of a certain frequency, by shock waves and micro-jets resulted from the implosion of the cavitation bubbles.

So, in time, on the attacked surface will appear elastic and plastic deformations and micro-crackings. These modifications are determined by the crystalline structure and the micro-structural dislocations, macles, crystalline network faults etc. of which density and positioning depend themselves on the conditions of fabrication of the material [18].

This is the reason why, the analyzing of the destruction of the material by cavitation erosion, respectively, of the resistance they have to cavitation attack, will be done from the point of view of crystalline network, grain sizes, structural faults and phase transformations. This analysis will be made on each category in part even if during the cavitation attack they can not be separated.

2.1. The influence of the grain size

Preece et. al. [14] analyzed the influence of the incubation period of cavitation erosion as a function of the grain size for the three crystalline networks types: cfc, cvc and hc. In the same time they analyzed the influence on the erosion process of the packaging faults respectively the packaging energy. So, in the study of Ni (cfc) one can ascertain:

1. If the grains are large (more than 750 μm) the creep is being achieved rather easy and the deformation is being shared in all the grains, fact that brings high concentrations of local tensions and the forming of craters at the surface of the sample. The resistance to cavitation erosion is very low.
2. If the grains have sizes between 50 μm and 750 μm the forming of craters is due to the macroscopic deformation of a few grains. So, the resistance to cavitation depends only on the characteristics of deformation of each grain.
3. In the case of the grains under 50 μm a rapid enhancement of the cavitation resistance was seen, linked with the decrease of the grain size. Also for the obtaining of craters of the same sizes with those formed in big size grains materials, a larger number of grains must be deformed. In this case the material behaves more like a polycrystal (having continuity at the grains intersections), fact that claims a higher tension.

The observations of Preece et. al. are sustained also by Rao et. al. [15] who mentioned that in a mono-phasic material, at the grain boundaries, the deformation can be transferred to the neighbor grain where it glides on an another plan interior to

the grain and has as a consequence the consolidation of the structure and the implied grains, in the polycrystal behaves like obstacles for creeping.

When the size of Ni grains become very small, erosion takes place mostly at the grain boundary.

A phenomenon similar to the influence of the sizes of Ni grains was seen in the Cu-30Zn (α alloy) cfc.[14] which has a packaging energy rather small 0.006J/mm^2 [5].

At this alloy Preece et.al. observed that during cavitation the deformation occur at the grains boundaries, the grain core staying smoother.

The phenomenon was put on the low interaction forces between dislocations and the small energy of the packaging faults that determines a high tensional concentration at the boundaries between grains determining the deformation of the entire grain surface.

These results are again sustained by Rao et.al [15] and their researches on bronze. Thus, if the metals have a small packaging energy, for obtaining a deviated creep it is needed a rather high shearing tension. For calculating the value of the tension produced by a group of grains Preece [14] gives the relation:

$$\tau_e = (\tau_a - \tau_f) \cdot \left(\frac{d}{x}\right)^{1/2} \quad (1)$$

where: - τ_e – the effective shearing tension produced by the superposition of dislocations (a powerful obstacle);

τ_a – the shearing tension acting on the packaging;

τ_f – the friction tension;

d – the distance from the dislocation source to the obstacle;

x – the distance from the dislocation of the packaging head to the obstacle.

For establishing a relation for the shearing tension Roa et.al [15] considers that this tension acts on a gliding plan on a certain direction on which a traction tension develops:

$$\sigma = M \cdot \tau \quad (2)$$

σ – the traction tension after the gliding direction

$$M = 1/(\sin(\phi) \cdot \cos(\lambda))$$

ϕ – the angle between the creeping plan and σ tension axis;

λ – the angle between the creeping direction and σ tension axis.

The shearing tension will have the following relation:

$$\tau_e = \frac{1}{M} \cdot \left(\frac{\sigma}{M} - \tau_0\right) \cdot \left(\frac{d}{x}\right)^{1/2} \quad (3)$$

where: τ_0 – the friction tension;

d – grain diameter;

x – the distance between the application point of the tension and the point when gliding starts.

For mono-phasic structures Vyas et.al. [20] considers that a reduced number of dislocations sources on the surface and the small packaging energy favorise a good cavitation resistance.

Similar results, from the point of view of grains sizes on the erosion cavitation resistance were obtained by Preece [14] on the pure Fe. The results, like for Ni and brass are linked on the period of incubation.

From the studies of Preece's [14] do not result any link between the erosion speed and the grain size after incubation. From the metals having a h.c. crystalline network, Preece studied a polycrystal of Zn and established that the grain size has a neglectable role in the incubation period of the cavitation and the mass loss speed enhances significantly with the grain size.

Analysing Co h.c., [18], Preece et. al. [14] have seen that during cavitation, inside the grains, a fine network of macles forms. In the same line forward, Vaidya et. al. [19] saw fine macles formation $\{1121\}$ and $\{1012\}$ in Co micro-crystals on surfaces $\{0110\}$ and $\{0001\}$.

These macles, generated by cavitation have as an effect the effective grain size diminishing at 0.1 μm from 1.0 μm . This fragmentation blocks the development of asperities formed at the surface and the erosion develops slowly by small particles expelling.

The results of the researchers from the above were obtained on materials with one or two components only.

Bordeasu [2] analysed the influence of various alloying elements upon the grains and defects induced in the crystalline structure correlated with the mass lost by cavitation erosion.

The studies made on non alloyed steels OL 370-3k and OT 500-3 shown that the resistance at cavitation erosion decreases because of P that leads to the occurring of segregations and growing of the fragilisation trend as well as of the presence of S that brings the fall of the fatigue resistance and tenacity with the forming of breaking amorses by sulphours FeS and MnS.

Also the researches on the Fgn 450-5 cast iron shown that the presence of graphite nodules lowers the resistance at cavitation attack because of their hardness and fragility high values.

The researches made on a steel having 12.5 % mn (coded D 32-1 [2]) have evidenced a rough and fragile structure due to high Mn, fact that lowered the cavitation resistance.

The same phenomenon registered on an austenite- ferritic stainless steel with 3.5 % Mn.

Through the alloying with Cr, ni, Mn, Mo the grain sizes decrease and the cavitation resistance enhances. These remark were done on the steels 18MoCrNi13, 41MoCr11, 33MoCr11, 40Cr10 [2].

So, from the researches made by Bordeasu it results that materials having the same granulation but different chemical compositions will resist differently at cavitation. Also one can see that through a combination between granulation and chemical composition it is possible to obtain different materials with various qualities and similar cavitation resistance.

2.2 The influence of martensitic transformation and macles

Studies made by Gould [9], Antony et. al. [1] and woodford [21] on alloys with Co base (stelite 6B) and stainless steels 301, 303 and 304 lead to various conclusions linked with the cavitation resistance, the energy developed in the cavitation process and the martensitic transformation $\gamma \rightarrow \varepsilon$.

So it is appreciated that the high resistance of stelite 6b comes exclusively from the transformation $\gamma_{\text{cubica cu fete centrate}} \rightarrow \varepsilon_{\text{hexagonala compacta}}$ and the benefic effect of the transformation is brought by the high energy of beaking of the phase ε_{hc} than of the energy absorbed during transformation $\gamma \rightarrow \varepsilon$.

In the same time, the studies of Woodford's on stelite 6B and stainless steels 301, 303 and 304 reveals that there is no simple correlation between the martensitic transformation ($\gamma \rightarrow \varepsilon$ and/or $\gamma \rightarrow \alpha'$) and the cavitation resistance.

In the same time woodford does not mention the existence or not of some mechanisms of deformation operating in ε_{hc} phase of the alloy co- 2% Fe, for example fine macles observed in pure Co by Vaidya et. al. [19].

The researches on cavitation achieved on various austenitic stainless steels [16] show that by plastic deformations created by the cavitation attack, some packaging defects occur leading at the martensitic transformation $\gamma \rightarrow \varepsilon$ [13].

The martensite formed by this method has an acicular shape and is surrounded by gliding strips made by macles and/or by martensite ε .

The models proposed for the transformation $\gamma \rightarrow \varepsilon$ during the cavitation attack are based on the super-positioning of packaging defects on the second compact plan $\{111\} \gamma$.

There are two ways of approach:

1. the transformation $\gamma \rightarrow \varepsilon$ is due to regular superposition of packaging defects [3];
2. the transformation $\gamma \rightarrow \varepsilon$ follows an irregular process of super-positioning of the packaging defects, i.e. the following of packaging defect is being made randomly at the beginning and then becomes regular, for minimising the energy associated with the packaging defects [8].

Even if a lot of authors do not have the same opinion on the exact nature of ε martensite germination, in the cavitation erosion process the majority of recent papers appreciate as the most probable mechanism of transformation $\gamma \rightarrow \varepsilon$ the one of the random super-positioning [4].

The crystallographic relations between the starting phase cfc (γ) and the hc phase (ε) in this case after [4] are:

$$\begin{aligned} (111)_{\gamma} // (0001)_{\varepsilon} \\ [1\bar{1}0]_{\gamma} // [1\bar{2}10]_{\varepsilon} \end{aligned}$$

The habitus plans of the martensite plates ε are the planes $\{111\}_{c.f.c.}$, formed by the superposition of the packaging defects.

Lecroisey et. al. [12] shows that the martensite ε forming occurs following to the decrease of the temperature, fact that means a reduction of the energy of packaging defects as one can see in figure 1.

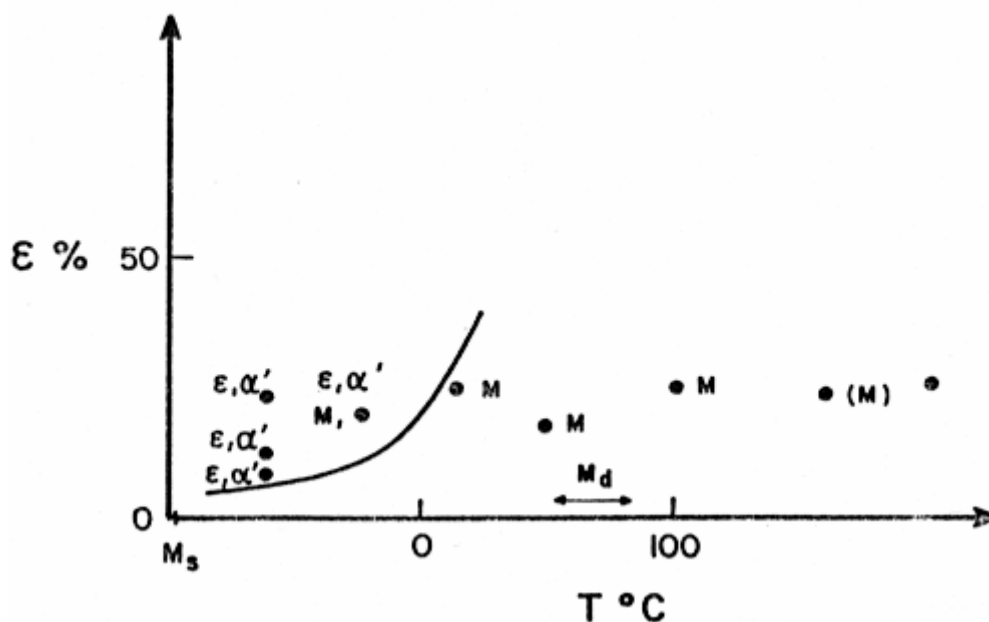


Fig. 1. The consequences of the temperature reduction on the transformations in an alloy 16-15. The curve represents the forming of approximate 1% of martensite α' (after Lecroisey and Pineau [12]): M – macling; ε – hc martensite; α' martensite cvc.

Using his own results and these of Thomas [1] Lecroisey [12] establish the following relation showing that martensite forming is easier than macles forming:

$$\frac{\gamma_0 - \gamma(1-x)}{\mu b} > \sqrt{2}\xi^2 \pm \sqrt{2}\alpha\xi \frac{\sigma}{\mu} \quad (3)$$

where:

γ_0 – intrinsic energy of packaging defects at T_0 temperature where $\Delta\sigma^{\gamma \rightarrow \varepsilon} = 0$;
 μ – shearing module; b – Burger's vector of Shockley partial dislocations; ξ – normal contraction in the plan $(111)_\gamma$ at the transformation $\gamma \rightarrow \varepsilon$; α - parameters that depends on the geometry of the germination location as a function of the applied tension; σ – the applied tension; $(1+x)$ the rapport between the extrinsic and intrinsic energy of the packaging defect.

This expression shows that the germination of martensite ε is not a function just of the intrinsic energy of the packaging defect but depends also by its extrinsic energy as well as on the slight contraction of the transformation c.f.c. $(\gamma) \rightarrow$ h.c. (ε) and is favored by a small temperature.

4. Conclusions

a) There have been shown various aspects about the influence of grain sizes on cavitation erosion of some categories of materials and the relations that put into evidence this influence.

Also it was discussed the mechanism of the transformation γ (c.f.c.) \rightarrow ε (h.c) produced by the deformations and packaging defects produced during the cavitation attack.

b) The transformation of the austenite in martensite h_c leads also to the enhancing of the resistance to cavitation of the material because the breaking of this kind of martensite needs higher energy.

c) If the cavitation stress produces macling the erosion resistance grows. If is the same stress produces cracking, the erosion resistance diminishes.

d) There were shown some aspects linked on the effects of some chemical elements on structure and grain size of steels and cast irons eroded by cavitation.

e) The results shown in the paper open new directions for studying the cavitation erosion. at the material testing, beside the characteristic curves of cavitation one must pay attention to the microstructural transformations in time of cavitation attack, especially macling and martensite h_c forming. Also it is compulsory to continue the study of the material at the level of crystallographic network. In this way, images about the cavitation behavior of the material, more advanced than a simple appreciation of the resistance, by using the comparison criterion.

References

1. Antony, K.C., Silence, W. L., Proc. 5th int. Conf. on Erosion by Solid and Liquid Impact, p. 67-1
2. Bordeasu I., - Eroziunea cavitațională asupra amterialelor utilizate in construcția mașinilor hidraulice și elicelor navale,. Efecte de scară, Teză de doctorat, Timișoara, 1997
3. Bollmann J.R., e.a. – Mechanical Physic of Solids, vol. 34, no.1, 1986, pp.29-54
4. Brooks, J. W., Thèse de doctorat (Ph. D.), Université de Birmingham, 1978
5. De, M. K. și Hammit, F.G., J. Phys. E. Sci. Instrum., vol. 15, p. 741
6. Franc J.P., e.a. - La Cavitation, Mecanismes phisiques et aspects industriels, Press Universitaires de Grenoble, 1995
7. Fujijama, S., Akamatsu, T., Proc. 10th Int. Shock Tube Symp., Dept. of Aeronautical Engineering, Kyoto University, Japan, 1975, p. 174
8. Fujita H., et Veda S., - Acta Met., Vol. 20, 1972, pp.759
9. Gould, G.C., Proc. 3^e Int. Conf. on Rain Erosion, 1970, p. 881
10. Graham, A. J., și Youngblood, J. L., Metall. Trans., vol. 1, 1970, p. 423
11. Karimi, A., Proc. 7th Int. Conf. on Strength of Metals and Alloys, vol. 2, 1985, p. 1607
12. Lecroisey, F. Pineau, A., Metall. Trans., vol. 3, 1972, p. 387
13. Olson, G. B. Cohen, M., Met. Trans., vol. 7A, 1983, p. 267
14. Preece, C.M.e.a, ASTM STP 664, 1977, p. 409
15. Rao, B.C.S. Buckley, D.H., Mat. Sci. and Eng., vol. 67, 1984, p. 55
16. Simoneau, R., e.a., - Cavitation_Erosion and Deformation mechanisms of Ni and Co Austenitic Stainless Steels, Erosion by Liquid and Solid Impact – Proceedings of, ELSI-VII, Cambridge, 7-10.10.1987, p.32.1-32.8
17. Thomas G.P, e.a. journal of test. And Eval., vol. 9, no.3, 1981, pp.189-197
18. Trusculescu, Studiul metalelor, Editura Didactica si Pedagogica, Bucuresti,
19. Vaidya, S.e.a, Metall. Trans., vol. 11A, 1980, p. 1139
20. Vyas, B. și Preece, C.M., Metall. Trans. A., vol. 8A, 1977, p. 915
21. Woodford, D.A., Metall. Trans., vol. 3, 1972, p. 1137

ILARE BORDEASU, Assoc. Prof. Department of Hydraulic Machinery "Politehnica" University of Timisoara

E-mail ilarica@mec.utt.ro

VICTOR BALASOIU, Prof. Department of Hydraulic Machinery "Politehnica" University of Timisoara

E-mail balasoIU@mec.utt.ro

RODICA BADARAU, Assist. Department of Hydraulic Machinery "Politehnica" University of Timisoara

E-mail badarau_r@yahoo.com

MIRCEA OCTAVIAN POPOVICIU, Prof. Department of Hydraulic Machinery "Politehnica" University of Timisoara E-mail mpopoviciu@mec.utt.ro

EUGEN DOBANDA, Lecturer Department of Hydraulic Machinery "Politehnica" University of Timisoara E-mail eugendobanda@yahoo.com

ASUPRA TRANSFORMARILOR STRUCTURALE PRODUSE DE SOLICITARILE CAVITATIONALE

Rezumat: In lucrare se discuta aspecte privind comportamentul microstructurii diverselor tipuri de materiale solificate la eroziune cavitationala. Pentru aceasta se face o grupare a rezultatelor obtinute in diverse laboratoare, inclusiv in cadrul Laboratorului de Masini Hidraulice din Timisoara, prezentate in literatura de specialitate si comunicate la diverse congrese si simpozioane, cu privire la raspunsul structurii materialelor la atacul cavitational, precum si la transformarile microstructurale ce au loc in timpul acestui atac. Scopul este de a intelege fenomenul cavitational erozional si de creare a unei imagini globale, mai clare, asupra modului in care materialul se distruge prin cavitate.

CONSIDERATIONS CONCERNING THE CAVITATIONAL DESTRUCTION OF THE COMPOSITE MATERIAL ARMURED WITH 20% CERAMIC PARTICLES

BY

**RODICA BADARAU, ILARE BORDEASU, VICTOR BALASOIU,
ION SPOREA, and MIRCEA NICOARA**

***ABSTRACT** : The use of composite materials in the air-plane building implies a series of tests in view of enhancing the flight safety. As this kind of materials are obliged to fly in rainy conditions it was compulsory to study the composites from the point of view of cavitation destruction, knowing the fact that some components of the plane are eroded through cavitation during the impact with the rain water drops [1]. In this sense the paper shows and discuss the results obtained by cavitation attack upon an aluminium based alloy armured with 20% ceramic particles. The attack was performed in the magnetostrictive vibrating apparatus with Ni tube from the Laboratory of Hydraulic Machines from Timisoara [2]. The results obtained are being compared with those of the etalon steel 40Cr10, considered as having a good cavitation resistance.*

***KEY WORDS:** erosion, cavitation, ceramic composite*

1. Introduction

Because of the very low specific weight and high mechanical characteristics they have, the composites are used today for many applications as machine building, airspace industry, sport equipment etc.

The researchers desire to obtain machines and equipment having low mass and high performances, involves the studying of various composites materials from the point of view of the technology of fabrication, of obtaining of some high physico - mechanical characteristics and of enhancing of their resistance of different types of stresses.

In countries like Canada, USA, France, Japan etc., a special attention for these materials is given by the aeroplanes builders. Because the aeroplanes are obliged to fly also in rainy conditions, one must achieve studies of the composites from the point of view of the resistance to the destruction by cavitation, knowing the fact that some elements like the wings and the ogive are subject to erosion by cavitation during their impact with the water drop [1].

In this paper we show and discuss the results obtained through the cavitation attack on an aluminium based composite alloy armoured with ceramic particles. This attack was achieved in the magnetostrictive apparatus with Ni tube, from the Laboratory of Hydraulic Machines from Timisoara [2].

2. The tested material

The composite material submitted to cavitation destruction has a metallic matrix, an aluminium alloy (AlCuSiMg) in which are being inserted using specific procedures ceramic carbides particles SiC type, in various proportions.

Table 1 shows the chemical composition of the metallic matrix of the composite, known as Alumix 123.

Table 1 The chemical composition of the Alumix 123 alloy

| Cu | Mg | Si | Lubricant type Steramida (Microwax C) | Al |
|----|------|------|--|------|
| | 0.5% | 0.7% | 1.5% | rest |

At the alloy mentioned in table 1 there were added Si carbides in 5% and 20% proportions.

In table 2 there are shown the densities of the armoured composites with Si carbides.

Table 2 The density of the armoured composite with Si carbides [4]

| SiC [%] | 0 | 5 | 20 |
|------------------------------|-------|-------|-------|
| Density [g/cm ³] | 2.600 | 2.631 | 2.724 |

The technology of obtaining of the composite armoured with Si carbides is specific for the powder metallurgy, namely (mechanical mixing, compacting by pressing and consolidation by a sintering heat treatment) [4].

The tested materials were submitted to heat treatments which led to an another enhancing of the mechanical characteristics. These are:

T1 – sintering followed by a cooling down to the environmental temperature ;

T2 – thermal ageing, consisting in a heating in air at 495 – 505 °C for 30 minutes followed by a cooling in water and then an ageing at 160 °C during 18 hours.

In table 3 there are given the mechanical characteristics of the Alumix 123 matrix obtained following the heat treatments applied and in table 4 there are given the hardness values for the armoured composite after ageing.

Table 3. Mechanical properties of Alumix 123 after heat treating

| Treatment | T 1 | T2 |
|-----------------------|-----|-----|
| R _m [N/mm] | 190 | 320 |
| HB [daN/mm] | 60 | 100 |
| A ₅ [%] | 5 | 1 |

Table 4 Mechanical properties of the composite material after heat treating

| % SiC | 0 | 5 | 20 |
|------------------------------|-----------|---------|-----------|
| HB [daN/mm ²] | 73,2-85,7 | 79,5-87 | 86,2-88,8 |

3. Installation and experimental methodics

The cavitation destruction of the composites was achieved in the magnetostrictive apparatus with Ni tube, from the Laboratory of Hydraulic Machines from Timisoara. The operational parameters of this apparatus are:

- Electric power = 500 W
- Amplitude of oscillations = 47 μm
- Frequency of oscillations = 7000 \pm 3% Hz
- Usual diameter of the sample = 14 mm
- Temperature of the cavitant liquid = 20 \pm 1 $^{\circ}\text{C}$

The methodology used during the cavitation attack is that described by the ASTM rules [6] and accepted by all the specialised laboratories.

So, at the start of each cavitation attack, the samples were degreased and then washed successively in water under pressure, distilled water, alcohol and acetone. Then they were dry out in hot air current and finally they were weighted on an analytical balance type Zaklady with five significant digits. The eroded mass was determined by difference between the mass of the sample at the start and at the end of the attack period.

During all the cavitation attack the parameters mentioned in table 5 were maintained at the prescribed value.

Because the samples had the sizes less than that necessary for fixing in the mantle corbel (M 12x1) of the Ni vibrating tube, for achieving the experiment the solution shown in figure 1 was adopted.

So, the samples, having the shape of a tablet were fixed by hooping in the appropriate parts who were fixed themselves in the Ni tube by screw. For enhancing the safety of fixing it was used also an adhesive for metals.

The fixing parts were made in duraluminium, in view of not enhancing the weight sample-fixing part beyond the protection limit (max. 7.8 g), ensured by the tube cracking resistance [2].

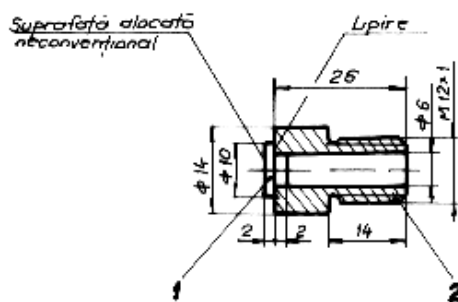


Fig. 1 The constructive solution for fixing the composite tablets in view of testing

Before starting the attack, the surfaces of the sample surfaces were carefully grinded in view of eliminating the influence of the roughness toward the material losses at the beginning of the attack.

4. Experimental results

In table 6 there are shown the mass losses corresponding to the three periods of cavitation attack, with the duration of 5, 10 and 15 minutes.

For a comparison, from the point of view of the cavitation erosion resistance, in the same table, there were inscribed the losses registered for the etalon steel 40Cr10, considered as having a good cavitation resistance.

Table 6 Mass losses during the cavitation attack

| Minute of the test/test duration | Mass losses [mg] | | | | | | |
|----------------------------------|------------------|----------------------------|------|-------|------|-------|------|
| | 40Cr10 | Composite material, [%SiC] | | | | | |
| | | 0 | | 5 | | 20 | |
| | FT | FT | TT | FT | TT | FT | TT |
| 5/5 | 0,94 | 5,13 | 5,74 | 3,10 | 3,97 | 3,10 | 3,97 |
| 15/10 | 2,65 | 5,27 | 4,99 | 6,99 | 6,63 | 6,99 | 6,63 |
| 30/15l | 4,1 | 5,5 | 5,01 | 23,87 | 7,68 | 23,87 | 7,68 |

FT – samples without ageing treatment; TT – heat treated samples

Analysing the results given in table 6 the following conclusions can be driven:

1. No matter the content in SiC, the treated material has a better resistance at cavitation attack than the material without the ageing treatment;
2. With the enhancing of the SiC content the cavitation resistance decreases (the mass losses grows)

The high mass losses during the first 5 minutes of cavitation attack are determined both by the eroded material mass and by the removing of the adhesive material used at the samples fixing. This is the reason why these losses can not be taken into consideration in comparing the results

During the following two periods of attack (10, and 15 minutes), the only material eroded was that of the composite.

Visually analysing the surfaces submitted to the attack and using the optic microscope (enhancing 16x), there were seen greater caverns on the non treated samples than those existent on the heat treated materials. This fact shows that by the ageing treatment the structure became more homogenous, fine and the level of the mechanical characteristics are higher.

It is a surprise the very high level of eroded mass at the non-treated sample with 20% SiC, at the minute (30– see table 6). Comparing the results obtained with those of the etalon steel 40Cr10, registered on standard samples (D = 14 mm, for the composite D = 10 mm) one can say that the cavitation resistance of the aluminium based composite armoured with SiC particles is not satisfactory.

Normally, with the decreasing of the diameter, the level of losses decreases [3, 5] but here, the enhanced fragility of the composite, and probably the bigger size of the Si carbide particles determined this so high enhancement.

5. Discussions concerning the distructions achieved by cavitation

a) General elements of the distruction

The cavitation distruction achieved in the vibratory apparatus is being caused by the impact between the shock waves and micro-jets that occur at the drifting of the

cloud of cavitation bubbles attached to the surface of the sample [2, 3]. This impact being iterative and locally distributed determines the breaking of the links between the carbides and the metallic matrix, cracking network around the impact point. As the attack continues, carbides are being expelled as well as base metal pieces.

Obviously before the final cracking there takes place a process of radial flowing (elasto-plastic deformation), but very small, because of the hardness and high fragility. The phenomenon is well put into evidence in the figures.

At all the samples, figure 2 – 6 it can be seen a central cavern. It appears even during the first minutes of the cavitation attack, because of the shape of the cloud of cavitation bubbles that determines, in this phase, through the specific cavitation mechanism a maximum intensity in its central zone. After a time, around the central cavern appear more other caverns placed in an approximate circle shape.

It must be remarked that with the growing of the content in SiC, the size of the caverns and their number becomes greater. The phenomenon is normal because of the fragility of the carbides. this phenomenon can be registered at all the samples no matter if the material was or was not heat treated. The difference is linked only by the size of the caverns, less at the treated materials grace to the enhancing of hardness and structural homogeneity.

b) Distruction analysis

The composite with 0% SiC without heat treatment, figure 2

The figure shows that the attacked surface is eroded in a pitting shape but the central zone is more affected. The caverns around the central zone are being produced following the breaking of the deformed material in the previous attacks. The shape of these suggests the expelling of a group of grains. The tilted shape shows the existance of a plastic deformation, radial flowing, produced under the influence of micro-jets and shock waves.

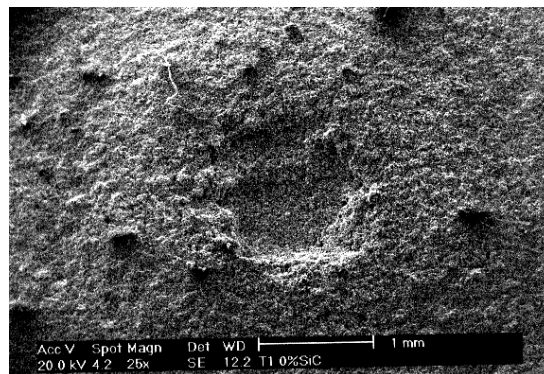


Fig.2 (0 % SiC, FT)

The composite material with 5% SiC without heat treatment, figure 3

At this material, the sizes of the caverns are slightly larger. The edges of them suggests also the radial flowing under the action of micro-jets and shock waves but the shape of the cavern looks more like an active vulcano crater. This phenomenon is determined by the polyedric shape of the SiC. The way in which they are dispersed in the metallic matrix and the patern of cracking propagation leads to the expelling of

pieces of the metallic matrix. This is why the sizes of the caverns grows with the content of SiC.

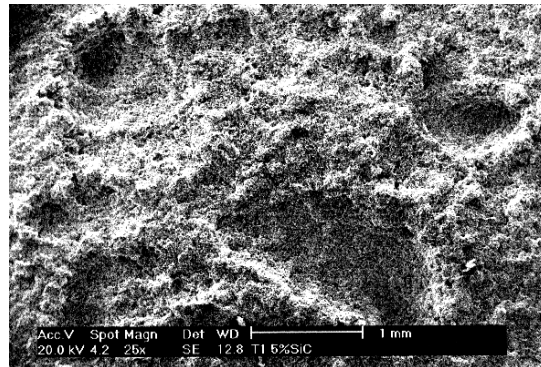


Fig.3 (5% SiC FT)

The composite material with 20% SiC without heat treatment, figure 4

In this figure it can be better seen the stratification of the composite. Here one can see clearly how the breaking of the material takes place at the boundaries between the carbides particles and the metallic matrix and how the destruction of the carbides leads at the expelling of the grains of the metallic matrix. The phenomenon resembles, at a lower scale with the breaking of the rocks using dynamite.

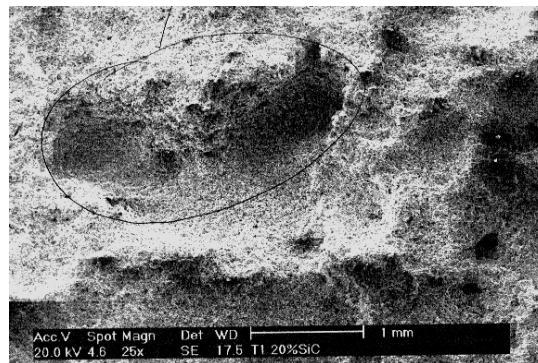


Fig. 4 (20 % SiC FT)

The heat treated composite material, figure 5 - 7

In these figures it can be seen that:

- the structures of these composite materials have a finer and more homogenous degree;
- the caverns have smaller sizes;
- the occlusions are being present in these cases too, fact that suggests some problems of the technology of obtaining the composite;
- the pittings are smaller than in the non-treated materials, showing the benefit of the ageing from the point of view of cavitation resistance.

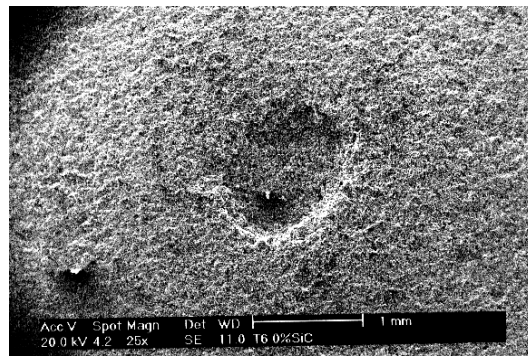


Fig.5 (0% SiC TT)

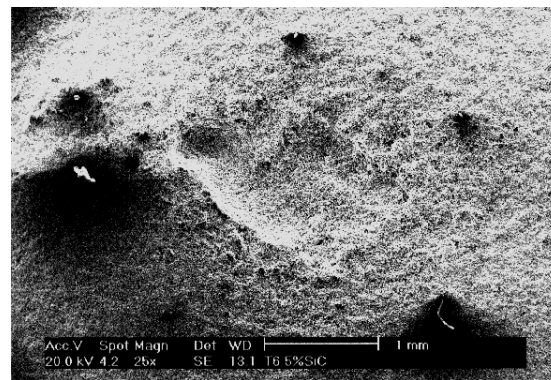


Fig.6 (5 % SiC TT)

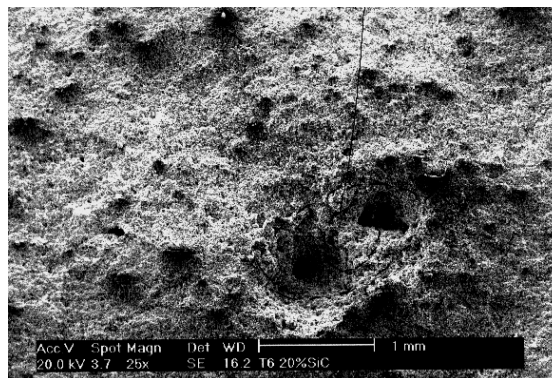


Fig. 7 (20% SiC TT)

It must be remarked , figure 7, that the too much content of SiC makes the decreasing of the cavern size in the horizontal plane but the deepness of the cavern is bigger. This can be explained due to the heat treatment applied.

The basic material suffered structure transformations that enhanced the mechanical characteristics (breaking resistance, hardness, elongation table 3), but the carbide, independently from the treatment suffers distructions on the vertical direction. Obviously, after a greater time of attack, this will lead at the situation of caverns coalescence and expelling of the entire group of grains of the metallic matrix comprised between these caverns.

6. Conclusions

The cavitation resistance of the composite material is not satisfactory and can not enable its' use in the fabrication of parts strongly submitted at cavitation attack as hydraulic machines rotors, rotor pumps or ship propellers.

The use of heat treatments ensures a better cavitation resistance but it must also be improved the technology of fabrication of the composite in view of enhancing the level of homogeneity and finishing of the structure.

The enhancing of the content of SiC make the resistance to cavitation attack to diminish because of the high fragility of the particles.

In the air plane industry the material can be used because the intensity of the cavitation phenomenon is much less than that created in the hydraulic machines or in the apparatus used for the experiment.

The enhancing of the content of SiC, made the cavitation resistance to diminish because of the high fragility of the carbides.

References

1. Anton I., - Cavitatia, Vol.I, Editura Academiei R.S.R, 1984.
2. Bordeasu I., - Eroziunea cavitationala asupra materialelor utilizate in constructia masinilor hidraulice si elicelor navale. Efecte de scara, Teza de doctorat, Timisoara, 1997.
3. Franc, J.P, e.a., - la cavitation, Mecanismes physiques et aspects industriels, Press Universitaires de Grenoble, 1995.
4. Nicoara, M., - Nicoara, M., - Contributii la studiul compozitelor metalice armate cu particule ceramice privind producerea si modificarea structurii si proprietatilor prin prelucrare mecanica, Teza de doctorat, Timisoara, 1998
5. Steller, J.K., - International cavitation erosion test. Test facilities and experimental results, 2-emes Journes cavitation, Paris, March, 1992.
6. Standard Test Method for Cavitation Erosion Using Vibratory Apparatus, ASTM G32-98.

RODICA BADARAU, Assist. Department of Hydraulic Machinery "Politehnica" University of Timisoara

E-mail badarau_r@yahoo.com

ILARE BORDEASU, Assoc. Prof. Department of Hydraulic Machinery "Politehnica" University of

Timisoara E-mail ilarica@mec.utt.ro

VICTOR BALASOIU, Prof. Department of Hydraulic Machinery "Politehnica" University of Timisoara

E-mail balasoiu@mec.utt.ro

ION SPOREA, Prof. Department of Mechanical Tehnology "Politehnica" University of Timisoara

E-mail mh@mec.utt.ro

MIRCEA NICOARA, Assoc. Prof. Department of Materials Scientifique "Politehnica" University of

Timisoara E-mail mnicoara@eng.utt.ro

Bv. Mihai Viteazu 1, 300222, Timisoara, Romania Telefon (+40) 236 403681, Fax (+40) 236 403682,

E-mail mh@mec.utt.ro

CONSIDERATII PRIVIND DISTRUGEREA PRIN CAVITATIE A MATERIALULUI COMPOZIT ARMAT CU 20% PARTICOLE CERAMICE

Rezumat: Utilizarea materialelor compozite in constructia aeronavelor implica o serie de incercari in vederea cresterii sigurantei zborului. Cum acestea sunt obligate sa zboare si in conditii atmosferice ploioase, s-a impus studierea compozitelor si din punctul de vedere al distrugerii prin cavitate, stiut fiind faptul ca unele componente, precum ogiva si aripile, sunt erodate prin cavitatia realizata din impactul lor cu picatura de ploaie [1]. In ceast sens , in lucrare se prezinta si discuta rezultatele obtinute prin atacul cavitational realizat asupra unui aliaj compozit pe baza de aluminiu armat cu 20 % particole ceramice. Atacul a fost realizat in aparatul vibrator magnetostriktiv cu tub de mchel, din cadrul Laboratorului de Masim Hidraulice din Timisoara [2]. Rezultatele obtinute sunt comparate cu ale otelului etalon 40Cr10, considerat cu buna rezistenta la cavitate.

**STRUCTURE – THERMAL AND VISCOMETRIC PROPERTIES
RELATIONSHIP FOR SOME
POLY (N-SUBSTITUTED MALEIMIDE-co-N-VINYL-2-PYRROLIDONE)S**

BY

CAMELIA HULUBEI and SIMONA MORARIU

Abstract: *Two N-substituted maleimide monomers, N-(4-carboxyphenyl)maleimide and N-(4-formylphenoxy-4'-carbonylphenyl)maleimide were copolymerized with N-vinyl-2-pyrrolidone at 90 °C in the presence of 2,2'-azobisisobutyronitrile as initiator in dimethylsulfoxide. The monomers reactivity ratios were calculated by Fineman-Ross, Kelen-Tüdös, extended Kelen-Tüdös, Joshi-Joshi and Mao-Huglin methods. Also, Alfrey-Price Q, e values were estimated. The copolymers microstructure was calculated using a statistical method based on the obtained reactivity ratios. Thermal properties of the new synthesized copolymers were studied by thermogravimetric analyses and differential scanning calorimetry. The intrinsic viscosities of copolymers were also discussed.*

Keywords: *radical copolymerization, N-substituted maleimide, N-vinyl-2-pyrrolidone, monomer reactivity ratio*

1. Introduction

During the last few years, increasing need in the high technology industries has been the driving force for the development of new polymers combining thermal stability with specific functional properties. N-substituted maleimides (RMI) which belong to 1,2-disubstituted ethylenic monomers are radically polymerizable. Polymers of maleimides have been reported for their special properties such as: high thermal stability, optical and catalytic activities, high sensitivity and versatility in lithographic applications or, for the ability to function as ion-exchanger or photoinitiator [1],..., [8]. One outstanding property of RMIs is their susceptibility to a variety of chemical reactions as a result of the electron withdrawing effect of the two adjacent carbonyl groups in the maleimide ring, which create a very electron-deficient double bond. Thus, RMIs are known to copolymerize with electron-rich monomers, to produce alternating copolymers [8], [9]. N-substituted maleimide/vinyl monomers copolymers found application in many fields as positive photoresists, non-linear-optical materials (NLO), Langmuir-Blodgett film, or related to their dielectric, nuclear magnetic resonance or asymmetric induction polymerization properties [9],..., [11]. On the other hand, poly(N-vinyl-2-pyrrolidone) is one of the most frequently investigated classes of polymers due to its remarkable properties (hydrophilicity, complexing ability, biocompatibility, etc.) [12], [13]. Thus, it is expected that the copolymers of N-substituted maleimides with N-vinyl-2-pyrrolidone will combine the interesting properties of these two type of monomers and, also, of its homopolymers.

The aim of this paper is to describe the synthesis and characterization of the copolymers of *N*-(4-carboxyphenyl) maleimide (MICOOH) and *N*-(4-formylphenoxy-4'-carbonylphenyl) maleimide (MICHO) with *N*-vinyl-2-pyrrolidone (NVP). The effect of the *N*-substituents on the intrinsic viscosities and thermal properties of the obtained copolymers was discussed.

2. Experimental

N-(4-carboxyphenyl)maleimide (MICOOH) was obtained, typically, by the reaction of maleic anhydride with *p*-amino-benzoic acid, in dried acetone at ambient temperature followed by cyclodehydration using sodium acetate and acetic anhydride [14]. Yield 82%, mp: 241°C (lit. m.p. 244°C [15]).

4-Maleimido-benzoyl chloride was synthesized by the reaction of MICOOH with thionyl chloride, according to the procedure reported by Liu [16]. Yield 78%, m.p. 165-168°C (lit. m.p. 168-169°C [16]).

N-(4-formylphenoxy-4'-carbonylphenyl)maleimide (MICHO) was prepared from 4-maleimido-benzoyl chloride and *p*-hydroxy-benzaldehyde by a Schotten-Baumann type-reaction presented in detail elsewhere [17]. Yield 88.6%, m.p. 221-223°C.

All copolymerizations of MICOOH and MICHO with *N*-vinyl-2-pyrrolidone were performed at 90°C in a sealed ampules with a radical initiator (AIBN) in DMSO, under nitrogen atmosphere. The resulting copolymers were isolated by precipitation in methanol and dried under vacuum at room temperature.

¹H-NMR spectroscopy was recorded in DMSO-d₆, using a JEOL 60 MHz NMR spectrometer. The IR spectra were recorded on a Specord M 90 Carl Zeiss Jena Spectrophotometer with KBr pellets. Differential scanning calorimetry (DSC) measurements were performed by a Mettler DSC 12E with a heating rate of 10°C/min under a nitrogen atmosphere. Thermal gravimetric analysis (TGA) was carried out in air with a F Paulik Derivatograph at a heating rate of 12°C/min. The number average molecular weights and the polydispersity indices of the copolymers were determined by means of gel permeation chromatography (GPC) using a PL-EMD 950 Evaporative Mass Detector equipped with 2xPLgel 5 μm MIXED-C, 300x7.5 mm columns. The viscometric measurements were carried out in dimethylformamide at 30°C, with an Ubbelohde viscometer. The intrinsic viscosities ([η]) were determined by using the Huggins method (copolymer concentrations: < 1.5 g/dl). Polymer solubilities were determined at room temperature, at a concentration of 1% (wt/v).

3. Results and discussion

The radical copolymerizations of both RMIs (*monomer 1*) with NVP (*monomer 2*) in dimethylsulfoxide (DMSO), using 2,2'-azobisisobutyronitrile (AIBN) as initiator, were carried out in order to elucidate the effect of the comonomers structure and copolymers composition on the resulting polymers properties. The copolymerizations were studied in a wide composition interval with mole fractions of RMI ranging from 0.10 to 0.90 in the monomer feed (Table 1).

The copolymers solubility was evaluated qualitatively and all copolymers are soluble in aprotic dipolar solvents such as: *N*-methylpyrrolidone, dimethylformamide,

dimethylsulfoxide and tetrahydrofuran. The high solubility in these polar solvents is due to the flexible linkages in the polymer main chain, which prevents the tight packing of the macromolecules. The bulk pendant groups are expected to reduce the polymer close packing too. The disturbed packing facilitates the diffusion of small molecules of solvents between the polymer chains and, by consequence, leads to a better solubility.

Table 1 Copolymerization of *N*-substituted maleimides (monomer 1) with NVP (monomer 2) in solution at 90°C

| Sample | Monomer 1 | Feed M ₁ (mole fraction) | Conv. ^c (wt %) | Copolymer m ₁ (mole fraction) | \bar{M}_n^d x10 ⁻³ | \bar{M}_w / \bar{M}_n^d | $[\eta]^e$ (ml/g) | IDT ^f (°C) |
|--------|---------------------|--|------------------------------|---|------------------------------------|---------------------------|----------------------|--------------------------|
| 1 | MICOOH ^a | 0.10 | 32.80 | 0.2794 | 30.50 | 1.325 | 0.635 | 252 |
| 2 | | 0.30 | 46.70 | 0.3884 | 10.50 | 1.238 | - | 262 |
| 3 | | 0.50 | 62.06 | 0.5652 | 7.80 | 1.162 | 0.374 | 265 |
| 4 | | 0.70 | 42.60 | 0.5456 | 3.70 | 1.236 | 0.247 | 258 |
| 5 | | 0.90 | 11.50 | 0.6842 | - | - | 0.130 | 255 |
| 6 | MICHOb | 0.10 | 27.24 | 0.2941 | 21.03 | 1.379 | 0.055 | 230 |
| 7 | | 0.30 | 34.18 | 0.5296 | 8.30 | 1.395 | 0.045 | 245 |
| 8 | | 0.50 | 29.16 | 0.6000 | 3.50 | 1.320 | 0.024 | 250 |
| 9 | | 0.70 | 10.44 | 0.6629 | 2.70 | 1.236 | 0.023 | 272 |
| 10 | | 0.90 | 8.13 | 0.8462 | 1.40 | 1.069 | - | 276 |

^a Solvent: DMSO = 5 ml; [AIBN] = 0.3 mol% (with respect to the monomers mixture);

Wt_{M1} + Wt_{M2} = 1 g; polymerization time = 1.5 h.

^b Solvent: DMSO = 10 ml; [AIBN] = 0.3 mol% (with respect to the monomers mixture);

Wt_{M1} + Wt_{M2} = 1 g; polymerization time = 72 h.

^c Polymer insoluble in methanol.

^d Estimated by GPC.

^e Determined in dimethylformamide at 30°C.

^f Initial decomposition temperature (onset on the TGA curve).

The chemical structures of the synthesized copolymers are represented in Fig. 1. The chemical structures were determined by IR and ¹H-NMR spectroscopy.

The IR spectra of the obtained copolymers present characteristic absorptions at: 3100-3070 cm⁻¹ (=CH), 2900-2850 cm⁻¹ (symmetrical and asymmetrical stretching vibrations of the aliphatic groups), 1780 cm⁻¹ (ν_{C=O} in plane), 1710-1730 cm⁻¹ (ν_{C=O} out of plane), 1400-1380 (ν_{C-N-C}), 740-700 cm⁻¹ ((ν_{O=C-N}). The large band between 2900-3300 cm⁻¹ and others, at about 1660 cm⁻¹ and 1200 cm⁻¹ respectively, are all ascribed to the carboxylic pendant groups. Special bands, at 2820, 2750 and 950 cm⁻¹ are associated with the aldehyde functionality.

The ¹H-NMR spectra recorded in DMSO-d₆, without internal reference, showed the presence of all the chemical shifts corresponding to the protons in the proposed structures. The proton from the CHO group was detected by offset, at about 9.70 ppm. A multiplet absorption, mostly between 8.20-7.15 ppm was assigned to the aromatic protons, while the peak at 5.23 ppm was associated with the methine proton resonance of NVP. The methine protons of maleimide ring, around 3.20 ppm and the side chain

methylene proton signals around 3.40 ppm are overlapped with the H₂O protons signal. The other methylene protons can be assigned in the range 2.00-2.25 ppm.

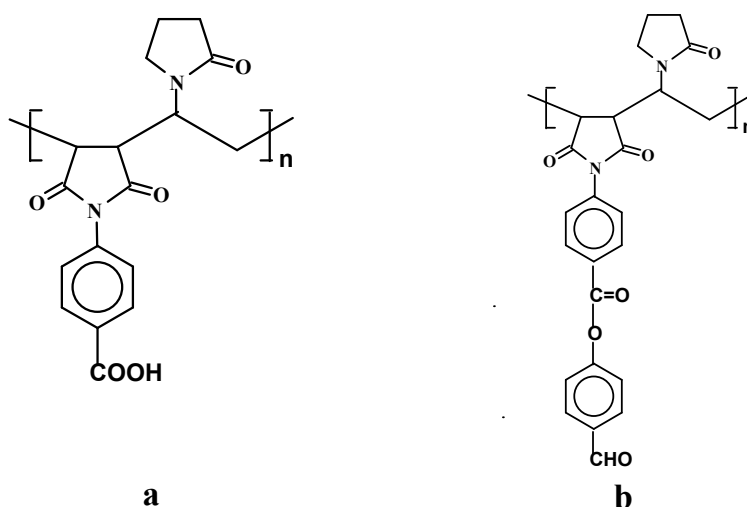


Fig. 1 Chemical structures of the copolymers: a) poly(*N*-(4-carboxyphenyl)maleimide-co-*N*-vinyl-2-pyrrolidone) (poly(MICOOH-co-NVP) and b) poly(*N*-(4-formylphenoxy-4'-carbonylphenyl)maleimide-co-*N*-vinyl-2-pyrrolidone) (poly(MICHO-co-NVP))

The copolymers compositions were estimated by ¹H-NMR analysis and were achieved by comparing the intensity of the aromatic protons signal from the functional maleimides (MICOOH and MICHO, respectively) and the intensity of NVP methine proton signal.

The reactivity ratios of the functional RMIs and NVP were determined according to the general copolymer composition equation by using the Fineman-Ross (F-R) [18], Kelen-Tüdös (K-T) [19], extended Kelen-Tüdös (ext K-T) [20], Joshi-Joshi (J-J) [21] and Mao-Huglin (M-H) [22] methods. The obtained reactivity ratios data are given in Table 2.

Table 2 Reactivity ratios calculated by different methods for copolymerization of some *N*-substituted maleimides (*monomer 1*) with NVP (*monomer 2*)

| <i>Monomer 1</i> | Method | r ₁ | r ₂ |
|------------------|----------|----------------|----------------|
| MICOOH | F-R | 0.133 | 0.137 |
| | K-T | 0.156 | 0.168 |
| | ext K-T | 0.117 | 0.105 |
| | J-J | 0.172 | 0.158 |
| | M-H | 0.124 | 0.116 |
| | Average: | 0.140 | 0.137 |
| MICHO | F-R | 0.506 | 0.110 |
| | K-T | 0.515 | 0.105 |
| | ext K-T | 0.500 | 0.066 |
| | J-J | 0.500 | 0.083 |
| | M-H | 0.500 | 0.067 |
| | Average: | 0.504 | 0.086 |

The type of the obtained copolymer could be understood from the values of the monomers reactivity ratios. The calculated average reactivity ratios of NVP are 0.137 for the copolymerization with MICOOH and 0.086 for the copolymerization with MICHO. The corresponding values for MICOOH and MICHO are 0.140 and 0.504, respectively. It can be seen that the reactivity values are similarly for the MICOOH / NVP monomers pair while r_1 value is greater than r_2 for MICHO / NVP system. It can observe that the reactivities of the growing radicals (regardless of the ending) are higher towards the other monomer than itself. The $r_1 \cdot r_2$ values of the both copolymerizations are closer to zero, indicating a greater tendency to alternation (e.g. 0.019 for MICOOH / NVP and 0.043 for MICHO / NVP systems). However, this tendency is lower than that of the MICOOH / Styrene or MICHO / Styrene systems [15], [17].

The Q , e values of MICOOH and MICHO were calculated by employing the following equation [23], using the average reactivity ratios (Table 2).

$$e_1 = e_2 + (|\ln r_1 r_2|)^{1/2} \quad Q_1 = (Q_2 / r_2) \exp[e_2(e_1 - e_2)]$$

The values of $Q_2 = 0.14$ and $e_2 = -1.14$ for NVP are from the literature [24]. The calculated Q_1 and e_1 parameters are found to be 0.106 and 0.848, respectively, for MICOOH and 0.216 and 0.632, respectively, for MICHO. The obtained positive e values indicate that maleimide monomers have an electron-poor double bond. Also, the obtained Q , e parameters for both maleimide monomers suggest that the electron-acceptor character of the substituent with carboxylic group is stronger than that having aldehyde pendant function.

It is also interesting to compare the sequence distribution in copolymers. From the average values of the reactivity ratios r_{RMI} and r_{NVP} given in Table 2 and using the statistical relations it was calculated the "run number" R . This parameter, defined by Harwood and Ritchey [25] as the average number of monomer sequence in a copolymer per 100 monomer units, provides a useful picture of the sequence distribution in a copolymer chain. R was determined with the following relations:

$$R_{random} = \frac{\%RMI_i \cdot \%NVP_i}{50}; \quad R_{experimental} = \frac{200}{2 + r_{RMI} \cdot \frac{\%RMI_i}{\%NVP_i} + r_{NVP} \cdot \frac{\%NVP_i}{\%RMI_i}}$$

where: i represents initial; R_{random} and $R_{experimental}$ are the run numbers for a random copolymer and for our samples with initial concentrations of monomers $\%RMI_i$ (mol% N -substituted maleimide) and $\%NVP_i$ (mol% N -vinyl-2-pyrrolidone); r_{RMI} and r_{NVP} are the reactivity ratios of N -substituted maleimide and N -vinyl-2-pyrrolidone, respectively. When $R_{experimental} > R_{random}$ the system of copolymerization tends to an alternant character. Fig. 2 shows the variation of $R_{experimental}$ and R_{random} with the molar fraction of RMI in feed. The $R_{experimental}$ values are higher than R_{random} for the both systems. The statistical distribution of the dyad monomer sequences RMI-RMI, NVP-NVP, RMI-NVP were calculated using the method proposed by Igarashi [26]. Fig. 3 shows the variation of the dyad monomer sequence fractions in copolymer

as a function as the *N*-substituted maleimide fraction in feed. The maximum value of RMI-NVP fraction in the copolymers corresponds to a mole fraction of RMI in feed of 0.4 for poly(MICHO-*co*-NVP) and 0.5 poly(MICOOH-*co*-NVP) respectively.

It is known that polymaleimides are polymers with a good thermal stability and high glass transition temperature (T_g) over 200°C which usually are not obtained using conventional vinyl polymerization [27]. The thermal behavior of the obtained polymers was evaluated by thermogravimetric analysis (TGA) and the results are summarized in the Table 1. The initial decomposition temperatures (IDT) of copolymers are in the range 230-276°C.

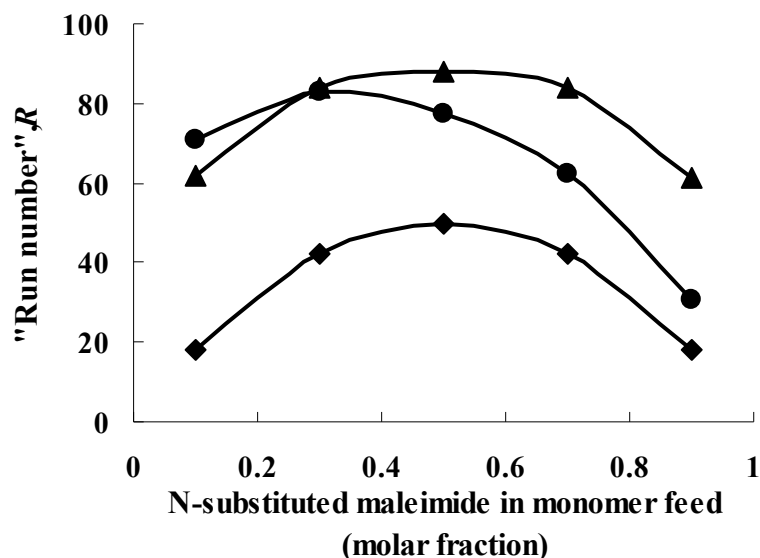


Fig. 2 Variation of the "run number" with the *N*-substituted maleimide in feed: (♦) variation of R_{random} ; (▲) variation of $R_{experimental}$ for poly(MICOOH-*co*-NVP); (●) variation of $R_{experimental}$ for poly(MICHO-*co*-NVP)

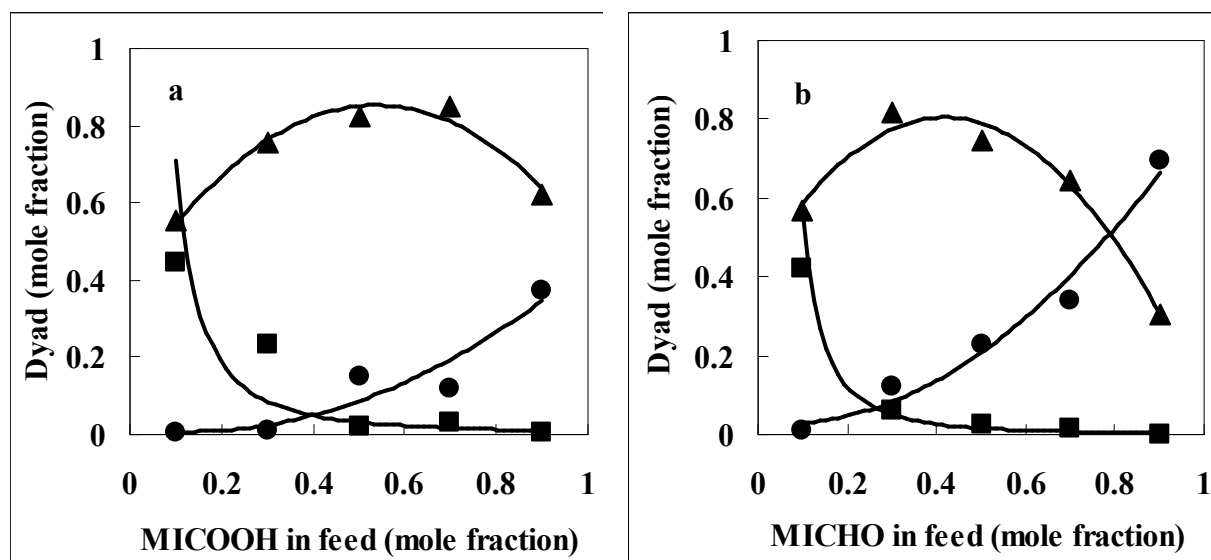


Fig. 3 Variation of the dyad monomer sequence fractions vs the *N*-substituted maleimide fraction for: a) poly(MICOOH-*co*-NVP) and b) poly(MICHO-*co*-NVP); (●) RMI-RMI dyad, (■) NVP-NVP dyad and (▲) RMI-NVP dyad.

The glass transition temperatures determined by differential scanning calorimetry was in the range 120-128°C for poly(MICHO-*co*-NVP). No T_g was observed for poly(MICOOH-*co*-NVP) below to decomposition temperature. This may be the result from the bulkiness and the strong polarity of the carboxylic group located at the *para* position of the aromatic ring side group.

The variation of RMIs concentration in the monomer feed on the intrinsic viscosities of copolymers is shown in Fig. 4.

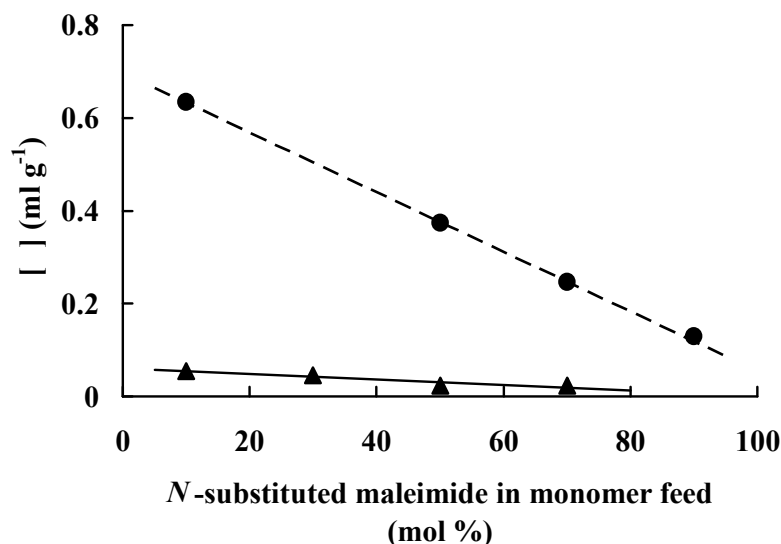


Fig. 4 Relation between *N*-substituted maleimide concentration in feed and the intrinsic viscosity of poly(MICOOH-*co*-NVP) (●) and poly(MICHO-*co*-NVP) (▲)

There are differences between the intrinsic viscosities of the prepared copolymers. A possible explanation for the higher intrinsic viscosities of poly(MICOOH-*co*-NVP) could be the intermolecular hydrogen bonds between the carbonyl group of NVP (proton accepting site) and carboxyl group of MICOOH (proton donor site). In addition, the formation of intermolecular hydrogen bonds increase the T_g values (i. e., copolymers with MICOOH). The intrinsic viscosities of the both copolymers decrease in the region with excess of maleimide derivatives in feed.

4. Conclusions

Two reactive maleimide monomers, characterized by the presence of a COOH or CHO functionality in the *N*-substituted group, *N*-(4-carboxy-phenyl)maleimide and *N*-(4-formylphenoxy-4'-carbonylphenyl)maleimide respectively, were copolymerized with *N*-vinyl-2-pyrrolidone (NVP) in solution by radical polymerization. The average reactivity ratios obtained by different methods were found to be $r_1=0.140$, $r_2=0.137$ for the MICOOH (1)/NVP (2) system and $r_1=0.504$, $r_2=0.086$ for the MICHO (1)/ NVP (2) system. The evaluated Q , e parameters for the both RMIs confirmed these structures as monomers with an electron-poor double bond. The radical copolymerizations of these functional RMIs with NVP present a marked tendency

toward alternation. The alternation tendency is higher for MICOOH / NVP system. These results were confirmed by the calculation of the monomer sequences distribution. The existence of planar maleimidic ring in the backbone chain, the polar structure of the *N*-phenyl ring substituents and the intermolecular hydrogen bonds have an important influence on the intrinsic viscosities and thermal stability of the synthesized copolymers.

REFERENCES

1. Şenel S., Rzaev Z.M.O., Pişkin E., Polym. Int., **52**, 713 (2003).
2. Jannasch P., J. Mater. Chem., **11**, 2303 (2001).
3. Wulff G., Krieger S., Macromol. Chem. Phys., **195**, 3665 (1994).
4. Lee Y.K., Kitamura S., Onimura K., Tsutsumi H., Oishi T., J. Polym. Sci., Part. A: Polym. Chem., **42**, 6157 (2004).
5. Amou S., Nishimura S., Takahashi A., Hagiwara T., Hamana H., Narita T., J. Polym. Sci., Part. A: Polym. Chem., **37**, 341 (1999).
6. Ahn K.D., Chung C.M., Jo H.S., Rhee J.M., Polym. Int., **47**, 407 (1998).
7. Chiang W.J., Lu J.Y., Macromol. Chem. Phys., **195**, 591 (1994).
8. Clark S.C., Hoyle C.E., Jonsson S., Morel F., Decker C., Polymer, **40**, 5063 (1999).
9. Soykan C., Erol I., J. Appl. Polym. Sci., **91**, 964 (2004).
10. Major J.S., Blanchard G.J., Chem. Mater., **14**, 2567 (2002).
11. Schmidt-Naake G., Drache M., Leonhardt K., Macromol. Chem. Phys., **199**, 353 (1998).
12. Barabas E.S., Encyclopedia of Polymer Science and Engineering. Ed. John Wiley, New York, **17**, 204 (1986).
13. Ng L.T., Jonsson S., Swami S., Lindgren K., Polym. Int., **51**, 1398 (2002).
14. Mikroyannidis J.A., J. Polym. Sci., Part. A: Polym. Chem., **28**, 669 (1990).
15. Oishi T., Iwahara M., Fujimoto M., Polym. J., **23**, 1409 (1991).
16. Liu F.J., Munukutia S., Levon K., Tesoro G., J. Polym. Sci., Part. A: Polym. Chem. **30**, 157 (1992).
17. Hulubei C., Morariu S., High. Perform. Polym., **12**, 367 (2000).
18. Fineman M., Ross S.D., J. Polym. Sci., **5**, 259 (1950).
19. Kelen T., Tüdös T., J. Macromol. Sci.-Chem., **A9**, 1 (1975).
20. Kelen T., Tüdös T., Földes-Bereznich T., Turcsányi B., J. Macromol. Sci.-Chem., **A10**, 1513 (1976).
21. Joshi R.M., Joshi S.G., J. Macromol. Sci.-Chem., **A5**, 1329 (1971).
22. Mao R., Huglin M.B., Polymer, **34**, 1709 (1993).
23. Alfrey T.J., Price C.C., J. Polym. Sci., **2**, 101 (1947).
24. Young L.J., J. Polym. Sci., **54**, 411 (1961).
25. Harwood H.J., Ritchey W.M., J. Polym. Sci., **B2**, 601 (1964).
26. Igarashi S., J. Polym. Sci., Polym. Lett. Ed., **1**, 359 (1963).
27. Turner S.R., Arcus R.A., Houle C.G., Schleigh W.R., Polym. Eng. Sci., **26**, 1096 (1986).

CAMELIA HULUBEI and SIMONA MORARIU

“Petru Poni” Institute of Macromolecular Chemistry, Jassy

RELAȚIA STRUCTURĂ-PROPRIETĂȚI TERMICE ȘI VÂSCOZIMETRICE PENTRU POLY(MALEIMIDĂ *N*-SUBSTITUITĂ-*co-N*-VINILPIROLIDONĂ)

Rezumat: S-au sintetizat doi monomeri maleimidici, *N*-(4-carboxifenil)maleimida și *N*-(4-formilfenoxi-4'-carbonilfenil)maleimida, care au fost copolimerizați cu *N*-vinil-2-pirolidona la 90°C, în dimetilsulfoxid, utilizându-se drept inițiator 2,2'-azobisisobutironitrilul. Rapoartele de reactivitate au fost calculate prin diferite metode. De asemenea, s-a determinat microstructura și proprietățile termice și vâscozimetrice ale copolimerilor sintetizați.

STUDIES AND RESEARCH AS REGARDS SPECTRAL REFERENCE MATERIALS FOR NI-CR ALLOYS

BY

VRAPCEA MARINELA , STOIAN PETRE and PREDA NICULINA

Abstract: *Nickel-chrome alloys are used for a wide variety of application , the majority of which involve corrosion resistance and heat resistance. One of these include medical applications(implantable metallic materials and dental restoration materials).This present paper shows the achivement and analysis of spectral referance materials for Ni-Cr alloys, which can satisfy the last generation spectrometers (optical and x-ray fluorescence) from Romania.For first the research presumed a very attentive theoretical study about Ni-Cr alloys and researches for providing the optimal cast shape of spectral reference material, chemical and structural homogeneous for each reference material.The spectral and microstructure investigations was done on the spectral reference materials, series 13 M.B.S. 81-88MBH -Great Britain .The structural homogeneous for each reference material was obtained on three successive layers from centre to edge . The results obtained will be very important in practical activity for research and achivement of spectral reference materials for Ni-Cr alloys used as stainless materials and biomaterials (metallic materials for dental application and metallic implants) .*

Keywords: Ni-Cr alloys, stainless materials, dental applications, metallic implants

Introduction

Nichel-chrome alloys are well known as high temperature and corrosion resistant materials. Thus, they are used for a wide variety of applications: aircraft gas turbines, steam turbines power plants , medical applications, nuclear power systems, chemical and petrochemical industries.

The existing last generation spectrometers in Romania (optical emission spectrometers and X-fluorescence) is good justification for spectral reference materials for Ni-Cr alloys as achivement study. In this sense UPB-University Politehnica Bucharest in co-operation with ICEM -Mettalurgical Research Institute-Bucharest realized spectral reference materials from Ni-Cr alloys. However, UPB-University Politehnica Bucharest have in Laboratory of ecological and mettalurgical analysis a Foundry-Master (AES-SDAR Atom Emission Spectrometer-Spark Discharge in Argon), with a analitical program for Ni-Cr alloys which can make the determination on the nichel alloys.

Theoretical and experimental investigation

One of these applications is medical applications (implantable metallic materials and dental restauration material).

Removable partial dentures of cobalt-chromium alloys have been in clinical since 1929. Traditionally , cast metal prosthetic devices were made of gold alloys due to their ductibility, low corrosion and durability in the oral environment. The non-gold

alloys used were base metal alloys that contained cobalt, chromium and nickel. These alloys are still being used in the construction of removable partial dentures as an alternative to gold alloys for economical reasons and because of their low density compared to traditional gold alloys. Table 1 shows the elements and their weight percentage for nickel-chromium containing base metal alloys.

Table 1. Examples of elemental composition (weight percent) of Ni-Cr base metal alloys[1]

| Element | Cr | Co | Ni | Fe | Mo | W | Mn | Si | C | Be | Al |
|---------|----|----|----|----|----|---|----|-----|-------|----|----|
| Wt% | 17 | - | 67 | - | 5 | - | 5 | 0.5 | trace | - | - |

Table 2 shows the elemental composition of several base metal nickel-chromium alloys for small dental castings:

Table 2. Elemental composition (%) of some examples of base nickel-chromium alloys for small dental castings [2,3]

| Element | Alloys | | | | | | | | | | |
|------------|--------|-------|-------|-------|-------|-------|-------------------|-------|-------|-------|--|
| | A | B | C | D | E | F | G | H | I | J | |
| Nickel | 80.75 | 79.67 | 78.51 | 68.96 | 80.86 | 68.75 | 63.36 | 67.21 | 71.20 | 77.36 | |
| Chromium | 12.58 | 13.24 | 19.47 | 16.54 | 11.93 | 19.57 | 20.95 | 12.88 | 15.89 | 12.27 | |
| Iron | 0.34 | 0.11 | 0.43 | 0.37 | 0.20 | 0.38 | 1.73 | 2.40 | 0.10 | 0.14 | |
| Aluminum | 3.42 | 3.87 | 0.21 | 4.15 | 2.95 | - | 0.16 | - | 3.31 | 2.76 | |
| Molybdenum | 1.53 | 1.52 | - | 5.10 | 1.87 | 4.22 | 8.40 | 6.80 | 4.50 | 4.84 | |
| Silicon | 0.29 | 0.30 | 1.10 | 0.83 | 0.18 | 2.72 | <1 | <1 | <1 | <1 | |
| Beryllium | 0.57 | 0.65 | - | - | 1.55 | - | - | - | 0.57 | 1.67 | |
| Copper | 0.15 | - | - | - | 0.13 | 1.54 | - | - | - | - | |
| Manganese | 0.13 | 0.12 | - | 3.05 | 0.1 | 1.24 | <1 | <1 | 4.28 | - | |
| Cobalt | - | - | - | 0.42 | - | - | - | <1 | - | <1 | |
| Tin | - | - | - | - | - | 1.25 | - | - | - | - | |
| Others | | | | | | | Nb 4.1 Ti<1 | Ga7.0 | | Ti<1 | |

Nickel-chrome alloys can be regarded as a low-cost alternative to precious-metal alloys in the field of crown and bridge technology. Nickel-chrome alloys are used for a variety of dental application including removable partial denture frame works, components of appliances in orthodontics and pediatric dentistry and crowns and fixed bridges.

Table 3. Chemical composition (wt%) of the NiCr alloys for dental restoration [5]

| Elem. | Ni | Co | Fe | Cr | Mo | Nb | Ti | W | Be | Ga | Si | C |
|-------|-------|-----|-----|-------|--------|-----|-----|-----|-------|-------|-----|------|
| C(%) | 58-82 | 0-2 | 0-9 | 12-26 | 0.5-16 | 0-7 | 0-3 | 0-4 | 0-1.5 | 0-7.5 | 0-3 | ≤0.5 |

Altele: Al, Ce, B, Mn, Sn, Ta, V, Cu, Y, La.

Results

Practical of the spectral reference materials for Ni-Cr alloys must be done using different casting forms made by film sand, and an furnace CIA and CIV was used.

For this step must be make investigations spectral and microstructure investigations regards as structural homogeneous for spectral reference material series: 13 M B.S. 81-88-MBH -Great Britain.

The spectral analysis was done with an optical emission spectrometer (Foundry - Master and 3460-ARL). The investigation was obtained on three successive layers from centre to edge (spiral form).

Table 4 shows chemical composition of the spectral reference material from centre to edge of the 13 M B.S. 86 MBH-Great Britain sample:

Table 4. Chemical composition (wt%) of the spectral reference material from centre to edge of the 13 M B.S. 86 MBH-Great Britain sample.

| | C | Si | S | P | Mn | Ni | Cr | V | Mo | W | Co | Ti | Nb | Cu |
|----------|------|------|-------|-------|------|-------|-------|-------|-------|-------|-------|--------|--------|-------|
| (centre) | 0.06 | 1.38 | 0.001 | 0.021 | 1.45 | 35.23 | 18.43 | 0.072 | 0.153 | 0.052 | 0.112 | 0.0092 | 0.008 | 0.222 |
| Standard | 1 | | 2 | | | | | | | | | | | |
| sample | 0.06 | 1.37 | 0.001 | 0.022 | 1.46 | 35.28 | 18.42 | 0.071 | 0.151 | 0.053 | 0.113 | 0.0093 | 0.009 | 0.223 |
| 13M B.S | 0 | | 1 | | | | | | | | | | | |
| 86 | 0.06 | 1.38 | 0.001 | 0.021 | 1.46 | 35.34 | 18.45 | 0.072 | 0.151 | 0.051 | 0.111 | 0.0091 | 0.009 | 0.221 |
| (edge) | 2 | | 1 | | | | | | | | | | | |
| | 0.06 | 1.37 | 0.001 | 0.022 | 1.45 | 35.29 | 18.41 | 0.073 | 0.152 | 0.051 | 0.112 | 0.0092 | 0.008 | 0.223 |
| | 1 | | 2 | | | | | | | | | | | |
| | 0.06 | 1.39 | 0.001 | 0.021 | 1.46 | 35.32 | 18.44 | 0.072 | 0.151 | 0.053 | 0.112 | 0.0092 | 0.008 | 0.222 |
| | 1 | | 1 | | | | | | | | | | | |
| Average | 0.06 | 1.38 | 0.001 | 0.021 | 1.45 | 35.28 | 18.42 | 0.072 | 0.152 | 0.052 | 0.112 | 0.0092 | 0.0085 | 0.222 |
| | 1 | | 1 | | 5 | | | | | | | | | |
| Wt% | 0.06 | 1.37 | 0.001 | 0.021 | 1.45 | 35.3 | 18.43 | 0.07 | 0.15 | 0.05 | 0.11 | 0.009 | 0.008 | 0.22 |
| Errors | ±0.0 | ±0. | ±0.0 | ±0.00 | ±0.0 | ±0.1 | ±0.0 | ±0.0 | ±0.0 | ±0.0 | ±0.0 | ±0.0 | ±0.0 | ±0.0 |
| device | 005 | 006 | 003 | 03 | 06 | 0 | 6 | 01 | 02 | 01 | 02 | 003 | 01 | 02 |

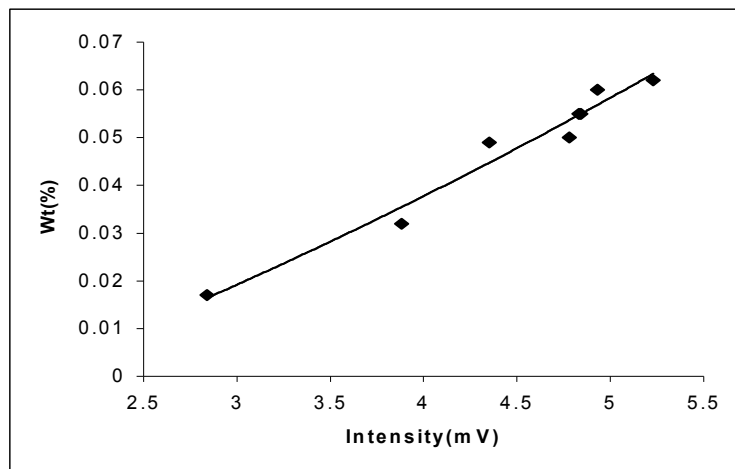
These results show us a high degree of chemical homogeneous for alloying elements and residual elements.

The diagrams $I = f(C)$ (intensity as a function of concentration), for each element, was done for quantitative spectral analysis on series: 13 M B.S. 81-88 MBH-Great Britain. Table 5 shows the wt% and intensities for spectral lines on spectral reference material 13 M B.S. -87 MBH-Great Britain.

Table 5. Weight percent and intensities for 13 M B.S. -87 MBH-Great Britain. spectral reference material.

| 13M B.S 87 | C | Si | S | P | Mn | Ni | Cr | V | Mo | W | Co | Ti | Nb | Al | Cu |
|------------|-------|-------|-------|-------|-------|-------|-------|-------|------|------|-------|-------|------|-------|-------|
| Wt% | 0.055 | 0.67 | 0.025 | 0.024 | 1.64 | 10.12 | 17.30 | 0.13 | 0.29 | 0.05 | 0.17 | 0.004 | 0.57 | 0.004 | 0.28 |
| I(mV) | 4.84 | 32.04 | 4.56 | 6.92 | 172.2 | 14.88 | 222.1 | 22.05 | 14.3 | 2.0 | 31.51 | 2.35 | 9.43 | 3.6 | 166.3 |

The spectral standard samples achievement give us the possibility to drawing the diagrams for each element. The figure 1 shows that diagram.



Caption:

13 M B.S. 81-MBH (3.88, 0.032)
 13 M B.S. 82-MBH (4.93, 0.06)
 13 M B.S. 83-MBH (4.83, 0.055)
 13 M B.S. 84-MBH (2.84, 0.017)
 13 M B.S. 85-MBH (4.35, 0.049)
 13 M B.S. 86-MBH (5.23, 0.062)
 13 M B.S. 87-MBH (4.84, 0.055)
 13 M B.S. 88-MBH (4.78, 0.05)

Fig. 1. Carbon concentration values in spectral reference material series 13M B.S. 81-88 MBH -Great Britain

The microstructure investigations of the spectral reference material series 13 M B.S. 84 and 87 MBH -Great Britain (fig. 2, 3) shown us the this series are obtained from forged bars with homogeneity treatments.



Fig. 2. Optical microstructure investigations on the 13M B.S. 84 MBH -Great Britain spectral reference material.(x200)

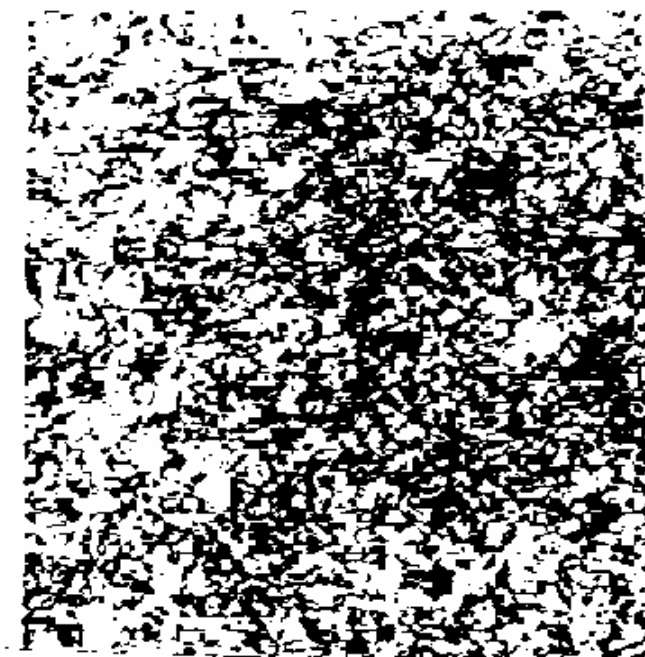


Fig. 3. Optical microstructure investigations on the 13M B.S. 87 MBH -Great Britain spectral reference material .(x200)

Conclusions

The chemical homogeneity of samples was confirmed by the optical emission spectrometry results and the analysis from centre to edge.

The concentration values different repartition of the alloying elements demand specifys diagrams for each element. The study of these shows the influence of the other alloying element on spectral reference material series 81-88 MBH - Great-Britain.

The results obtained will be very important in practical activity in our country for a reserch and achivement of spectral reference materials for Ni-Cr alloys used as stainless materials and biomaterials (metallic material for dental application and metallic implants).

References

- 1.Morris HF, Asgar K, Rowe AP, Nasjleti CE (1979). The influence of heat treatments on several types of base-metal removable partial denture alloys. *J Prosthet Dent.* 41(4):388-95.
- 2.Moffa J (1977). Physical and mechanical properties of gold and base metal alloys. In: *Alternatives to gold alloys in dentistry.* DHEW publication No. (NIH) 77-1227
3. Bumgardner JD, Lucas LC (1993). Surface analysis of nickel-chromium dental alloys. *Dent Mater.* 9(4):252-9.
4. M. Ienciu, P . Moldovan. *Elaborarea si turnarea aliajelor neferoase speciale* -Ed.Didactica si Pedagogica, Bucuresti ,1985, p.45-78.
5. J.Helsen, J.Breme. *Metals as Biomaterials*, 1998, p 62-63.

VRAPCEA MARINELA UNIVERSITY POLITEHNICA FROM BUCHAREST
STOIAN PETRE METALLURGICAL RESEARCH INSTITUTE FROM BUCHAREST
PREDA NICULINA

STUDII SI CERCETARI PRIVIND MATERIALELE DE REFERINTA
SPECTRALE PENTRU ALIAJE NI-CR

REZUMAT: Aliajele Ni-Cr au o varietate de aplicatii datorita proprietatilor deosebite pe care le poseda: caracteristici mecanice foarte bune atat la temperaturi ridicate cat si la temperaturi scazute, refractaritate si rezistanta la coroziune , rezistenta la uzura si proprietati antifriciune corespunzatoare, mare rezistenta electrica, etc. Un domeniu important in care sunt folosite aliajele Ni-Cr este medicina, pentru implanturi metalice si aliaje dentare. Lucrarea are ca obiectiv principal studiul realizarii si analizei in tara a unor materiale de referinta spectrale utilizate la caracterizarea spectrometrica a aliajelor Ni-Cr cu utilizare ca materiale biocompatibile (implanturi metalice, aliaje dentare).Aceasta presupune intr-o prima faza cercetarea analitica si metalografica a unor materiale de referinta spectrale pentru aliaje Ni-Cr produse de firme cu renume international. Astfel, s-au realizat investigatii spectrale privind gradul de omogenitate si investigatii metalografice pe etaloanele spectrale seria 13 M B.S.81-88 MBH -Marea Britanie. Rezultatele obtinute in prima faza vor constitui repere in activitatea de cercetare si realizare practica a seturilor de etaloane pentru aliaje Ni-Cr folosite ca materiale biocompatibile pentru implanturi metalice si aliaje dentare.

THE INTERELEMENT EFFECT STUDY IN SPECTRAL ANALYSIS ON THE SPECTRAL REFERENCE MATERIALS FOR CR-NI STAINLESS STEELS

BY

MARINELA VRAPCEA and PETRE STOIAN

Abstract

The materials with ecological impact are new type of materials, which are developed due to progress in many disciplines: materials science, biotechnology, surgery, dental technique, and medicine. This paper presents interelement effect study in spectral analysis on the spectral reference materials for Cr-Ni stainless steels. In the same time, the paper shows the achievement and study on the binary standard samples FeX_i ($X_i=Cr, Mn, Si, C, Mo, Cu, V, Ti, Al, Co, Mg, etc.$). The binary standard samples gave us the possibility to drawing the calibration diagrams for each alloying elements. The ability to use more than one wavelength for each element adds confidence to the analytical results and provides the flexibility to detect interferences and interelement effect in samples. The diagrams for representative spectral samples (UPB-ICEM) for Cr-Ni stainless steels and spectral reference materials from Great Britain, comparative with binary standard samples, give us the possibility to detect interelement effect. The microstructure investigations on the binary standard samples FeX_i , shows the different structures and the analysis errors. The achievement possibility in our country of the spectral reference materials for Cr-Ni stainless steels is very important, especially for the steels analysis as biomaterials.

Keywords: Cr-Ni stainless steels, biomaterials, dental technique

Introduction

Stainless steels are high-alloy steels that have superior corrosion resistance than other steels because they contain large amounts of chromium. Stainless steels can contain anywhere from 4-30 percent chromium, however most contain around 10 percent. Chromium-nickel steels are the most general widely used steels and are also known as 18-8(Cr-Ni) steels.

The last generation spectrometers from Romania (e.g. Foundry -Master spectrometer -UPB -University Politehnica from Bucharest which can analyse in maximum ten seconds the alloying elements in steels), is a good justification for a achievement study for spectral reference materials.

The achievement possibility in Romania of the spectral reference materials for Cr-Ni stainless steels is very important for steels analysis as biomaterials (metallic implants).

Theoretical and experimental investigation

Simple austenitic steels usually contain between 18 and 30% Cr, 8 to 20% Ni, and between 0.03 and 0.1% carbon. The presence of chromium greatly improves the corrosion resistance of the steel by forming a very thin stable oxide film on the surface, so that chromium-nickel stainless steels are now the most widely used

materials in a wide range of corrosive environments both at room and elevated temperatures. The chromium nickel ratio can be modified to improve formability; carbon content can be reduced to improve intergranular corrosion resistance. Molybdenum can be added to improve corrosion resistance; additionally the Cr-Ni content can be increased.

Chromium -nickel stainless steels are used as implantable materials, which involve the human body coming into contact with metallic materials and in which nickel is undesirable.

The chemical composition of austenitic stainless steels are given in table 1.

Table 1. Chemical composition (wt%) of austenitic stainless steels [9]

| Alloy | C | Cr | Ni | Si | Mn | P | S | Mo |
|---------------|-------|-----------|-----------|------|------|--------|-------|---------|
| X12CrNi177 | ≤0.15 | 16.0-18.0 | 6.0-8.0 | ≤1.0 | ≤2.0 | ≤0.045 | ≤0.03 | - |
| X5CrNi1810 | ≤0.08 | 18.0-20.0 | 8.0-10.5 | ≤1.0 | ≤2.0 | ≤0.045 | ≤0.03 | - |
| X25CrNi2522 | ≤0.25 | 24.0-26.0 | 19.0-22.0 | ≤1.5 | ≤2.0 | ≤0.045 | ≤0.03 | - |
| X2CrNiMo17133 | ≤0.03 | 16.0-18.0 | 10.0-14.0 | ≤1.0 | ≤2.0 | ≤0.045 | ≤0.03 | 2.0-3.0 |
| X5CrNiMo18164 | ≤0.08 | 18.0-20.0 | 11.0-15.0 | ≤1.0 | ≤2.0 | ≤0.045 | ≤0.03 | 3.0-4.0 |
| X2CrNiMo18164 | ≤0.03 | 18.0-20.0 | 11.0-15.0 | ≤1.0 | ≤2.0 | ≤0.045 | ≤0.03 | 3.0-4.0 |

The binary standard samples give us the possibility to drawing the calibration diagrams for each alloying elements. The ability to use more than one wavelength for each element adds confidence to the analytical results and provides the flexibility to detect interferences and interelement effect in samples.

Table 2. Chemical composition (wt%) of binary spectral standard samples (FeXi).

| No. | FeC | FeMn | FeSi | FeS | FeP | FeCr | FeNi | FeMo | FeV | FeW |
|-----|------|-------|------|-------|-------|-------|-------|-------|-------|-------|
| | C | Mn | Si | S | P | Cr | Ni | Mo | V | W |
| 1 | 0.03 | 0.05 | 0.08 | 0.015 | 0.016 | 0.05 | 0.12 | 0.04 | 0.01 | 0.01 |
| 2 | 0.21 | 0.52 | 0.23 | 0.085 | 0.034 | 0.84 | 0.64 | 0.17 | 0.36 | 0.21 |
| 3 | 0.52 | 1.35 | 0.51 | 0.12 | 0.089 | 0.96 | 1.14 | 0.23 | 0.79 | 0.52 |
| 4 | 1.42 | 3.55 | 0.99 | 0.14 | 0.16 | 3.45 | 3.44 | 0.51 | 1.42 | 1.03 |
| 5 | 2.21 | 6.85 | 2.51 | 0.42 | 0.32 | 9.65 | 7.23 | 1.06 | 3.27 | 2.45 |
| 6 | 2.65 | 10.23 | 3.22 | 0.76 | 0.72 | 14.12 | 14.33 | 1.28 | 4.75 | 7.23 |
| 7 | 3.12 | 12.16 | 4.43 | 1.04 | 0.98 | 19.98 | 23.12 | 2.94 | 7.21 | 9.11 |
| 8 | 3.36 | 14.35 | 5.34 | | | 25.52 | 34.55 | 3.81 | 10.21 | 12.14 |
| 9 | 3.55 | 20.52 | | | | 30.69 | 39.76 | 6.06 | | 13.29 |
| 10 | 3.87 | | | | | 40.33 | | 6.75 | | 17.62 |
| 11 | | | | | | | | 10.23 | | 18.65 |
| 12 | | | | | | | | | | 21.55 |

The charges elaboration was carried by using as alloying elements, pure metals such as Mn metallic, Si metallic, etc. , and iron alloys such as FeS 32% si FeP 24%. For this step was used an furnace CIA 5kg .

The sample was obtained by using different casting forms made by film sand . The sample shapes for binary and representative standars samples can be seen in figures1 and 2.

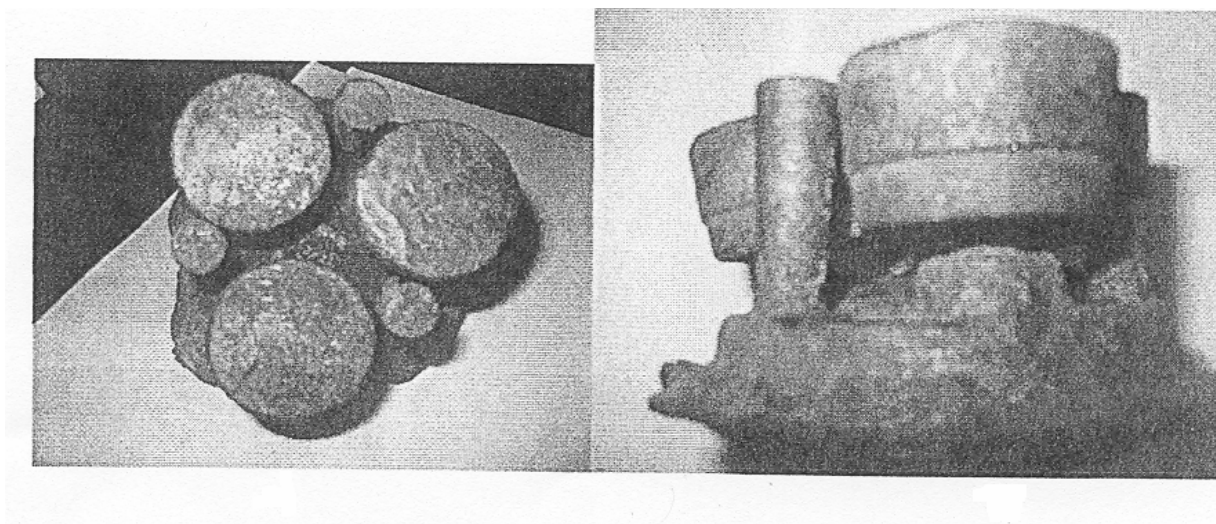


Fig. 1. Sample shapes for binary spectral standard samples.

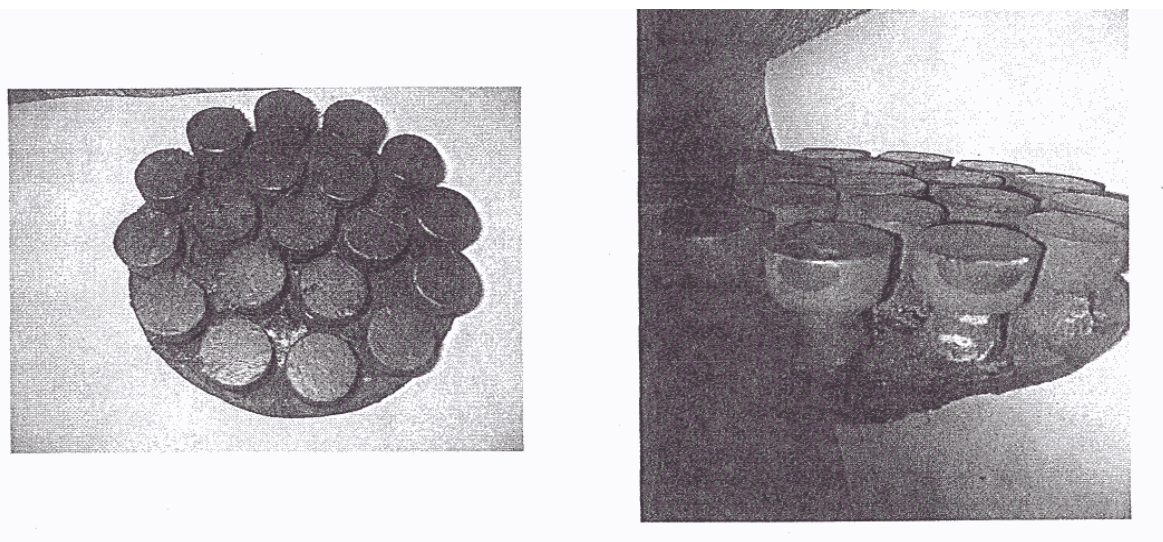


Fig. 2. Sample shapes for representative spectral standard samples.

Chemical composition of representative spectral standard samples for stainless steels was obtained by using chemical methods (clasical and instumental methods). Thus, the chemical composition of IA1-IA9 (UPB-ICEM) stainless steels was determined as follows:

Table 3. Chemical composition of the representative spectral standard samples for IA1-IA9(UPB-ICEM) stainless steels :

| Standard samples | | C | Si | Mn | P | S | Cr | Ni | Mo | V | Cu | Nb | Co | Ti | Al |
|------------------|-----|-----------|------|------|-----------|-----------|-----------|-----------|------|-----------|------|------|-------|------|-------|
| IA1 | Wt% | 0.10 | 0.38 | 0.88 | 0.03 4 | 0.03 4 | 6.62 | 30.0 8 | 1.34 | 0.22 | 0.24 | 0.01 | 0.24 | 0.03 | 0.024 |
| IA2 | Wt% | 0.19 | 1.23 | 0.56 | 0.02 2 | 0.00 8 | 29.9 4 | 5.12 | 0.14 | 0.12 | 0.12 | 0.44 | 0.064 | 0.08 | 0.036 |
| IA3 | Wt% | 0.22 | 0.78 | 0.74 | 0.02 8 | 0.03 8 | 14.4 4 | 15.2 8 | 0.52 | 0.04 4 | 0.18 | 0.12 | 0.12 | 0.12 | 0.12 |
| IA4 | Wt% | 0.04 2 | 0.67 | 2.28 | 0.01 4 | 0.01 5 | 16.0 8 | 7.26 | 0.84 | 0.02 8 | 0.14 | 0.84 | 0.086 | 0.16 | 0.18 |
| IA5 | Wt% | 0.34 | 0.86 | 4.04 | 0.02 4 | 0.04 2 | 22.1 8 | 8.98 | 0.42 | 0.32 | 0.28 | 0.25 | 0.044 | 0.22 | 0.24 |
| IA6 | Wt% | 0.11 | 0.97 | 2.11 | 0.05 4 | 0.04 8 | 17.5 4 | 13.7 4 | 3.84 | 0.11 | 0.05 | 0.08 | 0.18 | 0.26 | 0.04 |
| IA7 | Wt% | 0.13 | 1.64 | 1.63 | 0.01 1 | 0.01 2 | 9.12 | 22.2 4 | 0.11 | 0.16 | 0.46 | 0.18 | 0.03 | 0.31 | 0.08 |
| IA8 | Wt% | 0.05 5 | 0.68 | 1.85 | 0.01 8 | 0.05 6 | 18.4 2 | 10.1 5 | 0.34 | 0.04 | 0.09 | 1.54 | 0.01 | 0.01 | 0.16 |
| IA9 | Wt% | 0.07 5 | 1.17 | 1.26 | 0.03 8 | 0.01 8 | 20.4 3 | 11.9 8 | 2.44 | 0.18 | 0.11 | 0.04 | 0.36 | 0.64 | 0.05 |

Spectral investigations regarding the structural homogeneous representative spectral standard samples for stainless steels was done with an optical emission spectrometer (Foundry -Master- University Politehnica Bucharest).

The interelement effect study was done with binary spectral standard samples and spectral standard samples stainless steels from import . The spectral analysis is shown by the calibration diagram (intensity as a function of concentration $I = f(c)$).

Interelement effects cause intensity changes in the analytical spectral and/or reference line by the presence of one or more other elements in the base. They may have various causes:

- change in inclusion form of the element to be analysed;
- change in solidification form;
- changing discharge due to new non-oxidic cathode points of attack formed from simple components and discharge atmosphere;
- change in vaporisation enthalpy and thermal conductivity;
- change in spectral background due to alloying components.

Results

The diagrams for representative spectral samples (UPB-ICEM) for Cr-Ni stainless steels and spectral reference materials from Great Britain, comparative with binary standard samples, give us the possibility to detect interelement effect (fig. 3, 4).

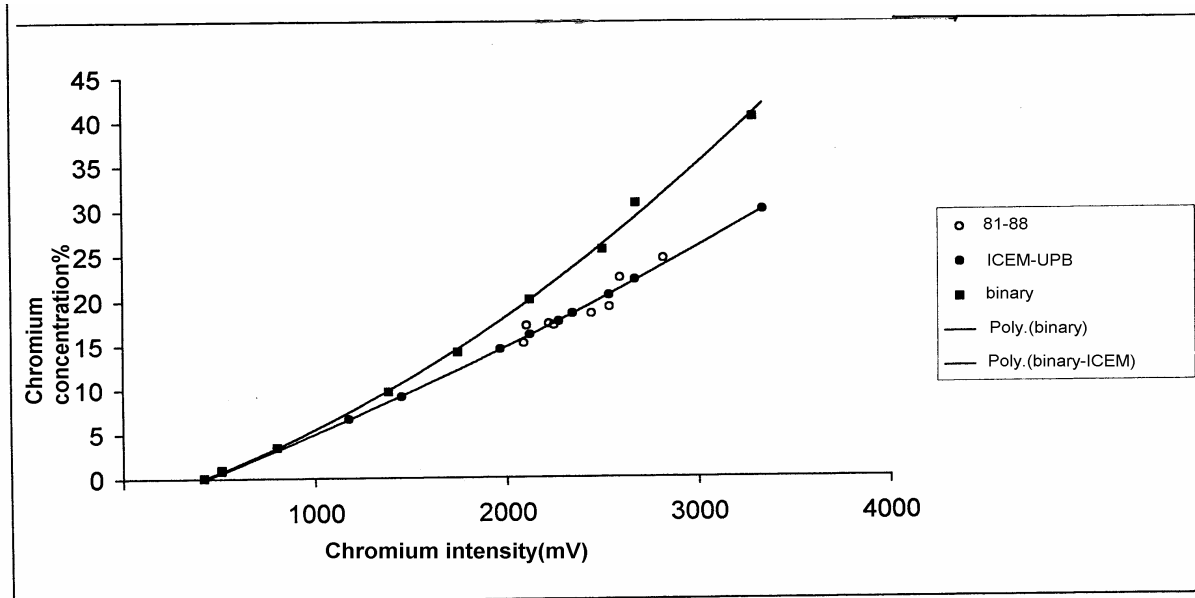


Fig. 3. Comparison of Cr concentration values on the representative spectral samples for stainless steels (UPB-ICEM), from import standard samples (series 81-88 MBH-Great Britain), and Fe-Cr binary spectral standard samples.

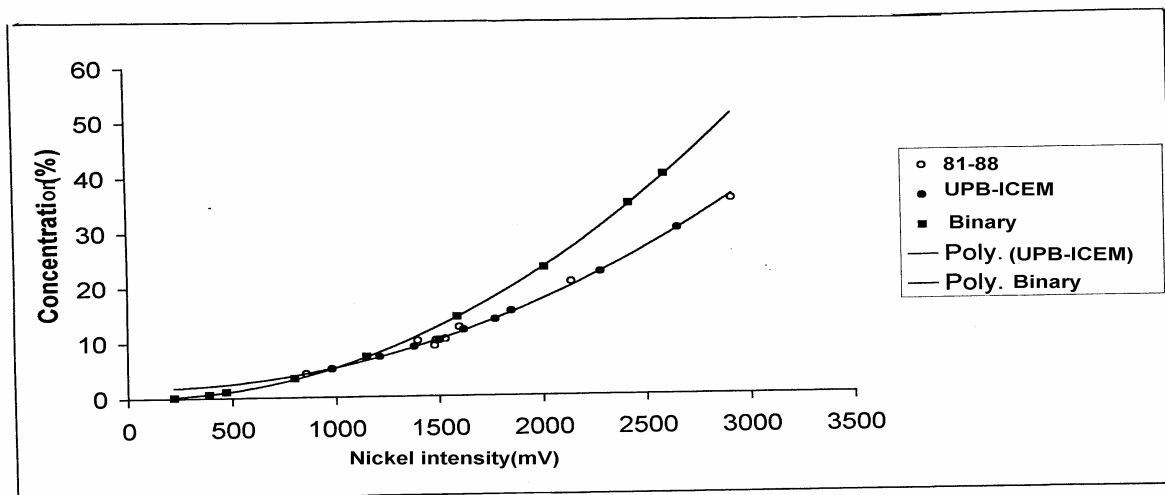


Fig. 4. Comparison of Ni concentration values on the representative spectral samples for stainless steels (UPB-ICEM), from import standard samples (series 81-88 MBH-Great Britain), and Fe-Cr binary spectral standard samples.

These analysis show the other alloying element influence. Chemical composition provides modified values for spectral lines intensity of analysed elements. Thus, is

indicate which the spectral standard samples will be most near to representative samples.

The microstructure investigations of three binary samples with different concentrations can be seen in fig. 5 and 6. These investigations with other physical-chemical phenomenous (plasma spectral source), are responsible of the being of analysis errors.

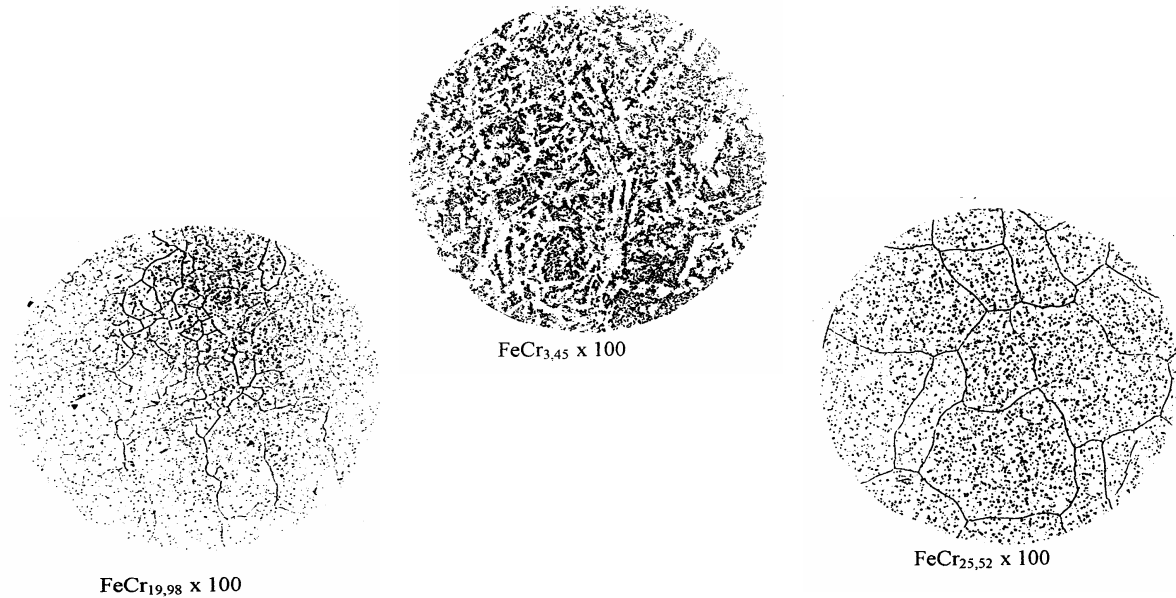


Fig. 5. Microstructure investigations on the FeCr binary spectral standard samples (UPB-ICEM) for different Cr concentrations values.

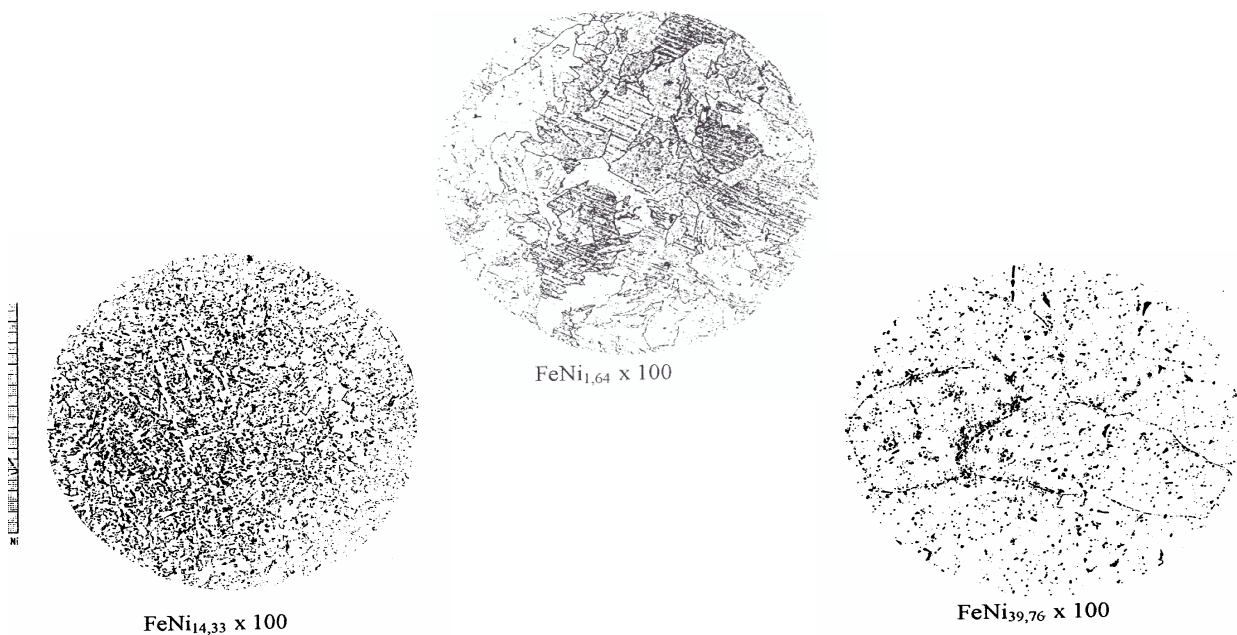


Fig. 6. Microstructure investigations on the FeNi binary spectral standard samples (UPB-ICEM) for different Ni concentrations values.

Conclusions

The results obtained are very important for steels analysis as bimetals.

The research and studies was done in UPB-University Politehnica Bucharest in co-operation with ICEM-Metallurgical Research Institute from Bucharest give us the achievement conditions of binary standard samples FeXi and representative standard samples (UPB-ICEM) for Cr-Ni stainless steels.

The calibration diagrams for representative spectral samples and spectral reference materials from Great Britain , comparative with binary standard samples , shown the possibility to detect interelement effect . The study of these diagrams done the influence of the interelement effect by the intensity changes in the analytical spectral.

References

1. H.M.Mark - Principles and practice of Spectroscopy Calibration, Ed. John Wiley (1991)
2. K. Slickers - Automatic Emission Spectroscopy, Ed. Bruhlshe (1993)
3. J. W Robinson - Handbook of Spectroscopy , vol I-III, CRC Press , Ohio (1974)
4. Athanasie Trutia - Spectrometrie optica aplicata, Ed. Univ. Buc. (1990)
5. Kubashewski O. - Binary Phase Diagrams, Springer Verlag, 1982, Berlin.
6. Cuida Oleg - Influenta elementelor reziduale si de microaliere asupra plasticitatii otelurilor -Ed. Image 2000 , Bucuresti.
7. Annual Book of ASTM Standards, part 46, 1992.
8. Bundy K.J., Luedemann R. - Factors which influence the accuracy of corrosion rate determination of implant materials- Ann. Biomed. Eng. 17, 1989, p 159-175.
9. J.Helsen, J.Breme. Metals as Biomaterials, 1998, p 40.

Marinela Vrapcea
Petre Stoian

UNIVERSITY POLITEHNICA FROM BUCHAREST
METALLURGICAL RESEARCH INSTITUTE FROM BUCHAREST

STUDIUL EFECTULUI INTERELEMENT IN ANALIZA SPECTRALA PE MATERIALE DE REFERINTA SPECTRALE PENTRU OTELURI INOXIDABILE CR-NI

REZUMAT

Aceasta lucrare are ca obiectiv studiul efectului interelement pe materiale de referinta spectrale pentru oteluri inoxidabile Cr-Ni cu spectru larg de utilizare atat ca materiale inoxidabile , dar si ca materiale biocompatibile care sa satisfaca cerintele spectrometrelor (de emisie optica si fluorescenta de raze X) din tara. Astfel , prezenta lucrare prezinta studiul si realizarea unor aliaje binare FeXi (Xi= C, Mn, Si, Ni, Mo, etc.) si reprezentative pentru oteluri inoxidabile Cr-Ni. Utilizarea etaloanelor binare FeXi , a dus la punerea in evidenta a efectului interelement asupra elementului considerat in analiza spectrala, prin reprezentarea grafica, in aceleasi coordonate, a dependentei $I=f(C)$, pentru etaloanele binare raportate la cele reprezentative si a celor din import, pentru otelurile inoxidabile Cr-Ni. Din studierea graficelor se observa ca datorita prezentei in matricea aliajului , in afara elementului considerat in analiza si a celorlalte elemente de aliere sau reziduale , valoarea intensitatii liniei spectrale a elementului analizat este modificata in directia cresterii acesteia. De aceea este indicat sa se realizeze etaloane a caror compozitie chimica sa fie cat mai apropiata de a probelor curente.

THE INFLUENCE OF MODIFICATION ON THE PHYSICO-MECHANICAL PROPERTIES OF SOME TIN BRONZES

Mircea Beloiu*, Ioan Alexandru**, Romeo Chelariu**, Costel Roman**, Ioan Carcea**

Abstract. This paper show the experimental results about the influence of modification on the some physico-mechanical properties of some tin bronzes. The processing in liquid state by microalloying determines structural and mechanical properties changes of the investigated tin bronzes.

Keywords. tin bronze, modification, properties

1. INTRODUCTION

The primary solidification structure obtained for the majority of as-cast non-ferrous metallic materials is characterized by coarse grains. The phase transitions and structural changes made by the subsequent metallurgical processing, such as plastic deformation or heat treatment are strongly influenced by the characteristics of primary structure /1/.

The grains of metallic materials grow during the solidification beginning from the initial nuclei. If the nuclei number increase then the grains number increase and the grain size decrease. The refinement of coarse grains can be made by treatment of melts before casting or during solidification process. The treatment in liquid state is performed using additions which limit the growth of grains. These additions are either alloying elements or alloys for which take place a constitutional undercooling during solidification. The growth of constitutional undercooling zone before front solidification is shown in Figure 1 /2/.

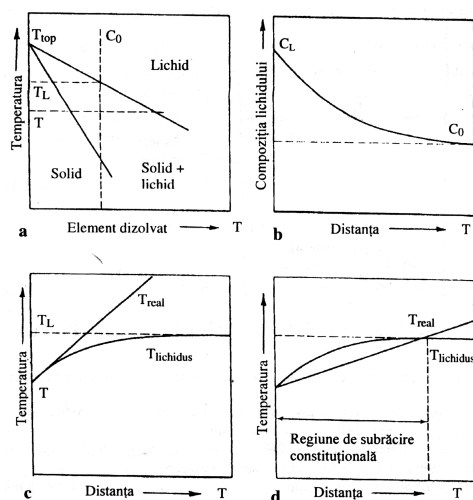


Figure 1. The constitutional undercooling during solidification of a alloy: a-phase diagram; b-enrich film with solvate before solidification interface; c-solid interface; d - non-steady interface.

The undercooling zone from Figure 1,d can be removed if the temperature slope is equal or great than the liquidus curve slope. This is described by the equation:

$$\frac{G}{R} \geq \frac{mC_0(1-k_0)}{Dk_0} \quad (1)$$

in which: G - temperature gradient, K/mm;
 R – growth rate, mm/s;
 m- liquidus curve slope, K/wt.%;
 D- diffusivity, mm²/s;
 C₀ – solvate concentration, wt.%;
 K₀ – equilibrium partition coefficient.

2. MATERIALS AND METHODS

The chemical compositions of investigated tin bronzes are shown in Table 1.

Table 1

The chemical compositions and treatment types of the alloys

| Chemical composition, [%] | | | | | | Modification | Code |
|---------------------------|-------|------|--------|------|------|--------------------------------------|--------------|
| Sn | Zn | Ni | Mn | Al | Cu | | |
| 10,80 | 3,12 | 1,43 | 0,04 | 0,90 | rest | - | CuSn9Zn5//00 |
| 8,14 | 3,00 | 1,35 | 0,01 | 0,70 | rest | 0,02 % B | CuSn9Zn5//01 |
| 8,10 | 2,07 | 1,42 | 0,01 | 0,70 | rest | 0,04 % B | CuSn9Zn5//02 |
| 7,95 | 3,25 | 1,36 | 0,01 | 0,70 | rest | 0,06 % B | CuSn9Zn5//03 |
| 7,75 | 3,00 | 1,25 | 0,01 | 0,50 | rest | 0,03 % B+ 0,05 % Zr | CuSn9Zn5//04 |
| 8,51 | 3,36 | 1,11 | 0,05 | 0,2 | rest | 0,03 % B+ 0,1 % Zr | CuSn9Zn5//05 |
| 8,80 | 3,35 | 1,13 | 0,01 | 0,40 | rest | 0,03 % B+ 0,15 % Zr | CuSn9Zn5//06 |
| 8,16 | 3,52 | 1,14 | 0,02 | 0,20 | rest | 0,02 % B+ 0,10 % Zr+ 0,20 % Ti | CuSn9Zn5//07 |
| 8,68 | 3,69 | 1,19 | 0,00 | 0,17 | rest | 0,02 % B+ 0,10 % Zr+ 0,60 % Ti | CuSn9Zn5//08 |
| 9,36 | 3,69 | 1,34 | 0,00 | 0,07 | rest | 0,02 % B+ 0,10 % Zr+ 0,80 % Ti | CuSn9Zn5//09 |
| 10,09 | 0,005 | 1,13 | 0,0008 | 0,05 | rest | - | CuSn10//10 |
| 10,90 | 0,026 | 1,20 | 0,0010 | 0,05 | rest | 0,02 % B | CuSn10//11 |
| 11,00 | 0,021 | 1,09 | 0,0020 | 0,05 | rest | 0,06 % B | CuSn10//12 |
| 12,10 | 0,018 | 1,26 | 0,0009 | 0,05 | rest | - | CuSn12//20 |

The elaboration of these alloys was performed using a induction furnace with a 35 kg capacity of graphite crucible and a 8 kHz frequency.

The treatment in liquid state by micro-alloying with Cu-B, Cu-Ti, and Cu-Zr master alloys was performed in casting ladle preheated at 780÷800 °C.

Some samples were subjected to a homogenization heat treatment in order to makes evident the influence of the processing in liquid state on the homogenized tin

bronzes (TT). The technological parameters of homogenization annealing are shown in Table 2. From cast and heat treated semi-finished products were made samples for optical microscopy and micro-hardness measurements.

Table 2

Technological parameters of homogenization annealing

| Technological parameters | | As-cast sample code | Heat treated sample code |
|---------------------------------------|-------------------------------|---------------------|--------------------------|
| $T_{\text{ment}}, [^{\circ}\text{C}]$ | $d_{\text{ment}}, [\text{h}]$ | | |
| 650 | 2,5 | 00 | 10 |
| | | 01 | 11 |
| | | 03 | 13 |
| | | 04 | 14 |
| | | 06 | 16 |

The chemical compositions of tin bronzes were determined by chemical methods, in accordance with current standards. To perform the chemical analysis the small quantities of metallic materials were cut from semi-finished products.

The samples prepared for hardness test were used for both hardness and electric conductivity measurements.

Electrical conductivity was measured in % IACS, using Magna Flux method and a FM Conductivity Meter. The electric resistivity was calculated using the equation:

$$\rho = \frac{172,41}{\% \text{IACS}}, (\mu\Omega \cdot \text{cm}) \quad (2)$$

The Brinell hardness was measured on the plane-parallel surfaces with small rugosity, in accordance with SR EN 10003/1-1997 standard, in the following test conditions: 2,5 mm ball diameters, 62.5 daN force and 60 s time.

The tensile tests were performed in accordance with SR EN 10002/1-1994, using samples with circular cross section.

To measure the micro-hardness a PMT 3 the microdurometer was used. The tests were performed using the following test conditions: 50 g load weight and 15 s loading time. The metallographic samples were used for micro-hardness measurements. To calculate the values of micro-hardness the following equation was used:

$$H_V = 17816.94 \cdot \frac{P}{N^2}, [\text{daN}/\text{mm}^2] \quad (3)$$

where P is the loading weight, in grams, and N represents the number of divisions measured on the diamond-pyramid impression.

The tin bronze microstructure was analyzed by optical microscopy. The metallographic samples were prepared by mechanical polishing and smoothing followed by chemical etching. The micrographs were obtained by digital capture from a METAVAL optical microscope.

3. EXPERIMENTAL RESULTS

The micrographs of as cast tin bronzes are shown in Figures 2÷7.

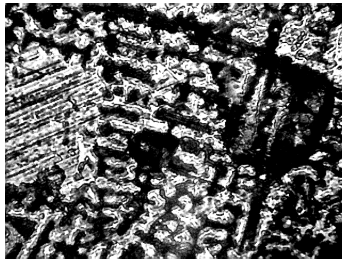


Figure 2.
The microstructure of
CuSn9Zn5/00 sample.

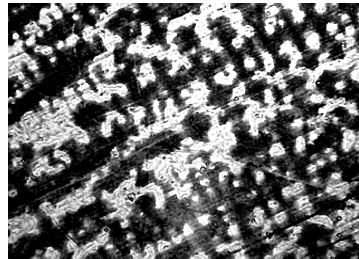


Figure 3.
The microstructure of
CuSn9Zn5/01 sample.

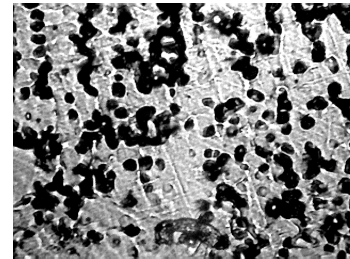


Figure 4.
The microstructure of
CuSn9Zn5/05 sample.

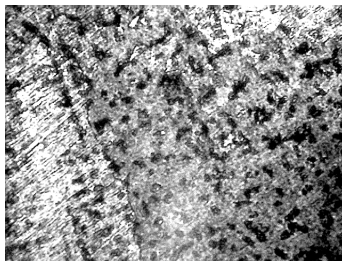


Figure 5.
The microstructure of
CuSn9Zn5/09 sample.

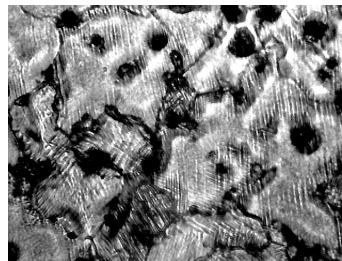


Figure 6.
The microstructure of
CuSn10/12 sample.

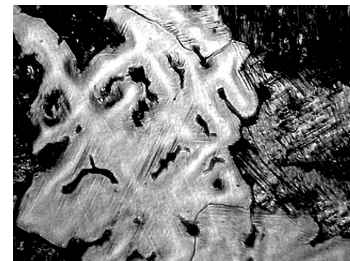


Figure 7.
The microstructure of
CuSn10/20 sample.

The few microstructures of heat treated CuSn9Zn5 shown in Figures 8÷10.

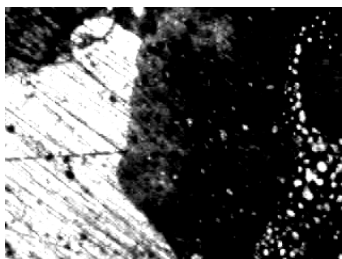


Figure 8.
The microstructure of
CuSn9Zn5/10 sample.

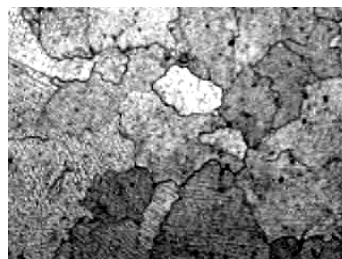


Figure 9.
The microstructure of
CuSn9Zn5/11 sample.



Figure 10.
The microstructure of
CuSn9Zn5/13 sample.

The analysis of micrographs shown in previous figures can be formulated the following conclusions:

- a 0,02wt.%B addition in liquid bronzes refines the dendrite sizes by comparison with the dendrite sizes of non-treated bronzes; the increase of content of boron up to 0,06 wt.% determines the decrease of refinement effect because of overmodification;

- a 0,03wt%B+0,15wt.%Zr complex addition determines a evident refinement of the dendrite sizes;

- in the case of the 07, 08, 09 samples the addition of titanium has the same effect as well as the addition of boron and zirconium.

The micrographs analysis showed that the solid solution morphology of cast samples differs from the heat treated samples. The processing of tin bronzes in liquid state determines the change of shape and dimension of primary dendrites. This effect influences the subsequent homogenization process.

The microhardness was measured only for the bronzes which were both cast and heat treated. Ten measurements of the diamond-pyramid impression were performed for each sample. This fact allowed a statistical analysis of experimental data. The calculated values of principal statistical parameters (mean, variance and standard deviation) for each sample are showed in Table 3. To test the statistical hypothesis concerning the equality of means the Student test for independent variables, unknown variances and a volume of selection less than 30 /3,4/.

Table 3

The principal statistical parameters of micro-hardness measurements

| Sample | HV, [daN/mm ²] | Variance | Standard deviation | Sample | HV, [daN/mm ²] | Variance | Standard deviation |
|--------|----------------------------|----------|--------------------|--------|----------------------------|----------|--------------------|
| 00 | 117.56 | 154.42 | 12.43 | 10 | 97.18 | 106.65 | 10.33 |
| 01 | 103.67 | 100.12 | 10.00 | 11 | 118.98 | 192.31 | 13.60 |
| 03 | 100.38 | 234.76 | 15.32 | 13 | 110.44 | 116.29 | 10.32 |
| 04 | 107.48 | 415.23 | 20.38 | 14 | 85.60 | 100.17 | 15.50 |
| 06 | 135.37 | 447.93 | 21.16 | 16 | 87.69 | 154.99 | 12.84 |

The analysis of experimental data from Table 3 shows that the processing in liquid state determined different values of micro-hardness of the two tin bronzes, both as-cast and heat treated. The influence of micro-alloying on the micro-hardness depends on the chemical composition of alloy, the micro-alloying element(s), and condition of material.

The electrical conductivity was measured only for as-cast samples. For each sample were performed at least three measurements, so that the experimental data could be statistically analyzed. The means values of the electric conductivity are graphically shown in Figure 11.

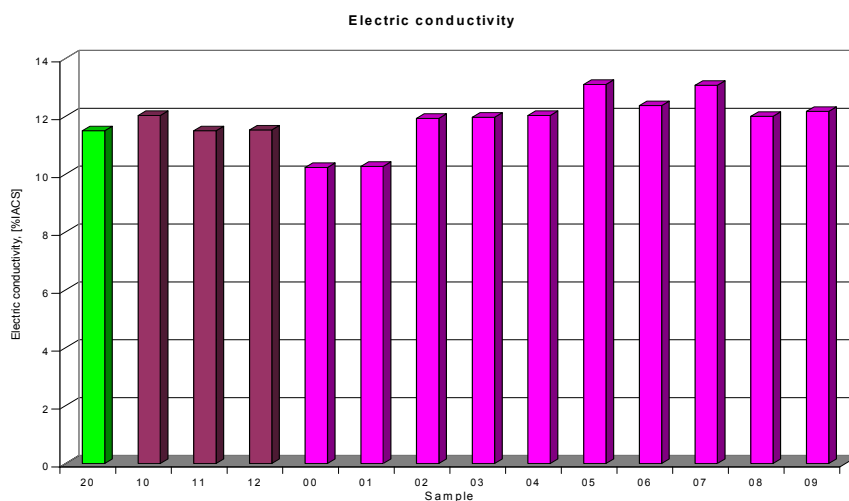


Figure 11. Mean values of electric conductivity.

The experimental data show that the regardless of the chemical composition of alloy, processing of bronze in liquid state by micro-alloying determines different values of the electric conductivity. The micro-alloying with titanium determines a new decrease of values of this physical property. In case of CuSn9Zn5 alloy the micro-alloying determines the increase of the electric conductivity, the high values of electric conductivity being obtained when the complex additions of boron, zirconium and titanium were used. The increase of titanium concentration determines decrease of the electric conductivity.

The hardness was measured only as-cast samples. The means values of this mechanical property are shown in Figure 12.

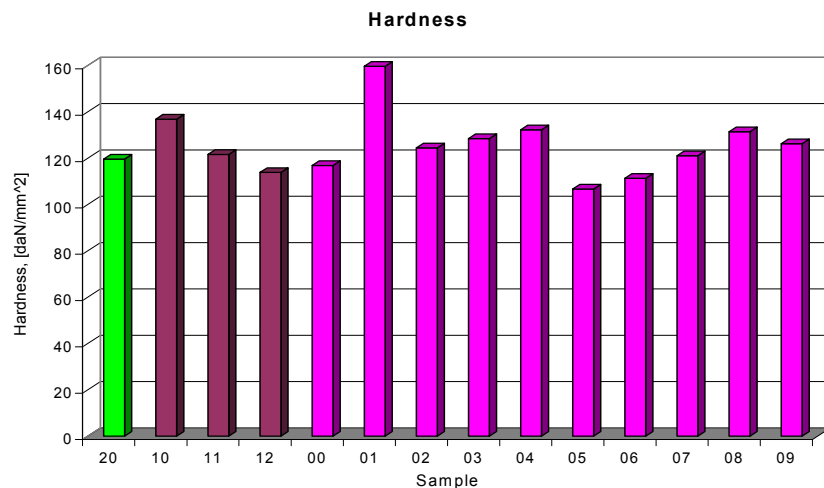


Figure 12. Mean values of hardness of tin bronzes treated in liquid state.

The micro-alloying determines the decrease of hardness excepting CuSn10 bronze with a greater lead concentration micro-alloyed with boron, and CuSn9Zn5 micro-alloyed with boron or boron+zirconium+titanium. This fact is evidently for CuSn10 alloys. It is worthy to note that the micro-alloying with boron determines either increase or maintaining of hardness values close by the values of samples which weren't micro-alloyed. The hypothesis testing of means equality shows significant differences between samples processed in liquid state and the other samples. A distinct influence is observed in the case of samples micro-alloyed with boron. The samples micro-alloyed with zirconium, titanium or mixture of these elements have the hardness values less than the hardness values of the other samples.

From as-cast semi-finished products were made tensile test sample. Using experimental data obtained by tensile test, the tensile strength, yield strength and elongation were measured. The mean values of the three mechanical characteristics are shown in Figures 13, 14, and 15. The graphics showed that the processing in liquid state determines a decrease of mechanical properties. The evident decrease of mechanical properties there is for CuSn9Zn5 bronze. The micro-alloying with boron have a less evident influence on the mechanical properties of tin bronzes.

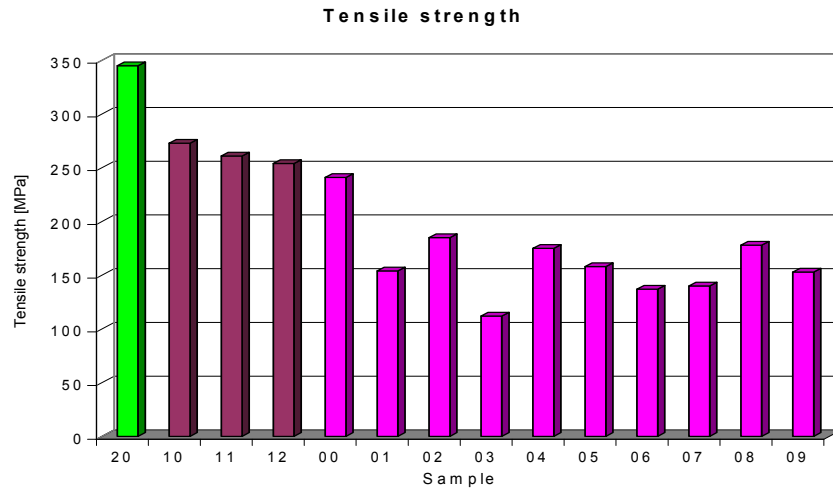


Figure 13. The tensile strength of investigated tin bronzes.

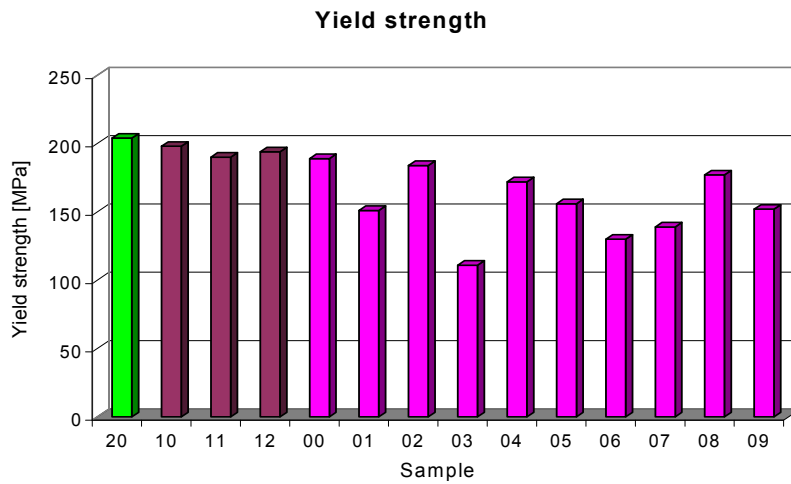


Figure 14. The yield strength of investigated tin bronzes.

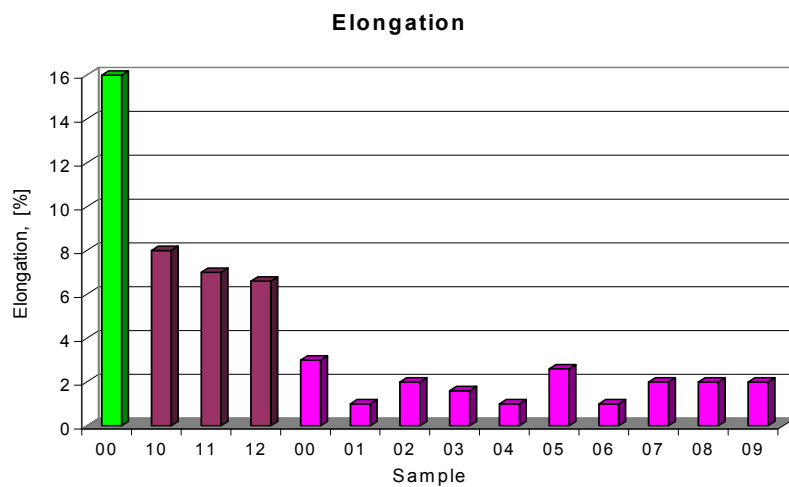


Figure 15. The elongation of investigated tin bronzes.

4. CONCLUSIONS

The processing in liquid state by microalloying determines structural and mechanical properties changes of the investigated tin bronzes.

Received 25 April, 2005

* S.C. Petrotub S.A. Roman

** Technical University „Gh. Asachi” Iasi

References

1. Ienciu, M., Moldovan, P., Panait, N., Groza, Ioana, Buzatu, M., Marinescu, Daniela, *Elaborarea și turnarea aliajelor neferoase*, Editura Didactică și Pedagogică, București, 1982.
2. Moldovan, P., Panait, N., Mărginean, St. *Bazele tratării topiturilor metalice neferoase*. Editura Intact, București, 1998.
3. Taloi, D., Bratu, C., Florian, E., Berceanu, E., *Optimizarea proceselor metalurgice*, Editura Didactică și Pedagogică, București, 1983.
4. Andrei, T., Stancu, S., *Statistica-teorie și aplicații*, Editura All, București, 1995.

INFLUENȚA MODIFICĂRII ASUPRA UNOR PROPRIETĂȚI FIZICO-MECANICE ALE UNOR BRONZURI CU STANIU

(REZUMAT)

Această lucrare prezintă rezultate experimentale despre influența modificării asupra unor proprietăți fizico-mecanice ale unor bronzuri cu staniu. Prelucrarea în stare lichidă determină modificarea structurii și proprietăților mecanice ale bronzurilor cu staniu studiate.

WEAR BEHAVIOUR OF SOME BRONZES

BY

MIRCEA BELOIU*, IOAN ALEXANDRU, COSTEL ROMAN**,
ROMEO CHELARIU**, IOAN CARCEA****

Abstract. This paper contains a comparative investigation of wear behaviour of some bronzes used as wearplates. Two tin bronzes (CuSn12, CuSn14), one aluminium bronze (CuAl9Fe3), and one tin-zinc-lead bronze (CuSn6Zn4Pb4) were subjected to testing. For wear test an apparatus *pin-on-disk* was used. The weight wear rate and linear wear rate were calculated using experimental data. The experimental results showed that the aluminium bronze had the lowest values of wear rates, and tin-zinc-lead bronze had the highest values of these.

Keywords: *bronze, wearplate, wear*

1. INTRODUCTION

The forces and momenta, as well as power and moving are transferred by surface contact between pair components of mechanical systems. The correlation between quality, durability, and reliability involves also the assurance of tribological properties of materials used to make the pair components.

Between pair components that have a relative motion there is the friction, which leads to the power losses as well as to the wear of components. The fretting wear represents a destructive process of material surface, which has the consequences like fracture or plastic deformation of materials.

The wear resistance is a material property that characterizes the behaviour of materials in certain fretting conditions. Points, lines, and cylindrical, spherical and plane surfaces can make the contact of fretting surfaces of pair components (Table 1) /1/.

Table 1

The classification of fretting coupling vs. type and number of contacts

| Contact type | Coupling class | Class | Number of contacts | Examples |
|-----------------------------------|----------------|-----------------|--------------------|--|
| Pointlike | Superior | 1 st | 1-4 and more | Tip contact, ball-plane, ball bearing etc |
| Linear | Superior | 2 nd | 1-4 | Roller-plane, two rollers, three rollers, spur gearing etc |
| Cylindrical and spherical surface | Inferior | 3 rd | 1-2 and more | Roller-one(two) heel(s), piston-liner, screw-nut etc |
| Plane surface | Inferior | 4 th | 1-2 | two rings, slide rods with one (two) surface contact etc |

Any contact surface, even if it is high finishing, has macroscopic or microscopic roughness, and also small waves. By contact friction, these surface irregularities are

either destroyed or plastic deformed, these effects resulting in adherence of soft material on the surface of hard material. The wear resistance of materials of components that form a coupling fretting depends on the materials nature, finishing degree of contact surface, and values of contact forces.

The structure of engineering tribological system (*tribosystem*) depends on three parameter types: external (Q), internal (M), and interaction (I). The wear rate of a tribological system (Δ_u – material loss/time) depends on three types of parameters: $\Delta_u = \Delta_u(Q, M, I)$.

The wear behaviour of a tribological system can be analyzed by use of a *tribomodel*. This involves that the interactions between surfaces of both tribomodel and tribosystem are similarly.

The superficial layers of tribosystem components are characterized by micro-geometry, hardness, structure, chemical composition, and induced stresses.

The paper shows the initial researches on the wear behaviour of some bronzes. The bronzes were both as-cast and heat treated. The materials of tribomodel components were steel and bronze.

2. MATERIALS AND METHODS

The chemical compositions of studied bronzes are shown in Table 2.

Table 2

| Bronze type | Code sample | Chemical composition, [%wt.] | | | | | | | | |
|-------------|-------------|------------------------------|------|-------|------|------|------|------|------|------|
| | | Sn | Zn | Al | Fe | Ni | Mn | Si | P | Cu |
| CuSn6Zn4Pb4 | 1 | 7.88 | 5.32 | 0.93 | 0.59 | 0.10 | 0.08 | 0.02 | 0.02 | bal. |
| CuSn12 | 2 | 11.90 | 0.16 | - | - | 0.03 | - | - | - | bal. |
| CuSn14 | 3 | 13.32 | 0.30 | 0.05 | 0.02 | 0.04 | - | - | 0.03 | bal. |
| CuAl9Fe3 | 4 | 0.98 | 0.29 | 10.11 | 2.02 | - | 0.01 | 0.11 | - | bal. |

The bronzes were heat treated as follows: (1) tin bronzes and tin-zinc-lead bronze were subjected to homogenization annealing in two stages (620⁰C, 1h-720⁰C, 1h, air cooling), (2) aluminium bronze was subjected temper hardening (720⁰C, 1.5h, water cooling-500⁰C, 2h, air cooling).

For all samples, both cast and heat treated, the hardness tests were performed.

Before wear tests, the disks of bronzes were polishing with up to 800 grit abrasive papers. Also, each disk was washed with deionized water, and degreased with ethanol.

A *pin-on-disk* apparatus was used to test wear behaviour of bronzes (Figure 1).

The circular support 1, which has a diameter of 90 mm, sustains the sample that is fixed by adjustable system 9. The mechanical gripping device is rotated by a direct current motor 10. The rotation velocity of electromotor can be changed using speed variator 4. The normal pressure force is obtained by placement of standard weights on the mobile lever 12, which is attached to the annular support 7. The counterweight 5 was used to balance the levers 7 and 12. The number of rotations was recorded with speed counter 11.

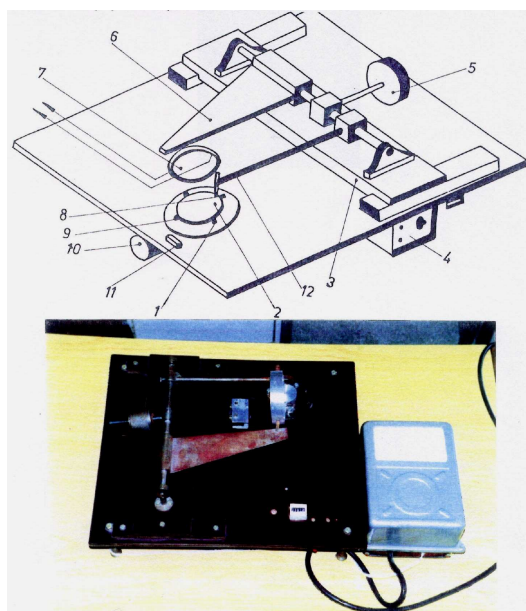


Figure 1. Layout of *pin-on-disk* apparatus: 1-mechanical gripping device; 2-sample; 3-mobile plate; 4-speed variator; 5-counterweight; 6-lever; 7-annular support for strain gauge; 8-steel ball; 9-adjustable system for sample fixing; 10-electromotor; 11-speed counter; 12-mobile lever.

The wear tests were used to calculate the *weight wear rate*, Δ_{um} , and *linear wear rate*, Δ_{ul} , using the following equations:

$$\Delta_{um} = \Delta m / L_f, [g / km] \quad (1)$$

$$\Delta_{ul} = \Delta m / (L_f \cdot A_f \cdot \rho), [m / km] \cdot 10^{-6} \quad (2)$$

in which Δm is loss weight, L_f is friction distance, A_f is area of pin surface, and ρ is bronze density.

The normal pressure force of pin on disk was obtained by placement of a 0.1 daN weight on the mobile lever of test apparatus. The dry friction was used during wear tests.

3. RESULTS AND DISCUSSIONS

The hardness experimental data of bronzes and results of statistical analysis are shown in Table 3.

Table 3

The hardness values of as-cast and heat treated bronzes

| Bronze type | Code sample | Mean hardness, HB | | Statistical analysis (Anova) |
|-------------|-------------|-------------------|--------------|------------------------------|
| | | as-cast | heat treated | |
| CuSn6Zn4Pb4 | 1 | 104.26 | 83.02 | Significant difference |
| CuSn12 | 2 | 95.53 | 83.02 | Significant difference |
| CuSn14 | 3 | 91.18 | 99.18 | Insignificant difference |
| CuAl9Fe3 | 4 | 171.07 | 182.38 | Insignificant difference |

The calculated values of *weight wear rate*, Δ_{um} , and *linear wear rate*, Δ_{ul} are shown in Table 4, and Figures 2÷5.

Table 4

Values of wear rates of cast and heat treated bronzes

| Bronze type | Sample state | Hardness | Weight wear rate, [g/km] $\times 10^{-6}$ | | | | Linear wear rate, [m/km] $\times 10^{-3}$ | | | |
|-------------|--------------|----------|---|------|------|------|---|-------|-------|-------|
| | | | 0.25 | 0.50 | 0.75 | 1.00 | 0.25 | 0.50 | 0.75 | 1.00 |
| CuSn6Zn4Pb4 | C | 104.26 | 7.2 | 5.4 | 5.6 | 6.1 | 0.022 | 0.016 | 0.017 | 0.019 |
| | HT | 83.02 | 7.8 | 6.3 | 5.1 | 6.4 | 0.024 | 0.020 | 0.016 | 0.020 |
| CuSn12 | C | 95.53 | 12.2 | 7.6 | 5.0 | 3.8 | 0.032 | 0.020 | 0.013 | 0.010 |
| | HT | 83.02 | 14.1 | 6.8 | 6.2 | 4.0 | 0.037 | 0.018 | 0.016 | 0.011 |
| CuSn14 | C | 91.18 | 9.6 | 6.4 | 4.4 | 3.4 | 0.030 | 0.020 | 0.014 | 0.011 |
| | HT | 99.18 | 9.8 | 7.2 | 5.1 | 4.0 | 0.031 | 0.023 | 0.016 | 0.013 |
| CuAl9Fe3 | C | 171.07 | 5.2 | 4.4 | 2.1 | 2.0 | 0.020 | 0.017 | 0.008 | 0.008 |
| | HT | 182.38 | 3.2 | 1.6 | 1.6 | 1.2 | 0.012 | 0.006 | 0.006 | 0.005 |

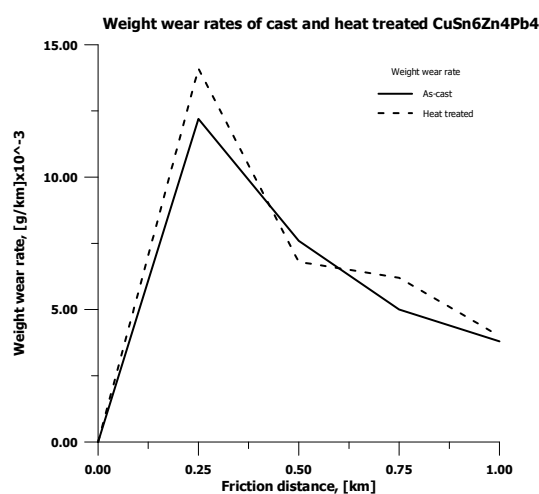


Figure 2. The weight wear rate of CuSn6Zn4Pb4.

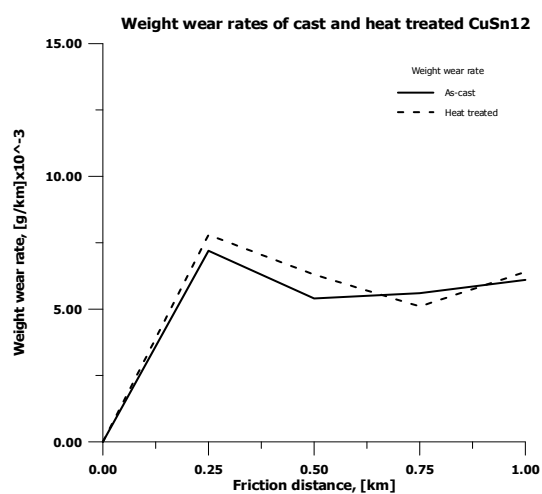


Figure 3. The weight wear rate of CuSn12.

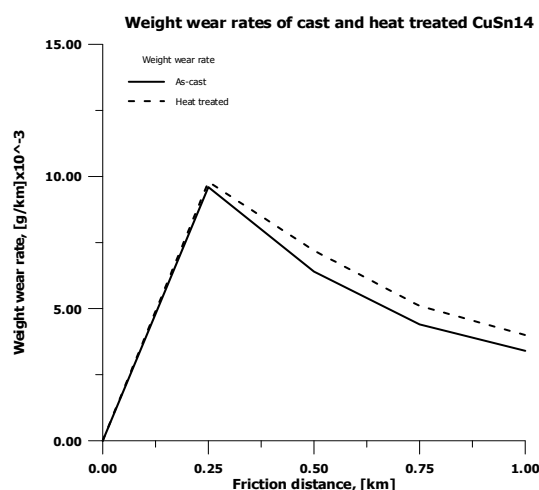


Figure 4. The weight wear rate of CuSn14.

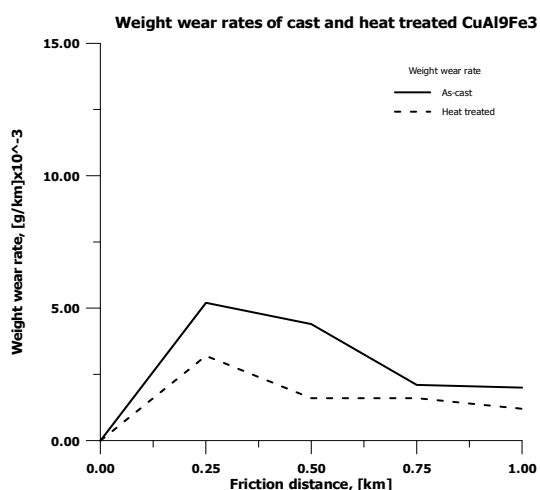


Figure 5. The weight wear rate of CuAl9Fe3.

The weight and linear wear rate had high values for friction distance of 0.250 km. This fact indicates that for beginning time of wear, an accommodation of

surface there is. This initial time period is named lapping. During lapping the weight loss was high, and contact surface topography was changed. After the initial stage was passed, the weight loss significantly decreases, and wear rate reaches a constant value.

The heat treated tin bronzes had wear rate greater than as-cast samples, but heat treatment decreased wear rate of aluminium bronze.

4. CONCLUSIONS

Beside another conditions, the wear behaviour of investigated bronzes depends on both the chemical composition and metallurgical processing.

The aluminium bronze had the lowest wear rates. The heat treatment decreased the wear rates of aluminium bronze, although a statistic insignificant increase of hardness was obtained.

Received 25 April, 2005

* *PETROTUB S.A. Roman*
** *Technical University of Iasi*

REFERENCES

1. Pavelescu, D., *Tribotehnica*, Editura Tehnica, Bucuresti, 1983.
2. Hosking, F.M., Folgar Portillo, F., Wunderlin, R., Mehrabian, R., *Composites of aluminium alloy: fabrication and wear behaviour*, Journal of Materials Science, vol. 17, 1982, pp. 477-498.
3. Roman, C., *Contributii privind obtinerea si caracterizarea materialelor compozite cu matricea metalica si particule*, Teza de doctorat, Iasi, 2001.

COMPORTAREA LA UZARE A UNOR BRONZURI

(REZUMAT)

Aceasta lucrare contine un studiu comparativ a comportarii la uzare a unor bronzuri utilizate pentru piese solicitate la uzura. Au fost supuse studiului doua bronzuri cu staniu (CuSn12, CuSn14), un bronz cu aluminiu (CuAl9Fe3) si un bronz cu staniu-zinc-plumb. Pentru testele de uzare a fost utilizata o instalatie *pin-on-disk*. Vitezele de uzura masica si liniara au fost determinate din datele experimentale. Rezultatele experimentale au aratat ca cele mai mici valori ale vitezelor de uzare au fost pentru bronzul cu aluminiu, iar cele mai mari pentru bronzul cu staniu-zinc-plumb.

DIAGNOSIS METHOD AND EVALUATION OF THE METALIC MATERIALS CHOICE

BY

D.C.

GHEORGHE BADARAU*, VALENTINA BADARAU, IULIAN IONITA* and MIHAI STEFAN***

***ABSTRACT:** In the material choice, experience plays a big role and for the young engineers an instrument for evaluating and diagnosis of the materials choice might be valuable. This paper introduces an original method of evaluation of the materials choice.*

***KEYWORDS:** materials choice, method of evaluation*

1. Introduction

Some times, in the metallic materials choice it occurs the situation in which, two or three possible variants of materials are not too easy to rank according to the choosing criteria established and then the experience of the engineer is the one which decides.

For an experienced person in the materials engineering field there is always a trend in using the materials one knows better and disregard other possibilities of choice, excluding the new materials and losing, in this manner, from many points of view both economically and technically.

For the young engineers and for the beginners especially, the problem of materials choice in these given conditions can be a big one and a method of evaluation of the material choice can be very appealing. On the other hand, for an expert in materials such a method can be more than that, an independent argument in sustaining a judgement.

2. Method of evaluation and diagnosis of the metallic materials choice

Because the way of judgement in the choice of a variant or another often remains "hidden" from being, in this way hard to discuss into the technical councils a method to enhance transparency in this domain would be very valuable.

Moreover, in the situation in which it is the case to discuss the correct or incorrect choice of a material for a given purpose, an impartial judgement tool would be desirable. In the following the principles of such a method will be shortly presented.

The idea of conceiving this calculation method started from the matrix of rapid evaluation of the environment impact method, from the Environment Impact Assessment field.

The method, called by the authors MEAMM (metoda de evaluarea a alegerii materialelor metalice), is based on a standard definition of the important criteria of evaluation as well as of the ways through which quasiquantitative values can be deducted for each of these criteria.

The variants of choosing a material are being evaluated by rapport to the criteria and one determines for each component a mark, using the defined criteria, ensuring in this manner a measuring of the performance for the properties discussed.

The important criteria of choice can be grouped in two categories:

A. Criteria that can change individually the obtained score;

B. Criteria that can not change individually the obtained score.

The values associated for each of the groups of criteria can be determined by using a simple formula. The formulas enable the determination of marks for individual components on an equal well defined base.

The ranking system is constituted as follows:

- the marks for the group A are obtained by multiplying of the values for each criteria

$$(a1) \times (a2) = aT \quad (1)$$

(a1), ... (ai) – are the marks given for the individual criteria for the group A.

Using the multiplication for the A criteria is important because it ensures the expressing of the weight of each mark, but the simple adding would expressed identical results for different conditions.

- the marks for the group B of criteria are being added, giving a single sum

$$(b1) + (b2) + (b3) = bT \quad (2)$$

(b1), ... (bi) – are the marks given for the individual criteria for the group B.

This gives the certainty that the individual marks can not influence the general score but as well as the sum importance of the values from the group B is also in view as a hole.

The sum of marks from the group B is then multiplied with the value resulted from the group A ensuring in this way a final evaluation score (ES).

$$(aT) \times (bT) = ES$$

aT is the result of multiplying of all marks A;

bT is the result of the sum of all marks from the B group;

ES is the average score for the analyzed property.

The reasoning for each property are given according the criteria and the ranking levels shown in table 1.

Table 1 Criteria and ranking levels

| Criterion | Scale | Description |
|--|-------|---------------------------------------|
| A1 The importance of the property for the functioning | 4 | Indispensable for the functioning |
| | 3 | Very important for the functioning |
| | 2 | Important for the functioning |
| | 1 | Little importance for the functioning |
| | 0 | Not influencing the functioning |

| Criterion | Scale | Description |
|---|-------|---|
| A2 Processing possibilities of the material during the technological route | +2 | High technological properties for all the needed procedures |
| | +1 | High technological properties for the most part of the needed procedures and average for the others |
| | +0 | Medium technological properties for the needed procedures |
| | -1 | Low technological properties for some of the needed procedures |
| | -2 | Impossible to be processed efficiently at least in one needed procedure |
| B1 Complexity of the equipment of primary processing | 3 | Simple |
| | 2 | Average |
| | 1 | Complex |
| B2 Complexity of heat treatment | 1 | Low |
| | 2 | Average |
| | 3 | High |
| B3 Processing cost | 1 | High |
| | 2 | Average |
| | 3 | Low |

3. The definition of the components of the evaluation discussion

To define the components of the evaluation discussion means to select the properties that might influence the producing, operation, maintaining and material recovery in the best economical conditions.

The components can be included in classes, like for example:

- properties of the metallic material (PMM) (physical, chemical, mechanical, technological, operational);
- economical and operational properties (EOP);
- ecological properties (Ec P).

For evaluating each variant of material one must build a matrix comprising cell showing the criteria by report of each component. In each cell the mark is being written for each individual criterion. With the given formulas one calculates the ES score. Then the scores are being compared following the table of categories shown bellow.

After being classified into a category the scores can be represented on a graphic or in a numerical presentation.

Table 2 Scores conversion in choice motivation

| Average score | Category | Category description |
|---------------|----------|----------------------|
| +48 at +72 | + D | Best choice |
| +24 at +47 | + C | Excellent choice |
| +13 at +23 | + B | Very good choice |

| | | |
|--------------|-----|----------------------------|
| + 1 at +12 | + A | Good choice |
| 0 | N | Functions without problems |
| - 12 at - 1 | - A | Not recommended |
| -23 at -13 | - B | Bad choice |
| - 47 at - 24 | - C | Very bad choice |
| - 48 at -72 | - D | Worst choice |

An evaluation matrix looks like in the example below but the construction of it remains at the appreciation of the user.

Table 3 - The matrix of evaluation of the metallic materials choice (MEAMM)

| Component | ES | Category | A1 | A2 | B1 | B2 | B3 |
|----------------------|----|----------|----|----|----|----|----|
| Material 1 | | | | | | | |
| PMM | | | | | | | |
| Tensile strength | | | | | | | |
| Elongation | | | | | | | |
| Young module value | | | | | | | |
| Specific mass | | | | | | | |
| Thermal conductivity | | | | | | | |
| | | | | | | | |
| EOP | | | | | | | |
| Acquisition price/kg | | | | | | | |
| Disponibility | | | | | | | |
| | | | | | | | |
| EP | | | | | | | |
| Toxicity | | | | | | | |
| Polluting potential | | | | | | | |
| | | | | | | | |

4. Conclusions

The steps that must be followed in the applying of the MEAMM method are:

- the establishment of the criteria and steps of evaluation;
- the definition of the components and grouping them on classes;
- ranking and computing the evaluation scores;
- conversion of scores in categories;
- the establishing of the category for each class of component;
- graphical representation: score on each class for each variant and category.

The building of the matrix is one of the most important steps in this method because choosing the components can be rather difficult. After it, the evaluation with marks and the calculation are not difficult to perform.

This method ensures the same treatment for each variant of material and because the most of the components (properties) can be measured, ranking them is very easy and the subjectivity, even if it exists is highly diminished.

Nevertheless, the most important advantage of the method is the transparency of the marks, so, of the judgement of each component, or of each criteria of evaluation.

The method is efficient because is more easy to compare numbers obtained in an objective manner than to evaluate opinions or recommendations.

In this initial phase, the preliminary tests made with this method gave results in good agreement with those obtained in the classical manner, but the method is still subject to further improvement.

References

1. Badarau ,V., Evaluarea impactului asupra mediului privind activitatea de depozitare a deseurilor menajere prin metoda MERI, Lucrarea de Disertatie, U.T. Iasi, Facultatea de Chimie Industriala, Master Managementul Mediului, 2004
2. Barrow, C., D., Environment and Social Impact Assessment. An Introduction, John Whilley and Sons, Inc., New York, 1997
3. Palmer, P.,J., Evaluarea impactului asupra mediului- Manual IMC Consulting, prezentat la Seminarul de Evaluare a impactului asupra mediului, Bucuresti ianuarie, 2001
4. Sheate, W., Making an Impact, a Guide to EIA Law & Policy, Cameron May Ltd., London, 1994
5. Negrei, C., C., instruemnte si metode in managementul mediului, Ed. Economica, bucuresti, 1999.

GHEORGHE BADARAU,
VALENTINA BADARAU,
IULIAN IONITA
MIHAI STEFAN

* **Technical University “ Gh.Asachi Iasi”**
** **S.C. HABITAT PROIECT S.A. IASI**
* **Technical University “ Gh.Asachi Iasi”**
* **Technical University “ Gh.Asachi Iasi”**

METODA DE DIAGNOSTICARE SI EVALUARE A ALEGERII MATERIALELOR METALICE

REZUMAT: In alegerea materialelor experienta joaca un rol important si pentru tinerii ingineri un instrument pentru evaluarea si diagnoza alegerii materialelor poate fi valoros. Acesata lucrare introduce o metoda originala de evaluare a alegerii materialelor.

THE WEAR OF THE METALIC SURFACES IN ABRASIVE TRIBOSYSTEMS I: WEAR TYPES AND MODIFICATIONS OF THE ABRADED SURFACES

By

MIREA CONSTANTIN

***Abstract.** Abrasive wear represents one of the most complex degradation phenomena of the solid bodies' surfaces. In the special literature, it is considered as being the characteristic type of the mechanical phenomena that, comparative with physical or chemical phenomena, contributes with the greatest weight at quick wear of the surfaces. From applicative point of view, one of the fundamental problems relating to the abrasive wear is the reduction of the negative effects that this generates, especially those in conjunction with the important costs that imply. To get out such as problems it is possible just in measure in that can be clarified the phenomenological fundament of abrasive wear processes.*

This paper presents, on the basis of special literature survey, some definitive aspects for the abrasive wear processes and attempts, concomitantly, to formulate some observations and points of view on some fundamental elements for the approach of the problems in connection with this type of wear. Without to minimize the importance of other aspects, in the first part of the paper are presented some considerations about the classification system of the abrasive wear types and the surface modifications induced by these.

Key words: abrasive wear, tribosystem, types of abrasive wear, surface modifications

1. Introduction

In the theory of surface degradation, the abrasive wear is considered an intense degradation process that involves loss of material from solid surfaces. This process is determined by the exercised action, in conditions that supposes applied load and relative motion, by hard particles or hard protuberances of one other surface. In this context, the wear of surface is produced by progressive loss of material due to the removal of micro-particles by micro-cutting, plastic deformation and other specific mechanisms of the abrasive wear process.

In the real tribosystems, the abrasive wear phenomena are disturber phenomena cause by the environment work, external actions or even as result of other types wear phenomena.

The special literature consider the abrasive wear as being the characteristic type of mechanical phenomena that, comparative with physical or chemical phenomena, contributes with the greatest weight at quick wear of surfaces.

In the economical field, the effects generated by abrasive wear are principally connected to the important costs that implies, these being estimated for high industrialized states as ranging from 1% to 4% of the gross national product, [12]. This

fact is not surprising if one has in view that abrasive wear, as is encountered in the context of the various industrial situations, have a high appearance frequency by comparison with other types of wear, [3], [13], figure 1.

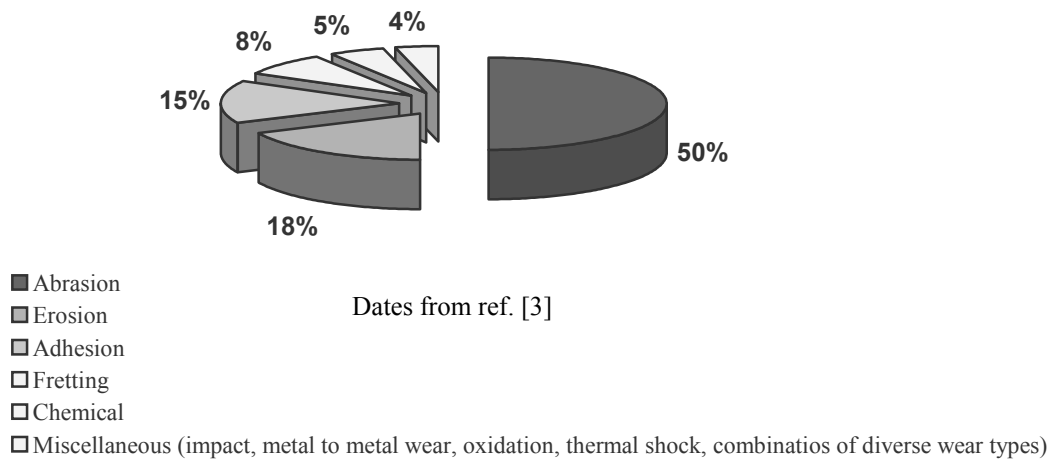


Fig. 1. The frequency with which the various wear types occur

From applicative point of view, the fundamental problem of abrasive wear consist in limitation and reduction of the negative effects generated, especially those in conjunction with the important costs that wear imply and the materials loss due to such surface processes.

The complexity of abrasive wear process and the considerable positive effects, especially from economic nature, which can be obtained by wear reduction, was represent and continue to represent the motivation of development on scientific bases of the studies and researches undertaken in the abrasive wear field.

This paper presents, on the basis of the special literature survey, some aspects and points of view considered that can constitute fundamental elements for the approach of the problems connected to abrasive wear processes and not in last instance to the behavior and abrasive wear resistance of the metallic materials. Without to minimize the importance of other aspects relating to the abrasive wear, are presented some aspects relative to the abrasive wear types classification and to surfaces modifications that have place during the wear process.

2. Types of abrasive wear

One of the characteristic aspects for the abrasive wear is the fact that on the surface of active elements this type of wear can manifest in different forms, function of concrete conditions that define the wear process. It can appreciate that the understanding and knowledge of abrasive wear phenomenon can't be complete than insomuch as these forms of manifestation become parts in the same knowledge process.

Generally, abrasive wear is represented, or classified, through some characteristic types of abrasive wear, identified and defined in report with different criteria. The necessity to identify, define and to classify the characteristic types of abrasive wear is argued by the fact that can offer a reference base for accurate

identification of the abrasive wear type, essential aspect for identification of some effective solutions to decrease the wear. Therefore, is very important to define an adequate system for classification and, implicit, classification criteria that can describe with enough accuracy the diverse manifestation forms of abrasive wear. In this way, must have in view both aspects connected to work conditions of active elements (load, speed, characteristics of abrasives, etc.) and the results observed in operating conditions, through the mechanisms and the manifestation forms of wear, inclusive the correspondence with the wear processes.

Frequently, the abrasive wear classification includes criteria such as the aspect of abraded surfaces, the characteristic wear mechanism, the functional structure of the tribosystem, nature and level of the solicitations. Owing to the very complex character of the abrasive wear, none of the wear types observed can't be described in all aspects only just one criterion.

The survey of special literature shows that this no offer a unitary classification of abrasive wear types. On remark the classifications having as criteria the type or functional structure of the contact, the contact environment, the mechanism of wear, and, mostly, the nature and level of the solicitations correlated with the aspect of worn surfaces. In figure 2 and table 1 are presented two more complex classifications systems which include some of the most used classifications criteria.

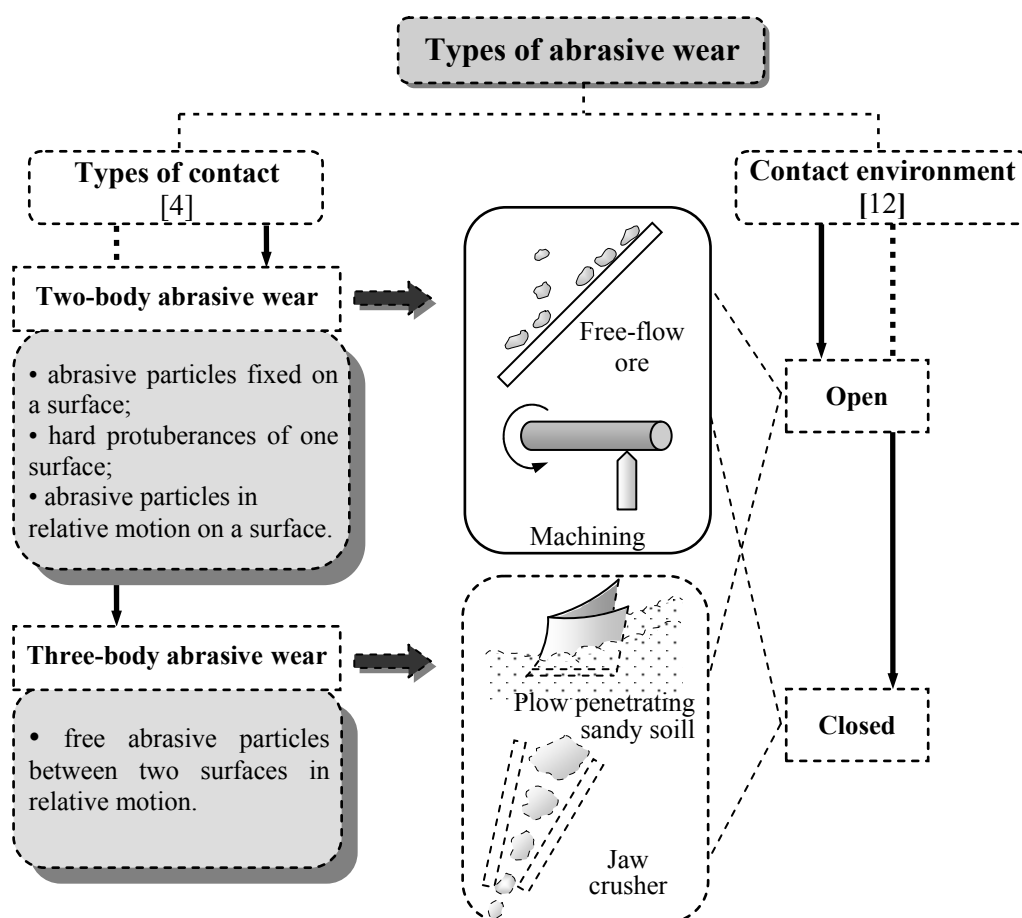
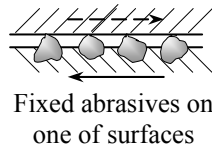
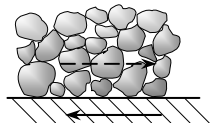
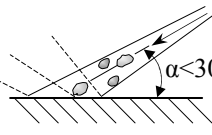
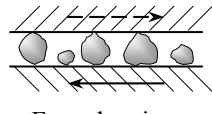
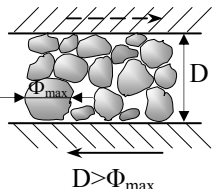


Fig. 2. The classification of the abrasive wear types according to contact type and contact environment

Tabelul 1

Principal types of abrasive wear

| Abrasive wear type | Nature and dynamic level of solicitations | Mechanical configurations, [7] | | Aspects of wear surfaces |
|--------------------------------|--|--|--|---|
| Gouging abrasion | <ul style="list-style-type: none"> Abrasion with high loads (with or no shocks) | <ul style="list-style-type: none"> Two body abrasive wear free abrasives bonded abrasives Three body abrasive wear hard and very hard coarse abrasives | <p>Two body abrasive wear</p>  <p>Fixed abrasives on one of surfaces</p>  <p>Free abrasives</p> | <ul style="list-style-type: none"> Macroscopic penetration of surfaces Very high wear rates |
| High-stress grinding abrasion | <ul style="list-style-type: none"> Abrasion with moderate loads (with or no shocks) high specific local stresses | <ul style="list-style-type: none"> Two body abrasive wear free abrasives bonded abrasives Three body abrasive wear $D > \Phi$ $D < \Phi$ |  <p>Abrasive erosion</p> <p>$\alpha < 30^\circ$</p> <p>Three body abrasive wear</p>  <p>Free abrasives between two surfaces</p> | <ul style="list-style-type: none"> Scratches, cuts local plastic flows, microcracks High wear rate |
| Low-stress scratching abrasion | <ul style="list-style-type: none"> Abrasion with high loads negligible impact shocks high speed of abrasive particles | <ul style="list-style-type: none"> Two body abrasive wear free abrasives bonded abrasives Three body abrasive wear $D > \Phi$ |  <p>Free abrasives between two surfaces</p> <p>$D > \Phi_{max}$</p> | <ul style="list-style-type: none"> Microscopic penetration of surfaces Intense abrasion of surfaces depend on the abrasive particles geometry Intense abrasion |

The previous model (table 1) of the abrasive wear types classification corresponds practically to the approach mode on the conceptually system adopted in the field of the wear processes. This concept places in first plan the interdependence relations between solicitations (entrance parameter), the materials characteristics (transformation block) and the aspects of worn surfaces (exit parameter), [2].

The integration of the concept system in the field of abrasive wear processes confers one more complete image for the abrasive wear types and some unity of the relations between solicitations, materials and the aspect of worn surfaces.

On an abrasive tribosystem, the solicitations that acts on the active elements can't be always quantized, but in the most frequently cases these can be appreciated by means of one integrant factors, or parameters, such as: load, speed, temperature, etc. The load is considered to be the most important factor for evaluation of the solicitations level.

3. Surfaces modifications during the abrasion processes

During abrasive wear processes, the surfaces of the metallic materials suffer some mechanical, structural, chemical modifications, inclusive modifications of the stress state, figure 3. On principle, owing to such modifications (that depends on the characteristics of the tribosystem elements and of solicitations), the metallic materials obtains one stratified structure formed from one modified surface layer and one non-affected substratum that preserves his initial properties and characteristics.

It can be therefore appreciated that, owing to such modifications, the abrasive wear behavior of the materials is much better defines in report with the properties and characteristics of these surface layers. This point of view can be argued by the fact that, once formed, the modified surface layer takes over the active function in the contact with abrasive material, his characteristics determining directly the wear resistance of the material.

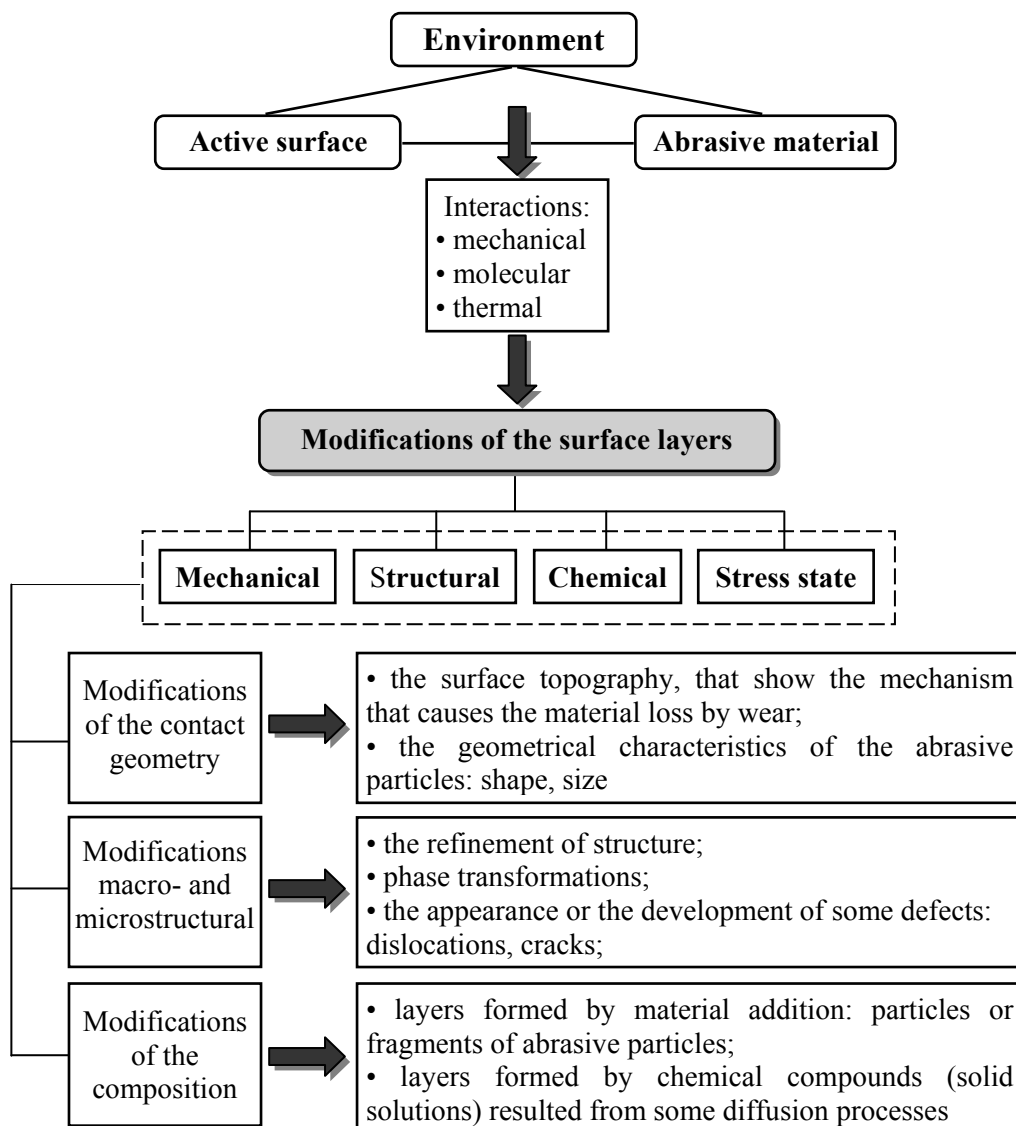


Fig. 3. Modifications types induced into surface layers of the metallic materials by abrasive wear processes

Because the modifications caused of the surfaces by the abrasive wear processes depends on the characteristics of abrasive tribosystem elements and solicitations, the analysis of the modified surface layers must takes in considerations the possible causes for development of structural modifications:

- plastic deformations in the surface layers;
- thermal processes in the surface layers;
- diffusion processes in the surface layers;
- chemical interaction of the surface with the environment work;
- concerted actions of the mechanical and thermal factors.

The structurally modifications generated by plastic deformations of the material during the wear process are one of the determinant factors for abrasive wear process. Such structural modifications are causal elements of the initial hardness surface modification, with adequate consequences on the wear behavior.

The structurally modifications and especially those produced on the microstructure, must be considered by means of the determinant role that microstructure have on the materials properties and in consequence on the wear resistance and material loss mechanisms.

The type and nature of the structural surface modifications depend on the material type, his microstructure and properties, but and on the wear conditions, [6], [8], [9], [10], [11].

In the matter of surface modifications founded behind abrasive wear of some steels with different microstructure it can be concluded that:

□ the microstructure and the hardness of surfaces are modified generally in the initial period of the wear process, [1], [10];

□ hardness modifications depend by the initial microstructure and hardness of the steels, [6], [10];

□ emphasized refinement of the microstructure at near worn surfaces of annealed steels is caused by intense plastic deformation of the material and the friction heat generated in certain conditions during wear process, [8], [9], [10], [11], that produces localized faze transformations (reaustenitizing, followed by martensitic transformation);

□ the surface layers regions that suffer intense plastic deformations during wear process are characterized by one great dislocations density, inherent of such phase transformations, [10];

□ volume modifications, caused by the microstructure modifications, determine cracks propagation from surface layers, which increase material loss especially when these cracks joint at surface, [10];

□ the material loss mechanisms are determined by the microstructure modifications produced during wear process; owing to some such modifications, ductile materials behave (from point of view of the mechanisms that determine material loss) likewise brittle materials, and vice versa, [10].

In certain conditions, the surface layers can suffer composition modifications, too, by abrasive material addition: fragments or even abrasive particles that penetrate and fix in the surface, figure 4, offering thus an additional protection against abrasion. The abraded materials benefits by this effect insomuch as these are able to sustain these particles that act like hard microstructural constituents. Also, on the worn surface

have identified layers formed of compounds resulted from diffusion processes. With regard to the forming and role of such layers in the wear processes on conclude, [5]:

□ from quantitative point of view, the penetration of particles or fragments particles in the wear surfaces increases with the increase of the wear surface temperature;

□ the alloys that no contain hard carbides are much susceptible to form such layers because the presence of the carbides can gives to the abrasive particles a unfavorable roll movement (mechanical stresses at the contact abrasive particle-surface are much less in the case of roll movement than in the case of sliding movement);

□ in the case of abrasive wear processes at elevated temperature, the hot resistance of the alloy matrix is essential to assurance an efficient base for particles or fragments particles embedded in the surface;

□ the forming of some thin solid solutions layers on the wear surfaces, figure 5, at relatively lower temperature than those at that it can produce in normal conditions such reactions, can be caused by the tribological stress state;

□ the connection between these layers and abraded surface is formed by means of some mechanical connections and by adhesion.

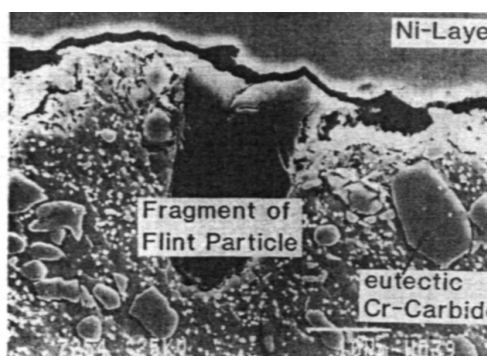


Fig. 4 Flint fragment embedded in the worn surface of a cold worked tool steel, [5]

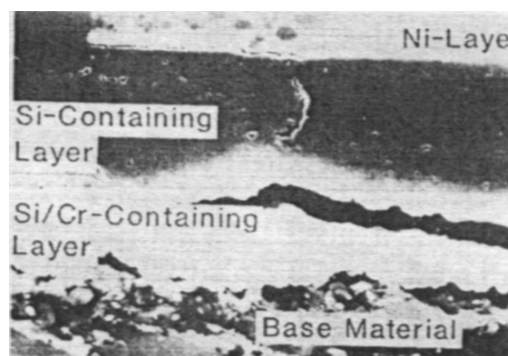


Fig. 5. Twin layer on worn surface of NiCr20AlTi containing silicon and Si-Cr, [5]

Experimentally, in the abraded surfaces layers of some steel samples with different microstructures and hardness, obtained by heat treatments, has been found modifications of the stress state caused by the friction-wear process, [6]. In the most cases, it has found the presence of some compression residual stresses. This stresses type is favorable to increase the abrasive wear resistance.

4. Conclusions

The abrasive wear is a phenomenon characterized by a high degree of complexity and by the important weight that have on quick surface degradation. The very complex character of abrasive wear is reflected and at the level of the wear manifestation forms, that often constitute a classification criterion for the different wear types.

The utilization of a unitary classification system of abrasive wear types and mostly the establishment of the most explicit criteria for classification are necessary

for correct identification of different wear types and must be understanding like an essential aspect for development of some solutions for wear decrease.

The abrasive wear processes determine complex modifications on surface of active elements. Owing to these, the abrasive wear behavior is much better defined in report with the properties and characteristics of worn surface. From this point of view, the micro structural modifications and the residual stresses state become much relevant indicators for the behavior or abrasive wear resistance of the metallic materials.

References

1. Das, S., Prasad, B., K., Jha, A., K., Modi, O., P., Yegneswaran, A., H., 3-Body Abrasive Wear of 0,98-Percent Carbon-Steel. *Wear*, vol. 162, 1993, p. 802-810
2. Dumon, P., Hubert, M., Lot, J., I. Le rechargement anti-usure. Méthode pour la résolution de cas industriels d'usure. *Soudage et Techniques Connexes*, vol. 32, nr. 5/6, 1978, p. 169-182
3. Dumovic, M., Repair and Maintenance Procedures for Heavy Machinery Components. *Welding Innovation*, vol. XX, nr. 1, 2003
4. Finkin, E., F., The wear phenomenon. *The Engineers' Digest*, nr. 9, 1970, p. 67-73
5. Fischer, A., Mechanism of high temperature sliding abrasion of metallic materials. *Wear*, vol. 152, nr. 1, 1992, p. 151-160
6. Garbar, I., I., Influence of residual stresses on abrasive wear resistance of steels. The 27th Israel Conference of Mechanical Engineering, Haifa, Israel, Mai 19-20, 1998, p. 647-649
7. Leger, M., T., Aciers et revêtements anti-abrasion. *Fonderie-Fondeur d'Aujourd'hui*, nr. 93, 1990, p. 31-17
8. Mashloosh, K., M., Abrasive wear and its applications to digger teeth. *Tribology International*, vol. 18, nr. 5, 1985, p. 259-266
9. Moore, M., A., A preliminary investigation of frictional heating during abrasive wear. *Wear*, vol. 17, nr. 1, 1971, p. 51-58
10. Prasad, B., k., Prasad, S., V., Abrasion-induced microstructural changes during low stress abrasion of a plain carbon (0,5%C) steel. *Wear*, vol. 151, nr. 1, 1991, p. 1-12
11. Scheffer, O., Allen, C., The abrasive wear of steels in South African soil. *Tribology*
12. Tylczak, J., Abrasive wear. *ASM Handbook*, vol. 18, Lubrication and Wear Technology, USA, 1995, p. 184-190
13. Womersley, D., Hardfacing: not merely a reclamation process. *Surface Engineering*, vol. 11, nr. 1, 1995, p. 43-46

Technical University "Gh. Asachi" Iassy

UZAREA SUPRAFETELOR METALICE ÎN TRIBOSISTEME ABRAZIVE I: TIPURI DE UZARE ȘI MODIFICĂRI ALE SUPRAFETELOR UZATE PRIN ABRAZIUNE

Rezumat. Uzarea abraziva reprezintă unul dintre cele mai complexe fenomene de degradare a suprafețelor corpurilor solide. In literatura de specialitate este considerat ca fiind tipul caracteristic al fenomenelor de natură mecanică care, comparativ cu fenomenele fizice sau chimice, contribuie cu ponderea cea mai mare la uzarea rapidă a suprafețelor. Din punct de vedere aplicativ, una din problemele fundamentale care privesc uzarea abrazivă vizează reducerea efectelor negative pe care aceasta le generează, în special a celor legate de costurile importante pe care implică. Soluționarea unor astfel de probleme este posibilă doar în măsura în care poate fi clarificată baza fenomenologică a proceselor de uzare abrazivă.

Aceasta lucrare aduce în discuție, pe baza cercetării literaturii de specialitate, o serie de aspecte definitorii pentru procesele de uzare abrazivă și totodată încearcă să formuleze unele observații și puncte de vedere asupra unor elemente fundamentale pentru abordarea problemelor legate de acest tip de uzare. Fără a minimaliza importanța altor aspecte, in prima parte a lucrării sunt aduse în discuție unele considerații privind sistemul de clasificare al tipurilor de uzare abrazivă și modificările induse de acestea la nivelul straturilor de suprafață.

**THE WEAR OF THE METALIC SURFACES IN ABRASIVE TRIBOSYSTEMS
II: THE INFLUENCE OF SOME PROPERTIES AND CHARACTERISTICS OF THE
MATALIC MATERIALS ON THEIR ABRASIVE WEAR RESITANCE**

By

MIREA CONSTANTIN

***Abstract.** In this paper are summarizing presented, on the basis of existing dates in the special literature, some definitive elements for abrasion resistance of metallic materials, begin considering the functional structure of the abrasive tribosystems, inclusive those properties and characteristics of the metallic materials that influence abrasion resistance of these. Owing to the complexity of the abrasion processes, one correct approach of any problems regarding to abrasion resistance suppose to include in the context of the hypotheses the fact that the abrasion resistance of the metallic materials is not an inherent property of these but a result of concrete conditions that have place the wear process. With other words, both abrasion process, and his consequence, wear, and abrasion resistance are determined by those properties and characteristics that, in report with abrasion process, define the structural elements of the abrasive tribosystems and by the parameters that describe the interaction between abraded material and abrasive material.*

The abrasive wear of metallic materials is influenced to begin with their microstructure. For this reason, the relation between abrasion resistance and structure must be placed in the more complex context of the dependence between chemical composition, structure, material properties. On impose thus a unitary approach of all the aspects in connection with microstructural characteristics, alloy degree, type and intensity of the solicitations.

The structural state of the metallic materials represents one of the most relevant indicators for abrasion resistance of the metallic materials.

***Key words:** abrasive wear resistance, abrasive tribosystems, microstructural characteristics, mechanical properties*

1. Introduction

The abrasive wear resistance of the metallic materials is, as the theoretical and experimental researches demonstrate, a problem with a very complex character, determined by the herself very complex nature of the abrasive wear process.

The evaluation of the abrasive wear resistance, or abrasive wear behavior, of a metallic material can't be correctly and efficiently tackled without to include in the context of the hypotheses the fact that the wear resistance of a metallic material in not an inherent property of this, but a result of the conditions that have place the wear in one abrasive tribosystem, [13], [21]. With other words, both wear process, and his consequence (the wear), and wear resistance are determined by those characteristics and properties that, in report with wear process, define the structural elements of one

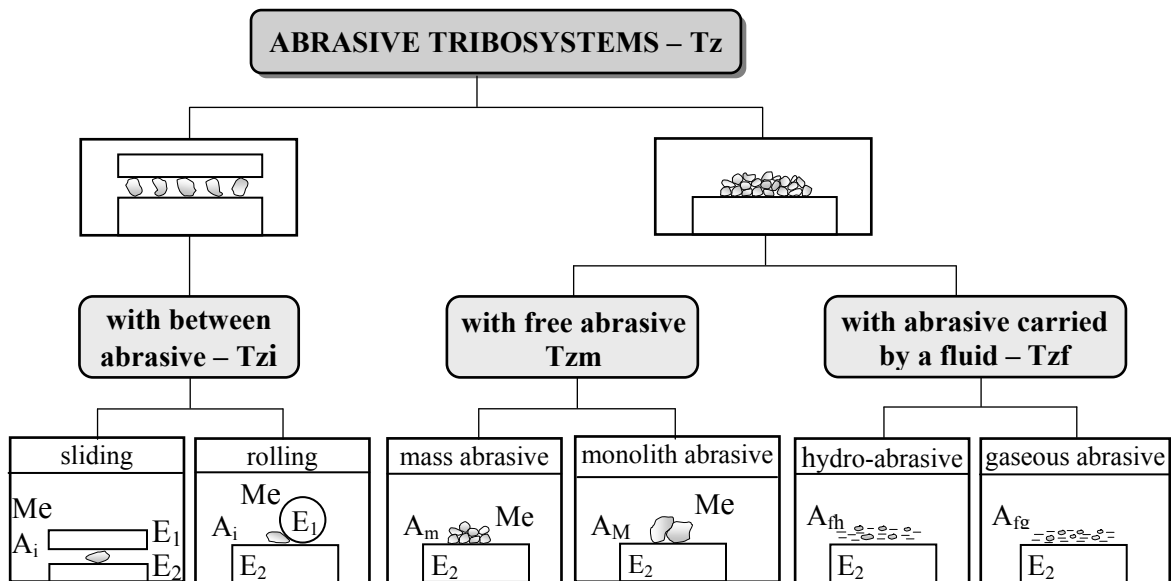


Fig. 1. Abrasives tribosystems (E1, E2: active elements; A: abrasive material; Me: environment), [4]

tribosystem, figure 1, and by the parameters that describe the interaction conditions between metallic material and abrasive material.

2. The influence of some properties and characteristics of the metallic materials

2.1 Metallurgical factors and characteristics

The abrasive wear of the metallic materials is determined to begin with by their microstructure. From this point of view, the relation between abrasive wear resistance and structure must be placed in the context of one much complex dependence between chemical composition, structure and material properties. These considerations impose a unitary treatment of the aspects concerned to microstructural characteristics (carbide and matrix characteristics), alloying degree, nature and level of solicitations.

One of the most important methods to ordering the process to form alloys microstructure and properties by means of chemical composition is the alloying and modification. Experimentally, it was found that, owing to the effects generated at microstructure level by saturation of the melted alloy with alloying elements and modifiers addition, the abrasive wear resistance of white irons can be reduced by 2,5-2,7 time, [22].

The carbon is one of the most important elements of the chemical composition of the abrasive wear resistant steels and white irons, being found the increase of the wear resistance with the increase of carbon percent, [1], [7], [9], [11], [13], [17], but the influence of carbon percent on abrasive wear is in one evident connection relation with the entire chemical composition and the structural constituents that form the alloy matrix. In the case of the steels it was found that the carbon have a more important influence on the abrasive wear resistance comparatively with other alloying elements, the influence of these being analyzed by means of equivalent carbon, [7].

For the alloy systems composed from a hard carbides phase and a metallic matrix (generally softer), the material losses by abrasion is the result of two interdependent wear processes of these phases. Consequently, the wear resistance of these materials can be described as being function of wear behavior of respectively constitutive phases, [8]:

$$\varepsilon = \alpha\varepsilon_1 + \beta\varepsilon_2 \quad (1)$$

where: ε is the wear resistance of the alloy
 ε_1 and ε_2 – wear resistance of phases;
 α and β – volume fractions of phases.

The way in which the hard phases determine the abrasive wear resistance of one alloy depend on the properties, characteristics and microstructural parameters of the respective phases.

Carbides type (*chemical composition, structure, hardness*). A good abrasion resistance is obtained by presence of the M_7C_3 chromium type carbides and, especially, by presence of extra carbides or complex carbides of some carbides formed elements, such as Mo, W, V, Ti, Nb, B, [2], [10], [13], [16], [17], [20], [22].

Carbides orientation. For example, owing to hardness differences of $(Cr,Fe)_7C_3$ carbide in report with her axes, the orientation of these with the maximum hardness axis perpendicularly on wear surface determine an importance increase of wear resistance, [17].

Carbides percent. Abrasive wear resistance increases with increase of this, [5], [10], [13], [14], [17], [21], [22], the maximum values corresponding to a *critical carbides content*, that commonly correspond to eutectic composition, [13], [17], and that depend on carbides type, matrix, abrasive material, abrasive wear type, figures 1 and 2.

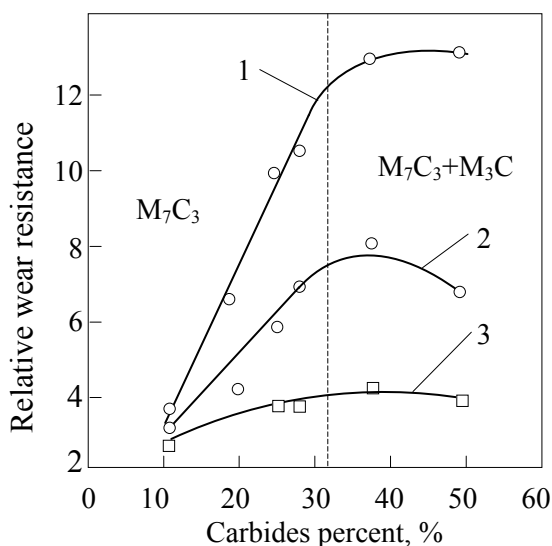


Fig. 1. The influence of carbides content, type carbide and metallic matrix on abrasive wear resistance of one Cr-Mo iron (1- martensite; 2- austenite; 3- pearlite), [17]

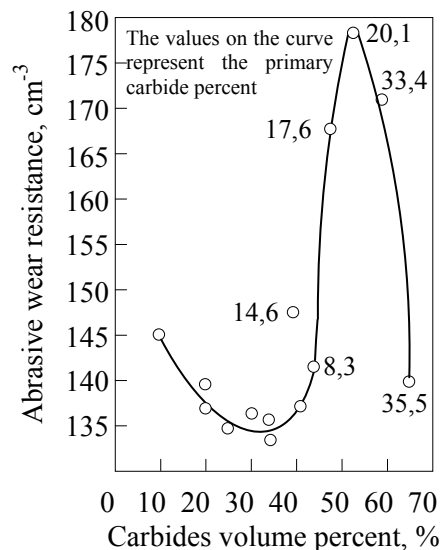


Fig. 2. The influence of carbides volume percent on the high stress abrasive wear resistance of the high chromium white irons, [10]

The increase of carbides percent signifies practically the increase of the **carbides occupied surface**, which will decrease the wear owing to matrix protections against abrasive particles action. The effect is more meaning if the **carbides toughness** is better, the **carbide dispersion** is more uniform and the *average distance between carbide particle*, or *the mean free path*, λm , [14] is lesser.

Carbides size. The abrasive wear resistance is improved with decrease of carbides size, [10], [14], [17], [21], owing to the fact that in the case of carbides with reduced size, the stresses are assumed by the matrix too, [17].

The effects of the refinement and dispersion of the microstructural phases depend on ratio between λm and *abrasive particles size*; for lesser values is counteract the preferential wear of matrix, which should determine the carbide removing, in this way being maintained the integrity of the matrix-carbides system, [14].

In accordance with the solicitations, it can be found a preponderant influence of either carbides or matrix, but the role of the two phases can't be dissociated because of the existing cohesion between these. In abrasion with low stresses, wear resistance depend principally on carbides percent and dispersion of these, the matrix hardness having a secondary importance, whereas in abrasion with high stresses, the material loses by wear is determined by the more accented wear of the matrix, [10], [14].

Matrix type. The influence that have on abrasive wear depends principally on solicitations type: the alloys with martensitic matrix have demonstrated a good abrasion resistance in wear conditions with low or average loads and shocks, while the alloys with work hardenable austenitic matrix have a good abrasion behavior when the intensity of the loads and shocks is enough to determine austenite transformation, [10], [13], [14], [17],

The influence of the austenite from matrix on abrasive wear resistance depend on ratio, composition and his stability degree, abrasive type, conditions of sollicitation, [10], [13], [14], [17].

The consolidation and the stability of the carbide-matrix connection are determined in positive sense by:

- a matrix with low plasticity that can assures an efficient base, countering to damaged of these owing to the shear stresses generated in abrasive wear process, [5], [14], [17];
- the existence of secondary precipitated carbides, that determine the increase of the ultimate strength, thus ensuring of the carbides a more efficiently mechanical base, [14], [21];
- carbides shape, that them offers a steady consolidation in matrix and that them confers resistance at solicitations; in the matter of carbides shape, it can be remark the like-hood niobium shape carbides, [2], and globular and compact carbides, suitable for abrasion and impact, [10], [17].

2.2. Physical and mechanical properties and characteristics

One of the more important properties that characterize the abrasive wear resistant materials is the **hardness**, being found that abrasion resistance is increased with hardness increase.

In report with abrasion resistance, the hardness notion implies two aspects: the one that refers to the *bulk hardness* and the one that refers to the *surface hardness*. Significant is the fact that the abrasion resistance is improved with hardness increase, indifferently if bulk hardness or surface hardness is the reference parameter.

For alloy steels it was found that abrasive wear resistance has a nonlinear increase with bulk hardness, slower for less hardness values and more accented for higher values. This fact, as well as the fact that for some steels with the same hardness was obtained, in similarly wear tests, different wear resistance values suggests that abrasion resistance must be correlated with other factors too, which can better describe the wear process. Moreover, the hardness being a complex characteristic that depends on a number of internal and external factors (crystalline lattice parameters, sliding elements, formation and multiplication of dislocations, impurities content, temperature) can't be considered one primary property of the metallic materials, [3].

When bulk hardness was replaced with surface hardness it was found that between this and abrasive wear resistance exist one correlation and much obvious adequacy, [12], [15]. This is explicable by the surface modifications that occur in wear processes, modifications that implies and hardness modifications. Additionally, this confirms the fact that surface modifications can explain and describes more really the wear processes. Thus, worn surface hardness becomes a more relevant indicator for abrasive wear resistance.

The linear dependence of abrasive wear resistance against annealed pure metals hardness was explained, [19], as being in reality just a manifestation of the **melting temperature** of these (owing to the proportionality relation between this temperature and hardness), the apparent effect of hardness (strength) being the result of the proportionality between temperature coefficient of flow stress and melting temperature, that in turn is proportional with the hardness. In this assumption, the argued in accordance with the higher hardness, strength respectively, the higher melting point, is more really in the case of one adiabatic regime of the material deformation under abrasive particles action.

The fact that at the same hardness values, pure metals have show a greater abrasive wear resistance than some alloyed steels can be explained and by greater **deformation capacity** of these. The correlation between deformation capacity and abrasive wear resistance is expressed, [23], although not explicitly, by relation:

$$w = f_{ab} \cdot A_v \cdot d \quad (2)$$

where: A_v is the cross-sectional area of the wear groove;

d - sliding distance of abrasive particle;

f_{ab} - fact that accounts for the proportion of displaced material to removal material:

$$f_{ab} = \frac{A_v - (A_1 + A_2)}{A_v}, \quad (3)$$

where $(A_1 + A_2)$ is the cross-sectional area of the material displaced to the side of the groove.

Function of material deformation capacity, $f_{ab} \in [0,1]$; for the materials with a great deformation capacity $f_{ab} \rightarrow 0$, that signifies with other words that the wear will produces with local plastic deformation (plowing) and not by cutting or microcutting,

mechanisms through it can produces abrasive wear of the materials with less deformation capacity, for which $f_{ab} \rightarrow 1$.

The materials that are **work hardened** under abrasive wear action have showed an increase of the abrasion resistance owing to both increase of the wear surface hardness and some modifications of the wear mechanisms. In accordance with the theoretical model based on plastic flow localization concept, [18], [19], *the work hardened capacity* of the material influence the plastic flow localization both from point of view of the extension and its profile, figure 3, with implications on the material volume possible to be later loses at the contact with other abrasive particles, therefore on the abrasive wear of the material.

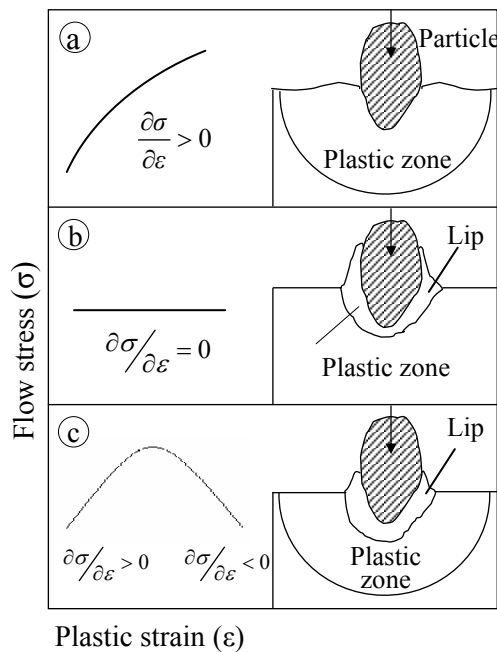


Fig. 3. The influence of the strain-hardening capability of a material on its localization during abrasion or erosion, [19]

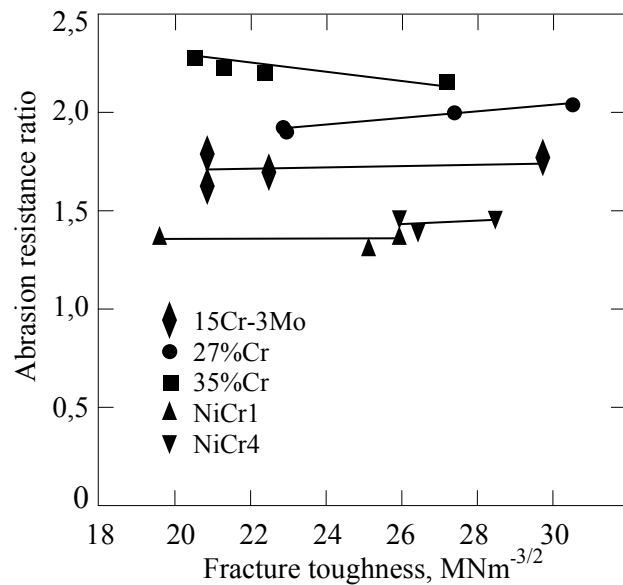


Fig. 4. Abrasion resistance ratio v. plane-strain fracture, [14]

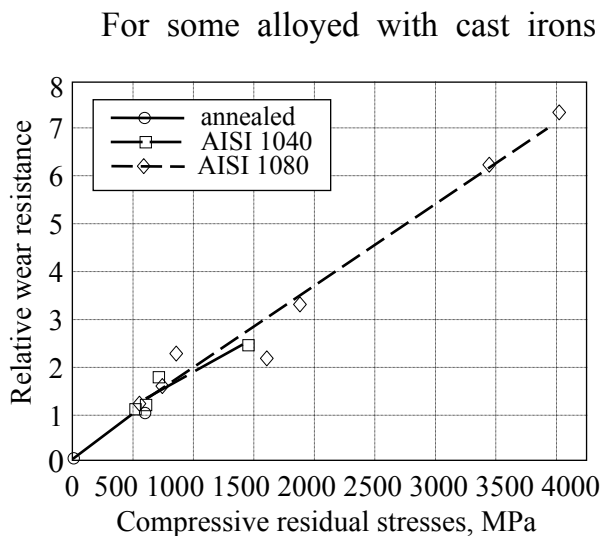


Fig. 5. Relative wear resistance as a function of compressive residual stress, [6]

For some alloyed with cast irons it was found, [14], the existence of one correlation between low stress abrasion and **fracture toughness** of these, the laboratory tests showing that in the case of the austenitic irons exists the better combination between abrasion resistance and their fracture toughness, figure 4.

On the basis of experimental results, that have showed that abrasion processes generate compression residual stresses in the wear surface, it was established one relation between abrasion resistance and the magnitude of these stresses, [6]. This relation shows a linear increase of the abrasion resistance with

the increase of the compression residual stresses, figure 5. Related to these results, it was concluded that abrasion resistance can be more really characterized by the residual stresses of the work hardenable materials than their bulk hardness and initial structure.

3. Conclusions

Abrasive wear resistance of the metallic materials is not an inherent property of these, but a result of the concrete conditions that have place the wear process. Both abrasion process and abrasion resistance are determined by those properties and characteristics that define the structural elements of the abrasive tribosystems and by the parameters that describe the interaction between the abraded material and abrasive material.

The microstructure of the metallic materials is one of the most adequate indicators for the abrasive wear resistance of these, but this relation must be extended in a more complex plan that includes in one unitary approaches the microstructural characteristics, alloy degree, nature and intensity of the solicitations.

The microstructure, hardness, type and magnitude of the residual stresses of the surfaces characterize more really abrasion resistance than material bulk hardness.

In that compression residual tensions generated by abrasion have observed in surface layers of some steels, and wear resistance increases with the increase of these tensions, can be considered for surface designed with pre-stressed surface layers that conduces to the abrasion increase.

References

1. Borik, F., Scholtz, W., G., Gouging Abrasion Tests for Materials used in Ore and Rock Crushing-Part. II: Effect of Metallurgical Variables on Gouging Wear. *Journal of Materials*, nr. 3, 1971, p. 590-605
2. Chen, H.-X., Chang, Z.-C., Lu, J.-C., Lin, H.-T., Effect of niobium on wear resistance of 15% Cr white cast iron. *Wear*, nr. 466, 1993, p. 197-201
3. Crețu, T., S., Mirica, R., F., Hârcu, I., Știuca, P., Fenomene fizice care determină duritatea materialelor. *Tribotehnica'87*, vol. II, 1987, p. 105-112
4. Crudu, I., Gramaticu, M., asupra criteriilor de tribomodelare în condiții de uzura abrazivă. *Tribotehnica'84*, vol. IV, 1984, p. 49-55
5. Fischer, A., Mechanism of high temperature sliding abrasion of metallic materials. *Wear*, vol. 152, nr. 1, 1992, p. 151-160
6. Garbar, I., I., Influence of residual stresses on abrasive wear resistance of steels. The 27th Israel Conference of Mechanical Engineering, Haifa, Israel, Mai 19-20, 1998, p. 647-649
7. Gramaticu, M., Crudu, I., Cercetări privind influența compoziției chimice asupra rezistenței la uzură în tribosistemele abrazive. *Tribotehnica'84*, vol. III, 1984, p. 153-158
8. Mutton, P., J., Watson, J., D., Some effects of microstructure on the abrasion resistance of metals. *Wear*, vol. 48, nr. 2, p. 385-398
9. Neculăiasa, V., Contribuții la studiul uzurii abrazive, factor al durabilității sculelor de prelucrat solul. Teză de doctorat, I. P. Iași, 1974
10. Parent-Simonin, S., Influence des facteurs métallurgiques essentiels sur la résistance à l'abrasion des fontes blanches. *Fonderie Fondateur d'Aujourd'hui*, nr. 399, 1980, p. 197-202
11. Pavelescu, D., Dumitrescu, C., Dependența rezistenței la uzura de abraziune a materialelor metalice de duritate, conținutul de carbon și structură. *Construcția de Mașini*, nr. 5, 1986, p. 253-257
12. Richardson, R., C., D., The Maximum Hardness of Strained Surfaces and the Abrasion Wear of Metals and Alloys. *Wear*, vol. 10, 1967, p. 353-382

13. Röhrig, K., Relations between structure and abrasion. Resistance of white cast iron. *Tribologia e Lubrificazione*, vol. XII, nr. 4, 1977, p. 148-150
14. Sare, I., R., Abrasion resistance and fracture toughness of white cast irons. *Metals Technology*, vol. 6, 1979, p. 412-419
15. Sare, I., R., Arnold, B., K., Dunlop, G., A., Lloyd, P., G., Repeated impact-abrasion testing of alloy white cast irons. *Wear*, vol. 162-164, 1993, p. 790-801
16. Shadrov, N., Sh. Korshunov, L., G., Cheremnyh, Blianie molibdena, vanadia, niobia na abraziynuyu iznosostoikost vysokohromistogo chuguna. *Metallovedenie i termicheskkaia obrabotka metallov*, nr. 4, 1983, p. 33-36
17. Sofroni, I., Ripoșan, I., Chira, I., Fonte albe rezistente la uzare. Editura Tehnica, București, 1987
18. Sundarajan, G., A New Model for Two-Body Abrasive Wear Based on the Localization of Plastic Deformation. *Wear*, vol. 117, 1987, p. 1-35
19. Sundarajan, G., The differential effect of the hardness of metallic materials on their erosion and abrasion resistance. *Wear*, nr. 162-264, 1993, p. 773-781
20. Ștefănescu, D., Crăciun, S., Fontes à 15% de chrome alliées au manganèse et au vanadium. *Fonderie*, nr. 364, 1977, p. 51-60
21. Tylczak, J., Abrasive wear. *ASM Handbook*, vol. 18, Lubrication and Wear Technology, USA, 1995, p. 184-190
22. Voinov, B., A., Vlianie legirovania i modifitsirovania belyh chgunov na strukturno-fazovoe sostoianie i iznosostoikost. *Trenie i iznos*, vol. 10, nr.1, 1989. p. 131-137
23. Zum Gaar, K., H., Modeling of Two-body Abrasive Wear. *Wear*, vol. 124, 1988, p. 87-103

Technical University "Gh. Asachi" Iassy

UZAREA SUPRAFETELOR METALICE ÎN TRIBOSISTEME ABRAZIVE

II: INFLUENȚA UNOR PROPRIETĂȚI ȘI CARACTERISTICI ALE MATERIALELOR METALICE ASUPRA REZISTENȚEI LA UZARE ABRAZIVĂ

Rezumat. Lucrarea își propune să prezinte într-o formă rezumativă, pe baza datelor existente în literatura de specialitate, o serie de elemente definiții pentru rezistența la abraziune a materialelor metalice, considerând în primul rând structura funcțională a tribosistemelor abrazive, precum și acele proprietăți și caracteristici ale materialelor metalice care influențează rezistența la abraziune a acestora. Datorită faptului că procesele de abraziune s-au dovedit a fi deosebit de complexe, o abordare corectă a oricărei probleme privitoare la rezistența la abraziune presupune includerea în contextul ipotezelor a faptului că rezistența la abraziune a materialelor metalice nu este o proprietate inerentă a acestora, ci un rezultat al condițiilor concrete în care are loc respectivul proces de uzare. Cu alte cuvinte, atât procesul de uzare și consecința acestuia, uzura, cât și rezistența la uzare sunt determinate de acele proprietăți și caracteristici care, în raport cu procesul de uzare, definesc elementele structurale ale tribosistemelor abrazive și de parametrii care descriu interacțiunea dintre materialul supus abraziunii și materialul abraziv.

Uzarea abrazivă a materialelor metalice este influențată în primul rând de microstructura acestora. Din acest considerent, relația dintre rezistența la abraziune și structură trebuie privită în contextul mult mai complex al dependenței dintre compoziția chimică, structură, proprietățile materialului. Se impune astfel o tratare unitară a tuturor aspectelor legate de caracteristicile microstructurale, gradul de aliere, tipul și nivelul solicitărilor.

Starea structurală a materialelor metalice constituie astfel unul dintre indicatorii cei mai relevanți pentru rezistența la abraziune a materialelor metalice.

THE WEAR OF THE METALIC SURFACES IN ABRASIVE TRIBOSYSTEMS III: THE INFLUENCE OF THE ABRASIVE MATERIAL, SOLICITATIOES AND ENVIRONMENT

MIREA CONSTANTIN

***Abstract.** The paper desire to presents synthetically the way in that the behavior and abrasive wear resistance of the metallic materials is influenced by some properties and characteristics of the abrasive materials, environment, as well as by the character of solicitations. The dates who is based the content of this paper constitute the result of one attentive survey of the special literature. Alongside the properties and characteristics of the metallic materials that influence their abrasive wear behavior or their abrasive wear resistance, intervene obviously and those properties and characteristics of the other elements that define the abrasive tribosystems, inclusive one series of elements of the interaction between abrasive material and surface who act. Abrasive wear resistance is influenced by the hardness, resistance, shape, size of the abrasive particles, compactness degree and humidity of the abrasive mass. One important property for the abrasive materials is considered their abrasion capability, expressed by an abrasion capability coefficient. The influence who the environment characteristics have on the abrasive wear is determined by some modifications of the surface, by modifications of some abrasive particles characteristics and of their motion way, by some modifications that can intervene in the wear mechanisms, as well as by interaction character between abrasive particle and surface. Because abrasive wear processes involve, in accordance with definition, relative motion and applied load, both worn surface aspect and wear evolution are determined by way that have place the motion and by the character of interaction between abrasive particle and surface.*

***Key words:** abrasive wear, abrasive wear resistance, abrasive particles, environment, solicitations*

1. Introduction

The abrasive wear of the metallic materials is influenced not only by their properties and characteristics but and a series of properties and characteristics of the abrasive materials, environment, as well as by the character of the solicitations. It can be found so, that abrasive wear depends by a great number of parameters and influence factors. The analysis of wear processes supposes to considering the whole ensemble of parameters, because how it was demonstrated, the influence of any parameter must be analyzed in the context of the all influence factors that act in one tribosystem.

Abrasive material, environment type and not at last the type and the nature of solicitations influence a large measure the behavior and the abrasive wear resistance of one material. The modification of some characteristics of the abrasive material, environment or solicitations determines characteristic aspects of the wear.

The paper presents on the basis of one attentive research of the special literature a date series and considerations regarding to influence of abrasive material, environment and solicitations on abrasive wear resistance of the metallic materials.

2. The influence of some properties and characteristics of the abrasive materials

Significantly for the character of the interaction between abrasive material and metallic surface is that for to be possible the predominant mechanical action of the abrasive it is necessary a hardness of the abrasive particles greater than that of the abraded material, a favorable geometry of particles and a certain orientation against the surface, [2].

For the abrasive tribosystems study, the essential property of any abrasive material is considered the **abrasion capability**, defined to being the capacity of the abrasive materials to degrade through wear the surface layers. It is a complex property that depend on physical and mechanical properties of the abrasive material, on his aggregate state (density, hardness, humidity, compactness, etc.), but and on the interaction character of the abrasive particles. Quantitatively, it is expressed by means of the *abrasion capacity coefficient*, k_d , [3]:

$$k_d = \frac{m_r}{m_{et}}, \quad (1)$$

where m_r is the wear in the considered abrasive material and m_{et} is the wear of the same material for standard abrasive material.

Abrasive hardness. Function of these, the wear evolution have, generally, an upward trajectory, but which can have particular aspects owing to some characteristics of the abrasive material, abraded material, corrosive action of the environment or dynamic character of the solicitations, [18], [23]. For abrasives with lesser hardness than those of abraded material on found a reduced wear, that can be determined to the abrasive characteristics loss and/or, in some cases, to the corrosive action of environment. When the abrasive hardness tends to the abraded material hardness it was found an important increase of the wear; the increase is more emphasized and more twisted for heterogeneous materials (steels with hard carbide insertions, alloy cast irons) owing to the different abrasive wear of the structural phases.

The **toughness** of abrasive particles is an important property of these and in the same time an important factor for abrasive wear processes. It was found that abrasive wear increases with the increase of the abrasive particles toughness, [16]. If during wear process in the abrasive particles appear tensions that, owing to solicitations, exceed their toughness, the abrasive particles can be destroyed, being formed other new particles and other contact surfaces for that will correspond other characteristic of the tensions state, [16].

The **shape and sizes** of the abrasive particles, inclusive their **orientation** against surface, determine characteristic aspects for the abrasive wear process, materialized by a certain wear evolution. The abrasive particles size (round, pointed) determines the wear groove shape and influences the contact load and the transition from elastic to plastic contact. Experimentally, it was found that the wear of one

metallic material is more reduced when the abrasive particle have rounded shapes comparative with the wear produces by abrasive particles with pointed edges and angles. This fact is explains by the different mechanisms that generate the material loss. Geometrical orientation of the abrasive particles, defined by their *attack angle*, can determine the predominant wear mechanism. For attack angle values lesser than *critical angle* the wear it can produces through plowing or scratching, and for upper values and the friction coefficient decrease the wear it can produces through microcutting.

In report with abrasive particles size, the wear increases with the size increase of these, [7], [8], [13], [15], [16], [20]. From some experimental researches results the existence of one *critical size* of the abrasive particles (that practically not depends on

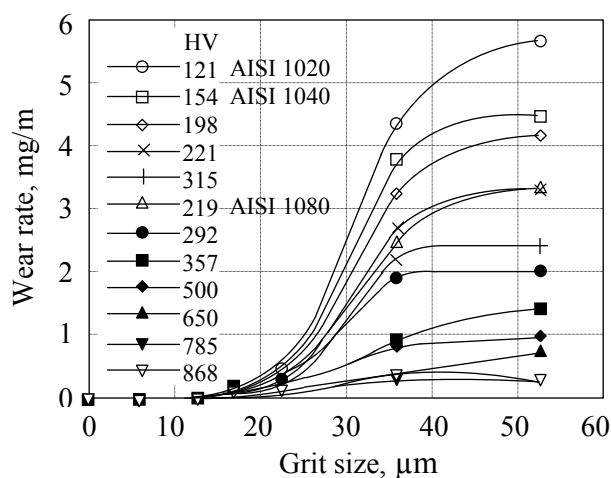


Fig. 1. Wear rate as a function of abrasive grit size, [7]

material hardness), [7], [8], in report with that the increase tendency of wear is more firmly for lesser abrasive particles, or more slowly for abrasive particle with greater sizes, figure 1. The wear evolution function of the abrasive particles size is influenced both by wear particles removed from wear surface, that decreases the abrasive particles action the more the lesser are these, and by the applied load, the wear being little influenced by the abrasive particles size in the low load application case.

Experimentally, it was found a relationship which shows that abrasive

wear varies with abrasive particle diameter at fourth power, [16]:

$$u = \frac{\gamma_a \cdot \text{tg}\gamma}{4 \cdot \tau_{\max}^2 \cdot C^2} \cdot k \cdot d^4, [\text{g}] \quad (1)$$

where: γ_a is the specific weight of abrasive particles;

γ - the point angle of abrasive particle;

τ_{\max} - maximum shear of abraded material, in daN/cm²;

C - constant in accordance with γ and friction on the contact surface;

k - pressure unity on surface, 1 daN/cm²;

d - the abrasive particle diameter, in cm;

For inhomogeneous abrasive mediums from point of view of the granulometric composition, it was found, [16], that abrasive wear varies with the percent fractions, the wear increasing with the increase of the abrasive particle percent of certain diameter, figure 2. For such abrasive mediums the relation (1) becomes:

$$u = \sum_{i=1}^{i=m} \frac{\gamma_a \cdot \text{tg}\gamma}{4 \cdot \tau_{\max}^2 \cdot C^2} \cdot d_i^4 \cdot n_i, [\text{g}] \quad (2)$$

where n_i is the abrasive particles number contained in the granulometric fraction "i".

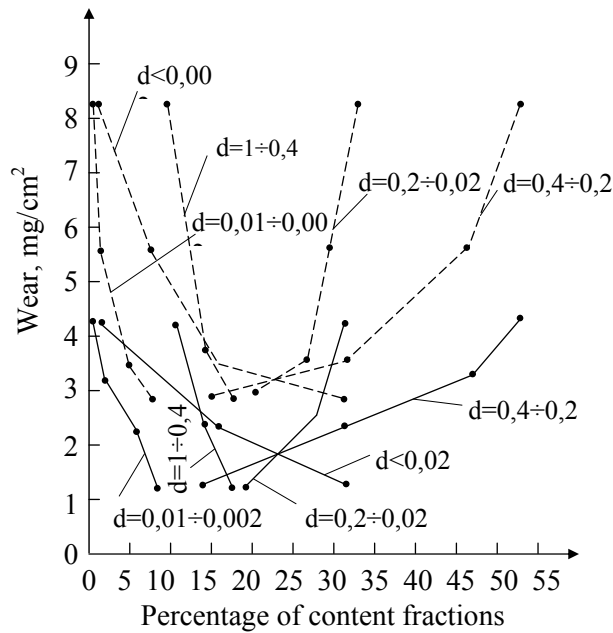


Fig. 2. Abrasive wear as function of the abrasive particles percentage, [16]

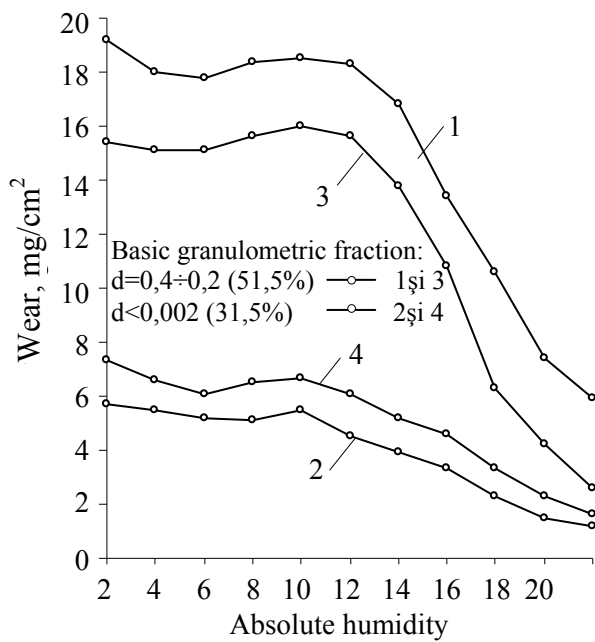


Fig. 3. Abrasive wear as function of the mass abrasive humidity, [16]

In the abrasive wear processes that have place in abrasive mass, the wear depends on the **compactness** of abrasive mass, increasing with the *compactness degree* increase, [1]. It is found also that metallic surface wear is influenced and by the abrasive mass **humidity**, the wear evolution with humidity increase depending however on abrasive mass composition, [16]. The wear decrease with humidity increase is argued through the modification of the abrasive particles interaction character with friction surface. The causative elements in this process are considered: the reduction of the abrasive particles efficiency because of the edges and angles damage, of the pressure decrease on the friction surface and of the formation of one molecular layer at interface between abrasive particle and abraded surface, [16].

3. The influence of the dynamic and cinematic characteristics of the contact

Because the abrasive wear process implies, in accordance definition, relative motion between abrasive material and one surface, the way in which have place the relative motion and the contact characteristics determine both wear aspects and his evolution.

Function of **friction way type** (closed or open), the wear evolution have an upward tendency that depends on the abraded material, abrasive medium, inclusive on the abrasive process type, [14], [15], [16]. The linear tendency of the wear increase with the **friction way length** in closed circuit is due to the fact that the wear surface is in permanent contact with abrasive material with non-modified characteristics by the previous actions. In open circuit, the wear tends to decrease after one spell owing to modification of some abrasive material characteristics, or owing to the accumulation of some wear particles between abrasive particles and/or some abrasive particles embedded on the wear surface, [2], [8].

The influence of the **wear process standing** is similarly to the friction way length.

In the abrasive tribosystems the solicitations are frequently expressed by **force** or **pressure on friction surface**. In similarly abrasive wear conditions, it can be seen an upward tendency of the abrasive wear evolution with the applied force increase. The wear magnitude and the function type that describes this connection depend on applied force magnitude, [2], [4], [15], [20], [22], abraded material type, shape, dimensions and abrasive particles toughness, [15], [20]. The applied pressure on the friction surface differently influences the abrasive wear evolution, being found experimentally that this depends on abrasive particles mobility: slow decreasing tendency with the applied pressure increase, for tests effected with bounded abrasives, [17], and upward tendency with pressure increase, figure 4, for tests effected with abrasive mass (free abrasives), [16]. The exercised influence by the pressure is greater when the abrasive hardness and abraded material hardness are lower, [16].

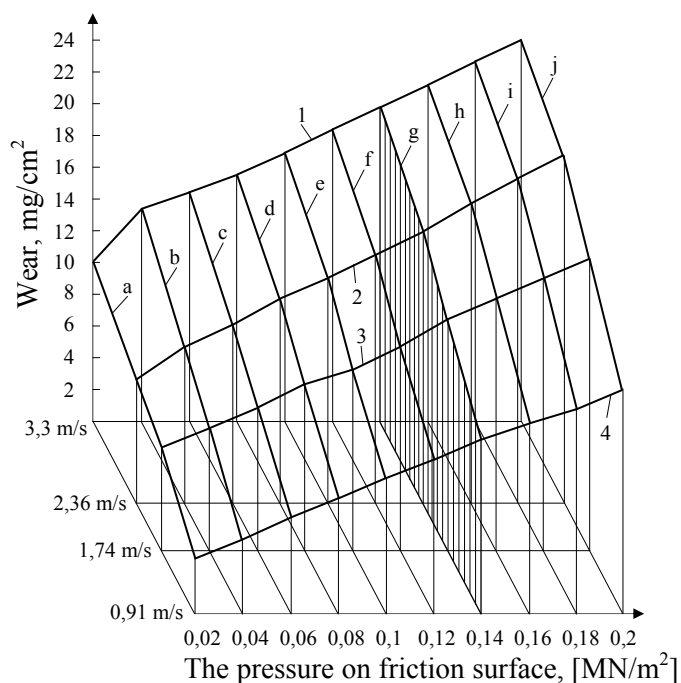


Fig. 4. Abrasive wear as function of applied pressure and speed on friction surface, [16]

increase, because of pressing dynamic force of the abrasive medium; with speed increase have place and an kinetic energy increase of the abrasive particle on the friction surface, [16], which conduces to conclusion that one particular influence can have and mobility degree of the abrasive particles.

3. The influence of some characteristics of the environment

The influence of the characteristics that define the environment on abrasive wear is determined by some modifications of active surface, of abrasive material, by

The results of some experimental tests as regards to the influence of **speed motion** on abrasive wear have distinguish different aspects that show either wear increase with speed motion increase, [2], [16], or an evolution that not follows a definite trend, [4]. The wear increase is argued by;

- the decrease of the mechanical characteristics under friction temperature effect, [2], effect considered to be reduced due to the fact that abrasive wear processes are near adiabatic, which should signify that temperature in the abrasive particle-abraded material local contact area is not influenced by the speed increase, [20];

- the pressure increase on friction surface with speed

modifications of the abrasive particles character motion, or by wear mechanisms modifications, inclusive by interaction character between abraded material and abrasive material.

The **water** presence like intermediary medium in the abrasive wear processes, can determines, in accordance to some special literature dates, contradictory aspects of abrasive wear:

- the wear increase, or wear rate increase, founded in laboratory tests, [5], and behind observations concerning the active elements wear of some crushing and pulverizing installations, [23], or of some rock drilling tools, [21], fact attributed and corrosion influence, [23];

- the wear decrease of some cobalt base alloys that contain titanium carbides insertions, used in sandstone cutting works, [12];

- minor modifications of wear speed, comparatively with the values obtained in dry air, founded for one Al-Mg-Si alloy, for copper and for an 0,45C steel, [10].

The abrasive wear increase in presence liquid mediums or in presence of **water vapors** is explained by fact that these mediums facilitate the material particles removal on wear surface, which have as consequence the preservation of the abrasive particles efficacy, [8].

The influence who liquid mediums, either water or aqueous solutions, have on abrasive wear, is principally determined by their **ph value**, [23]. In acid or corrosive medium the wear increase is due to the fact that the abraded metallic surfaces are more affected by corrosion, and oxide layers are removed by the abrasive particles, [20], [23]. Abrasive wear tests in corrosive mediums (siliceous sand-water, siliceous sand-sea water, siliceous sand-CuSO₄ solution) of some alloy Fe-C-Cr irons have showed that the wear metal loss are increased by the corrosive effects of the medium, the wear being started by one corrosion process between phases, matrix-carbide, followed by abrasive wear and corrosion of the matrix, [19].

Atmospheric humidity can differently influences the wear evolution, function of the test conditions, humidity level, abraded material, [20], [9], [10]. The wear rate increase with atmospheric humidity increase is principally due to the fact that humidity favors the abrasive particles fracture, [9], [10], [20], the fracture resistance of these decreasing with the increase of the partial pressure of water vapors from atmosphere, [11]. This phenomenon can contribute at wear increase in two ways:

- by fracture of the great abrasive particles, so resulting a greater number of abrasive particles, but with lesser sizes, in contact with wear surface;

- by self sharpening of the abrasive particles, due to some micro-volume fracture at surface level, there where exist cracking source in form of some surface defects.

The humidity is a factor that favors the deformation and fracture destruction of the resistant and adherent oxides layers formed on wear surface, [9].

The differences founded in wear evolution function of atmospheric humidity, figures 5 and 6, can be determined and by different modes testing, respective by more severe conditions that characterize the two-body abrasion tests, [10].

With the **environment temperature** increase, when the material hardness and ultimate strength decrease, it can be anticipated an increase of the abrasive wear, but in

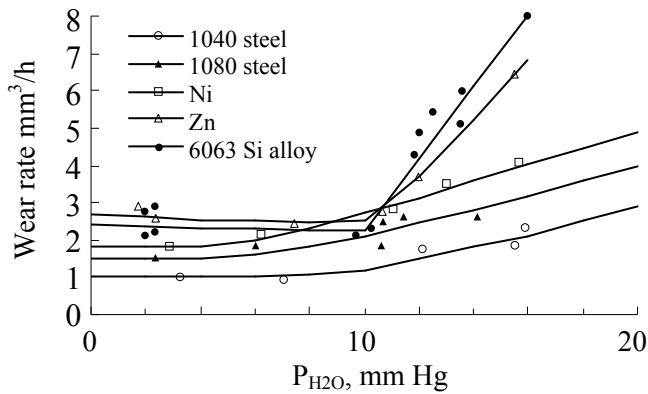


Fig. 5. Wear rate in 3-body abrasion vs. humidity, [9]

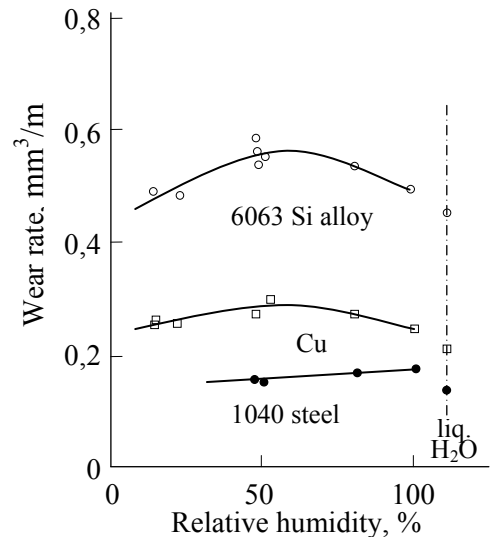


Fig. 6. Wear rate in 2-body abrasion vs. relative atmospheric humidity, [10]

the case of some experimental tests it was found nevertheless particular aspects, interpretable in the context of real tests conditions:

- minor modifications of the wear rate (for aluminum and copper), in the temperature range comprised between ambient temperature and 673K (400°C), fact explained in hypothesis of adiabatic heating of the micro-volumes from areas where the material is removed, [20];

- wear rate decrease for some Fe, Ni or Co base alloys with the temperature increase from 25°C to 650°C, figure 7. This tendency, more pronounced in the case of the alloys with softer metal matrix, is caused by the forming of some adherent layers on the wear surfaces and by the embedment of particles or fragment particles on the wear surfaces, both protecting the surfaces against abrasion and compensating in this way the effect of matrix softening with the temperature increase, [6].

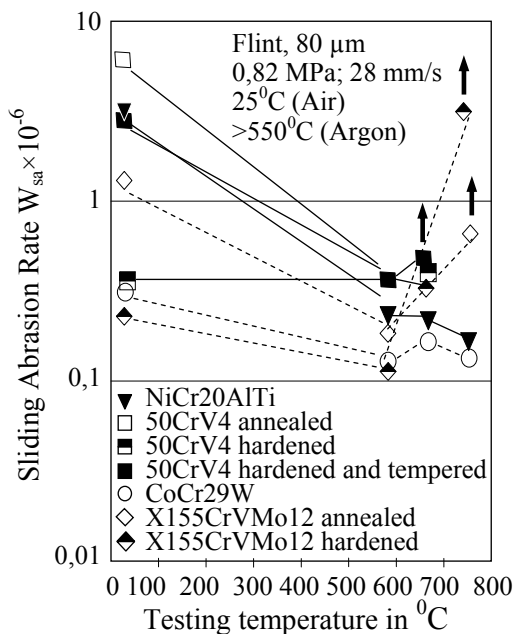


Fig. 7. Sliding abrasion rate of metallic materials up to 750 °C, [6]

4. Conclusions

An important property for any abrasive material is considered the abrasion capability, quantitatively expressed by an abrasion capability coefficient. The hardness, resistance, shape and size of the abrasive particles, their orientation against wear surface, granulometric composition, the compactness and humidity of the abrasive mass are characteristics that influence the abrasive wear resistance of the metallic materials.

Both wear aspects and his evolution are determined by the way in which have place the relative motion and by the contact characteristics between abrasive particles and surface against act.

In the abrasive tribosystems the solicitations are frequently expressed by force or pressure on friction surface. In similarly abrasive wear conditions, the abrasive wear evolution have an upward tendency with the applied force increase. The applied pressure on the friction surface differently influences the abrasive wear evolution, being found experimentally that this depends on abrasive particles mobility. The exercised influence by the pressure is greater when the abrasive hardness and abraded material hardness are lower.

The influence of the characteristics that define the environment is determined by some modifications of active surface, of abrasive material, by modifications of the abrasive particles character motion, or by wear mechanisms modifications, as well as by the interaction character between abraded material and abrasive material. It is not clear how the atmospheric humidity influence the wear process.

References

1. Bilik, S., M., Papy trenya metall-plastmassa v machinah i mehanismas. Izdatelstvo Mashinostroenie, Moskva, 1966
2. Blouet, J., Etudes de laboratoire en liaison avec des cas industriels. Soudage et Techniques Connexes, vol. 32, nr. 5/6, 1978, p. 199-126
3. Crudu, I., Gramaticu, M., Asupra criteriilor de tribomodelare în condiții de uzură abrazivă. Tribotehnica'84, vol. IV, I. P. Iași, 1984, p. 49-55
4. Das, S., Prasad, B., K., Jha, A., K., Modi, O., P., Yewngneswaran, A., H., 3-Body Abrasive Wear of 0,98-Percent carbon-Steel. Wear, vol. 162, 1993, p. 802-810
5. Dawihl, W., Frisch, B., Wear properties of tungsten carbide and aluminum oxide sintered materials. Wear, nr. 12, 1968, p. 17-25
6. Fischer, A., Mechanism of high temperature sliding abrasion of metallic materials. Wear, vol. 152, nr. 1, 1992, p. 151-160
7. Garbar, I., I., Influence of residual stresses on abrasive wear resistance of steels. The 27th Israel Conference of Mechanical Engineering, Conference Proceeding, Mai 19-29, Technion City, 1988, Haifa, Israel, p. 647-649
8. Larsen-Basse, J., Influence of grit diameter and specimen size on wear during sliding abrasion. Wear, Nr. 12, 1968, p. 35-53
9. Larsen-Basse, J., Influence of Atmospheric Humidity on Abrasive Wear-I. 3-Body Abrasion. Wear, vol. 31, nr. 2, 1975, p. 373-379
10. Larsen-Basse, J., Influence of Atmospheric Humidity on Abrasive Wear-I. 2-Body Abrasion. Wear, vol. 32, 1975, p. 9-14
11. Larsen-Basse, J., Effect of Atmospheric Humidity on the Dynamic Fracture Strength of SiC Abrasives. Wear, vol. 166, nr. 1, 1993, p. 93-100

12. Latin, A., The properties of tungsten carbide-cobalt alloys used for mineral cutting tools. *Metallurgia*, nr. 64, 1961, p. 211-216, 267-273
13. Maratray, F., Le procès d'usure des matériaux soumis à l'abrasion. *Revue de l'Industrie Minérale*, nr. 11, 1970, p. 713-734
14. Mulhean, T., O., Samuels, L., E., The abrasion of metals. A model of the process. *Wear*, nr. 5, 1962, p. 478-498
15. Nathan, G., K., Jones, J., D., The empirical relationship between abrasive wear and the applied condition. *Wear*, nr. 9, 1966 p. 300-309
16. Neculăiasa, V., Contribuții la studiul uzurii abrazive, factor al durabilității sculelor de prelucrat solul. Teză de doctorat, I. P. Iași, 1974
17. Richardson, R., C., D., The Wear of Metals by Hard Abrasives. *Wear*, vol. 10, 1967, p. 291-309
18. Rohrig, K., Relations between structure and abrasion resistance of white cast iron. *Tribologia e Lubrificatione*, vol. XII, nr. 4, 1977, p. 141-150
19. Sofroni, I., Ripoșan, I., Chira, I., Fonte albe rezistente la uzare. Editura Tehnică, București, 1987
20. Tylczak, J., Abrasive wear. A.S.M. handbook, vol. 18, Friction, Lubrification and Wear Technology, U.S.A., 1995, p. 184-190
21. Wahl, H., Kantenwein, G., Schafer, W., Wear in rock drilling (laboratory tests). *Wear*, vol. 4, nr.3, 1961, p. 234-245
22. Xu, L., Vose, C., St. John, D., Abrasive wear study of selected White cast irons as liner materials for the mining industry. *Wear*, nr. 162-164, 1993, p. 820-832
23. *** La résistance a l'usure des matériaux. *Fonderie-Fondeur d'Aujourd'hui*, nr. 25, 1983, p. 33-35

Technical University "Gh. Asachi" Iassy

UZAREA SUPRAFETELOR METALICE ÎN TRIBOSISTEME ABRAZIVE III: INFLUENȚA MATERIALULUI ABRAZIV, A SOLICITĂRILOR ȘI A MEDIULUI INTERMEDIAR

Rezumat. Lucrarea încearcă să prezinte într-un mod sintetic modul în care comportarea și rezistența la uzare abrazivă a materialelor metalice este influențată de unele proprietăți și caracteristici ale materialelor abrazive, mediului intermediar, precum și de caracterul solicitărilor din tribosistemele abrazive. Datele pe care se bazează conținutul lucrării constituie rezultatul unei cercetări aprofundate a literaturii de specialitate. Alături de acele proprietăți și caracteristici ale materialelor metalice care influențează comportarea și rezistența la abraziune a acestora, intervin în mod evident și acele proprietăți și caracteristici ale celorlalte elemente care definesc tribosistemele abrazive, precum și o serie de elemente proprii ale interacțiunii dintre materialul abraziv și suprafața asupra căreia acționează. Rezistența la abraziune este influențată de duritatea, rezistența, forma și dimensiunile particulelor abrazive, gradul de compactitate și umiditatea masei abraziv. O proprietate importantă pentru materialele abrazive este considerată abrazivitatea acestora, exprimată prin coeficientul de abrazivitate, k_a . Influența pe care caracteristicile mediului intermediar o au asupra uzurii abrazive este determinată de unele modificări care se produc la nivelul suprafețelor, de modificări ale unor caracteristici ale particulelor abrazive și ale modului de mișcare a acestora, de unele modificări care pot interveni la nivelul mecanismelor de uzare, precum și de caracterul interacțiunii particulă abrazivă-suprafață. Deoarece procesele de uzare abrazivă implică, conform definiției, mișcare relativă și sarcină aplicată, atât aspectul suprafețelor uzate cât și evoluția uzurii sunt determinate de modul în care are loc mișcarea și de caracterul interacțiunii particulă abrazivă-suprafață.

MICROSTRUCTURAL CHARACTERISATION AND ELECTROCHEMICAL BEHAVIOUR OF THE NEW BETA Ti-12Mo-5Ta ALLOY FOR BIOMEDICAL APPLICATIONS

D.M. Gordin^{*}, T. Gloriant^{*}, R. Chelariu^{**}, Gh. Nemtoi^{***}, N. Aelenei^{**}

Abstract. *We have synthesized a new Ti-based alloy that combines Ti with the non-toxic elements Ta and Mo. Ingot of composition Ti-12Mo-5Ta was prepared by melting pure elements in an arc-melting furnace. The alloy was annealed at 950°C for one hour under high vacuum and quenched in water at room temperature. The alloy was characterized by X-ray diffraction, observed by microscopy and found to have a body-centered-cubic structure (β -type). We have measured the Young's modulus of Ti-12Mo-5Ta by ultrasonic technique and found a lower value (about 74GPa) than the classical $\alpha+\beta$ Ti-6Al-4V alloy (120GPa). As long-term stability in biological environment is required, we have evaluated the electrochemical behavior of both alloys. Experiments, i.e. measurements of open-circuit potential (OCP) versus time and the observation of linear and cyclic potentiodynamic polarization curves, were carried out in simulated body fluid (Ringer's solution) for two immersion times. Under these conditions both titanium alloys exhibit spontaneous passivity and high corrosion resistance. The excellent electrochemical properties combined with low elastic modulus make the new beta-type Ti-12Mo-5Ta alloy suitable for use as a bone substitute.*

Keywords: *Metals and alloys; X-ray diffraction; Microstructure; Electrochemical properties*

1. INTRODUCTION

The great complexity of conditions imposed for a biomaterial makes its choice for a certain application very difficult. Selecting materials for different components in biomedical devices depends especially on several factors. First, the material must be biocompatible to human body. On top of that, it must have an excellent corrosion resistance in the body environment and appropriate mechanical properties in service. For a material used as bone substitute the Young's modulus is a key factor in order to transfer the adequate mechanical stress to the surrounding bone. Decreasing this modulus, thereby increasing elasticity, enhances implant-to-bone stress loading and minimizes bone atrophy due to stress shielding. Titanium and titanium alloys are well-suited as clinically used biomaterials because their biological, mechanical and physical properties play significant roles in the longevity of the prostheses and implants [1]. The "standard" Ti-6Al-4V (currently used in aircraft industry) was one of the first titanium biomaterial introduced in implantable components and devices (particularly for orthopedic and osteosynthesis applications [2]). Although this alloy is still widely used in medicine, some concern has been recently expressed over its use since it appears that small amounts of both vanadium and aluminum, released in the human

body, induce possible cytotoxic effect and neurological disorders, respectively [3-5]. Thus, toxicity of alloying elements like V and Al and high elastic modulus (due to the 2 phases $\alpha+\beta$ microstructure) of the conventional Ti-6Al-4V alloy has required the development of new β -titanium alloys with non-toxic elements (Nb, Zr, Ta, Mo, Pd...). Advantages of β /near- β titanium alloys over α near- α or $\alpha+\beta$ alloys include their lower modulus [8-10] and better formability [11-16]. Consequently, β -titanium alloys allow a greater load transfer from the artificial implant to the adjacent remodeled bone. The bone resorption is then minimized and a possible loosening of the prosthetic device is avoided [17,18]. Recently, many materials research groups in the field of metallic biomaterials have oriented their activities towards the modification of the available β -titanium alloys or exploring new compositions. The most investigated β -titanium alloys for biomedical applications were included in the Ti-Ta, Ti-Zr-Nb-Ta, Ti-Nb-Zr, Ti-Nb, Ti-Sn-Nb-Ta, Ti-Sn-Nb-Ta-Sb and Ti-Nb-Ta-Mo systems. For these alloys the Young's modulus varies between 60 GPa and 90 GPa [19] while the Ti-6Al-4V modulus is \sim 110-120 GPa [20].

Our research activity deals with the metallurgical aspects and the mechanical properties of new β titanium alloys in the Ti-Mo-Ta and Ti-Mo-Fe-Ta systems [21,22]. Because the biocompatibility/biofunctionality is related to the corrosion behavior in physiological fluid, this papers presents our first electrochemical experiments of a β -type Ti-12Mo-5Ta alloy in Ringer's solution. The results were compared to those obtained on the Ti-6Al-4V commercially alloy in similar experimental conditions.

2. EXPERIMENTAL PROCEDURES

Because of the high reactivity of titanium with both oxygen and nitrogen, synthesis must be carried out under high vacuum conditions. Appropriate amounts of metals (83wt%Ti-12wt%Mo-5wt%Ta) were arc melted in a laboratory scale arc furnace (7400 TUBINGEN, Edmund Bühler), with a tungsten alloy electrode on a water-cooled copper heart. The pure elements were melted in a high purity argon atmosphere (0.5 bar) and the ingot were melted many times to improve chemical homogeneity. The obtained ingot (shape almost cylindrical with a diameter of about 8-10mm and weight of about 12 g) was solution treated at 950°C under high vacuum (10^{-6} mbar) for one hour into a tubular furnace and then quenched in water at room temperature. The purpose of this heat treatment is to produce the desired homogenous β -microstructure alloyed with β -stabilizers (Ta and Mo).

The commercially Ti-6Al-4V alloy (90wt%Ti-6wt%Al-4wt%V) was produced by CEZUS-Ugine (France) and was supplied in a 7mm diameter rod after a heat treatment at 730°C for 1 hour.

The phase analysis of the synthesized Ti-12Mo-5Ta and Ti-6Al-4V alloys were carried out by X-ray diffraction (XRD) using a PHILIPS PW 1830/00 (X-ray generator) diffractometer operated at 40kV and 30 mA ($\text{CuK}_{\alpha 1}$ radiation (1.54060Å wave length) was used).

The microstructures of the alloys were investigated both by optical microscopy (OM, LEICA DM/RM) and by scanning electron microscopy (SEM, JEOL JSM 6400). To be observed, the samples were embedded in an electrically conducting cold-setting resin (Polyfast 485) and then mirror polished by standard metallographic techniques followed by etching with 5% HF, 25 % HNO_3 and the balance H_2O . The

chemical composition of the Ti-12Mo-5Ta alloy was checked by EDS (energy-dispersive spectroscopy coupled with the scanning electron microscope).

Elastic modulus (Young's modulus E) of designed alloy was determined by ultrasonic method from the density (ρ) and from the measurements of the longitudinal V_L and the transversal V_T wave velocities. A piezo-electric transducer (10 MHz), in contact with the sample via a coupling gel, was used for these measurements. Thus, the value of the Young's modulus for the infinite mode can be obtained from equation 1:

$$E = \rho \frac{3V_L^2 - 4V_T^2}{\frac{V_L^2}{V_T^2} - 1} \quad (1)$$

The corrosion behavior of titanium alloys was carried out in a simulated body fluid, namely Ringer's solution, supplied by SICOMED S.A., Bucharest, Romania. The ionic composition of this medium was: $\text{Na}^+=3.38$ g/l ; $\text{K}^+=0.157$ g/l ; $\text{Ca}^{2+}=0.0195$ g/l ; $\text{Cl}^-=5.525$ g/l and the pH was maintained at 5.13. To investigate the electrochemical behavior a three electrodes corrosion cell and an electrochemical system VOLTALAB 32 were used.

Samples (with a surface of 0.283 cm² for Ti-12Mo-5Ta and 0.302 cm² for Ti-6Al-4V) were mounted on a teflon suitable holder and polished to a mirror finish. A saturated calomel electrode and a platinum wire were used as the reference and auxiliary electrodes, respectively. The electrochemical testing sequence was consisted of the recording open circuit potential (*OCP*), linear and cyclic potentiodynamic polarization curves. Open circuit potentials were recorded with a 15 min time increment over a 20 h time period. The linear potentiodynamic polarization curves, tracing between (*OCP*-150; *OCP*+150, mV) with a 0.5 mV/s scanning rate, were used to measure the polarization resistances (R_p , $\Omega \cdot \text{cm}^2$) and Tafel's slopes (b_c and b_a , mV/mA $\cdot\text{cm}^2$) from which the corrosion current densities (J_{corr} , mA/cm²) were deduced. The cyclic potentiodynamic polarization curves, tracing between -400, 2000, -400 mV with a 50 mV/s scanning rate, were used to evaluate the passivation potentials (E_p , mV) and critical current densities (J_{cr} , mA/cm²). Also, cyclic polarization curves indicated the pitting tendencies of investigated alloy specimens in the given electrochemical systems. All the experimental data were statistically analyzed using *t*-test from independent variables.

3. RESULTS

Figure 1.a. shows the XRD pattern of the Ti-12Mo-5Ta alloy after melting and quenching operations. The desired bcc (body-centered-cubic) single β -phase is detected and corresponding diffraction planes are well identified.

The X-ray diffraction profile presented in Figure 1.b. clearly shows the duplex microstructure of the "standard" Ti-6Al-4V alloy. All the diffracted peaks, related to the α -phase and the β -phase, are identified and the corresponding Miller indices are indicated on the pattern. With this alloy composition, it is well known that Al stabilizes the low-temperature α -phase (hexagonal close packed, hcp), while V stabilizes a small amount of the high-temperature β -phase (body-centered cubic, bcc).

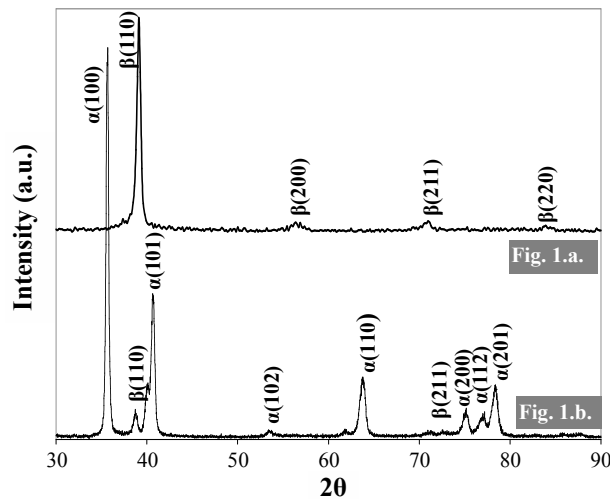


Figure 1. XRD patterns of Ti-12Mo-5Ta (a) and Ti-6Al-4V (b).

The two alloys were observed by microscopy and the optical micrographs are presented in Figure 2. For the Ti-12Mo-5Ta alloy, few hundred micrometer large granular β -type structure (Figure 2.a) is observed, while the typical equiaxed 2 phases $\alpha+\beta$ microstructure is observed in Ti6Al4V alloy (Figure 2.b).

The Young's modulus, E , evaluated by ultrasonic technique (see *experimental procedures*), are found to be very different from the two alloys studied in this work. A value of 120GPa is measured on the Ti-6Al-4V alloy while 74GPa is obtained in the case of the beta Ti-12Mo-5Ta alloy.

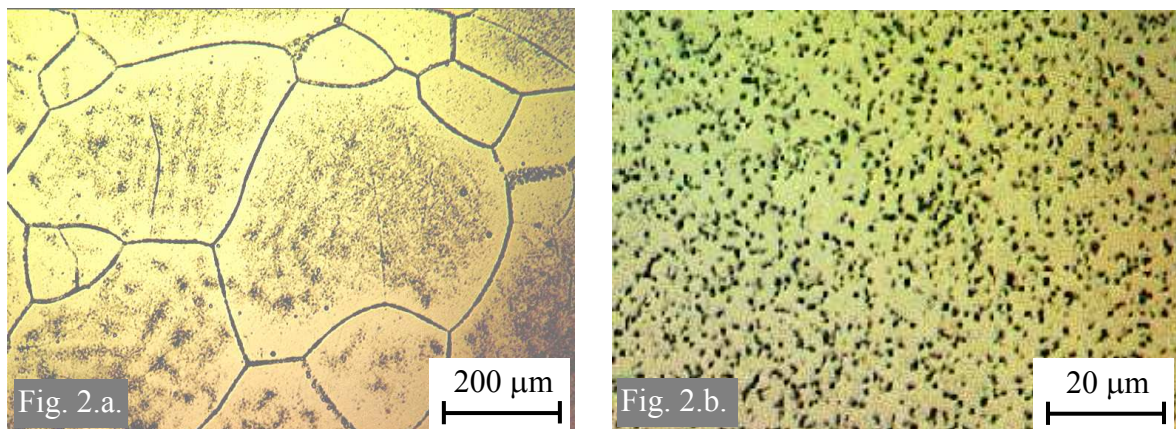


Figure 2. Optical micrographs of Ti-12Mo-5Ta (a) and Ti-6Al-4V (b).

To evaluate the electrochemical properties of the metallic materials, examples of experimental measurements are presented in Figures 3, 4 and 5. Figure 3 shows the evolution of the open-circuit potential (OCP) versus time for both alloys. As it is shown on this diagram, it is observed a very similar behavior among OCP mean values of Ti-Mo-Ta alloy and Ti-Al-V alloy.

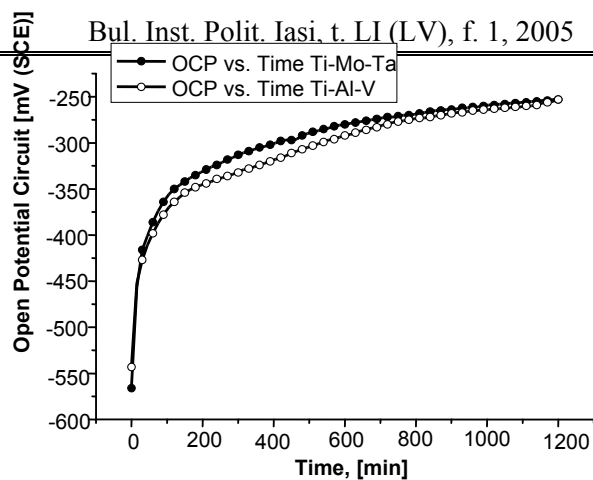


Figure 3. Open potential circuit (OCP) versus time for the studied titanium-based alloys: Ti-12Mo-5Ta alloy (black circles) and Ti-6Al-4V alloy (white circles).

Some curves concerning the new Ti-12Mo-5Ta alloy, which were obtained by linear and cyclic voltammetry, are presented, for two different immersion time, in Figure 4 and Figure 5, respectively.

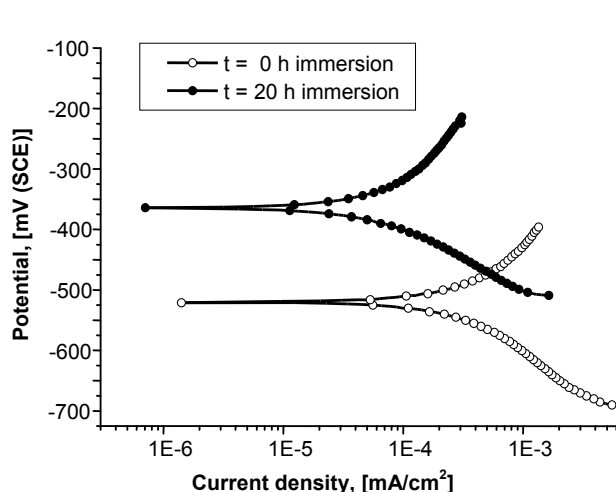


Figure 4. Linear potentiodynamic polarization curves (potential versus current density) of Ti-12Mo-5Ta alloy for two immersion times: 0h (white circles) and 20h (black circles).

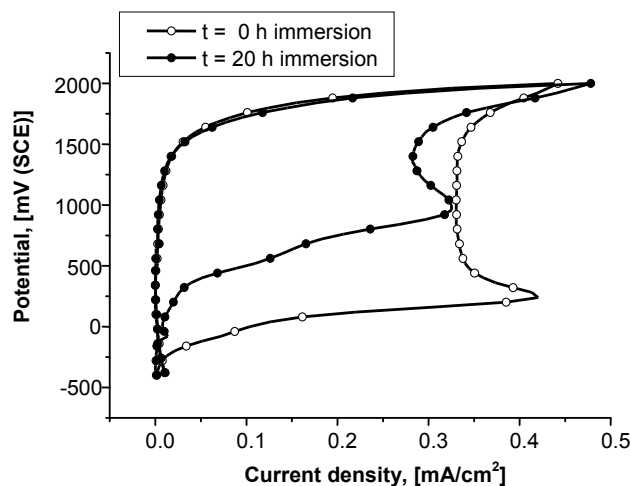


Figure 5. Cyclic potentiodynamic polarization curves of Ti-12Mo-5Ta alloy for two immersion times: 0h (white circles) and 20h (black circles).

In Table 1 are reported all the data for both Ti-12Mo-5Ta and Ti-6Al-4V alloys after immersions of 0h and 20h. In this table are indicated the mean values (with the corresponding standard deviation) of the corrosion parameters deduced from the linear voltammetry potential (such as the corrosion rate, R_{corr} , for example) and those obtained from the cyclic voltammetry evaluation (such as the passivation potentials, E_{pas}).

The corrosion potential (E_{corr}), the Tafel slopes (b_a and b_c), the polarization resistance (R_p), the corrosion current density (J_{corr}) and the corrosion rate (R_{corr}) are measured from the linear potentiodynamic curves. The critical anodic current densities (J_{cr}), the primary passivation potentials (E_{pas}) and the minimum passivation current density (J_{pas}) are obtained from the cyclic potentiodynamic polarization curves.

Table 1

Electrochemical measurements of Ti-12Mo-5Ta and Ti-6Al-4V in Ringer's solution

| CORROSION PARAMETERS (mean value (std. dev.)) | TITANIUM ALLOYS | | | |
|---|--|---|--|---|
| | Ti-12Mo-5Ta | | Ti-6Al-4V | |
| | 0 h immersion | After 20 h immersion | 0 h immersion | After 20 h immersion |
| E_{corr} , [mV (SCE)] | -532.5 (16.26) | -321.0 (60.81) | -549.5 (20.51) | -317.0 (9.90) |
| b_a , [mV/decade] | 75.72 (6.060) | 54.25 (31.247) | 94.65 (7.573) | 59.23 (2.482) |
| $-b_c$, [mV/decade] | 71.38 (5.388) | 33.04 (21.920) | 72.26 (10.946) | 31.45 (4.978) |
| $10^{-6} R_p$, [ohm cm ²] | 0.09 (0.004) | 0.76 (0.488) | 0.11 (0.014) | 1.08 (0.389) |
| J_{corr} , [mA/cm ²] | 17.50×10^{-5} (0.849×10^{-5}) | 1.18×10^{-5} (0.021×10^{-5}) | 16.40×10^{-5} (4.101×10^{-5}) | 0.87×10^{-5} (0.240×10^{-5}) |
| R_{corr} , [μm/an] | 2.590 (0.1273) | 0.175 (0.0071) | 3.455 (0.8556) | 0.185 (0.0495) |
| E_{pas} , [mV] | 260.0 (28.28) | 921.0 (56.57) | 302.5 (139.30) | 861.0 (28.28) |
| J_{cr} , [mA/cm ²] | 0.396 (0.0339) | 0.344 (0.0262) | 0.336 (0.0403) | 0.392 (0.0679) |
| J_{pas} , [mA/cm ²] | 0.331 (0.0007) | 0.294 (0.0169) | 0.243 (0.0014) | 0.235 (0.0078) |

4. DISCUSSION

As observed, a new single phase beta-type titanium alloy was successfully synthesized with the Ti-12Mo-5Ta chemical composition. The value of the beta-stabilizer equivalence (%Mo_{eq}) is calculated to be 13.1 wt%, more than 10.0 wt%, which classified this alloy in the β-metastable category. The elementary cell parameter of the structure can be evaluated from the determination of each peak position in the X-ray diffraction pattern (computed by the Rietveld method, MAUD software) and a value of $3.2625 \pm 0.0008 \text{ \AA}$ is found. This value is reduced of 1.32% by comparison with the elementary cell parameter of pure titanium (3.3060 Å) and can be explained by the difference between the atomic radius of pure titanium (1.47 Å) and the atomic radius of substitutional alloying elements Ta (1.49 Å) and Mo (1.39 Å) in the solid solution.

The elastic modulus measured on Ti-12Mo-5Ta (74GPa), much lower than the one obtained on Ti-6Al-4V (120GPa), presents a similar order of magnitude by comparison with the modulus of recent developed β type alloys. This is due to the fact that the Ti-12Mo-5Ta alloy is purely a beta body-centered cubic (bcc) structure (Ti-6Al-4V is a two-phase alloy: hexagonal (hcp) alpha + body-centered cubic (bcc) beta); but it is also well known that, as far as an alloy with fixed fractions of different phases is concerned, elastic modulus mainly depends on chemical composition [14]. It has been shown [19] that the value of Young's modulus decreased with the increase of both the bond strength (between Ti and alloying elements) and the metal d-orbital energy level (which is correlated with electronegativity and the metallic radius elements).

Statistical analysis of the electrochemical measurements of both alloys presented in Table 1 showed a similar electrochemical behavior. The two mean values of the both primary passivation potentials (E_{pas}) and critical anodic current densities

(J_{cr}) are not significantly different. On the other hand, the cyclic potentiodynamic polarization curves showed that the pitting corrosion there is not.

Due to the microstructure difference between Ti-6Al-4V and Ti-12Mo-5Ta, different mechanical properties are observed. Alpha-beta alloys are shown to exhibit tensile strength of about 850-950 MPa (and hardness of 330-340HV), while in beta titanium alloys a tensile strength from 490 to 1000MPa is observed. On the other hand, microhardness can vary between 180 and 330HV, depending on the type and the amount of β -stabilizer alloying element (Nb, Zr, Ta, Mo). In literature, β -type titanium alloys show excellent wear resistance when zirconia ball is used as a mating material, while opposite trends are observed when alumina ball is used as a mating material in air and Ringer's solution. Consequently, "tribocorrosion" aspect of titanium as biomaterials must be investigated further and will be the subject of our future work.

5. CONCLUSIONS

We have characterized the new Ti-12Mo-5Ta alloy by X-ray diffraction and by microscopy, and measured the elastic modulus (Young's modulus) by ultrasonic technique. The results were compared to the standard Ti-6Al-4V alloys. The Ti-12Mo-5Ta alloy has a body-centered-cubic structure (β -phase). It had a lower Young's modulus (about 74GPa) than the classical α/β Ti-6Al-4V alloy (120GPa), which is much better in order to use it as hip prostheses and to avoid stress shielding and thus prevent bone resorption.

We have investigated the electrochemical properties of both titanium alloys in a simulated body fluid. Consequently, we have measured the open-circuit potential (OCP) upon time and observed the linear and cyclic potentiodynamic polarization behavior in Ringer's solution for two different immersion times. Similar passivation potentials (E_{pas}) and critical anodic current densities (J_{cr}) are observed in both cases: the passive film has a very good stability and is not influenced by the chemical composition.

As titanium alloys are to be used as implants or prostheses, they must be highly biocompatible and have essential properties such as a good resistance to corrosion, a small modulus, and a good adhesion to tissues. Thus, the new β -metastable Ti-12Mo-5Ta alloy represents a good compromise in order to use it as a bone substitute.

Acknowledgements

The authors would like to thank the following organizations: "Région Bretagne" and "Rennes Métropole" for support and for providing help to purchase equipment.

Received, April 25th, 2005

* *Institut National des Sciences Appliquées de Rennes (INSA Rennes),
Groupe de Recherche en Chimie-Métallurgie, France*
** *"Gh. Asachi" Technical University of Iasi*
*** *"Al. I. Cuza" University of Iasi*

References

- [1] M. Niiomi, Metall. Mater. Trans. A 33 (2002) 477.
- [2] M.C. García-Alonso, L. Saldaña, G. Vallés, J.L. González-Carrasco, J. Gonzáles-Cabrero, M.E. Martínez, E. Gil-Garay, L. Munuera, Biomaterials 24 (2003) 19.

- [3] S.G. Steimann, in: G.D. Winter, J.L. Leray and K. de Groot (Eds.), *Biomaterials*, John Willey & Sons Inc., 1980, p.1.
- [4] Y. Okazaki, E. Nishimura, *Mater. Trans.* 41 (2000) 1247.
- [5] Y. Okazaki, S. Rao, S. Asao, T. Tateishi, S. Katsuda, Y. Furuki, *Mater. Trans.* 39 (1998) 1053.
- [6] U. Kamachi Mudali, T.M. Sridhar, B. Raj, *Sādhanā* 28 (2003), 601.
- [7] M.A. Khan, R.L. Williams, D.F. Williams, *Biomaterials* 20 (1999) 631.
- [8] Z. Cai, T. Shafer, I. Watanabe, M.E. Nunn, T. Okabe, *Biomaterials* 24 (2003) 213.
- [9] J.A. Davidson, A.K. Mishra, P. Kovacs, R.A. Poggie, *Bio-Med. Mater. Eng.* 4 (1994) 231.
- [10] K. Maehara, K. Doi, T. Matsushita, Y. Sasaki, *Mater. Trans.* 43 (2002) 2936.
- [11] M.J. Donachie, in: M.J. Donachie (Ed.), *Titanium: a technical guide*, vol.31. ASM International: Metal Park, OH, 1989, p. 218.
- [12] D.J. Lin, J.H. Chern Lin, C.P. Ju, *Biomaterials* 23 (2002) 1723.
- [13] M. Niiomi, T. Hattori, K. Morikawa, T. Kasuga, A. Suzuki, H. Fukui, S. Niwa, *Mater. Trans.* 43 (2002) 2970.
- [14] Y. Song, R. Yang, Z-X. Guo, *Mater. Trans.* 43 (2002) 3028.
- [15] I. Weiss, S.L. Semiatin, *Mater. Sci. Eng. A* 243 (1998) 46.
- [16] S. Ankem, C.A. Greene, *Mater. Sci. Eng. A* 263 (1999) 127.
- [17] M. Niiomi, *Mater. Sci. and Eng. A* 243 (1998) 231.
- [18] M. Long, H.J. Rack, *Biomaterials* 19 (1998) 1621.
- [19] D. Kuroda, M. Niiomi, M. Morinaga, Y. Kato, T. Yashiro, *Mater. Sci. and Eng. A* 243 (1998) 244.
- [20] Y-H. Hon, J-Y. Wang, Y-N Pan, *Mater. Trans.* 44 (2003) 2384.
- [21] D.M. Gordin, T. Gloriant, G. Texier, I. Thibon, D. Ansel, J.L. Duval, M.D. Nagel, *J. Mater. Sci. : Mater. Med.* (2004), submitted.
- [22] F. Guillemot, F. Prima, R. Bareille, D.M. Gordin, T. Gloriant, M.C. Porté-Durrieu, D. Ansel, *Ch. Baquey, Med. Biol. Eng. Comp.* 42 (2004) 137.

CARACTERIZAREA MICROSTRUCUTRALA SI COMPORTAREA ELECTROCHIMICA A NOULUI ALIAJ Ti-12Mo-5Ta PENTRU APLICATII BIOMEDICALE

(REZUMAT)

Un nou aliaj Ti-12Mo-5Ta a fost elaborat prin topirea elementelor pure intr-un cuptor cu incalzire prin arc electric. Aliajul a fost caracterizat structural prin difractie cu raze X si microscopie optica, observandu-se ca are o structura cvc (tip β). Valoarea modulului de elasticitate longitudinal (circa 74 GPa) a acestui aliaj este sensibil mai mica decat cea a aliajului clasic Ti-6Al-4V (circa 120GPa). Testele asupra comportarii electrochimice in medii biologice simulate a celor doua aliaje nu au aratat existenta unor diferente semnificative. Comportarea electrochimica corespunzatoare combinata cu modulul de elasticitate longitudinal scazut, indica noul aliaj Ti-12Mo-5Ta ca fiind adecvat aplicatiilor medicale.

A NEW NANOMATERIAL FOR QUANTUM COMPUTING PROCESSORS AND QUANTUM CELLULAR AUTOMATA. I. INTUITIVE MODELS

BY

CARMEN-IULIANA CIUBOTARIU, CORINA MARIN, CIPRIAN CIUBOTARIU,
and CORNELIU CIUBOTARIU

Abstract: *We describe a continuous variable quantum processor based on the electron collision experiment of Franck and Hertz. The qubits are represented by neon atoms in a Franck-Hertz macroscopic tube. We have chosen the neon atom because its De Boer quantum parameter has a value of the order 0.5, i.e. the theory can be semiclassical and thus we can define a new type of qubit for quantum computing (QC) registers and also, a semiquantum bit ('squbit') for quantum cellular automata (QCA). The aim of the paper is threefold. First, to show that pure quantum logic gates (e.g. square-root-of-NOT and Hadamard gates) can be realized even in a student laboratory. Second, the external manipulation of (s)qubits in QC and QCA can be implemented by using electron collisions and periodically kicked rotator principle (frequently encountered in bio-material processors), and third, we propose a Franck-Hertz nanomaterial, i.e. neon atoms (as 1D quantum gas) confined (by physisorption or by 'physical doping' with 'physical impurities', not a nano-peapod system) to nanotubes or 1D interstices between tubes in ropes as waveguides or yet simple quantum dots. The Franck-Hertz current in nanostructures as a function of the acceleration voltage (displayed on an oscilloscope or a classical computer) may represent an (analog or digital) readout of QC or QCA.*

Keywords: *Nanomaterials, Qubit, Quantum processor, QCA, Continuous variable readout.*

1. Introduction

The starting point for the present paper is represented by the fact that electrons carrying a small current through a nanostructure (generally, a mesoscopic quantum well material) can be considered as probes for the internal energy states of the well. For example, the harmonic series of energy levels (eigenvalues $E_n = n^2 \pi^2 \hbar^2 / 2m_0 a^2$) is the signature of a quantum dot (a 0D-zero dimensional well) and thus, whenever the voltage across the well corresponds to the energy of one of its eigenvalues (resonant stationary states), current increases. If the 'diameter' a of the nanostructure is very small (e.g. on the order of electron wavelength $\approx 20 \text{ \AA}$, which corresponds to an energy of 1/40 eV) its current-voltage spectrum displays a harmonic series of peaks that indicates a quantum confinement. Also, regular peaks appear in the optical absorption spectra of a quantum dot (QD) energy structure [1].

In the present paper we show that a new type of quantum processor can be elaborated on the basis of a simple Franck-Hertz (FH) device. With this device, for example, the square-root-of-NOT gate and (pseudo-) Hadamard gate (which are a mystery for classical computing) can be visualized even in a student laboratory. Our proposal of using electron collisions and periodically kicked rotator principle may become a new method for external manipulation (control) and read-out of qubits. In order to keep the character of a selfcontained paper we discuss, with intuitive

explanations, quantum nanobits, quantum logic gates and circuits in terms of a FH experiment concerning quantization. Finally, an exact definition of a nanomaterial, the newly proposed FH quantum processor and FH readout are presented.

It is interesting that any information (any readout) about the result of a quantum computing based on a FH processor is obtained from a I-V characteristic, that is from the conductance of a FH device. This ‘principle’ represents the key of our new ideas in the present paper because it appears in any experimental study of a nanostructure.

2. Definition of the Franck-Hertz qubit

Neutral neon atoms have 10 electrons in a ground-state configuration $1s^2 2s^2 2p^6$, the $n=1$ and $n=2$ shells being closed (see Fig. 1).

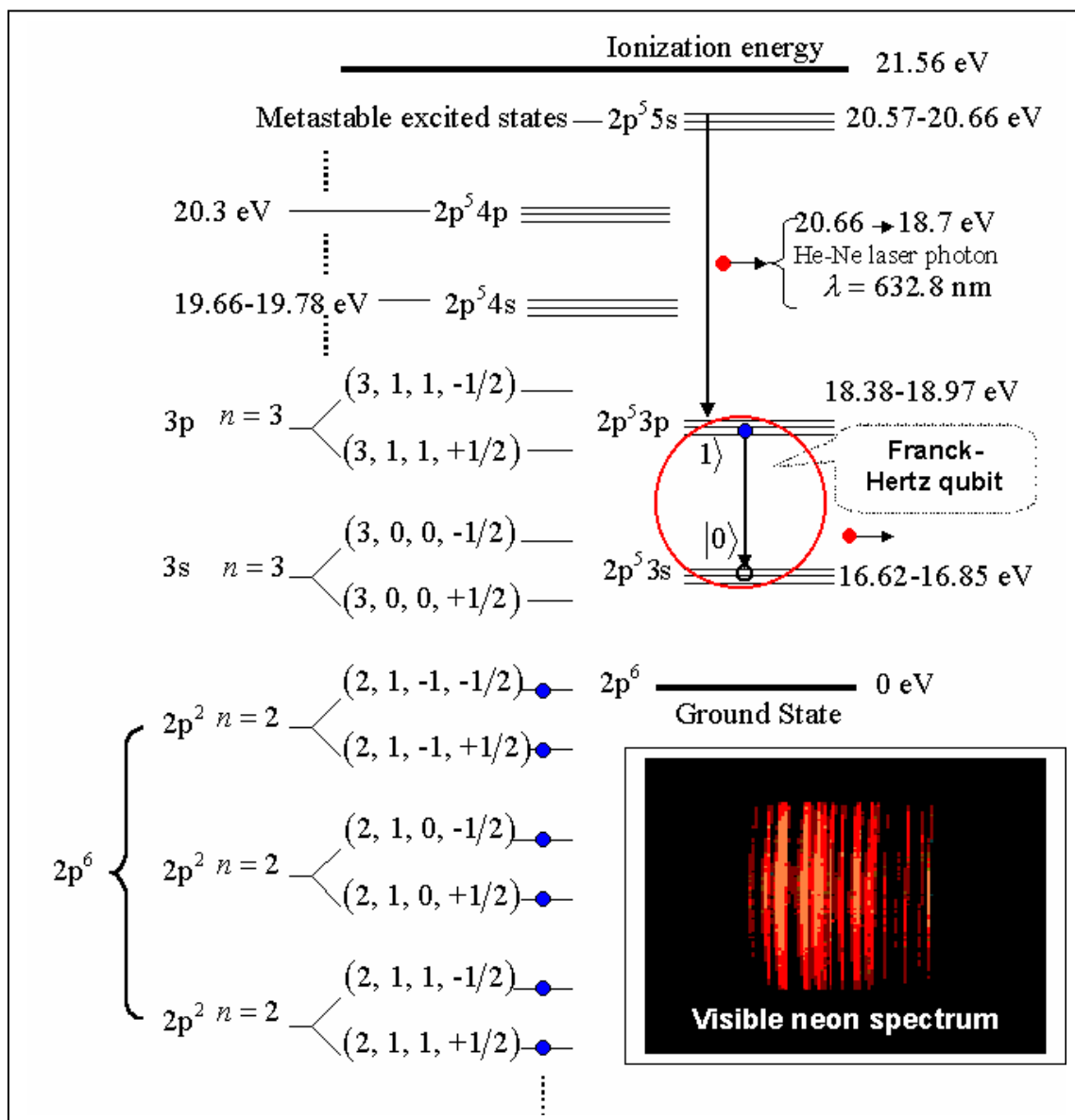


Fig. 1. Grotrian diagram showing some energy levels in neon. Inset: the red part of the spectrum of neon [2]. A spectral line may represent a read out of an atomic qubit; the ensemble of lines, a qudit.

Due to electron spin-related selection rules, collisions with electrons excite neon atoms from the ground state to, for example, the $2p^53p$ and $2p^54p$ states. When falling back toward the ground state by emitting photons the $2p^53s$ state (e.g. a $|0\rangle$ -state, which has $l_1=0$, $s_1=1/2$, $l_2=1$, and $s_2=1/2$, for the pair of particles 1–2, electron-hole, defined below) is also allowed. If the upper level (a $|1\rangle$ -state) for the transitions is $2p^53p$ then $l_1=1$, $s_1=1/2$, $l_2=1$, and $s_2=1/2$. Recall that we can calculate the wavelength of the photons emitted from $\Delta E = h\nu = hc/\lambda$. The transitions to be studied (in the Franck-Hertz experiment, see Fig. 2) are between initial states with one electron to a $3s$ level (not transitions to the ground state). In a way, these transitions are simple to model theoretically (in a self-consistent field approximation [3]), because the neon atom may be considered as a pair of particles, namely a ‘hole’ (in the $n=2$ shell) and an excited electron (labeled as particle 1) in the $n=3$ shell. In other words, all nine unexcited electrons (in the $n=1$ and $n=2$ shells) are considered as a single particle, a hole, labeled as particle 2. The pair electron-hole (a kind of Wannier-Mott atomic exciton), 1–2, and the states $|0\rangle$, $|1\rangle$ (a standard quantum computational basis in the Hilbert space H^2) represent a quantum two-level system and thus a potential candidate for an ‘atomic orbital’ ($\Delta l = \pm 1 \neq 0$) qubit.

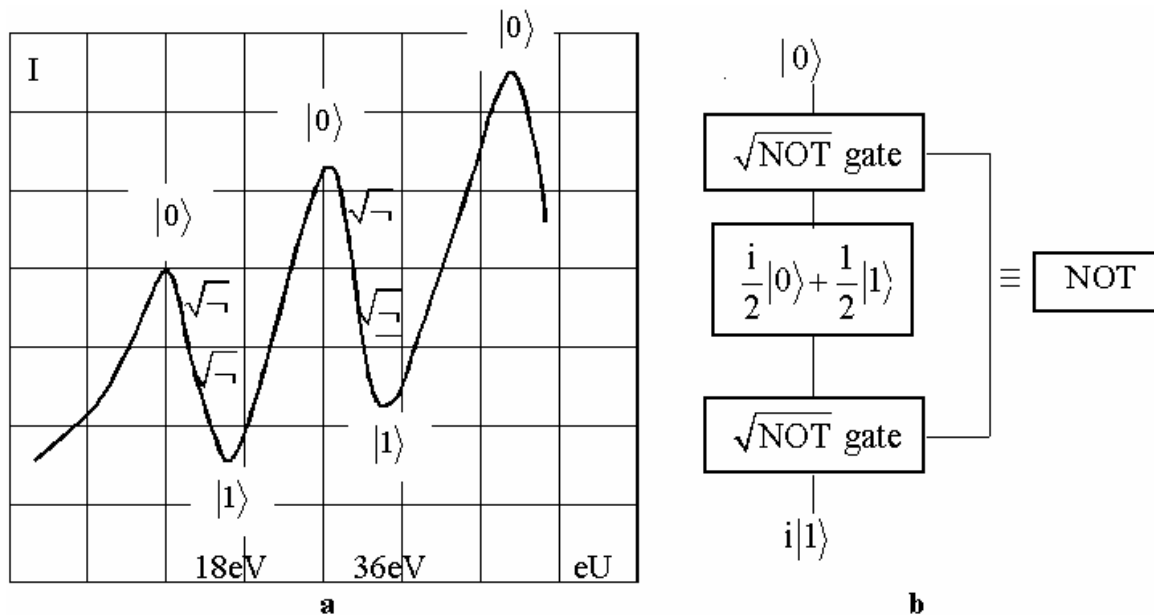


Fig. 2. Point-by-point (or oscilloscope) readout of the neon Franck-Hertz quantum processor. (a) We identify the ground and first excited states of the neon atom (qubit) with the states $|0\rangle$ and $|1\rangle$, respectively. (b) A simple quantum FH circuit with $\sqrt{\text{NOT}} \equiv \sqrt{-}$ gate, which is obtained by a half pulse of light or half the kinetic energy of electrons which collide nanostructures (neon atoms).

One problem with this scheme is that, for example, there are about ten excited levels in the range 18.3 to 19.5 eV. They deexcite by dropping to lower states, for example, at 16.57 and 16.79 eV. This energy difference gives photons in the visible range. Since the accelerated electrons undergo inelastic collisions with the neon atoms and are then accelerated again, they can undergo a series of such collisions if the accelerating voltage is high enough. The accelerating voltage from the Franck-Hertz

(FH) device used to produce the collector current peaks (see Fig.2a) was capable of producing about 80 volts, so we could get up to four inelastic collisions. This can be seen under proper conditions as four bands of light from the deexcitation in the collision regions. Each of these bands represents a (spectroscopic) signature of the existence of a FH qubit with a corresponding asymmetric FH quantum gate $|1\rangle \rightarrow |0\rangle$ (deexcitation with photons), and $|0\rangle \rightarrow |1\rangle$ (excitation with electrons). Thus, a single neon atom may be the ‘headquarters’ of at least four Franck-Hertz qubits, and can be used as a quantum processor (or a quantum memory). This is in agreement with the Volovich’s idea [4] that multi-qubit states may be implemented as multi-electron states in a single atom. Spin-orbit, spin-spin interactions and collisions can realize the coupling between qubits.

Finally this section we emphasize that in today’s (classical, conventional) computers, the most part of information is transported from one place to another by electric currents, whereas in QCs information is transferred with the use of propagation of quantum (polarization) states [5].

3. Franck-Hertz experiment with quantum dots

Even if a quantum dot (QD) represents an ‘artificial atom’ (Figs. 3-6), for the time being, the release of information from it seems to be more rich and easier to exploit up than from the corresponding ‘natural’ atom.

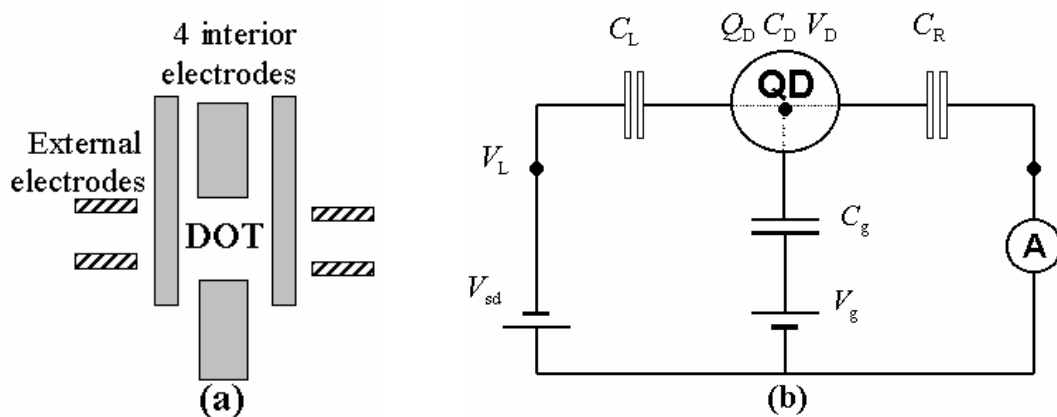


Fig. 3. Controlling the energy levels and number of electrons in a ‘laterally structured’ QD. (a) A voltage applied to interior electrodes confines (squeezes) electrons inside QD and controls the harmonic series of energy levels E_n . (b) Equivalent circuit.

Energy levels of QDs are determined at least by two quantization rules: (i) energy quantization (which is determined by the size of QD, the de Broglie wavelength – few angstroms, and effective mass of the conduction electron in the dot; the size of a QD approaches the Fermi wavelength in order to display quantized energy levels and quantum ballistic – free of impurities - electron transport), and (ii) quantization of electron charge (e). Thus, the electrical QD capacitance (C) and the amount of charge ($Q = a$ multiple of e) contained within a QD may also have an important role in the distribution of energy levels.

Furthermore, generally, a quantum dot has an irregular shape, like an irregular stadium in which the motion of an electron is similar to a bouncing-ball motion which

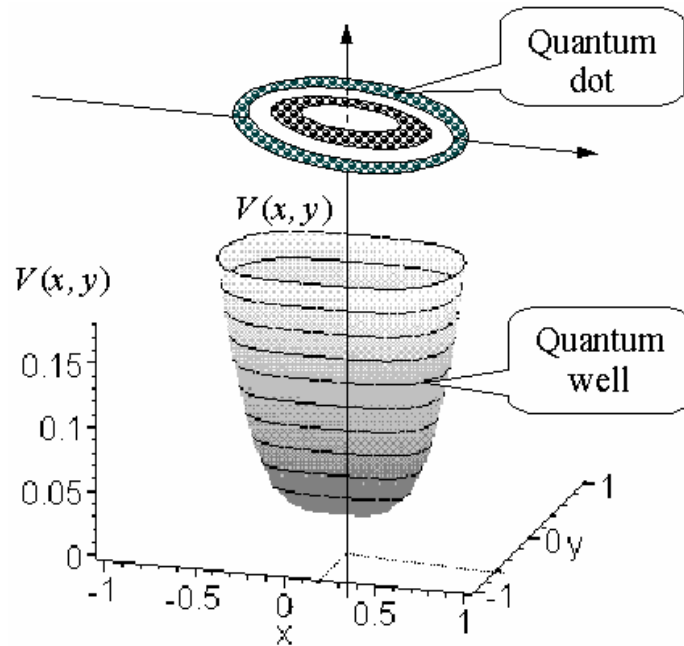


Fig. 4. A 2D (circular) quantum dot with a parabolic confining potential.

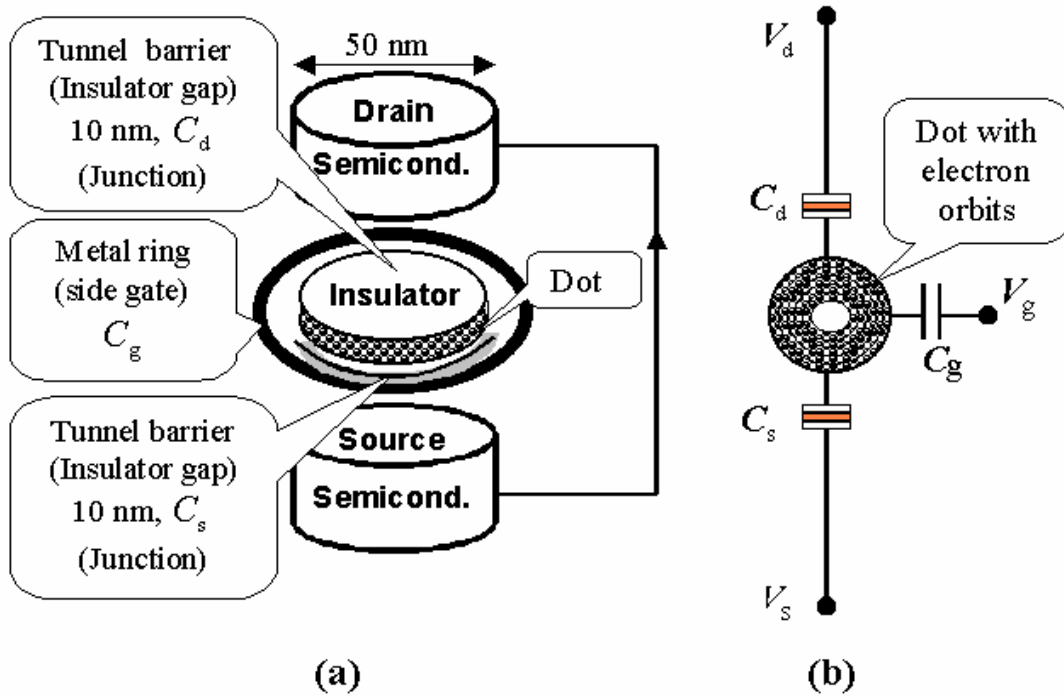


Fig. 5. Controlling the energy levels and number of electrons in a ‘vertically structured’ QD (‘round pillar model’ of QD). (a) The physical structure. The source and drain are doped semiconductor layers, which are separated from the QD by tunnel barriers. If a negative voltage is applied to the side gate (metal ring) around the pillar QD, its diameter (i.e. the quantum well diameter) is gradually reduced from 50 nm to about zero, and the electrons leave the QD one by one [6]. (b) Equivalent circuit of a QD.

generates (quantum) chaos. The variation of squeezing voltage (electrostatic confining) permits to endow the QD with as many or as few electrons as desired, and thus one can scan a true ‘artificial periodic table’ (e.g. it is possible to have even a single electron in a QD, an artificial hydrogen atom, and then electrons can be added one by one, in a digital way. Also, an artificial neon-like atom can be generated). External (gate) electrodes induce quantum contacts for electrons to tunnel in or out the QD and carrying a small current which displays the properties of the internal energy levels of QD. Quantum tunneling effect (which can be controlled by the height and the thickness of the quantum confining barriers) is strengthened when electron energies match the QD’s energy levels, i.e. $eV = E_n$. The valence (i.e. the number of electrons on ‘exterior orbits’) is also determined by the external gate voltage. The shape of the gate electrodes influences the size, shape and symmetry of the squeezing potential, the transparency of the barriers, and thus can realize a wavefunction technology. Particularly, one can realize wavefunctions for electrons in square or rectangular quantum wells (‘artificial atoms’).

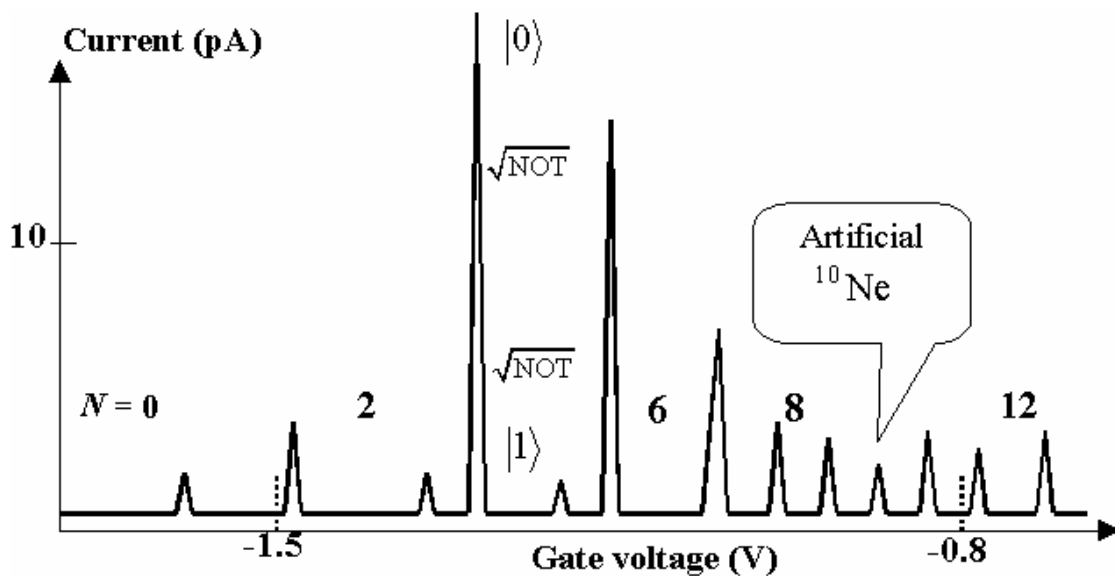


Fig. 6. Coulomb blockade and the series of peaks in the current. At any peak, the number of electrons on the dot changes between N and $N+1$, and between peaks the N is constant (zero current). The first peak on the graph corresponds to the energy at which the first electron enters the dot, the second peak corresponds to the second electron and so on [6]. One can observe that the spacing between the peaks are not constant and this shows that a QD behaves indeed as an artificial 2D - atom in the sense that electrons fill some orbits (shells with ‘magic numbers’, spin states, Hund’s rules, etc) with different energy states inside the QD.

4. Exact definition of a nanomaterial

The current experimental implementations of quantum processors (e.g. in the framework of NMR [7], trapped ions [8], cavity QED [9], quantum dots – QDs [10] etc, with their corresponding limitations) may be considered as molecular computers in the sense that they contain a number of coupled natural and artificial atoms (quantum dots), each of these atoms being a qubit. The coupling between these qubits represents

the difficult task of any QC and this coupling can generate various quantum gates. In essence, researchers considered qubits from the magnetic spin ($|\uparrow\rangle, |\downarrow\rangle$) of atomic nuclei or molecules, or from the polarization of light ($|\uparrow\rangle, |\leftrightarrow\rangle$ or $|\square\rangle, |\square\rangle$, or $|\dot{O}\rangle, |\ddot{O}\rangle$) in QCs, and from the (charge or spin) polarization states $\begin{bmatrix} \dot{Y} & \dot{U} \\ \dot{U} & \square \end{bmatrix}, \begin{bmatrix} \dot{U} & \dot{Y} \\ \dot{Y} & \dot{U} \end{bmatrix}$ of four-QD structure in QCA [11]. All these quantum processors are hard to scale, to miniaturize up an atomic or molecular system, in order to obtain a desktop quantum computer.

Because a qubit (or generally, a qudit) is characterized by easily distinguishable on-off states, for the time being, a solid state component cannot be considered for quantum computing, the electrons in solids having innumerable quantum states with transitions between them which cannot be controlled. However, in semiconductor QDs ('artificial atoms'), charge carriers (electrons and holes) can only occupy a reduced number of energy levels, like the electrons in an atom ('a natural QD'). Even if the wave function of a QD electron, and its hole, propagates over many thousands of lattice atoms, the corresponding exciton behaves in a quantized and coherent fashion. Thus, QDs may represent individual qubits in a lattice of solid-state environment.

Thus, a nanomaterial (in the proper sense of this concept) is characterized by the fact that its components (nanoparticles) can be individually controlled, e.g. by their distinctive energy levels, even if the nanoparticles are embedded in a macroscopic environment. Only in the framework of this definition a nanomaterial can be used as a quantum (atomic, molecular etc) memory or quantum processor in order to push further the Gordon Moore's law. We recall the Coulomb blockade (CB) tunneling. That is, in a QD, the charging energy (generated by electron-electron interactions) equals $Q^2/2C$, and an electron tunneling is blocked if the potential energy eV for a voltage V is less than the elementary charging energy $e^2/2C$. Also, tunneling should not be initiated by quantum fluctuations and this imposes a restriction on the conductance. In essence, CB represents a combined effect of the discreteness of energy levels and the charging energy. The diameter of a QD is small enough to make its charging energy greater than (the thermal fluctuation energy) $k_B T$ and trap individual electrons. Present QDs only works at $T=0.1$ K, and smaller QDs may increase the temperature (T) of operation. For a $1\ \mu\text{m} \times 1\ \mu\text{m}$ QD, the temperature T must be less than $e^2/2k_B C \approx 30$ mK, and this shows the difficulty of realizing a practical nanomaterial at an accessible temperature. It is interesting that, in some magnetic field regions, one can also define a spin blockade (an inhibition of single-electron tunneling because of a spin selection rule) in the case of a QD in the framework of an anharmonic (or even rectangular hard wall shape) confinement potential [12]. QDs can be used as qubits, i.e. as two-level quantum systems, based on charge or spin (or both). For example, one such two-level system is a coupled electron-hole pair - an exciton. The absence (state $|0\rangle$) and presence (state $|1\rangle$) of an exciton in a semiconductor QD could represent the two levels of a qubit.

Finally, we emphasize that for example a quantum well (QD or nanotube) material offers numerous advantages over 'natural atoms' materials, including a greater control over the artificial atom size, composition, and shape, and in this sense a QD material is *programmable*, i.e. can be controlled by external potentials.

5. Conclusions

We have shown that the Coulomb blockade in a quantum nanostructure may be interpreted as an analogue effect with the decrease of current in a Franck-Hertz (FH) tube as a result of elastic collisions electron-neon atom. Thus, the I-V continuous variable readout of a FH tube can be considered as an output of a quantum processor with FH qubits. The I-V (peak) characteristic of a quantum nanostructure (empty or filled with neon) may be used as a discrete variable readout of a FH processor based on new quantum materials as dots and nanotubes.

Received September 20, 2004

*Department of Electrical and Computer Engineering, University of Calgary (AB), Canada
Ministry of Education and Research, General Berthelot 28-30, Bucharest 010168, Romania
Université Laval, Faculté des Sciences de l'Administration, Québec G1K 7P4, Canada
Physics Department, Technical University "Gh. Asachi", Bv. Mangeron 67, Iasi-700050, Romania*

REFERENCES

1. Reed, M. A. – *Quantum dots*, **Scientific American**, **268** (1), 1993, **118-123**
2. <http://chemlab.pc.maricopa.edu/periodic/Ne.html>
3. Sobelman, I. I. - *Atomic Spectra and Radiative Transitions*, SpringerVerlag, Berlin, 1991.
4. Volovich, I.V. – *Atomic quantum computer*, **Physics of Elementary Particles and Atomic Nuclei** (in Russian), **31** (7A), 2000, **133-136**; <http://www1.jinr.ru/Archive/Pepan/v-31-7a.html>; arXiv:quant-ph/9911062; Ohya, M. and Volovich, I. V. - *Quantum Computing, NP-complete Problems and Chaotic Dynamics*, arXiv:quant-ph/9912100
5. Smith, C. G. – *Computation without current*, **Science**, **284**, 1999, **274**.
6. Kouwenhoven, L. and Charles Marcus, C. – *Quantum dots*, **Physics World**, June 1998, **35-39**
7. Laflamme, R. et al. - *Introduction to NMR Quantum Information Processing*, quant-ph/0207172, 44 pages.
8. Zoller, P. et al. - *Implementing quantum information processing with atoms, ions and photons*, **les Houches summer school proceedings**, session 79, Ed. D. Estève, J. M. Raimond and J. Dalibard, Elsevier, Amsterdam (2004), quant-ph/0405025.
9. Cirac, J. I. et al. - *Quantum optical implementation of quantum information processing*, **Proceedings of the International School of Physics Enrico Fermi 148**, Experimental Quantum Computation and Information, Ed. F. De Martini and C. Monroe, IOS Press, Amsterdam (2002), quant-ph/0405030.
10. Loss, D. and DiVincenzo, D. P. - *Quantum Computation with Quantum Dots*, **Phys. Rev. A****57**, 1998, 120-138; cond-mat/9701055.
11. Wang, W., Walus, K. and Jullien, G. A. - *Quantum-Dot Cellular Automata Adders*, **IEEE Nano 2003 Conference**, San Francisco, CA, vol. 1, 2003, **461-464**
12. Imamura, H., Maksym, P. A. and Aoki, H. - *Vertically coupled double quantum dots in magnetic fields*, **Physical Review B** **59**, 1999, **5817-5825**

UN NOU NANOMATERIAL PENTRU PROCESOARELE DE CALCUL CUANTIC SI AUTOMATELE CELULARE CUANTICE. I. MODELE INTUITIVE

Rezumat: Se arata ca ideea experimentului Franck-Hertz poate fi folosita pentru a construi un nou tip de procesor cuantic in care portile logice sunt activate atat de fotoni cat si de ciocniri cuantice. Oprirea electronului (in urma unei ciocniri elastice) si micsorarea brusca a curentului in tubul Franck-Hertz este interpretata ca un efect analog blocadei Coulomb din cazul nanostructurilor. Ca urmare, este posibil un experiment de tip Franck-Hertz in cadrul nanostructurilor simple sau umplute, de exemplu, cu neon.

**THE CONFIGURATION OF THE REUSABLE MATERIALS'
RECYCLATION PROGRAMMES INSIDE
THE EUROPEAN UNION**

By

NECULAI SCANTEIANU

***ABSTRACT:** Nowadays ,at the level of the countries in EU, we are assisting at a global approach in the field of the recycle of reusable materials and of residues' managerial problems. The definition for SOCIAL ENVIRONMENT or FUNCTIONING ENVIRONMENT is extremely complex within the firms which have as the main activity the recycle of materials, because it includes a number of different types of elements: politics, social, economics ,ecology, etc. these elements have a local, national and international impact upon the firm, and not each at a time, but in a tight interdependency.*

***KEYWORDS:** residual recycle, the extern environment, functioning environment.*

1. INTRODUCTION

This integration was realized on two plans connected with each other:

-inside the firms which have as the main activity domain the retrieving and the recycle of materials, between the number of activities and the compartments inside the firm

-between the firms and the extra organizational environment in which they function.

On the basis of this type of approach, there has been a succeed in developing some important activities for the community, such as the recycle of the residues and the cleaning of the localities, made by particular firms which assured profitableness. These activities are supported by local and regional organisms and function in a well defined legislative and fiscal background.

2. THEORETICAL CONSIDERATIONS

A complex and dynamical socio-economical system looks like this: the firm, which has as the main activity domain the recycle of materials, has an active and opened character, being part of bigger systems such as the economy or the society. The integration of the firm in these systems is made through multiple connections, fact that reflects not only the relative dependency in front of the environment, but also the manifestation possibilities of the firm's dynamism, which is an important factor of conditioning the firm's viability. Due to the fact that it is an opened system, the recycle firm modifies its products, structures and socio-economical functioning mechanism, if there are changes in its system. But through the active character of its economical involvement, it has also a direct influence upon the environment. The general view of the firm is a complex ensemble, which integrates organically in the

socio-economical life as a well defined element, but which has multivalent relationships with its organizational environment.

The definition for **SOCIAL ENVIRONMENT** or **FUNCTIONING ENVIRONMENT** is extremely complex within the firms which have as the main activity the recycle of materials, because it includes a number of different types of elements: politics, social, economics, ecology, etc. these elements have a local, national and international impact upon the firm, and not each at a time, but in a tight interdependency.

A. THE SOCIAL ENVIRONMENT

In general, the rhythm of changes from the social environment which affect first the size and the density of population, the values and social structures, is slow, but cannot be ignored in the process of choosing the recycle firm's strategy. All these changes affect the corresponding services, the type of work within the firm, certain aspects of productivity, the ratio between the number of direct and indirect productive workers.

The specific tendency for the EU countries is the direct influence of this environment through direct interventions at a regional / local level, through educational programs for the population. These programs are supported, in general, by the local budget as well as from the taxes imposed to the producers of industrial products and consumer goods.

B. THE TECHNOLOGICAL ENVIRONMENT

The quickness of the technological modifications in certain industries has an impact upon the length of the products' cycle of life.

The technological evolutions are of great value especially for high-technical industries. Although some industries are less affected by the technologies' dynamic, changes appeared in connected industries can have immediate effects. For example, the technological innovations used in the packing industry had considerably influenced both the technologies used food industry and in the modalities of recycling the wrappings.

In EU countries this environment has a strong institutional-administrative influence. Thus, through legislative configurations, technological measurements are imposed to help the recycle process. Due to the assimilation of modern technology, from the early stage of project, the conceiving of reusable products has become possible nowadays.

The new concept of "clean" technology represents an elder one, which covers more aspects concerning the economical activities, as well as safety measurements of the environment. The fields which are assured by this category of technology are:

- the reduction of noxious residues and compounds
- a more pleasant place to work in, both inside buildings and in the nearby area
- the decrease of pollution
- the decrease of the consumption of natural resources

The traditional way of thinking concerning the technological development was in favor of the solutions assuring maximum efficiency, the flexibility of the technical system, the accomplishment of achieving products of the best "technical" quality. But from another point of view, the technological estimation was too little oriented

towards the effect of consuming resources or the noxious emissions and residues. The types of projects that were preferred those which responded well to some strictly economical criteria and less to those that exerted reduced pressure on the environment.

3.THE ANALYSIS AND THE ESTIMATION OF THE TECHNOLOGICAL PROCESS

Nowadays, the analysis and the estimation of a technological process must start from pointing out the existing relationship between the elements of an industrial process (picture 1).

The analysis of this scheme must start from the premise that the unit of a “clean” technology is that of decreasing the use of energy and resources and improving the living conditions for people. Consequently, the decrease of the following factors is necessary:

- the use of resources
- the impact upon human health
- the impact upon the quality of the environment

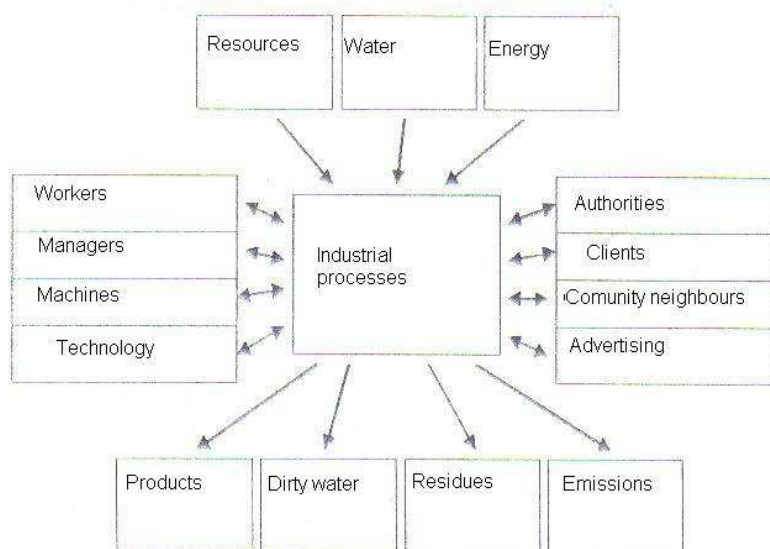
These demands can be found in the EU programs for the approach concerning the environment and the lasting development, which has the following characteristics:

- providing accessible resources permanently
- keeping the superior quality of life
- preventing the irremediable deteriorations of the environment

Nowadays, a 100% prevention of the human activities side effects is impossible. But it is possible to create some activities which have positive effects upon the ecological conditions. These effects depend on the entrances and exits from the processes of production and consuming. In picture one can see the relationship between entrances, processes and exits from these two pictures we can elude the relationship between the dynamic of the partners

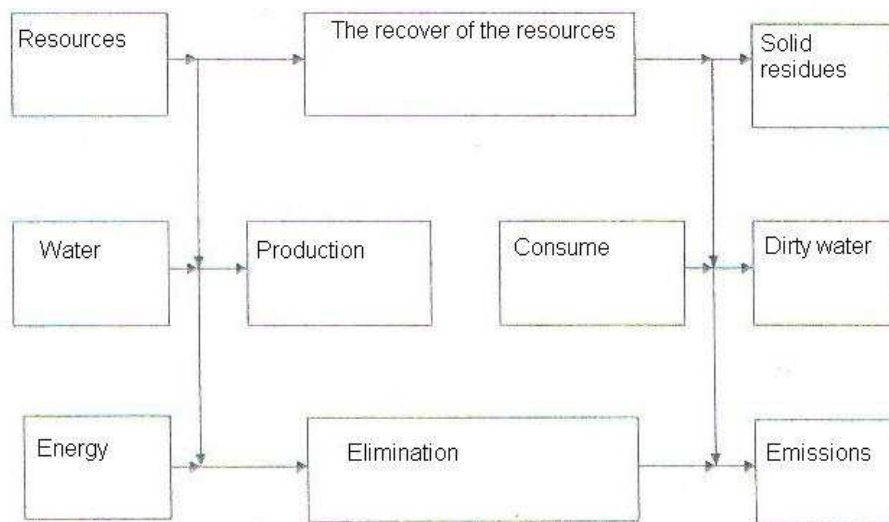
An analysis of these changes can indicate for each technology:

- the current consumption of resources



Picture 1

- the level of these consumptions in comparison to those than can be realized on the basis of the best possible or available technology
- the reduction possibilities of these consumptions
- the quality of emissions and liquid / solid residues
- the level of these quantities in comparison to those obtained from the best possible / available technologies
- the possibilities of reduction of these quantities



Picture 2

C.THE POLITICAL ENVIRONMENT

The EU governments can influence the firm's recycle process, collecting the reusable materials activities, both at a national or a local level, not only through legislative applications, but also strategically, through implementing some new opportunities or, otherwise, through imposing new limits and compulsions. Due to their prerogatives, governments have the possibilities to:

- establish the structure of the collecting-recycle-neutralizing the residues and the reusable materials process, through a juridical framing of their display of practices
- contact goods and services from the sphere of the activities of collecting, recycle, neutralizing the reusable materials and the residues, being a beneficiary of those mentioned before
- ask and encourage the execution of civil constructions which are useful in this field (ecological storehouse holes, cleaning stations for water, cremation stations for rubbish, etc.)
- promote programs which involve regional development and reorganization politics for the industry of processing reusable residues through fiscal facilities

The economical instruments with the help of which such tasks can be accomplished are:

- taxes for the generation of reusable materials
- subventions for collecting and recycle of materials
- marketing authorizations
- taxes for products

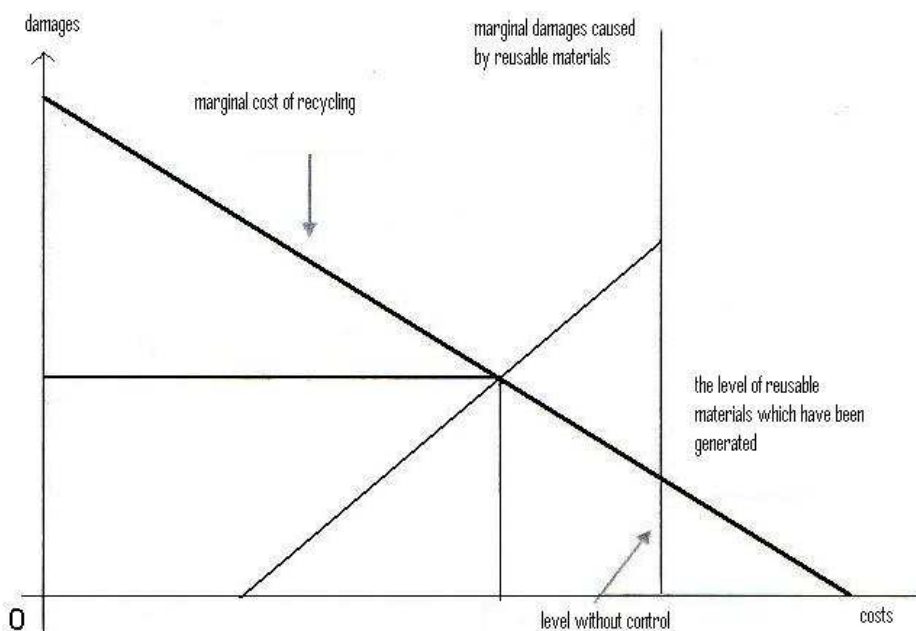
The most frequently used instruments for direct reglementations are:

- the quotas concerning technologies
- the quotas concerning the level of reusable materials generated

The theoretical model substantiates the use of economical instruments refers to the comparison between the marginal costs and involved by recycling the materials and the marginal loss caused by the generation of reusable materials and the lack of concern for their recycling (picture 3). For a firm that produces residues, the optimal level of generation can be considered equal to the OP interval below.

The main ways of touching the equilibrium point are:

- the application by the authorities of a tax for generation of reusable materials equal with the OT interval. This tax will oblige the generator of reusable materials (to save the money paid for the tax) to reduce the quantities until it is reached the P situation of equilibrium. As a result of introducing some collecting systems, in 2004, the quantity of recycled materials in occidental countries increased at 25% (on an average). on the first place is Germany, which overcame 40% through the application of the DSD system. This system was conceived due to the initiative of the producers preoccupied by solving the problem concerning the recycling their used products. The dual system is financed by the "green point" sign, symbol that certifies that the producers of wrappings paid the recycling tax, and that the amount of money obtained is used with the target of:
 - paying the services performed by the specialized firms in collecting, sorting, recycling residues



Picture 3

-developing the infrastructure necessary for collecting and sorting residues
 The taxes imposed by DSD are differentiated on types of residues, depending on the costs and the difficulties of the processes of collection-recycling

| MATERIAL | TAX(€/KG) |
|------------|-----------|
| Plastic | 1.5 |
| Aluminum | 0.5 |
| Cardboard | 0.83 |
| Sheet iron | 0.28 |
| Paper | 0.165 |
| Glass | 0.08 |

The dual system assures selective collection, which means that every type of material is separated by the others.

-subsiding the reduction of generating residues, with a value equal with OT. This measurement will determine the firm to reach the equilibrium point to gain the offered subsidy

- laws which will impose that the level of quantities of reusable materials generated to be equal to OP

In the table below there are presented arguments pro and con the using in practice of different economical instruments meant to control the generation of reusable materials.

Arguments pro and con the use of different economical

Table 1

| Instruments | Pros | | Cons | | |
|--------------------------|---|--|--|---|--|
| Taxes | Rise the budget venue | Offer the possibility of a flexible response | If the tax is not well established, the target will not be reached | | The firm can suffer decrease of the volume of activity |
| Subsides | The firm will not restrict its activity | | Possibility of appearing corruption | If the value of the subsidy is wrong calculated, the target will not be reached | |
| Laws | Lead to reaching the target rapidly | | Rapidity | Involve the existence of some complex administration structures | Higher costs |
| Marketing authorizations | Reaching the target in a relatively inexpensive way | | The rise of the production costs of the firm | | A limited experience in trade |

The economical instruments impose the use of some taxes which are in direct connection with the quantity and composition of recyclable materials generated and the methods of elimination or recycling retrieving.

Also, there have been elaborated more stimulus concerning the reduction of the quantity of recyclable materials which are not reintroduced in the economical circuit.

4. CONCLUSIONS

Nowadays there are applied taxes for the volume of recyclable materials which have been generated in: Austria, Denmark, Belgium, France, Germany, Italy, Holland, Switzerland etc. The cost of these taxes varies between 1€/tonn and 26€/tonn of residues that have been generated. As mentioned before, the level of taxes can be established depending on the destination of the residues.

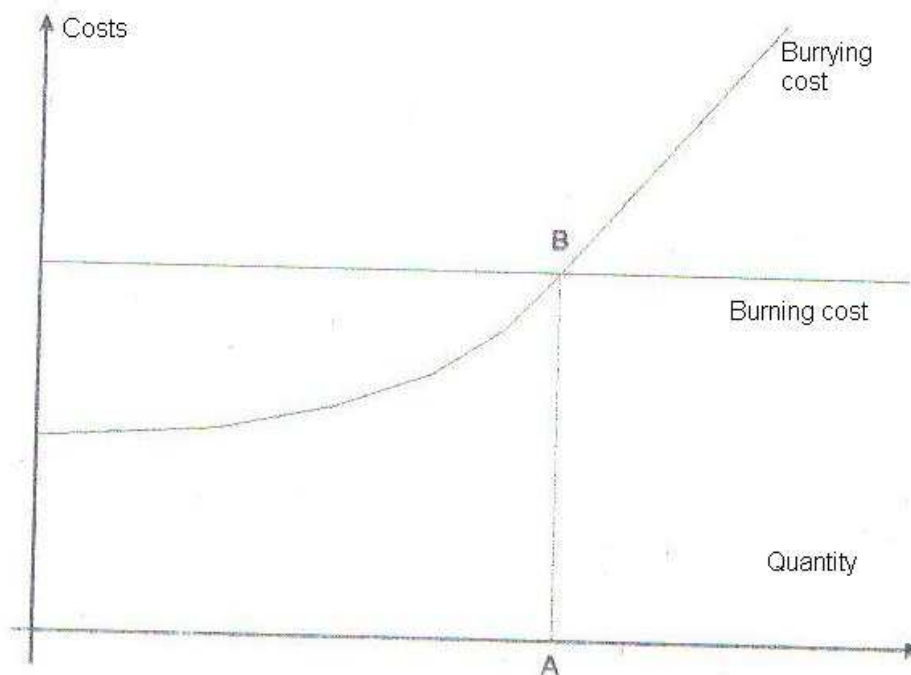
The use of such system of taxes has rise, however, some problems:

- part of the social costs of retrieving are paid by collectors
- the stimulants for recycling materials are not always based on the level of costs imposed by residual elimination
- the marginal social costs of different recycling methods are not equal

As an example, if we suppose that the level of marginal costs for the elimination through burning of some residues is constant (does not vary, if the quantity varies) and the level marginal costs of burying rise once the quantity rise, the optimal situation which minimalise the costs is marked by the equilibrium point B from picture 4.

- a rise of the level of taxes can reduce the volume of activities
- the subventions for recycling can decrease the budget balance
- the marketing authorizations can exclude some small but dynamical firms

These measurements need a propitious economical and political environment. The experience of the last years allow the identification of the conditions that must be fulfilled so that their application is efficient.



Picture 4

References

1. Legea protectiei mediului nr.137/1995- Monitorul oficial nr.304 din 30.12.1995
2. Scanteianu, N. – contributions concerning the improvement of some operations parameters of thermal heating equipment for meeting the ecological ruler in force – Teza de doctorat, Universitatea Tehnica “Gh.Asachi”, Iasi, 2001

Neculai Scanteianu – Faculty of Materials Science and Engineering, Technical University “Gh.Asachi” Iasi, Bd. D.Mangeron, nr.63, Iasi, Romania.

**CONFIGURAREA PROGRAMELOR DE RECICLARE A MATERIALELOR REFOLOSIBILE IN
UNIUNEA EUROPEANA**

Rezumat: In prezent, la nivelul tarilor UE, asistam la o abordare globala, integratoare, a problemelor manageriale din domeniul reciclarii materialelor refofosibile si a deseurilor.

In cadrul firmelor de reciclare a materialelor din UE, notiunea de **MEDIU EXTERN** sau **MEDIU DE FUNCTIONARE** este deosebit de complexa, deoarece include o serie de elemente de natura foarte diferita – politica, sociala, economica, ecologica etc. – care se manifest ape plan local, national si international, actionand asupra firmei nu in mod izolat, ci in stransa interdependenta.

MECHANICAL PROPERTIES OPTIMISATION OF AN AlCu4Mg1 ALLOY

BY

ALINA-ADRIANA MINEA

Abstract. This paper presents experimental and theoretical studies regarding the behavior after heat treatment of an AlCu4Mg1 aluminum alloy. Therefore, I choused a typical charge of parts for studying the optimization of the mechanical properties. The theoretical and experimental studies that I have done can reveal the advantage of controlling the heating process at heat treatment of aluminum alloys. Also, I have obtained some equations that can express the process and can determine the values of the mechanical properties obtained after a specific heat treatment.

Keywords: mechanical properties, heat treatment, hardness, stress, mathematical model

1. INTRODUCTION

This paper presents an Al – Cu – Mg alloy, AlCu4Mg1 that is used for aeronautical parts. This alloy is heat treated in order to establish the optimum mechanical properties, and I am referring especially at microhardness and tensile strength. So, I took 10 parts, of identical measures, from this alloy and apply the final heat treatment. At the end there is a study of the microhardness and the mechanical properties and the results are compared with a test part.

2. RESULTS AND DISCUSSIONS

This paper contains an experimental and theoretical optimisation regarding the improvement of heating processes, which determine a better heat treatment technology for aluminum alloys and low energy consumption.

The charge is from aluminum alloy AlCu4Mg1. The composition for this alloy is illustrated in table 1.

Table 1.

| | Chemical composition, % | | | | | | | |
|----------|-------------------------|---------|---------|-----|-----|------|----|------|
| | Cu | Mg | Mn | Si | Fe | Zn | Ni | Ti |
| AlCu4Mg1 | 3,8-4,9 | 1,2-1,8 | 0,3-0,9 | 0,2 | 0,3 | 0,25 | - | 0,15 |

The parts have the geometrical configuration like in figure 1 and the dimensions are in table 2.

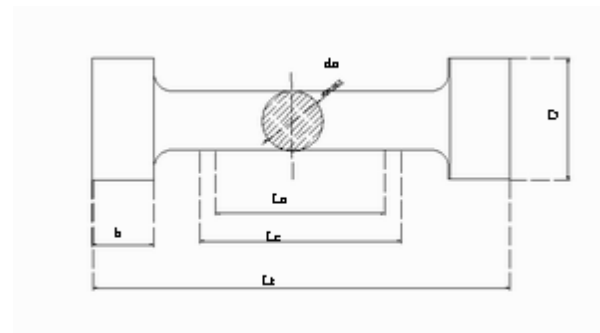


Figure 1

Table 2

| | d_0 | S_0 | D | h | L_t | L_0 | L_c |
|----------|-------|-------|-----|-----|-------|-------|-------|
| AlCu4Mg1 | 12 | 113 | 15 | 40 | 160 | 60 | 72 |

I have made experiments in the same conditions of preheating for the furnace, and I used the same equipment for the stress and hardness determinations.

Every part got a code, that was inscribed on it.

In figure 2 and 3 are illustrated the stress diagrams for the test part and for one treated part. The experimental results are in table 3 and 4.

In order to obtain the proposed mathematical model, I have made the experiments that are illustrated in table 3,4.

Table 3

| experiment | Code | $T_c, ^\circ\text{C}$ | $T_i, ^\circ\text{C}$ |
|------------|--------|-----------------------|-----------------------|
| 0. | N | - | - |
| 1. | 1.1.1. | 485 | 185 |
| 2. | 1.1.2. | 485 | 195 |
| 3. | 1.2.2. | 485 | 205 |
| 4. | 2.2.1. | 495 | 185 |
| 5. | 2.1.1. | 495 | 195 |
| 6. | 2.2.2. | 495 | 205 |
| 7. | 3.2.1. | 505 | 185 |
| 8. | 3.1.2. | 505 | 195 |
| 9. | 3.2.2. | 505 | 205 |

Table 4

| code | Stress, R_m | hardness |
|--------|---------------|----------|
| | MPa | HV |
| 3.1.2. | 276.36 | 168.4 |
| 3.2.1. | 392.42 | 132 |
| 3.2.2. | 331.17 | 138.5 |
| 2.1.2. | 329.24 | 140 |

| | | |
|--------|--------|-------|
| 2.2.1. | 436.32 | 177.4 |
| 2.2.2. | 355.31 | 136.6 |
| 1.1.1. | 367.85 | 142.3 |
| 1.1.2. | 224.19 | 177 |
| 1.2.2. | 316.42 | 134.3 |

With the results illustrated in table 3 and 4, using 3^k factorial experiment model and with a specific computer program I obtained the tridimensional variation of hardness and stress, depending on heating temperatures

Also, the regression equation, which describes the process is:

$$R = 313,634 + 15,246x_1 - 32,282x_2 - 2,455x_1x_2 - 55,554x_1^2 + 89,984x_2^2$$

$$HV = 139,822 + 2,45x_1 - 18,9x_2 - 3,2x_1x_2 - 2,583x_1^2 + 17,266x_2^2$$

In these equations, x is the factor that describes the variation of hardness and stress.

So, we considered two cases:

- case 1: quenching heat treating temperature is constant and imposed.
- case 2: artificial aging heat treating temperature is constant.

Case 1 In this situation, according to Table 3 we have three equations, for the three values of the quenching temperature:

$$1. \quad x_1 = -1, T_c = 485^\circ\text{C}$$

$$T_i = 283,373 + 0,19 R_m - 0,98 HV$$

$$2. \quad x_1 = 0, T_c = 495^\circ\text{C}$$

$$T_i = 257,676 + 0,14 R_m - 0,77 HV$$

$$3. \quad x_1 = 1, T_c = 505^\circ\text{C}$$

$$T_i = 47,68 - 0,32 R_m + 1,66 HV$$

These relations represents the variation equations between artificial aging heat treating temperature of the AlCu4Mg1 aluminum alloy and the hardness and mechanical stress. In these conditions it can be determined the necessary artificial aging temperature in some certain conditions needed in industry.

Case 2 In this situation, according to table 3 we have three equations, for the three values of the artificial aging heat treating temperature:

$$4. \quad x_2 = -1, T_i = 185^\circ\text{C}$$

$$T_c = 735,66 + 0,07 R_m - 1,54 HV$$

$$5. \quad x_2 = 0, T_i = 195^\circ\text{C}$$

$$T_c = -224,376 - 0,26 R_m + 5,7 HV$$

$$6. \quad x_2 = 1, T_i = 210^\circ\text{C}$$

$$T_c = 1395,307 + 0,34 R_m - 7,4 HV$$

These relations represent the variation equations between quenching heat treating temperature of the AlCu4Mg1 aluminum alloy and the hardness and mechanical stress.

In these conditions the technology designers can determine the necessary quenching temperature in some certain conditions needed for an AlCu4Mg1 aluminum alloy part.

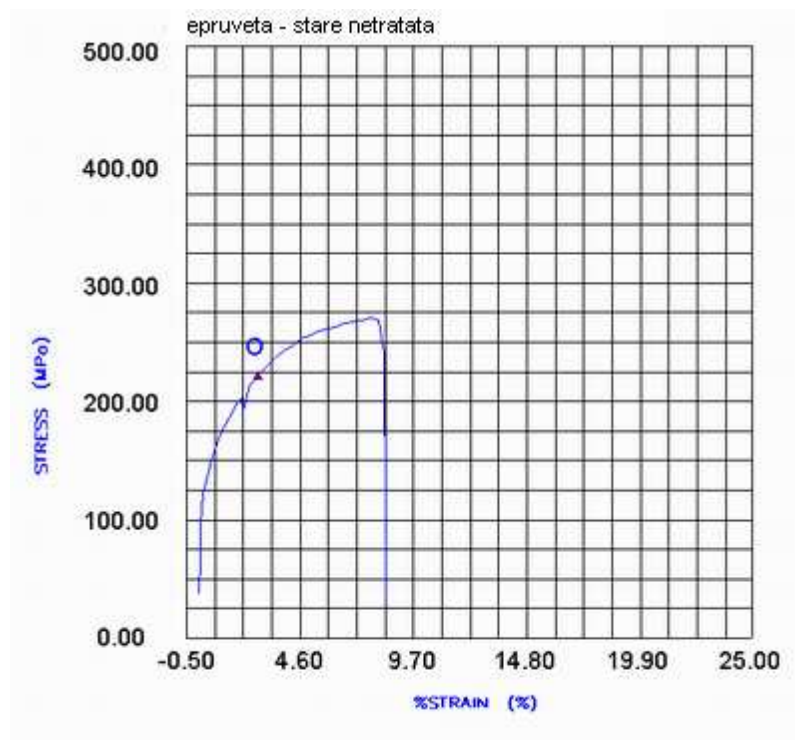


Figure 2. Stress diagram – test part

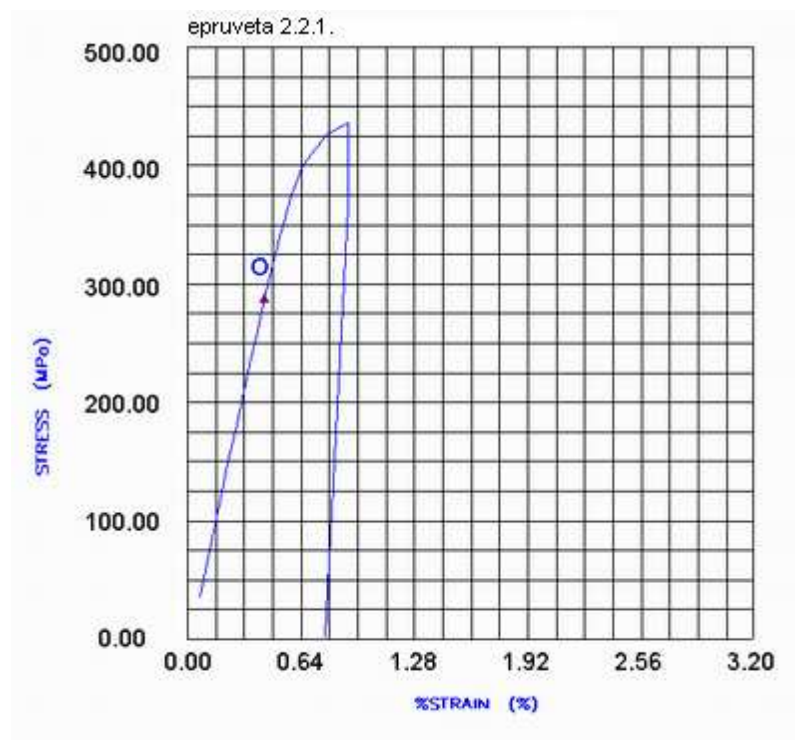


Figure 3. Stress diagram – 2.2.1. treated part

We must mention that the calculated temperatures must be between standard limits for the studied alloy. In case that the calculated temperature it is not in standard limits, it

must give up of imposing some characteristics and must use just the one – variable functions.

As a conclusion, the paper presents the algorithm for applying the optimum heat treatment in order to obtain the necessary properties for the working parts.

4. CONCLUSIONS

So, in this paper is presented the variation of the hardness and tensile strength with aging and quenching heating temperature. Also, we were obtaining the equations for theoretical determination of some properties in standard or special heat treatment conditions.

Using the equations determined, we impose some characteristics needed for the final working part and we calculate the parameters for the quenching heat treating and artificial aging heat treating. Also, in some given conditions of final heat treating it can be predict the mechanical characteristic of a treated part; and we are referring at mechanical stress and hardness. This is a very important matter because in duty it is absolutely necessary to know the behavior of a working part, which can influence the stability of a machine or a mechanism.

REFERENCES

1. Comsa, D. - *Instalatii electrotermice industriale*, E. T. Bucuresti, 1986
2. J.E. Hatch - *Aluminum Properties and Physical Metallurgy* (American Society for Metals, 1984, p. 165-166
3. Banno, T. - *Heat Treatment Furnace Technology - Present Status and Challenges*, Heat Treatment of Metals, 1994.

MINEA ALINA – ADRIANA - TECHNICAL UNIVERSITY “GH. ASACHI” – IASI, BD. D. MANGERON NR.63

OPTIMIZAREA PROPRIETATILOR MECANICE ALE UNUI ALIAJ AlCu4Mg1 (Rezumat)

Aceasta lucrare prezinta un studiu privind un aliaj Al-Cu-Mg, si anume AlCu4Mg1. Din acest aliaj s-au realizat 10 epruvete, care s-au supus tratamentului termic final de calire de punere in solutie. ~n urma experimentarilor realizate, am obtinut ecuatii de legatura intre temperatura finala de incalzire si rezistenta la tractiune, respectiv duritatea. Aceste ecuatii au fost determinate prin metoda experimenntului activ. Cu ajutorul relatiilor se pot impune anumite caracteristici mecanice necesare in exploatarea pieselor si se pot calcula temperaturile necesare de calire de punere in solutie si/sau imbatranire pentru aceste aliaje, prin impunerea uneia dintre ele. Totodata, se pot calcula teoretic duritatea, rezistenta la tractiune, rezistenta la curgere a unei epruvete in functie de parametrii de incalzire in vederea tratamentului termic final al aliajului de aluminiu cercetat. Trebuie sa mentionez ca temperaturile calculate cu ajutorul ecuatiilor prezentate trebuie sa se incadreze in limitele prevazute de standardul aliajului. In cazul in care acestea nu se incadreaza, se renunta la impunerea a mai multor caracteristici mecanice, folosindu-se ecuatiile de o singura variabila.

NEW HYBRID NANOCOMPOSITES OF MgAlHT ANIONIC CLAYS INCORPORATED WITH ACETAMIPRID

BY

GABRIELA CARJA, MIHAELA FRUNZA, MARCEL IONEL POPA and CRISTINA
POPESCU

Abstract: New organic – inorganic hybrid nanostructures were synthesized and characterized by incorporation of acetamiprid, the active component of Mospilan insecticide, in the layered structure of hydrotalcite – like anionic clays. MgAl hydrotalcite (HT) was used as clay matrix while two methods of incorporation have been applied: direct coprecipitation of metal nitrates and acetamiprid aqueous solutions and reconstruction method of the thermal treated anionic clays. The FT-IR spectroscopy (FTIR) and thermogravimetric (TG -DTG) analysis point out that the presence of the organic compound in the network structure of the synthesized MgAlHT. The SEM analysis shows that the acetamiprid – clay nanocomposites are formed by well dispersed particles with average sizes of about 120 nm. Considering together the insecticide activity of acetamiprid and the biocompatibility of the HT – like anionic clays the new synthesized materials could open interesting perspectives for obtaining more environmentally friendly insecticides.

Keywords: hydrotalcites, acetamiprid, hybrid – nanostructures, FTIR, TG-DTG

1. Introduction

Hydrotalcite (HT) is a class belonging to the naturally occurring anionic clay with the formula $Mg_6Al_2(OH)_{16}CO_3 \cdot 4H_2O$. It presents a positively charged brucite-like layers ($Mg(OH)_2$) in which some of Mg^{2+} are replaced by Al^{3+} in the octahedral sites of the hydroxide sheets. Interstitial layers formed by CO_3^{2-} anions and water molecules compensate the excess of the positive charge resulting from this substitution. The layers are stacked one on top of the other and are held together by weak interactions of hydrogen bonds [1-2]. Both magnesium and aluminium can be isomorphously substituted by other divalent or trivalent cations so a wide range of compositions containing various combinations of M(II), M(III) and different anions A^{n-} can be synthesized. The large variety of anions that can be incorporated in the brucite-like layer and the high anionic exchange capacity of these materials allow using them as matrices for tailoring specific organic – clay hybrid nanostructures with new potential applications [3]. The incorporation of the organic pesticides in the structure of anionic clays can offer premises to increase the pesticide active life by reducing its volatilization, controlling the release of the pesticide from the layered structure and decreasing the pesticide adsorption in soil and groundwaters.

Taking into account this information we selected acetamiprid the active component of Mospilan insecticide, to be incorporated into layered network of MgAl anionic clays.

The present paper aims to report the tailoring synthesis and some physical - chemical properties of MgAl hydrotalcite – like anionic clays incorporated with acetamidrid.

2. Experimental procedure

2.1. General procedures

All chemicals were commercially purchased and used without further purification. Thermal analyses (TG and DTG) were carried out in air on a Netzsch TG 209C thermal analyzer, from 298 to 1123 K, at a heating rate of 5 K /min. FTIR spectra were recorded on a FT-IR BOMEM MB 104 spectrometer under the following experimental conditions: 200 scans in the mid-IR range (400-4000 cm^{-1}) using KBr (ratio 5 / 95 wt %) pellets, and a resolution of 4.0 cm^{-1} . A Hitachi S-800 scanning electron microscope was used for scanning electron microscopy (SEM).

2.2 Preparation of the samples

2.2.1 Preparation of reference MgAlHT

100 ml of an aqueous solution of $\text{Mg}(\text{NO}_3)_2 \cdot 6\text{H}_2\text{O}$ (0.03 mol) / $\text{Al}(\text{NO}_3)_3 \cdot 9\text{H}_2\text{O}$ (0.01mol) and an aqueous solution of NaOH / Na_2CO_3 ($\text{CO}_3^{2-}/\text{Al}^{3+}+\text{Mg}^{2+}=0.67$, $\text{HO}^-/\text{Al}^{3+}+\text{Mg}^{2+}=2.25$), were added dropwise together, in such a way that the pH remained at a constant value of 9.5. The resulting white precipitate was aged at 338 K for 24 h under stirring. After an aging step, the obtained precipitates were separated by centrifugation, washed extensively with warm deionized water until sodium free and dried under vacuum at 40°C.

2.2.2 Preparation of acetamidrid containing samples

Acetamidrid – MgAlHT hybrid nanopowders were prepared by using direct synthesis by coprecipitation method or the reconstruction method; the amount of acetamidrid was optimized to the 4 times the content of Al^{3+} cations defined as anionic exchange capacity of the clay.

Direct synthesis by coprecipitation method (denoted as A1MgAlHT):

100 ml of an aqueous solution of $\text{Mg}(\text{NO}_3)_2 \cdot 6\text{H}_2\text{O}$ (0.03 mol) / $\text{Al}(\text{NO}_3)_3 \cdot 9\text{H}_2\text{O}$ (0.01mol) and an aqueous solution of acetamidrid 0.02 M were slowly added dropwise together; pH=10 was maintained by the continuous addition of 0.1 M NaOH . The obtained white precipitate was separated by centrifugation, washed extensively with warm deionized water until sodium free and dried under vacuum at 30°C.

Synthesis by reconstruction method (denoted as A2MgAlHT):

0.5 g MgAlHT sample was calcined at 500°C for 5 h, under air flow. 1 g of freshly calcined hydrotalcite – like sample was added in an aqueous solution

containing 3 g of acetamiprid, under bobbling N_2 in the medium and aged for 36 h at $45^\circ C$. The obtained white precipitate was separated by centrifugation, washed with warm deionized water until sodium free and dried under vacuum at $30^\circ C$.

3. Results and discussion

The FTIR spectra of the studied samples are shown in Figure 2. Between $2700 - 3700\text{ cm}^{-1}$ the broad adsorption band is assigned to the OH stretching mode of both layer hydroxyl groups and of interlayer water molecules [4]; for acetamiprid containing samples the characteristic peaks of aliphatic C-H stretch can be also identified at 2858 and 2927 cm^{-1} though the broad adsorption band of the hydroxyl stretching mode partially overlap the ν_{CH_3} vibrations. The band around 1620 cm^{-1} and the band between $1370 - 1380\text{ cm}^{-1}$ are characteristic for HT-like materials and are due to δ_{OH} bending vibrations of water molecules in the interlayer space and to the ν_3 antisymmetric stretching of interlayer carbonate respectively [5].

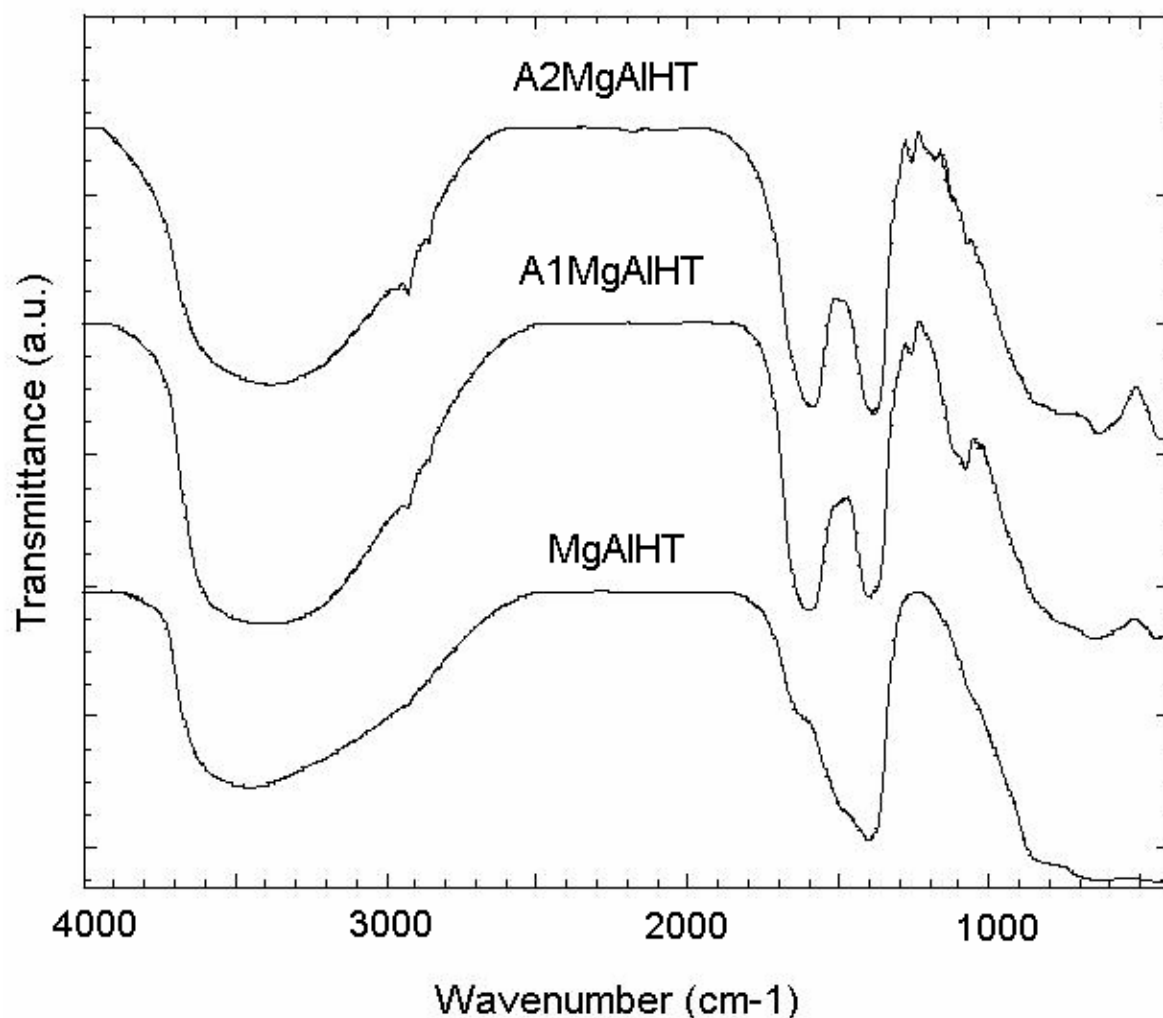


Fig.1 The FTIR spectra of A1MgAlHT, A2MgAlHT and MgAlHT

For acetamiprid containing samples two strong adsorption bands appear in the wavenumber range $1300 - 1700 \text{ cm}^{-1}$; the broadness of these bands can be assigned to the specific vibrations of interlayer water molecules, the specific vibrations of substituted pyridine [5] the characteristic vibration of $\nu_{\text{C}=\text{N}}$ and the characteristic vibrations of accidentally adsorbed CO_3^{2-} . Further the weak band that appears at 1255 cm^{-1} can be ascribed to $\nu_{\text{C}-\text{N}-\text{C}}$ vibration mode. The bands recorded below 1000 cm^{-1} can be mainly attributed to the M - O and M - O - M LDH lattice vibrations though the intense band that appears around 690 cm^{-1} in acetamiprid containing samples can be attributed to the specific vibrations of pyridine.

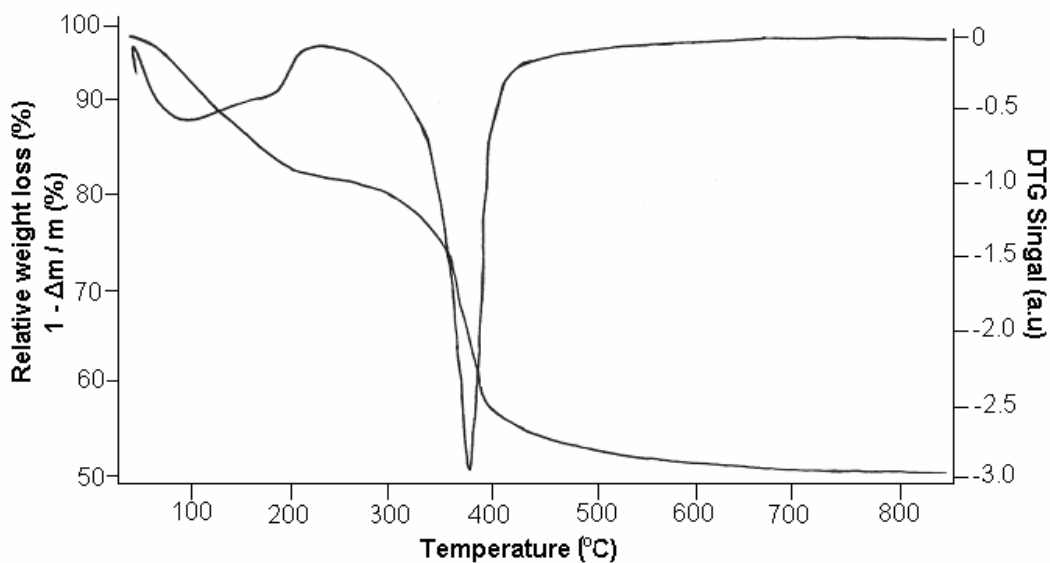


Fig.2 The TG-DTG diagram of AlMgAlH.

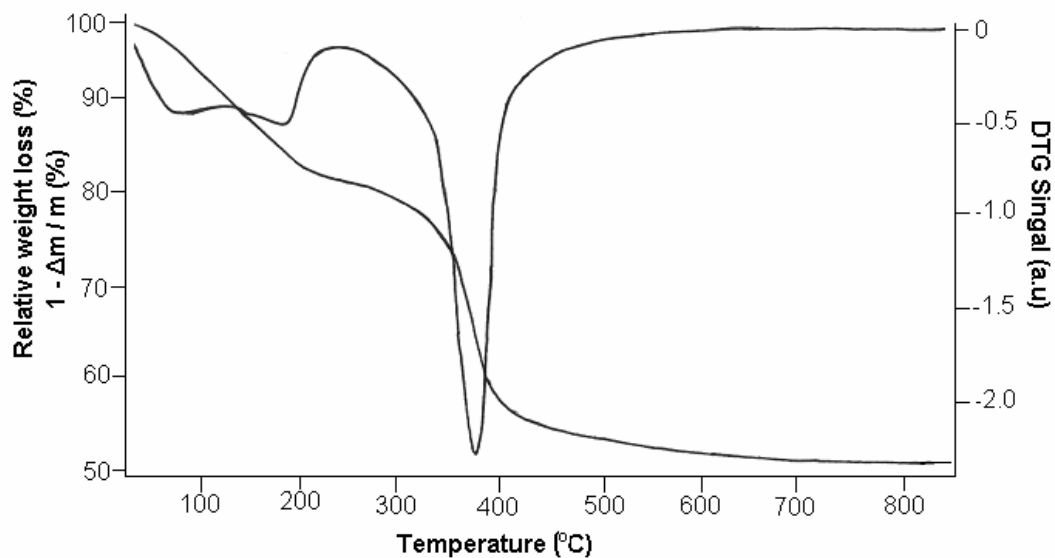


Fig.3 The TG-DTG diagram of A2MgAlHT.

The TG-DTG diagrams of A1MgAlHT and A2MgAlHT samples are displayed in Figure 2 and Figure 3 respectively and indicate that only a very small quantity of acetamiprid could be intercalate in the MgAlHT interlayer.

Both FTIR and TG-DTG analysis points out the presence of a small quantity of acetamiprid in the clay network.

The SEM picture of MgAlLDH sample is shown in Figure 4; it reveals well shaped particles characteristic to the HT –like materials with an average size of about 120 nm.

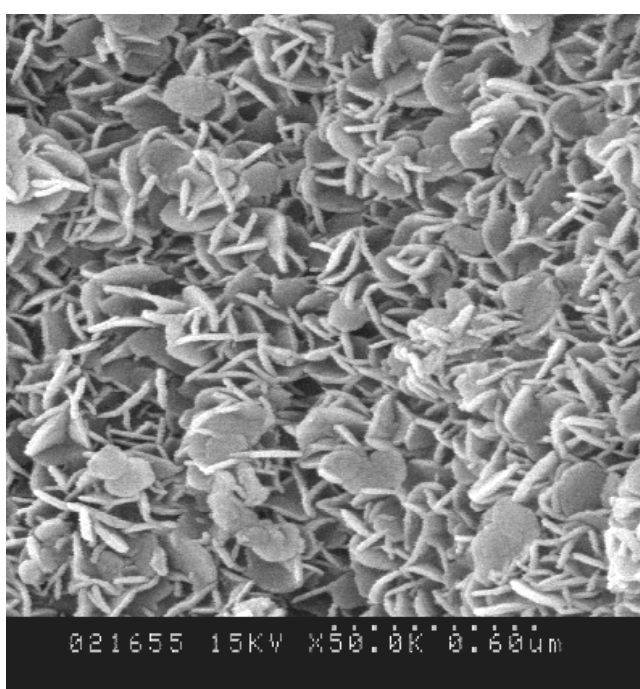


Fig.4. The SEM micrograph of MgAlHT

4. Conclusions

These preliminary results have shown that is enough difficult to intercalate acetamiprid in the layered network of hydrotalcite – like anionic clay though the partial intercalation of organic insecticide in the HT – like anionic clay structure has achieved; the experimental work on this subject has been continued in our laboratory for optimizing the synthesis conditions for obtaining well crystallized acetamiprid – anionic clay hybrid nanostructure.

REFERENCES

1. F. Cavani, F. Trifiro, A. Vaccari, **Catal. Today** **11** (1991) 173 and references therein.
2. W. Jones, M. Chibwe, in: I.V. Mitchel (Ed.), **Pillared Layer Structures Current Trends and Applications, Elsevier, London, 1991, p. 67.**
3. G. Carja, R. Nakamura, H. Niiyama, **Appl. Catal. A** 236 (2002) **91.**
4. G. Carja, R. Nakamura, T. Aida, H. Niiyama, **J. Catal.** 218 (2003) **104.**
5. FTIR data base catalogue of Tokyo Institute of Technology, Japan.

NOI NANOCOMPOSITE HYBRIDE A ARGILELOR ANIONICE DE TIP MgAlHT INCORPORATE CU ACETAMIPRID

Rezumat: Noi nanostructuri hibride organice – anorganice au fost sintetizate si caracterizate prin incorporarea acetamipridului, componenta activa a insecticidului de tip Mospilan, in structura stratificata a argilelor anionice de tip hidrotalcit. MgAl hidrotalcit (HT) a fost utilizat ca matrice de argila si 2 metode de incorporare a acetamipridului au fost studiate: coprecipitarea directa a nitratilor metalici si a solutiei apoase de acetamiprid si de asemenea metoda reconstructiei argilelor anionice tratate termic. Analiza prin spectroscopie FTIR cat si analiza TG-DTG arata prezenta compusului organic in matricea argilei MgAlHT sintetizate. Analiza SEM ne arata formarea unor nanocomposite de tip argila acetamiprid bine cristalizate formate din particule bine dispersate si cu o dimensiune medie de 120 nm. Considerand impreuna activitatea de insecticid a acetamipridului cat si biocompatibilitatea argilei anionice noile structuri sintetizate pot deschide perspective interesante pentru a obtine insecticide mai putin poluante.

LUBRICANT PERFORMANCES AND ENVIRONMENTAL PROBLEMS

BY

MARIA BERCEA

Abstract: *The paper discusses the rheological behavior and some performances of mineral oils additived with polymers. The environmental impact of the lubricants used in modern technologies imposes the reconsideration of the performances by taking into account the adverse effect on the environment.*

Keywords: *lubricants, polymer additive, viscosity, biodegradability*

1. Introduction

The basic functions of a lubricant are friction and wear reduction, heat removal and contaminant suspension. Apart from important application in internal combustion engines, vehicles and industrial gear boxes, compressors, turbines or hydraulic systems, there are vast number of other applications, which mostly require specifically tailored lubricants. Designing a lubricant to perform above stated functions in different systems is a complex task, involving a careful balance of properties both in the lubricant base stocks and the performance enhancing additives.

Lubrication has always implied the use of lubricating oil, usually formulated by blending appropriate quality lube base stocks(s) and additives. An average lubricating oil consists of about 93% base stock(s) and 7% chemical additives and other components. Base stocks used to formulate lubricants are normally of petroleum origin along with synthetic and vegetable oils, which may be incorporated for specialized applications. The performance of a finished lubricant, therefore essentially depends upon the type and quality of base stocks and on the additives used. The physico-chemical and performance requirements define a lubricant identity and its ability to reduce friction, resist oxidation, minimize deposit formation, prevent corrosion and wear. The lubrication efficiency and the application of lubricants is further dependent upon key parameters like consistency, flow properties or viscosity, which also appear in nearly all lubricant specifications.

The lubricant choice depends on the application, cost, temperature range, loading, oxidation stability, volatility, system compatibility, dispersant and detergency requirements and demulsification or emulsification properties. A long period of time, the cost and technical performances were priority criteria for the selection of lubricants. More recently, everyone has become more aware of the environmental

issues affecting our planet. Environmental behavior such as biodegradability, toxicity, occupational health and safety, and emissions has come into consideration.

The polymers are incorporated as additives into the base oils, increasing the viscosity and therefore the lubricant film thickness [1],..., [5]. Friction between two surfaces is one of the most important interactions, which controls the behavior of mechanical components in a wide range of applications. In concentrated contacts, the relative sliding velocity is superposed on nominal rolling velocity and the resulting friction is often referred to as traction. By using polymers as additives it is possible to modify the traction behavior of the lubricant oils. Due to the mechanical, thermal and physical-mechanical interactions, the modeling of the traction behavior is a complex problem, which has gained much interest [6],..., [8].

The paper is focused on the rheological behavior of additived and non-additived lubricants in the temperature range of 10°C to 95°C. These investigations are useful to improve our understanding of the lubricant performances at different temperatures and to forecast the influence of the polymer.

2. Experimental

A mineral oil, containing mainly paraffins and a low content of iso-paraffins and cycloparaffins was used as base oil. As additive was selected low density polyethylene (PE) with branched structure and $M_w = 1.2 \cdot 10^5$ g/mol.

The additivation of mineral oil with polyethylene was realized by mixing the polymer solid particles with the base oil under continuous magnetic stirring at 60°C. The following samples were selected for the experimental investigations: 0.0% (base oil), 0.1% PE, 0.5% PE, 1.0% PE, 1.5% PE and 2.0% PE (the concentration is expressed in grams of polymer dispersed into 100mL of base oil). More concentrated systems, i.e. 3.0% concentration, contain associated polymer particles and therefore no tests were performed with concentrations greater than 2.0%. The range of temperature for this study was from 10°C to 95°C.

Rheological investigations were performed for all samples using a Bohlin CVO rheometer equipped with a Peltier device for temperature control. The measurements were performed by using parallel-plate geometry. Both plates are from stainless steel, the upper plate having the radius of 60 mm. The upper plate was set at the separation distance of 500 μm . The viscosity and the shear stress of the additived oil samples were measured at shear rates ranging from 10^{-2}s^{-1} to 10^4s^{-1} , at different temperatures in the domain of 10°C - 95°C. The samples were pre-sheared before testing and the values of the viscosity were obtained after stabilization of the shear stress.

3. Results and Discussion

Viscosity is one of the most important properties of the lubricating oil. It is one factor responsible for the formation of lubricating films under both thick and thin film conditions. Viscosity affects heat generation in bearings, cylinders and gears due to internal fluid friction. It affects the sealing properties of oils and the rate of oil consumption. It determines the ease with which machines can be started at various temperatures, particularly cold temperatures. The satisfactory operation of any given

piece of equipment depends on using oil with the proper viscosity at the expected operating conditions.

The simple assumptions made in discussing fluid film lubrication are hardly ever valid in practice. Under certain conditions - such as shock loading, steady heavy load, high temperature, slow speed, and critically low viscosity - the lubricant system no longer remains in the hydrodynamic regime. A situation arises wherein there is intermittent contact between the surfaces, resulting in a significant rise in temperature and subsequent destruction of the contacting surfaces. Under these circumstances, the fluid film is no longer capable of adequately protecting the surfaces, and other approaches must be employed such as adding film-forming additives.

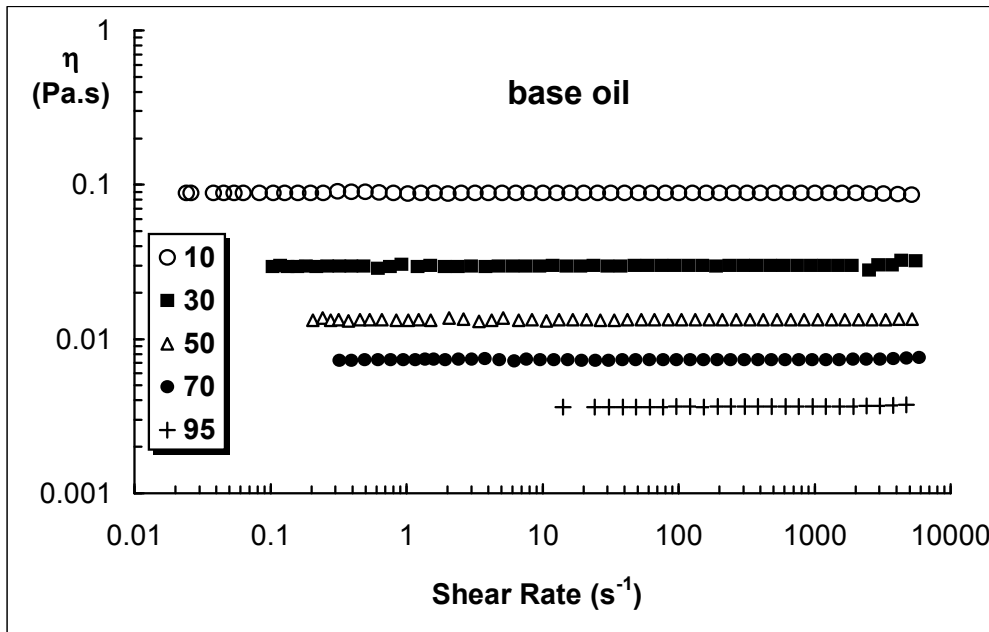


Fig. 1. – The flow curves obtained for the base oil at different temperatures.

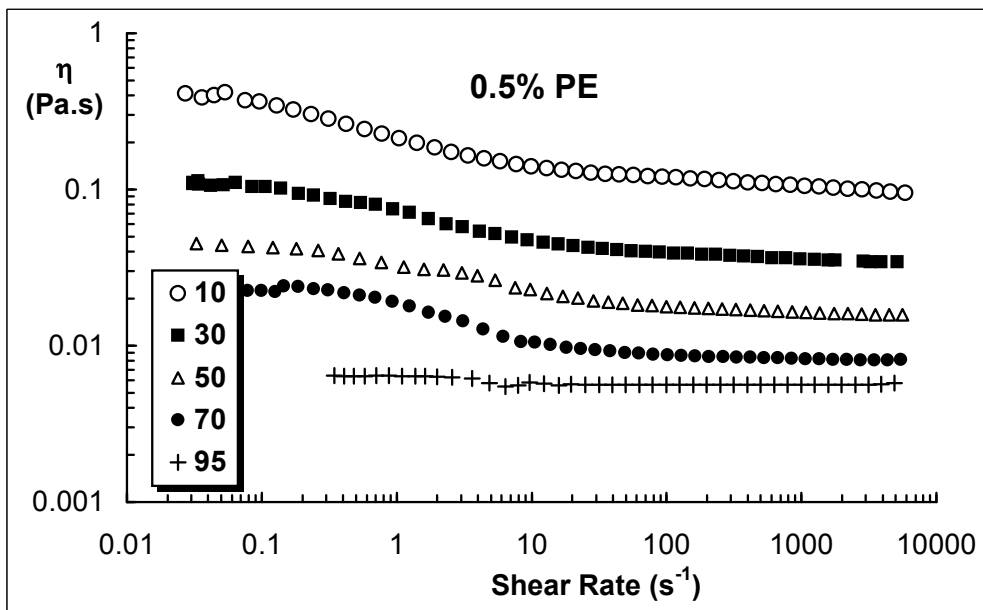


Fig. 2. – The flow curves obtained for the sample of 0.5% PE at different temperatures.

Figures 1 and 2 give the flow curves obtained at different temperatures for base oil (Figure 1) and a sample of base oil additived with 0.5% PE (Figure 2). For the base oil, the Newtonian behavior is observed for all studied temperatures. For all additived samples one observes a behavior similar with those given in Figure 2: the first Newtonian plateau at low shear rates, followed by a power-law shear-thinning region and then by a second Newtonian plateau at high shear rates ($> 100 \text{ s}^{-1}$).

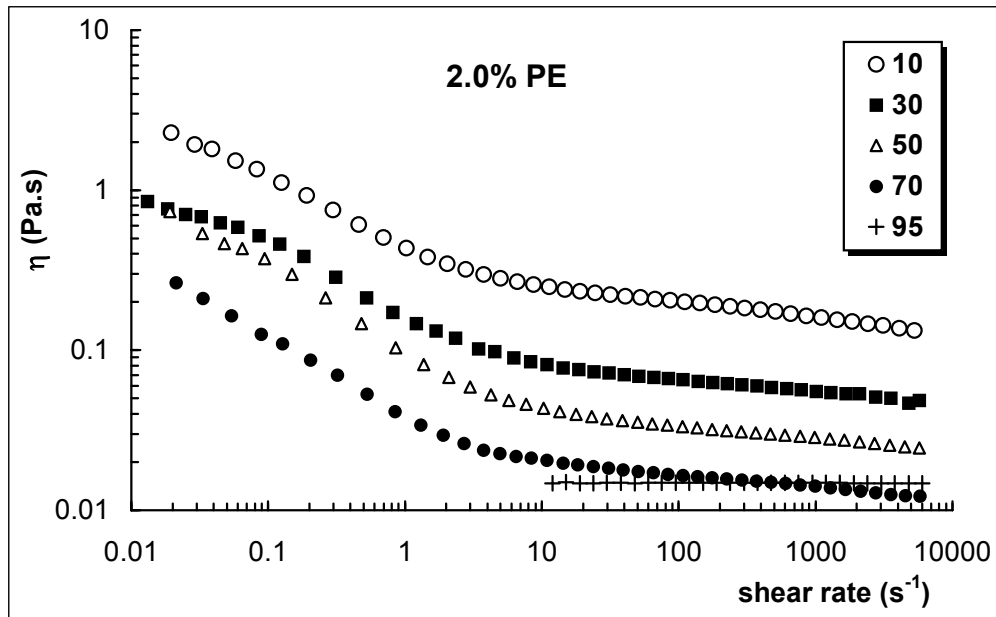


Fig. 3. – The flow curves obtained for the sample of 2.0% PE at different temperatures.

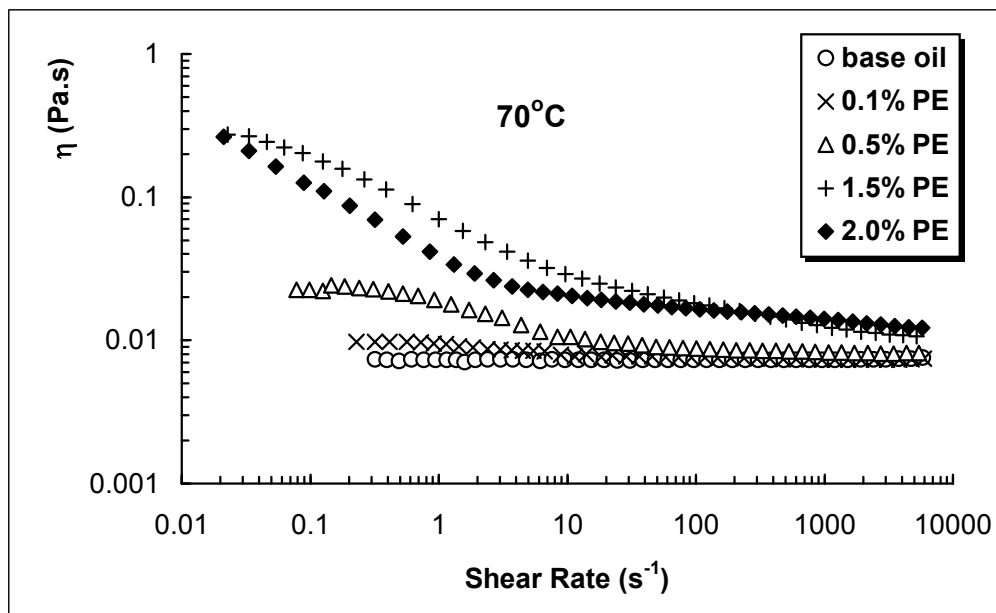


Fig. 4. – The flow curves obtained for samples with different concentrations of PE at 70°C .

Figures 3 and 4 present the effect of the polymer concentration on the flow curves at two different temperatures: 10°C and 70°C, respectively. In the region of very low shear rate, one observes an increase of viscosity with increasing the PE concentration up to 1.5% PE. For high shear rates, the differences between different samples diminish. The sample of 2% PE presents a peculiar behavior: up to 300 s⁻¹ the viscosity is lower than those of 1.5% PE, for higher shear rate the behavior changes. This behavior could be attributed to the entanglement formation. By analysing the viscometric data, the systems with concentration lower than 1.5% PE correspond to dilute regime, while the 2.0% concentration of PE indicated a solution in semidilute regime. Up 70°C, the dilute solutions exhibit non-Newtonian behavior, whereas at temperatures higher than 80°C all studied systems become Newtonian and sample of 2% PE have a viscosity higher than those of 1.5% PE.

The variation of the lubricant viscosity as a function of temperature can be described by using the Roelands relationship:

$$\log[\log \eta_T + 4.2] = \log K1 - K2 \cdot \log \left[1 + \frac{T}{135} \right] \quad (1)$$

where η_T is lubricant absolute viscosity (Pa·s) at temperature T (°C), K1 and K2 are constants determined for each lubricant at different temperatures.

A semi-empirical approach for determining the effect of the flow conditions on the effective rheological parameters of the lubricant (the elastic shear modulus, the viscosity of the lubricant and the limiting and Eyring stresses) at different temperatures can be considered [9], [10]. The tribological properties are strongly dependent on the polymer concentration. Previous experimental investigations [5], [10] have shown that there is an optimum value of the polymer concentration at which the polymer coils begin to overlap each other. This value is close to the critical concentration at which the polymer coils begin to overlap each other.

Schipper et al. [11] have observed that, under certain operating conditions, a constant low friction coefficient was obtained in the boundary or mixed lubrication regime. This behavior was attributed to microelasto-hydrodynamic lubrication with local solid-state lubrication. Under very high pressure such as the one found between contacting asperities, the lubricant becomes extremely viscous and behaves like a solid. It has been also shown that the lubricating films formed in rolling, concentrated contacts have two components [1]. At very slow speeds, the polymer forms an immobile film of thickness equivalent to two radii of gyration of the polymer molecules. This film thickness is independent of speed but is gradually squeezed from the contact when motion is halted. The film likely to represent maximum two monolayers of polymer on each surface (Figure 5) and can be regarded as a boundary lubricating film. As the rolling speed is raised, a conventional elastohydrodynamic is formed which is superimposed on the immobile film. By using low density polyethylene as additive, a considerable reduction of friction ($\approx 60\%$) due to the film formed by the adsorption of macromolecular coils on the solid surface was observed. It was observed that a low PE concentration (up to 1%) is enough to enhance the friction behaviour [6].

Generally, a chemical substance is said to be biodegradable if it can be broken down (degraded) by the metabolic action of living organisms such as bacteria, fungi, algae and yeasts. This is different from the processes of physical or chemical degradation (as for example an acid destroys), but biodegradation can take place at the same time as chemical or physical processes.

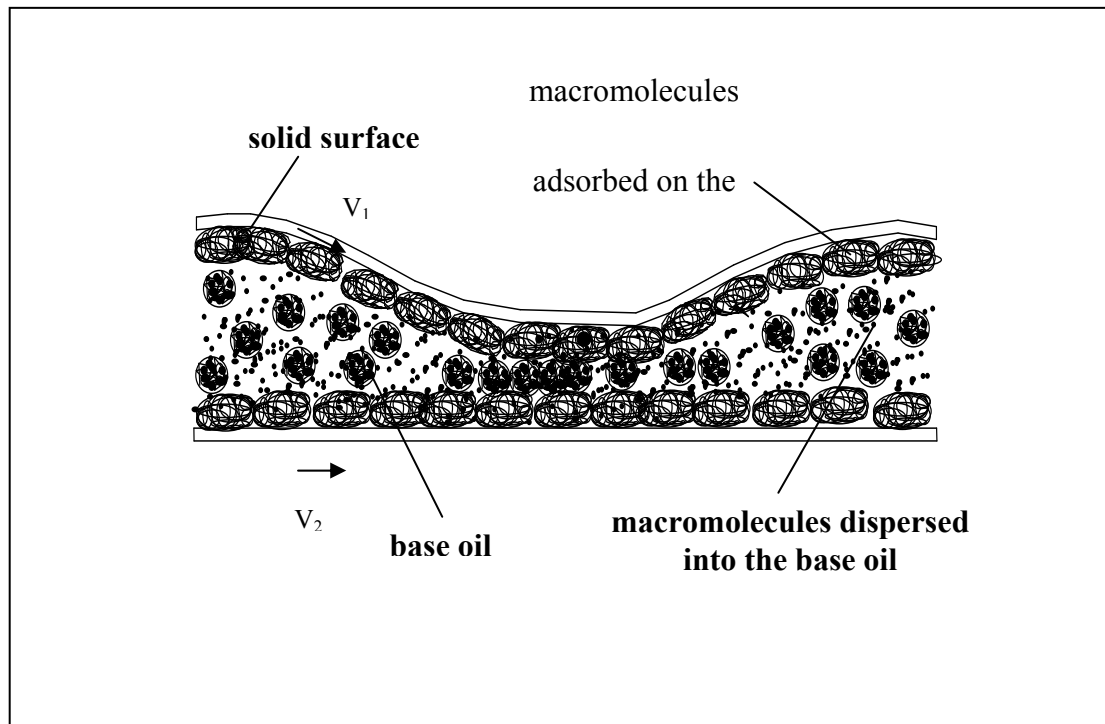


Fig. 5 – Schematic representation of the lubricant action in the presence of polymer.

Conventional lubricants based on mineral oils and certain synthetic base fluids will not be degraded by living organisms, or at least only to a small extent, so if such materials get into the environment they will stay there for a very long time presenting a contamination hazard to wildlife and the public alike. Some examples of environment contamination could be: railway lubrication; automotive lubricant leaks and overlubrication; catastrophic failures, water craft lubrication, forestry equipment lubrication, mining industry, unauthorized disposal, a.s.o. Such contamination hazards could be significantly reduced by using biodegradable lubricants. Such lubricants are attacked by natural microbes, consumed as a form of nutrient and energy resulting in breakdown of the lubricant. In reality, this process would be far more complex and it is unlikely that 100 per cent ultimate biodegradation would ever take place [12].

The biodegradability of the product's main components must be greater than 80%. (Main components are defined as components weighting more than 5% of product weight.) The product shall not contain organic halides or nitrite compounds. The biodegradability of the product's additives must be greater than 80% or meet the following requirements: (1) Toxicity to aquatic organisms should be > 1 mg/l in the acute test, or > 0.01 mg/l in the long-term test; and should have no bioaccumulation potential; (2) Toxic effect on higher plants should be > 100 mg/kg; (3) 3-hour bacteria inhibition test show a 50% inhibitory concentration $IC_{50} > 100$ mg/l.

The plastic packaging must not contain polyvinyl chloride (PVC) or other chlorine containing plastics. Also codes should be used to indicate types of plastic. The product or the packaging material shall bear a label reading "High Biodegradability". The following text should appear in the instructions for use and on product container: "Do not let residues escape into waste water or ground. Please bring residues to qualified disposal facility for separate disposal".

Different biodegradable lubricants and functional fluids are continuously developed [13], [14]. They are based on naturally occurring plant and rapeseed oils which make them harmless to the environment and cleaner for the operative to use. The technical properties of these products are equal to normal mineral oil based products and, in some characteristics, even show an improvement offering industrial end users benefits through lower consumption, rationalisation of product mix, excellent corrosion protection and reduced environmental and health and safety concerns.

By employing environment-friendly lubricants, pollution of and damage to the environment can be kept at bay. The use of fast biodegradable oils is especially required in areas with non-circulating lubrication.

Acknowledgements

This work was supported by a GRANT for Scientific Research financed by CNCISIS (cod 918).

REFERENCES

1. Cann P.M., Spikes H.A. – *The Behavior of Polymer Solutions in Concentrated Contacts: Immobile Surface Layer Formation*, **Trib. Trans.**, 1994, 37, **580-586**.
2. Georges E., Georges J.M., Diraison C. – *Rheology of Olefinic Copolymer Layers Adsorbed on the Solid Surfaces*, **Trib. Trans.**, 1996, 39, **563-570**.
3. Georges J.-M. – *Some Surface Science Aspects of Tribology in New Directions in Tribology*, Ed. Hutchings I.M., Mech. Eng. Publ. Ltd, 1997, **67**.
4. Mitsui, H., Spikes, H.A. – *Predicting EHD Film Thickness of Lubricant Polymer Solutions*, **Trib. Trans.**, 1998, 41, **1-10**.
5. Bercea M., Bercea I., Nélias D., Olaru D.N. – *Polyethylene as an Additive for Mineral Oils – Part I: Influence of the Polymer Concentration on the Film-Forming Properties in Rolling Bearing* **Trib. Trans.**, 1999, 42, **851-859**.
6. Bercea M., Bercea I., Nélias D., Flamand L. – *Polyethylene as Additive for Mineral Oils. Part II. EHD Traction Behavior*, **Trib. Trans.**, 2002, 45, **145-152**.
7. Bercea M., Bercea I. – *A Rheological Model Based on Primary Laboratory Data of the Lubricants Additived with Polymers*, **Macromol. Symp.**, 2002, 181, **353-362**.
8. Bair S., Qureshi F. – *The High Pressure Rheology of Polymer-Oil Solutions*, **Trib. Int.**, 2003, 36, **637-643**.
9. Bercea M., Paleu V., Bercea I. – *Lubricant Oils Additived with Polymers in EHD Contacts: Part I. Rheological Behavior*, **Lubr. Sci.** 2004, 17-1, **3-24**.
10. Paleu V., Bercea I., Cretu S., Bercea M., – *Lubricant Oils Additived with Polymers in EHD Contacts: Part I. Tests using a Four-Ball Machine*, **Lubr. Sci.** 2005, 17-2, **173-184**.
11. Schipper D.J., Gee A.W.J. – *On the Transitions in the Lubrication of Concentrated Contacts*, **ASME J. of Tribology**, 1994, 117, **250-254**.

12. Bercea M., Bercea I. – *Des Nouveaux Lubrifiants et l'Environnement*, Actes du Deuxième Colloque Franco-Roumain de Chimie Appliquée, 10-12 Oct. 2002, Bacau, Romania, p. 309-314.
13. <http://www.fuchs-oil.com>.
14. <http://www.ime.rwth-aachen.de>.

MARIA BERCEA

*“Petru Poni” Institute of Macromolecular Chemistry
Iasi*

**PERFORMANTE ALE LUBRIFIANTILOR SI PROBLEME LEGATE DE MEDIUL
INCONJURATOR**

Lucrarea prezinta aspecte privind comportarea reologica si performantele uleiurilor minerale aditivate cu polimeri. Impactul lubrifiantilor utilizati in tehnologii moderne impun reconsiderarea performantelor acestora in raport cu efectele nocive asupra mediului inconjurator.

EFFECT OF ADSORPTION ON THE VISCOSITY OF POLYMER SOLUTION AT VERY LOW CONCENTRATIONS

BY

MARIA BERCEA and SIMONA MORARIU

Abstract : *Measurements of viscosities in the dilute solution and in the region of very low concentrations were carried out for polystyrene in ethyl acetate. The curves of the reduced viscosity plotted against concentration shows an upward turn as the concentration is below a certain value. The anomalous behaviour of the η_{sp}/c vs. c dependence is explained as being due to the adsorption of the polymer on the glass walls of the viscometer.*

Keywords: *viscosity, polymer solution, low concentration, adsorption phenomena*

1. Introduction

Experimental and theoretical papers have established the existence of three concentration regimes: dilute, semidilute and concentrated. Generally, the transition from one region to another does not occur abruptly, but rather gradually. It is not always possible to establish a well-defined transition concentration separating regimes with distinctive features, i.e., to find a measurable quantity displaying a different behaviour depending on the actual regime [1], [2].

The behaviour of polymer solutions at extreme dilutions has attracted considerable interest during the last years and a series of investigations has been carried out to elucidate such problems [3],..., [7]. The experimental works present some difficulties due to the very low concentration of polymer and high precision measurements are necessary. The viscosity of a polymer solution in the extremely dilute concentration region usually reveals some abnormalities such as the curves of reduced viscosity plotted against concentration that shows either an upward or a downward turn as the concentration us below definite concentration.

Dondos et al. [3],..., [10] detected the critical concentration c' for poly(methyl methacrylate), polystyrene and their mixtures in different solvents, from the dependence of η_{sp}/c versus c . In all cases two different straight lines having positive slopes (depending on the capillary size of the viscometers for the extremely dilute domain) were obtained and their intersection clearly determined a crossover point c' . Above the c' concentration they supposed that a compression of the macromolecular coils occurs due to the resistance of the macromolecular coils to mutual interpenetration. The gradual compression of the chains is shown by a continuous deviation of the observed values of η_{sp}/c from the "ideal" values. Also, they have

found that c' varies with $[\eta]^{-1}$ or M^{-a} , where a is the exponent in the Mark–Houwink equation.

The present paper is concerned with a viscometric study of polystyrene in ethyl acetate in the dilute and extremely dilute regimes. The critical concentrations c' as well as their dependence on the molecular weight were determined.

2. Experimental procedure

Four standard polystyrene (PS) samples narrowly distributed ($M_w/M_n < 1.05$) with molecular weights in the range $4.37 \cdot 10^4 \leq M_w \leq 1.07 \cdot 10^6$ (from Polymer Laboratories Ltd.) were studied. Also, a ultrahigh molecular weight polystyrene (PS) sample with $M_w = 6.386 \cdot 10^6$, $M_w/M_n \cong 1.2$, obtained by plasma induced polymerization [11] was investigated.

The viscometric measurements were carried out in ethyl acetate over a large domain of concentrations, at 25°C, with an Ubbelohde suspended-level viscometer. The flow time for the solvent was 172.2 sec ($\pm 0.03\%$). The intrinsic viscosities were determined by using the Huggins method, in the domain of concentrations for which the relative viscosity $1.2 < \eta_{rel} < 1.80$. The present study is focused on the viscometric behaviour in the region $\eta_{rel} < 1.2$.

3. Experimental results and discussion

The dependence between the intrinsic viscosity and the molecular weight obtained for polystyrene ($4.3 \cdot 10^4 < M_w < 1.9 \cdot 10^7$) in ethyl acetate at 25°C was recently reported [12]:

$$[\eta] = 48.3 \cdot 10^{-5} \cdot M_w^{0.55} \quad (\text{dl/g}) \quad (1)$$

Table 1 presents the weight average molecular weights, the polydispersity indices, the intrinsic viscosities and the Huggins constants for the PS samples studied in ethyl acetate.

In Table 1 are also given the values of the critical concentration c^* , at which the polymer coils begin to overlap each other (the concentration which separates the dilute - semidilute regimes), calculated according to:

$$c^* = \frac{0.77}{[\eta]} \quad (2)$$

The dependence of reduced viscosity (η_{sp}/c , dl/g) versus concentration (c , g/dl) for sample 5 (Table 1) in ethyl acetate is presented in Figure 1. For all samples, at the critical concentrations c' and c^* , changes in the slope of the straight lines were observed. The values of critical specific viscosity (η_{sp}^{cr}) and critical concentration c' which separates the extremely dilute to dilute domains were determined (Table 2).

Table 1 Weight and number average molecular weights, polydispersity indices, intrinsic viscosities, Huggins constants and critical concentrations c^* (eq. (2)) for polystyrene samples in ethyl acetate at 25°C

| Sample | $M_w \cdot 10^{-6}$ (g/mol) | M_w/M_n | $[\eta]$ (dl/g) | k_H | c^* (eq. (2)) (g/dl) |
|--------|--------------------------------|-----------|--------------------|-------|---------------------------|
| 1 | 0.0437 | 1.03 | 0.172 | 0.220 | 4.477 |
| 2 | 0.5260 | 1.04 | 0.753 | 0.257 | 1.023 |
| 3 | 0.6470 | 1.03 | 0.832 | 0.266 | 0.997 |
| 4 | 1.0700 | 1.20 | 0.874 | 0.278 | 0.881 |
| 5 | 6.3860 | 1.20 | 2.606 | 0.374 | 0.295 |

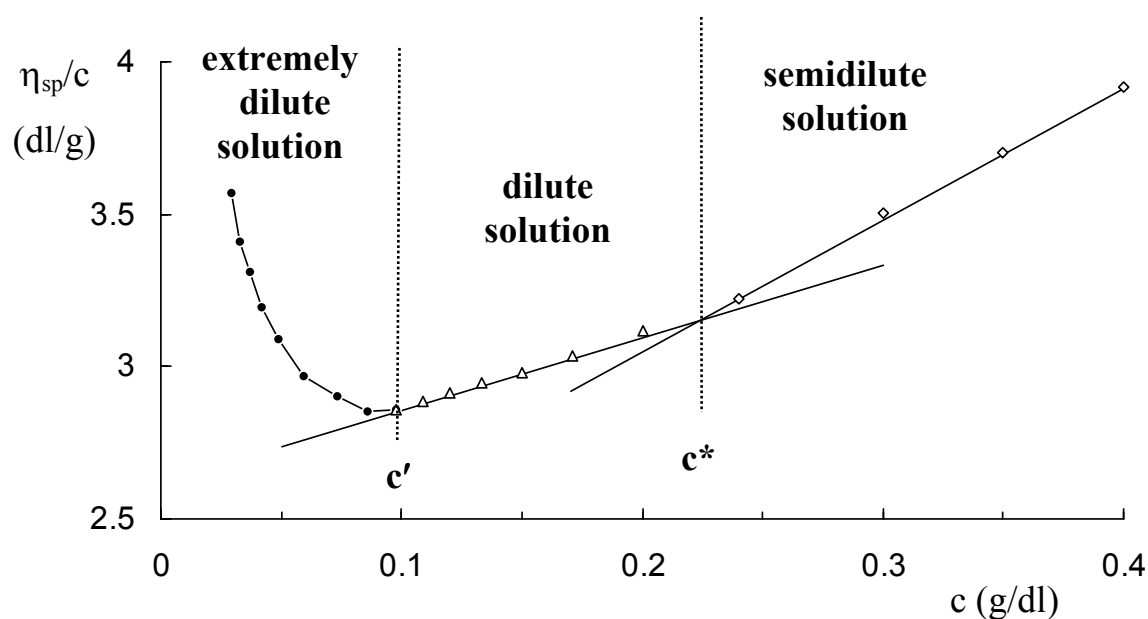


Fig. 1 Plot of reduced viscosity (η_{sp}/c) versus concentration (c) for polystyrene with $M_w = 6.386 \cdot 10^6$ in ethyl acetate at 25 °C

At crossover concentration c' the chains of the polymer first come into contact. Figure 1 suggests that an expansion of the coil below this concentration occurs as shown by the deviation of the observed values of η_{sp}/c versus c from the straight line obtained in the dilute regime. The crossover point c' changes with the molecular weight of the samples and moves to lower concentrations as the molecular weight of the samples increases (Table 2).

According to the data from Table 2, over the molecular weight range investigated, we obtain the following relation:

$$c' = \frac{0.19}{[\eta]} \quad (\text{g/dl}) \quad (3)$$

If in equation (3) $[\eta]$ is replaced by the Mark – Houwink dependence (equation (1)), the following relation is obtained for c' :

$$c' \cong 393.4 \cdot M_n^{-0.55} \quad (\text{g/dl}) \quad (4)$$

Also, for the critical specific viscosity the following empirical equation was established:

$$\eta_{sp}^{cr} = e^{-0.18 \cdot \ln[\eta] - 1.951} \quad (5)$$

Table 2 c' and η_{sp}^{cr} values determined from experimental curves and from equations (3) and (5), respectively, and the exponent b calculated from experimental curves

| Sample | c' (g/dl) | | η_{sp}^{cr} | | b |
|----------------|----------------|---------|------------------|---------|-------|
| | experimental | eq. (3) | experimental | eq. (5) | |
| 1 | 1.103 | 1.105 | 0.194 | 0.195 | 0.227 |
| 2 | 0.250 | 0.252 | 0.165 | 0.150 | 0.198 |
| 3 | 0.226 | 0.228 | 0.148 | 0.147 | 0.180 |
| 4 | 0.209 | 0.217 | 0.153 | 0.146 | 0.140 |
| 5 | 0.068 | 0.073 | 0.116 | 0.120 | 0.183 |
| average value: | | | | | 0.186 |

Table 2 shows that the equations (3) and (5) verify satisfactorily the experimental data.

From the experimental data obtained for PS samples in ethyl acetate, an empirical equation was established:

$$\frac{\eta_{sp}}{c} = [\eta] \cdot c^b \quad \text{for } c < c' \quad (6)$$

with the exponent b given in Table 2.

Also, for $c' < c < c^*$, the Huggins equation is valid:

$$\frac{\eta_{sp}}{c} = [\eta] + K_H \cdot [\eta]^2 \cdot c \quad \text{for } c > c' \quad (7)$$

From equations (3), (5) and (6), for $c = c'$, the b exponent is found to be 0.180, very close to the mean value of 0.186 resulting from the studied samples (Table 2).

The upturn in the reduced viscosity below the critical concentration c' was also reported in a previous paper for polyacrylonitrile in dimethylformamide in very dilute solutions [11]. The relative viscosity of an extremely dilute solution is very close to unity and high accuracy is demanded for the measurement.

The viscometric results obtained in the extremely dilute regime can be explained in different ways. During polymerization, some polymer chains intermesh in a complex fashion and they will not become completely untangled unless dissolved with strong agitation to concentration below the critical one. Thus, the upturn of the

η_{sp}/c curves could be due in part to the final untangling of the molecules but also in part to an expansion of the individual coils. On the other hand, the anomalous behaviour of the η_{sp}/c vs. c dependence at low concentrations could be caused by adsorption of the polymer on the glass walls of the viscometer. The reduction in radius of the viscometer capillary and actual concentration of solution may also influence the result for the measurement [12].

The adsorption of the macromolecular chains on the viscometer walls may have two effects. Firstly, a decreasing of the concentration occurs and, consequently, the efflux time decreases. The other effect is a change of the shape of the η_{sp}/c vs. c curve at very low concentrations and can be attributed to the decrease of the capillary radius of the viscometer due to the adsorbed film (Figure 2), when:

$$\eta_{rel} = \eta_{rel}^* \left(\frac{r-a}{r} \right)^4 \quad (8)$$

or

$$\frac{\eta_{sp}^*}{c} = \frac{\eta_{sp}}{c} + \frac{4a}{r \cdot c} \left(\frac{\eta_{sp}}{c} + 1 \right) \quad (9)$$

where: r is the capillary radius and a is the film thickness; η and η^* are the true and observed viscosities, respectively.

For $\eta_{rel} \sim 1$, equation (9) can be approximated as:

$$\frac{\eta_{sp}^*}{c} = \frac{\eta_{sp}}{c} + \frac{4a}{r \cdot c} \quad (10)$$

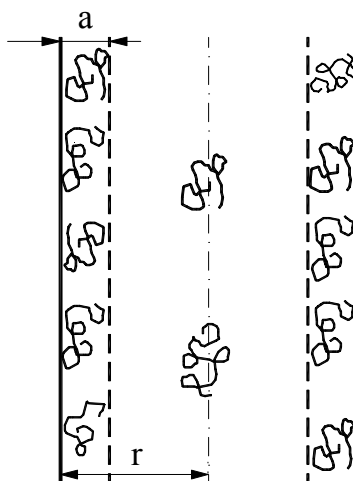


Fig. 2 The decrease of the capillary radius of the viscometer due to the adsorbed film

The correction terms, $\frac{r-a}{a}$ in eq. (8) or $\frac{4a}{r \cdot c}$ in eq. (10), are negligible at higher concentrations when a is much smaller than r . The value of this term increases at very

low concentrations c and the observed value η_{sp}^*/c can be considerably greater than the true one. Also, it is observed that the correction term varies linearly with $1/r$ and this effect should be corrected by extrapolation to $1/r = 0$ (i.e. to infinite radius) from a series of measurements with different capillary radii.

4. Conclusions

This work presents the viscometric behaviour of polystyrene in ethyl acetate at 25°C in dilute and extremely dilute solutions. The experimental investigations show that the critical overlapping concentration depends on the molecular weight and on the viscosity of the polymer in solution. Moreover, a scaling law between the reduced viscosity η_{sp}/c and the concentration c in extremely dilute regime was established.

Also, from experiments it was observed that the change of the viscometer capillary size determines a change of the b parameter from equation (6).

Acknowledgements

This work was supported by a GRANT for Scientific Research financed by CNCSIS (cod 918).

REFERENCES

1. Graessley W.W., *The entanglement concept in polymer rheology*, **Adv. Polym. Sci.**, 1974, 16, 1-179.
2. Bercea M., Ioan C., Ioan S., Simionescu B.C., Simionescu C.I. - *Ultrahigh molecular weight polymers in dilute solutions*, **Prog. Polym. Sci.**, 1999, 24, 379-424.
3. Dondos A., Tsitsilianis C. - *Viscometric Study of Extremely Dilute Macromolecular Solutions: Critical Concentration c^{**} and the Huggins constant*, **Polymer International**, 1992, 28, 151-156.
4. Dondos A., Tsitsilianis C., Staikos G. - *Viscometric study of aggregation phenomena in polymer dilute solutions and determination of the critical concentration c^{**}* , **Polymer**, 1989, 30, 1690-1694.
5. Papanagopoulos D., Dondos A. - *Viscometric study of extremely dilute solutions of two polymers with different molecular weights*, **Macromol. Chem. Phys.**, 1994, 195, 439-448.
6. Papanagopoulos D., Pierri E., Dondos A. - *Influence of the shear rate, of the molecular architecture and of the molecular mass on the critical overlapping concentration c^** , **Polymer**, 1998, 39, 2195-2199.
7. Dondos A., Papanagopoulos D. - *Difference between the dynamic and static behaviour of polymers in dilute solutions : 1. The critical concentration c^{**}* , **Polymer**, 1995, 36, 365-369.
8. Papanagopoulos D., Dondos A. - *Difference between the dynamic and static behaviour of polymers in dilute solutions : 2. The critical concentration c^** , **Polymer**, 1995, 36, 369-372.
9. Gosa K.L., Uricanu V., Pierri E., Papanagopoulos D., Dondos A. - *Study of the critical concentration c^{**} in dynamic and static state*, **Macromol. Chem. Phys.**, 2000, 201, 621-626.
10. Gosa K.L., Papanagopoulos D., Dondos A. - *Study of the conformational transition of polystyrene-poly(methyl methacrylate) block copolymers with temperature using measurements of the c^{**} critical concentration*, **Colloid Polym. Sci.**, 2003, 282, 84-87.
11. Bercea M., Morariu S., Ioan C., Ioan S., Simionescu B.C. - *Viscometric study of extremely dilute polyacrylonitrile solutions*, **Eur. Polym. J.**, 1999, 35, 2019-2024.
12. Cheng R., Shao Y., Liu M., Qian R. - *Effect of adsorption on the viscosity of dilute polymer solution*, **Eur. Polym. J.**, 1998, 34, 1613-1619.

*“Petru Poni” Institute of Macromolecular Chemistry
Iasi*

**EFFECTUL ADSORBTIEI ASUPRA VISCOZITATII SOLUTIILOR DE POLIMERI LA
CONCENTRATII FOARTE MICI**

Rezumat: Lucrarea prezintă date viscozimetrice obținute în soluție diluată și în regiunea concentrațiilor foarte mici pentru polistiren în acetat de etil. Sub o anumită valoare a concentrației polimerului, curbele care prezintă variația vîscozității reduse cu concentrația au înregistrat deviații pozitive de la liniaritate. Anomaliile de comportare a dependenței η_{sp}/c funcție de c sunt explicate ca fiind datorate adsorbției polimerului pe pereții viscozimetrului.

METALLURGICAL TREATMENT AND SURFACE INFLUENCE ON THE CORROSION RESISTANCE OF NICROMALSOFT ALLOY

D. MARECI*, DELIA-MARINELA AELENEI**, GH. NEMTOI*** and GINA UNGUREANU*

In recent years a number of a new highly corrosion resistant alloys combining Nickel, Chromium and Molybdenum have been introduced as biomaterials. Between these the NicromalSoft alloy (IMNR Bucuresti) presents superior corrosion resistance in biological human fluids. Using the electrochemical methods, namely linear and cyclic polarization curves, was studied the influence of surface quality and metallurgical treatments on the corrosion process of this alloy in an artificial saliva of Afnor type. The main parameters of the corrosion process were evaluated. Alloy surface was also analyzed by optical microscopy

Keywords: NicromalSoft, pitting, corrosion, polarization curves, corrosion parameters

Introduction

The utilization of nickel in dental alloys is due to the fact that, at a content of 55 ... 65 percentages, the alloy's properties satisfy the essential wants of dental replacements: corrosion resistance, strong, thin and low cost. The alloy itself with Chromium and Cobalt provide the mechanical properties accepted by dentistry. It was demonstrated that Nickel dissolves from dental devices into natural saliva, the dissolution rate being accelerated if beryllium is present in the alloy

On the other hand, the Nickel is recognized as the most carcinogenic metal on Terra. Thus alloys delivering nickel ions can generate cancer through readily absorption across the cell membranes. In other direction, Nickel has the ability to bind oxygen, nitrogen, and sulfur from bio-compounds, replacing the usual catalysts (magnesium and calcium), which are essential in many metabolic activities. More, Nickel is considered as a metal that can create reproductive toxicity, create chromosomal aberrations, is immunosuppressive, etc.

Nevertheless, twenty years ago about 85% of the dental crowns were made from nickel based alloys, while in the last decade we are still faced with over 50% of the crowns being allied nickel. Between the most used nickel based alloys one can mention the Wiroloy and Wiron NT produced in Germany. These alloys exhibit a good corrosion resistance in artificial saliva and in Ringer type solution [1]. Corrosion behavior of some Ni-Cr alloys in Rondelli saliva was also studied earlier [2,3].

As recommends the American Dental Association (no. 14 ANSI specification), the total weight of chromium, cobalt and nickel do not be lower than 85 %, and chromium percentage do not be lower than 20. American Dental Association can

accept other compositions only when the alloy satisfies the conditions of toxicity, hyper sensibility and corrosion.

Thus, was accepted the VeraSoft alloy (Alba Dent SUA) which contain 68,1% Ni and 14,5% Cr. A similar alloy was realized in Romania (INMR, Backrest), named as NicromalSoft. This alloy was studied previously regarding the corrosion behavior in Ringer solution [4].

This paper presents the effects of the thermal treatments about to the corrosion resistance comparatively with the corresponding casting alloy.

Experimental

The composition of NicromalSoft alloy is: 64.6Ni, 17.8Cr, 9.8Cu, 3.5Mn, 1.8Si, 1.5Al, 0.5Ti and 0.5Fe. Phase diagram of the binary system Ni-Cr shows that this mixture is a system with partial isomorphism and eutectic. The eutectic temperature is 1344 °C. By addition copper, manganese and aluminum the alloy melting temperature was reduced till 1150 °C.

The corrosion medium was an aerated artificial saliva of Afnor type having the composition: NaCl – 0.7 g/L, KCl – 1.2 g/L, Na₂HPO₄H₂O – 0.26 g/L, NaHCO₃ – 1.5 g/L, KSCN – 0.33 g/L, urea – 1.35 g/L [5] (Carter-Brugirard AFNOR/NF (French Association of Normalization) and pH = 8.

The thermal treatment applied to this alloy was conducted at two main temperatures: 1100 °C for the domain of the Ni predominanting mixed crystals and 750 °C for the domain of the heterogeneous mixture of mixed crystals. The treatment parameters are presented in Table 1.

Table 1

| NicromalSoft alloy | Applied thermal treatment |
|--------------------|-------------------------------|
| Sample 1 | Commercial material (casting) |
| Sample 2 | 1100°C/2h/AC |
| Sample 3 | 750°C/20h/AC |
| Sample 4 | 1100°C/2h/FC/750°C/3h/AC |
| Sample 5 | 1100°C/2h/FC/750°C/20h/AC |

AC-air cooling, FC-furnace cooling

The determination of open circuit potential and the cyclic polarization curves recording were performed with the electrochemical system VOLTALAB-32, which consists of a potentiostat, a three-electrode cell, an electrochemical interface and a PC. Experimental data were acquired and processed with the VoltaMaster 2 software. The saturated calomel electrode (SCE) was used as reference electrode) and platinum as a counter electrode.

The working electrode, made from alloy sample was processed into a cylindrical shape and mounted in a Teflon support. In these conditions the surface exposed to corrosion was a one-dimensional circular aria.

Before experimental measurements the samples were mechanically polished successively up to a granulation number of 2500 mesh, by using different SiC abrasive

papers. Then they were washed with water, degreased with ethyl alcohol and preserved in double-distilled water.

Linear polarization measurements were performed, in aerated solution, at potentials near the corrosion potential (E_{corr}) in the potential range ($E_{\text{corr}} - 10$) mV ... ($E_{\text{corr}} + 10$) mV and a potential scan rate of 0,5 mV/s. The polarization resistance (R_p) was calculated as tangent slope at the electrode potential vs. current density curve, in the E_{corr} point. Subsequently, potentiodynamic cathode polarization was initiated at E_{corr} and terminated at 200 mV below the E_{corr} value at a rate of 0,5 mV/s in aerated medium.

The current density at the corrosion potential (J_{corr}), which is a measure of the corrosion rate, was calculated with the Stern-Geary equation [6, 7]:

$$J_{\text{corr}} = \frac{\beta_a \beta_c}{2,3 R_p (\beta_a + \beta_c)}$$

Three additional corrosion parameters: breakdown potential (E_{br}) and repassivation potential (E_{rep}), were determined from the cyclic potentiodynamic polarization curves, which were registered at a potential scan rate of 10 mV/s, over the electrode potential range: $-350 \dots +1500$ mV.

Results and Discussion

Figures 1 and 2 show the dependence of the electrode potential as function of the current density on a potential interval of ± 10 mV around the corrosion potential for sample 2 and sample 3. From this dependence was calculated the polarization resistance, R_p .

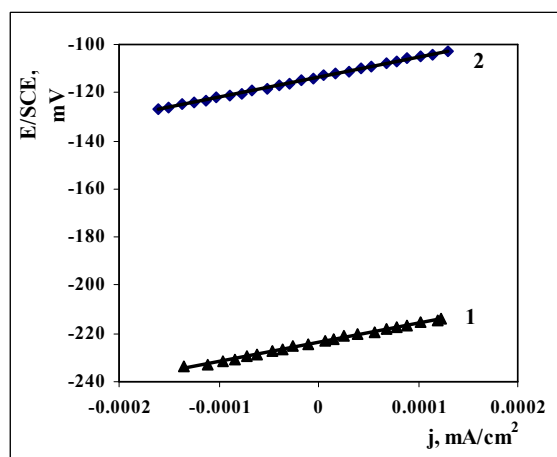


Fig.1. E-j dependence for sample 2
1-fresh polished surface, 2-surface maintained for 3 day in solution

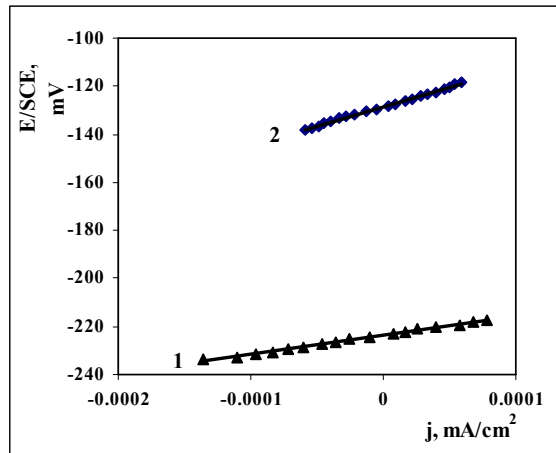


Fig.2. E-j dependence for sample 3

1- fresh polished surface, 2- surface maintained for 3 day in solution

Figures 3 and 4 presents the cyclic polarization curves for sample 1 and sample 3 in the domain $-300 \dots +1500$ mV.

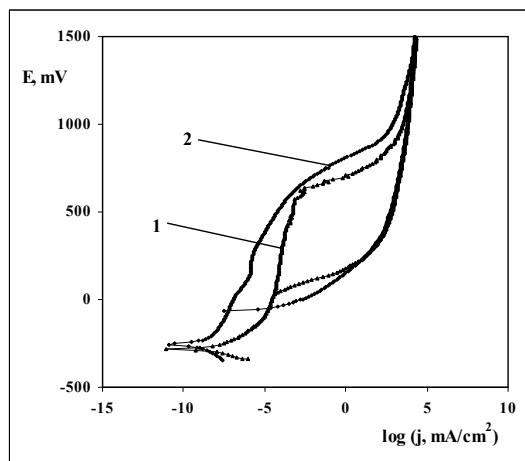


Fig. 3. Cyclic polarization curves for sample 1

1- fresh polished surface, 2- surface maintained for 24 hours in solution

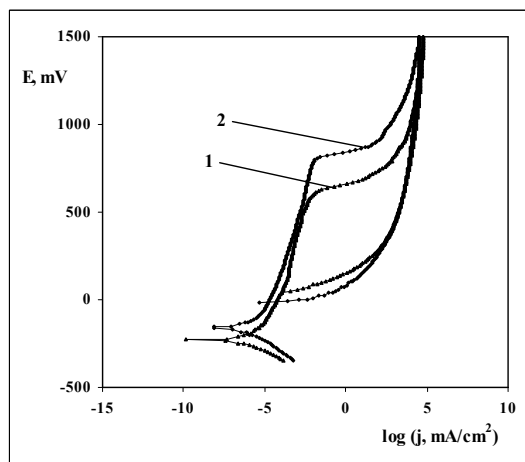


Fig. 4. Cyclic polarization curves for sample 3

1- fresh polished surface, 2- surface maintained for 24 hours in solution

One can see that both casting sample and thermal treated samples pass directly in a stable state, namely do not presents a classical active-passive transition.

On the basis of the two polarization curves, linear and cyclic, the main parameters of the electrochemical corrosion process are presented in Table 2.

Table 2

Electrochemical corrosion parameters for NicromalSoft alloys in Afnor type saliva

| NicromalSoft | Fresh polished surface | | | | | |
|--------------|--|-------------------------------------|--|-------------------------|--------------------------|-----------------|
| | E_{corr} (mV) | R_p ($K\Omega \text{ cm}^2$) | J_{cor} (nA/cm^2) | E_{br} (mV) | E_{rep} (mV) | ΔE (mV) |
| Sample 1 | -350 | 37,8 | 278 | 620 | 120 | 500 |
| Sample 2 | -229 | 79,5 | 163 | 667 | 172 | 495 |
| Sample 3 | -205 | 55,9 | 204 | 643 | 140 | 503 |
| Sample 4 | -166 | 26,9 | 458 | 675 | 156 | 519 |
| Sample 5 | -205 | 18,7 | 650 | 627 | 147 | 480 |
| | Old surface (3 day in artificial saliva) | | | | | |
| Sample 1 | -290 | 40,1 | 252 | 720 | 110 | 610 |
| Sample 2 | -157 | 83,8 | 137 | 851 | 116 | 735 |
| Sample 3 | -173 | 162,8 | 59 | 840 | 140 | 700 |
| Sample 4 | -157 | 33,5 | 292 | 859 | 133 | 726 |
| Sample 5 | -213 | 20,46 | 605 | 843 | 52 | 791 |

E_{br} – breakdown potential, E_{rep} – repassivation potential, $\Delta E = E_{\text{br}} - E_{\text{rep}}$.

From these data one results that the casting NicromalSoft alloy shows a great negative corrosion potential in the case of fresh polished surface which is reduced after that the alloy was maintained three day in artificial saliva. This indicates a certain passivation. The corrosion currents are enough lower, of 200...300 nA

The lower values of the breakdown potential indicate a high susceptibility to pitting corrosion on the alloy surface. The repassivation take place at small potentials, closed on the corrosion potential, both in the case of fresh surface and old surface.

The corrosion behaviour depend on the applied thermal treatment. The corrosion potentials are closed for all treated samples but these are greater than for non-treated sample, indicating a certain passivation. Important differences appear in the case of the polarization resistances and, consequently, in the case of corrosion currents. As can be seen, the sample 3 (treated at 750 °C) presents a significant passivation after maintenance in solution, this being single sample for that the corrosion current density diminish less than 100 nA/cm^2 . As compared with commercial sample the samples 2 and 4 presents a higher resistance to corrosion, while, contrary, the sample 5 is more corrosive than casting sample, indifferently on the surface state.

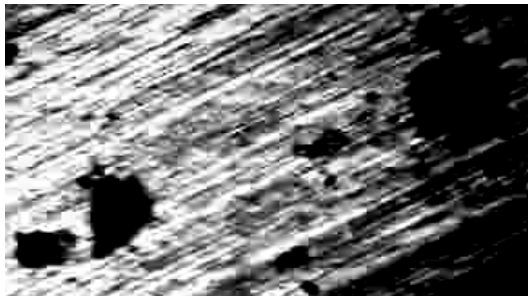
As an effect of the applied thermal treatment the corrosion type do not modify. More, the repassivation potential is very closed for all treated and non-treated samples, while the breakdown potential is higher with approximately 100 mV for old surface measurements.

However, a potential difference of +800 mV, corresponding to the breakdown potential, is hardly probable to achieve in the oral cavity.

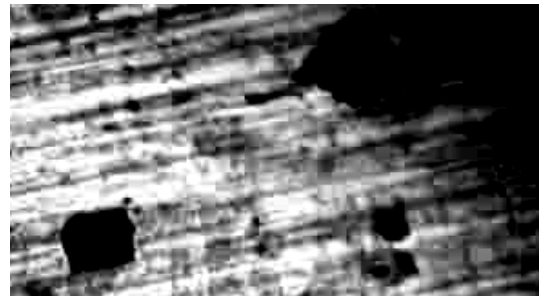
By optical microscopy was evidenced the surface quality after anodic polarization. In Figure 5 are presented the surface photographs for all of the five samples after polarization at +1500 mV.



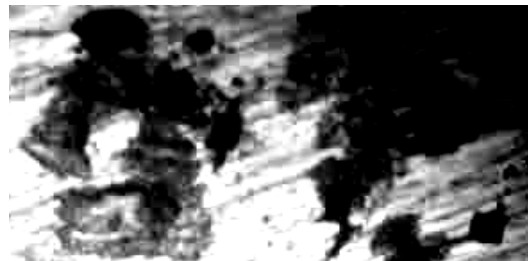
Sample 1



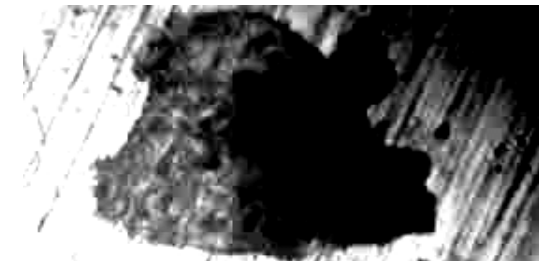
Sample 2



Sample 3



Sample 4



Sample 5

Fig. 5. The surface structure photographs obtained by optical microscopy

From the optical microscopy analysis one finds that after the polarisation all the samples were locally attacked, but the size of the corrosion points differs. Over the surface of sample 1 and 2 the corrosion points have a low size and are dispersed, while in case of the samples 3, 4 and 5 the points exist on a larger surface.

Conclusions

1. The thermal treatment applied to the samples may determine the decrease of the corrosion rate or reverse. In this sense one finds that the maintaining of the alloy for 20 hours at 750⁰C, followed by a sharply cooling in air, has a positive effect in alloy passivation.
2. Independently of thermal treatment applied, the samples show the same type of corrosion (pitting corrosion), the same as the cast alloy. More, the

electrochemical parameters of this process have almost the same values. The only difference that occurs is between the sizes of the corrosion points.

References

1. Nemțoi Gh., Aelenei D., Mareci D., Chelariu R., Petreuş I., Annals of West University of Timisoara, **12** (3) 619 (2003).
2. Chiper C., Burlui V., Forna N., Nemțoi Gh., Aelenei D., Andronache M, Aelenei N., Mareci D., Medicina Stomatologică, **5** (5) 29 (2001).
3. Chiper C., Burlui V., Forna N., Nemțoi Gh., Aelenei D., , Andronache M, Aelenei N., Mareci D, Medicina Stomatologică, **5** (3) 37 (2001).
4. Mareci D., Aelenei D., Nemțoi Gh., Cârjă G., Bocanu C., International Conference on Materials science and engineering, Brasov, 19 (2005).
5. Grosogeat B., Reclaru L., Lissac M., Dalard F., Biomaterials, **20**, 933 (1999).
6. Philippe Marcus, eds., Corrosion Mechanisms in Theory and Practice, Marcel Dekker Inc. 203 (2002).
7. Kelly R.G., Schully J.R., Shoesmith D.W., , Electrochemical Techniques in Corrosion Science and Engineering, Marcel Dekker Inc., New York, (2003).

*Gh.Asachi" Technical University of Iasi, Faculty of Industrial Chemistry,
Department of Physical Chemistry

**Gh.Asachi" Technical University of Iasi, Faculty of Materials Science and Engineering

***Al.I. Cuza University of Iasi, Faculty of Chemistry, Department of Physical and Theoretical Chemistry

INFLUENTA TRATAMENTULUI METALURGIC SI SUPRAFETEI ASUPRA REZISTENTEI LA COROZIUNE A ALIAJULUI NICROMALSOFT

In ultimii ani au fost introduse în categoria biomaterialelor noi aliaje pe bază de nichel, crom și molibden foarte rezistente la coroziune. Printre acestea aliajul NicromalSoft (INMR București) prezintă rezistență la coroziune superioară în fluide biologice umane. Prin metode electrochimice, respectiv prin polarizare liniară și ciclică, s-a studiat influența calității suprafeței și influența tratamentului metalurgic asupra procesului de coroziune a acestui aliaj în salivă artificială de tip AFNOR. S-au calculat parametrii principali ai procesului de coroziune. Suprafața aliajului a fost analizată și prin microscopie optica.

STABILITY OF IRON IN THE SYSTEM METHANOL – ADIPIC ACID – WATER

D. SUTIMAN, M.T.NECHITA, A.CĂILEAN, and D.MARECI

The behavior of tree type of steel, with a variable carbon concentration (from 0.20 to 0.40%) is studied in medium of methanol – 5% adipic acid with water concentration varying between 1% to 5%. The weight losses are measured; also the polarization curves plotted and the corrosion parameters are established. SEM visualized the metallic surface. The corrosion compounds are analyzed by IR spectroscopy, X-Ray diffraction and elemental chemical analysis.

Keywords: iron, corrosion, methanol, adipic acid, water

Introduction

This paper is a continuation of studies of the behavior of iron with low carbon concentration in organic media with methanol and/or ethylene glycol, having as corrosion reagents saturated mono- and di-carboxyl organic acid [1-9]. This corrosion system and also the studied acids are the main responsible agents for the corrosion process that appears in the synthetic fiber industry.

Experimental

The iron samples that are used for corrosion are the chemical composition presented in table 4.

Table 4.

The chemical composition of the samples of iron used in the experiments

| Sample | %C | %Mn | %S | %Si | %P |
|--------|------|------|------|------|------|
| I | 0.20 | 0.80 | 0.06 | 0.40 | 0.06 |
| II | 0.30 | 0.80 | 0.05 | 0.40 | 0.05 |
| III | 0.40 | 0.80 | 0.05 | 0.40 | 0.05 |

The iron samples of 5 cm² active metallic surface were cut up from a cylindrical bar. They were polished and dyeing protected the surface that should not be corroded. The corrosion system contained methanol, 5% adipic acid, HOOC—(CH₂)₂—COOH, and the water concentration varied between 1% and 5%. Karl-Fisher method was used to determine the water concentration. We used Merck reagents and the water was bi-

distilled, having electrical conductivity of $12 \mu\text{S cm}^{-1}$. Also the pH-variation of the corrosion medium was measured with a HACH pH-meter.

Before introducing the samples in the corrosion medium, they were submitted to a degreasing process in boiling benzene for 30 minutes and degreased in solution of hydrochloric acid 3% for 3 minutes. The corrosive system was open, allowing the permanent access of oxygen from the atmosphere. For every value of water concentration, six metallic samples were used and were placed in the same time in the corrosion system, being subsequently taken off from 10 to 10 days, degreased with HCl (3%) for 15 seconds and then were weighed by an analytical balances. From the values of weight losses, the gravimetric figure K ($\text{g m}^{-2} \text{h}^{-1}$) and the penetration figure (mm year^{-1}) were calculated. SEM visualized the metallic surface on a TESLA B300 microscope. For the value of 5% water concentration, the polarization curves were plotted on a Digital Electrochemical Analyzer DEA 332, made by RADIOMETER, Copenhagen, Denmark. The kinetics parameters ϵ_{cor} , ϵ_{st} and I_{cor} were determined by the VOLTMASTER 2 program. The corrosion final compounds, for every value of water concentration, were insoluble in the system. They were analyzed by X-ray diffraction on a HZG 4C Karl Zeiss Jena diffractometer using Co (K_{α}) radiation, by IR spectroscopy on a SPECORD M82. The chemical composition (C, H, O and Fe), of the final compounds were also determined.

Results and Discussion

The pH-metric study of the system methanol - 5% adipic acid – water show that the influence of water on acid dissociation is insignificant. The initial value of pH in anhydrous medium is 2,80 and if we add water until the system contains 5%, the pH value decrease to 2.68. In the table 1, the experimental data for weight losses expressed by K and P figures are presented.

Table 2.
The values of K and P figures.

| %H ₂ O | Sample I K/P | Sample II K/P | Sample II K/P |
|-------------------|-----------------|------------------|------------------|
| 1 | 0.030/0.027 | 0.029/0.026 | 0.028/0.025 |
| 2 | 0.031/0.028 | 0.029/0.026 | 0.029/0.026 |
| 3 | 0.031/0.028 | 0.031/0.028 | 0.030/0.027 |
| 4 | 0.033/0.030 | 0.032/0.029 | 0.031/0.028 |
| 5 | 0.034/0.031 | 0.033/0.029 | 0.032/0.029 |

From these values, resulted that the corrosion rate increases with the increase of water concentration without reaching an optimal value of it accomplishing the passive layer. Even a molar ratio water/acid of 6.53/1 the passive layer is not obtained. In corrosive medium of inorganic acids the ratio water/acid necessary for obtaining the passive layer is 4/1 [10, 11]. In organic medium, because of the polar character of the solvent molecules of methanol is possible that water is stronger bonded through hydrogen bridges and so it does not participate in passive oxy-hydroxide layer formation.

From experimental data resulted also the iron with the best behavior in corrosive medium is from the sample III that have the highest carbon concentration.

The metallic surface, from the sample III visualized by electronic microscopy is presented in figure 1.



Fig. 1. The metallic surface of sample III.
(x1200)

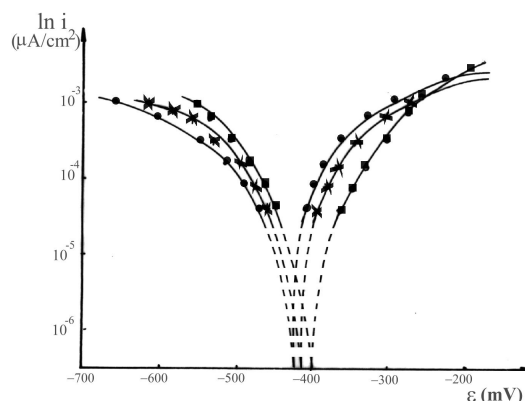


Fig. 2. The polarization curves; ● sample I;
x sample II; ■ sample III

It is observed that the adipic acid determines a pitting corrosion, a fact uncommon to the organic acid. The pitting corrosion is for all sample of iron.

The polarization curves were plotted for 5% water concentration (figure 2) and the values of kinetic parameters are presented in table 2. It is also observed that the iron with the highest stability is from the sample III, with the 0.4% carbon concentration.

Table 2.

The values of kinetic parameters of the corrosion in the system methanol – 5% adipic acid – 5% water.

| Sample | ϵ_{st} , mV | ϵ_{cor} , mV | I_{cor} , $\mu\text{A cm}^{-2}$ |
|--------|----------------------|-----------------------|-----------------------------------|
| I | -422 | -440 | 6.55 |
| II | -416 | -435 | 6.21 |
| III | -403 | -420 | 6.04 |

In order to establish a corrosion mechanism, the corrosion compounds were analyzed. These were insoluble in the system and presented a red color. The X-ray diffraction spectra do not show the existence of crystalline compounds in any of the obtained products at any water concentration. The IR spectra are identical for all system at any water concentration, meaning that they present absorption maximum points at the same wave number. The IR spectra of the corrosion compounds at 5% water concentration are present in figure 3.

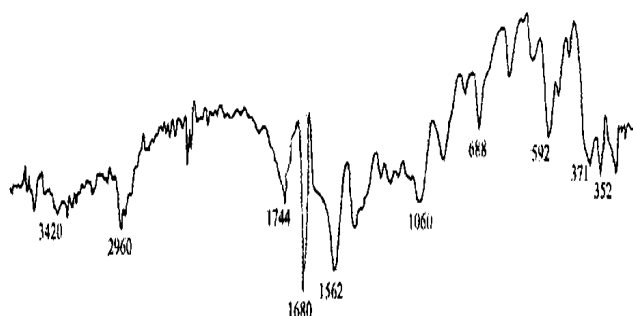


Fig. 3. The IR spectra of the corrosion compound in the system methanol – 5% adipic acid – 5% water from the sample III

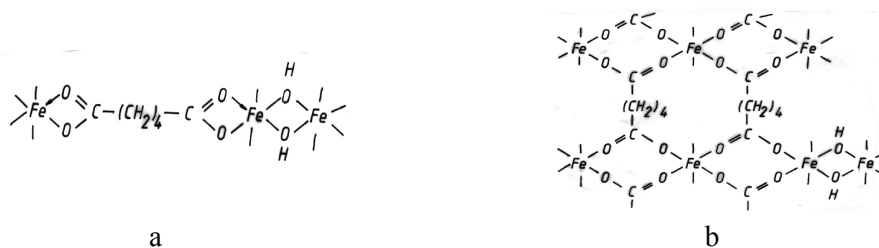


Fig. 4. The proposed structure of the adipate iron III; a – linear and b – cyclic.

In this spectrum is observed the displacement of the absorption frequency of the group COO^- from 1695 cm^{-1} to 1600 cm^{-1} due to a stronger bonding of oxygen. Also, the displacement of the absorption band characteristic for the alcoholic group HO^- from the value 1080 cm^{-1} to 1060 cm^{-1} show that the solvent participate to the coordination bond in the obtained compound. The HO group from water presents to 3420 and 2960 cm^{-1} fact that is explained by the existence of water bonded in two different ways: a group HO is coordinative bonded and the other in bridge linkage. Is a well-defined peak at 1700 cm^{-1} characteristic to the ester type bond. The bond Fe-O is clearly showed by to peaks situated at 371 and 352 cm^{-1} . The other peaks from IR spectra are characteristic to the C—C and C—H bonds [12, 13].

The chemical analysis of the corrosion compounds is presented in table 3.

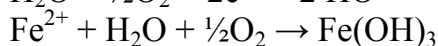
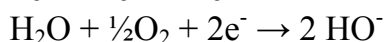
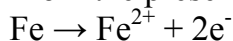
Table 3.

The chemical composition of the corrosion products in the system methanol – 5% adipic acid – 5% water.

| % | Compound of sample I | Compound of sample II | Compound of sample II |
|----|----------------------|-----------------------|-----------------------|
| C | 36.67 | 37.05 | 36.12 |
| H | 4.11 | 4.05 | 4.78 |
| O | 32.76 | 32.45 | 33.06 |
| Fe | 24.46 | 26.45 | 26.04 |

The analysis corresponds to a compound in which the ratio Fe/adipate is 1/1 with a small surplus of oxygen and hydrogen. This ratio can be explained only a polymer compound.

From the presented data, the following corrosion mechanism is assigned:



The structure of the resulted compound is presented in the figure 4. The hexacoordination of iron is accomplished through both water molecules and the solvent ones. Also the polymeric chain is extended through ether type bonds.

Conclusions

1. All types of iron are corroded in the studied medium
2. The best behavior is presented by the iron with highest carbon concentration (0.4%). That is due to the existence in the iron structure of a solid Fe—C solution that determines a superior stability on the material [14].
3. Water is not used in the passive layer formation even if it is present in molar rates higher than 4/1 (when the system contains 5% water the molar ratio water/adipic acid is 8.10/1). The fact that water does not participate in anticorrosive protection can be justified by the existence of two groups COO⁻ in the structure of acid that requires a higher quantity of water in order to accomplish the oxy-hydroxilic passive layer formation, using the dissolved O₂ molecules. The water molecules is possible to be stronger bonded through hydrogen bridges of the organic solvent so it does not participate in passive oxy-hydroxilic layer formation.
4. The corrosion mechanism is a complexing one with formation of insoluble compounds non-adherent on the surface of the corroded metal. These compounds presented an amorphous polymer structure.
5. Remarkable is the fact that the adipic acid determines a pitting corrosion process.

References

1. Sutiman D.M., Cretescu I., Cailean A., *Revista de Chimie*, 49 (11) 813 (1998).
2. Sutiman D.M., Cretescu I., Nemtoi Gh., *Revista de Chimie*, 50 (10) 766 (1999).
3. Sutiman D.M., Cioroianu T., Georgescu O., *Hung. Jour. Ind. Chem.*, 27, 107 (1999).
4. Sutiman D.M., Cretescu I., Rusu I., Cailean A., *Revista de Chimie*, 51 (11) 889 (2000).
5. Sutiman D.M., Cailean A., *Hung. Jour. Ind. Chem.*, 29, 17 (2001).
6. Sutiman D.M., Cailean A., *Hung. Jour. Ind. Chem.*, 30, 37 (2002).
7. Sutiman D.M., Vizitiu M., *Hung. Jour. Ind. Chem.*, 30, 33-37 (2002).
8. Sutiman D.M., *Hung. Jour. Ind. Chem.*, 30, 187 (2002).
9. Sutiman D.M., *Hung. Jour. Ind. Chem.*, 30, 285 (2002).
10. Stypula B., *Coor. Resit. Alloy*, 1, 252 (1965).
11. Banas J., Stypula B., *Metallurgy and Foundry Engineering*, 6, 112 (1995).
12. Avram M., *Infrared Spectroscopy*, Ed. Tehnica, Bucuresti, (1960).
13. ****, *The Sadler of Handbook of Infrared Spectra*, Sadler and Hayden, London, (1978)
14. Cartis Gh., *Thermal Treatments*, Ed. Facla, Timisoara, (1982).

*Gh.Asachi" Technical University of Iasi, Faculty of Industrial Chemistry,

STABILITATEA FIERULUI ÎN SISTEMUL METANOL-ACID ADIPIC-APĂ

S-a studiat comportarea la coroziune a 3 tipuri de oțel, de diverse concentrații în carbon (de la 0,20 la 0,40%) într-un mediu apos de metanol – 5% acid adipic de concentrații variate, cuprinse între 1 și 5%. S-a măsurat pierderea de material, după trasarea curbelor de polarizare și s-au stabilit parametrii procesului de coroziune. Suprafața metalelor a fost analizată prin microscopie SEM. Compușii de coroziune au fost analizați prin spectroscopie IR, difracție de raze X și analiză chimică elementară.

STRUCTURAL CHARACTERISTICS AND MAGNETICAL PROPERTIES OF SILICON STEEL SHEETS

by

G. GHERGHISOR, G. COSMELEATA, V. MIRON and I. GEORGESCU

Abstract: Silicon steel sheets for electrical purposes like great power engines are realized at a superior quality under European standards, low core losses and high magnetic induction.

It was realized research concerning the performances improvement of the silicon steel sheets correlated with technological upgrading of the operating.

The research works have proposed to obtain practical technological data and to emphasize the influence of the main technical hot and cold processing parameters on the structure development, texture strengthening and final grain diameter which have important influence on the magnetic properties.

Keywords: non-oriented and oriented grain, silicon steel sheets.

1. INTRODUCTION

Silicon Steel Sheets production in Romania has been started in 1980 under the know-how of U.S.Steel. Important investments, specific for silicon steel production had to be done in the slabbing and hot rolling sheet mill, including furnaces for slow cooling of more than 2.60% silicon steel slabs and high temperature reheating furnaces (1380-1420° C). For processing of the hot rolled sheets has been put into operation a new plant, which include cold rolling, heat treatments and electro-insulating coating.

As regarding grain oriented silicon steel sheets technology, during the beginning of the production major efforts were necessary to adapt the existing facilities at know-how. Specific technologies were developed in order to obtain the necessary chemistry of the steel, to decrease manganese content in the hot metal fabrication and using of high purity ferrosilicon with no aluminum and titanium, and argon bottom stirring of steel.

Another key parameter in the fabrication of grain oriented silicon steel sheets was the high entering temperature at finishing train in hot rolling mill. Rough rolling into three stands instead of five stands and the speed of the bar between roughing stands and finishing train and a large bar entering thickness increasing were applied to get entering temperature at first finishing stand over 1150° C /1/.

The recent researches /2,3/ are regarding the development of a simplified technology to produce grains oriented silicon steel sheets with AlN as a

recrystallization inhibitor, which needs slabs heating for hot rolling at lower temperatures situated between 1220° and 1250° C.

An intensive industrial research program was promoted in the '90-es to modernize the technology of non-oriented steel sheets. Thus, the technology has turned from BOF steelmaking, re-ladling alloying, ingot casting to BOF steel-making, vacuum decarburizing, the ladle alloying with argon stirring of steel and continuous casting.

2. EXPERIMENTS AND OBTAINED RESULTS

2.1. Grain Oriented Silicon Steel Sheets

The research programmers in the field of grain oriented silicon steel were focused to a better understanding the bases for increasing the performances of products and technology. Some of the main results are presented below.

2.1.1. Structure development during hot deformation

The industrial investigations were done in order to study the structure development during hot rolling. The results obtained proved the followings:

a) *Roughing rolling*

With rolling temperatures over 1200°C at the last roughing stand mill, the structure are fully recrystallized at reduction degrees ranging from 38 to 62 %; the higher the reduction degree, the finer the structure (fig. 1.a and 1.b). With rolling temperatures of less than 1200°C the grains remain not recrystallized and more elongated the higher was the reduction degree (fig. 1.c and 1.d).

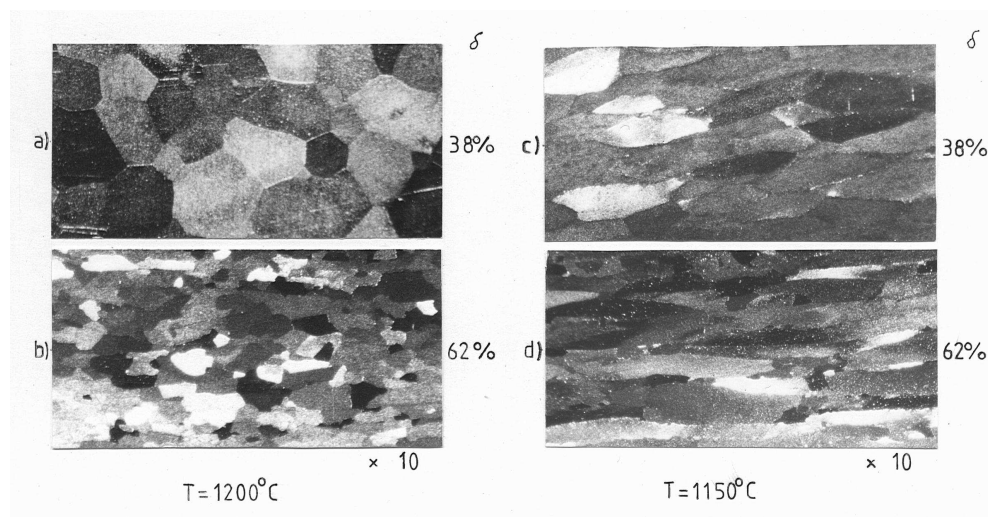


Fig. 1. Structure appearance in roughing rolling conditions

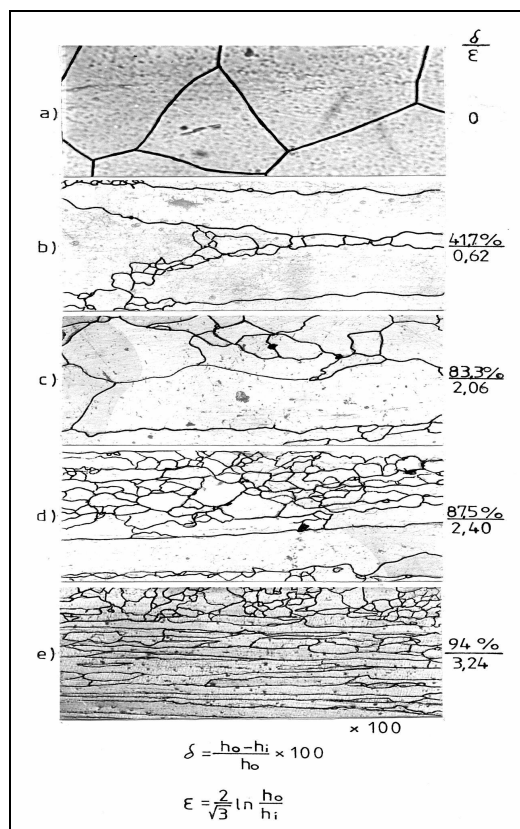


Fig. 2. Structure development at industrial finishing rolling

2.1.2 Texture enhancement in hot rolling

Early investigations [4-6] achieve that for Goss texture enhancement at hot rolled sheet it should either roll with lower temperatures and maintain a certain content of partially recrystallized grains or to microalloy steel with molybdenum for sluggish recrystallization.

The samples which had a more pronounced Goss texture in hot rolled stage, keeps the same texture until the final sheet.

To verify the efficiency of these methods in industrial conditions, silicon steel sheets only with MnS inhibitor and final temperatures between 850° and 1030° C or silicon steel sheets with MnS inhibitor and 0,03% Mo-addition were hot rolled.

The texture development on thickness sheet shows that Goss texture intensity increases whit the final temperature diminution (fig. 3).

At temperatures between 850° to 870° C, the Goss texture intensity ($I_{(110)} / I_0$ ratio) has the 2.0 value in a region with the thickness of 0.3 mm and the distance of 0.2 mm from the surface of the hot rolled sheet; at higher temperatures the $I_{(110)} / I_0$ ratio has this value only in a region with the thickness of 0.1 mm.

In the case of the sheets with final temperature 950° C, by Mo-addition the Goss texture intensity has increased from 2.0 at 2.7 in the region with the thickness of 0.3 mm in the surface vicinity.

A comparative analysis of the effect of decreasing rolling mill temperature and of Mo-addition on the Goss texture enhancement in hot rolled sheets, shows the stronger influence of Mo-addition.

b) Finishing rolling

Investigation of specimens from industrial rolling proved that recrystallization starts in finishing stand mill no.3, from 80% total deformation and temperature at about 1100° C (figure 2). At a total deformation of 85–90% in finishing stands mill no. 4 and 5 was formed one distinct layer of fully recrystallized grains in the border region and partially recrystallized grains in great central region was. After the last finishing stands mill, at lower rolling temperatures and total deformation over 90%, in the central regions a fully non-recrystallized structure was formed, a typical deformation structure, while the intermediary regions between center and surface of the sheet was partially recrystallized.

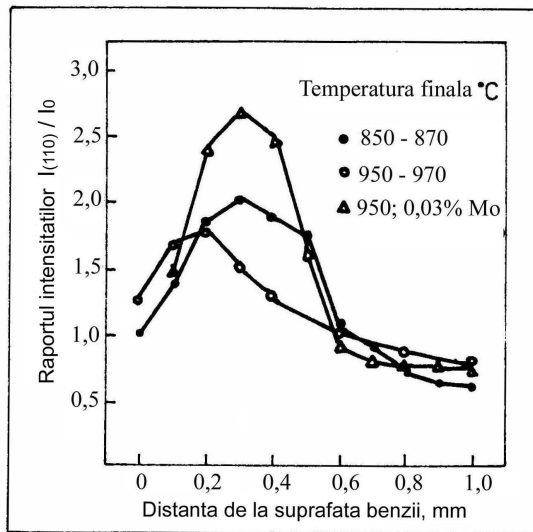


Fig. 3. The influence of decreasing rolling temperature and Mo-addition on texture enhancement

2.1.3. Grain secondary recrystallization capability

The determination of the secondary recrystallization capability through a laboratory simulation method like cold processing and verification of primary and secondary grains recrystallization was done [7]. This method quickly determined MnS capability to conduct secondary recrystallization and finally to obtain the grains with a length of 5 - 10 μm ; it is considered satisfactory whose grains length more than 3 μm .

The stages of the 2.20 mm hot rolling sheet processing has been:

- cold rolling at 0.70mm thickness;
- recrystallization annealing at 900° C temperature;
- second cold rolling at 0.30 mm thickness;
- decarburizing heat treatment of the cold rolled sheet at 840° C in an controlled atmosphere, with nitrogen, hydrogen and clean steam (dew point + 60° C);
- high annealing at 1175° C in a hydrogen atmosphere for a secondary recrystallization and grain size increase.

After was done all heat treatments was taken sheet samples to analyze the grain size and the recrystallization degree.

The samples, which not suffered the secondary recrystallization after annealing and primary recrystallization (namely intermediary and decarburizing) had relatively big grains – more than 30 and 20 μm respectively. This proves the low effect of the MnS inhibitor on the Goss texture control.

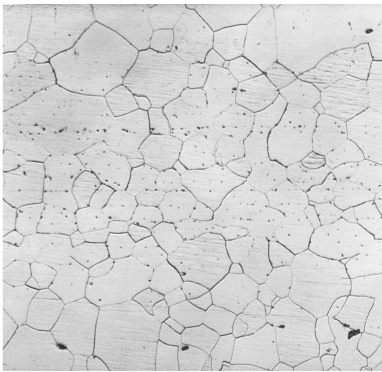
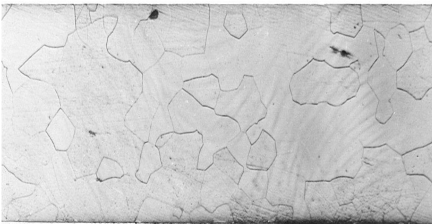
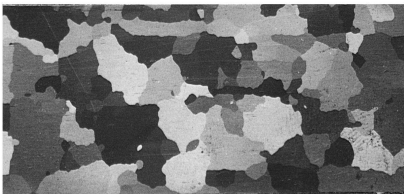
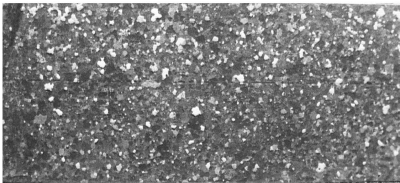
When the steel sheet has a correct chemical composition and the hot rolling technology is adequate, the MnS inhibitor distribution do not allow a more than 20 μm grain size increase, after annealing and primary recrystallization under 900° C.

In the process of high annealing at 1175° C in hydrogen atmosphere the MnS inhibitor is eliminated and the grain size increase take place.

Considering the difficulty to control the inhibitor precipitation at lower rolling temperatures resulted that Mo - microalloying of the steel with MnS inhibitor is a more efficient solution for the industrial applications, comparably using only MnS inhibitor.

In the table no. 1 are given the sheet metallographies in the various technology stages, proving adequate and inadequate structures which satisfactory or non-satisfactory magnetic characteristics.

Tab. 1 The sheet metallographies in the various technology stages

| Technology stages | Good metallographic aspect | Wrong metallographic aspect |
|--|--|---|
| Intermediary annealing; Temperature: 900° C; Thickness: 0.70mm |  5% Nital etching, 100:1 Medium grain diameter: 10 – 40 μm |  5% Nital etching, 100:1 Medium grain diameter: 20 – 70 μm |
| Decarburizing hot treatment; Temperature: 840° C; Furnace atmosphere: nitrogen, hydrogen and clean steam; dew point: + 60° C; Thickness: 0,30 mm |  5% Nital etching, 100:1 Medium grain diameter: 10 – 20 μm |  5% Nital etching, 100:1 Medium grain diameter: 20 – 40 μm |
| High annealing; Temperature: 1175° C; Furnace atmosphere: hydrogen |  Macro etching, 1:1 Macrostructure on the sample surface; Grains length: 5 – 10 mm |  Macro etching, 1:1 Macrostructure on the sample surface; Grains length: 1 – 3 mm |

2.2. Non oriented silicon steel sheets

The research works concerning non oriented steel sheets pursued the diminution of the core losses $P_{1,5/50}$ under 2.90 w/kg, the increase of magnetic induction over 1.60

T and a magnetic anisotropy until 17%, at a superior quality according to European standards.

To improve the core losses, the silicon contents of steel has been between 2.80 and 3.25%, and aluminum content of 0.50– 0.53%; the sulphur content under 0.008%, to remove the inhibitor character of MnS to the increasing grains size.

Following the industrial investigations on the cold rolled and heat treatments flow at ERDEMIR România Târgoviște, the influence of silicon content on the core losses and grain size on the magnetic induction were studied. In figures 4 and 5 it can be seen that for a high category of sheet with superior magnetic characteristics, corresponding to M290-50A quality, the silicon content must be over 3.05% and the medium grain diameter of 100 - 150 μm .

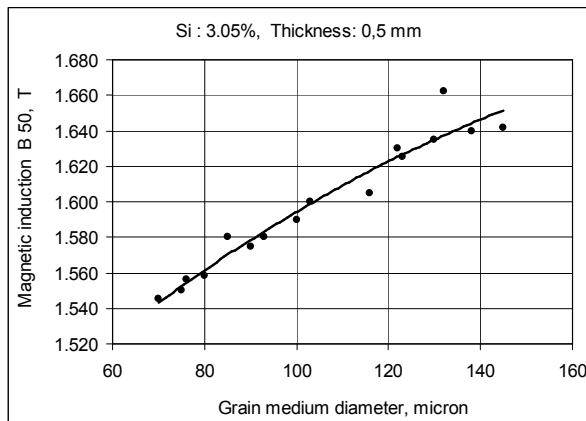


Fig. 4. The influence of final grain size on the magnetic induction B_{50}

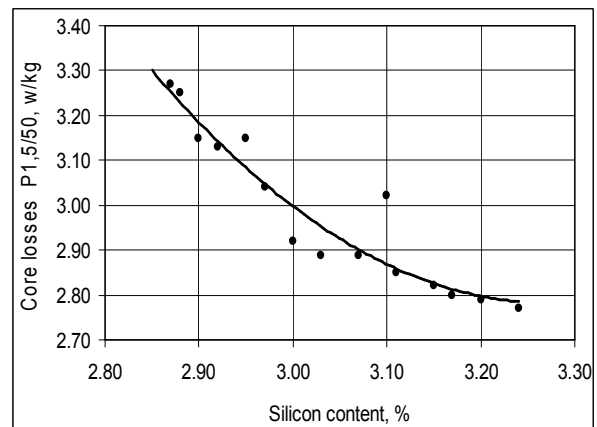
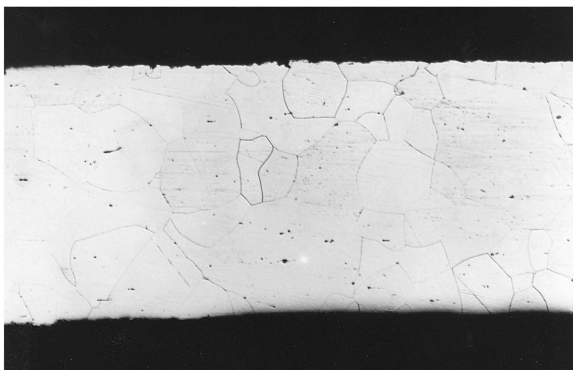
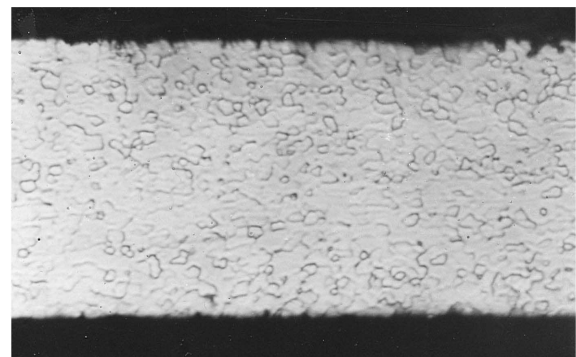


Fig. 5. The influence of silicon content on the core losses $P_{1,5/50}$

The investigation of the samples taken over the heat treatments proved that for achievement an optimal final grain size (figure 6.a), after decarburizing hot treatment in an controlled atmosphere with nitrogen, hydrogen and clean steam (dew point +25° C) for the decreasing the carbon content under 0.003%, it is necessary that the medium grain diameter must be about 30 μm and not occurs the recrystallization of grains with large grains (figure 6.b).



5% Nital etching, 100:1



5% Nital etching, 100:1

Fig. 6. Microstructure achieved after decarburizing hot treatment at 820° C and recrystallization annealing at 970° C

3. CONCLUSIONS

The results of the laboratory and industrial investigations concerning grain oriented silicon steel sheets and achieve in this paper have shown:

- At deformation in the last roughing stand mill, at rolling temperature of over 1200° C, the structure are fully recrystallized at industrial reduction degrees.
- Investigation of specimens from industrial rolling proved that recrystallization starts in finishing stand mill no.3, from 80% total deformation and temperature about 1100° C.
- The texture development on thickness sheet shows that Goss texture intensity increases whit the final temperature diminution. A comparative analysis of the effect of decreasing rolling mill temperature and of Mo-addition on the texture enhancement in hot rolled sheets, shows the stronger influence of Mo-addition. Considering the difficulty to control the inhibitor precipitation at low rolling temperatures resulted that Mo- microalloying is a more efficient solution for the industrial applications, comparably using only MnS inhibitor.
- The determination of the secondary recrystallization capability through a laboratory simulation method like cold processing and verification of primary and secondary grains recrystallization was done. This method quickly determined MnS capability to conduct secondary recrystallization and finally to obtain grains with the length of 5-10 mm; it is considered satisfactory whose grains length more than 3 mm.
- For a high category of non-oriented silicon steel sheet with superior magnetic characteristics, corresponding to M290-50A quality, with the core losses $P_{1,5/50}$ under 2.90 w/kg, the magnetic induction over 1.60 T and a magnetic anisotropy until 17%, the silicon content must be over 3.05% and the medium final grain diameter of 100 - 150 μm ; the aluminum content was of 0.50 – 0.53% and the sulphur content under 0.008%.
- For achievement an optimal final grain size after decarburizing heat treatment it is necessary that the medium grain diameter must be about 30 μm and not occurs the recrystallization of grains with large grains.

REFERENCES

1. V. Miron, Gh. Pârnu, ş.a; Brevet de invenție nr. 102068/1990
2. XXX – French patent acts: 2.202.944; 2.249.957; 2.313.344; 1.275.315
3. XXX – French patent acts: 2.202.943; 2.194.788; 2.192.180; 2.222.442
4. Y.Shimizu, Y.Ito, Y.Iida; Met,Trans., vol. 17A. aug. 1986, p.1323-1333
5. M.Matsuo, T.Sakai, Y.Suga; Met.Trans., vol. 17A, aug.1986, p.1313-1322
6. Y.Inokuti, C.Maeda, Y.Ito; Trans.of ISIJ, vol. 25, 1985, p.233-240
7. Gh. Pârnu, A.T.Dumitrescu, ş.a; Revista Metalurgia nr. 11, 1987, p. 542-545
8. Gh. Pârnu, V.Miron, ş.a; Revista Metalurgia nr. 4, 1991, p. 21-28

GABRIEL GHERGHISOR – UNIVERSITY POLITEHNICA BUCHAREST
GEORGETA COSMELEATA – UNIVERSITY POLITEHNICA BUCHAREST
VASILE MIRON – METALLURGICAL RESEARCH INSITUTE – ICEM S.A. –
ION GEORGESCU – S.C. ERDEMIR ROMANIA TARGOVISTE

CARACTERISTICILE STRUCTURALE ȘI PROPRIETĂȚILE MAGNETICE
ALE BENZILOR DIN OȚEL SILICIOS

Rezumat

Benzile din oțel silicios, utilizate în industria electrotehnică pentru realizarea mașinilor electrice de mare putere, sunt la nivelul calităților superioare din normele europene, având pierderi magnetice scăzute și inducție magnetică ridicată.

Au fost efectuate lucrări de cercetare referitoare la îmbunătățirea performanțelor benzilor din oțel silicios, în corelație cu modernizările tehnologice ale fluxurilor de fabricație.

Lucrările de cercetare efectuate și-au propus obținerea de date utilizabile tehnologic și evidențierea influenței principalilor parametri tehnologici de procesare la cald și la rece asupra dezvoltării structurii, intensificării texturii și mărimii granulației, cu implicații majore asupra proprietăților magnetice.

ALUMINUM DEPOSITION BY CVD METHOD ON NICKEL- BASED SUPERALLOY SUPPORTS

BRANDUSA GHIBAN and GEORGETA COSMELEATA

Abstract

In order to increase the oxidation/corrosion resistance at high temperatures of the NIMONIC 80 parts during service, aluminide coatings were employed on the surface. This is due to the fact that the high near surface content of aluminium increases the ability of forming an Al_2O_3 protective film. The coatings were obtained using the Fluidised Bed Chemical Vapour Deposition Technique. The aim of present paper is to put in evidence the behaviour of aluminide deposition by CVD method of nickel based superalloy, type NIMONIC 80. The metallic supports for the experiments were a nickel based superalloy type NIMONIC 80, with the composition: Cr20%, Co19%, C0,06%, Ti 2,5%, balance Ni. According to the experimental results, the formation of high-quality aluminide coatings on a Ni-based superalloy substrate at relatively low temperatures (600 °C) is successfully accomplished by the FBCVD process. It is observed that the coating thickness increases with treatment time: 5 μ m (2h treated sample), 8 μ m (6h treated sample) and 10 μ m (6h treated sample after annealing for 2h). For all experiments the coatings obtained are continuous, homogeneous, dense and very adherent onto the substrate.

Keywords: CVD method, aluminum deposition, nickel, nimonic

1. INTRODUCTION

In order to increase the oxidation/corrosion resistance at high temperatures of the NIMONIC 80 parts during service, aluminide coatings were employed on the surface. This is due to the fact that the high near surface content of aluminium increases the ability of forming an Al_2O_3 protective film. The coatings were obtained using the Fluidised Bed Chemical Vapour Deposition Technique, which is characterised by the following features:

- uniform temperature distribution over the whole reactor volume;
- uniform concentration of the reactive gases, which prevents the development of localized coating growths;
- higher mass transfer rates at the substrate surface;
- an easier introduction and extraction of the specimens, the furnace being at the treating temperature.

The aim of present paper is to put in evidence the behaviour of aluminide deposition by CVD method of nickel based superalloy, type NIMONIC 80.

2. MATERIALS AND EXPERIMENTAL PROCEDURE

The scheme of the CVD installation is shown in figure 1.

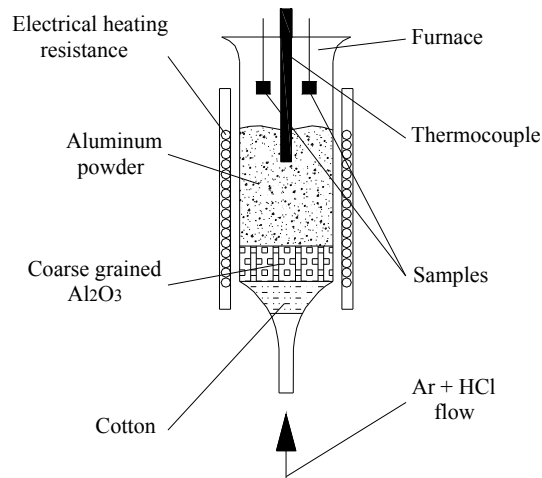


Figure 1- Scheme of CVD installation used in present experiments

A fine aluminium powder was used as donor, placed over a thick layer of coarse grain alumina. HCl was used as activator and was inserted in the process through a tube placed in the lower part of the furnace. The fluidization was obtained due to the flow of the inert gas, Ar. The working temperature was set at 600 °C and was controlled by means of PID controllers. The gas flow rates were manually controlled by means of gas flow meters. All samples were polished before treatment up to a 400-grit SiC paper and ultrasonically cleaned in acetone. The specimens were inserted within the Fluidised Bed from the top of the Fluidised Bed furnace, removed after specific treatment time and left to cool in ambient air. The main features of the experiments are illustrated in table 1.

Table 1. The main features of the experiments

| No. | Substrate | Inert gases | Bed's Charact. | Activator | Temp. | Time |
|-----|------------|------------------------|---|-----------|-------|----------|
| 1 | NIMONIC 80 | Ar+ 10% H ₂ | AlCl ₃ 6H ₂ O Al ₂ O ₃ coarse Al powder | - | 600°C | 2h;4h;6h |
| 2 | | Ar | Al ₂ O ₃ coarse | HCl | | 2h;4h;6h |
| 3 | | Ar | Al powder | HCl | | 1.5h |
| 4 | | Ar | | HCl | | 2h;4h;6h |

Some of the coated specimens were segmented in two: a part was Ni electroplated for the protection of the coating during metallographic preparation and the other half was annealed at 950 °C for 2 hours; in the end, the resin mounted samples were polished up to 1- μ m diamond paste. The coatings were characterised by optical microscopy and by SEM.

The metallic supports for the experiments were a nickel based superalloy type NIMONIC 80, with the composition: Cr20%, Co19%, C0,06%, Ti 2,5%, balance Ni.

3. RESULTS AND INTERPRETATION

The aluminide coatings on NIMONIC 80 deposited by the Fluidized Bed Chemical Vapor Deposition Technique are characterized by optical microscopy and SEM. The results are presented in the figures below (*Figure 2 through figure 8*).

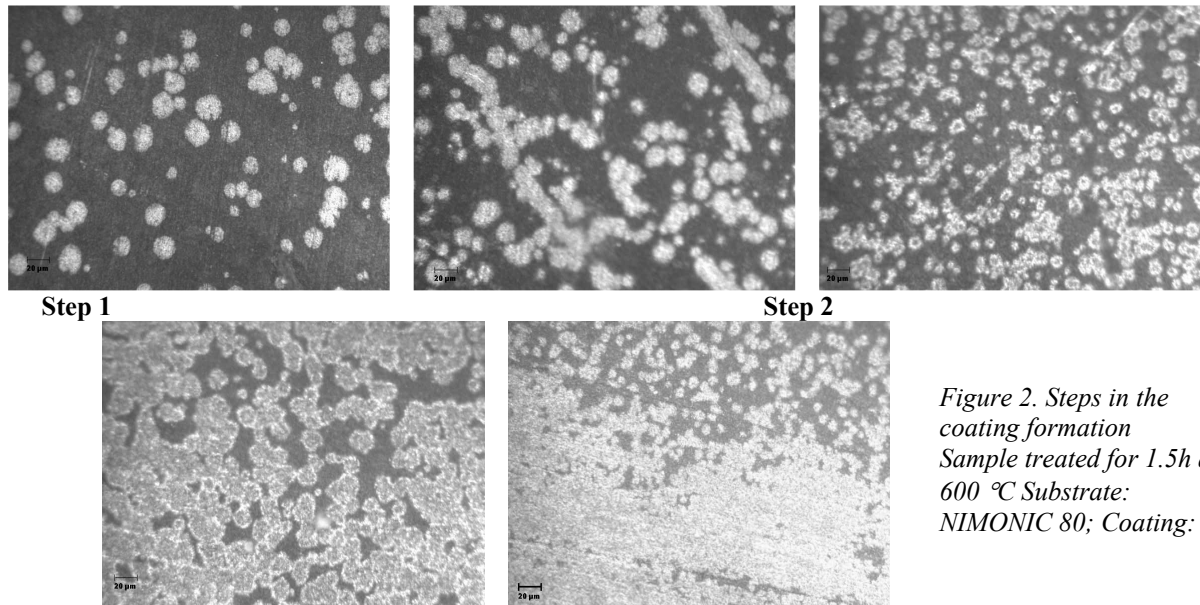
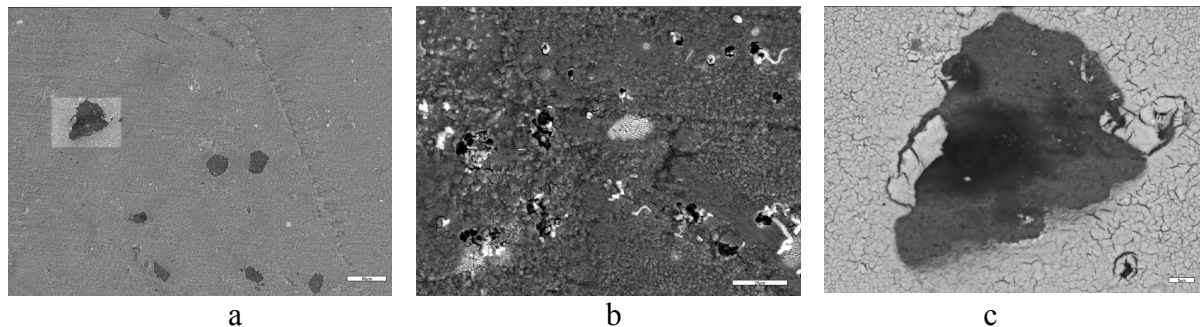


Figure 2 shows the evolution of the aluminide coating. In the first step it is clearly observed the formation of Al islands on the surface, followed by the nucleation growth in step two. In the last stage it is evidenced the formation of the aluminide coating onto the surface of the alloy.



*Figure 3. The formation of the aluminium islands
Sample treated for 1.5h at 600 °C (Substrate: NIMONIC 80; Coating: Al)*

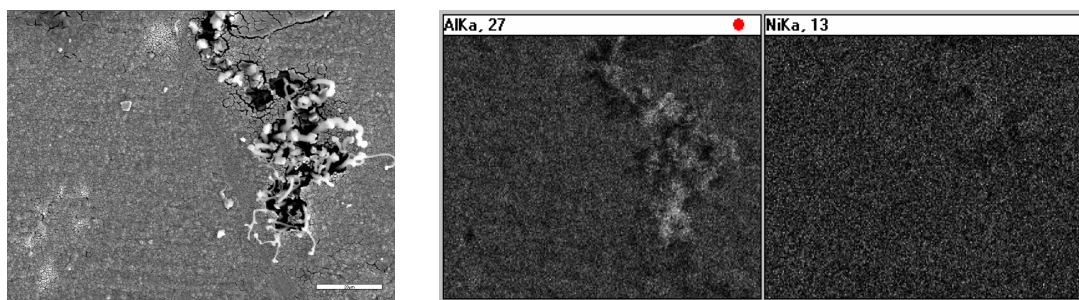


Figure 4. Comparison between the amount of Al and the amount of Ni on the surface of the sample

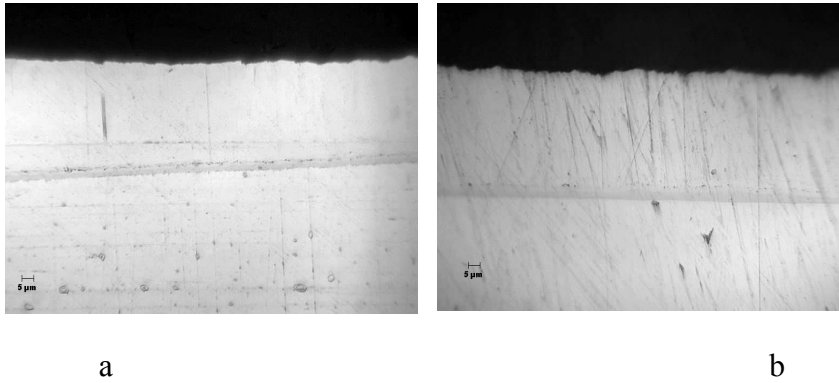


Figure 5 Optical microscopy aluminide coatings of the NIMONIC plated samples treated at 600 °C for: a- 2h; b 4h

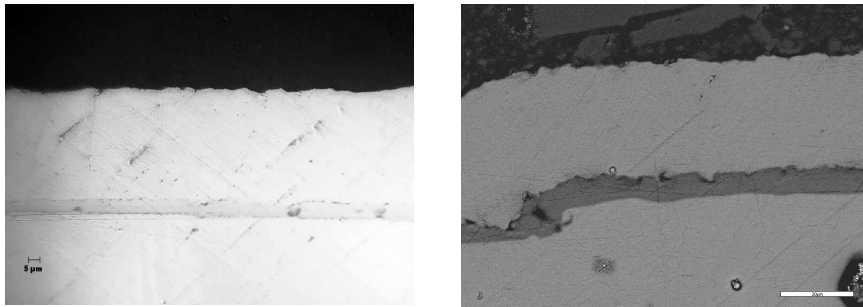


Figure 6. Optical microscopy of aluminide coatings of the NIMONIC plated sample treated for 6h at 600 °C

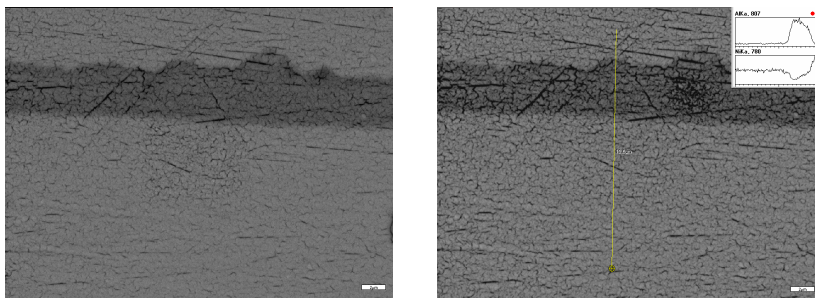


Figure 7- SEM of aluminide coatings of the NIMONIC plated sample treated for 6h at 600 °C

Figure 7 shows a detailed perspective of the appearance of the coating of the sample treated for 6h at 650 °C. The yellow line represents a line scan and it analysis the evolution of the Al and Ni content in the substrate and coating.

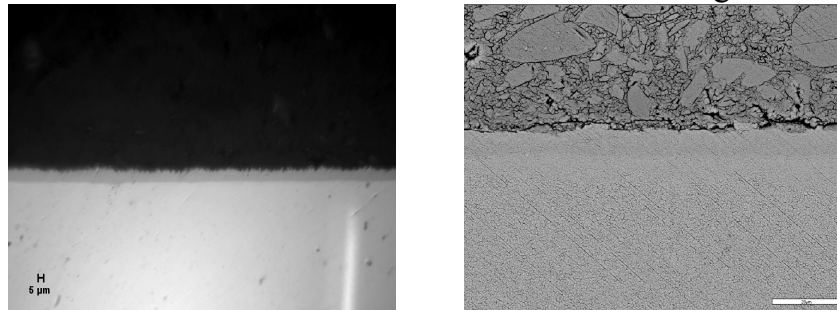


Figure 8. Optical and SEM characterization of aluminide coating at the 6h sample after annealing at 950 °C for 2h

It is easily noticed that the coating thickness increases with treatment time: the sample treated for 2h has a coating thickness of $5\mu\text{m}$, the 4h one has $8\mu\text{m}$ and the 6h one, $10\mu\text{m}$. The *Figure 9* shows this evolution.

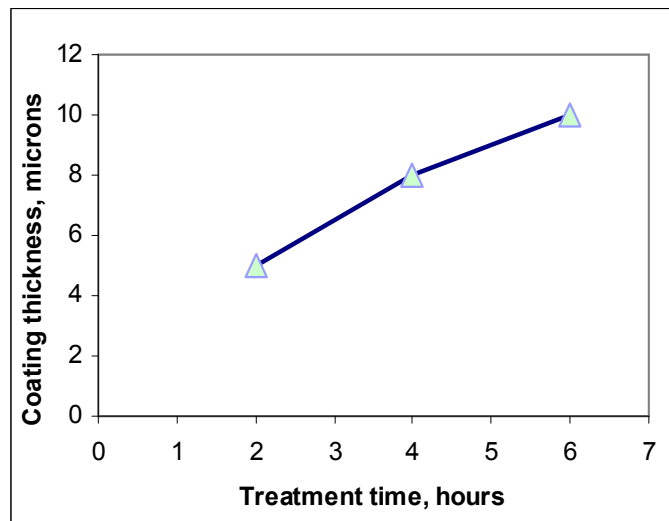


Figure 9. The coating thickness of the deposited layers as function of treatment time

4. CONCLUSIONS

- ❖ According to the experimental results, the formation of high-quality aluminide coatings on a Ni-based superalloy substrate at relatively low temperatures ($600\text{ }^{\circ}\text{C}$) is successfully accomplished by the FBCVD process.
- ❖ It is observed that the coating thickness increases with treatment time: $5\mu\text{m}$ (2h treated sample), $8\mu\text{m}$ (4h treated sample) and $10\mu\text{m}$ (6h treated sample after annealing for 2h).
- ❖ Characteristic for all experiments is that the coatings obtained are continuous, homogeneous, dense and very adherent onto the substrate.

REFERENCES

- [1]. H. Gabrisleh, D. Mukherji, *Character of Dislocations of the γ/γ' interfaces and internal stresses in Nickel-Based Superalloys*, Acta Materialia, 48, 2000, 3157-3167
- [2]. C.H. Jwashita, R.P. Wei, *Coarsening of Grain Boundaries Carbides in a Nickel-Based Ternary Alloy During Creep*, Acta Materialia, 48, 2000, 3145-3156.
- [3]. C.M. Reylands, M.D. Wilkes, W.M. Bainfort, *Materials Science*, 1994, 29, 1985.
- [4]. E. M. Lehorkey, G. Palumbo, *Material Science and Engineering*, A, 1997, A237, 168.
- [5]. J. Ardell, *Material Science and Engineering*, 1997, A238, 108
- [6]. G. B. McFadden, S. R. Coriell, R. F. Sekerna, *Effect of Surface Free Energy Anisotropy on Dendrite Shape*, Acta Materialia, 2000, 3177-3181.

Brandusa GHIBAN, Georgeta COSMELEATA, University Politehnica of Bucharest- ROMANIA

DEPUNEREA ALUMINIULUI PRIN METODE CVD PE SUPPORT DIN SUPERALIAJE PE BAZA DE NICHEL

In scopul imbunatatirii rezistentei la oxidare/coroziune la temperaturi inalte a pieselor NIMONIC 80 in timpul functionarii s-au folosit depuneri aluminoase pe suprafata.

KINETIC CONSIDERATION OF COPPER REFINING PROCESS

BY

VASILE HOTEA, GHEORGHE IEPURE, ELENA POP, EMILIA TALPOȘ,
JOSZEF IUHAZS, AURICA POP

Abstract: The study made on impurities removal kinetic was materialised through an adoption of a kinetic model in conditions of refining flux injections with use of an oxidant agent. This work is focussed on copper refining by the injection of Na_2CO_3 powder. Experiments were carried out using 15 kg copper bath at two temperatures, 1200 and 1250°C. The carrying gas used for the injection trials was air with flow rates of 3,5 and 10 l/min. The results show that the copper refining process is more efficient at temperatures for the Na_2CO_3 injection process where as high temperatures produce better antimony removal for the injection of Na_2CO_3 powder. Na_2CO_3 injection with the air flow rate (10 l/min) produced higher removal rates. The kinetic model was adapted to the copper refining process to predict the rate antimony removal.

Keywords: kinetic model, copper refining, antimony removal, Na_2CO_3 injection

1. Introduction

The following model was originally proposed by Ohguchi and Robertson [1] for desulphurisation of liquid iron and it is adapted of the to the injection of copper refining processes to the injection of powder Na_2CO_3 to eliminate antimony from molten copper.

The overall rate of antimony can be written as the sum of the contributions of permanent and transitory reaction zones.

The chemical reactions of interest for the antimony removal whit Na_2CO_3 were:



The rate equation for the permanent reaction zone between the metal and the slag is given by:

$$-\frac{d[\%Sb]}{dt} = K_p \{ [\%Sb] - [\%Sb]_{eq} \} \quad (3)$$

where $[\%Sb]$ –is antimony concentration in the metal at time (t) in mass (%), and $[\%Sb]_{eq}$ is the equilibrium antimony content of the metal;

K_p – is apparent rate constant of the permanent reaction zone and is function of the mass transfer conditions:

$$K_p = \frac{A \cdot k_p}{V} \quad (4)$$

where A is the total interfacial area, V – is the volume of metal phase and k_p is the rate constant for the permanent contact reaction zone.

The antimony removal rate for the transitory reaction is determined by the number of particles ascending through the bulk metal about to join the slag, the injection rate Na_2CO_3 and the antimony content of these particles. Based on the stoichiometric of the equation (1-2) the process at each time increment may be described as:

$$-\frac{d[\%Sb]}{dt} = J_{\text{Na}_2\text{O}_3} \frac{(\%Sb)_{zg}}{W_{Cu}} \quad (5)$$

where $(\%Sb)_{sl}$ is the antimony content of a particle Na_3SbO_4 when it reaches the slag, W_{Cu} -is the mass of copper and $J_{\text{Na}_2\text{CO}_3}$ - is the injection rate powder in terms of mass per unit time.

The antimony content of floating particle which is about to join slag is expressed by:

$$(\%Sb)_{zg} = E \cdot L_{Sb} \cdot [\%Sb] \quad (6)$$

where the equilibrium antimony (L_{Sb}) between the slag phase and metal is:

$$L_{Sb} = \frac{(\%Sb)_{eq}}{[\%Sb]_{eq}} \quad (7)$$

$(\%Sb)_{eq}$ -is the equilibrium antimony content in the slag in mass percent. The parameter (E) is a measure of the efficiency of the transitory reaction and its value can vary between 0 and 1.

By substituting equation (6) in (5) the final expression is obtained for the antimony removal rate:

$$-\frac{d[\%Sb]}{dt} = J_{\text{Na}_2\text{CO}_3} E L_{Sb} \frac{[\%Sb]}{W_{Cu}} \quad (8)$$

The progress of the antimony removal rate with time can be obtained by solving equations (3) and (8) through a numerical technique such as the fourth-order Runge-Kutta method [2].

The method parameters in this work are the apparent rate constant for the top slag reaction (K_p), the equilibrium antimony partition ratio (L_{Sb}) and the efficiency of the transitory reaction (E). The values of these parameters will be defined in the Results and Analysis Section.

Sawada and Ohashi [3] developed a hydrodynamic model of a gas and powder injection system. Their analysis of the buoyancy driven plume generated through gas injection showed that plume velocity (U) can be predicted using the relationship:

$$U = 19,9 \frac{Q}{D^2} \left(\frac{gD^5}{Q^2} \right)^{0,24} \left(\frac{H}{D} \right)^{0,2} \left(\frac{H}{L} \right)^{0,52} \quad (9)$$

where (Q) is the gas flow rate, (D) the diameter of vessel and (H) the immersion depth of lance. The knowledge of plume velocity allows one to determine the particle residence time in the metal bath (τ) as follows:

$$\tau = \frac{H}{U} \quad (10)$$

2. Calculation Method

The calculation method, shown in figure 1, considers two interfaces as reaction sites:

- (a) interfaces between injected Na_2CO_3 (transitory reaction) and
- (b) an interfaces between slag on a bath surface and metal (permanent reaction).

In the sites, the following steps were repeated as shown in figure 2.

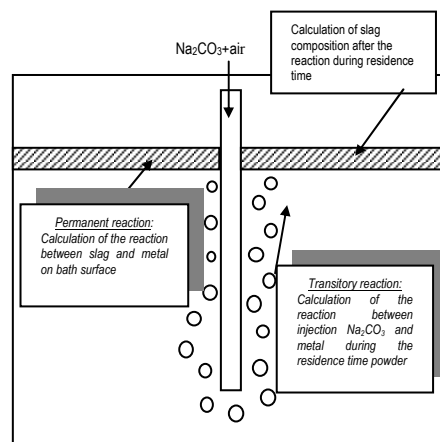


Figure 1 Calculation method for the permanent and transitory reaction zones.

1. The reaction by the injected Na_2CO_3 was calculated during the residence time of the powders (τ) determined by equation (9) and (10). The interval was fixed at $\Delta t = \tau / 20$. The equilibrium antimony content in the melt and antimony partition ratio were calculated by the FACT system [4] and then the instantaneous ($\%Sb$) was estimated with equation (8).
2. The top slag composition was calculated by a mass balance of the preexisting top slag and the injection Na_2CO_3 powder which floated on the bath surface after the end of the transitory reaction was calculated by Step 1.

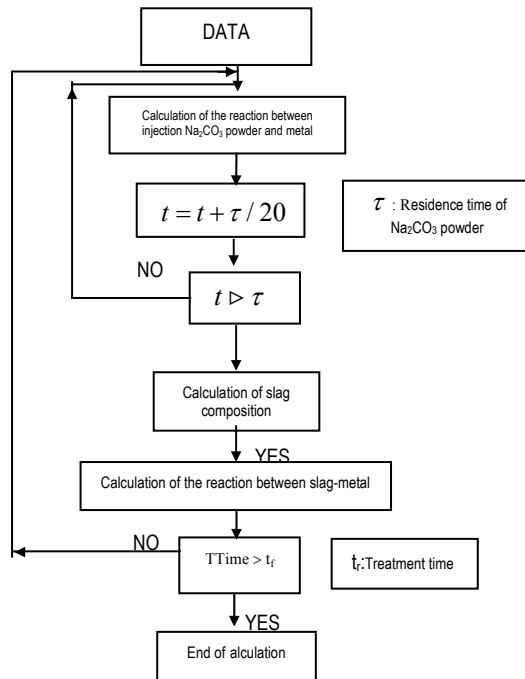


Figure 2 Calculation step for the kinetic model.

3. The calculation of [%Sb] for the permanent reaction was carried out using the top slag composition obtained in Step 3 and Equation (3). K_p is calculated from the top addition Na_2CO_3 . It is assumed in this model that although $[\%Sb]_{eq}$ may change it is low enough does not affect the value of K_p .

Na_2CO_3 injection Trials

Experiment were conducted to study the effects of temperature and gas flow rate at 3,5 and 10 l/min on the antimony content in the melt. The experimental conditions are shown in the Table 1.

Table 1. Injection trials conditions

| No. | Parameter | T=1200°C | | T=1250°C | |
|-----|-----------------------|----------|----|----------|----|
| | | 3,5 | 10 | 3,5 | 10 |
| 1 | Gas flow rate (l/min) | 3,5 | 10 | 3,5 | 10 |
| 2 | Time injection (s) | 80 | 28 | 80 | 28 |

The distance between the lance and crucible bottom was established at 100 mm and total injection time was 80 seconds with a flow rate 3,5 l/min and 28 seconds with a flow rate 10 l/min ensuring that the same total volume of gas was used in both trials. Four additions of 10 g of Na_2CO_3 each were injected during the injection period and a metal was taken after each injection.

3. Results and analysis

The application of the mathematical model requires the experimental estimation of the following unknown parameters [5]:

- Equilibrium Antimony Content and Antimony Partition Ratio

The equilibrium antimony content in the melt and the antimony partition ratio are difficult to estimate experimentally. Therefore, $[\%Sb]_{eq}$ and L_{Sb} are thermodynamically estimated with the FACT [4] database for the slag and the parameters proposed in this work for the molten copper refining. $[\%Sb]_{eq}$ and L_{Sb} depend on the temperature, composition and mass metal and the slag phase.

- Apparent Rate Constant for the Permanent Reaction Zone

The value of K_p can be obtained taking the following solution of the Equation (3) if K_p and $[\%Sb]_{eq}$ are assumed to be constant [6]:

$$-\ln\left(\frac{[\%Sb] - [\%Sb]_{eq}}{[\%Sb]^0 - [\%Sb]_{eq}}\right) = K_p \cdot t \quad (11)$$

Approximating the time dependence of the left hand side of Equation (11) to a straight line gives an estimation of the apparent rate constant for the reaction (K_p). The values of $[\%Sb]$ and $[\%Sb]^0$ can be obtained experimentally. $[\%Sb]_{eq}$ was estimated from thermodynamic calculation using the FACT system [4] assuming 15 kg of copper melting and 10 g of Na_2CO_3 . The results were $[\%Sb]_{eq} = 0.00052$ at $1200^\circ C$ and $[\%Sb]_{eq} = 0.00087$ at $1250^\circ C$.

The Na_2CO_3 injection trials in molten copper at $1200^\circ C$ and $1250^\circ C$ were used to estimate K_p . Figure 3 presents the $[\%Sb]/[\%Sb]^0$ ratio as a function of the processing time for the Na_2CO_3 injection trials. These results show that the best removal of antimony is achieved at a temperature $1250^\circ C$ which is in good agreement with the results of the thermodynamic analysis. These experiments also show that for a given temperature the antimony is reduced to a steady level after long reaction times. The mean estimated values of K_p are $1,6 \cdot 10^{-4} s^{-1}$ at $1200^\circ C$ and $4,6 \cdot 10^{-5} s^{-1}$ at $1250^\circ C$.

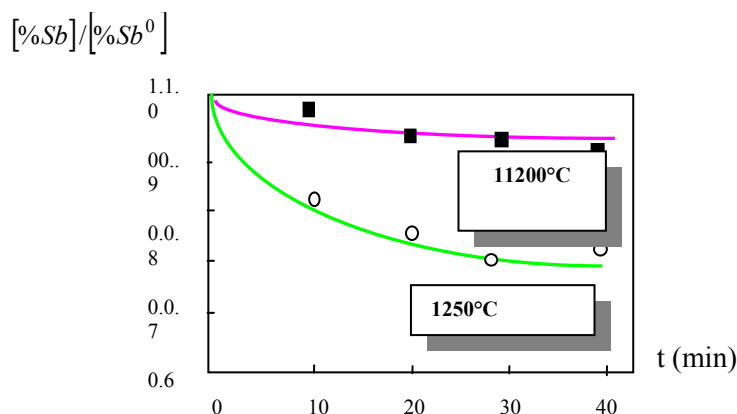


Figure 3. Effect of temperature and reaction time of the antimony removal rate.

- Efficiency of the Transitory Reaction

The efficiency of the transitory reaction (E) is a parameter that depends on many aspect: the geometry of the system, the contact area of the powders with the liquid and the hydrodynamics of the injection process.

The injection trials at 1200°C and 1250°C were used to estimate the values of the efficiency parameter by means of trial and error by comparing the mathematical predictions with the experimental data.

The results of the injection are shown in Figures 4 for high (10 l/min) air flow rate. The lines in these figures represent the results calculated by the kinetic model. The selected values of E are summarized in Table 2. It is clear that even though the values of E are low, the transitory reaction promotes a much higher the rate of antimony removal than the permanent reaction zone.

Table 2. Efficiencies of the transitory reaction

| No. | Temperature (°C) | Air flow rate (l/min) | Efficiency of the transitory reaction (E) |
|-----|------------------|-----------------------|---|
| 1. | 1200 | 3,5 | 0,04 |
| | | 10 | 0,07 |
| 2. | 1250 | 3,5 | 0,10 |
| | | 10 | 0,1 |

In the injection experiments four times as much Na_2CO_3 was added. After each injection the rate of antimony removal changed because it depended on the equilibrium antimony partition ratio and the initial copper content in the melt.

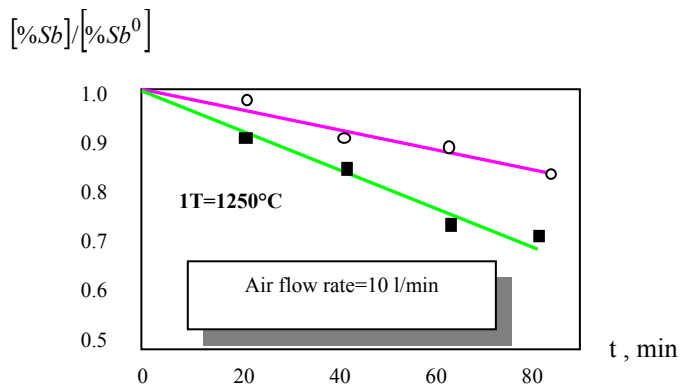


Figure 4 Experimental (points) and calculated (lines) of the effect injection time and temperature on antimony content in the molten copper.

- Effect of Temperature

Figure 3 shows the effect of temperature and reaction time for the injection Na_2CO_3 in bath molten. Rate of antimony removal is increased as temperature; the reason for this improvement is that the thermodynamic effects of the activities of antimony in the metal and Sb_2O_3 in the slag which produce a higher antimony coefficient distribution at lower temperature

At higher temperatures the viscosity of the metal diminishes, the agitation of the melt by the gas injection is increased, better mass transfer along the process is

obtained and therefore a better rate of antimony removal is obtained. These effects give higher values of the efficiency parameter at higher temperatures, as shown in Table 2.

- Effect of air flow rate

The stream of Na_2CO_3 in the injection process is transported with the carrier gas forming a two phase jet which makes contact with the molten copper at the gas-liquid interface. Initially, only a fraction of the total amount of the amount of injected Na_2CO_3 entrained into the metal. This fraction will actually react with the dissolved antimony. As expected, at given particle size the entrained fraction of solids increases with the gas flow rate since the momentum transfer provided to the particle is favoured by such a parameter. Figures 4 show that the rate of antimony removal increases with higher flow rates of carrier gas and higher temperatures.

4. Conclusions

The study made on impurities removal kinetic was materialised through an adoption of a kinetic model in conditions of refining flux injections with use of an oxidant agent. The kinetic model consists of studies the following interface reactions:

- interfaces between injected Na_2CO_3 (transitory reaction) and
- an interfaces between slag on a bath surface and metal (permanent reaction).

The application of the mathematical model requires the experimental estimation of the following unknown parameters:

- the apparent rate constant for the top slag reaction (K_p),
- the equilibrium antimony partition ratio (L_{Sb})
- efficiency of the transitory reaction (E);
- effect of temperature (T);
- effect of gas flow (Q_a).

The progress, rate of antimony removal can be calculated the following relation:

$$-\frac{d[\%Sb]}{dt} = J_{\text{Na}_2\text{CO}_3} E L_{Sb} \frac{[\%Sb]}{W_{Cu}}$$

The antimony removal from the liquid copper through the injection of Na_2CO_3 with use of air, was more efficiency at higher air flow rate and higher temperatures.

The kinetic model was adapted to the copper refining process to predict the rate antimony removal in terms of temperature and air flow rate.

REFERENCES

1. Ohguchi S., Robertson, D.G.C., *Kinetic Model for refining by Submerget Powder Injection, Ironmaking and Steelmaking, vol.II*, 1984, 262-273
2. Sawada I., Ohashi T., *Hydrodynamics of gas Stirred Melts, Tetsu-to-hagane, vol.73*, 1987, 669-674
3. Tsitouras, Ch., ELSEVIER, *Applied Mathematical Modelling, vol.26*, 2002, 77-88
4. Thompson W.T., Bale C.W., and Pelton A.D., *F* A * C * T * -Facility for the Analysis of Chemical Thermodynamics, User's Manual*, 1999,

5. Hotea V., *Studies and researches regarding interaction between slag-metallic bath in copper refining process*, **M.Sc.Thesis**, Politechnic Institute of Bucharest, 2002
6. Plascencia-Barrera, G., *Copper and Nickel Removal From Liquid Lead*, **M.Sc.Thesis**, Instituto Politecnico Nacional, Mexico, 1999

Conf.dr.ing. VASILE HOTEA, Ș.I.dr.ing. GHEORGHE IEPURE, Ș.I.dr.ing. ELENA POP, Ș.I.drd.ing. EMILIA TALPOȘ, Ș.I.drd.ing. JOSZEF IUHAZS, Asist.drd.ing. AURICA POP

UNIVERSITATEA DE NORD BAIA MARE, STR. VICTOR BABEȘ 62A, BAIA MARE, MARAMUREȘ, ROMANIA, email: vhotea@yahoo.com

CONSIDERAȚII CINETICE PRIVIND PROCESUL DE RAFINARE TERMICĂ A CUPRULUI

Rezumat: În acest studiu cinetica îndepărtării impurităților s-a materializat prin adoptarea unui model cinetic în condițiile insuflării fluxurilor de rafinare cu ajutorul unui agent oxidant. Lucrarea abordează în principal insuflarea Na_2O_3 sub formă de pulbere în procesul de rafinare termică a cuprului. Experimentele au fost constat în utilizarea a 15 kg de cupru în stare topită, la 1200 și 1250°C. Agentul de transport utilizat la insuflarea Na_2O_3 a fost aerul la debite de 3,5 și 10 l/min. Rezultatele au arătat că în procesul de rafinare termică a cuprului, îndepărtarea stibiului la insuflarea Na_2O_3 este mult mai eficientă la temperaturi mai ridicate. Gradul de îndepărtare al stibiului este mai mare la debite mai mari ale aerului (10 l/min.). Modelul cinetic a fost adoptat pentru a prezice gradul de îndepărtare al stibiului în procesul de rafinare termică a cuprului.

CREEP OF SOME POLYURETHANIC ELASTOMERS

BY

PAUL DORU BÂRSĂNESCU, CONSTANTIN BÎTCĂ and MIHAI MIHĂLCUȚ

Abstract: This paper presents some aspects with regard to the creep of the polyurethanic elastomers, concerning especially the concomitant action of the ultraviolet radiations and the effect of the successive loads and unloads of these polymers. The study of the creep behavior realized according to ASTM-D674.

Keywords: polyurethanic elastomer, creep, aging, UV radiation

1. Introduction

In general, a polymer specimen loaded to creep can present one of the next results [6]:

- Specimen fractures immediately after the stress application;
- Specimen fractures after a certain time;
- Specimen resists an undefined time period.

Last cases are representative for practical applications.

To establish the region of the admissible forces during the exploitations it is necessary to study the behavior of a polymer under a constant stress depending on time, therefore under creep conditions. More methods were proposed to predict the creep behavior. These methods base on the theory of visco – elasticity or on the experimental representations $\varepsilon(t)$ or $J(t)$, [1, 2, 3, 7, 14]. Investigation of the influence of the ultraviolet radiations on the mechanical properties shown that these have an accelerator effect on the creep fracture of the polymers, what can be explained by the summation of the mechanical processes and of the effect of the ultraviolet irradiation, [10, 11, 12].

This paper presents some aspects with regard to the creep of the polyurethanic elastomers, concerning especially the concomitant action of the ultraviolet radiations and the effect of the successive loads and unloads of these polymers.

2. Experimental details

The study of the creep behavior ha been realized according to ASTM-D674 using the experimental device, shown in *figure 1*, [8, 9].

The specimens have been made from polyurethanic elastomer, called Moldotan – D, made in *Petru Poni* Macromolecular Chemistry Institute of Iași, [4].

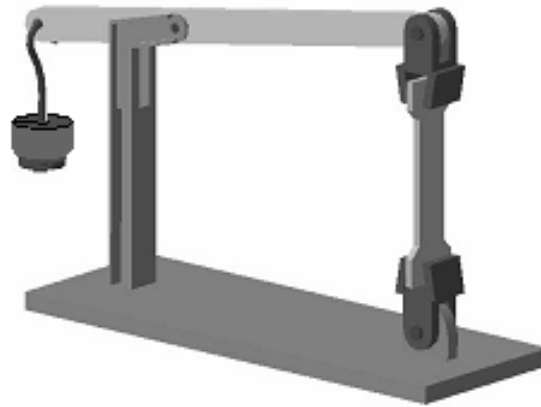


Fig. 1. Loading mechanism with constant force, [8]

Accelerated aging was realized by means of ultraviolet irradiation, with a lamp with mercury vapors, at de 25°C, for 200 hours.

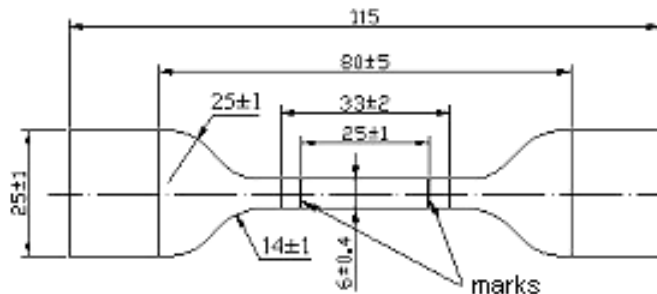


Fig. 2. Shape and size of polyurethane specimen, according to ISO R 527/66 E

3. Results and discussions

3.1. Effect of UV irradiation on the behavior of the polyurethane elastomers under tensile creep conditions

The experimental ε – time diagrams have been assigned for a specimen loaded in creep conditions without ultraviolet irradiations (*figure 3, curve 1*) and for another specimens with UV irradiation. The stress was for the both cases $\sigma = 8.97$ MPa (*fig. 3*).

It can observe the aged specimen fractures after 55 hours from the start of the test, while the specimens unloaded to ultraviolet irradiation do not fracture for sollicitation time by 1000 hours, after what the unload follows. Also, in the case of the specimen under concomitant aging, the appearance of some cracks was observed, what produce the macromolecular fracture of the specimens by means of coalescence and increase. The same experimental data were presented by means of the creep compliance, calculated with the equation

$$J(t) = \frac{\sigma_0}{\varepsilon(t)}$$

where σ_0 is the constant stress [MPa] and $\varepsilon(t)$ is the specific deformation measured strain (*fig. 4a and 4b*).

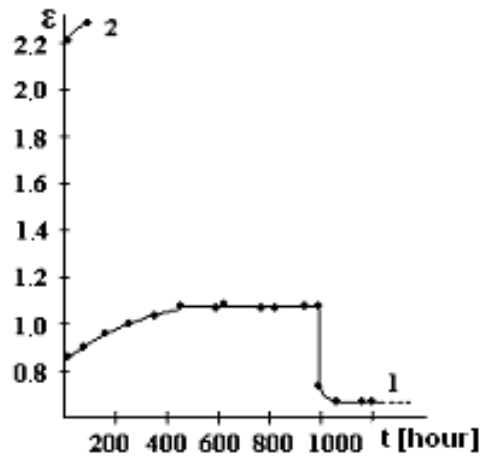


Fig. 3. Experimental (ε - t) diagrams for a specimen loaded in tensile creep ($\sigma = 8,97$ MPa): 1. without UV irradiation, 2. with concomitant UV irradiation UV

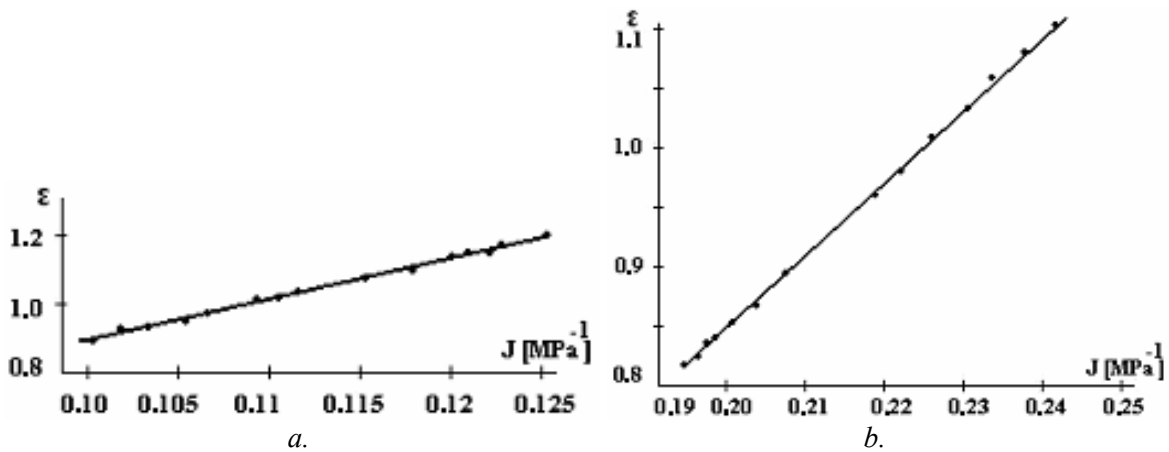


Fig. 4. ε - $J(t)$ diagrams at $\sigma = 8,97$ MPa: a) stressed specimens without UV radiation, b) stressed specimens and UV irradiated during the loading

In *fig. 5*, the $\varepsilon - t$ diagram for two-aged specimen preliminary and after this stressed is presented. In this case, also $\varepsilon - J(t)$ diagram were represented (*fig. 6a* and *6b*). It observes that the preliminary uniaxial loading of the aged specimen do not conduct to failure after 1000 hours under loading. Though, the strains presented by these specimens are greater than in the case of the unaged specimens (*table 1*).

Tab. 1. Typical strains in the case of the stressing and UV aging

| σ [MPa] | 8.97 | 8.97 concomitant UV irradiation | 10.06 preliminary UV irradiation |
|---|-------|---------------------------------|----------------------------------|
| Strain, ε | | | |
| Instant strain, ε_1 | 0.88 | 0.885 | 1.79 |
| Residual strain, ε_3 | 0.75 | - | 1.75 |
| Total strain, $\varepsilon_3 + \varepsilon_3 + \varepsilon_3$ | 1.135 | 2.32 | 1.92 |

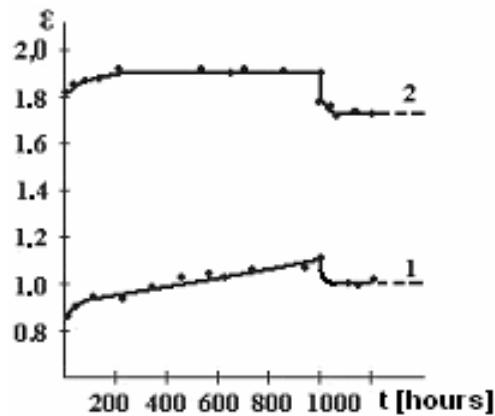


Fig. 5. Experimental (ε - t) diagram in the case of the preliminary aged specimens:
1. $\sigma = 4.22$ MPa, 2. $\sigma = 10.06$ MPa

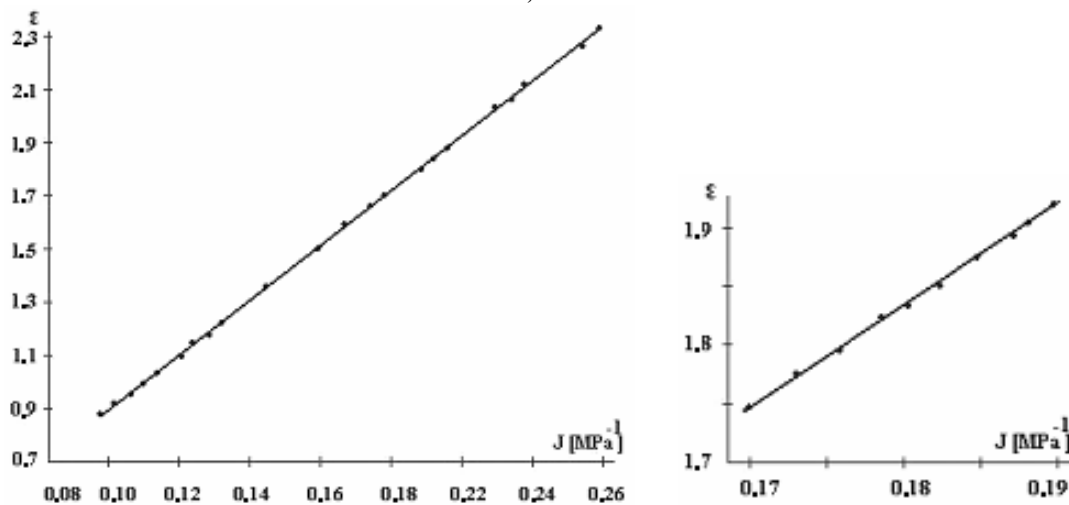


Fig. 6. $\varepsilon - J(t)$ diagrams for preliminary UV aged specimens: a) $\sigma = 4.22$ MPa, b) $\sigma = 10.02$ MPa

Also, after accelerated aging, a modification of the colors and hardness of the specimen, without to observe the appearance of the cracks. These results conduct to the follow interpretations:

- It is known that the action of the UV radiations, with a particular wavelength, determines the rupture of the valence chemical bond inside polymers, [13]. In the case of concomitant loading with UV irradiation, the tensile stresses accelerate the photo-destructible process of the macromolecules. Such as acceleration is produced in the first instance by the stressed state decelerating the regeneration process of some broken bonds because of the UV irradiation.

- Another cause is the decrement of the dissociation energy of the stressed bonds, becoming possible the acceleration of the scission process under UV irradiation. Acceleration of the photo-destructive process under mechanical loading is finalized with the breaking of polymer specimens, through cracking, process observed with the naked eye.

Some valence bonds of the previous irradiated specimens fracture, that produce a significant increase of the deformation under ulterior loading, toward unirradiated specimen (*table 1*). A photo-destructive process occurs under UV irradiation. This think decreases the strength of the polymer under the next action of the mechanical energy. Though this decrease is not enough to produce the rupture of the polymers in the experimental conditions studied.

These results are concordantly with the data obtained by E.E. Tomaşevskii et al. [10, 11, 12] for methyl polymethacrylate, poly ϵ – caprolactam and natural silk. They studied also the kinematics of the free radical accumulation under mechanical loading and concomitant irradiation, by means of the spin electrical resonance.

In the same time, these data show that a scission process of the valence bonds from macromolecular chains occurs in the case of the *Moldotan D* polyurethaneic elastomers in creep conditions because only the valence bonds break off by UV irradiation. These processes base on the same phenomenon, namely the scission of the primary chemical bonds.

In this way, new proof is brought to sustain the macromolecular failure mechanism of the specimens, developed by Jurkov, [5].

3.2. Influence of successive loadings and unloadings on the strain – time curve

More loading – unloading solicitations of the same specimens were effectuated with the same stress ($\sigma = 8.89$ MPa), and the same recovering period between them (figure 7).

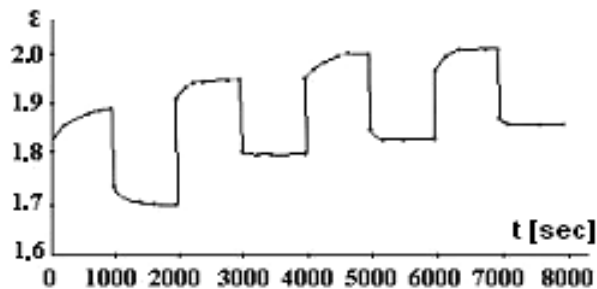


Fig. 7. Experimental curve $\epsilon - t$ in the case of successive loading and unloading with $\sigma = 8.89$ MPa

From experimental data, presented in the table 2, it observe that the total and residual strain increase with the loading number. Some chemical bonds rupture under solicitation. This think is shown by the size of the residual strain, what does not renew during the recovering period.

Table 2. Comparative typical strains in the case of successive loading and unloading (cyclical)

| Cycle | I | II | III | IV |
|--|------|-------|-------|-------|
| Typical strain, ϵ | | | | |
| Instant strain, ϵ_1 | 1.65 | 0.16 | 0.137 | 0.087 |
| Residual strain, ϵ_3 | 1.70 | 1.795 | 1.82 | 1.845 |
| Total strain, $\epsilon_3 + \epsilon_3 + \epsilon_3$ | 1.89 | 1.94 | 1.99 | 1.998 |

Number of broken bonds increase with the residual strain, under a new solicitation.

Also, by means of this experiment, it confirms that the interatomic chemical bonds fracture because of creep. This process constitutes the major act of the deformation and the macroscopic failure of the polymers. It is expected as the macroscopic failure of the polymers occurs after more cyclic solicitations.

Because the applied effort was the same in the case of loads, the process has some similarities with the creep phenomenon of the polymers.

4. Conclusions

1. The study confirms the molecular mechanism of the creep failure for the polyurethanic elastomers.

2. Accelerator effect of mechanical loading on the aging of the polymers by UV irradiation was emphasized. This phenomenon occurs usually during the exploitation conditions. Some data are offered by this study regarding the aging process of the polyurethanic elastomers.

3. Modification of some properties of the elastomers studied, under mechanical solicitations and UV irradiation, shows that the deformation and the failure in creep conditions bases on the scission of chemical bonds existing in the atomic lattice of the polymer. This is the major act of the final macroscopic failure.

Received April 18, 2005

The "Gh.Asachi" Technical University Iași

REFERENCES

1. Brüller O.S., Pütz D., *Rheol. Acta* 15, 1967, p.143
2. Cherry B.W., Kinder D.F., *Mater. Sci. Eng.* 49, 1981, p.285
3. Dieter G. (vol. chair) et. al., *ASM Handbook*, vol. 20, Material Selection and Design, ASM Int., dec. 1997
4. Geanău L., Caraculacu A., Taranu V., Seiler S., Popescu V., Brevet RSR 100.965, 1980
5. Jurkov S.N., Korsukov V.E., *J. Polym. Sci, Polym. Phys. Ed.* 12, 385, 1974
6. Kausch H.H., *Polimer Fracture*, Springer-Verlag, Berlin, 1978, p. 211
7. McCrum N.G., *J. Mater. Sci.* 13, 1978, p.1596
8. Oprea C.V., Constantinescu A., Bârsănescu P., *Proc. Of the 29th Symposium IUPAC MACRO'83, Bucharest, Section IV*, 1983, p. 697
9. Oprea C.V., Constantinescu A., *Comunicarea la Conferința de chimie și tehnologie chimică a I.P.B., București, nov.*, 1983
10. Samoïlov T.T., Tomașevskii E.E., *Fizika Tverdogo Tela* 10, 1968, 1094
11. Samoïlov T.T., Tomașevskii E.E., *Fizika Tverdogo Tela* 10, 1968, 3039
12. Samoïlov T.T., Tomașevskii E.E., *Fizika Tverdogo Tela* 11, 1969, 1729
13. Schnabel W., Kiwi J., *Aspects of degradation and stabilization of polymers*, H.H.G. Jellinek ed., Elsevier, Amsterdam, 1978, p. 150
14. Wineman A., Rajagopal K.R., *Mechanical Response of Polymers*, Cambridge University Press, 2000

STUDIUL LA FLUAJ A UNOR ELASTOMERI POLIURETANICI LA TRACȚIUNE

Rezumat: Lucrarea își propune să studieze unele aspecte ale fluajului elastomerilor poliuretanic, legate în special de acțiunea concomitentă a radiațiilor UV și efectul pe care îl exercită asupra deformării acestor polimeri încărcările și descărcările succesive. Studiul comportării la fluaj s-a făcut conform cu ASTM-D674.

COMPARATIV STUDY ON THE BEHAVIOR OF THE RUBBER AND SOME POLYURETHANS UNDER CREEP CONDITIONS

BY

PAUL DORU BÂRSĂNESCU, BÎTCĂ CONSTANTIN AND CARMEN BEJENARIU

Abstract: This paper studies the difference between the behaviors of some conventional polymers and the thermoplastic polyurethanic elastomer (Moldotan D). Loading in tensile under creep conditions accomplished according to ASTM D-674, using specimens in concordance with ISO R527/66E. The creep study of the Moldotan D polyurethanic elastomers shows the presence of the permanent deformations, because of the scission of low intermolecular bonds.

Keywords: polyurethane, rubber, creep

1. Introduction

The physical and mechanical properties of polyurethanes (high abrasion resistance, ultimate elasticity, stability at oils and other petrochemicals, etc) result from their complex structures (present rigid and flexible segments, the density of the intermolecular interactions, sometimes the reticulation advanced, etc), [1, 3, 5, 6].

Intention of this paper is to emphasize the difference between the behaviors of some conventional polymers (butadiene - styrene rubber) and the thermoplastic polyurethanic polymers (Moldotan D). Therewith the modification of some physical properties is shown (solubility, bulking, viscosity, thermal stability) reflecting the transformations what produce at molecular level under tensile conditions with a constant effort, a long time.

2. Experiments

Polyurethanic elastomers used were obtained by casting, from 4.4'-dibenzylidiazocyanate și polyetilenglycoladipate, like catena extension using ethylenglycole. Behavior under creep conditions was studied comparatively with that of a butadiene - styrene rubber. Loading in traction under creep conditions accomplished according to ASTM D-674, for 3 values of stresses: 3.5, 7.0, and 14.0 MPa, using specimens in concordance with ISO R527/66E. All determinations accomplished at room temperature, [2, 4, 7].

Structural variations happened under sollicitation can be studied by means of some physical and mechanical properties, as: bulking at equilibrium, solubility, viscometry, and thermal stability.

3. Results and discussions

After the processing of experimental data, the creep diagrams were plotted, in ε – time coordinates, for Moldotan D and butadiene - styrene rubber vulcanized, at a stress of $\sigma = 3.5$ MPa (figure 1).

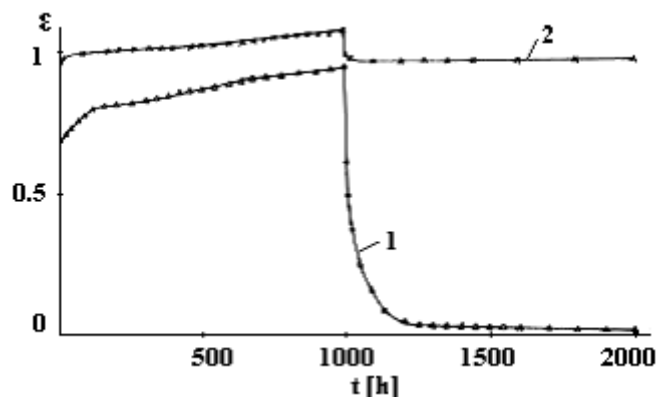


Fig. 1. Creep curves for a stress of 3.5 MPa: 1. Moldotan D, 2. butadiene - styrene rubber vulcanized

With these data, deformations due to the visco – elastical behavior computed (table 1). It observes from this table that the polyurethanic elastomer presents, for the same stress σ , a bigger maximal strain. If the force is removed (recovering period), the polyurethane remains with an emphatic permanent strain after 1000 hours, while in the case of the vulcanized elastomers (with strong transversal bonds) this strain tends to zero. This behavior is due to the thermoplastic character of the polyurethanic elastomer.

Table 1. Deformations due to the visco – elastical behavior

| Material \ Strain, ε | $\varepsilon_{el.instant}$ | $\varepsilon_{el.delay}$ | ε_{max} | Recovering <i>el.instant.</i> | Recovering. <i>el. delay</i> | ε_{perm} |
|----------------------------------|----------------------------|--------------------------|---------------------|----------------------------------|---------------------------------|----------------------|
| Moldotan D | 0.94 | 0.13 | 1.07 | 0.9 | 0.06 | 0.96 |
| Rubber | 0.68 | 0.27 | 0.95 | 0.33 | 0.31 | 0.02 |

During the creep conditions, the scission of the weak intermolecular bonds occurs, what at the removal of the stress do not recover totally, generating the permanent strain. For an elastomer vulcanized, the regeneration of the transversal chemical bonds broken occurs totally, but with a delay, determined by the rate of the realignment at macromolecular level.

Plotting of experimental data in semilogarithmic and logarithmic coordinates (figures 2 and 3), conducts to a partial linearization of the creep curves, phenomenon more accentuated in the case of the elastomer vulcanized, that approach more to linear visco – elastical behavior.

Calculation of the creep compliance realizes with the equation

$$D(t) = \frac{\varepsilon(t)}{\sigma_0} \text{ [MPa}^{-1}\text{]}$$

The plotting of the $\varepsilon - D(t)$ and $\varepsilon - \log D(t)$ curves (figure 4 and 5) conducts to some right lines, what can constitute a base to predict the behavior of these polymers under load conditions a long time.

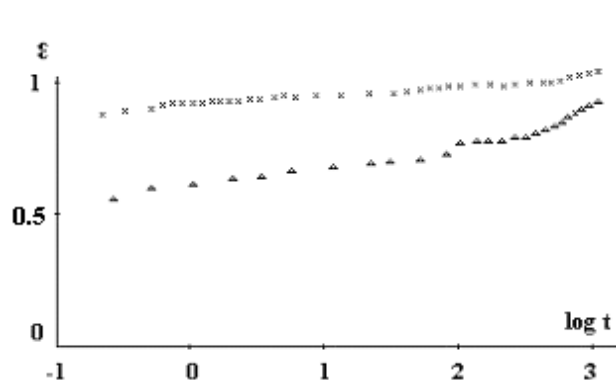


Fig. 2. Creep curves in semilogarithmic coordinates

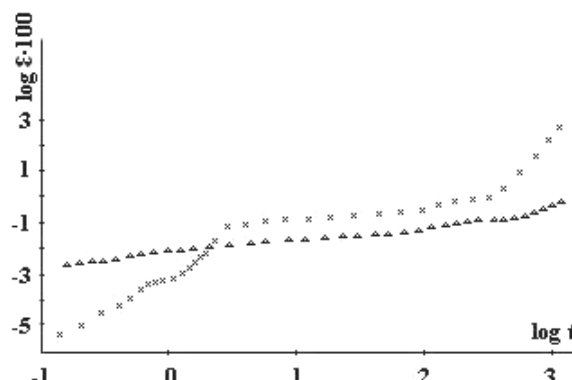


Fig. 3. Creep curves in logarithmic coordinates

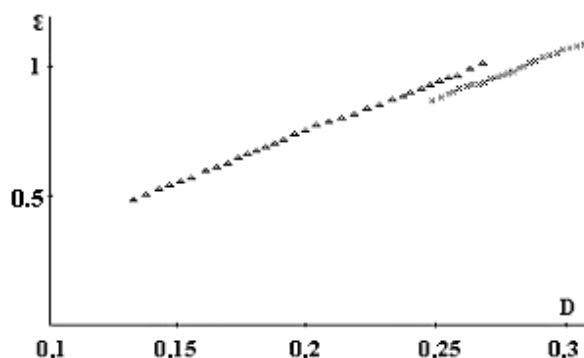


Fig. 4. $\varepsilon - D(t)$ curves

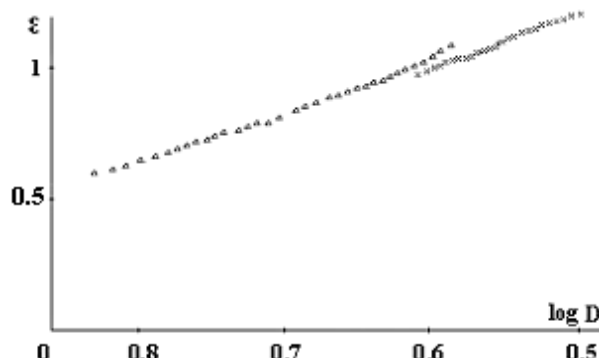


Fig. 5. $\varepsilon - \log D(t)$ curves

The experimental data regarding to the modifications of some physical properties pursuant to the loading of the Moldotan D polymer are explicable by the physical and mechanical properties that occur in traction in creep conditions. Polymer studied is constituted from catena what represents some relative rigid segments, because of the presence of the aromatic nucleus and other flexible that contain esteric bonds. It has numerous intermolecular bonds (van der Waals and hydrogen bonds), evidence being the low solubility and good thermal stability.

Existence of rigid segments constitutes a concentrator coefficient at this level. The concentration of mechanical energy on these segments determines the scission of some intermolecular bonds that produces a pronounced aeration of the molecular and supramolecular structure of the polymer, inducing the increasing of the bulking and the decreasing of the thermostability. With the increasing of the stress (σ), also the scission of chemical valence bonds occurs, phenomenon emphasized by the decrease of the logarithmic viscosity coefficient (Table 2).

With the increasing of the unit stress, an accumulation of the physical and mechanical phenomenon occurs inside microvolume destroyed, which manifests by an exquisite diminution of the molecular mass and the strength of the polyurethane studied under the action of some solvents and the heat.

4. Conclusions

The creep study of the Moldotan D polyurethanic elastomers shows the presence of the permanent deformations, because of the scission of low intermolecular bonds. In the same time, the permanent deformation of an elastomer vulcanized tends temporally to zero, because of the stronger nature of the transversal bonds. The scission of intermolecular bonds (van der Waals, hydrogen), as well as of some chemical valence bonds, produces a strong aeration of the polymer structure, what constitutes the cause of the increase of the buckling and absorbing capacity. The molecular mass and thermostability decrease also.

Received April 19, 2005

The "Gh.Asachi" Technical University Iași

REFERENCES

1. *Developments in Polyurethanes*, J.M. Buist ed., Appl. Sci. Publ., London, 1978
2. Dieter G. (vol. chair) et. al., *ASM Handbook*, vol. 20, Material Selection and Design, ASM Int., dec. 1997
3. Lipatov O.C., Kercea I.I., Sergeeva L.M., *Struktura i svoistva poliuretannov*, Naukova Dumka, Kiev, 1970
4. Oprea C.V., Popa M., Bârsănescu P.D., *Izmenenia mehaniceskih svoistv polichorida v sledsvie polzucesti*, Mekch. Kompoz. Mat., no. 3, 1985, p. 401 - 403
5. Saunders J.H., Frisch K.C., *Polyurethanes Chemistry and Technology*, Part I, Interscience, New York, 1976
6. Saunders J.H., *Polymer Chemistry of Synthetic Elastomers*, J.P. Kennedy, E.G.M. Tornqvist ed., Interscience, New York, 1969
7. Wineman A., Rajagopal K.R., *Mechanical Response of Polymers*, Cambridge University Press, 2000

STUDIUL COMPARATIV ASUPRA COMPORTĂRII LA FLUAJ A CAUCIUCULUI ȘI A UNOR POLIURETANI

Rezumat: Această lucrare studiază diferența dintre comportarea unor polimeri convenționali și a unor elastomeri poliuretatici termoplastici (Moldotan D). Solicitarea la tracțiune în condiții de fluaj s-a efectuat conform normelor ASTM D-674, utilizându-se epruvete conform ISO R527/66E. Studiul fluajului elastomerului poliuretanic Moldotan D arată prezența deformației permanente, consecință a scindării legăturilor intermoleculare slabe.

STRUCTURAL ASPECTS OF A $\text{Ni}_{50}\text{Ti}_{48}\text{Nb}_2$ SHAPE MEMORY ALLOY REVEALED BY SCANNING AND TRANSMISSION ELECTRON MICROSCOPY

IOANA GHERGHESCU¹ and SORIN CIUCĂ²

This paper presents structural aspects obtained by scanning and transmission electron microscopy of a shape memory $\text{Ni}_{50}\text{Ti}_{48}\text{Nb}_2$ alloy. The alloy was chosen in order to obtain a shape memory alloy having a wider hysteresis than equiatomic NiTi, that involves a better thermomechanical stability. Prior to all investigation, the ingot was annealed at 900°C/48 h. Transmission electron micrographs, scanning electron micrographs, electron diffraction patterns and X-ray microanalysis (EDAX) results were obtained. Both scanning and transmission electron microscopy give informations on the structure of the different phases found in NiTi alloys: austenite, martensite and secondary phases. The austenite in this alloy has nearly the same characteristics as in an equiatomic NiTi alloy; the martensite suffers supplementary distortions. Complex precipitate particles of NiTiNb were analyzed by EDAX, an approximate chemical composition being determined; two new types of complex precipitates were found. Their composition is not modified by annealing at 800°C; these two phases are stable, having equilibrium structures and chemical compositions.

Key words: Shape memory alloy, scanning and transmission electron microscopy

A shape memory $\text{Ni}_{50}\text{Ti}_{48}\text{Nb}_2$ alloy was chosen in order to obtain a shape memory alloy having a wider hysteresis than equiatomic NiTi, that involves a better thermomechanical stability, therefore a higher reliability [1].

The raw materials employed in order to obtain NiTiNb alloys were the following: Ti (Ugine) refined in vacuum (99,99%), electrolytic (99,98%) Ni (INCO) and master alloy TiNb, containing 44 (wt%) titanium. All three were grinded and then pickled in a 1/3 HF + 2/3 HNO₃ solution. The metals were melted in a high induction furnace (0,5 MHz) having 25 kW maximum power. This furnace allows melting the materials in neutral atmosphere in a cavity made in a copper pipe, continuously cooled by water. A satisfactory homogeneousness is obtained thanks to the electromagnetic induction and the quick final cooling allows segregation reduction.

The resulting ingot had a cylindrical shape of 6 mm. radius and 50 mm. length. Its mass was 40 grams. A homogenizing annealing was applied, at 900°C/48 h.. The hot rolling was performed at 800°C, until 40 mm² of the ingot section, followed by cold rolling.

I. Scanning electron microscopy investigation

Scanning electron microscopy investigation was used in order to determine the chemical composition of the compounds existing in the structure of this alloy. X-ray diffraction gives unidentified peaks, except those attributed to the austenite, martensite and Ti₂Ni, currently found phases in NiTi alloys [2].

Taking into account the 2% niobium concentration of this alloy, we had to verify the existence of rich niobium compounds, found in the $\text{Ni}_{47}\text{Ti}_{44}\text{Nb}_9$ system.[1]

The obtained micrographs are images of secondary electron emission ejected by atoms by disexcitement. The lighter zones correspond to atoms or atom mixtures having greater atomic mass. X-ray microanalysis (EDAX), frequently associated with scanning electron microscopy, allows to obtain qualitative informations concerning elements repartition on the material surface; the results are less accurate in quantitative analysis.

The experiments were the following:

1) Determination of the alloy chemical composition on the whole of the ingot by WDX, more accurate than EDAX, using accumulation times of 1000 seconds.

The results were: a) 51,03%Ni, 47,12%Ti, 1,85%Nb and b) 51,32%Ni, 46,85%Ti, 1,83%Nb, which is close to the expected composition, 50%Ni, 48%Ti et 2%Nb.

2) Scanning electron micrographs and X-ray diffraction patterns concerning Ni, Ti and Nb distribution for three kinds of samples: a) cast; b) hot rolled; and c) annealed at 800°C/12h. and submitted to thermal cycles consisting in alternative heating and coolings.

a) For the cast sample, the following results were obtained:

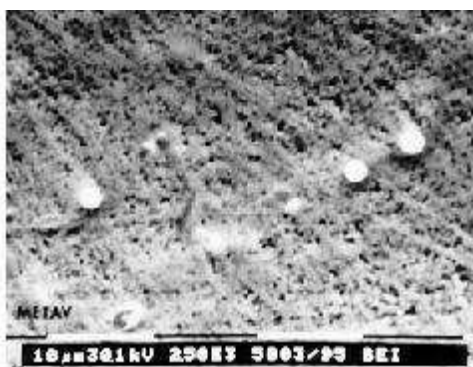


Figure 1. Scanning electron micrograph, distribution electrolytical attack 5% $C_6H_3O_7N_3$ in CH_3-COOH

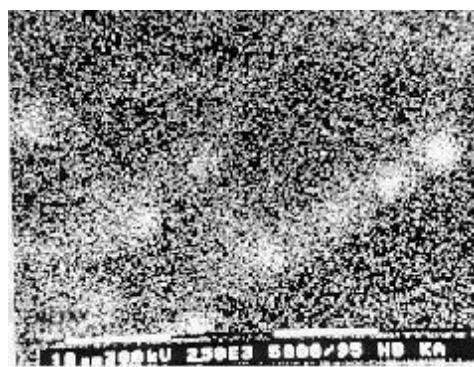


Figure 2. X-ray image concerning Nb

In spite of all difficulties related to samples preparation, we have succeeded in obtaining matrix + compounds zones. The X-ray images concerning niobium distribution clearly show the existence of a higher niobium content in the considered compounds. It is to be noticed that examining these compounds was extremely difficult, because of their very weak coherence with the matrix. Every tested attack was pulling out the compound particles; on the scanning electron micrographs, what we presumed to be compounds were in fact cavities from which they have been pulled out.

The compounds distributed at grain boundaries belong to an eutectic, consisting in a NiTiNb solid solution, Ti_2Ni compounds, but also rich-niobium compounds.

The morphology of some idiomorph-like compounds found on the scanning electron micrograph (figure 3) suggest their cubic-like symmetry.

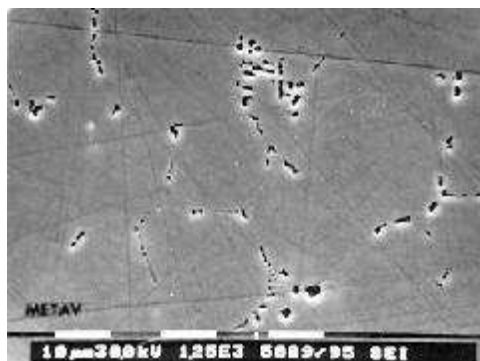


Figure 3. Scanning electron micrograph showing rich niobium compounds, HF attack.

The structure of the cellular eutectic is also easy to observe on the scanning electron micrograph, figure 4. Niobium has a greater atomic number, therefore can be observed as a light coloured network surrounding darker crystals of NiTiNb.

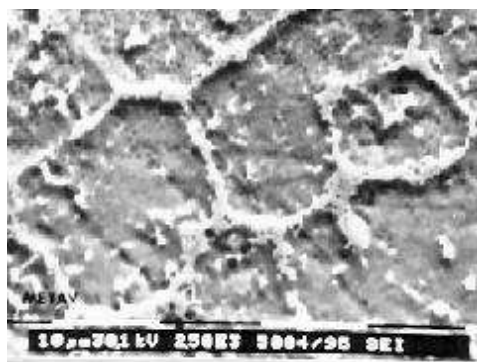


Figure 4. Rich niobium light coloured network, electrolytical attack.

b) For the hot rolled sample, several changes were noticed: the characteristic eutectic morphology is partially modified by shattering of eutectic cells. The compound crystals are somewhat rounder, keeping a distribution that still suggest former grain boundaries. X-ray diffraction pattern concerning every element gives a regular distribution of Ni, Ti and Nb on the examined surface, which confirms compounds pulling out by attack.

c) For the 800°C/12 h. annealed sample, form and distribution of crystals are not radically changed, still suggesting former grain boundaries.

The explanation concerning compound distribution change can be given by admitting the existence of a solvus curve of solubility variation in the solid state (Ni-Nb equilibrium diagram); on heating, rich niobium compounds are partially dissolved; on further cooling they re-precipitate as finer crystals, having a different distribution from the original state.

3) Chemical composition of the compounds by EDAX. Two types of rich niobium compounds were found, having the following approximate chemical compositions:

- I – Ni_{53,5}Ti₄₂Nb_{4,5} (atomic %)
- II - Ni₄₆Ti_{32,5}Nb_{21,5} (atomic %)

These two compounds were found in the three samples: cast, hot rolled and annealed; they are primary compounds, formed during solidification. We can suppose they are stable phases, having equilibrium structures and chemical compositions. It is to be noticed that annealing at 800°C does not change the chemical composition of the two compounds.

II. Transmission electron microscopy investigation

Specimens for transmission electron microscopy were obtained from hot and than cold rolled strips of 0,5 mm. thickness, attacked in a mixture of 1V H₂O₂+ 1V HNO₃+ 1V HF in order to make them as thin as possible. In these strips, disks of 3 mm. were cut up. The final operation was piercing them by ionic bombing. TEM experiments were carried out using a Philips CM 35 microscope; matrix and compounds chemical composition were also determined by TEM/EDAX.

According to the critical point temperatures determined by differential scanning calorimetry (DSC) [3], we can anticipate that austenite is mainly to be found in the material structure. Owing to deformations induced by sample preparation, we can also expect to find martensite; nevertheless, we cannot neglect the thermal effect of the electron beam, that rises the specimen temperature, leading to martensite-to-austenite transformation.

Typical electron diffraction patterns of the premartensitic phase showing 1/3 <110>, 1/3<111>, 1/3 <112> superlattice reflections are not found in any specimen; therefore premartensitic phase reported in some NiTi alloys [4] is not found in Ni₅₀Ti₄₈Nb₂; DSC and internal friction experiments also did not show peaks related with premartensitic phase [3], [5].

We expected to find [2]:

- austenite, CsCl (B₂) type structure, cubic centered (ordered), with a lattice constant of $a_0 = 3,012\text{\AA}$
- martensite, B'₁₉, monoclinic, with lattice constants:

$$a = 2,898\text{\AA}; \quad b = 4,66\text{\AA}; \quad c = 4,12\text{\AA}$$

$$\alpha = 90^\circ; \quad \beta = 90^\circ; \quad \gamma = 97,78^\circ$$

After electron diffraction patterns interpretation, we can observe that austenite is submitted to the following structural changes:

- the angle between reciprocal lattice reflections having <111> zone axis become 59° or 61°;
- a systematical increase of the austenite lattice constant, from 3,01Å to 3,12÷3,15 Å.

These changes are related to the niobium presence in the solid solution.

As far as martensite is concerned, electron diffraction patterns similar to those already reported [2] were obtained, but also different patterns systematically repeated. These diagrams could not be interpreted because of particular angles and interplanar

distances found. We could not obtain electron diffraction patterns for the compounds found in the material structure; these have been pulled out during polishing or specimens haven't been thin enough for revealing compound areas, appropriate for electron microdiffraction.

Transmission electron micrographs for austenite, martensite, a compound and their electron microdiffraction patterns are further on shown:

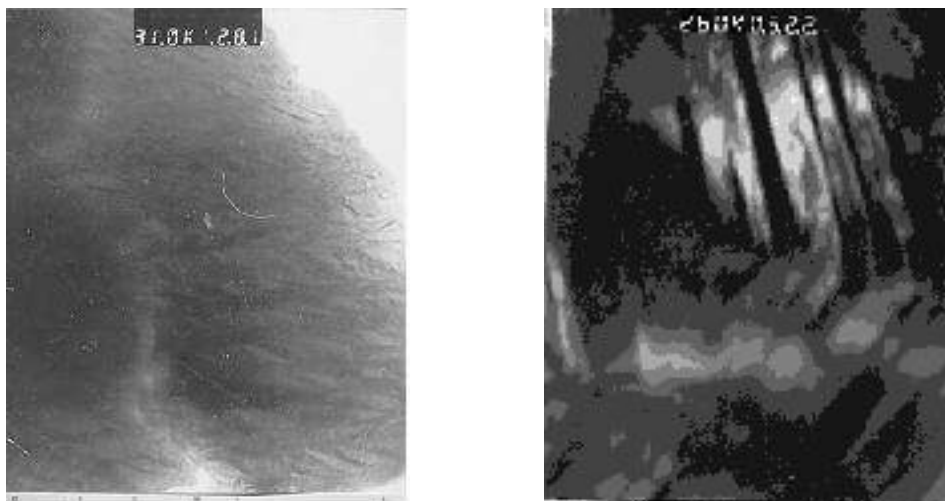


Figure 5. Transmission electron micrographs of martensite twins. M = 31.000, U = 250 kV.



Figure 6. Transmission electron micrograph revealing both austenite and martensite; M = 42.000

By TEM/EDAX we were able to determine the chemical composition for some precipitate particles, taking into account measurement dispersion inherent to such a method, of 5% or even greater. Medium chemical composition was: 4%Nb, 49%Ni and 47% Ti (atomic percentage).

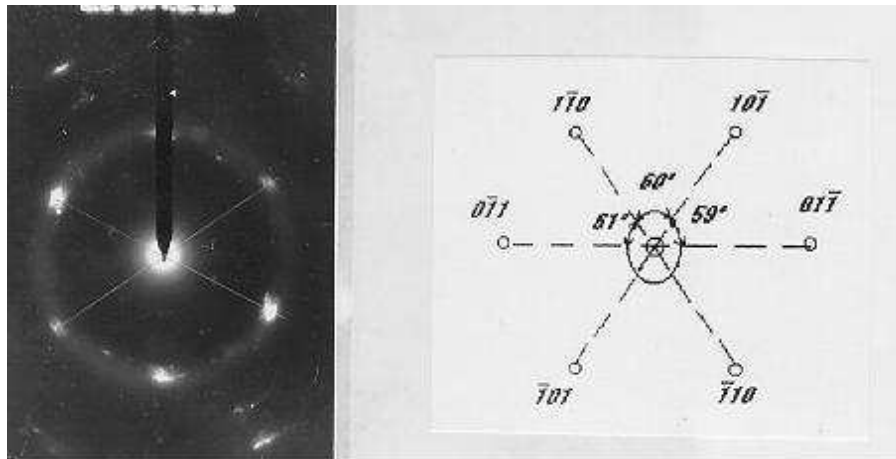


Figure 7. Electron diffraction pattern of a distorted austenitic zone, zone axis $\langle 111 \rangle$, $a=3,16\text{\AA}$, $\alpha=61^\circ$.

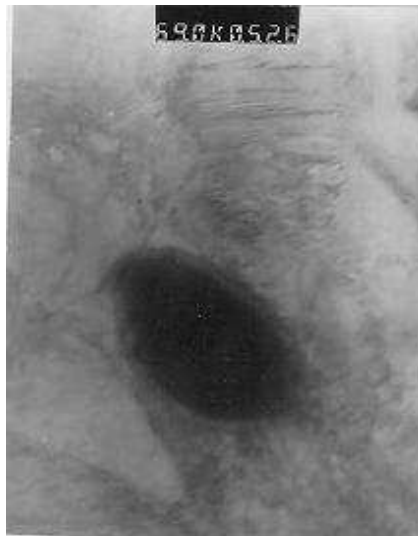


Figure 8. Transmission electron micrograph of a precipitate. $M = 69.000$.

Conclusions

Two types of ternary compounds were identified in the structure of a shape memory $\text{Ni}_{50}\text{Ti}_{48}\text{Nb}_2$ alloy by complementary investigations, scanning electron microscopy and EDAX.

Transmission electron microscopy gives indications on the structure of NiTi alloys typical phases: austenite, martensite, secondary phases. Austenite has nearly the same characteristics as in equiatomic NiTi alloy; martensite suffers supplementary distortions. Complex NiTiNb precipitate particles were analyzed by EDAX, their approximate chemical composition being determined.

REFERENCES

1. Melton K.N., Proft J.L., Duerig T.W., Wide hysteresis SMA based on the NiTiNb system, MRS Int'l. Mtg. On Adv. Mats., Vol.9, pp. 165-170, 1989.
2. Goubaa K., Thèse de doctorat, ENSCP, 1991.
3. I.Gherghescu, E.Florian, Evaluation par DSC des effets des différents traitements thermiques sur les points de transformation d'un alliage à mémoire de forme de composition $Ni_{50}Ti_{48}Nb_2$, U.P.B.Sci.Bull., Vol.54, no.1-2, pp.24-30, 1992.
4. E.Goo, R.Sinclair, The B_2 to R transformation in TiNiFe and TiNi alloys, Acta metall. Vol.33 No.9, pp.1717-1723, 1985.
5. I.Gherghescu, Aspects concernant le frottement intérieur d'un alliage à mémoire de forme $Ni_{50}Ti_{48}Nb_2$, U.P.B.Sci.Bull., Vol.60, no.1-2, pp.175-180, 1998.

IOANA GHERGHESCU^{1,2}, SORIN CIUCĂ²

1,2 – Lecturer, Faculty “Materials Science and Engineering”, “POLITEHNICA” University of Bucharest

**ASPECTE STRUCTURALE ALE UNUI ALIAJ CU MEMORIA FORMEI
 $Ni_{50}Ti_{48}Nb_2$ RELEVATE PRIN MICROSCOPIE ELECTRONICĂ PRIN
BALEIAJ ȘI TRANSMISIE**

Lucrarea prezintă aspecte structurale obținute prin microscopie electronică prin baleiaj și transmisie ale unui aliaj cu memoria formei $Ni_{50}Ti_{48}Nb_2$. Această compoziție a fost aleasă în vederea obținerii unui aliaj cu memorie având un histerezis mai mare decât al unui NiTi echiatomic, ceea ce implică o fiabilitate ridicată. Înaintea oricăror experimentări, materialul a fost supus unei recoaceri în condițiile 900 °C/48 h. Au fost obținute imagini de microscopie electronică prin baleiaj și transmisie, microdifracții de electroni și analize EDAX. Metodele de investigare expuse furnizează informații asupra diferitelor faze ce se găsesc în aliajele NiTi: austenită, martensită și faze secundare. Austenita din aliajul studiat are caracteristici apropiate de cele ale austenitei din aliajul NiTi echiatomic; martensita suferă distorsiuni suplimentare. Au fost analizate particule ale unor compuși complecși prin EDAX, fiind determinată compoziția chimică aproximativă a acestora; două noi tipuri de compuși au fost astfel identificate. Compoziția lor nu se modifică prin recoacere la 800 °C; aceste faze sunt deci stabile, având structuri și compoziții chimice de echilibru.

CONSIDERATIONS ON MECHANICAL PROPERTIES OF THE HUMAN BONES

BY

BÎTCĂ CONSTANTIN, MIHALCUT MIHAI AND PAUL DORU BÂRSĂNESCU

Abstract: The behaviour of the biological structures has a great influence on the design of the prosthesis. The experimental studies can contribute to the understanding of the phenomenons from biomechanical field, to increase the quality of the prosthesis and the service time of these. Geometry, structure and elastic and plastic characteristics of the bone are an obstacle to realize correctly a numerical and experimental analysis. Recent biomechanical studies presented an important increase of the utilization of the femur prosthesis and artificial femur from composite materials in orthopaedics field.

Keywords: bone, elastic and plastic properties, Young's modulus, strength, fatigue, and stiffness

1. Introduction

Bone is a dynamic biologic tissue composed from two-phases: a mineral phase and a phase from flexibly collagen fiber and a ground substance. The fact that the bone is a composite materials has an important influence on the strength and its stiffness which has all considerably greater that the values for collagen fibers alone. Mechanical properties of the bone structures depend on the kind of bone, the age, anatomical location and the testing conditions. Although these conditions are usually recorded, some aspects of the testing conditions and the sample preservation are sometimes overlooked (bone hydration, temperature, etc). *Figure 1* shows the microscopic structure of the cortical and cancellous bone.

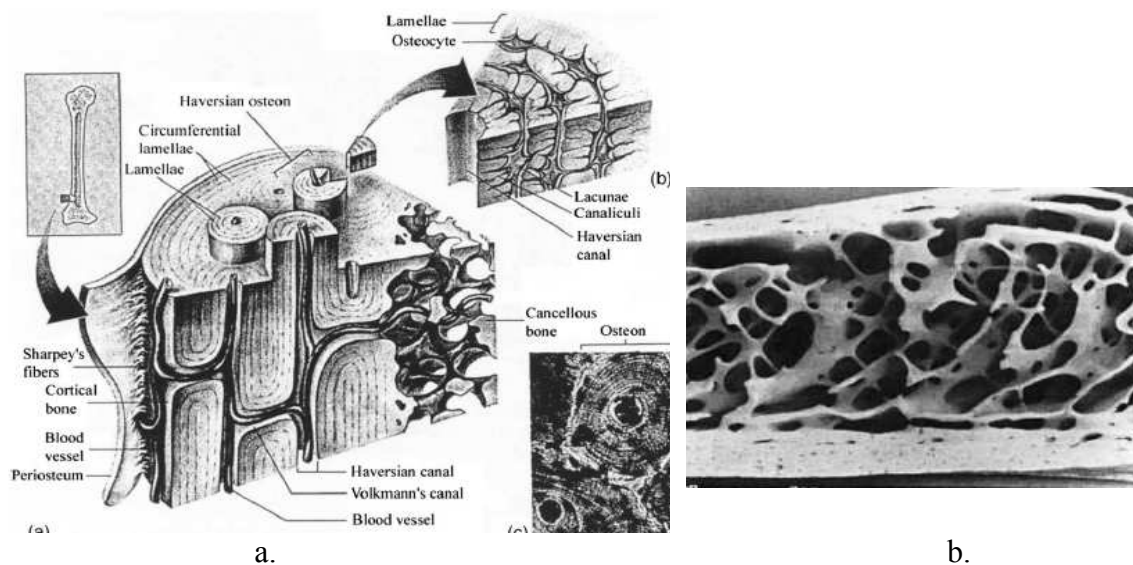


Fig. 1. Microscopic structure of the bone tissue: a) cortical bone, b) cancellous bone

For the cancellous bone, the determination of the stiffness is more difficult than for other materials. More of these studies are concentrated on the structural properties because the material properties of the bones are complicated to measure. These properties vary and depend on the anatomical position, the density of the cancellous bone and the trabecular orientation.

2. Mechanical properties of the human bones

The most important mechanical properties of bones are its strength and stiffness. These and other characteristics can be best understood by examining its behaviour under loading and under the influences of the external applied forces. If a specimen is loaded, a deformation of this will appear. The relation between the stress applied to a structure and its strain is called a stress – strain curve. This curve can be divided into two regions: elastic strain region and plastic strain region (*fig. 2*). The initial part of the curve (elastic region) shows the stiffness of the structure and its capacity to recover its original shape when unloaded. The strain increases with the increase of the load, [6].

In practice, the bone does not behave like a perfect elastic material because of the viscosity and the fluids from the bone matrix that causes to lose a part of the elastic energy. In bone, like in wood and other biological structures, there is a preferred direction. Because of this, the Young's modulus depends on this direction. For instance, the Young's modulus of a long bone varies between 17 GPa in longitudinal direction and 12 GPa in transversal direction, [8]. Also, the modulus depends on the region from bone where the measurements occur. The Young's modulus can vary between 0.1 and 4.5 GPa, depending on the bone density and trabecular orientation, [7, 9].

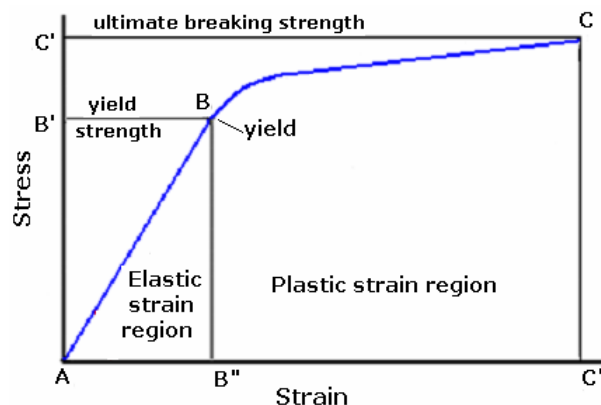


Fig. 2. Stress – strain curve

The yield point *B* from the stress – strain characteristic divides elastic and plastic region. This point represents an imaginary boundary over what the stresses cause residual strains in the bone structure. These strains are called plastic strains. Usually, the bone is not a ductile material and has possibilities reduced to sustain the deformation over the yield point. The area under characteristic represents the quantity of the energy storage. The yield point is rarely good defined. Some methods were suggested to measure the yield point. For instance, this point is often defined as the point where the stress – strain curve begins to become nonlinear, [4, 5]. Other techniques contain *offset* methods where an offset line is constructed with the linear

portion of the stress – strain curve, [10]. The point where this line intersects the curve is arbitrarily called yield point. The point *C* shows the ultimate failure point or ultimate breaking strength. The slope of curve in elastic region indicates the stiffness of the bone structure. This value is called modulus of elasticity (Young's modulus).

The knowledge of the stress – strain is useful to study the behaviour during failure, the response of the structure under loads or the influences of various treatments. Sometimes, characterizing a bone depending on the constitutive material, apart from its geometry, it is necessarily to standardize the testing conditions and the size and shape of the specimen loaded. Such standardized tests are useful to compare the mechanical properties for two or more materials. The strength of the cortical bone depends on the kind of stress applied to the bone. For instance, the ultimate tensile strength of femoral bone in the longitudinal direction is 135 MPa, the ultimate compressive strength is 205 MPa and the shear strength is 67 MPa, [8]. Like the Young's modulus, the strength of cortical bone also varies with the direction. The tensile strength of a femur in transversal direction is only 53 MPa, [8]. The strength of the cancellous bone varies between 1 ÷ 20 MPa and is strongly dependent upon apparent density and trabecular orientation, [3].

When a material is loaded with loads within the elastic region of the stress – strain curve, its properties gradually degrade over a period of time. This degradation of the strength and modulus of elasticity depending on the time is called fatigue. The decrease of these properties is attributed to the formation of small cracks within the bone structure. The fatigue strength of the bone, as for more composite materials is more less than its static strength, allowing the failure to occur at loads below those that would normally cause fracture, [1].

The mechanical properties differ depending on the kind of bone. The cortical bone is stiffer than the cancellous bone, withstanding greater stress but less strain before failure. The cancellous bone *in vitro* does not fracture until the strain exceeds 75%, but cortical bone fracture when the strain exceeds 2%. Because of its porous structure, the cancellous bone has a large capacity for energy storage, [10]. In *figure 3* is presented the stress – strain curve of the cortical bone, metal and glass what shows the differences in mechanical behaviour between these materials. The variations in stiffness are reflected in the different slopes of the curves in the elastic region. Metal has the steepest slope and is thus the stiffest material, [5].

The elastic region of the characteristic for metal is a straight line, indicating linearly elastic behaviour. The fact that the metal has a long plastic region indicates that this typical ductile material deforms extensively before failure. Glass, a brittle material, exhibits a linearly elastic behaviour but fails abruptly with little deformations. This thing is indicated by the lack of a plastic region on the stress – strain curve. Cortical bone, which possesses both ductile and brittle qualities, exhibits nonlinear elastic behaviour. This behaviour is demonstrated by a slight curve in the elastic region, which indicates some yielding during loading within this region, [5, 11]. Cortical bone continues to deform before failure, but no so much that in the case of the metal.

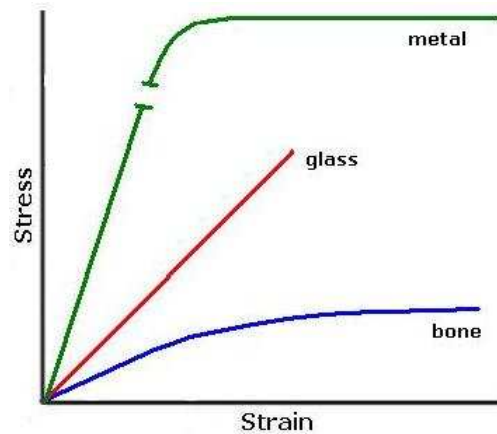


Fig. 3. Stress – strain curve for three materials (bone, metal, glass), [5]

The differences concerning the plastic behaviour for metal and bone is due to differences in micromechanical events during the yield. Yielding in metallic materials (tested in tension) is caused by plastic flow and formation of plastic slip lines. The slip lines are formed when the molecules of the lattice structure of metal will be dislocated. For bones, debonding of the osteons at the cement lines and microfracture causes the yielding.

Because the bone structure is dissimilar in the transverse and the longitudinal directions, it manifests diverse mechanical properties when it is loaded along different axes. In *figure 4* is presented the variation of the strength and the stiffness for a cortical bone specimen, tested in tension in four directions, [12].

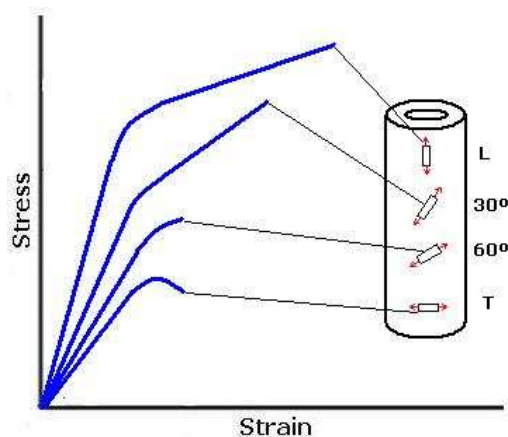


Fig. 4. Anisotropic behavior of cortical bone specimen from a human femur tested in tension in four directions: longitudinal (L), 30° with respect to the neutral axis of the bone, 60° and transversal (T), [12]

The values for both parameters are highest for the samples loaded in the longitudinal direction. Although the relationship between loading patterns and the mechanical properties of bone throughout the skeleton is extremely complex, it can generally say that the bone strength and the stiffness in the direction in which loads are most commonly imposed, [12].

Bone exhibits more brittle or more ductile behaviour depending on its age (younger bone being more ductile) and the rate at which is loaded (bone being more brittle for higher loading speeds), [2]. In *figure 5* is presented a comparison between the stress – strain curve for two specimens from a human adult tibiae. The ultimate stress was approximately the same for the young and the old bone. The old bone specimen could withstand until half of the strain that the young bone could. This thing indicates a greater brittleness and a reduction in energy storage capacity.

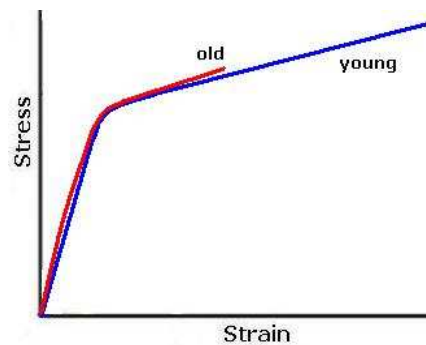


Fig. 5. Stress – strain curve for specimens of adult human tibiae of two widely differing ages tested in tension, [2]

3. Conclusions

Bone is an anisotropic material, exhibiting different mechanical properties when is loaded in different directions. Because of the bone structure is very complex, the elastical and mechanical properties are not the same for all bones, depending on the anatomical position, the bone age, etc. Each bone is unique. These characteristics are important for the realization of new materials used for different prosthesis, what must have the same or superior properties.

Received April 19, 2005

The “Gh.Asachi” Technical University Iași

REFERENCES

1. Agarwal B.D., Broutman L.J., *Analysis and performances of fiber composites*, New York: John Willey and Sons, 1980
2. Burstein A.H., Reilly D.T., *Aging of bone tissue: Mechanical properties*, J. Bone Jt. Surg., 58A, 1976, p. 82 – 86
3. Carter D.R., Hayes W.C., *The compressive behavior of bone as a two-phase porous structure*, J. Bone Jt. Surg., 59A, 1977, p. 954 – 962
4. Hvid I., Jensen J., *Cancellous bone strength at the proximal human tibia*, Engineering in Medicine, 13, 1984, p. 21 – 25
5. Nordin M., Frankel V.H., *Biomechanics of Bone*, in: *Basic Biomechanics of the Musculoskeletal System*, Second Edition, Lea & Febiger, Philadelphia, 1980
6. Reifnider K.L., Henneke E.G., Stinchomb W., Duke J.C., *Mechanics of composite materials*, Pergamon Press, New York, 1983, p. 399

7. Reilly T.D., Burstein A.H., *The elastic and ultimate properties of compact bone tissue*, J. Biomech., 8, 1975, p. 393 - 405
8. Turner C.H., Burr D.B., *Basic Biomechanical Measurements of bone: A tutorial*, Bone, 14, 1993, p. 595
9. Turner C.H., Cowin S.C., Rho J.Y., Ashman R.B., Roce J.C., *The fabric dependence of the orthotropic elastic constants of cancellous bone*, J. Biomech, 23, 1990, p. 549 – 561
10. Carter D.R., Hayes W.C., *Bone compressive strength: The influence of density and the strain rate*, Science, 194:1174, 1976
11. Bonefield W., Li C.H., *Anisotropy of nonelastic flow in bone*, J. Appl. Physics, 38:2450, 1976
12. Frankel V.H., Burstein A.H., *Orthopaedics Biomechanics*, Lea & Febiger, 1970

CONSIDERAȚII ASUPRA PROPRIETĂȚILOR MECANICE ALE OASELOR UMANE

Rezumat: Comportarea structurilor biologice are o mare influență asupra proiectării protezelor osoase. Analizele experimentale pot contribui la înțelegerea fenomenelor care apar în domeniul biomecanic, la creșterea calității protezelor și a timpului lor de utilizare. Geometria, structura și caracteristicile elastice și plastice ale osului reprezintă un obstacol în realizarea corectă a analizelor numerice și experimentale. Recente studii biomecanice au arătat o importantă creștere a utilizării protezelor de femur sau a femurului artificial din materiale compozite în domeniul ortopedic.

SOME ASPECTS REGARDING THE DESIGN OF NAIMOV SAMPLES FOR STRESS RELAXATION BENDING TESTS

BY

**CORNELIU COMANDAR¹, NICUȘOR AMARIEI¹, DOREL LEON¹
and CONSTANTIN DUMITRACHE²**

Abstract: The paper presents the design of the slotted ring sample with constant rectangular cross-section, used for the study of stress relaxation in metals. The ring specimens are constrained by the introduction of a calibrated wedge, and the remaining stresses are calculated by elastic springback at the end of test period. The influence of the rapport between radius and height of cross-section at the variations of maximum normal stress are presented.

Keywords: stress relaxation, bending tests, slotted ring samples, elastic springback

1. Introduction

The phenomenon of time-dependent decrease of the stresses in conditions of constant strains is called stress relaxation, [2], [3], [13].

The general stress relaxation test is performed by isothermally loading a specimen to a fixed value of constraint. The constraint is maintained constant and the constraining force is determined as a function of time.

Bending tests for stress relaxation covers the determination of the time-dependent decrease in stress in a specimen subjected to long duration, constant bending strain, in a uniform environment, and negligible vibration [8].

The initial and remaining bending stresses are determined from either of the methods:

- readings are taken continuously from a force indicator while the apparatus adjusts the force to maintain constrain within specified bounds;
- the force required to lift the specimen just free of one or more constrains during the test period is periodically measured;
- the elastic springback is measured after unloading at the end of the test period.

For the first two methods a single specimen is enough to obtain all the necessary data to plot the relaxation curve, while the third method requires a specimen for each point on the curve. Still, the last method has the advantage of a much simpler testing device.

For the remaining stress study using the elastic spring back method, one of the samples used is in the shape of a slotted ring with a wedge inserted in the slot to put the test-piece under load [4], [5]. When are used constant rectangular section rings, the samples are called Naimov rings.

2. The elastic spring back method

The width of the slot in the ring test-piece is carefully measured, after which the test-piece is loaded by means of a wedge of suitable thickness, and placed in a furnace, from which it is removed and cooled after set intervals of time. The stresses in the ring depend on the difference between the wedge thickness and the width of the slot. After removing the wedge, the width of the slot is measured again; this can easily be done with the aid of two marks (holes) on the adjacent faces of the ring.

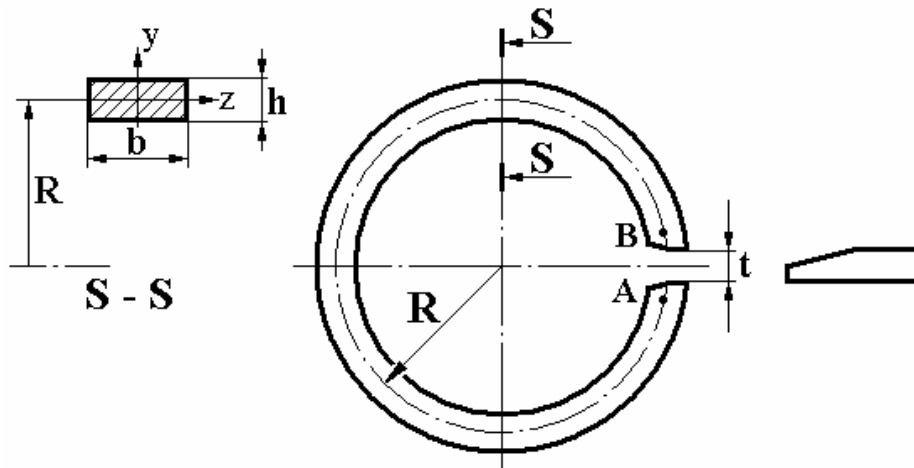


Fig. 1. Naimov sample

The distance between the marks can be measured to an accuracy of microns on a measuring microscope. The slot will widen in time as a result of increasing plastic strain in the gauge-length of the ring. By measuring the slot width we can construct a relaxation curve converting strains to stresses.

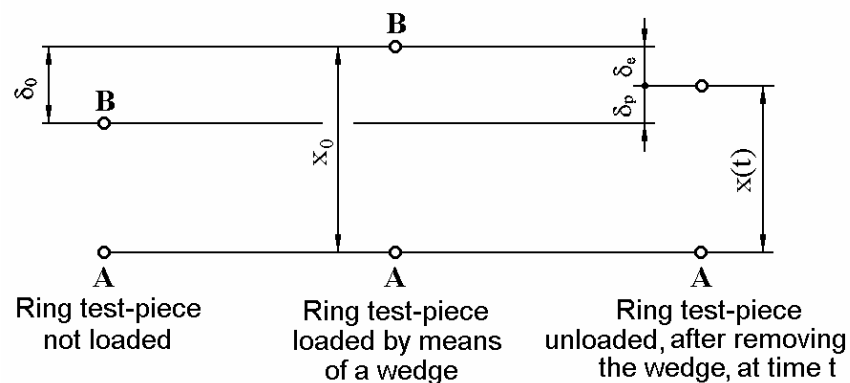


Fig. 2. The mark positions of the ring test-piece in relaxation tests

The remaining stress σ is:

$$\sigma(t) = C \cdot \delta_e \quad (1)$$

where t -time;

C - constant depends on the geometry and material

$\delta_e = x_0 - x_t$ elastic deformation (see fig. 2)

3. Calculus

For the normal stress calculus the following scheme are adopted:

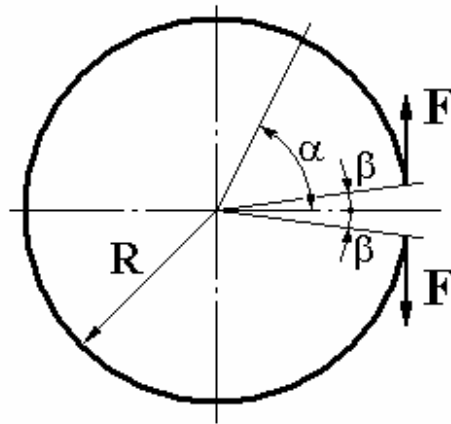


Fig. 3. The geometrical and loaded scheme

The normal force and the bending moment are calculated with the relations:

$$N(\alpha) = -F \cdot \cos \alpha \quad (2)$$

$$M(\alpha) = -F \cdot R \cdot (\cos \alpha - \cos \beta) \quad (3)$$

In figure 4 the variation with the angle α of the normal force and of the bending moment, are presented.

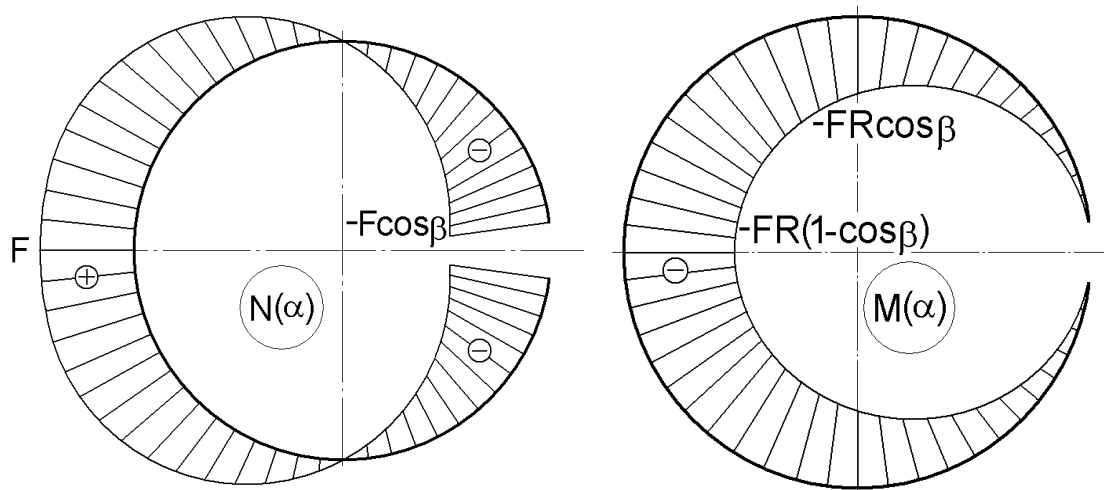


Fig. 4. The variation of normal force and bending moment

The dimension t of the slotted ring is adopted to be a fraction of R . This dimension influenced the angle β (see fig. 2 and 3). The relation between $\cos \beta$ and t/R is:

$$\cos \beta = \frac{1}{2} \cdot \sqrt{4 - \left(\frac{t}{R}\right)^2} \quad (4)$$

The variation of the $\cos \beta$ with the t/R rapport is presented in the figure 5.

The normal stress in a cross section at the angle α can be calculated with the relation:

$$\sigma(\alpha) = \frac{1}{A} \left[N(\alpha) + \frac{M(\alpha)}{\rho} + \frac{M(\alpha)}{\rho \cdot k} \cdot \frac{y}{\rho + y} \right] \quad (5)$$

where: $A = b \cdot h$ - the cross section area;
 ρ - radius curvature;
 k - shape coefficient for cross section;
 $y \in \left[-\frac{h}{2}, \frac{h}{2} \right]$ - the distance from the geometrical axis to the fibre where the stress is calculated.

The shape coefficient for the cross section is:

$$k = -\frac{1}{A} \cdot \int_{(A)} \frac{y}{\rho + y} \cdot dA \quad (6)$$

For the rectangular cross section (see fig. 1) the relation (6) become:

$$k = -1 + \frac{R}{h} \cdot \ln \frac{\frac{2 \cdot R}{h} + 1}{\frac{2 \cdot R}{h} - 1} \quad (7)$$

The variation of the shape coefficient k with the R/h rapport is presented in the figure 6.

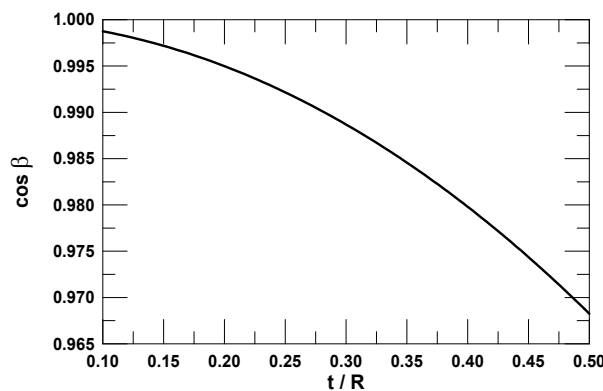


Fig. 5. Variation of $\cos \beta$ with t/R

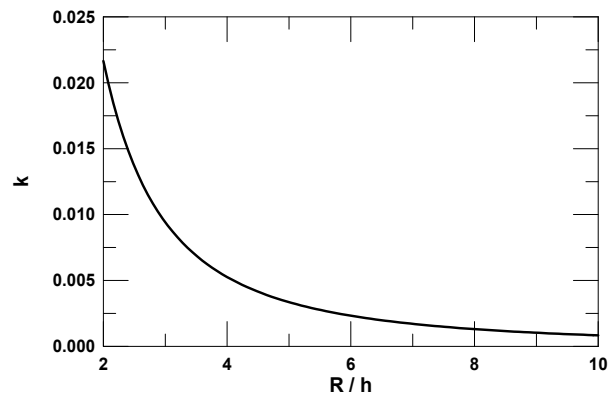


Fig. 6. Variation of k with R/h

Replacing the relations (2) and (3) in the relation (5) we obtain:

$$\sigma(\alpha) = -\frac{F}{b \cdot h} \cdot \left[\cos \beta + \frac{(\cos \beta - \cos \alpha) \cdot y}{k \cdot (R + y)} \right] \quad (8)$$

For the interior fibre and for exterior fibre, the relation (8) become:

$$\sigma_{\text{int}}(\alpha) = \sigma(\alpha) \Big|_{-\frac{h}{2}} = \frac{F}{b \cdot h} \left[-\cos \beta + \frac{\cos \beta - \cos \alpha}{k \cdot \left(\frac{2 \cdot R}{h} - 1 \right)} \right] \quad (9)$$

$$\sigma_{ext}(\alpha) = \sigma(\alpha)_{+\frac{h}{2}} = \frac{F}{b \cdot h} \left[-\cos \beta - \frac{\cos \beta - \cos \alpha}{k \cdot \left(\frac{2 \cdot R}{h} + 1 \right)} \right] \quad (10)$$

The variation of the σ_{int} and the σ_{ext} with the angle α at different rapport R/h are presented in figure 7.

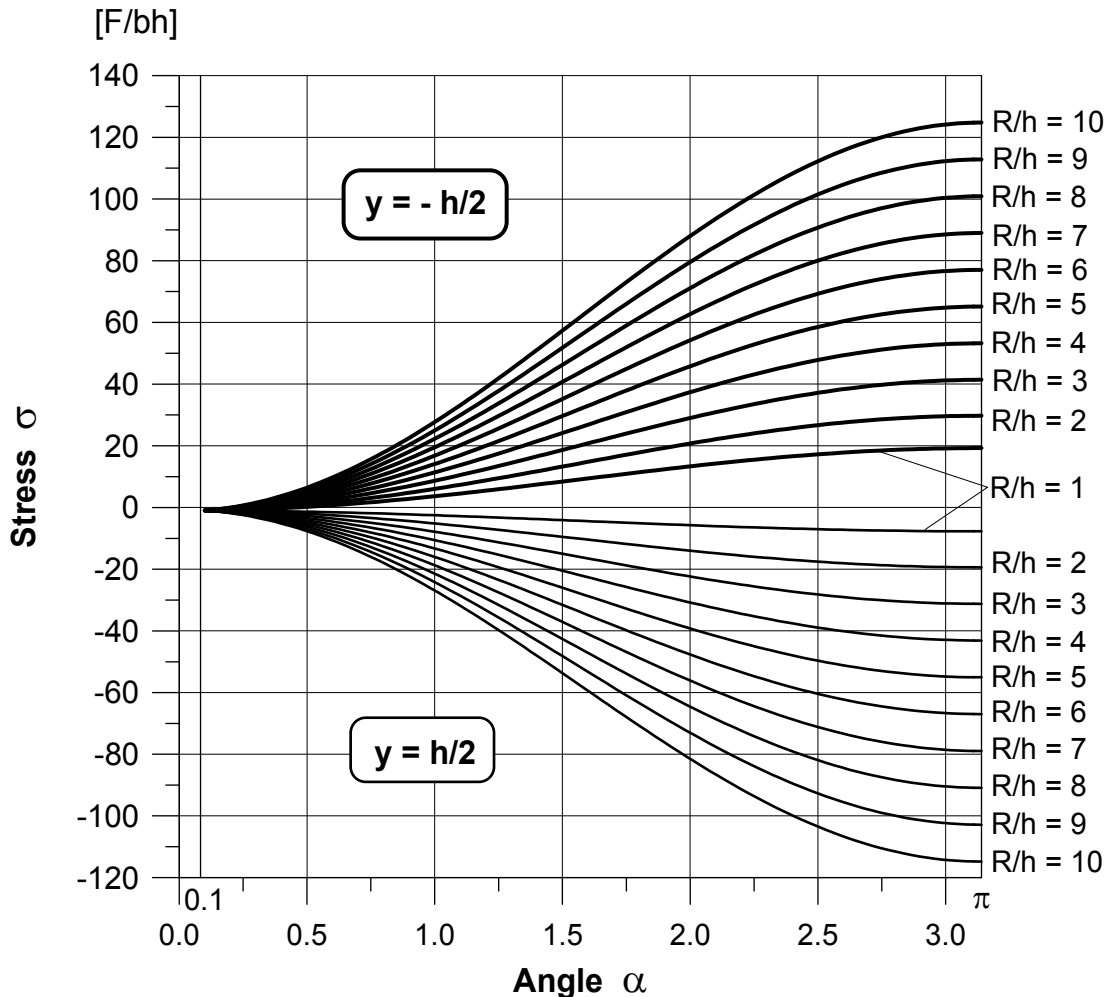


Fig. 8. The variation of the normal stress σ at the interior and exterior fibre with the angle α , for different rapport R/h

4. Conclusions

The maximum normal stress is located at interior fibre and absolute value increase with the rapport R/h .

The maximum normal stress is nonuniform distributed (it is a function of angle α); the gradient increase with the rapport R/h .

The slotted ring samples with constant rectangular cross section are the advantage of simplicity but for uniformity distribution of maximum normal stresses is recommended used of the samples with variable cross section, Oding [9], [10], [11], [12] or by patent RO 116985, [1], [6], [7].

Acknowledgements

The present investigation was conducted with the financial support of the National University Research Council (CNCSIS), the main Romanian funding organisation for university and postgraduate research programmes, Grant A cod CNCSIS 498/2005.

Received April 20, 2005

¹ The "Gh.Asachi" Technical University Iași

² The Maritime University Constanța

REFERENCES

1. Comandar, C., Miroș, I., Leon, D. - *Epruvetă inelară pentru studiul relaxării tensiunilor*, Brevet de invenție nr. 116985, 1995.
2. Comandar, C., Leon, D., Amariei, N. - *Study of stress relaxation using the vibrating string method in prestressed steel wires*, 17th Danubia-Adria Symposium on Experimental Methods in Solid Mechanics and Workshop "Future of the Experiment", October 11-14, 2000, Prague, ISBN 80-01-02234-X, 2000, 71-74
3. Comandar, C., Leon, D., Amariei, N. - *Determination of equation of stress relaxation curves based on creep experimental research for 16 Mo 3 steel*, Proceedings of the Fifth European Rheology Conference, Portoroz, Slovenia, September 6 - 11, Steinkopff Verlag Darmstadt, Editor Igor Emri, 1998, 258-259.
4. Comandar, C., Miroș, I., Leon, D., Aignătoaie, M. - *Stress and strain analysis of the ring specimens used in stress relaxation studies*, Buletinul I.P. Iași, Tomul XL (XLIV), Fasc. 3-4, Vol. 2, Secția IX, Știința și ingineria materialelor, 1994, ISSN 1453 -1690, 814-817.
5. Comandar, C., Miroș, I., Leon, D., Palihovici, V., Popa, S., Isbășescu, A. - *Contribuții teoretice și experimentale la cercetarea fenomenului de fluaj pe epruvete inelare*, Simpozionul "70 de ani de la înființarea laboratorului de rezistența materialelor", Timișoara, 1993, 88-92.
6. Comandar, C., Amariei, N., Leon, D. - *Stress relaxation using ring test-piece* - Annals of the Oradea University, CD-ROM Edition, Volume III, 2004, ISSN 1583-0691.
7. Comandar, C., Leon, D., Amariei, N. - *Experimental validation for a new ring type of test piece use to stress relaxation testings* - Buletinul I. P. Iasi, Tomul L (LIV), Fasc. 6B, 2004, ISSN 1011-2855, 197-202.
8. Comandar, C., Palihovici, V., Amariei, N., Dumitrache, C. - *Bending test for stress relaxation*, Buletinul I. P. Iași, Tomul XLV (IL), Fasc. 1-2, Secția Știința și ingineria materialelor, 1999, ISSN 1453-1690, 77-82.
9. Giriadă, C., Miroș, I., Hopulele, I., Leon, D. - *Oding rings design*, Buletinul Institutului politehnic din Iași, tomul XXXIV (XXXVIII), fasc.1-4, secția IV- Construcții de mașini, 1988, ISSN 1453 -1690, 43-50.
10. Leon, D., Miroș, I., Comandar, C. - *Considerații privind proiectarea inelelor Oding*, Lucrări prezentate la al V-lea Simpozion Național de Tensometrie, vol. 1, Galați, 1989, 457-461.
11. Leon, D., Comandar, C., Amariei, N. - *Stress State in Oding Type Ring, Determined Analytically, Numerically and Experimentally* - Proceeding of the 35th International Conference Experimental Stress Analysis, EAN '97, Olomouc, Czech Republic, 1997, 268-272.
12. Oding, I. A., Ivanova, V. S., Burdukskii, V. V., Geminov, V. N. - *Creep and stress relaxation in metals*, Oliver and Boyd, Edinburgh, 1965.
13. ASTM E328 - 86 (reapproved 1991) - *Standard Methods for Stress Relaxation Tests for Materials and Structures*.

CÂTEVA ASPECTE PRIVIND PROIECTAREA EPRUVETELOR NAIMOV PENTRU ÎNCERCĂRI DE RELAXARE A TENSIUNILOR PRIN ÎNCOVOIERE

Rezumat: Lucrarea se referă la proiectarea epruvetelor inelare secționare, cu secțiunea transversală dreptunghiulară constantă, utilizate pentru studiul relaxării tensiunilor în metale. Epruvetele inelare sunt deformate prin introducerea unei pene calibrate iar tensiunea remanentă se calculează pe baza revenirii elastice la sfârșitul perioadei de încercare. Este prezentată influența raportului dintre rază și înălțimea secțiunii transversale asupra variației tensiunilor normale maxime.

THE ALLOYING ELEMENTS INFLUENCE OVER CORROSION RESISTANCE OF SOME BIOMATERIALS NICKEL BASED

D. MARECI, D. SUTIMAN, N.FOCA, GABRIELA CARJA and C.BOCANU

Four non-precious Nickel based alloys (VeraSoft, WironNT, Wirolloy and NicromalSoft) were analysed vis a vis to their corrosion behaviour. The correlation between the amount of the elements Chromium, Molybdenum and the corrosion behaviour, expressed by PREN index (pitting resistance equivalent number) in the case of the allied steels, was extended for Nickel-Chromium dental alloys characterization. The corrosion potentials and corrosion rates were determined in artificial saliva using the electrochemical methods. The Chromium and Molybdenum contents play a significant role in corrosion resistance: alloys with high Chromium and Molybdenum content exhibit a much wide passivation range and a better resistance to pitting corrosion. The alloys with $PREN \leq 32.9$ are susceptible of localized corrosion.

Keywords: nickel based alloy, pitting, corrosion, polarization curves, corrosion parameters

Introduction

Due to their electronic structure, the dental alloys react extremely easy with the buccal cavity medium, being degraded especially by chemical corrosion. In present, various types of dental alloys are used, both precious and non-precious.

In the actual socio-economical conditions, the dentist should select with discernment the alternatives alloys Ni-Cr-Fe, Ni-Cr-Mo and Co-Cr-Mo based, appeared on the Romanian market in the present. The selection takes place depending on the properties and corrosion resistance of the alloy and is a function of the clinical case. The inadequate choice of the dental alloy in order to realise certain prosthesis may lead to mechanical, chemical or biological failures that have undesirable consequences in time over the patient general state of health.

Studies concerning the corrosion resistance of both non-precious and precious materials were realised [1-3].

The present paper presents the influence of the main elements that form the structure of the alloys nickel based over the corrosion resistance and the corrosion type. The influence of chromium and molybdenum existing in the nickel alloys was studied as compared to the electrolytic nickel from the electrochemical behaviour point of view.

Experimental

Four non-precious dental alloys used in dental prosthetics construction and nickel were investigated. Their composition is shown in Table 1.

Table 1: The composition of the dental alloys

| Alloy | Main Components (%) |
|--------------|---|
| Wiroloy | 63.5 Ni 23Cr 9Fe 3Mo 0.5Mn 1Si |
| VeraSoft | 53.6Ni 19.5Mn 14.5Cr 9.5Cu 1.6Al 1.5Si |
| WironNT | 61.4Ni 22.9Cr 8.8Mo 2.5Fe 3.9Nb |
| NicromalSoft | 64.6Ni 17.8Cr 9.8Cu 3.5Mn 1.8Si 1.5Al 0.5Ti 0.5Fe |
| Nickel | 99,9Ni |

The electrolyte used as corrosion medium was a solution of the aerated artificial saliva (Carter-Brugirard AFNOR/NF (French Association of Normalization) 591-141) [4] that is composed of: NaCl – 0.7 g/L, KCl – 1.2 g/L, Na₂HPO₄H₂O – 0.26 g/L, NaHCO₃ – 1.5 g/L, KSCN – 0.33 g/L, urea – 1.35 g/L, pH = 8.

The determination of open circuit potential and the cyclic polarisation curves recording were performed with the electrochemical system VOLTALAB-32, which consists of a potentiostat, an electrochemical interface and a PC. Experimental data were acquired and processed with the VoltaMaster 2 software. The reference electrode was a saturated calomel electrode (SCE) and platinum as a counter electrode.

The working electrode, made from alloy sample was processed into a cylindrical shape and mounted in a teflon support. In these conditions the surface exposed to corrosion was a one-dimensional circular surface.

Before experimental determinations the samples were mechanically polished using abrasive SiC paper up to a granulation number of 2500 mesh. Then they were washed with water, degreased with ethyl alcohol and preserved in double-distilled water.

The linear polarisation curves were recorded at an electrode potential scanning rate of 0.5 mV/s, while the cyclic ones at 50 mV/s.

Currents densities of corrosion were determined by polarisation resistance method [5, 6].

After the electrochemical treatment, the analysis of the alloys surface was performed on a optical microscope MC1.

Results and Discussions

For each alloy, the main parameters of corrosion process were established using the cyclic polarisation curves.

In Figure 1 are presented the cyclic polarisation curves for the Nickel and WironNT alloy and Figure 2 shows the cyclic polarisation curves for the VeraSoft, NicromalSoft and Wiroloy alloys after maintaining 7 days in an artificial saliva solution.

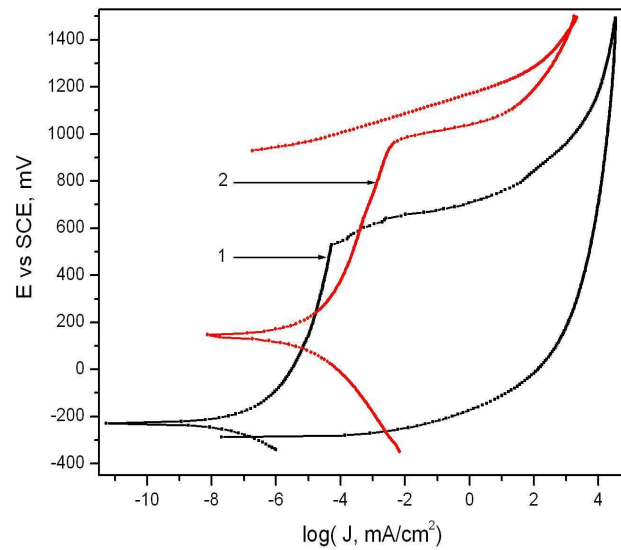


Figure 1: Cyclic polarisation curves for the Nickel and WironNT alloy after maintaining 7 days in an artificial saliva solution (1-Nickel, 2-WironNT)

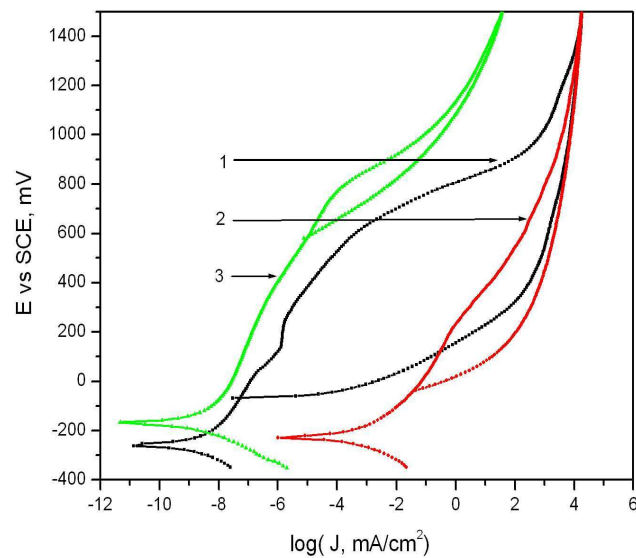


Figure 2: Cyclic polarisation curves for the VeraSoft, NicromalSoft and Wiroloy alloy after maintaining 7 days in an artificial saliva solution (1- NicromalSoft, 2- VeraSoft, 3- Wiroloy)

In table 2 there are presented the corrosion process parameters corresponding to the five materials studied after 7 days in artificial saliva.

Table 2: The main parameters of the corrosion process

| Alloys | E_{corr} (mV) | R_p ($K\Omega cm^2$) | J_{corr} (nA/cm^2) | E_{tr} (mV) | E_{br} (mV) | E_{rep} (mV) | ΔE (mV) |
|---|--------------------|-----------------------------|-----------------------------|------------------|------------------|-------------------|--------------------|
| The materials maintained for 7 days in artificial saliva | | | | | | | |
| Nickel | -229 | 38,4 | 312 | - | 531 | -287 | 818 |
| Wiroloy | -166 | 320 | 16,8 | - | 960 | 830 | 130 |
| WironNT | 147 | 210 | 38,5 | 1010 | - | - | - |
| VeraSoft | -229 | 0,78 | 7050 | - | 280 | 12 | 268 |
| NicromalSoft | -262 | 55 | 178 | - | 800 | 130 | 670 |

E_{corr} –corrosion potential, R_p –polarisation resistance, J_{corr} –density of corrosion current, E_{tr} –transpassivation potential, E_{br} –breakdown potential, E_{rep} –repassivation potential

After 7 days of maintaining in artificial saliva, one find that most of the materials shows negatives corrosion potentials characteristic of non-precious elements, excepting the case of Wiron NT alloy.

The corrosion currents have different values. In case of the NicromalSoft alloy, the corrosion current has a value close to the one recorded for nickel and the VeraSoft alloy presents a current that is ten times higher as compared to nickel. The lowest corrosion current was recorded for Wiroloy alloy, two times lower than WironNT alloy and 400 times lower than VeraSoft alloy.

Analysing the profiles of cyclic polarisation curves results that the only alloy showing a generalised corrosion is WironNT and the others alloys present a pitting corrosion. The highest breakdown potential exists in case of Wiroloy alloy, less susceptible to localised corrosion due to a high repassivation potential. The most susceptible to localised corrosion is the VeraSoft alloy, having a breakdown potential very low, with a value close to the corrosion potential. The nickel surface do not repassivates because the repassivation potential is more negative than the corrosion one.

Localized corrosion attack is one of the most commonly observed failure mechanisms of stainless steels and high Ni-Cr-Mo alloys. This form of localized attack being generally less predictable than general corrosion and more limiting to a materials performance. A Pitting Resistance Equivalent Number (PREN) is calculated, using the alloy chemical composition, to estimate relative pitting resistance alloy. The equation that most closely represents the performance of the high Ni-Cr-Mo alloys in the various media examined being:

$$PREN = Cr + 3.3(Mo + 0.5W)$$

The PREN calculations for each of the Ni-Cr-Mo alloy are:

$$PREN=51.94(WironNT) > PREN=32.9(Wiroloy) > PREN=17.8 \\ (NicromalSoft) > PREN=14.5(VeraSoft).$$

The Wiron NT alloy, presenting a PREN higher than 50 is not susceptible to the localised corrosion.

Figure 3 shows the influence of alloying elements, expressed by PREN, over the breakdown potential and Figure 4 shows the repassivation potential dependence of PREN.

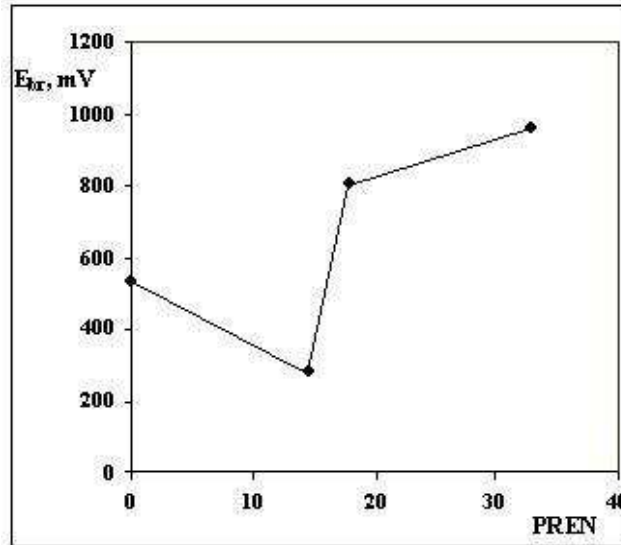


Figure 3: The dependence of breakdown potential of PREN

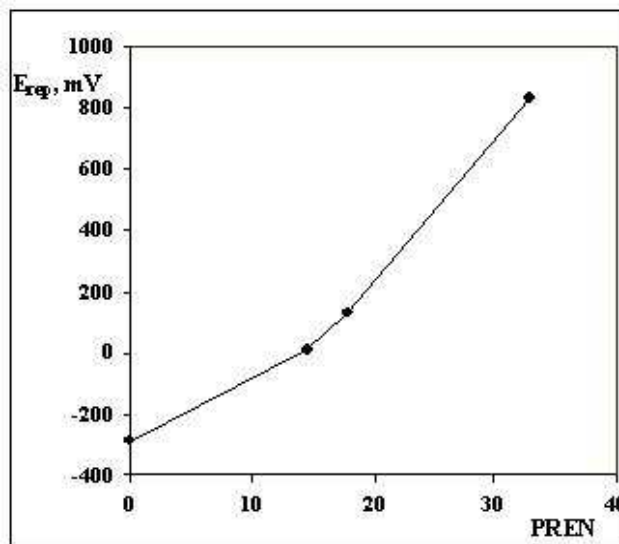


Figure 4: The dependence of repassivation potential of PREN

It is interesting the fact that the VeraSoft alloy shows a breakdown potential lower than the one corresponding to Nickel, although the alloying elements should have a positive role in this sense. This exception may be caused by the inadequate casting conditions. But the repassivation potential is higher as compared to the Nickel one.

At the same time as the PREN index increases, the susceptibility to localised corrosion decrease. This fact was confirmed by microscopic analysis of the samples surfaces after the polarisation at +1500 mV (Figure 5).

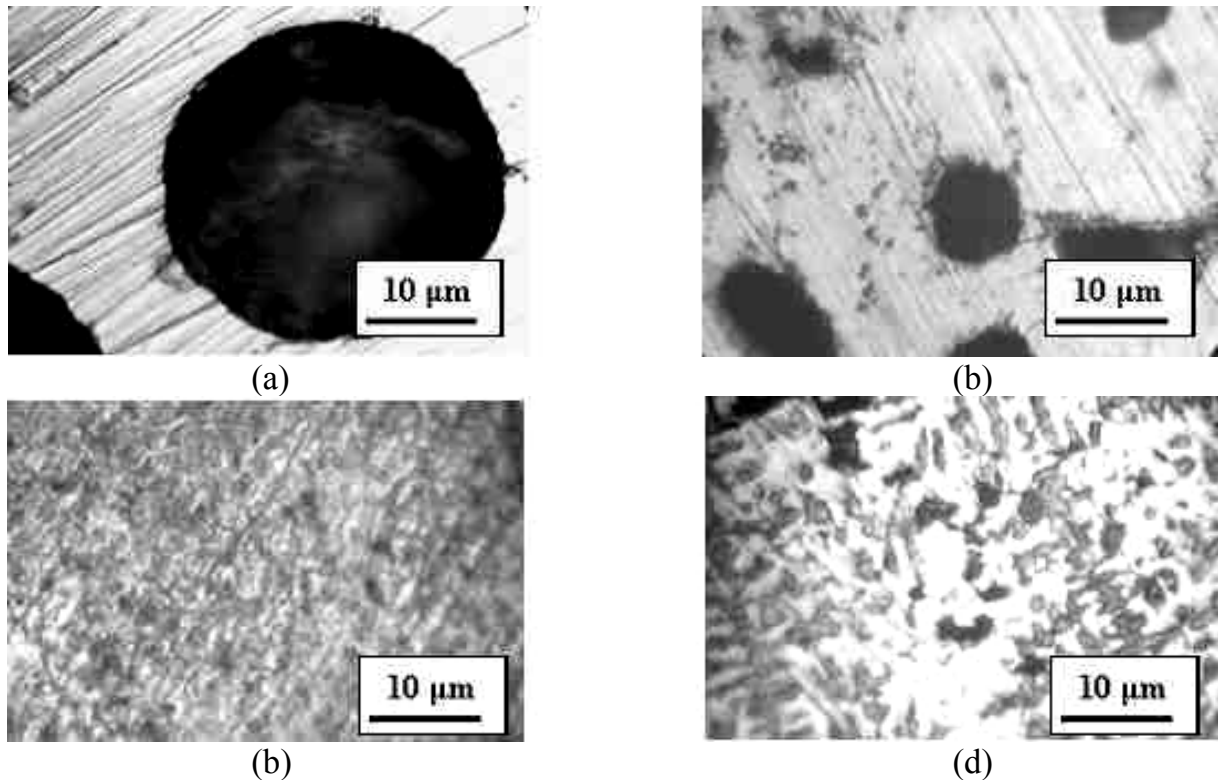


Figure 5: Micrographs of the alloys surfaces after polarisation at +1500 mV
 (a) Nichel, (b) VeraSoft, (c) WironNT, (d) Wirolloy

The effect of alloying over the nickel alloys may be established because the micrographs were realised using the same magnifying power. In case of pure nickel the corrosion point is well defined and has a dimension relatively high, but after alloying and depending on PREN value, the corrosion points become smaller and tend to cover uniformly the entire alloy surface, marking the passing from a localised corrosion to a generalised corrosion. The Wirolloy alloy surface shows a generalised corrosion passing and the WironNT alloy surface was attacked uniformly.

Conclusions

1. The alloying of nickel with chromium and molybdenum do not always determines a decrease of the corrosion rate. In case of the VeraSoft alloy the corrosion current is higher than the one corresponding to Nickel and in case of Wirolloy alloy is significantly lower.

2. The alloying determinates the modification of the corrosion type. Thus, for a PREN higher than 35, the corrosion is generalised.

3. An inadequate alloying beside the fact that does not modify the corrosion type, may determine an increase of corrosion rate. This is the case of VeraSoft alloy that shows a breakdown potential lower than the Nickel one, situated under 300 mV.

References

1. Aelenei N., Nemtoi Gh., Mareci D., Aelenei D., Chiper C., Chelariu R., volume Studia University Babes Bolyai Cluj **1-2** 314 (2002).
2. Mareci D., Aelenei Delia, Petreuş I., Aelenei N., Buletinul Institutului Politehnic Iaşi, XLIX (LIII), fasc. 5, 197 (2003).
3. Nemţoi Gh., Aelenei D., Mareci D., Chelariu R., Petreuş I., Dental alloys electrochemical behaviour in simulated human fluids, Annals of West University of Timisoara, Series Chemistry **12** 619 (2003).
4. Grosogeat B., Reclaru L., Lissac M., Dalard F., Biomaterials, **20**, 933 (1999).
5. Philippe Marcus, eds., Corrosion Mechanisms in Theory and Practice, Marcel Dekker Inc. 203 (2002).
6. Kelly R.G., Schully J.R., Shoesmith D.W., , Electrochemical Techniques in Corrosion Science and Engineering, Marcel Dekker Inc., New York, (2003).

*Gh.Asachi" Technical University of Iasi, Faculty of Industrial Chemistry,

INFLUENŢA ELEMENTELOR DE ALIERE ASUPRA COROZIUNII UNOR BIOMATERIALE PE BAZĂ DE NICHEL

In lucrare a fost studiată comportarea la coroziune a 4 aliaje pe bază de nichel (VeraSoft, WironNT, Wirolloy și NicromalSoft). Corelația dintre conținutul de crom și molibden și comportarea la coroziune s-a realizat prin indicele PREN, corespunzător oțelului inox care a fost extins și pentru caracterizarea aliajelor dentare pe bază de nichel-crom. Potențialele și curenții de coroziune utilizând ca mediu coroziv saliva artificială au fost determinați folosind metode electrochimice. Conținutul de crom și molibden joacă un rol semnificativ în rezistența la coroziune: aliajele cu un conținut ridicat în aceste elemente prezintă un interval de pasivare lag și o rezistență la coroziunea în puncte. Aliajele cu un PREN < 32.9 sunt susceptibile la coroziunea în puncte.

INFLUENCES OF ENVIRONMENT ON DEFORMATION AND CRACK OF ESTANE ELASTOMERS

BY

BÂRSĂNESU PAUL DORU, BÎTCĂ CONSTANTIN AND ADRIAN STOIAN

Abstract: In the present paper we have studied the influences of environment on deformation and crack of ESTANE elastomers. ESTANE is a thermoplastic polyurethane elastomer and reach a great interest due to their special properties. After experimental studies, we can conclude that the maximum strain in the electron acceptor environment is greater than in inert ones, for the same load, and the behavior during the creep shows general characteristics of the thermoplastic elastomers.

Keywords: polyurethane, creep, environment

1. Introduction

Thermoplastics polyurethane elastomers reach a greater interest from many technical fields. Actually they are important due to their special properties: very good strength to abrasion and creep, limited elongation, remarkable strength to petroleum products and ozone action, [1, 2, 3].

The strains, in creep condition, of this kind of elastomers show us that they have an important residual strain after removing the load, due to some mechanochemical reactions, [4, 5,6].

The paper presents the study of strain and creep phenomena of these elastomers.

2. Experimental tests

We will study the type of elastomer, so called ESTANE, manufactured by B.F. GOODRICH CHEM.CO. (SUA). It's a linear polymer, based on 4.4' dibenzyl – diisocyanate. The density is 1.22 g/cm^3 , and the softening point $160 \pm 10^\circ\text{C}$. For the present study we used elastomer films, manufactured by mixing melting polymer in water fenolate solution (9/1 vol.), at 80°C temperature. The films are cast on glass plates, the carrier evaporating through thermal treatment at 105°C in air and at 60°C for 24 hours in vacuum. The manufactured films have the following dimensions: $35 \times 15 \times 0.07 \text{ mm}$.

The device used for creep study (*fig. 1*), allow us to develop different gaseous and liquid environments, equipped with a self-seal and clamping in system.

In case of the gaseous environment (vacuum, nitrogen, air, nitrogen oxide, vinyl chloride), the value of tensile load was about $\sigma_o = 42.20 \text{ MPa}$, and in case of liquid environment (ethyl alcohol, DPPH alcohol, acrylonitrile alcohol), about 17.0 MPa . All experiments were conducted at room temperature.

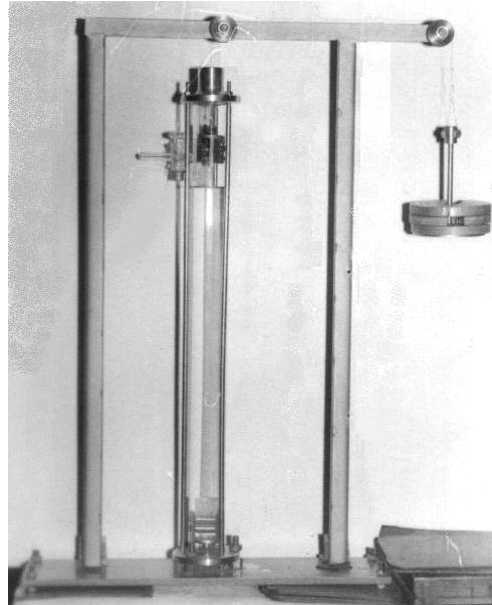


Fig. 1. Device for tensile loads

We have used an inert and electronic acceptor environment in order to study the deformation and crack phenomena, taking into consideration the confirmed radically nature of these processes.

In order to remove the air inside the device, it has been washed with nitrogen after vacuum, for many times, in case of the active environment (nitrogen oxide, vinyl chloride). Before loading, the films were dried at 60°C, for 24 hours under vacuum and weighted after that. After loading in gaseous environment, the samples were heated at 60°C, for 24 hours in vacuum.

After loading in the liquid environment above mentioned, the samples were washed with ethyl alcohol for 10 hours and then drying at 60°C in vacuum. After drying the samples were warmed again.

3. Results and discussions

Experimental study of loading tensile allows us to plot the creep diagram for different environments (gas, liquid).

The creep diagram in atmosphere (fig. 2) allows us to calculate the strains, characteristic to viscoelastic behavior, specific to studied thermoplastic elastomer (table 1).

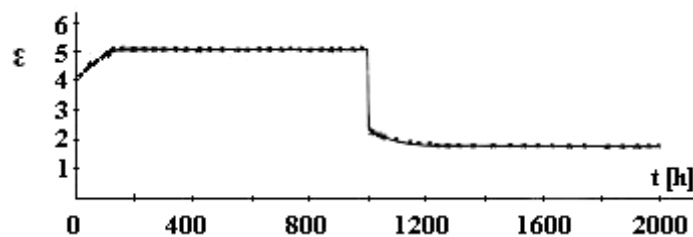


Fig. 2. Creep diagram ε – time for $\sigma_o = 42.2$ MPa, in atmosphere

Table 1. Strain values at $\sigma_o = 42.20$ MPa, for different environments

| Strain, ϵ , mm/mm | $\epsilon_{el.inst}$ | $\epsilon_{el.del}$ | ϵ_{max} | $\epsilon_{rev.el.inst}$ | $\epsilon_{rev.el.int}$ | $\epsilon_{permanent}$ |
|-------------------------------|----------------------|---------------------|------------------|--------------------------|-------------------------|------------------------|
| Atmosphere | 3.25 | 1.84 | 5.09 | 2.79 | 1.04 | 1.75 |
| Vacuum | 3.10 | 1.60 | 4.70 | | | |
| Nitrogen | 3.0 | 1.55 | 4.55 | | | |
| Nitrogen oxide | 3.45 | 2.50 | 5.95 | | | |
| Vinyl chloride | 3.50 | 2.15 | 5.65 | | | |

The great value of the permanent strain indicates the linear character of this polymer.

In the *fig. 3* are presented other creep diagrams in different gaseous environments.

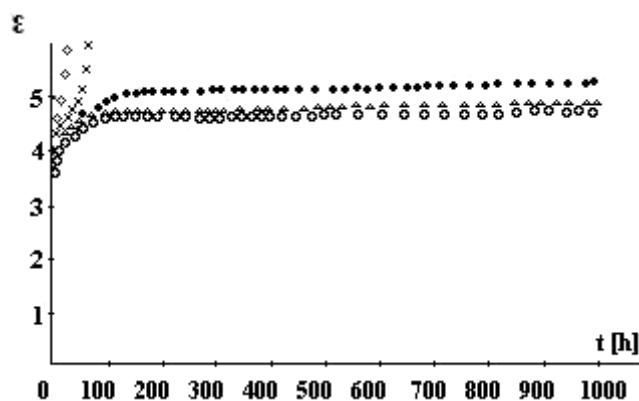


Fig. 3. Creep diagrams for different gaseous environments: ● – atmosphere, Δ – vacuum, × – nitrogen oxide, ◇ – vinyl chloride

We can see that the maximum strain in electronic acceptor environment is greater than those inert, for the same load (*Table. 1*). The samples loaded in vacuum, nitrogen and atmosphere, do not crack neither after 1000 hours of loading, but those loaded in nitrogen oxide and vinyl chloride there are cracked after 65 hours and 23 respectively, from the start point. This happened because of the strong electron-acceptor character that inhibits the recombining and disproportional reactions, accelerating the mechanochemical reactions that determine, finally, the macroscopic cracks.

Also the increased nitrogen content of the films from 3.87% (blank sample) to 4.36%, after loading in nitrogen oxide environment has an important influence. In the same time it was determined a difference of 0.5% of weight of the samples in vinyl chloride.

The load in creep condition, in liquid, electronic acceptor or different monomers allows us to plot the creep diagrams, presented in the *fig. 4*. The polymer does not crack after 1000 hours, reaching the maximum strain after 120 hours, but in DPPH alcoholic, isoprene and acrylonitrile, cracks after 140, 48 and 1 hour respectively.

The representation of experimental results in $\epsilon - \log t$ (*fig. 5*) and $\log \epsilon - \log t$ coordinates (*fig. 6*) permitted a partial linearization of the creep diagrams.

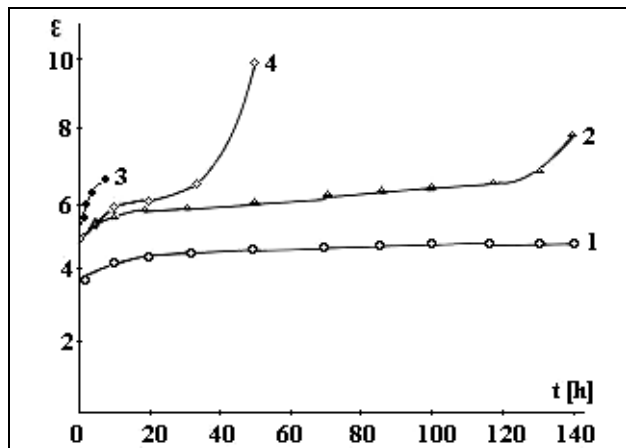


Fig. 4. Creep diagrams for the load $\sigma_0 = 17.0$ MPa, in: 1. ethyl alcohol, 2. DPPH, 3. acrylonitrile, 4. isoprene

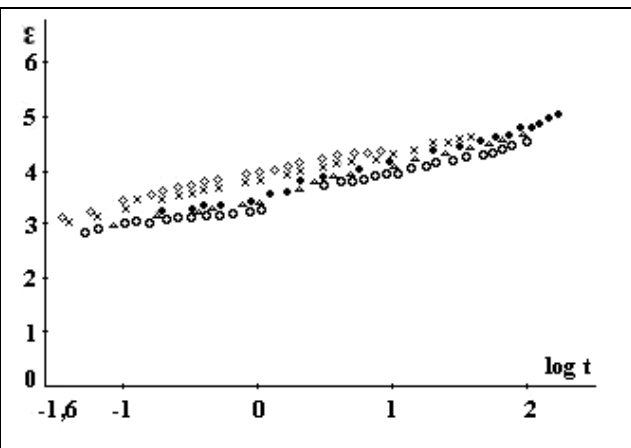


Fig. 5. Creep diagrams $\epsilon - \log t$ for $\sigma_0 = 42.2$ MPa in gaseous environment: \bullet – atmosphere, Δ – vacuum, \times – nitrogen oxide, \diamond – vinyl chloride

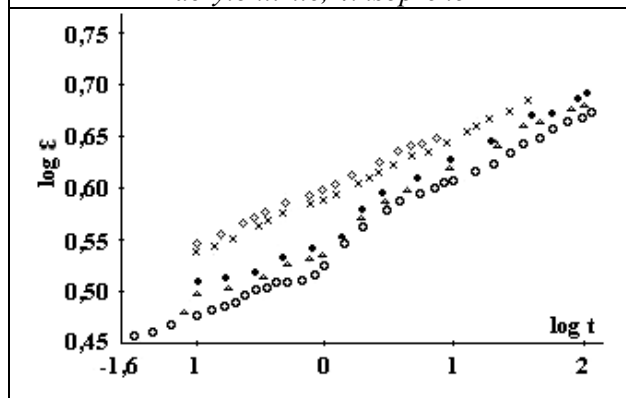


Fig. 6. Creep diagrams $\log \epsilon - \log t$ for different gaseous environment: \bullet – atmosphere, Δ – vacuum, \times – nitrogen oxide, \diamond – vinyl chloride

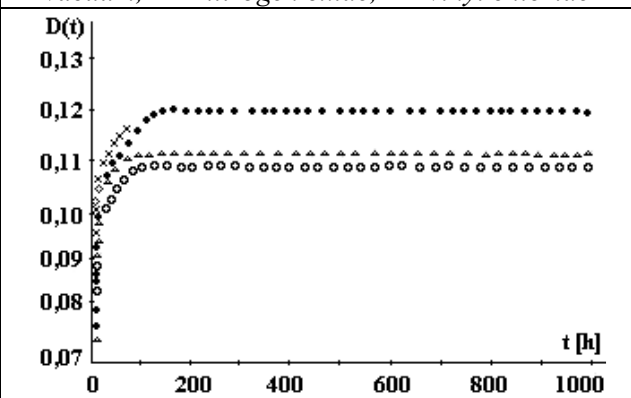


Fig. 7. $D(t)$ Diagrams – t : for different gaseous environment: \bullet – atmosphere, Δ – vacuum, \times – nitrogen oxide, \diamond – vinyl chloride

Also the determination of the creep compliance $D(t)$, parameter characteristic to viscoelastic behavior of polymers, calculated using the formula

$$D(t) = \frac{\epsilon(t)}{\sigma_0}, [\text{MPa}^{-1}] \quad (1)$$

allowed us to plot the diagrams $D(t) - t$ (fig.7), $\epsilon - D(t)$ (fig. 8) and $\epsilon - \log D(t)$ (fig. 9) in order to predict the long time behavior. We can observe that the linearity of the variations of experimental data for $\epsilon - D(t)$ and $\epsilon - \log D(t)$ coordinates, which are a strong argue to the possibility of using them for this purpose.

Utilization of acceptor electron environment (gas and liquid) permits us to distinguish the mechanochemical reactions that are producing during the creep processes of the polyurethane type of thermoplastic elastomers.

We established that in the presence of the air, the total strain is greater than in vacuum or nitrogen, because the free radicals, appeared after cleavage of chemical links, reacts with the oxygen, forming peroxide grouping, which are easily break-up. So, the presences of the oxygen accelerate the subsequent cleavage of the chemical links, process observed through the increased strain of the sample.

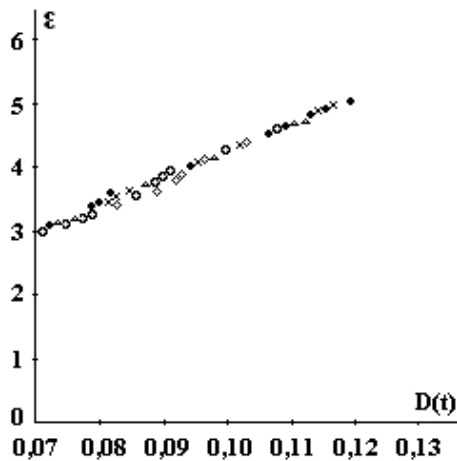


Fig. 8. Diagrams $\varepsilon - D(t)$ for different gaseous environment: \bullet – atmosphere, Δ – vacuum, \times – nitrogen oxide, \diamond – vinyl chloride

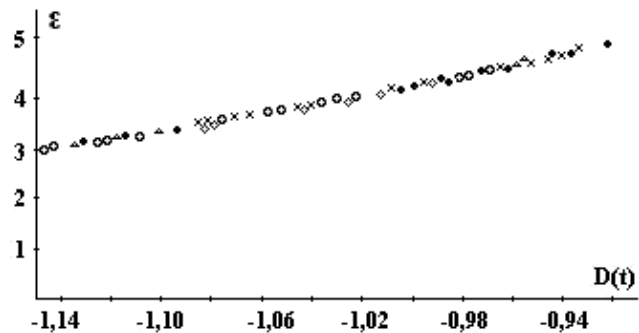


Fig. 9. Diagrams $\varepsilon - \log D(t)$ for different gaseous environment: \bullet – atmosphere, Δ – vacuum, \times – nitrogen oxide, \diamond – vinyl chloride

Using the electron acceptor environment conducts to their linking to the primary macro groups, preventing the reaction of recombination which intensify mechanodegradation and modification of some properties of the initial elastomer (colour and the nitrogen content).

The presence of monomers are involve in initiation of the grafting of the loaded films, because of the presence of the active chemical group centers formed during the cleavage of the valence chemical links.

The weight modification of the polymer is an argument for these reactions.

At the same time, it was establish that in all active environments (gas or liquid) the macromechanical crack was accelerated by consumed free radicals and brake of the transfer chain and recombination reactions.

The reactivity of the acceptor environments used against the polymer loaded in creep conditions prove the radical nature of the transformations that happened during the strain and crack of these polyurethane elastomers.

4. Conclusions

1. We can see that the maximum strain in the electron acceptor environment is greater than in inert ones, for the same load. The samples loaded in vacuum, nitrogen and atmosphere does not break neither after 1000 hours, but those in nitrogen oxide and vinyl chloride breaks after 65, 23 hours respectively, from the beginning of loading.

2. The ESTANE elastomers behavior during the creep shows general characteristics of the thermoplastic elastomers.

Received April 21, 2005

The "Gh. Asachi" Technical University Iassy
Strength of Materials Department

REFERENCES

1. Saunders J.H., Frisch K.C., *Polyurethanes Chemistry and Technology*, Part I, Interscience, New York, 1967
2. Saunders J.H., *Polymer Chemistry of Synthetic Elastomers*, J.P. Kennedy, E.G.M. Tornqvist ed., Interscience, New York, 1969
3. Lipatov O.C., Kercea I.I., Sergheeva L.M., *Struktura i svoistva poliuretannov*, Naukova Dumka, Kiev, 1970
4. Oprea C.V., Constantinescu Al., Bârsănescu, P.D., *Ruperea polimerilor*, Ed. Tehnică, București, 1992
5. Wineman A., Rajagopal K.R., *Mechanical response of Polymers*, Cambridge University Press, 2000
6. Dieter G. (chair vol.) *ASM Handbook, vol.20, Materials selection and design*, ASM, 1997

INFLUENȚA MEDIULUI ASUPRA DEFORMĂRII ȘI RUPERII ELASTOMERILOR ESTANE

Rezumat: Elastomerii termoplastici dobândesc o importanță crescândă în diferite domenii ale tehnicii prin proprietățile lor deosebite ca: rezistență foarte bună la abraziune și rupere, lungire limitată. Lucrarea de față abordează studiul mecanismului deformării și ruperii acestor elastomeri. În urma studiului s-a constatat că deformația maximă este mai mare în mediile acceptoare de electroni decât în cele inerte iar în urma solicitării, în condiții de fluaj prezintă caracteristicile generale ale deformării elastomerilor termoplastici.

ON THE D.C. CONDUCTION MECHANISM OF N-(p-R-PHENACYL)-1,7-PHENANTHROLINIUM BROMIDES IN THIN FILMS

By

L. LEONTIE^{1*}, I. DRUTA², T. DANILOAIA², G.I. RUSU¹

The investigation of temperature dependence of electrical conductivity, σ , and Seebeck coefficient, S , for six new synthesized N-(p-R-phenacyl)-1,7-phenanthrolium bromides, is reported. Thin film samples ($d=0.11-0.96 \mu\text{m}$) deposited by an immersion technique (from ethanol solutions) onto glass were used.

$\sigma(10^3/T)$ and $S(10^3/T)$ dependences evidence typical semiconducting (n-type) behavior of actual polycrystalline organic materials. The activation energy of electrical conduction lay in the range 1.71-1.94 eV, while the ratio of charge carrier mobilities ranged between 1.13 and 1.75.

Some correlations between semiconductor properties and molecular structure of the compounds were established. The model based on band gap representation can be satisfactory used for the explanation of electronic transport in investigated compounds.

Keywords: organic materials, thin films, electronic transport

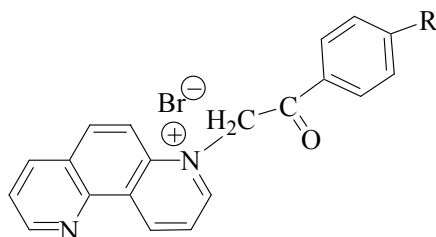
1. Introduction

In the last two decades, the study of electronic transport mechanism in semiconducting organic compounds has been the object of many theoretical and experimental investigations. The interest in this interdisciplinary topic is strongly stimulated by the wide applications of organic semiconductors in different domains of modern technology of solid-state devices [1-3].

Generally, by studying electronic transport properties of semiconducting materials very useful information can be obtained about the mechanism of electrical conduction, concentrations and mobilities of charge carriers, predominant scattering mechanism of carriers, etc. [4-8].

In a series of previous papers [9-19] we studied the temperature dependence of the electrical conductivity and Seebeck coefficient for a large number of new organic compounds (monomers, polymers, charge transfer complexes, etc.) showing typical semiconducting characteristics. Some correlations between these characteristics (thermal activation energy of electrical conduction, ratio of carrier mobilities, etc.) and the molecular structure of studied compounds were established [9, 11, 15, 18].

In present paper, we extend these investigations on some recently synthesized N-(p-R-phenacyl)-1,7-phenanthroline bromides, in thin films.



T (1 - 6)

- 1) R = CH₃
- 2) R = OCH₃
- 3) R = NO₂
- 4) R = H
- 5) R = Cl
- 6) R = Br

Scheme 1

2. Experimental

The molecular structure of synthesized compounds, as well the nature of substituents, are presented in Scheme 1.

For the study of temperature dependence of the electrical conductivity, σ , and Seebeck coefficient, S , thin-film samples deposited from ethanol solutions onto glass substrates were used. The used experimental conditions permitted obtaining films of uniform thickness on large areas of the substrate surface [9, 11].

Measurements were performed using surface-type cells. Indium thin films (deposited onto substrate by thermal evaporation under vacuum) were used as electrodes.

Film thickness ($d=0.11-0.96 \mu\text{m}$) was determined by an interferometric method.

The surface morphology of the films was studied by means of atomic force microscopy (AFM).

The experimental arrangements used to study the temperature dependence of σ and S were similar to those described previously [9, 11].

The Seebeck coefficient was determined using sonde electrodes [9]. The temperature difference between electrodes was chosen equal to 10-12 K. The Seebeck voltage was measured by a standard DC potentiometric method [20]. A Keithley model 6517 electrometer was used.

3. Results and Discussion

With a view to obtain thin-film samples with stable solid-state structure and reproducible properties, all films. After deposition, they were subjected to a heat treatment consisting of several successive heating/cooling cycles within a certain

temperature range, ΔT , characteristic for each studied organic compound (Table 1).

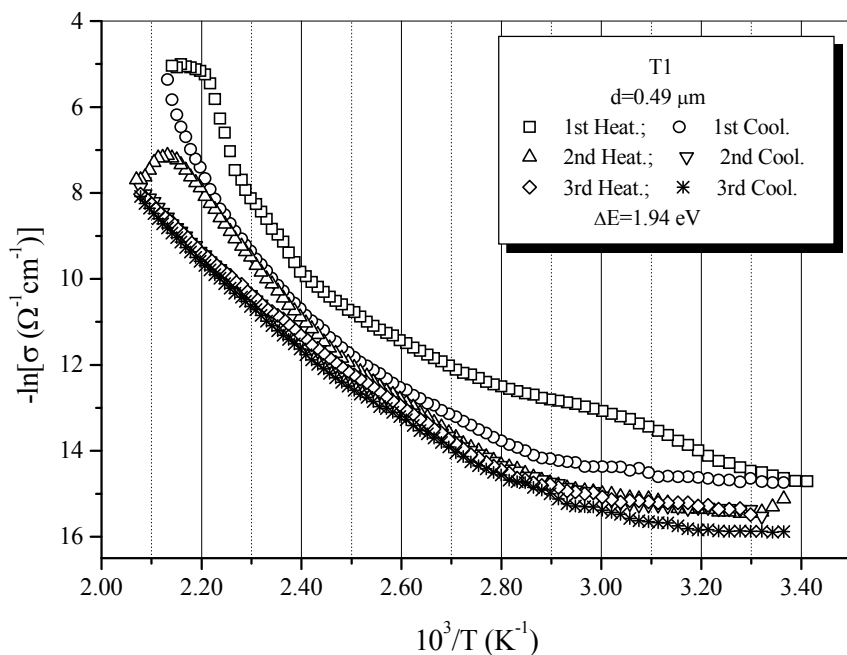


Fig. 1. Temperature dependence of electrical conductivity-compound T1.

The thermal stability of the compounds within these temperature ranges was verified.

In our previous papers related to the investigation of some organic compounds with similar chemical structures, we found that temperature dependence of electrical conductivity, σ , may be described by the exponential law [9, 13, 14]

$$\sigma = \sigma_0 \exp(-\Delta E / 2kT), \quad (1)$$

where ΔE is thermal activation energy of electrical conduction, σ_0 denotes a parameter depending on the compound nature, and k is Boltzmann's constant.

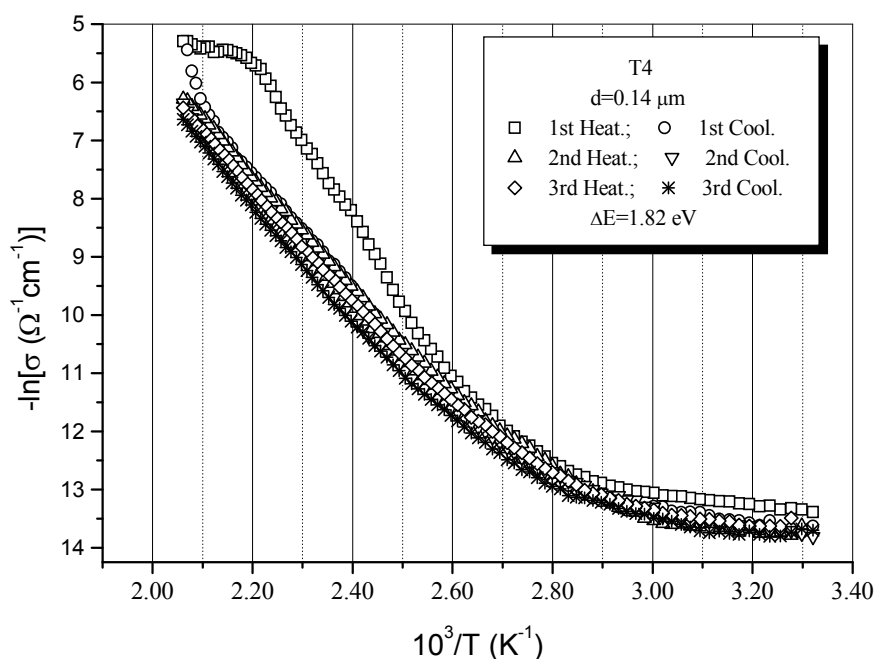


Fig. 2. Temperature dependence of electrical conductivity-compound T4.

Consequently, in present paper we supposed that an exponential increase of σ as a function on temperature is also possible for investigated compounds in thin films.

Figs. 1 and 2 show the typical obtained $\ln\sigma=f(10^3/T)$ curves during heat treatment for two studied samples.

A detailed analysis of these dependences has been performed in [9, 11]. It was established that after heat treatment the temperature dependence of the electrical conductivity becomes reversible. This fact indicated the stabilization of sample structure within respective temperature range.

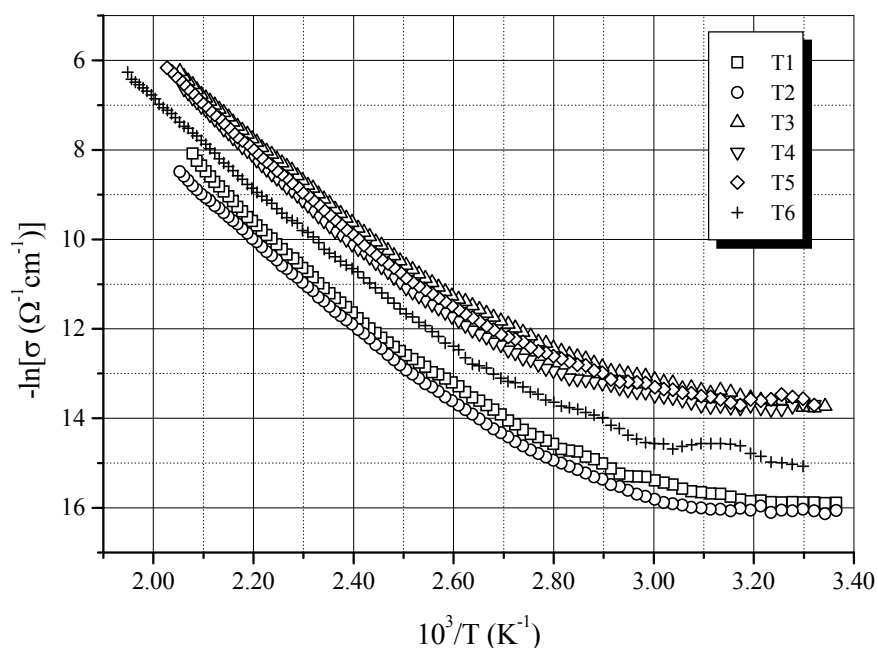


Fig. 3. Temperature dependence of electrical conductivity for heat-treated films.

In Fig. 3 the $\ln\sigma=f(10^3/T)$ curves are illustrated for some heat-treated samples. The values of the characteristic parameters of respective samples are listed in Table 1. In this table the values of the activation energy, ΔE , are also indicated. They were calculated according to Eq. (1) from $\ln\sigma=f(10^3/T)$ curves in the intrinsic conduction domain (higher temperature range).

The semiconducting characteristics of the compounds are determined by their specific chemical structure, which affords extended conjugation of the electrons. The nature of substituent R significantly influences the value of the activation energy, ΔE . These values are smaller for extended conjugation systems.

In order to obtain other information on the mechanism of electronic transport for studied compounds in thin films, the temperature dependence of the Seebeck coefficient, S , was investigated in temperature range 300-450 K.

The sign of the Seebeck coefficient was negative for all samples, indicating the predominance of electrons as majority charge carriers and confirming that investigated compounds have an n-type conduction.

The Seebeck coefficient is seen to decrease with increasing temperature within the intrinsic conduction domain (Fig. 4).

By analysing $\ln\sigma=f(10^3/T)$ and $S=f(10^3/T)$ experimental curves, one can state that the model based on the bandgap representation can be used in the study of

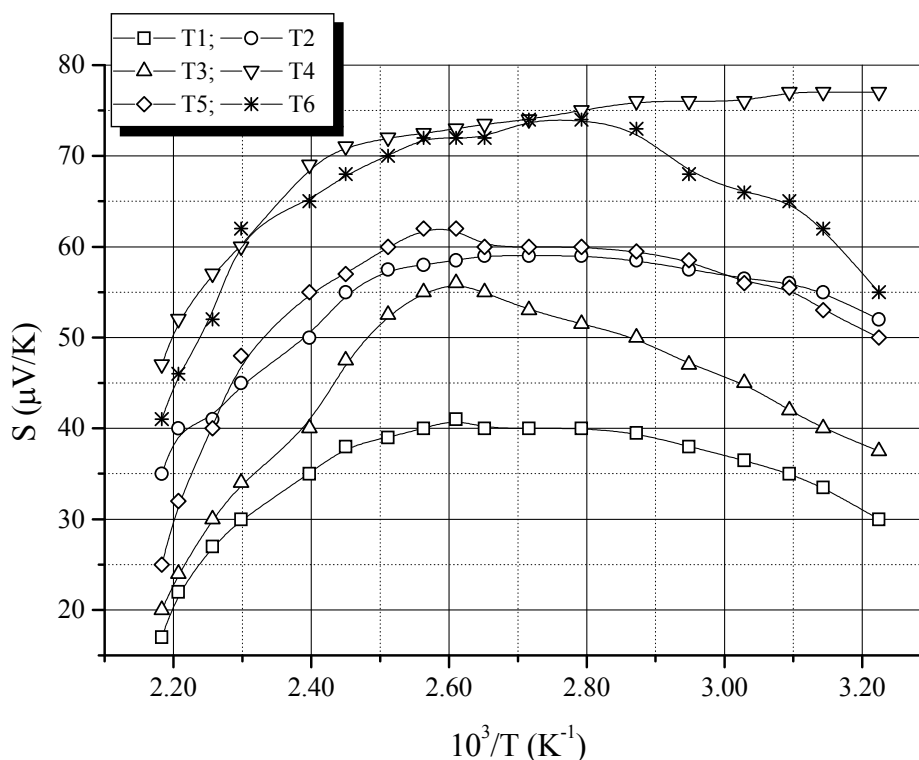


Fig. 4. Temperature dependence of Seebeck coefficient for T series.

electronic transfer mechanism in present organic compounds. Therefore, we have estimated some of the characteristic material parameters by means of the equations deduced for the domain of intrinsic conduction of a semiconductor.

Based on temperature dependence of the Seebeck coefficient within the intrinsic conduction domain [21, 22], the following expression can be obtained for the ratio of carrier mobilities [20]:

$$b = \frac{(\Delta E/2) \cdot \Delta(1/T) - |e| \cdot \Delta S}{(\Delta E/2) \cdot \Delta(1/T) + |e| \cdot \Delta S} \quad (2)$$

where $b = \mu_e/\mu_h$ denotes the ratio of charge carrier (electrons and holes, respectively) mobilities. ΔS is the variation of the Seebeck coefficient corresponding to a determined variation $\Delta(1/T)$ of the reciprocal temperature.

Table 1. Results of transport measurements

| Compound | d (μm) | σ_c ($\Omega^{-1} \cdot \text{cm}^{-1}$) | ΔT (K) | σ_T ($\Omega^{-1} \cdot \text{cm}^{-1}$) | ΔE (eV) | b |
|----------|---------------------|---|----------------|---|-----------------|------|
| T1 | 0.49 | 4.38×10^{-7} | 297-483 | 1.26×10^{-7} | 1.94 | 1.75 |
| T2 | 0.96 | 1.63×10^{-7} | 297-487 | 1.07×10^{-7} | 1.71 | 1.13 |
| T3 | 0.11 | 1.64×10^{-6} | 299-487 | 1.09×10^{-6} | 1.74 | 1.29 |
| T4 | 0.14 | 1.54×10^{-6} | 301-485 | 1.12×10^{-6} | 1.82 | 1.21 |
| T5 | 0.12 | 1.69×10^{-6} | 301-493 | 1.11×10^{-6} | 1.88 | 1.46 |
| T6 | 0.23 | 1.24×10^{-6} | 303-513 | 2.85×10^{-7} | 1.76 | 1.41 |

d-film thickness; ΔT -temperature range for heat treatment; σ_c and σ_T -electrical conductivity before and after heat treatment, respectively; ΔE -thermal activation energy of electrical conduction; b-ratio of charge carriers mobilities.

Eq. (2) is deduced by supposing that in respective temperature range, the value of the scattering parameter [23, 24] doesn't depend on the temperature.

In Table 1 the obtained values of b for some of the studied samples are shown. As can be seen, they are not very much different from the unity.

In the case of semiconductors, the electron mobility is much greater in comparison with that of holes and, consequently, b must be $\gg 1$ [21, 25, 26]. But in thin-film samples, free carriers are also scattered by the film and crystallite boundaries [26]. Besides, some structural particularities of actual compounds (grain size and shape, characteristics of inter-grain contacts, etc.) may contribute to substantial reduction of the electron mobility [11, 12].

4. Conclusions

The new synthesized organic compounds, N-(p-R-phenacyl)-1,7-phenanthroline bromides, in thin films behave as typical n-type semiconducting materials.

The electronic transfer in actual compounds is strongly dependent on their molecular structures, which favor presence of extended conjugation systems.

The model based on bandgap representation is suitable in studying the electron transport mechanism in investigated compounds.

References

- [1] M.C. Petty, M.R. Bryce, D. Bloor, *An Introduction to Molecular Electronics*, Edward Arnold, London, 1995.
- [2] J. L. Brédas and R. R. Chance (eds.), *Conjugated Polymeric Materials. Opportunity in Electronics, Optoelectronics and Molecular Electronics*, Kluwer, Dordrecht, 1990.
- [3] A. Ulman, *An Introduction To Ultrathin Organic Films: From Langmuir-Blodgett To Self-Assembly*, Acad. Press, Boston, 1997.
- [4] R. Schmechel, *J. Appl. Phys.* 93/8 (2003) 4653.
- [5] Y. Shen, K. Diest, Man-Hoi-Wong, B.R. Hsieh, D.H. Dunlap, G.G. Malliaras, *Phys. Rev. B-Cond. Matter Mater. Phys.* 68/8 (2003) 812041.
- [6] D.R.T. Zahn, T.U. Kampen, H. Mendez, *Appl. Surf. Sci.* 212-213/2003 423.
- [7] G. Paasch, T. Lindner, S. Scheinert, *Synth. Met.* 132/1 (2003) 97.
- [8] M.A. Baldo, S.R. Forrest, *Phys. Rev. B-Cond. Mat. Materi. Phys.* 64/8 (2001) 085201/1-17.
- [9] V. Şunel, G.I. Rusu, G. G. Rusu, L. Leontie, C. Şoldea, *Prog. Org. Coat.* 26/1 (1995) 53.
- [10] V. Şunel, M. Rusu, G.I. Rusu, N. Asandei, L. Leontie, *Cellulose Chem. Techn.* 31/5-6 (1997) 309.
- [11] G.I. Rusu, I. Căplănuş, L. Leontie, A. Airinei, E. Butuc, D. Mardare, and I.I. Rusu, *Acta Mater.* 49 (2001) 553.
- [12] L. Leontie, Mihaela Roman, I. Căplănuş, G.I. Rusu, *Prog. Org. Coat.* 44 (2002) 287.
- [13] L. Leontie, M. Roman, F. Brinza, C. Podaru, G.I. Rusu, *Synth. Met.* 138 (2003) 157.
- [14] L. Leontie, Ivona Olariu, and G.I. Rusu, *Mater. Chem. Phys.* 80 (2003) 506.
- [15] L. Leontie, I. Druta, R. Alupoae, and G.I. Rusu, *Mater. Sci. Eng. B* 100/3 (2003) 252.
- [16] M. Rusu, A. Stanciu, V. Bulacovschi, G. G. Rusu, M. Bucescu, and G. I. Rusu, *Thin Solid Films*, 326 (1998), 236.
- [17] G.I. Rusu, G.G. Rusu, M.E. Popa, *Mater. Res. Innov.* 7 (2003) 372.
- [18] G.I. Rusu, *Appl. Surf. Sci.* 65/66 (1993) 381.
- [19] M. Rusu and G.I. Rusu, *Appl. Surf. Sci.*, 126 (1998), 246.
- [20] A.S. Ohotin, A.S. Pushkarski, R.P. Borovikova, V.A. Simonov, *Metody Izmereniya Harakteristik Termoelektriceskih Materialov i Preobrazovatelej*, Izd. Nauka, M., 1974.

- [21] R. Smith, Semiconductors, Cambridge Univ. Press, London, 1980.
[22] H. Meier, Organic Semiconductors, Verlag Chemie, Weinheim, 1974.
[23] K. Seeger, Semiconductor physics, Springer, Berlin, Heidelberg, New York, 1999.
[24] H.P. Wolf, Semiconductors, Wiley, London, 1971.
[25] P.T. Landsberg (Ed.), Handbook on Semiconductors. Basic Properties of Semiconductors, vol. 1, North-Holland, Amsterdam, 1992.
[26] L.L. Kazmerski, Polycrystalline and Amorphous Thin Films and Devices, Academic Press, New York, 1980.

L. LEONTIE^{1*}, I. DRUTA², T. DANILOAIA², G.I. RUSU¹

¹ Faculty of Physics, "Al.I. Cuza" University, 11 Carol I Bd., R-700506 Iasi, Romania

² Faculty of Chemistry, "Al.I. Cuza" University, 11 Carol I Bd., R-700506 Iasi, Romania

* Corresponding author: dr. L. Leontie, Faculty of Physics, "Al.I. Cuza" University, 11 Carol I Bd., R-700506, Iasi, Romania

Phone: ++40-32-201168; Fax: ++40-32-201150/201201; E-mail: lleontie@uaic.ro

ASUPRA MECANISMULUI DE CONDUCTIE ELECTRICA IN STRATURI SUBTIRI DE BROMURI DE N-(PARA-R-FENACIL)-1,7-FENANTROLINIU

În lucrare se studiază dependența de temperatură a conductivității electrice, σ , și a coeficientului Seebeck, S , pentru șase compuși organici recent sintetizați, bromuri N-(p-R-fenacil)-1,7-fenantrolină. Au fost utilizate eșantioane sub formă de straturi subțiri ($d=0.11-0.96 \mu\text{m}$), depuse printr-o tehnică de imersie (soluții de etanol) pe suporturi de sticlă.

Dependențele $\sigma(10^3/T)$ and $S(10^3/T)$ evidențiază un comportament tipic semiconductor (de tip n) al materialelor policristaline studiate.

Energia de activare a conducției electrice se situează în intervalul 1.71-1.94 eV, în timp ce raportul mobilităților purtătorilor de sarcină are valori între 1.13 și 1.75.

Au fost stabilite corelații între proprietățile semiconductoare și structura moleculară ale compușilor. Modelul conducției în bandă poate fi utilizat cu succes în explicarea transportului electronic în compușii investigați.

FUNCTIONALIZED MATERIALS IN MONITORING AND REMEDIATION OF ENVIRONMENT

BY

DANIELA SUTEU, VALERIA - MARTA GORDUZA and LAVINIA TOFAN

Abstract: The technical and informational development and demographic explosion, characteristic to contemporary civilization, have been resulted in ecological unbalances, genetic mutations and resources of raw material waste. In this context the synthetic macromolecular materials sorptive potential in assurance of environmental factors quality and development of new economical strategies is of particular importance. The choice of sorbent is based on requirements concerning high selectivity, large capacity of sorption, favorable kinetic features, physico - chemical stability, mechanical strength, easy regeneration and availability at low cost. Because of compatibleness between these criteria and their sorptive features, the macromolecular synthetic materials (synthetic resins, polyamides, polyurethane foams) constitute, in many instances, a solution of election. The specialty studies are focused on synthetic resins, materials with a wide range of uses in environment depollution and processes of deficient metals concentration- separation. These materials can be used in untreated form or after physical and/or chemical functionalizations. On the other hand, the improvement of their features (degree of crosslink, size of pores, regular surface area) determined the extension of range of organic substances concentrated by sorption on synthetic resins, comparatively to activated carbon or silicagel.

Keywords: synthetic resins, ion exchangers, removal dyes, environmental protection

1. Introduction

The life quality assurance is a major demand of the modern and superindustrialized society which must offer biotechnological, ecological and efficient alternatives, in conditions of a demographic explosion unprecedented, crude materials exhausting, pollutants diversification and environment pollution, the presence in small amounts and time cumulative toxicity of the products with ecological risk are of major importance [1].

The dyestuff manufacturing and consuming industries are some of the leading consumers of water. Effluents of textile dyeing/finishing mills are often complex with intense color, chemical oxygen demand, suspended solids and a variety of refractory matter such as heavy metals and nonionic surfactants. It was been suggested that strong colours can reduce light penetration, thus affecting the growth of plants and impacting on invertebrate and other forms of wildlife. To remove dyes from the waste water in an economic fashion remains a major problem for the textile industry [2]. In order to retain dyes from aqueous media different types of sorbents, such as activated carbon, chitine, chitosan, ion exchange celluloses, lingo-cellulosic waste [3-12] have been used.

The choice of sorbent is based on requirements concerning high selectivity, large capacity of sorption, favorable kinetic features, physico-chemical stability, mechanical strength, easy regeneration and availability at low cost. Because of compatibleness

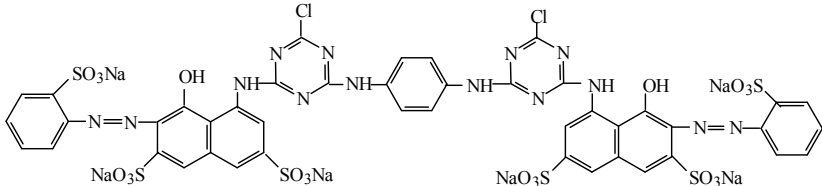
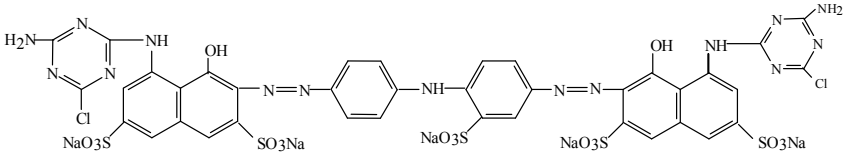
between these criteria and their sorptive features, the macromolecular synthetic materials (such as synthetic resins, polyacrilamide, cellulose ion exchange, polyurethane foams, crosslinked polymers) constitute, in many instances, a solution of election.

This paper is a synthesis of our experimental data concerning the testing of ion exchange synthetic resins (based on styrene-divinylbenzene copolymers) sorptive potential in dyes recovery (Brilliant Red HE-3b, Blue M-EM, Methyl Violet).

2. Experimental procedure

Dyes solutions. The selected dyes were used as commercial salts and are characterized in Table 1. Working solutions (in concentration of 0.05 – 0.3 mg/mL) were prepared by appropriate dilution of the stock solution (10mg/L).

Table 1. The characteristic of dyes tested

| Dye | Structure and characteristics |
|--|--|
| Brilliant Red HE-3B – reactive dye |  <p>MW = 1463; adsorption maximum, $\lambda_{\max} = 530 \text{ nm}$; $\epsilon = 40200.5 \text{ L/mol.cm}$</p> |
| Blue M-EB – reactive dye |  <p>MW = 1306; adsorption maximum, $\lambda_{\max} = 650\text{nm}$; $\epsilon = 235050 \text{ L/mol.cm}$</p> |
| Methyl Violet – triphenyl methanic dye |  <p>MW = 358, adsorption maximum $\lambda_{\max} = 580\text{nm}$</p> |

Ion exchangers. The experiments were carried out using a various type of ion exchangers resins (anionites and cationites), characterized in Table 2.

Table 2. The features of tested ion exchangers

| Characteristic | Type of resin | | | | |
|----------------------|--|-------------|----------------|----------------|--|
| | Amberlite IRA-401S | Vionit AT-1 | Purolite A-400 | Purolite A-500 | Purolite C-100 |
| Matrix | polystyrene-divinylbenzene | | | | |
| Structure | gel | gel | gel | macroporous | gel |
| Type of ion exchange | anionite with quaternary ammonium groups $R - (\text{CH}_3)_3\text{N}^+$ (type I) | | | | strong acid cationite (Na ⁺ form) |
| Capacity | 1.1-1.3 meq/mL | | 3.72 meq/g | 3.93 meq/g | 1.9 meq/mL |

Dye sorption procedure. The experimental studies of dyes retention on the ion exchangers were carried out in batch conditions. Thus, sample of resins (0.1-0.2g) were allowed to contact with 50-100mL of working solutions with known concentration. After equilibrium (24 hours) the phases were separated and in filtrate the unretained amount of dye were measured by spectrophotometric method with a HACH DR 20 UV-VIS spectrophotometer. The sorption capacity of sorbents was evaluated by amount of dye sorbed: q (mg dye/ g of resin).

3. Experimental results and discussion

In the previous works [13-17], the equilibrium sorption of the selected dyes onto ion exchange resins, on the basis of some experimental factors (pH, temperature, type and amount of resin, dye initial concentration, electrolyte amount) influence, have been studied. Dye retention on these types of ion exchangers is favourably influenced by solution – exchanger contact time, temperature, amount of resin and initial dye concentration increasing and is indifferent to the possible additions of electrolytes or pH variation (an exception is the triphenylmethanic dye where the experiments on $\text{pH} < 7$ are preferred).

Thus, the analytical potential of these materials under study in dyes retention from aqueous solutions at $18^{\circ} \pm 2^{\circ} \text{C}$ for a contact time of 24 hours has been tested. Plotting of data in $q = f(\text{concentration at equilibrium})$ represent the sorption isotherms (Fig. 1-3).

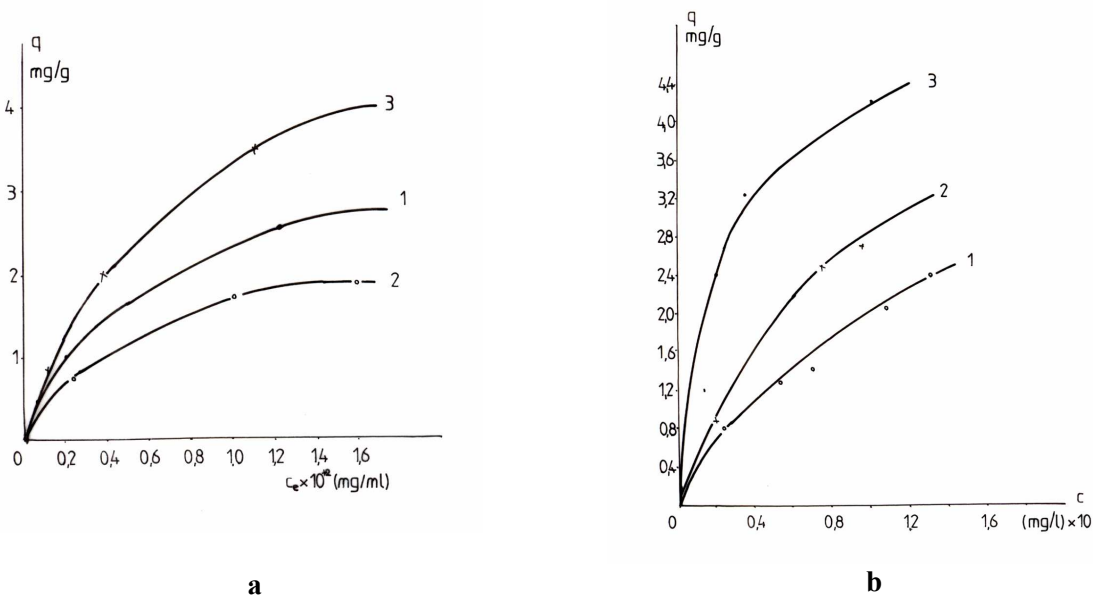


Figure 1. The sorption isotherm of the reactive dye Red Brilliant HE-3B on
 a) ion exchanger resins at 20°C : 1- Purolite A-400; 2- Vionit AT-1; 3- Amberlite IRA 401-S
 b) Amberlite IRA 401-S at: 1 – 20°C ; 2 – 20°C ; 3- 40°C

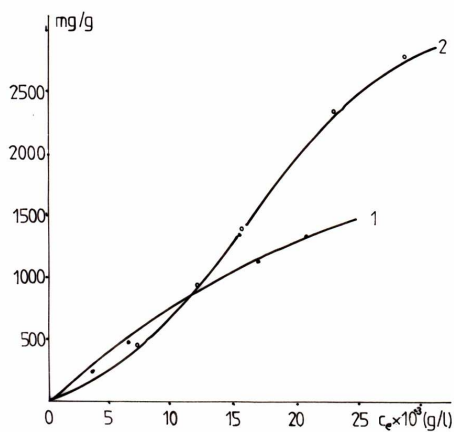


Figure 2. The sorption isotherm of the reactive dye Blue M-EB on ion exchangers resins: 1 – Purolite A-400; 2- Purolite A- 500 at 18⁰C

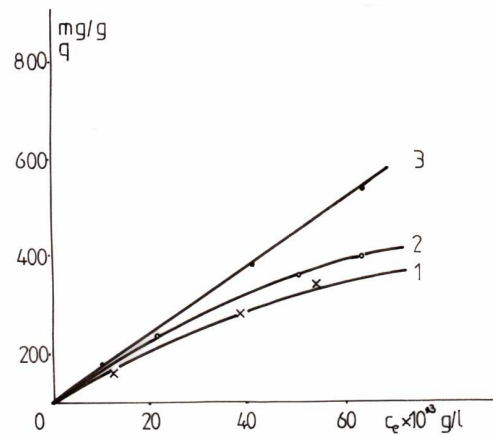


Figure 3. The sorption isotherm of the triphenylmethanic dye Methyl Violet on ion exchangers resin Purolite C-100 at: 1- 2⁰C; 2-8⁰C; 3-17⁰C

Due to high molecular weight the dyes diffusion into the internal structure pores of the ion exchangers is difficult, suggesting that the mechanism of the retention process is predominantly based on physical sorption and is completed with ion exchange.

In order to completed characterize the sorptive potential of ion exchange resins, the batch retention of three dyes has been studied using Freundlich [18] and Langmuir [19] model isotherm, the thermodynamic and kinetic data. The quantitative amounts of the sorption process have been calculated on the basis of Freundlich and Langmuir liniarized equations plots (Fig.4 and 5) and are recorded in Table 3.

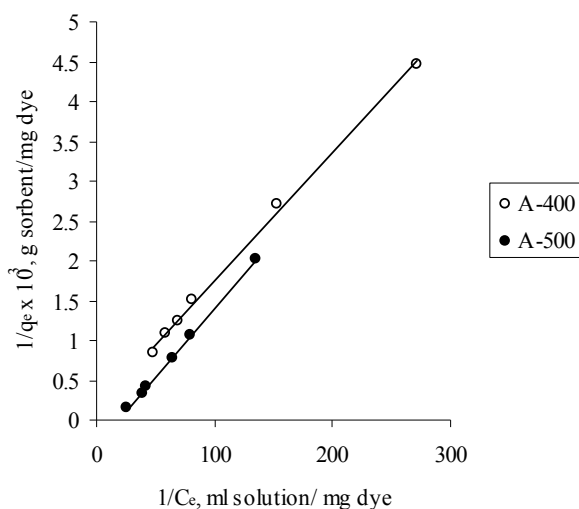


Figure 4. The representation of the Langmuir isotherm for reactive dye Blue M-EB sorption on ion exchangers resins at 20⁰C

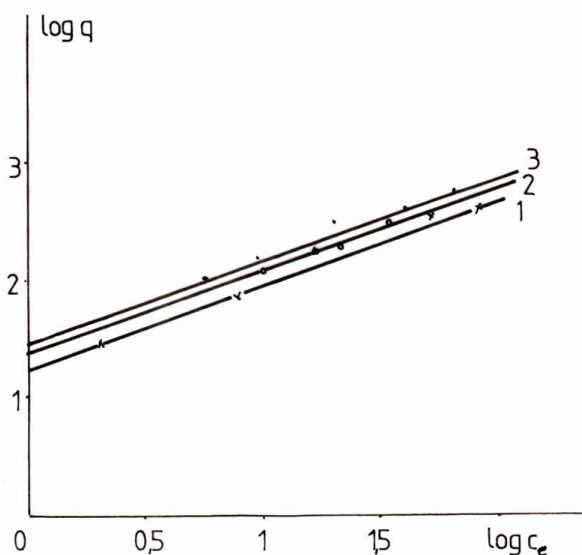


Figure 5. The representation of the Freundlich isotherm for triphenylmethanic dye Methyl Violet sorption on ion exchanger resin Purolite C-100 at three temperature:1- 2⁰C; 2-8⁰C; 3-17⁰C

Using the values of binding Langmuir constant, K_L , and following equations one can calculate the variations of enthalpy (ΔH , kJ/mol - from the equation 1 plots: $\lg K_L = f(1/T)$ Fig.6), free energy (ΔG , kJ/mol) and entropy (ΔS , J/mol.K) of dye sorption on activated charcoal. The data obtained are given in Table 3.

$$\ln K_L = -\frac{\Delta H}{R \cdot T} + \text{const} \quad (1)$$

$$\Delta G = -RT \ln K_L \quad (2)$$

$$\Delta S = \frac{\Delta H - \Delta G}{T} \quad (3)$$

where R is the gas law constant and T is the absolute temperature.

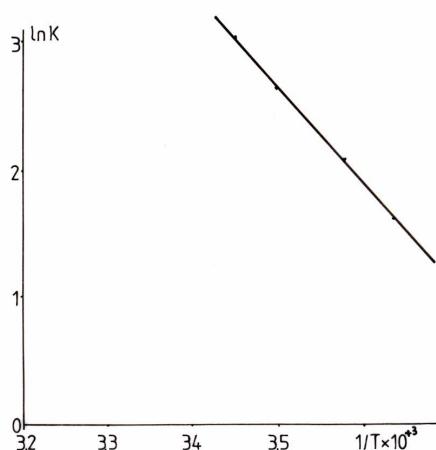


Figure 6. Plot of $\lg K_L$ versus $1/T$ in triphenylmethanic dye Methyl Violet – Purolite C-100 resin ion exchange sorption system

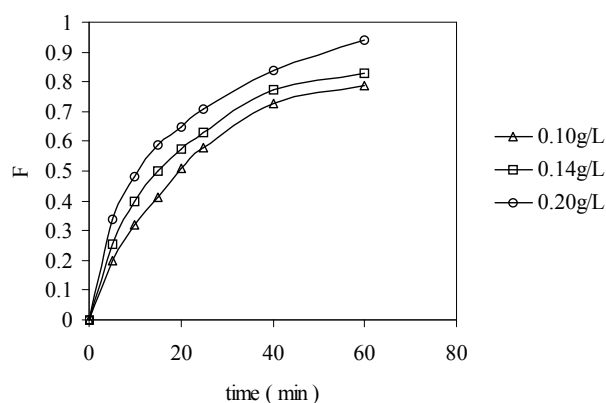


Figure 7. Rate of sorption of Blue M-EB dye on Purolite A – 400 resin at 20°C and at different initial concentration

According to Table 3, ΔH values being greater than 0 ($\Delta H > 0$), represent a process of endothermic sorption of dyes on ion exchangers. This findings is in good agreement with the increase of maximum capacity of dyes sorption as result of the temperature increase.

In order to obtain more information, the kinetic properties of ion exchangers have been tested. The values of the constant rate k' calculated on basis of different kinetic models [20] and the values of half life time $t_{1/2}$ (is the time required for $F=0.5$) from the plot $F = f(\text{time})$, were F represent the degree of equilibrium reaching at time t are given in Table 3.

From practical point of view the half life time is a suitable parameter for relative rate of sorption process characterization.

In order to obtain a cheap and effective method of removing dyes, the sorption, kinetic and thermodynamic parameters of some ion exchangers have been assessed (Table 3).

Tabele 3. The sorption study of some dyes on ion exchange resins

| Type of sorbent | Vionit AT-1 | Amberlite IRA 401-S | Purolite A-400 | Purolite A-500 | Purolite C-100 |
|--|---------------------|---------------------|----------------------|----------------------|----------------|
| References | 13,17 | 13,17 | 16,17,20 | 16,17,20 | 14,17,21 |
| Dye under study | Brilliant Red HE-3B | Brilliant Red HE-3B | Blue M-EB | Blue M-EB | Methyl Violet |
| <u>Langmuir parameters</u> | | | | | |
| * q_0 , mg/g | 4.000 | 4.760 | 6666.67 | 20000.00 | 980.40 |
| * K_L , L/g | 0.235 | 1.111 | 13.64 | 83.54 | 20.24 |
| <u>Freundlich parameters</u> | | | | | |
| * K_F | 0.0621 | 0.0505 | 31.62 | 79.43 | 29.85 |
| * n | 1.4300 | 1.2730 | 1.02 | 1.06 | 1.45 |
| <u>Thermodynamic parameters</u> | | | | | |
| ΔG , J/mol | 3538.916 | -258020.2 | -6321.84 | -10780.16 | -7271.116 |
| ΔH , J/mol | 23787.049 | 27737.8 | | | 26166.550 |
| ΔS , J/mol.K | 69595.900 | 95364.4 | | | 115.225 |
| <u>Kinetic parameters</u> ($C_0=0.1$ mg/mL; $T=284.15$ K) | | | | | |
| * $t_{1/2}$, s | | | 20 | 16 | |
| * k , s^{-1} | | | $5.33 \cdot 10^{-5}$ | $2.99 \cdot 10^{-4}$ | |

4. Conclusions

The experimental data processing points out that the synthetic ion exchange resins have the potential to be use as materials with efficient properties in dyes recovery from waste waters, in order to their optimum conditions of recycling assurance.

Received 2005

The "Gh.Asachi" Technical University Iași

REFERENCES

- Gorduza, V.M., Tofan, L., Ţuteu, D., Gorduza, E.V. – **Biomateriale – Biotehnologii – Biocontrol**, Editura Cermi, Iasi, 2002, ISBN973-8188-12-1
- Hu, T.L. – *Sorption of reactive dyes by aeromonas biomass*, **Water Sci.Tech.**,26(1-2),1992,**357-366**
- Figueiredo, S.A., Boaventura, R.A., Loureiro,J.M.- *Color removal with natural adsorbents : modeling, simulation and experimental*, **Sep. and Purif.Technol.**, **20**, 2000, **129-141**
- Hwang, M.C., Chen, K.M. –*Removal of color from effluents using polyamide-epichlorohydrin-cellulose polymer.II. Use in acid dye removal*, **J. Appl. Polym. Sci.**, **49**, 1993, **975-989**
- Hwang, M.C., Chen, K.M. –*Removal of color from effluents using polyamide-epichlorohydrin-cellulose polymer.III. Use in anionic dye removal in a batch process*, **J. Appl. Polym. Sci.**,**50**, 1993, **735-744**
- Vandevivere, P.C., Bianchi, R., Verstraete, W.- *Treatment and reuse of waste water from the textile wet-processing industrz: review of emerging technologies*, **J.Chem.Technol.Biotechnol.**, **72**, 1998, **289-302**

7. Karcher, S., Kornmüller, A., Jekel, M. *Screening of commercial sorbents for the removal of reactive dyes*, **Dyes and Pigments**, **51**, 2001, **111-125**
8. Voudrias, E., Fytianos, K., Bozani, E. – *Sorption-desorption isotherms of dyes from aqueous solutions and wastewaters with different sorbent materials*, **Global Nest: the Int. J.**, **4(1)**, 2002, **75-83**
9. Longhinotti, E., Pozza, F., Furlan, L., et al. – *Adsorption of anionic dyes on the biopolymer chitin*, **J. Braz. Chem. Soc.**, **9(5)**, 1998, **435-440**
10. Pala, A., Tokat, E., Erkaya, H. – *Removal of some reactive dyes from textile processing wastewaters using powdered activated carbon*, **Proceeding of the First International Conference on Environmental Research and Assessment**, Bucharest, Romania, march 23-27, 2003, 114-122, Ars Docendi Publishing House
11. Markovska, L., Meshko, V., Noveski, V., Marinkovski, M. – *Solid diffusion control of the adsorption of basic dyes onto granular activated carbon and natural zeolite in fixed bed columns*, **J. Serb. Chem. Soc.**, **66(7)**, 2001, **463-475**
12. Saraydin, D., Karadag, E. – *Adsorption of some anionic azo dyes onto crosslinked poly(N-vinylpyrrolidone) from aqueous solution*, **Rev. Roum. Chim.**, **43(2)**, 1998, **139-148**
13. Şuteu, D., Bîlbă, D., Gorduza, V.M. – *Removal of reactive dyes from waste waters using ion exchangers*, **Bul. I.P. Iaşi**, **II**, **43(1-2)**, 1997, **61-66**
14. Şuteu, D., Nacu, Al. – *Removal of triphenylmethanic dye from waste water using ion exchangers*, **Bul. I.P. Iaşi**, **II**, **44(3-4)**, 1998, **53-59**
15. Şuteu, D., Bîlbă, D., Nacu, Al. – *Studiul experimental privind posibilitatea de eliminare a coloranţilor reactivi din apele reziduale utilizând răşini schimbătoare de ioni*, **Revista de Chimie**, **49(4)**, 1998, **245-248**
16. Gorduza, V.M., Şuteu, D., Tofan, L. – *Removal of reactive dyes from waste waters using ion exchanger resins*, **J. of Balkan Ecology**, **4(1)**, 2001, **84-87**
17. Şuteu, D., Teză de doctorat: *Concentrarea prin sorbţie a substanţelor organice*, Universitatea Tehnică « Gh. Asachi », Iaşi, 1998
18. Namasivayam, C.N., Kanchana, C.N. – *Waste Banana pith as adsorbent for colour removal from waste waters*, **Chemosphere**, **25(11)**, 1992, **1691-1705**
19. McKay, G., Blair, S.H., Findon, A. – *Equilibrium studies of metal ions sorption onto chitosan*, **Indian J. Chem.**, **28a(5)**, 1989, **356-360**
20. Şuteu, D., Bîlbă, D., Zaharia, C. – *Kinetics of Blue M-EB dye sorption on ion exchange resins*, **Hung. J. Chem.**, **30**, 2002, **7-11**
21. Şuteu, D. – *The thermodynamic of Methyl Violet triphenylmethanic dye recovery from waste water effluents of dyehouse operation (II)*, **Bul. I.P. Iaşi**, **VIII**, **1-2**, 1999, **99-102**

MATERIALE FUNCȚIONALIZATE ÎN MONITORIZAREA ȘI REMEDIEREA MEDIULUI

Rezumat: Dezvoltarea tehnico-informațională și explozia demografică, caracteristicile civilizației contemporane s-au soldat cu dezechilibre ecologice, mutații genetice și epuizarea resurselor de materii prime. În acest context, se impune reconsiderarea potențialului sorbtiv al materialelor macromoleculare, naturale, artificiale și sintetice în asigurarea calității factorilor de mediu și în elaborarea de noi strategii economice. Alegerea unui sorbent se bazează pe cerințe corelate cu selectivitatea înaltă, capacitate de sorbție ridicată, caracteristici cinetice favorabile, rezistență mecanică, stabilitate fizico-chimică, regenerare ușoară și accesibilitate la preț redus. Datorită compatibilității dintre aceste criterii și caracteristicile lor sorbtive, materialele macromoleculare sintetice (rășini, spume poliuretanică, poliamide etc.) constituie, în multe cazuri, o soluție de elecție. Studiile de specialitate sunt focalizate asupra rășinilor sintetice, materiale cu un spectru larg de utilizări în depoluarea mediului și în procesele de concentrare-separare a unor metale deficitare. Pot fi folosite ca atare sau după modificări fizice și/sau chimice. Îmbunătățirea caracteristicilor unor sorbenți polimerici (grad de reticulare, dimensiunea porilor, suprafața specifică) a determinat extinderea concentrării prin sorbție a substanțelor organice pe rășini sintetice, comparativ cu cea pe cărbune activ sau silicagel.

STRUCTURAL PROPERTIES AND TRANSITION TEMPERATURES OF POLYCRYSTALLINE NiMnGa SHAPE MEMORY ALLOYS

BY

VIOREL DOBREA, HORIA CHIRIAC and MIHAIL-LIVIU CRAUS

Abstract: The Heusler alloys of Ni-Mn-Ga system are materials that reveal a reversible first-order structural phase transition and therefore they present shape memory effect. The critical temperatures (T_M , T_A) of direct and reverse martensitic transition are strongly depended of chemical composition. For some NiMnGa alloys with Ni content higher than the stoichiometric Ni_2MnGa , transformation temperatures are higher than room temperature, these attaining values of ~ 250 °C.

In this paper we present the results of structure and transition points investigations of some non-stoichiometric Ni-Mn-Ga alloys in polycrystalline state. Investigation of structure was performed by means X ray diffraction, using Cu $K\alpha$ radiation; martensitic and premartensitic temperatures were evidenced by study of electrical resistivity variation versus temperature in range of 240 to 430 K. The samples were prepared by arc-melting in argon atmosphere and further annealing.

Keywords: shape memory alloys, Heusler alloys, NiMnGa, martensitic transition

1. Introduction

Some of the Heusler alloys are known to exhibit a crystallographic reversibility and possess a thermoelastic martensitic transformation, resulting in the shape-memory effect (SME). The Ni_2MnGa Heusler alloy, which is a ferromagnetic intermetallic compound, undergoing a martensitic transition from cubic $L2_1$ structure (see Fig. 1) to a complex tetragonal structure, has been investigated as a potential smart material and also as a candidate for actuator materials. [1, 2, 3]

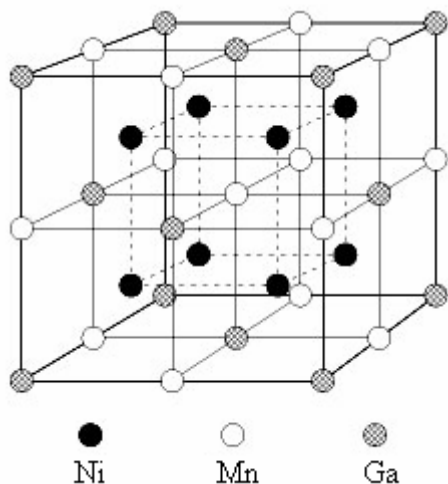


Fig.1 Cubic $L2_1$ structure of Ni_2MnGa intermetallic Heusler alloy. Ni ions occupy the corner sites of the body-centered-cubic structure, while Mn and Ga ions occupy alternate body-center sites.

The Ni_2MnGa Heusler compound exists in a wide compositional domain. For the stoichiometric Ni_2MnGa , the alloy was found to be ferromagnetic with a Curie

temperature of 376 K. Structural phase transition from the cubic austenite ($a=0.582$ nm at $T=295$ K) to the tetragonal martensite ($a=0.592$ nm and $c=0.557$ nm at $T=4.2$ K) takes place on cooling below $T_M=202$ K. This phase transition is hysteretic, but reversible on heating, showing the shape-memory effect. [4]

The potential of the Ni-Mn-Ga alloys as shape memory materials has led to much more careful studies of the structural transition. Work on alloys with nonstoichiometric compositions shows that both the Curie temperature and the martensitic transition can be varied with the concentration x [5, 6]. Some papers reported that the martensitic transition temperature increased and the magnetic transition temperature decreased with increasing nickel substitution for manganese and gallium content in the Ni_2MnGa system alloy. [3]

The aim of the present work was to prepare polycrystalline samples with a different Ni content (at the expense of Ga) and to study the composition dependence of their structural transitions in order to obtain a Ni-Mn-Ga shape memory-alloy (SMA) with higher structural transition temperature than Ni_2MnGa compound.

2. Experimental procedure

Polycrystalline $\text{Ni}_{50+x}\text{Mn}_{25}\text{Ga}_{25-x}$ alloys were prepared by three times arc-melting into buttons of the high-purity nickel, manganese and gallium under argon atmosphere. The composition of the alloys was characterized by Ni excess x in the range $x = 0 - 4$. Buttons were then remelted and drop-cast into a copper mold to obtain rods with a diameter of 1 and 5 mm and a length of 40 mm and lamella with 40x5x1 mm dimensions. For homogenization they were annealed at 1073 K for 4 days in a vacuum quartz ampoule. After homogenization the samples were quenched into ice-water. Although quenching increases the brittleness of the samples it was considered to be important to obtain the highest degree of chemical order. The phase structure of the samples was identified by X-ray diffraction measurements at room temperature using a DRON 2 diffractometer with Cu $K\alpha$ radiation. The structural transition (martensitic and premartensitic) temperatures of the alloys were evidenced by study of electrical resistivity variation versus temperature in range of 240 to 430 K using an X-Y recorder according to basic diagram showing in Fig. 2.

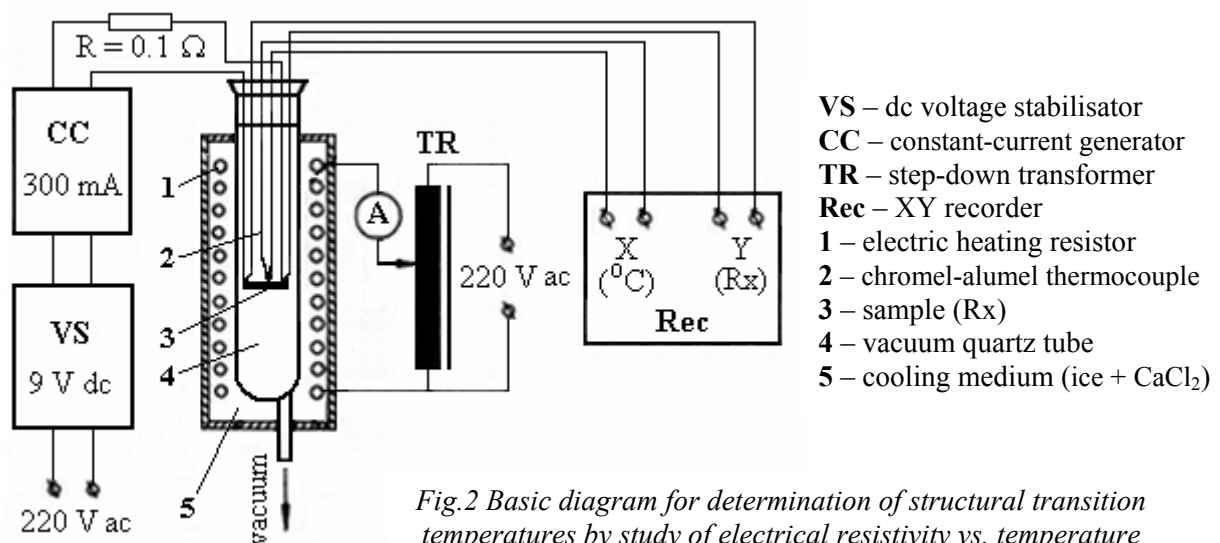


Fig.2 Basic diagram for determination of structural transition temperatures by study of electrical resistivity vs. temperature

3. Experimental results and discussion

The X-ray diffraction patterns of the annealed $\text{Ni}_{50+x}\text{Mn}_{25}\text{Ga}_{25-x}$ ($x = 2, 4$) polycrystalline alloys at room temperature indicate a cubic (austenitic) phase for $\text{Ni}_{52}\text{Mn}_{25}\text{Ga}_{23}$ alloy and a two phase mixture (austenite + martensite) for $\text{Ni}_{54}\text{Mn}_{25}\text{Ga}_{21}$ alloy, as shown in Fig. 3. Presence of two phases in structure of $\text{Ni}_{54}\text{Mn}_{25}\text{Ga}_{21}$ sample indicates that martensitic transition temperature for this alloy belongs the near room temperature, while the existence of a single phase $\text{Ni}_{52}\text{Mn}_{25}\text{Ga}_{23}$ sample shows that structural transition temperature is situated under the room temperature. We observed an unidentified phase (probably a compound of Mn with Ga: Mn_3Ga or similar) in the phase structure of the $\text{Ni}_{54}\text{Mn}_{25}\text{Ga}_{21}$, that is present in very small amount.

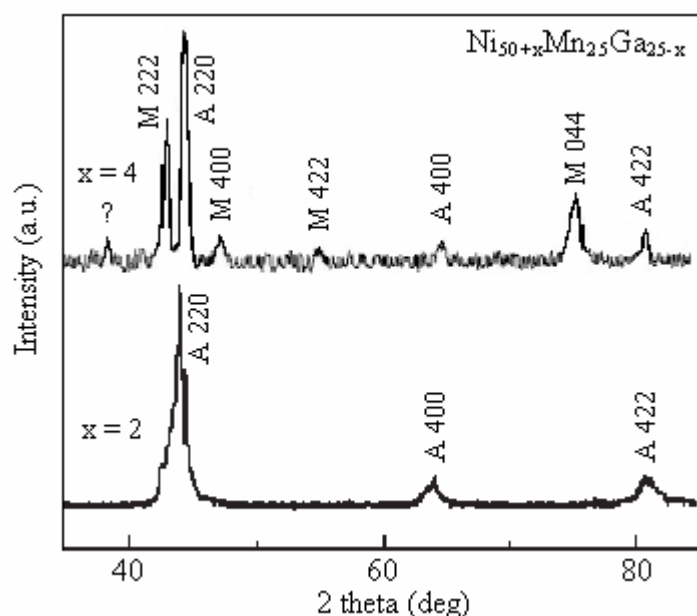


Fig.3 The X-ray diffraction patterns of the $\text{Ni}_{50+x}\text{Mn}_{25}\text{Ga}_{25-x}$ ($x = 2, 4$) polycrystalline alloys at room temperature after homogenized treatment at 1073 K for 4 days

In comparison with lattice parameters of stoichiometric $\text{Ni}_{50}\text{Mn}_{25}\text{Ga}_{25}$ Heusler compound, the lattice parameters of these structures at room temperature are presented in Table 1. The tetragonally coefficient of martensite (c/a) of the $\text{Ni}_{54}\text{Mn}_{25}\text{Ga}_{21}$ alloy has the value of 0.781 and for the $\text{Ni}_{50}\text{Mn}_{25}\text{Ga}_{25}$ stoichiometric compound (at 4.2 K) the value is 0.941. It is possible that this kind of martensitic structure should be different from that of the stoichiometric Ni_2MnGa .

Table 1 Lattice parameters of $\text{Ni}_{50+x}\text{Mn}_{25}\text{Ga}_{25-x}$ ($x = 0, 2, 4$) alloys structures at room temperature

| Sample | Austenite (cubic) | | Martensite (tetragonal) | |
|--|-------------------|--|-------------------------|-----------------|
| | a, nm | | a, nm | c, nm |
| $\text{Ni}_{50}\text{Mn}_{25}\text{Ga}_{25}$ [3] | 0.582 (at 295 K) | | 0.592 (at 4,2 K) | 0.557(at 4,2 K) |
| $\text{Ni}_{52}\text{Mn}_{25}\text{Ga}_{23}$ | 0.579 | | - | - |
| $\text{Ni}_{54}\text{Mn}_{25}\text{Ga}_{21}$ | 0.577 | | 0.767 | 0.599 |

The data presented in Table 1 show that the increase of Ni substitution in the Ga detriment from the alloy leads to an easy decrease of the lattice parameter of austenitic phase.

Direct current resistivity measurements provide a simple and effective tool to detect structural (martensitic and premartensitic) transitions. As shown in Figs. 4 and 5, at martensitic transition temperature (T_m) the resistivity exhibits a pronounced jumplike behavior, while at premartensitic transition temperature (T_p) only change in the slope takes place.

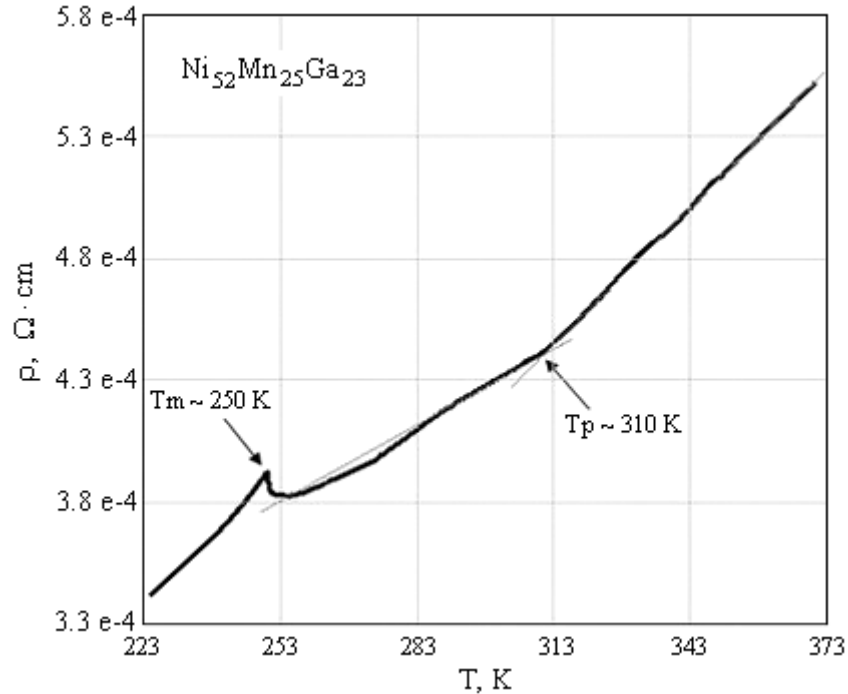


Fig.4 Resistivity as a function of temperature for the $\text{Ni}_{52}\text{Mn}_{25}\text{Ga}_{23}$ sample

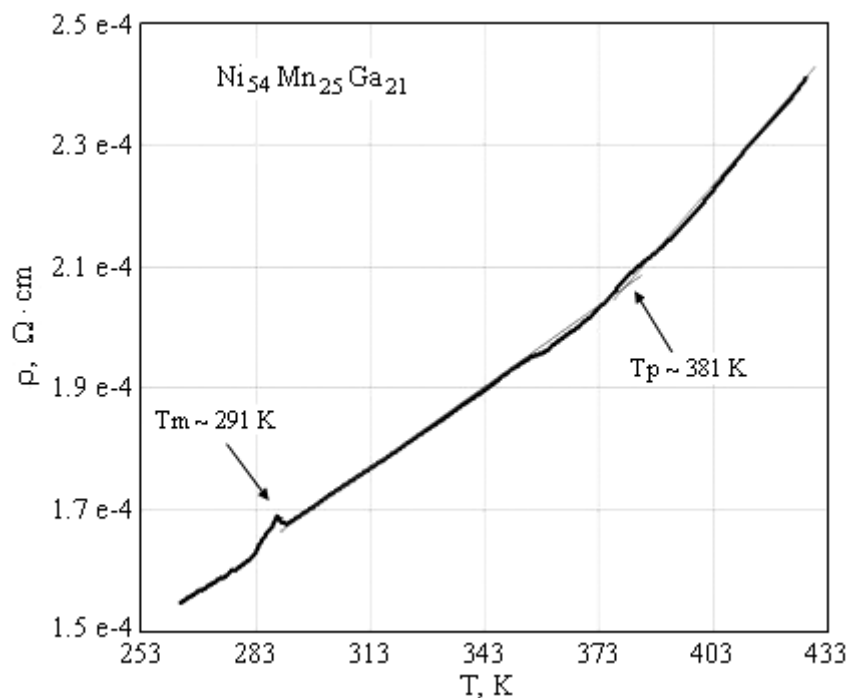


Fig.5 Resistivity as a function of temperature for the $\text{Ni}_{52}\text{Mn}_{25}\text{Ga}_{23}$ sample

In Table 2, martensitic and premartensitic transition temperatures determined by study of resistivity variation versus temperature are presented. For comparison there

are also shown structural transition temperatures values for $\text{Ni}_{50}\text{Mn}_{25}\text{Ga}_{25}$ stoichiometric alloy that were given in reference paper [3] and which were obtained by the same method.

Table 2 Structural transition temperatures for $\text{Ni}_{50+x}\text{Mn}_{25}\text{Ga}_{25-x}$ ($x = 0, 2, 4$) alloys

| Sample | Structural transition temperature | |
|--|-----------------------------------|---------------------------|
| | martensitic, T_m , K | premartensitic, T_p , K |
| $\text{Ni}_{50}\text{Mn}_{25}\text{Ga}_{25}$ [3] | 205 | 245 |
| $\text{Ni}_{52}\text{Mn}_{25}\text{Ga}_{23}$ | 250 | 310 |
| $\text{Ni}_{54}\text{Mn}_{25}\text{Ga}_{21}$ | 291 | 381 |

4. Conclusions

The martensitic transformation temperatures of the $\text{Ni}_{50+x}\text{Mn}_{25}\text{Ga}_{25-x}$ ($x = 0, 2, 4$) alloys monotonically increase with the increase of Ni substitution for Ga from around 205 K to 291K. In the same time, the premartensitic transition temperature arises from about 245 K to 381 K (see Fig.6).

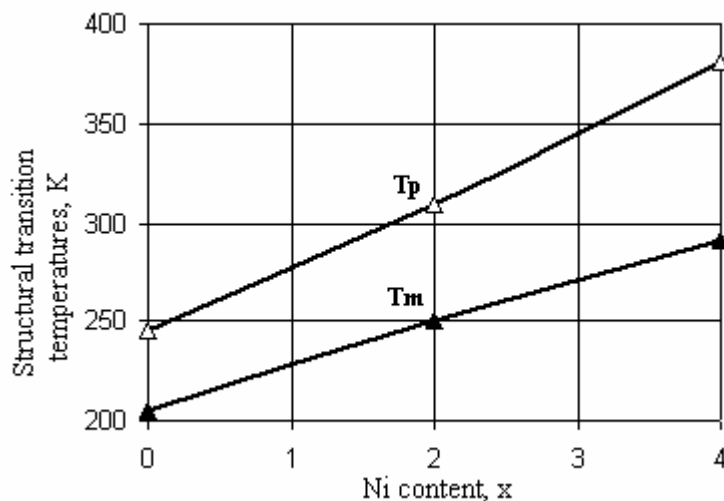


Fig.6 The structural transition temperatures T_m and T_p versus Ni content in $\text{Ni}_{50+x}\text{Mn}_{25}\text{Ga}_{25-x}$ ($x = 0, 2, 4$) alloys.

These experiments have proved that with increasing Ni content in stoichiometric $\text{Ni}_{50}\text{Mn}_{25}\text{Ga}_{25}$ Heusler compound, the structural transition temperature (T_m) increased significantly, and it can increase over the room temperature for higher Ni content. Also, it is interesting to study the evolution of the magnetic properties (magnetisation, Curie temperature) versus Ni content for $\text{Ni}_{50+x}\text{Mn}_{25}\text{Ga}_{25-x}$ ($x = 2, 4$) alloys.

Acknowledgements

This work is supported by Matnantech Program - Faculty of Industrial Chemistry Bucharest - by means of the research contract no. 159/2003.

REFERENCES

1. K. Ullakko, J. K. Huang, C. Kantner, R. C. O'Handley, and V. V. Kokorin, Appl. Phys. Lett. **69**, 1966 (1996)
2. Huibin Xu, Yunging Ma and Chengbao Jiang, Appl. Phys. Lett. **82**, 3206 (2003)

3. Gen Feng, Chengbao Jiang, Ting Liang and Huibin Xu, JMMM **248**, 312-317 (2002)
4. A. N. Vasil'ev, A. D. Bozhko and V. V. Khovailo, Phys. Rev. B **59**, 1113 (1999)
5. F. Zuo, X. Su, P. Zhang, G. C. Alexandrakis, F. Yang and K. H. Wu, J. Phys.: Condens. Matter **11**, 2821–2830 (1999)
6. F. Albertini, L. Pareti, A. Paoluzi, L. Morellon, P. A. Algarabel, M. R. Ibarra and L. Righi, Appl. Phys. Lett. **81**, 4032 (2002)

**PROPRIETĂȚI STRUCTURALE ȘI TEMPERATURI DE TRANSFORMARE
PENTRU UNELE ALIAJE NiMnGa POLICRISTALINE CU MEMORIA FORMEI**

Rezumat: Aliajele Heusler din sistemul Ni-Mn-Ga sunt materiale ce prezintă o transformare structurală de fază de ordinul I, reversibilă și ca urmare acestea prezintă efect de memoria formei. Punctele critice ale transformării martensitice depind puternic de compoziția aliajului. Pentru anumite aliaje NiMnGa cu conținut de Ni mai mare decât în Ni₂MnGa stoichiometric temperaturile de transformare sunt mult mai mari decât temperatura camerei, acestea atingând valori de ~ 250 °C.

În această lucrare se prezintă rezultatele investigațiilor structurii și punctelor de transformare ale unor aliaje Ni-Mn-Ga nestoichiometrice în stare policristalină. Investigațiile asupra structurii au fost efectuate prin difractometrie de raze X, utilizând radiația Cu K α , iar evidențierea temperaturilor de transformare martensitică și premartensitică s-a făcut prin studiul variației rezistivității electrice cu temperatura în intervalul 240 – 430 K. Probele au fost preparate prin topire sub arc electric în atmosferă de argon și apoi recoapte pentru omogenizare.

INFLUENCE OF TEMPERATURE AND STRAIN RATE ON MECHANICAL PROPERTIES OF A BORON STEEL

BY

DORU CANTEMIR^{a,b}, RENZO VALENTINI^b and MASSIMILIANO PAGLIARO^c

Abstract: Production of parts with high strength and light-weight is today the main target for automotive industries. New grade of high strength steel are used to realize parts with low thickness and high energy absorption capability. The weak formability of common high strength and ultra high strength steels is the major problem for their massive application. The boron steel is the best alternative in this field. The present paper is focused on the characterisation of a boron steel for hot forming process by means of hot tensile and hot compression tests. A series of tests have been conducted at temperatures of 820, 850 and 880 °C and strain rates of 0.1, 1 and 10 s⁻¹, using Gleeble 3800 thermo-mechanical simulator and the results are presented. The effects of temperature and strain rate on mechanical properties of the material are analysed and discussed.

Keywords: boron steel, mechanical properties, temperature influence, strain rate influence, hot tensile test, hot compression test, Gleeble 3800

1. Introduction

High-strength steel sheets (HSS) present some advantages that make them very attractive for automotive industry: improving of collision safety, reducing of automotive weight, contributing to fuel consumption reduction and, consequently, improving environmental problems [1-5]. With respect to light materials such Al, Mg and plastics, high-strength steel sheets have offer the benefit of using conventional forming technology without great investment. For these reasons, the use of HSS in automotive industry has significantly increased and an expansion in the range of its application is expected [4]. However, there are many factors hindering their broad application to automotive parts [2]: high production cost, poor formability, poor shape fixability, weldability problems etc.

An optimal solution is represented by the quench hardened boron steel which has good formability in as received conditions and allows very high strength levels to be obtained after heat treatment, with exceptional impact strength and fatigue resistance [3].

A boron steel for hot forming processing, produced by ILVA-Riva Group, Italy has been studied by means of various tests in order to determine the mechanical properties and to investigate its applications and in service behavior. In the present paper, the compression and tensile tests conducted at three temperatures, with three different strain rates are presented and the results are discussed. The effects of temperature and strain rate on material's mechanical properties are evaluated and the conclusions are included.

2. Experimental procedure

A 15 kg heat of steel was prepared by induction melting in argon protected atmosphere. The chemical composition is shown in Table 1.

Table 1 Chemical composition

| C | Si | Mn | P | S | Al | Cr | Cu | B | Ni | Fe |
|------|------|------|-------|-------|------|------|------|-------|------|------|
| 0.21 | 0.30 | 1.40 | 0.017 | 0.009 | 0.04 | 0.25 | 0.01 | 0.002 | 0.02 | bal. |

The material had been normalized in order to homogenize its properties. Specimens were made from the resulted ingots by cutting and machining to the required shape and size (Fig. 1 and Fig. 4).

A Gleeble 3800 thermo-mechanical simulator [6] was employed for hot compression and hot tensile tests and the strain-stress curves, along other parameters, were recorded. From engineering stress-engineering strain curves resulted during tensile tests the yield strength and tensile strength were determined, according to ASTM standard [7]. The specimen's length and diameter were measured before and after test. Using the maximum load recorded by the machine, F_{\max} , and the ultimate cross-section area, A_u , measured on the specimen, the true fracture stress is computed using the relation:

$$\sigma_f = \frac{F_{\max}}{A_u} \quad (1)$$

Reduction of area is calculated using the equation:

$$RA\% = \frac{A_0 - A_u}{A_0} \cdot 100 \quad (2)$$

where A_0 is the specimen initial cross-section area.

Hot compression tests (HCT) have been conducted at three different temperatures: 820, 850 and 880 °C and three different strain rates: 0.1, 1 and 10 s⁻¹. In order to avoid specimen oxidation, the specimens were tested in argon atmosphere. Specimens (Fig. 1) were heated up to 900 °C with a heating rate of 10 °C/s, were maintained at this temperature for 5 minutes and then cooled to the test temperature with a cooling rate of 10 °C/s. After compression, they were cooled with 10 °C/s to 600 °C and then to 200 °C with a cooling rate of 20 °C/s. The loading cycle is presented in Fig. 2.

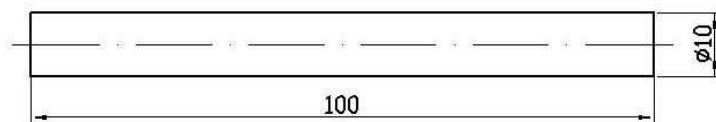


Fig. 1 Hot compression test specimen

Hot tensile tests have been conducted at the same temperatures (820, 850 and 880°C) and strain rates (0.1, 1 and 10 s⁻¹) as in the case of compression tests. Specimens were heated up to 900°C with a heating rate of 10 °C/s, maintained at this

temperature for 5 minutes, then cooled to the test temperature with a cooling rate of 10 °C/s. The loading cycle is shown Fig. 3 while the specimen is schematized in Fig. 4.

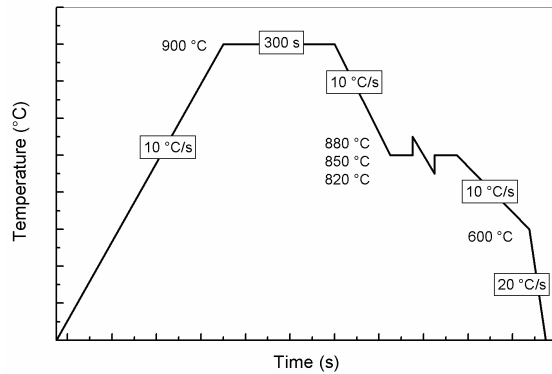


Fig. 2 Schematic diagram of testing cycle for HCT

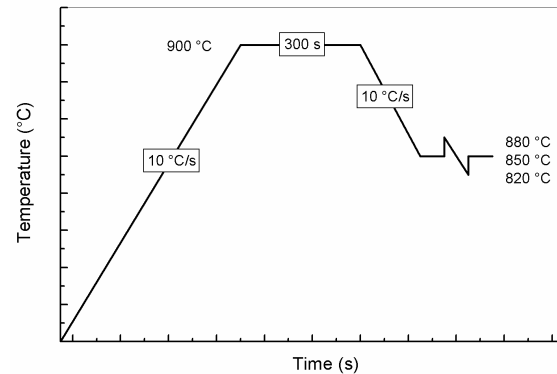


Fig. 3 Schematic diagram of testing cycle for HTT

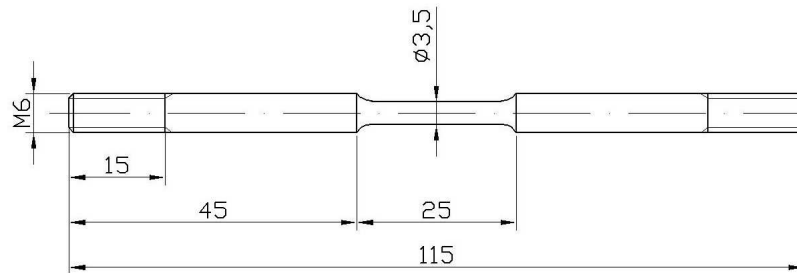


Fig. 4 Hot tension test specimen

Alumel thermocouples welded on the specimen central section were used for measurement and feedback control of specimen temperature. The specimen's longitudinal deformation during tests was measured using a LVDT type transducer mounted between machine's jaws. Since the system used for specimen holding is very stiff compared to the stiffness of the specimen, it is believed that the jaw-to-jaw measurements introduce little error in the elongation measurement.

3. Results and discussion

In Fig. 5, Fig. 6 and Fig. 7 the flow curves recorded during compression tests are depicted for a constant temperature, this way the effect of strain rate being visible. As could be seen, when the strain rate increase, the flow stress level is increasing too. The same thing is made for the engineering stress-engineering strain curves obtained by tensile tests, in Fig. 8, Fig. 9 and Fig. 10. A similar effect of strain rate on the curves can be noted. A further study was made in order to see the effects on the mechanical properties. The characteristics considered are yield strength, tensile strength, true fracture stress and reduction of area and the results are presented in Fig. 11 to Fig. 14.

From those results it is clear that by increasing the strain rate the tensile strength and yield strength are increasing, too, while the deformability is decreasing as well as the true fracture stress. However, this is right only in a limited range, as we well know from literature and from previous experience [8-10].

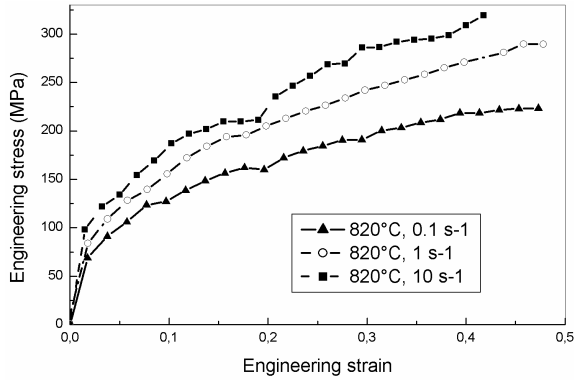


Fig. 5 Influence of strain rate on flow curves at 820°C

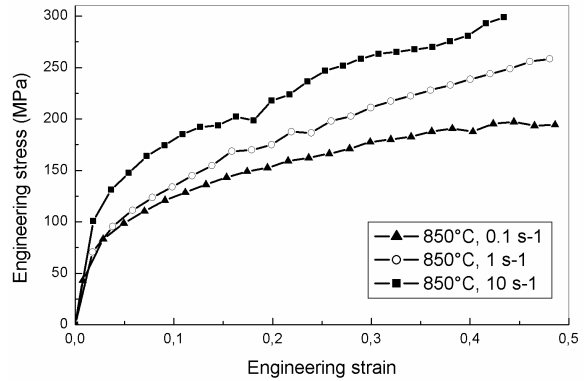


Fig. 6 Influence of strain rate on flow curves at 850°C

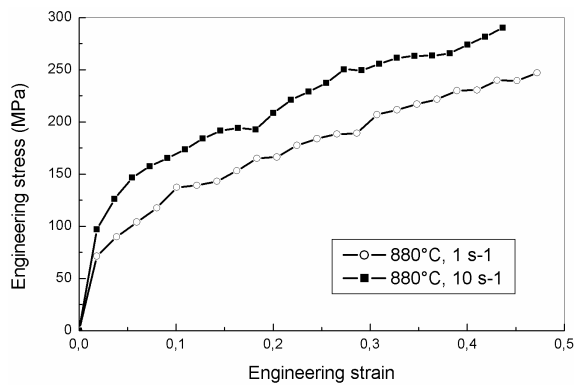


Fig. 7 Influence of strain rate on flow curves at 880°C

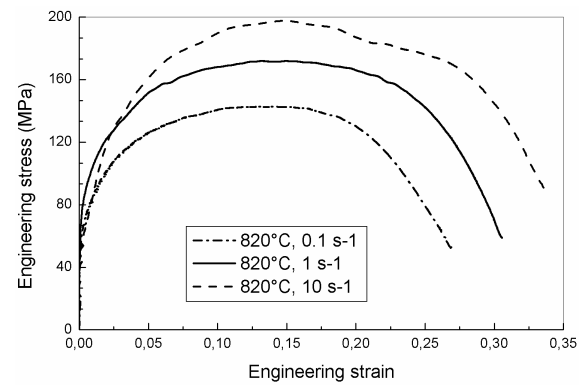


Fig. 8 Influence of strain rate on stress-strain curves at 820°C

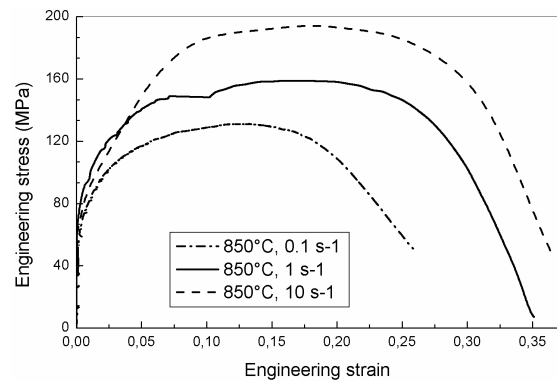


Fig. 9 Influence of strain rate on stress-strain curves at 850°C

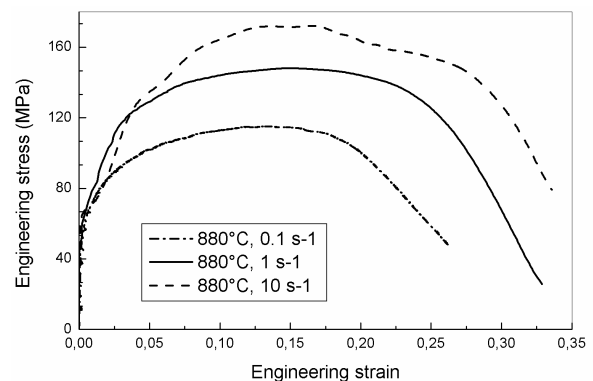


Fig. 10 Influence of strain rate on stress-strain curves at 880°C

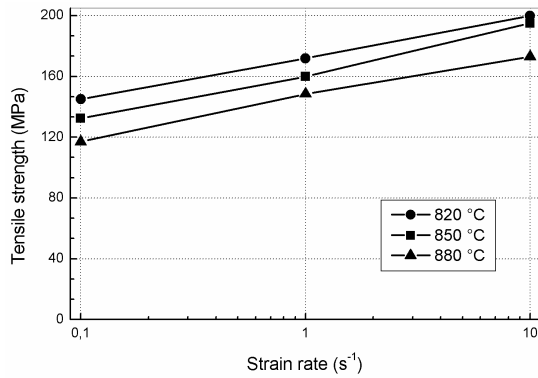


Fig. 11 Effect of strain rate on tensile strength

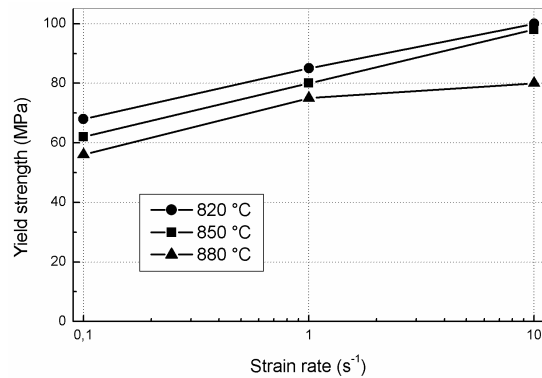


Fig. 12 Effect of strain rate on yield strength

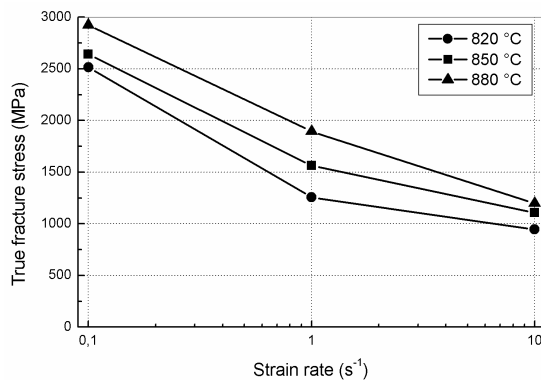


Fig. 13 Effect of strain rate on true fracture stress

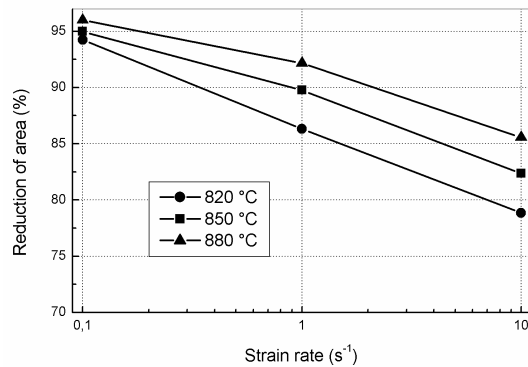


Fig. 14 Effect of strain rate on reduction of area

An analogous approach as in the case of strain rate influence study was applied to investigate the influence of temperature. The results are shown in Fig. 15 to Fig. 24. As could be seen, the effect of temperature is contrary to the one of the strain rate. The results are consistent with data from literature, for example Eriksson et al. [11].

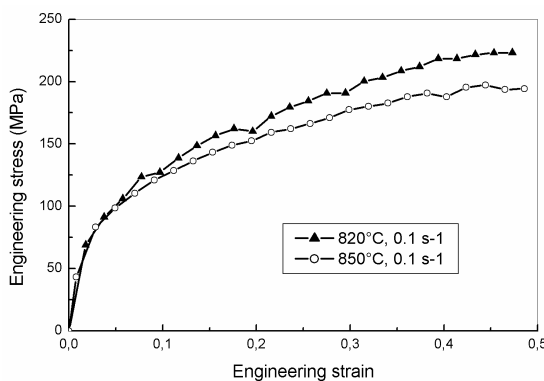


Fig. 15 Influence of temperature on stress-strain curves at a strain rate of 0.1 s^{-1}

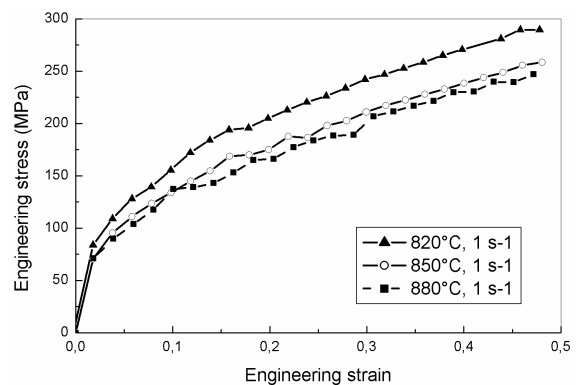


Fig. 16 Influence of temperature on stress-strain curves at a strain rate of 1 s^{-1}

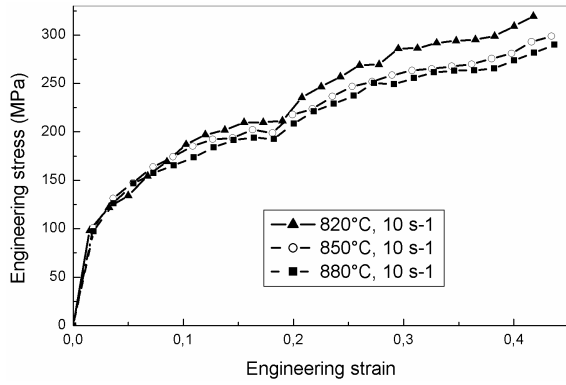


Fig. 17 Influence of temperature on stress-strain curves at a strain rate of 10 s^{-1}

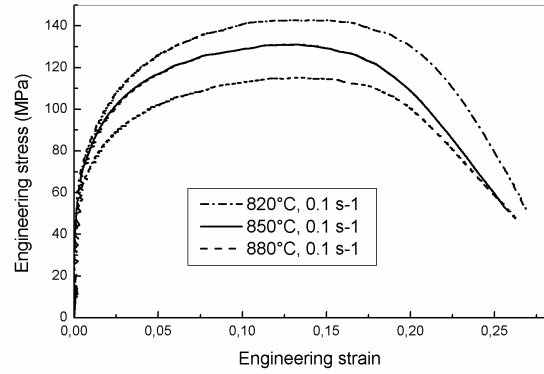


Fig. 18 Influence of temperature on stress-strain curves at a strain rate of 0.1 s^{-1}

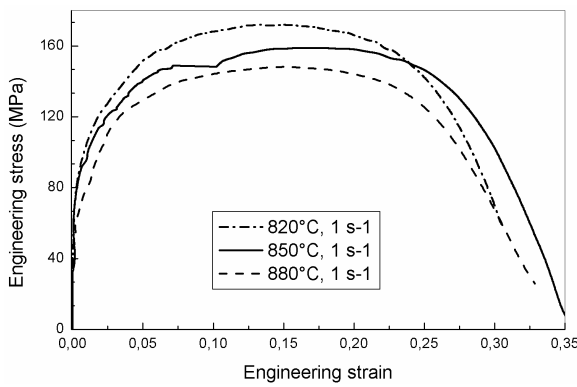


Fig. 19 Influence of temperature on stress-strain curves at a strain rate of 1 s^{-1}

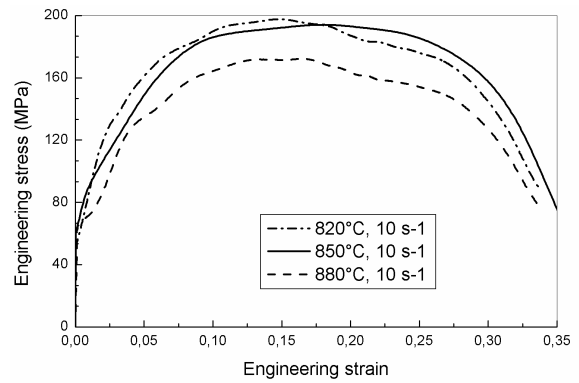


Fig. 20 Influence of temperature on stress-strain curves at a strain rate of 10 s^{-1}

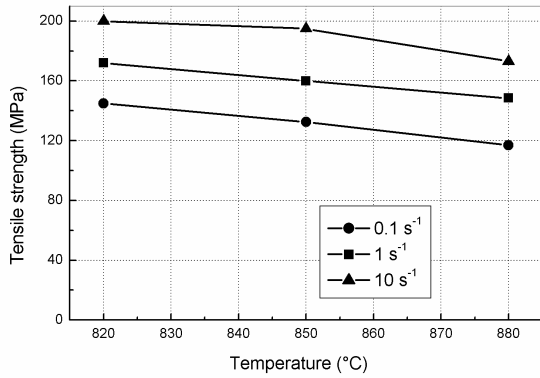


Fig. 21 Effect of temperature on tensile strength

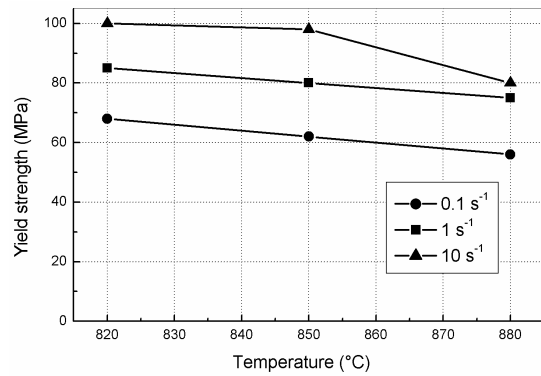


Fig. 22 Effect of temperature on yield strength

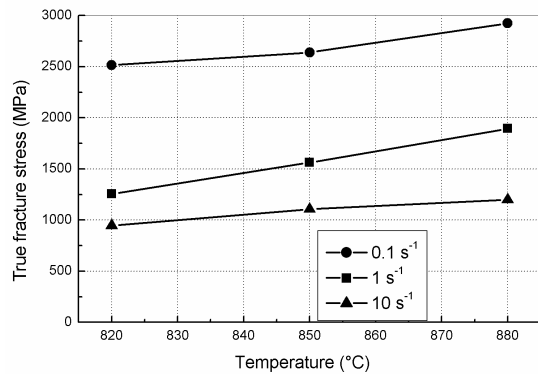


Fig. 23 Effect of temperature on true fracture stress

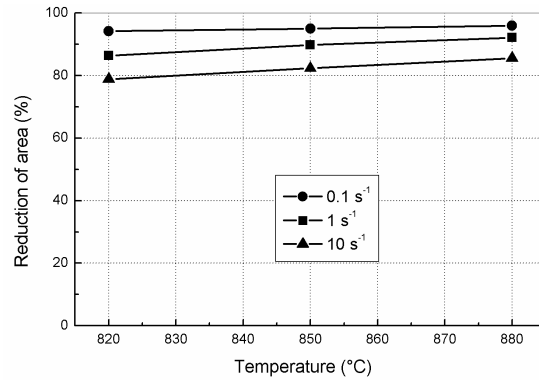


Fig. 24 Effect of temperature on reduction of area

4. Conclusions

A boron steel was produced in laboratory and its mechanical behavior was evaluated by means of hot tensile and hot compression tests at temperatures of 820, 850 and 880 °C and strain rates of 0.1, 1 and 10 s⁻¹. The results were processed in order to underline the effects of temperature and strain rate on the mechanical properties. It was seen that, in the studied temperature and strain rate range, the yield strength and tensile strength increase as strain rate increase, while the material ductility and true fracture stress decrease. The effect of temperature is contrary.

Acknowledgements

We thank Fabio Garelli for support in tests implementation. D. Cantemir acknowledges his Ph.D. grant from the University of Pisa, Italy.

Received April 20, 2005

^a“Gh.Asachi” Technical University Iași
^bUniversity of Pisa, Italy
^cILVA -Riva Group, Italy

REFERENCES

1. El-Kashif, E., Asakura, K., Shibata, K. - *Effect of cooling rate after recrystallization on P and B segregation along grain boundary in IF steels*, **ISIJ International**, 43, 12, 2003, **2007-2014**
2. Senuma, T. - *Physical metallurgy of modern high strength steel sheets*, **ISIJ International**, 41, 6, 2001, **520-532**
3. Jeanneau, M., Pichant, P. - *The trend of steel products in the European automotive industry*, **La Revue de Metallurgie**, 11, 2000, **1399-1408**
4. Takita, M., Ohashi, H. - *Application of high-strength steel sheets for automobiles in Japan*, **La Revue de Metallurgie**, 10, 2001, **899-909**
5. Suehiro, M., Kusumi, K., Miyakoshi, T., Maki, J., Ohgami, M. - *Properties of aluminium-coated steels for hot-forming*, **Nippon Steel technical report**, 88, 2003, **16-21**
6. Gleeble 3800 - Dynamic Systems Inc., <http://www.bleeble.com/Products/gleeble3800.htm>, 2004
7. ASTM Standard E 8m-95a - *Standard Test Methods for Tension Testing of Metallic Materials*, ASTM International, 1995
8. Marin, B, Jagintowicz, J. - *Effect of boron addition on the properties of ultra-low and low carbon steels*, technical report ECSC Steel RDT Project, Contract no. 7210-PR/355, 2004

9. Marin, B - *Optimisation of the influence of boron on the properties of steel*, technical report ECSC Steel RDT Project, Contract no. 7210-PR/355, 2005
10. Song, S.H. et al. - *Effect of boron on the hot ductility of 2.25Cr1Mo steel*, **Mat. Sc. Engng.**, A360, 2003, **96-100**
11. Eriksson, M., Oldenburg, M., Somani, M.C., Karjalainen, L.P. - *Testing and evaluation of material data for analysis of forming and hardening of boron steel components*, **Modelling. Simul. Mater. Sci. Engng.**, 10, 2002, **277-294**

INFLUENTA TEMPERATURII SI A VITEZEI DE DEFORMARE ASUPRA PROPRIETILOR MECANICE ALE UNUI OTEL ALIAT CU BOR

Rezumat: Una din principalele tendinte actuale in industria automobilelor este producerea de componente cu rezistenta mecanica ridicata si masa proprie redusa. Noi tipuri de otel sunt utilizate in vederea obtinerii de diverse repere matritate avand grosimi mici si capacitate ridicata de absorbtie a energiei mecanice. Principalul impediment in folosirea pe scara larga a otelurilor de inalta rezistenta este deformabilitatea redusa a acestora. Otelul aliat cu bor reprezinta o buna solutie la acesta problema deoarece are o deformabilitate buna si, in urma tratamentului termic, dobandeste si o rezistenta mecanica ridicata.

In aceasta lucrare sunt prezentate incercarile de tractiune si compresiune la temperaturi ridicate efectuate pentru determinarea proprietatilor mecanice ale unui otel aliat cu bor, elaborat in vederea matritarii la cald. Au fost efectuate o serie de probe la temperaturi de 820, 850 si 880 °C, cu viteze de deformare de 0.1, 1 si 10 °C/s. Sunt prezentate rezultatele si se discuta efectele temperaturii si a vitezei de deformare asupra caracteristicilor mecanice ale materialului.

CHARACTERIZATION OF LUBRICANT COATINGS

BY

ALINA VLADESCU¹, VIOREL BRAIC¹, MIHAI BALACEANU¹, MARIANA BRAIC¹,
ADRIAN KISS¹, COSMIN-MIHAI COTRUT²

Abstract: The goal of this study was to investigate the mechanical and tribological properties of lubricant coatings deposited on sliding shoes within radial bearings, in order to extend their life time. Ag, In and Sn films were prepared by vacuum evaporation, while In-Sn coatings were obtained by dc magnetron sputtering method in argon atmosphere. The characteristics of the films (thickness, adhesion and sliding friction coefficient) were determined by using various techniques (optical microscopy, scribe-grid and Amsler tests).

Keywords: lubricant coatings, vacuum evaporation, magnetron sputtering, friction coefficient

1. Introduction

Surface friction between various components and parts causes about 80%...90% of machine breakdowns. This fact forces us to constantly seek ways to lessen the effects of this phenomenon and to develop new and more effective methods of surface treatment.

As improving the life time of components is very important for industrial applications, in recent years there has been an increasing interest in achieving materials with good tribological properties, in particular low friction coefficients. Antifriction materials were successfully being used as lubricant coatings (2-20 μm), for which the most important coating characteristics are film adhesion and friction coefficient.

In the last years, interesting materials such as Ag, In, Sb, Cd, Sn, Pb, Te Mo, W, commonly characterized by a low friction coefficient and good adhesion, have attracted attention as possible candidates for antifriction coatings [1].

Our work was focused on In, Ag, Sn and In-Sn deposition. A significant advantage of these films is that they can be easily obtained by relatively simple and inexpensive experimental arrangements (e.g. vacuum evaporation or magnetron sputtering). Some mechanical and tribological properties (thickness, adhesion, friction coefficient) of these coatings deposited on sliding shoes within radial bearings were investigated.

2. Experimental procedure

Ag, In and Sn films, with thicknesses ranging from 8 to 20 μm , were prepared by vacuum evaporation, while In-Sn coatings - of the same thicknesses - were obtained by dc magnetron sputtering method in argon atmosphere (Fig.1). Details of the magnetron system were reported previously [2]. The coatings were deposited on Cu base alloy (Sn = 4.51%; Fe = 0.39%; Ni = 0.78%; Cu = 88.20%; Zn = 4.44% ; Pb = 1.67%). Ag, In and Sn evaporation was carried out at a basic pressure of about 10^{-5} mbar and substrate temperatures of 300°C , 160°C and 160°C , respectively. For the magnetron sputtering deposition of In-S, an argon pressure of 5×10^{-3} mbar and a substrate temperature of 150°C were chosen.

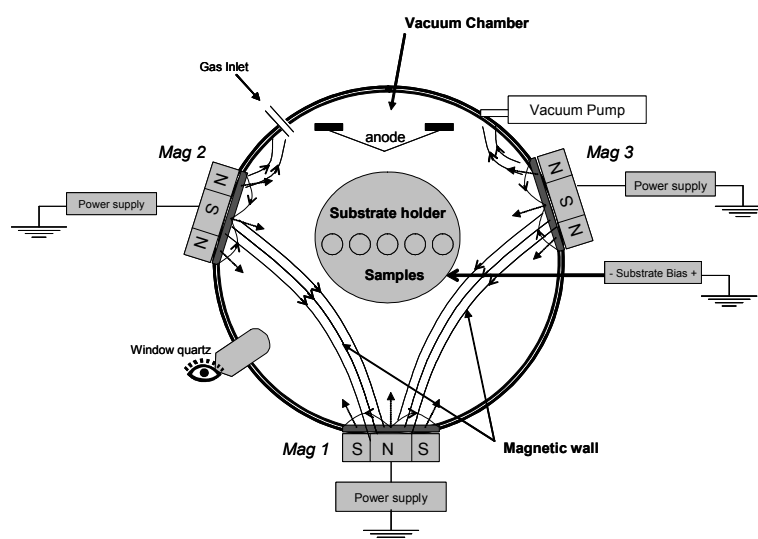


Fig. 1 Magnetron system

Scrib-grid tests were carried out to evaluate the coatings adhesion. The test consisted in scratching two or more parallel lines using a hardened steel tool ground to a sharp (30-deg) point, with a distance between the scribed lines approximately ten times the nominal coating thickness. In scribing the lines, we used sufficient pressure to cut through the coating to the substrate in a single stroke. If any portion of coating between the lines breaks away from the substrate, the adhesion is inadequate.

Film thickness was determined by optical microscope examination of the cross section through the coating.

Tribological behaviour of the coatings (sliding friction coefficient) was investigated by using the Amsler technique. The testing parameters used for tribological properties evaluation of all films were: environment – TK 21 oil, load – 10 daN and 25 daN, sliding speed – 0.4 m/s. Tribological performance was appreciated by the dependence of the friction coefficient on the sliding distance.

3. Experimental results and discussion

The thicknesses of the coatings were ranging between 8 and 20 μm . The scribe-grid test showed that the adhesion became worse with the increasing film thickness. The scratch test tracks for In-Sn and Ag thin films, with thickness of 8 μm , are illustrated in Figs. 2 and 3. The tracks obtained for the In-Sn films do not show film delamination, indicating a better adhesion.

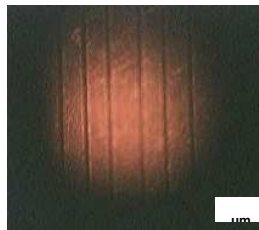


Fig. 2 Scratch test track for In-Sn coating

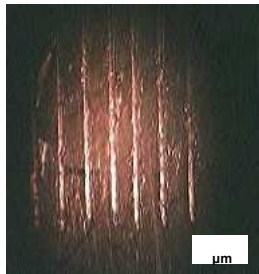


Fig. 3 Scratch test track for Ag coating

The dependences of the sliding friction coefficients (μ) on sliding distance (l), for each coating, at 10 daN, can be examined in figures 4 – 7. For comparison, the friction coefficient of the uncoated specimen is also illustrated.

It would be noticed that the coated samples exhibit lower friction coefficients than those of the uncoated specimen. The lowest μ values were observed for In-Sn layers. It can also be seen that the friction coefficients do not depend on the film thickness.

For some coatings, friction coefficients obtained at an applied load of 25 daN are shown in Fig. 8. In the case of Ag and Sn coatings, a partially delamination of the films was observed. In-Sn films exhibited the best behaviour.

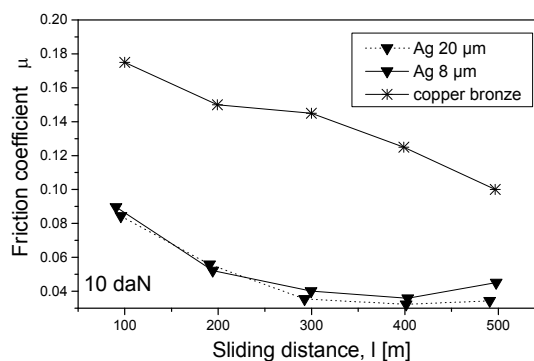


Fig. 4 Friction coefficient vs. sliding distance for Ag coatings (10 daN)

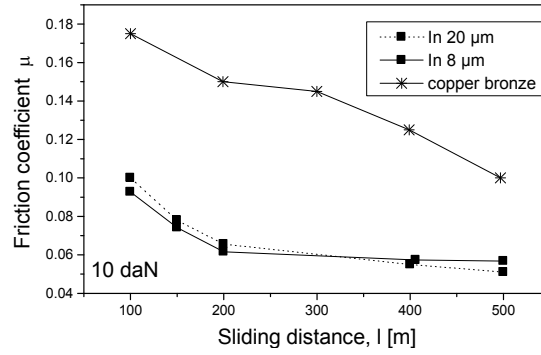


Fig. 5 Friction coefficient vs. sliding distance for In coatings (10 daN)

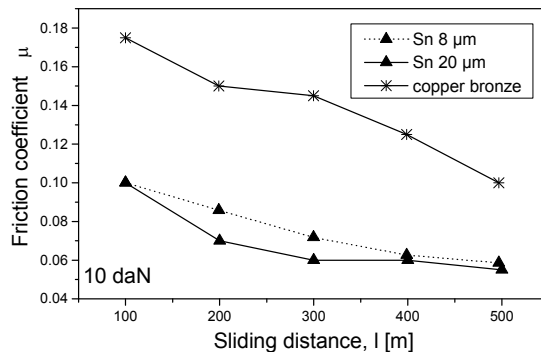


Fig. 6 Friction coefficient vs. sliding distance for Sn coatings (10 daN)

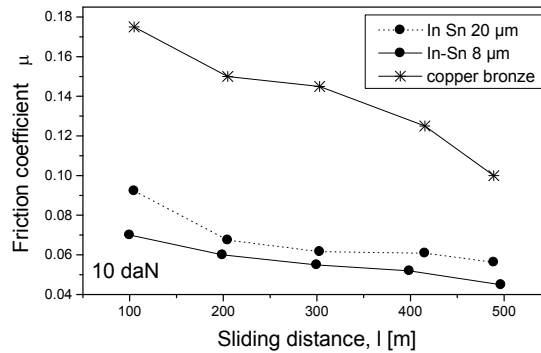


Fig. 7 Friction coefficient vs. sliding distance for In-Sn coatings (10 daN)

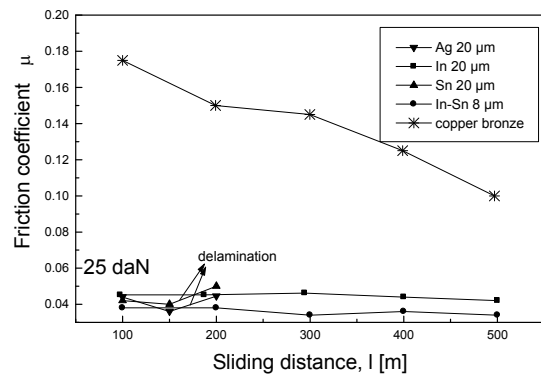


Fig.8 Friction coefficient vs. sliding distance for some coatings at 25 daN

4. Conclusions

The experimental research showed that the investigated coatings exhibited remarkable properties such as good adhesion and low friction coefficient, making them very useful as antifriction coatings for the sliding shoes.

The thicknesses of the coatings ranged between 8 and 20 μm . The scribe-grid test showed that the adhesion became worse with the increasing film thickness. The best adhesion was found for In-Sn films, followed by In, Sn and Ag.

It was observed that all coated samples exhibited lower friction coefficients than that of the uncoated specimen, whatever the load was used. The lowest values of the friction coefficient were observed for In-Sn layers. In the case of Ag and Sn coatings, a partial delamination of the films was observed at 25 daN load.

Acknowledgements

The work presented in this paper was supported by Romanian research project MATNANTECH 166/2003.

REFERENCES

- [1] Aurent F.D., Goodman S.D., Koschnick, J.M.Spaeth F.K., Beaumont B., Gibart G., *Appl.Phys.Lett.* **74**, 2172, 1999.
- [2] Balaceanu M., Braic V., Braic M., Pavelescu G., Vladescu A., *J.Optoel.Adv. Mat.* **5**, 1399, 2003.
- [3] Lungu C.P., Mustata I., Musa G., Lung AM., Zaroschi V., *Nanostructure influence on DLC-Ag tribological coatings*, Proc. 9th International Conference on Plasma Surface Engineering -September 13-17, Garmisch, Germany, 2004.

**ALINA VLADESCU¹, VIOREL BRAIC¹, MIHAI BALACEANU¹, MARIANA BRAIC¹,
ADRIAN KISS¹, COSMIN-MIHAI COTRUT²**

¹National Institute for Optoelectronics, Bucharest, PO Box MG 5 Bucharest-Magurele, RO

²Politehnica University of Bucharest, Spl. Independentei 313, Bucharest, 77206, RO

CARACTERIZAREA ACOPERIRILOR LUBRIFIANTE

Rezumat: Scopul prezentului studiu este acela de a investiga proprietatile mecanice si tribologice ale acoperirilor lubrifiante depuse pe sabotii oscilanti din componenta lagarelor radiale, in vederea cresterii timpului de viata. Straturile de Ag, In si Sn au fost depuse prin evaporare in vid, iar straturile de In-Sn a fost obtinute prin metoda pulverizarii magnetron dc in atmosfera de argon. Caracteristicile straturilor (grosime de strat, aderenta si coeficient de frecare) au fost determinate prin utilizarea a diverse tehnici (microscopie optica, teste Amsler si de aderenta).

CORROSION OF TiN COATINGS DEPOSITED ON CoCr ALLOY SUBSTRATES

BY

**ALINA VLADESCU¹, MIHAI BALACEANU¹, VIOREL BRAIC¹, MARIANA BRAIC¹,
RALUCA ZAMFIR²**

Abstract: TiN coatings were investigated as possible candidates to improve the performance of the dental implants and medical instruments used in dentistry. The biocompatible thin films were deposited on CoCr alloy substrates by cathodic arc evaporation in nitrogen atmosphere, under various deposition conditions. The chemical and phase composition, texture, hardness, adhesion and corrosion resistance of the resulting coatings were analyzed by EDX and XRD techniques, Vickers microhardness measurements, scratch testing and electrochemical polarization experiments.

Keywords: biocompatible thin films, TiN, cathodic arc,

1. Introduction

The recent rapid progress in biomedical requires materials of good mechanical properties and high resistance to wear and corrosion. These requirements can be satisfied by coating various implants, prosthesis or medical instruments with thin films having proper characteristics. Many transition metal nitride coatings, especially TiN, have achieved wide application in surface biomedical [1]. This is because these coatings exhibit many interesting properties such as high hardness, good wear and corrosion resistance, low friction and good electrical or thermal conductivity.

This article reports the deposition of biocompatible TiN films on CoCr alloy substrates using the cathodic arc technique. The influence of the main deposition conditions on the corrosion resistance of the coatings in artificial saliva was analyzed. In order to account for the corrosion behaviour of the coatings, some microchemical, microstructural and mechanical properties of the films prepared under various deposition parameters were also investigated.

2. Experimental procedure

The experimental setup has been described elsewhere [2]. The base pressure in the deposition chamber was of about 10^{-3} Pa. Specimens to be coated were ultrasonically cleaned with trichloroethylene and mounted on a rotating holder inside the deposition chamber. Prior to deposition, the samples were sputtered by Ti ion bombardment (1000 V; 5min).

The main process parameters for the various coatings were as follows: substrate material – CoCr alloy, cathode material - Ti; reactive atmosphere - N₂, nitrogen pressure $P_{N_2} = 5 \times 10^{-2} \div 8 \times 10^{-1}$ Pa, arc current $I_a = 60 \div 130$ A, substrate bias $V_s = 0 \div 220$ V; deposition time $t = 15 \div 60$ min.

To evaluate the corrosion behavior of the coatings, electrochemical measurements were carried out. The test consisted of potentiodynamic polarization from -2000 to +1100 mV with a scan speed of 20 mV/s of the coated samples in artificial saline (Table 1). The corrosion potential and current were measured by an Amel 2049 Potentiostat/Galvanostat. A saturated calomel electrode (SCE) and a platinum electrode were used as a reference and auxiliary electrodes, respectively. The pH and the temperature of the solution were kept constant at 7.4 and 25⁰C, respectively. The corrosion current and the critical current for passivation were used to compare the corrosion resistance of the coatings.

Table 1 The composition of artificial saline

| Compound | Composition (g/l) |
|----------------------------------|-------------------|
| K ₂ HPO ₄ | 0.200 |
| Na ₂ HPO ₄ | 0.260 |
| KSCN | 0.330 |
| NaHCO ₃ | 1.500 |
| NaCl | 0.700 |
| KCl | 1.200 |
| Uree | 0.130 |

The elemental composition of TiN films was determined by energy dispersive X-ray (EDX) analysis. EDX investigations were performed by means of a XL-30 – ESEM TMP scanning electron microscope.

Phase composition and texture were determined by XRD analysis using an X-ray DRON diffractometer with Cu K_α radiation.

Microhardness (Vickers) measurements were performed using a microhardness tester at 15g load. Film thickness was determined by optical microscope examination of the cross section through the coating. Scratch tests under standard conditions were undertaken to determine the coating adhesion.

3. Experimental results and discussion

The specimens for the corrosion tests consisted of TiN coated square plates (23x23x4mm) made of CoCr alloy, carefully polished. Potentiodynamic polarization curves in artificial saliva for the coatings are shown in Figs. 2 and 3, where the influence of nitrogen pressure and substrate bias on the film corrosion resistance can be examined. For comparison, the corrosion behaviour of an uncoated sample is also illustrated.

From the potentiodynamic curves, corrosion current densities (i_{corr}) and critical current densities for passivation (i_{cr}) were determined. It can be seen that the coatings improved the corrosion resistance of the uncoated specimens, by decreasing both the i_{corr} and i_{cr} currents. The measurements revealed that the nitrogen pressure has not significant influence on the corrosion behavior, while the increase of the substrate bias (in the range 15-220 V) resulted in an improvement of the corrosion resistance of the films.

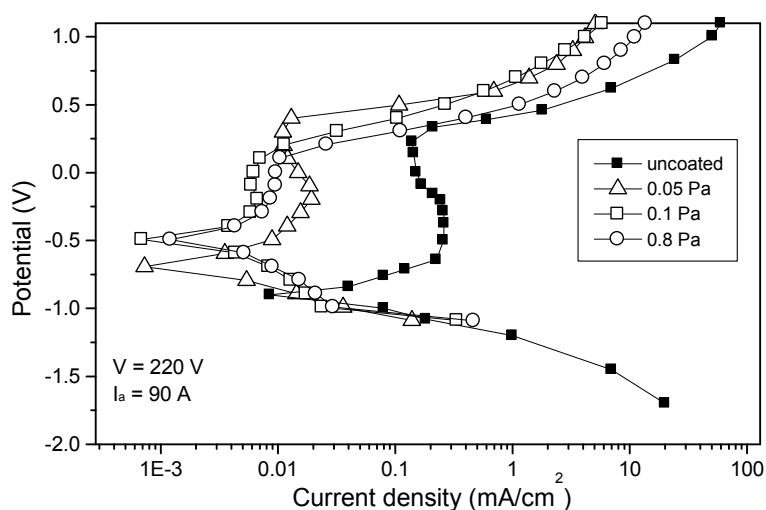


Fig.2. Polarization curves of TiN coatings deposited at different nitrogen pressures ($V_s = 220V$)

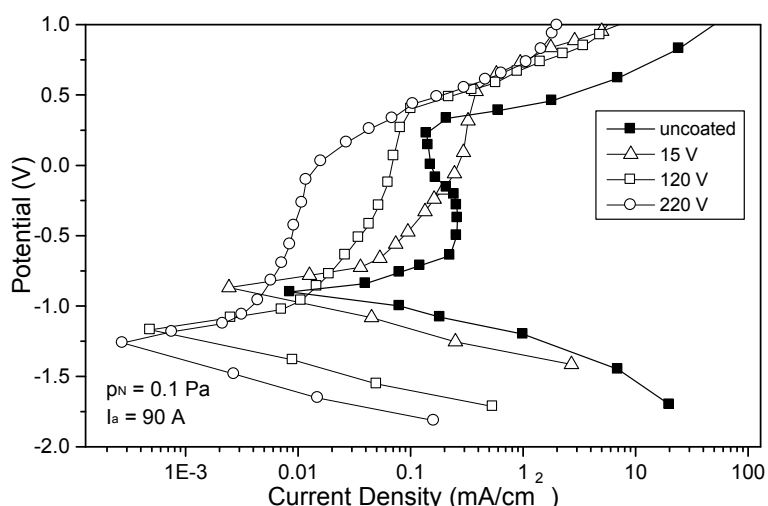


Fig.3. Polarization curves of TiN coatings deposited at different bias voltage ($p_{N_2} = 0.1Pa$)

The elemental composition of the coatings was obtained by EDX analysis (Table 2). The TiN showed that the N/Ti ratio was of about 0.68. The presence of oxygen is

mainly due to the film contamination, which is a typical phenomenon when coatings are exposed in atmosphere.

Table 2 Elemental composition of the TiN coating

| Coating | Elemental concentration (at.%) | | |
|---------|--------------------------------|-------|-------|
| | Ti | N | O |
| TiN | 52.96 | 36.26 | 10.78 |

X-ray diffraction analysis revealed that the films deposition for a nitrogen pressure ranging from 10^{-2} to 1 Pa consisted only of TiN phase ((111) and (200) diffraction peaks were detected).

As shown in Table 3, where the texture ($I_{(111)}/I_{(200)}$) of the coatings is presented, the films exhibit a (111) preferred orientation, which becomes stronger with the increasing N_2 pressure and substrate bias and does not depend on the arc current ($I_{(111)}/I_{(200)}=0.77$ for TiN random polycrystalline sample)

Table 3 Relative intensities of X - ray diffraction peaks for TiN coatings

| Deposition conditions | | | Texture for TiN $I_{(111)} / I_{(200)}$ |
|-----------------------|-----------|-----------|--|
| P_{N_2} (Pa) | V_s (V) | I_a (A) | |
| 5×10^{-2} | 220 | 90 | 4.14 |
| 1×10^{-1} | 15 | 90 | 4.70 |
| 1×10^{-1} | 120 | 90 | 5.43 |
| 1×10^{-1} | 220 | 90 | 6.64 |
| 8×10^{-1} | 220 | 90 | 9.22 |

The dependence of the Vickers microhardness ($HV_{0.015}$) on the main deposition parameters (N_2 pressure and substrate bias) revealed that the microhardness reaches its maximum value within a narrow range of the nitrogen pressure, from about 5×10^{-2} to 1×10^{-1} Pa. For a constant gas pressure, the microhardness increases with the substrate bias. The highest microhardness values ($\sim 3200 HV_{0.03}$) were obtained for N_2 pressures bellow 10^{-2} Pa.

The experiments carried out showed that the adhesion mainly depends on the film properties (thickness, microhardness), as it was already reported (e.g. [5]). The critical load increases with the film microhardness and thickness and with the substrate hardness. For a TiN layer with thickness and microhardness of about 2.5 μm and 2600 $HV_{0.02}$, respectively, critical loads of 38-44 N were measured. These values, compared with the data in literature, indicate an excellent adhesion that assures a good behaviour of various coated dental implants and medical instruments used in dentistry. Films with thickness from 2 to 4 μm were prepared for deposition times between 15 and 60 min.

4. Conclusions

These experiments have proved that the corrosion behaviour of CoCr alloy into artificial saliva can be improved by TiN thin film deposition prepared by cathodic arc deposition method. The increase of the substrate bias (in the range 15-220 V) resulted in an improvement of the corrosion resistance of the films.

Determination of the mechanical characteristics of the TiN coatings can predict, to a certain extent, the coating performance in various applications in dentistry. Vickers microhardness $HV_{0.015}$ and thickness values of about 2600 $HV_{0.02}$ and 2.5 μm , respectively, were measured. A good adhesion of the TiN coatings was found (critical loads of 38-44 N were obtained).

Acknowledgements

The work presented in this paper was supported by Romanian research project RELANSIN 1717/2003.

REFERENCES

- [1] Black S., "Biological performance of materials: fundamental of biocompatibility", 3rd edition, Ed. Dekker, New York, 1999.
- [2] Balaceanu M., Braic V., Macovei D., Genet M., Manea A., Pantelica D., Braic M., Negoita F., *J.Optoel.Adv.Mat.*, 4 (1), 2002, 107.
- [3] *Handbook of Vacuum Arc Science and Technology*, Ed.R.L.Boxman, D.M.Sanders, P.J.Martin, **Noyes Publications**, Park Ridge, N.J., U.S.A , 1995.
- [4] Vyskocil J., Musil J., *J.Vac.Sci.Technol. A* 10, 1992, 1740.
- [5] *Adhesion Measurement of Films and Coatings*, ed. **Mittal**, K.L., 1995, Utrecht.

**ALINA VLADESCU¹, MIHAI BALACEANU¹, VIOREL BRAIC¹, MARIANA BRAIC¹,
RALUCA ZAMFIR²**

¹National Institute for Optoelectronics, Bucharest, PO Box MG 5 Bucharest-Magurele, RO

²Politehnica University of Bucharest, Spl. Independentei 313, Bucharest, 77206, RO

COROZIUNEA STRATURILOR TiN DEPUSE PE SUBSTRATURI DE ALIAJ CoCr

Rezumat: Au fost investigate straturi de TiN, ca posibila solutie pentru imbunatatirea performantelor implanturilor dentare si a instrumentarului utilizat in stomatologie. Straturile subtiri biocompatibile de TiN au fost depuse pe substraturi din aliaj de CoCr prin metoda de evaporare cu arc catodic in atmosfera reactiva de azot, pentru diferite conditii de depunere. Straturile depuse au fost analizate din punct de vedere al compozitiei elementale si fazice, texturii, duritatii, aderenței si rezistenței la coroziune prin utilizarea tehnicilor EDX si XRD, masuratori de microduritate Vickers, teste de aderența si electrochimice.

CHARACTERIZATION OF PHOSPHOGYPSUM BY PHYSICAL AND CHEMICAL METHODS

BY

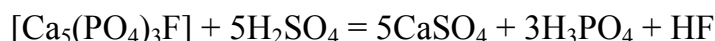
Nicolae Foca¹, Daniel Mareci², Catalin Bocanu² and Al. Tofan¹

Abstract: The phosphogypsum represents a residuum accumulated in large quantities, altering the environment. In the paper there are presented data regarding the phosphogypsum behaviour in water. Also, the pH of different phosphogypsum samples in distilled water were determined. The main components of phosphogypsum were identified using chemical methods of analysis. The thermal treatment of phosphogypsum was performed in the temperature range 105⁰C-1000⁰C. The samples calcined at 1000⁰C were studied by IR spectrometry. The radioactivity of phosphogypsum, given by the content of U₃O₈ was determined using a Geiger-Muller counter. Based on the experimental data, one establishes the structure, properties and the directions of utilization for the phosphogypsum.

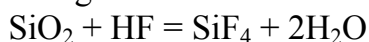
Keywords: phosphogypsum properties, IR spectrometry, chemical analysis

1. Introduction

At the industrial scale, the phosphoric acid is obtained usually in a process that consists on principle in the next main chemical reaction:



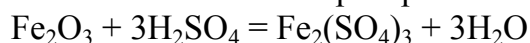
Besides the main reaction, presented earlier, there are reactions of decomposing of other minerals contained in calcium tri-phosphate as impurities. Thus, the silicium dioxide (SiO₂) reacts with HF, following the reaction:



The silicium tetra-fluoride is a volatile compound, but in solution it forms H₂[SiF₆]. The calcium carbonate CaCO₃, in contact with sulfuric acid is decomposed as CaSO₄, CO₂ and H₂O:



Also, other impurities react with sulfuric and phosphoric acid:



After the reaction between the raw material and sulfuric acid takes place, the solution will contain in a high percent the ions Fe²⁺, Fe³⁺, Al³⁺, Na⁺, K⁺, F⁻ and a reduced quantity of SiO₂. Filtrating the solution results a precipitate (phosphogypsum) insoluble in water. It contains in main CaSO₄ and a part of the minerals that did not decompose totally [1].

Besides CaSO₄, the main component, phosphogypsum contains a low quantity of SiO₂ resulted from aluminium-silicates, clays or dolomite.

In the present paper are presented data regarding the physical and chemical properties of phosphogypsum resulted in the fabrication process of phosphoric acid at the Chemical Factory Soffert-Bacau (Romania). The study was realized in order to obtain certain information regarding the possibility of using this residuum in civil engineering or other directions.

2. Experimental procedure

Two types of phosphogypsum samples were analyzed: both from the production line and samples washed with distilled water for the removal of the acidity given by the presence of the acids H_2SO_4 , H_3PO_4 , HF and $H_2[SiF_6]$, retained in the precipitate resulted from chemical process.

The behavior of phosphogypsum in water was studied by monitoring the variation of pH using a Consort C831 system connected to a personal computer.

A thermal treatment was realized for phosphogypsum in the temperature range $115..1000C^0$ to establish it's heating behavior. The calcined samples were analyzed by IR spectrometry. The radioactivity of phosphogypsum, given by the content of U_3O_8 was determined using a Geiger-Muller counter.

The chemical characterization of phosphogypsum was performed on the basis of the standard methods of analysis.

3. Experimental results and discussion

The phosphogypsum contains volatile substances, respectively HF, HCl, SO_3 , that are evacuated together with water, generating errors in chemical analysis. The measuring of the phosphogypsum initial humidity could decrease the errors for the components determination.

Six phosphogypsum samples were maintained for 72 hours at a constant temperature of $50 C^0$. Recording the mass variation of each sample, the relative humidity values expressed in percents (%) were calculated. They are presented in

Table 1: The relative humidity of phosphogypsum samples

| Sample Number | Sample mass (g) | Drying time (h) | Drying temperature (0C) | Relative humidity (%) |
|---------------|-----------------|-----------------|------------------------------|-----------------------|
| 1 | 10 | 72 | 50 | 2.210 |
| 2 | 10 | 72 | 50 | 0.069 |
| 3 | 10 | 72 | 50 | 0.064 |
| 4 | 10 | 72 | 50 | 0.440 |
| 5 | 10 | 72 | 50 | 0.067 |
| 6 | 10 | 72 | 50 | 3.580 |

The distribution of relative humidity values in a large range shows a high material non-uniformity.

The acidity of phosphogypsum was determined by mixing equal quantities from each of the six samples with distilled water in the ratio material/water = 1/5. The

solutions pH was recorded for a time interval of 24 hours and the values are given in Table 2.

Table 2: The pH of the aqueous solutions of phosphogypsum samples

| Sample Number | Sample mass (g) | Distilled water volume (mL) | Contact time (h) | pH |
|---------------|-----------------|-----------------------------|------------------|------|
| 1 | 10 | 50 | 24 | 2.15 |
| 2 | 10 | 50 | 24 | 2.60 |
| 3 | 10 | 50 | 24 | 2.65 |
| 4 | 10 | 50 | 24 | 2.45 |
| 5 | 10 | 50 | 24 | 2.85 |
| 6 | 10 | 50 | 24 | 2.30 |

From the Table 2 results that the recorded pH values indicate a pronounced acidic character of the phosphogypsum, from this point of view being very toxic for the environment.

The phosphogypsum resulted in the H_3PO_4 synthesis process was analyzed chemically determining the content of Si, S, Ca, Mg, Fe, Al and P. The amount of each of the elements mentioned earlier was measured experimentally for two samples with different acidity and then expressed numerically as mass percent of corresponding oxides (Table 3).

Also, the concentration of fluoride ions F^- in phosphogypsum was established in case of the same two samples: for the less acidic sample (pH = 2.85) %F = 0.21 and for the sample with a higher acidity (pH = 2.15) %F = 0.85.

The methods of chemical analysis used are presented in Table 4.

Table 3: The amount of main elements in phosphogypsum

| Sample Number | Mass percent of the elements oxides (%) | | | | | | | pH |
|---------------|---|--------------------------------|--------------------------------|-------|------|-----------------|-------------------------------|------|
| | SiO ₂ | Fe ₂ O ₃ | Al ₂ O ₃ | CaO | MgO | SO ₃ | P ₂ O ₅ | |
| 1 | 0.78 | 0.055 | 0.18 | 33.00 | 1.48 | 45 | 0.65 | 2.85 |
| 2 | 0.90 | 0.060 | 0.15 | 32.11 | 1.44 | 45.15 | 1.62 | 2.15 |

Table 4: The methods of analysis used for the determination of main elements

| Element | Method of analysis | Reference |
|---------|----------------------------|-----------|
| Si | Gravimetric | [2] |
| Fe | Titration with EDTA | [2] |
| Al | Titration with EDTA | [2] |
| Ca | Precipitation | [2] |
| Mg | Gravimetric and volumetric | [2] |
| S | Precipitation | [2] |
| P | Gravimetric | [2] |

Analyzing the data presented in Table 3 results that in the samples investigated the elements have almost the same concentration, excepting P. The content of phosphogypsum in P, as well as the fluoride ions concentration increases with the acidity of the sample. In conclusion, the acidity of phosphogypsum is determined in principal by the content of phosphoric acid and hydrofluoric acid.

The phosphogypsum samples non-uniformity is caused by the different retention of the phosphoric acid and HF in the precipitate in the process of maturation.

After the chemical analysis, the phosphogypsum was heated in the range of temperature 105..1000 °C. Mass loss of the samples, corresponding to various temperatures was established. Experimentally, one finds that in the range 900..1000°C at a constant mass, the material changes its color. The color modify may be determined by various chemical reactions or physical transformation that could affect the phosphogypsum structure. In a previous paper [3], the IR patterns of the samples calcined at 1000 °C were presented. From the IR spectra results that the calcined samples suffer structure modification due to the existing chemical reactions at this temperature.

The raw material used in the synthesis of the phosphoric acid contains uranium oxide and a high concentration of this compound is founded in phosphogypsum [4]. The uranium oxide (U_3O_8) causes the radioactivity of the phosphogypsum. The experimental determination of the phosphogypsum samples radioactivity shows values of 3-4 times higher than the cosmic background. The increased radioactivity suggests that the phosphogypsum could not be used as a material in civil engineering or other fields.

4. Conclusions

The phosphogypsum has a pronounced acidity and an increased radioactivity. As a consequence, it is a pollutant for the air, water and soil.

The phosphogypsum non-uniformity causes a different behavior to the heating. Due to the existing chemical reactions at the heating temperature, the structure of phosphogypsum is modifying, resulting that the material is thermal unstable.

The results of this study show the impossibility of phosphogypsum use in civil engineering or in the synthesis of other inorganic substances of practical use.

REFERENCES

1. Moutaouakil, A., Pineau, J.L. and Bouahaouss, A. – *Les possibilité d'une valorisation du phosphogypse provenant de l'industrie phosphatière marocaine*, **Les Techniques de l'Industrie Minérale**, **12**, 2001, **104-110**
2. Furman, N., *Standard Methods of Chemical Analysis*, New York, 1963, **212-246**
3. Foca N., Oancea, S., Mareci, D. and Airinei, A., - *Etude Physique et Chimique du Phosphogypse Resultant du Procédé de Fabrication de l'Acide Phosphorique*, **Colloque Franco-Roumain de Chimie Appliquée, Slanic Moldova, Bacau, Romania**, 22-24 September 2004
4. Smith, J.T., Comans, R.N.J., Beresford, N.A., Wright, S. M., Howard, B. J., and Camplin, W.C. – *Chernobyl's Legacy in Food and Water*, **Nature**, **24(1)**, 2004, 107-112

¹ Technical University Gh. Asachi Iasi, Faculty of Industrial Chemistry, Inorganic Chemistry Department

² Technical University Gh. Asachi Iasi, Faculty of Industrial Chemistry, Physical Chemistry Department

CARACTERIZAREA FOSFOGIPSULUI PRIN METODE FIZICE ȘI CHIMICE

Rezumat: Fosfogipsul este un reziduu acumulat în cantități mari, care alterează mediul înconjurător. În această lucrare sunt prezentate date privind comportarea fosfogipsului în apă. De asemenea, s-a determinat pH-ul pentru diferite probe de fosfogips în apă distilată. Prin metode chimice de analiză s-au pus în evidență cantitativ principalii componenți ai fosfogipsului. S-a realizat și un tratament termic pentru probele de fosfogips luate în lucru în intervalul de temperatură 105⁰C-1000⁰C. Probele calcinate la 1000⁰C au fost studiate prin spectroscopie IR. Radioactivitatea fosfogipsului, dată de conținutul în U₃O₈ a fost determinată cu ajutorul unui counter Geiger-Muller. Pe baza acestor date experimentale se pot stabili : structura, proprietățile și direcțiile de utilizare ale fosfogipsului.

POLYESTERS BASED ON EPICLON

BY

CAMELIA HULUBEI and ELENA HAMCIUC

Two new polymers have been synthesized by solution polycondensation reaction from a dicarboxylic acid containing imide rings based on EPICLON, [5-(2,5-dioxotetrahydrofurfuryl)-3-methyl-3-cyclohexyl-1,2-dicarboxylic acid anhydride], with biphenyl-4-4'- diol and phenolphthalein, respectively. The polymers were characterized by infrared and proton nuclear magnetic resonance spectroscopy. Thermal properties of the new synthesized copolymers were studied by thermogravimetric analyses and differential scanning calorimetry.

Keywords: polyesters; polyimides; thermal behavior

1. Introduction

The aromatic polyesters (polyarylates) possess high thermal stability and excellent mechanical properties [1]. However, their processing into articles is limited due to the high melting or softening temperatures, which are often close to those of decomposition [2]. Also, their poor solubility in most organic solvents make necessary to develop new chemical structures with the simultaneous preservation of their special mechanical properties and a favorable balance between solubility, thermal stability and processability [3, 4].

On the other hand, polyimides are important, both scientifically and commercially, because of their combination of outstanding key properties, including thermal, thermo-oxidative stability, high mechanical strength, high modulus, excellent electrical properties, and superior chemical resistance [5-7].

Generally, it is known that one of the successful approaches to increase the solubility and processability, of aromatic polyesters, without sacrificing high thermal stability, is the introduction of bulky and unsymmetrical groups, flexible bonds, large pendent or polar substituents into the polymer backbone [8-10].

Therefore, it is expected that the combination of imide units, aromatic rings, flexible ester bonds and epiclon moieties (a cycloaliphatic anhydride with flexible and asymmetrical structure) in one macromolecule, would develop new synthetic polyesters offering a compromise between processability and physical and thermal characteristics. Epiclon has been used as raw material for polyimides resins to enhance the solubility and to render other new properties [11,12].

The new polyesters reported in this paper were prepared by using direct polycondensation reaction of certain diphenols with an epiclon-based diacid, namely 5-[N-(4-carboxyphenyl)succinimido]-3-methyl-[N-(4-carboxyphenyl)]-1,2,5,6-

tetrahydrophthalimide. The reactions were performed at ambient temperature, with dicyclohexylcarbodiimide (DCC) as an activating agent and 4-(dimethylamino)pyridinium-4-toluenesulfonate (DPTS) as catalyst. The products have been characterized from the view point of their chemical structure and thermal behavior.

2. Experimental

Materials

Epiclone B-4400, [5-(2,5-dioxotetrahydrofurfuryl)-3-methyl-3-cyclohexyl-1,2-dicarboxylic acid anhydride], *p*-aminobenzoic acid, *p*-toluenesulfonic acid (PTS), glacial acetic acid, biphenyl-4-4'-diol, phenolphthalein, dicyclohexylcarbodiimide (DCC), 4-(dimethylamino)pyridine (DMAP) and pyridine were provided by different commercial sources and used as received. Dimethylformamide (DMF) was dried before using, by standard methods. The catalyst, 4-(dimethylamino)pyridinium-4-toluenesulfonate (DPTS), was synthesized according to [13].

Methods

The IR spectra were recorded on a Specord M80 Carl Zeiss Jena Spectrophotometer by using the KBr pellet technique.

¹H-NMR spectra were run on a Jeol 60 MHz ¹H-NMR spectrometer at 50 °C in DMSO-d₆.

Polymer solubilities were determined at room temperature at a concentration of 1%(w/v).

Thermogravimetric analysis (TGA) was carried out dynamically in air, with an F. Paulik Derivatograph at a heating rate of 12 °C/min. The initial decomposition temperature (IDT) is characterized as the temperature at which the sample achieves a 5% weight loss. The temperature of 10% weight loss (T₁₀) was also recorded.

Differential scanning calorimetry (DSC) measurements were done by using a Mettler TA instrument DSC 12E at a heating rate of 12 °C/min under nitrogen atmosphere, with the glass transition temperature (T_g) taken as the inflection point of the heat capacity versus temperature.

Synthesis of the dicarboxylic acid (I)

The preparation of dicarboxylic acid (I), 5-[N-(4-carboxyphenyl)succinimido]-3-methyl-[N-(4-carboxyphenyl)]-1,2,5,6-tetrahydrophthalimide, was carried out in a round-bottom flask equipped with a condenser, CaCl₂ drying tube, magnetic stirrer and heating source. 5.48 g (0.04 mol) of *p*-aminobenzoic acid and 52 mL of glacial acetic acid were placed in the flask and 5.28 g (0.02 mol) of Epiclone was added with rapid stirring. The reaction mixture was heated at reflux for 10 h. The resulting white product was filtered, washed with ethanol and dried (scheme 1). Yield 65 %; m.p. 311-314 °C.

Elemental analysis: calculated for C₂₇H₂₂N₂O₈: C, 64.54 %; H, 4.38 %; N, 5.57 %. Found: C, 64.29 %; H, 4.64 %; N, 5.22 %.

IR spectrum (KBr, cm^{-1}): 3100-2800 (-OH stretching); 1780 (imide carbonyl symmetric stretching); 1720 (imide carbonyl asymmetric stretching and carboxylic C=O); 1390 (C-N stretching); 730 (imide ring).

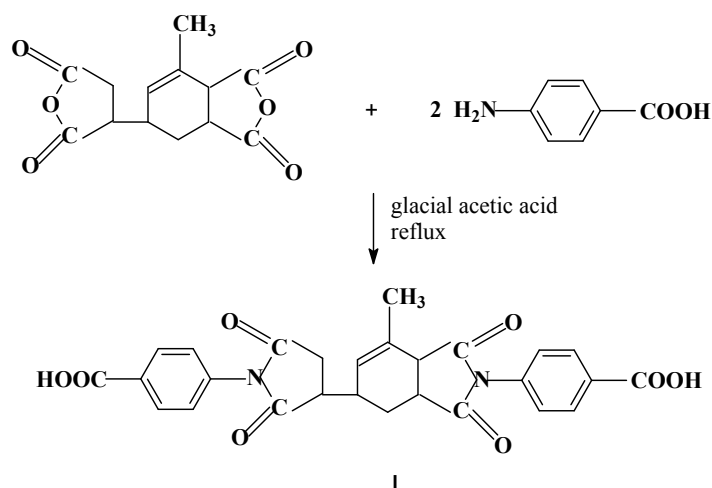
$^1\text{H-NMR}$ spectrum (60 MHz, DMSO-d_6 , TMS, δ , ppm) (figure 2): 7.42 – 8.23 (m, 8H), 5.56 (s, 1H), 2.74 – 3.62 (m, 8H), 1.87 (s, 3H).

Synthesis of the epiclone-containing polyesters (III)

The polyesters were prepared by direct solution polycondensation, at ambient temperature. A typical example is the follow: 0.7035g of diacid **I** (1.4mmol) were placed in a reaction vessel and dissolved in 5mL of dry DMF. Then, 0.4456g of phenolphthalein (1.4mmol of **IIb**) and 0.7828g of DCC, separately dissolved in a minimum quantity of dry DMF, were added. The catalyst, DPTS, 0.0847g (0.288mmol), was introduced at the end. The reaction was stirred at room temperature, under inert atmosphere, for 96 hours. The dicyclohexylurea (DCU) formed in reaction was filtered off, and the remained solution was poured into a water/methanol mixture 1/1. The resulting crude product was washed several time with water and methanol, and dried. To remove the remained DCU traces, the product was stirred with acetic acid for an hour, washed with water, dried and then, extracted with ethanol. Yield: 71%.

3. Results and Discussion

In order to obtain a favorable balance between processability, physical and thermal characteristics, new polyesters based on Epiclone have been synthesized. The synthetic chemistry for the dicarboxylic acid is outlined in Scheme 1.



Scheme 1. Synthesis of the dicarboxylic acid **I**

Figure 1 shows the $^1\text{H-NMR}$ spectrum for the obtained epiclone-containing diacid. The peak at about 5.6 ppm was assigned to the vinylic proton, while the multiplet at 2.74 – 3.62 ppm was associated with the resonance values of the methylene and methine protons in the succinimide and the unsaturated rings of the structure. The chemical

shift of the carboxylic acid protons are difficult to see, being very close to the water protons.

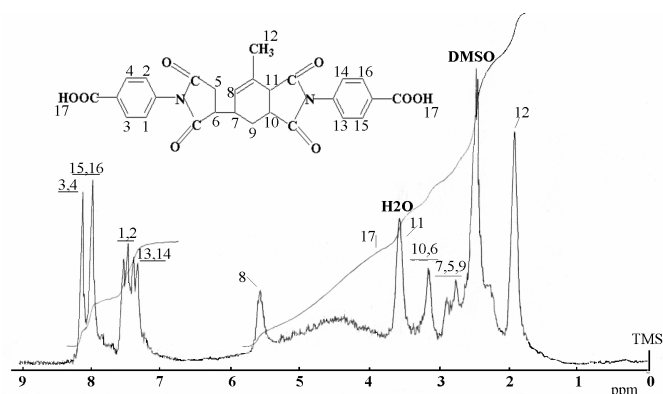
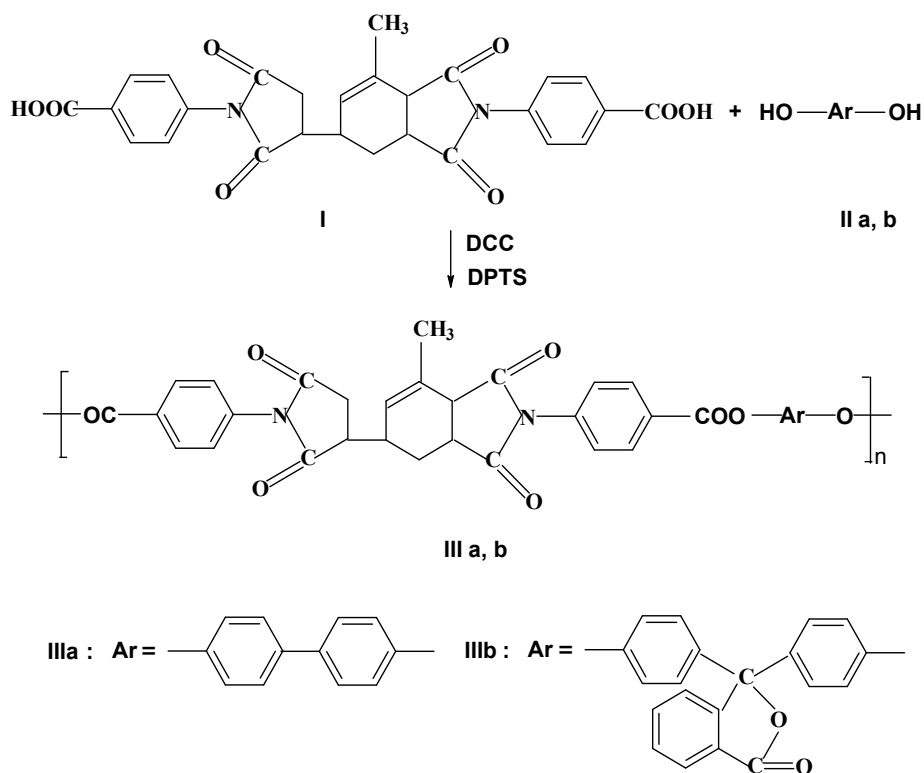


Figure 1. $^1\text{H-NMR}$ spectrum of the dicarboxylic acid **I**, 5-[N-(4-carboxyphenyl)succinimido]-3-methyl-[N-(4-carboxyphenyl)]-1,2,5,6-tetrahydrophthalimide, in DMSO-d_6 at room temperature

Polycondensation of equimolar amounts of dicarboxylic acid **I** and diphenols (biphenyl-4-4'-diol and phenolphthalein, respectively) in DMF, at room temperature, yielded solutions of poly(imide-ester)s **III** (scheme 2).



Scheme 2. Preparation of the polyesters **III**

The structure of polymers was identified by IR and $^1\text{H-NMR}$ spectroscopy. Strong bands at 1780 cm^{-1} and 1720 cm^{-1} are commonly attributed to the symmetrical and asymmetrical stretching vibrations of carbonyl groups of imide. The absorption band

at 1380 cm^{-1} is due to C-N stretching in imide ring and the absorption at $760\text{-}750\text{ cm}^{-1}$ is possibly due to imide ring deformation. All the polymers exhibited absorptions at 1610 , 1400 and 1080 cm^{-1} due to COO asymmetric and symmetric stretch, respectively (Figure 2).

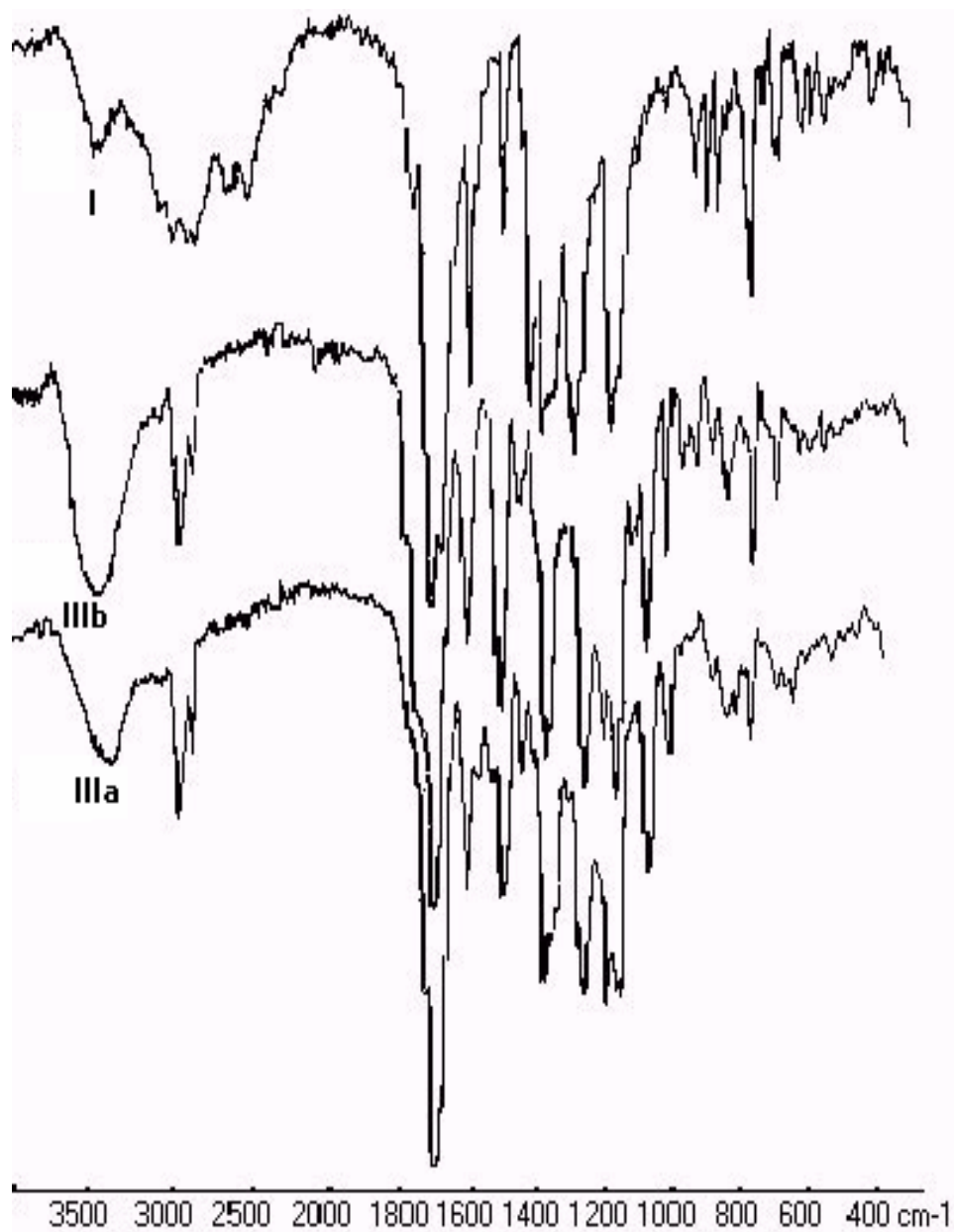


Figure 2. IR spectra of the dicarboxylic acid **I**, polyesters **IIIa** and **IIIb**

$^1\text{H-NMR}$ spectra confirmed the proposed structures. The $^1\text{H-NMR}$ spectrum of the polymer **IIIb** (figure 3) contains the signals characteristic to the diacid monomer and the corresponding diphenols. The majority of peaks in a relative downfield spectrum region are assigned to the aromatic protons, at about $7.20 - 8.30$ ppm. A characteristic peak was registered at about 5.7 ppm due to vinylic proton of the epichlor moiety.

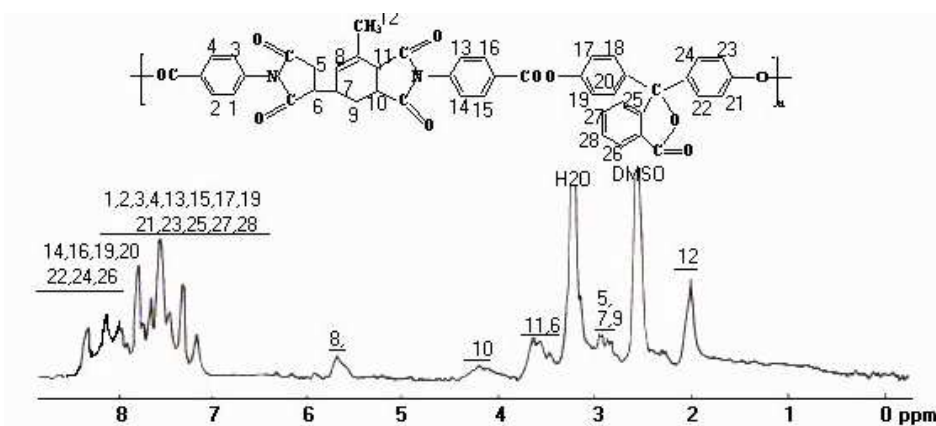


Figure 3. $^1\text{H-NMR}$ spectrum of the polymer **IIIb** in DMSO-d_6 at room temperature.

The new compounds dissolve easily in electro-donating organic solvent such as DMF, NMP, DMAc, DMSO as well as in chloroform. This good solubility is due to the relatively high flexibility of macromolecular chains, which was obtained by the introduction of epiclone units and ester linkages into the structure of the polyesters which induce asymmetry and steric hindrance and prevent a dense packing of the chains.

The thermal stability was evaluated by thermogravimetric analysis (TGA). These polymers do not show significant weight loss below 350°C . They begin to decompose in the range of 330°C - 340°C and show 10% weight loss in the range of 355°C - 370°C (table 1). One can assume that the degradation process could begin in the aliphatic segment of the backbone and then propagates to the entire structure [14].

Table 1. GPC data and thermal properties of the polymers **III**

| Polymer | Ar | Mw (g/mol) | Mn (g/mol) | IDT ^a ($^\circ\text{C}$) | T ₁₀ ^b ($^\circ\text{C}$) | T _g ^c ($^\circ\text{C}$) |
|-------------|----|---------------|---------------|--|--|---|
| IIIa | | 27383 | 24327 | 335 | 370 | 201 |
| IIIb | | 18636 | 16916 | 330 | 355 | 167 |

^a Initial decomposition temperature = the temperature of 5% weight loss.

^b Temperature of 10% weight loss.

^c Glass transition temperature.

The glass transition temperature (T_g) of the poly(imide-ester)s **III** were in the range of 167°C - 201°C (table 1, figure 4). It can also be noticed that there is a large interval between T_g and the decomposition temperature, which could be advantageous in the processing of these polymers by a thermoforming technique.

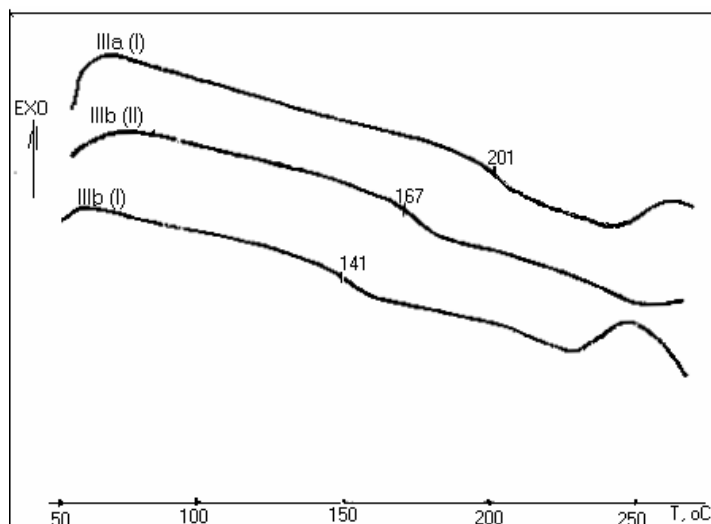


Figure 4. DSC curves of the polymers **IIIa** and **IIIb**: run I, run II

4. Conclusions

The incorporation of epiclone units together with ester linkages into the main chain of poly(imide-ester)s gave products with substantially improved solubility in electro-donating organic solvents. These polymers maintain high thermal stability, with the decomposition temperature being above 300°C and a glass transition in the range of 167°C - 201°C. The large interval between glass transition and decomposition temperature may be advantageous for their processing.

REFERENCES

1. Imai Y., Kakimoto M., *Handbook of Polymer Science and Technology, Vol. 1: Synthesis and Properties*, N.P. Cheremisinoff, Ed., Dekker, New York., 177, 1989
2. Hamciuc E., Bruma M., Schulz B., Kopnick T., *High. Perform. Polym.*, **15**, 347, 2003
3. Jacson W.J., *Br. Polym.*, **12**, 154, 1980,
4. Bruma M., Sava I., Hamciuc E., Hamciuc C., Belomoina N. M., Krongauz E. S., *Die Angew. Makromol. Chem.*, **194**, 3361, 179, 1992,
5. Sroog, C. E., *Prog. Polym. Sci.*, **16**, 561, 1991
6. Huang, S. J., Hoyt, A. E., *Trends Polym. Sci.*, **3**, 262, 1995
7. de Abajo J, de la Campa, J.G., *Adv. Polym. Sci.*, **140**, 23, 1999
8. Hamciuc E., Bruma M., Simionescu C. I., *Rev. Roum. Chim.*, **38**, 1311, 1993
9. Diakoumakos C.D., Mikroyannidis J. A., *Polymer*, **35**, 1986, 1994,
10. Hamciuc E., Hamciuc C., Sava I., Bruma M., *Eur. Polym. J.*, **37**, 287, 2001
11. Kim C., Tak T.M., *J. Appl. Polym. Sci.*, **74**, 272, 1999,
12. Mallakpour, S., Hajipour, A.R., Zamanlou, M.R., *J. Polym. Sci.: Part A: Polym Chem.*, **41**, 1077, 2003
13. Yeakel C., Gower K., Mani R. S., *Makromol. Chem.*, **194**, 2779, 1993
14. Arnold C.Jr., *Polym. Sci. Macromol. Rev.*, **14**, 265, 1979

CAMELIA HULUBEI
ELENA HAMCIUC

“Petru Poni” Institute of Macromolecular Chemistry Jassy

POLIESTERI PE BAZA DE EPICLON

(Rezumat)

Au fost sintetizati doi noi poliesteri prin policondensare directa in solutie. Reactia a avut loc intre 5-[N-(4-carboxifenil)succinimido]-3-metil-[N-(4-carboxifenil)]-1,2,5,6- tetrahidroftalimida, un nou acid dicarboxilic cu cicluri imidice preformate si 4-4'- dihidroxi-difenil, respectiv, fenolftaleina. Polimerii au fost identificati prin analiza chimica elementala, spectroscopie IR si ¹HRMN. Proprietatile termice ale noilor poliesteri au fost determinate prin analiza termogravimetrica si calorimetrie diferentia.

NONLINEAR BEHAVIOR IN CROSS-PLY GLASS/EPOXY COMPOSITE LAMINATES

ADRIAN CATANGIU

***Abstract:** Nonlinear stress-strain behavior in cross-ply glass/epoxy composite laminates has been investigated experimentally. We assumed that the nonlinear part of strain comes from plasticity and tried to describe the nonlinear behavior with the one-parameter plasticity model. In this paper the nonlinear behavior was predicted under an assumption that the nonlinear behavior of the unidirectional composite is known.*

***Keywords:** cross-ply composite, nonlinear behavior.*

1. Introduction

The rapidly expanding application of composites in the recent past have provided much optimism for the future of our technology. Although man-made composites have existed for thousands of year, the high technology of composites has evolved in the aerospace industry only in the last twenty years.

Usage of composites can be greatly enhanced if the cost is lowered and design more precise. Designing with any material is often more art than science. Composites design is no exception and there is much information to learn.

It is a common practice to limit the design of laminates to balanced (orthotropic) and symmetric construction. These restrictions are intended to simplify the design and manufacturing processes. In fact, the laminate may be designed to be balanced and symmetric before it is exposed to load and environments.

The polymer matrix composites reinforced with continuous fibers are an important class of materials, commonly used in thin laminates made up from individual plies stacked and consolidated in a proper way.

Polymer matrix composite laminates exhibit nonlinear stress-strain behavior under certain loading modes. Many models, phenomenological and of a physical nature have been proposed to describe the phenomenon using two approaches, one macroscopic and the other microscopic. In the macroscopic approach, composites are treated as a nonlinear elastic or plastic body.

Ogihara and Reifsninder [2] using a yield function which is quadratic in stress found an orthotropic plasticity model with three parameters for the woven composite. They show that is a difference between mechanical behavior of samples loaded in warp and yarn directions and is plastic deformation in the fiber direction..

Sun and Chen [3] developed the one-parameter plasticity model to describe the nonlinear behavior of unidirectional composites based on a quadratic plastic potential and the assumption that there is no plastic deformation in the fiber direction.

The response of a symmetric and balanced cross-ply glass/epoxy laminate is studied under uniaxial tensile loading at different angles to the material orthotropy axis.

The laminate configuration is $[0/90]_s$ (fig. 1) and the thickness is 3 mm.

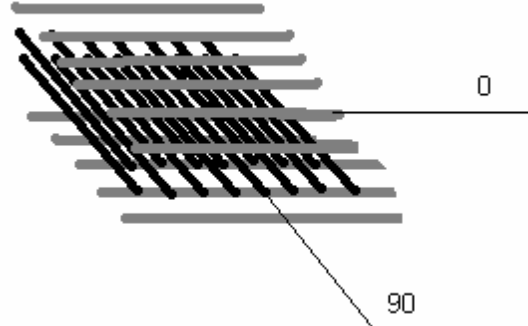


Figure 1. The cross-ply composite used in tests $[0/90/90/0]$ or $[0/90]_s$

Samples are cut out of the laminate in the direction of $\theta = 0^\circ, 15^\circ, 25^\circ, 45^\circ$ and 90° and encoded S-i (i – the angle between cutting direction and direction of fiber in external layer). Tensile tests were performed at all samples.

The mechanical response of such structure can be accurately modelled by the Classical Lamination Theory (CLT), if the mechanical properties of individual ply are known [4].

The two-dimensional composite analysis procedure apply when the through the thickness stresses are not significant. For orthotropic laminates that have low stresses in the thickness or 3-direction ($\sigma_3 = \tau_{23} = \tau_{13}$), plane stress), the stress strain relationships [4] is:

$$\begin{Bmatrix} \varepsilon_{11} \\ \varepsilon_{22} \\ \gamma_{12} \end{Bmatrix} = [S_{ij}] \begin{Bmatrix} \sigma_{11} \\ \sigma_{22} \\ \sigma_{12} \end{Bmatrix} \quad \begin{Bmatrix} \varepsilon_{11} \\ \varepsilon_{22} \\ \gamma_{12} \end{Bmatrix} = \begin{bmatrix} S_{11} & S_{12} & 0 \\ S_{12} & S_{22} & 0 \\ 0 & 0 & S_{66} \end{bmatrix} \begin{Bmatrix} \sigma_{11} \\ \sigma_{22} \\ \sigma_{12} \end{Bmatrix} \quad (1)$$

In terms of the engineering constants obtained by simple tests:

$$\begin{Bmatrix} \varepsilon_{11} \\ \varepsilon_{22} \\ \gamma_{12} \end{Bmatrix} = \begin{bmatrix} \frac{1}{E_1} & -\frac{\nu_{12}}{E_1} & 0 \\ -\frac{\nu_{21}}{E_2} & \frac{1}{E_2} & 0 \\ 0 & 0 & \frac{1}{G_{12}} \end{bmatrix} \begin{Bmatrix} \sigma_{11} \\ \sigma_{22} \\ \sigma_{12} \end{Bmatrix} \quad (2)$$

E_1 – longitudinal Young modulus;

E_2 – transversal Young modulus;

G_{12} – in-plane shear modulus;

ν_{12}, ν_{21} – in-plane Poisson ratio.

The reciprocity relationships for stiffness is $\frac{\nu_{12}}{E_1} = \frac{\nu_{21}}{E_2}$.

The engineering constants ($E_1, E_2, G_{12}, \nu_{12}$) only describe the initial linear elastic behavior.

2. Analytical procedure

Consider an orthotropic elastic-plastic laminate subjected to active in-plane loading. Total strain can be partitioned into two components: linear elastic strain ε_i^e and plastic strain ε_i^p .

$$\varepsilon_i = \varepsilon_i^e + \varepsilon_i^p \quad (3)$$

Elastic strain can be determined by:

$$\varepsilon_i^e = \frac{\sigma_x}{E_x} \quad (4)$$

σ_x - longitudinal stress (in cutting direction for each sample).

For a state of plane stress parallel to laminate plane the yield function proposed by Ogihara and Reifsninder is:

$$2f = a_{11}\sigma_{11}^2 + a_{22}\sigma_{22}^2 + 2a_{12}\sigma_{11}\sigma_{22} + 2a_{66}\sigma_{12}^2 \quad (5)$$

The effective stress [2]:

$$\bar{\sigma} = \sqrt{3f} \quad (6)$$

If x-axis (the uniaxial loading direction) make the angle θ with fiber direction, the stresses in the ply principal coordinate system are :

$$\begin{aligned} \sigma_{11} &= \sigma_x \cos^2 \theta \\ \sigma_{22} &= \sigma_x \sin^2 \theta \\ \sigma_{12} &= \sigma_x \sin \theta \cos \theta \end{aligned} \quad (7)$$

From (5, 6, 7), if

$$\bar{\sigma} = h(\theta)\sigma_x \quad (8)$$

$$h_{(\theta)} = \sqrt{\frac{3}{2} \{a_{11} \cos^4 \theta + a_{22} \sin^4 \theta + 2(a_{12} + a_{66}) \sin^2 \theta \cos^2 \theta\}} \quad [2] \quad (9)$$

The rule of flow is defined if the parameters a_{11} , a_{22} , a_{12} , a_{66} are determined (this is the most general rule of bidimensional model).

3. The model for cross-ply laminate

Sun and Chen show that there is no plastic deformation in fiber direction (quasi-linear stress-strain relations). Our tests performed in the fiber directions (0^0 and 90^0) confirm that (fig. 2).

That means:

$$d\varepsilon_{11}^p = 0 \text{ which leads to } a_{11} = a_{12} = 0.$$

Besides, the response of samples cutted in 0^0 and 90^0 are the same, which leads to:

$$a_{22} = 1.$$

The relation (5) becomes :

$$2f = \sigma_{22}^2 + 2a_{66}\sigma_{12}^2 \quad (10)$$

$$h(\theta) = \sqrt{\frac{3}{2}(\sin^4 \theta + 2a_{66} \sin^2 \theta \cos^2 \theta)} \quad (11)$$

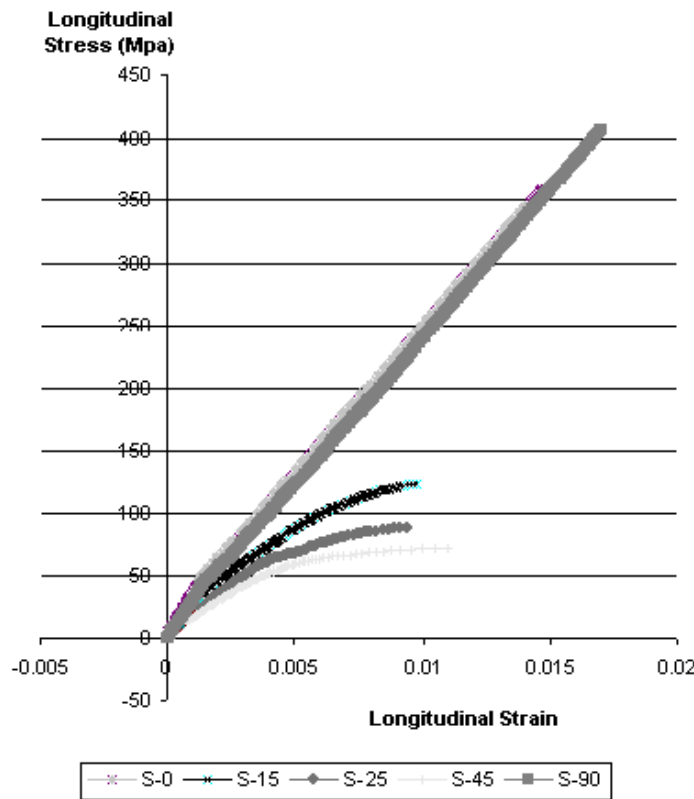


Figure 2. Stress-strain curve for $[0/90]_s$ glass/epoxy composite uniaxially loaded.

If the Sun-Chen one-parameter plasticity model can be used to predict the nonlinear behavior of an unidirectional, we try to perform an analytical response of cross-ply composite laminate using the model for each ply. The total incremental stress-strain relations [2, 3] for elastic-plastic unidirectional composite are:

$$\begin{Bmatrix} d\varepsilon_{11} \\ d\varepsilon_{22} \\ d\gamma_{12} \end{Bmatrix} = \begin{bmatrix} S_{11} & S_{12} & S_{16} \\ S_{21} & S_{22} & S_{26} \\ S_{61} & S_{62} & S_{66} \end{bmatrix} \begin{Bmatrix} d\sigma_{11} \\ d\sigma_{22} \\ d\sigma_{12} \end{Bmatrix} \quad (12)$$

$$\left. \begin{aligned} S_{11} &= \frac{1}{E_1} & S_{12} = S_{21} &= -\frac{\nu_{12}}{E_1} & S_{16} = S_{61} &= 0 \\ S_{22} &= \frac{1}{E_2} + \Omega \sigma_{22}^2 & S_{26} = S_{62} &= 2a_{66} \Omega \sigma_{12} \sigma_{22} \\ S_{66} &= \frac{1}{G_{12}} + 4a_{66}^2 \Omega \sigma_{12}^2 & \Omega &= \frac{9}{4} A \bar{\sigma}^{n-3} \end{aligned} \right\} \quad (13)$$

$$a_{66} = 2.2 [3]$$

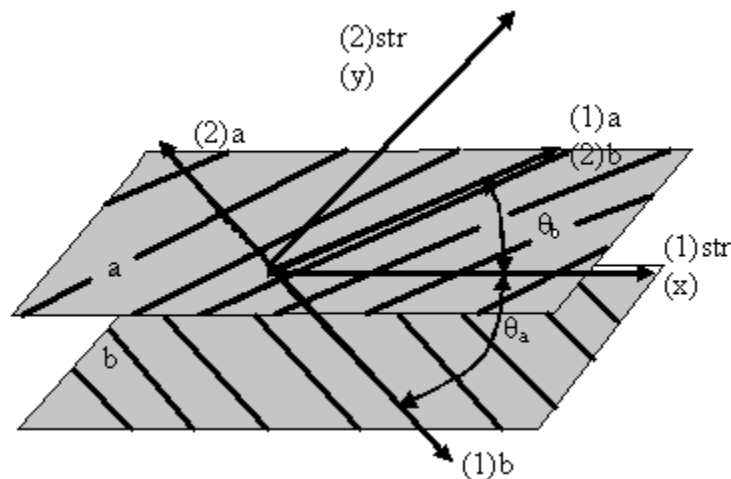


Figure 3. Coordinate system
 (1)a-(2)a – ply a local system (1)b-(2)b – ply b local system
 x-y ; (1)str-(2)str –global coordinate system

The laminate have two ply of type a and two ply of type b. The stress-strain relations of a multidirectional laminate in plane state of stress is obtained in a step-by-step manner. The increment of stress in loading direction for each ply ($d\sigma_{xi}$) is converted in the components of local coordinate system. The increment of strain (12, 13) is calculated and converted again in global coordinate system.

Total longitudinal strain of composite laminate is the same with the longitudinal strains of each ply in global coordinate system. We assumed that the total longitudinal strain of laminate is produced by the average of stresses which produces the same deformation in each ply (because the laminate have the same proportion of ply in each direction).

4. Experimental Procedure

The composite material used in this work is a cross-ply glass/epoxy composite. The raw material is a prepreg (long fiber unidirectional composite). The panel have four ply with configuration [0/90/90/0].

Vacuum bag processing is suited to components with thin section. The completed assembly, with vacuum applied, is placed inside an oven with good air circulation, and the composite is produced after 1h at 120⁰ C [5].

Samples are cut out of the panels in the direction of $\theta = 0^0, 15^0, 25^0, 45^0$ and 90⁰. Tensile test were conducted with an Instron 6025 universal testing machine. The strains, up to failure, were measured using two extensometers. The Young moduli were determined from the experimental data by linear regression analysis using Microsoft Excel.

Table 1. Initial longitudinal Young moduli

| θ | 0 ⁰ | 15 ⁰ | 25 ⁰ | 45 ⁰ | 90 ⁰ |
|-------------|----------------|-----------------|-----------------|-----------------|-----------------|
| Samples | S-0 | S-15 | S-25 | S-45 | S-90 |
| E_x (GPa) | 31.4 | 26 | 16.2 | 15 | 31 |

Fig. 4 shows the effective stress-effective plastic strain curves from the experimental data of all angles. Effective plastic strain is obtained by removing the elastic component from total strain (this is possible if σ_x and E_x are known). Effective stress is calculated with relations (8 and 11). This dependence is the same for all angles if material is homogeneous.

The curve is described by the power law $\bar{\epsilon}^p = A\bar{\sigma}^n$.

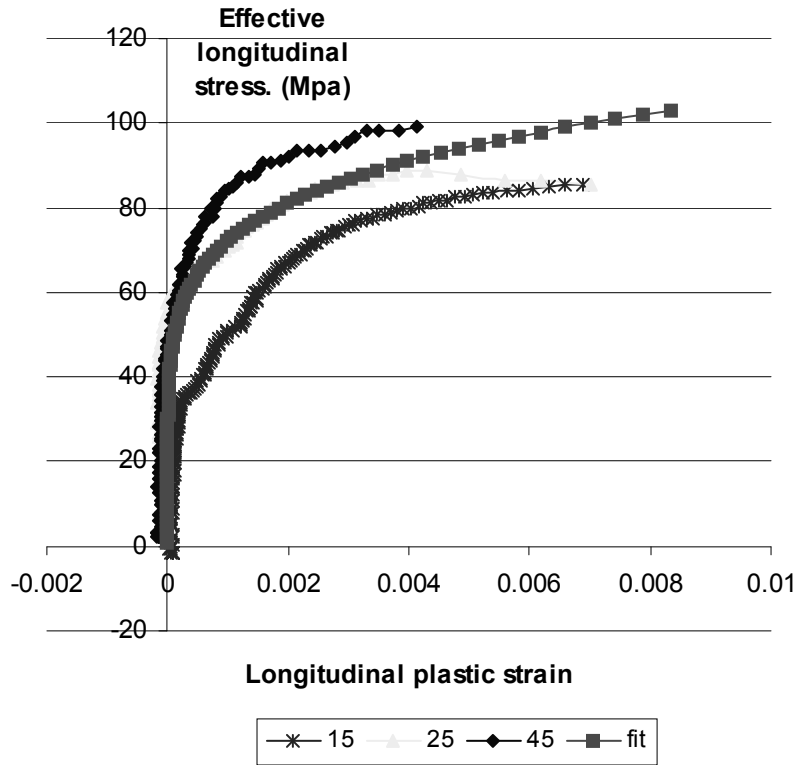


Figure 4. Effective stress – effective plastic strain curve.

The parameters which describe the curve ($A=7 \cdot 10^{-15}$, $n=5.77$) were found using an empirical procedure.

Table 2. Assumed properties of glass/epoxy unidirectional composite [5].

| | | |
|----------------------------|----------------|------|
| Longitudinal Young modulus | E_1 (GPa) | 43 |
| Transverse Young modulus | E_2 (GPa) | 8 |
| Longitudinal Poisson ratio | ν_{12} | 0.27 |
| Shear modulus | G_{12} (GPa) | 4 |
| a_{66} Sun Chen [3] | | 2.2 |

Figures (5,6) show stress-strain relations of glass/epoxy unidirectional laminate loaded at the angles specific to each ply of the samples predicted by Sun-Chen's one-parameter plasticity model, the predicted stress-strain relations of a cross-ply laminate and the curves obtained experimentally.

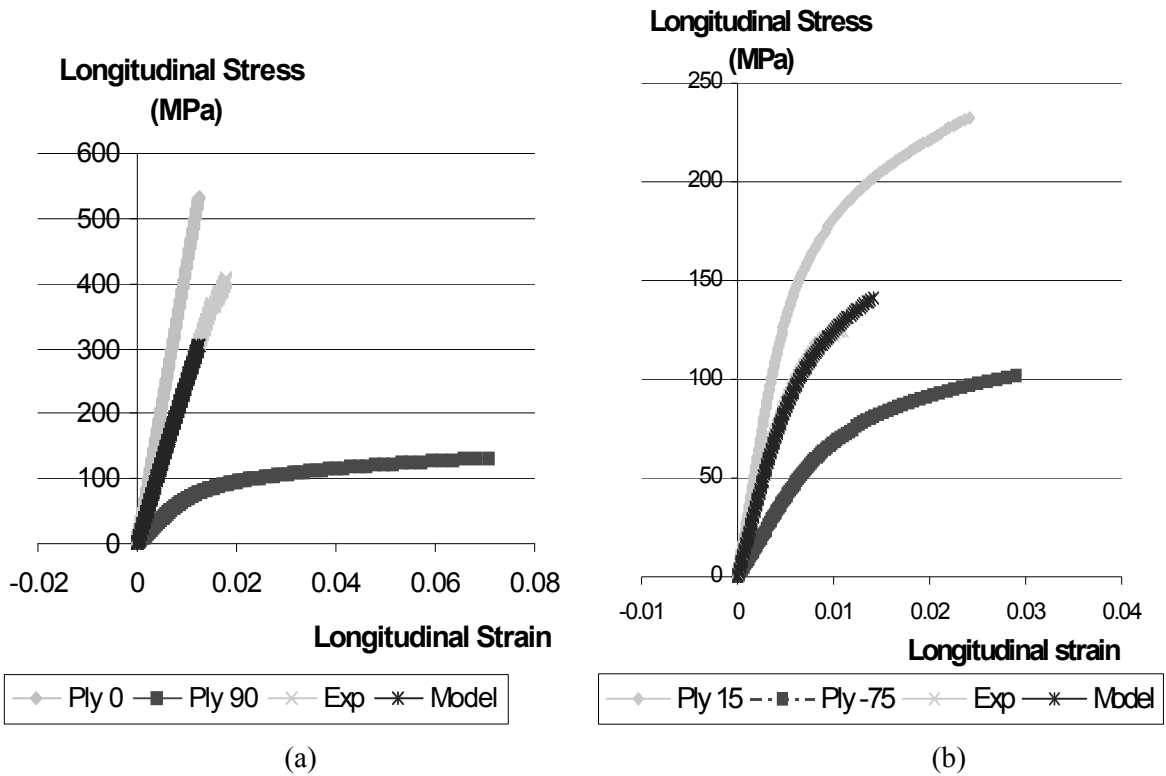


Figure 5. Comparison between the predicted stress-strain curve and the experimental one obtained for: (a) sample of type S-0 or S-90 and (b) sample of type S-15.

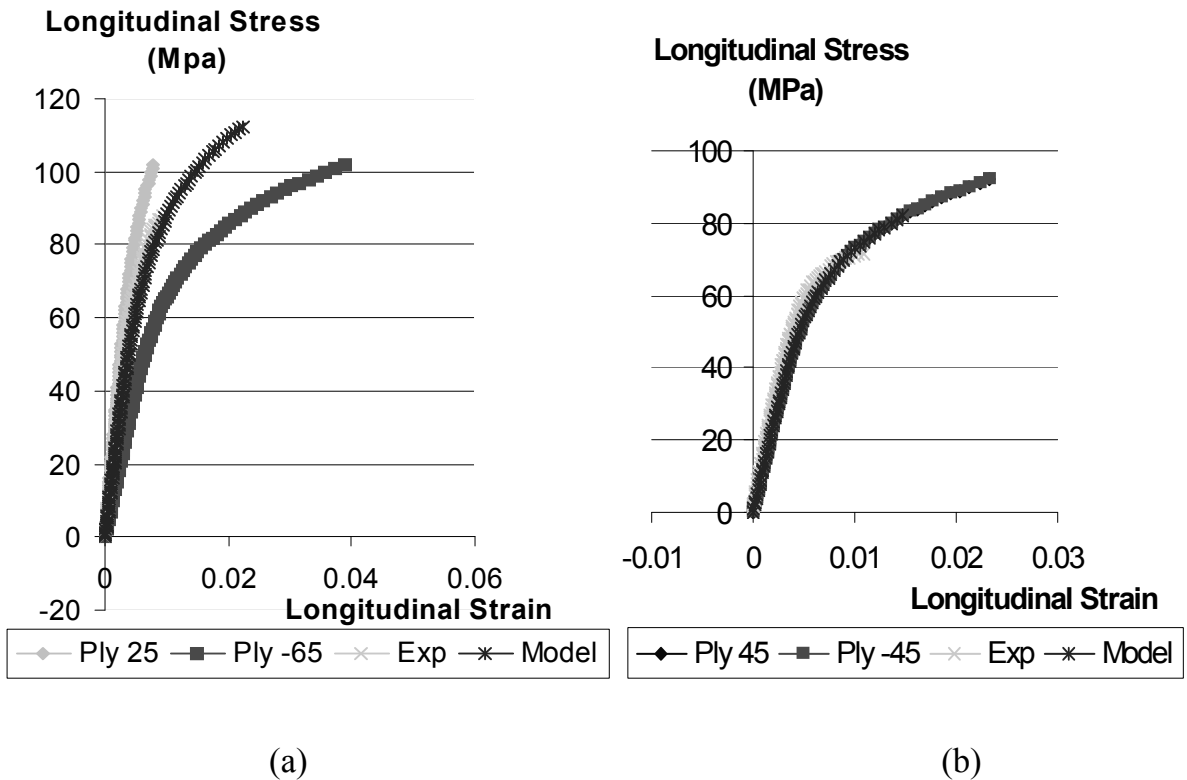


Figure 6. Comparison between the predicted stress-strain curve and the experiment one obtained for: (a) sample of type S-25 and (b) sample of type S-45.

4. Conclusions

These preliminary experiments have proved that, with increasing the angle between fiber and loading directions the nonlinear behavior increases.

Composite laminates exhibit much lower strength in the transverse direction, and at ply interfaces, making them particularly susceptible to matrix cracking and delamination.

The prediction exhibits less nonlinearity which may be due to empirical procedure for evaluation of parameters A and n .

Nonlinear behavior of cross-ply glass/epoxy composite laminates can be described by one-parameter plasticity model.

Our next step is to investigate a mechanical model which can describe the nonlinear behavior of uniaxial composites under off-axis loading and to verify if Sun Chen parameter a_{66} is appropriate for our composite system.

REFERENCES

1. Mazumdar, S.K. - **Composite Manufacturing**, CRC Press, London, 2002
2. Ogihara, S., Reifsnider, K.L. – *Characterization of Nonlinear Behavior in Wovwn Composite Laminates*, **Applied Composite Materials** **9**, 2002, 249-263.
3. Sun, C.T., Chen, J.L., *A Simple Flow Rule for Characterizing Nonlinear Behavior of Fiber Composites*, **Journal of Composite Materials** **23**, 1989, 1009-1020.
4. Jones, R.M. - **Mechanics of Composite Materials**, Taylor&Francis, Philadelphia, 1999
5. **Prepreg Technology**, Hexcel corporation, January 2004.
6. Gay, D. – **Matériaux composites**, Hermes, Paris, 1997.

CATANGIU ADRIAN

Universitatea Valahia Târgoviște
Facultatea Ingineria Materialelor Mecatronică și Robotică
B-dul Unirii nr.18 Târgoviște cod. 130082
Tel/fax 0040 245 206106
e-mail: catangiu@valahia.ro;
acatangiu@yahoo.co.uk

COMPORTAREA NELINIARA A COMPOZITELOR STRATIFICATE STICLĂ-EPOXI [0/90],

Rezumat: Au fost supuse încercării la tracțiune epruvete prelevate dintr-un stratificat sticlă/epoxy. În cazul epruvetelor pentru care direcția de aplicare a sarcinii face cu direcția fibrelor unghiuri diferite de 0^0 , comportarea în spațiul tensiune-deformație se abate de la liniaritate. Efectul de abatere de la liniaritate a fost atribuit plasticității și s-a încercat aplicarea unui model cu un parametru care să caracterizeze comportamentul neliniar. Modelarea se bazează pe ipoteza că este cunoscută comportarea neliniară a materialului unidirecțional.

TITANIUM/HYDROXYAPATITE GRADED MATERIALS FOR ENDOSSEUS IMPLANTS

BY

GABRIEL BATIN, CĂTĂLIN POPA and IOAN VIDA-SIMITI

Abstract: A good bone substitute, in bulk form, should be biocompatible and osteoconductive, allowing attachment and bone growth on and into its surface porosities. In addition, its mechanical properties should match to that of natural bone. We propose a novel material to meet these requirements. The samples were made of post-hydride titanium powder and hydroxyapatite powder obtained by sol-gel process. After die-compaction, the samples were sintered in vacuum at 1160 °C. Several concentrations of hydroxyapatite were studied: 5, 10, 20, 50 %. A high percentage of hydroxyapatite leads to poor mechanical properties and a sharp variation of the hydroxyapatite amount from one layer to another produces cracks, as experimental results show. Some reactions occurred at the titanium/hydroxyapatite interface and lead to the formation of solid solutions and other compounds, as revealed by microstructures.

Keywords: biomaterials, endosseus implants, titanium, hydroxyapatite

1. Introduction

To create a biomaterial simulating the structure and biological characters of natural bone is a priority for biomaterials research [1, 2]. A good bone substitute, in bulk form, should be biocompatible and osteoconductive, allowing attachment and bone growth on and into its surface porosities [1]. Titanium (Ti) is one of the best biocompatible metals and used most widely as material for oral, maxillofacial and orthopaedic implants because of its mechanical properties and biocompatibility [3,4]. Hydroxyapatite [HAP or $\text{Ca}_{10}(\text{PO}_4)_6(\text{OH})_2$] is widely used as bone replacement due to its excellent biocompatibility, bioactivity and osteoconductive properties. These properties are given by its unique chemical composition and crystal structure that is similar to the human skeletal apatite [2, 3, 5, 6].

A biomaterial with a single composition and a uniform structure doesn't satisfy all this requirements at the same time, that is why functionally graded materials are proposed for use.

The functional gradient refers to: the bone-insertion zones must contain hydroxyapatite as bioactive phase; the zones with no direct contact to bone must have cross-sectional functional gradient, in order to ensure a reduction of stiffness and the chemical stability leading to an as reduced fibrous capsule as possible and to allow blood to irrigate the tissue.

The implants must have interconnected pores to provide the space for vascular tissue required for continued mineralized bone growth [4]. The commonly accepted range of pore size is between 150 and 400 μm , but others reported a pore size between 200 and 900 μm [4,7].

2. Experimental procedure

In this study, samples composed of post-hydride titanium powder and hydroxyapatite powder obtained by sol-gel processes were made. Samples with a single composition as well as gradual composition samples were produced. The bioactive phase, represented by the hydroxyapatite powder, was used in different concentrations in samples: 5, 10, 20, 50 wt%.

The samples were made of post-hydride titanium powder and hydroxyapatite powder obtained by a sol-gel process. After mixing and die-compaction, the samples were sintered in vacuum (1160 °C). Several concentrations of the bioactive phase were studied: 5, 10, 20, 50 % wt. Samples with a single composition, as well as gradual samples were produced.

A mixed powder containing 5% wt HAP was compacted in a die without any lubricant. The die walls and the punch were lubricated with oil. The samples were compacted at 400, 500 and 600 MPa and sintered in vacuum (10^{-4} torr) at 1160 °C following a complex regime: isothermal dwellings were made at 250 °C for about 30 minutes, at 800 °C for another 30 minutes and finally at 1160 °C for about 60 minutes.

Samples with composition gradient were produced. The same die was used to compact layers with 5% wt, 20 % wt and 50 %wt. The samples were compacted at 500 MPa without lubrication. The sintering program (in vacuum at 10^{-4} torr) consisted in 4 dwellings: 15 minutes at 250 °C, 15 minutes at 600 °C, 30 minutes at 850 °C and 5 minutes at 1160 °C.

The samples were studied using images and EDX analyses on a scanning electron microscope JEOL 6500 LV.

3. Experimental results

The samples with 5% wt HAP were used to study the interface between the calcium phosphates and the titanium matrix function of compaction forces. The increase of the compacting forces lead to a higher compaction. An increase in volume was observed; the higher the compacting pressure, the more increase in volume.

As seen in Figure 1, the samples with 5% HAP are well sintered, with interconnected pores.

The swelling depends largely on the composition, also. The layers with 50 % wt HAP present the highest increase and the poorest mechanical properties. Up to 20 % wt HAP, the samples were completely sintered. For gradual samples, as in Figure 2, when the variation in composition was sharp, cracks were observed between the layers. These cracks appeared because of the differences in swelling. There is no apparent cracking for a variation of 5% HAP between layers.

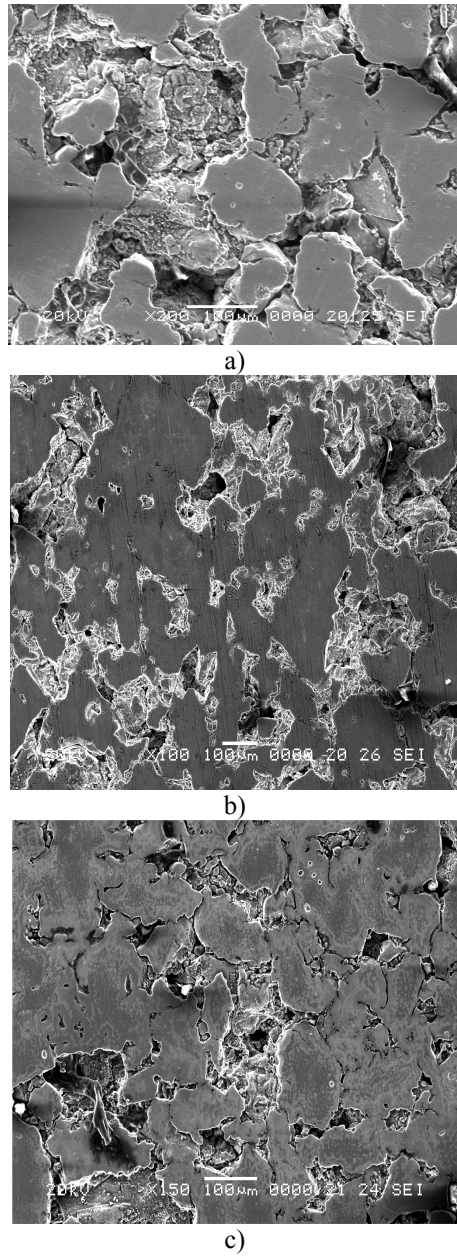


Fig. 1. Microstructures of Ti/ 5% wt HAP samples at : a) 400 MPa ; b) 500 MPa ; c) 600 MPa.

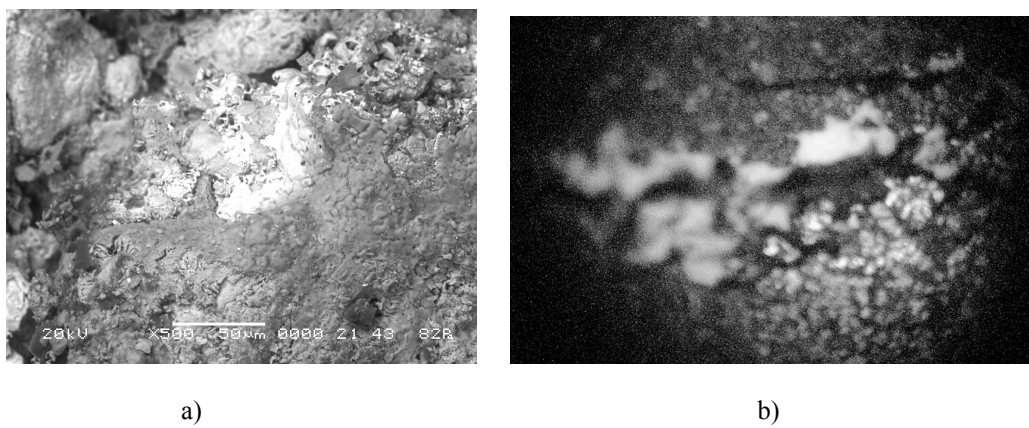


Fig. 2. Sample with functional gradient: a) microphotography; b) cracks between layers.

Between the titanium matrix and the ceramic phase, diffusion processes occurred, as observed on the EDX spectrum, Fig.3.

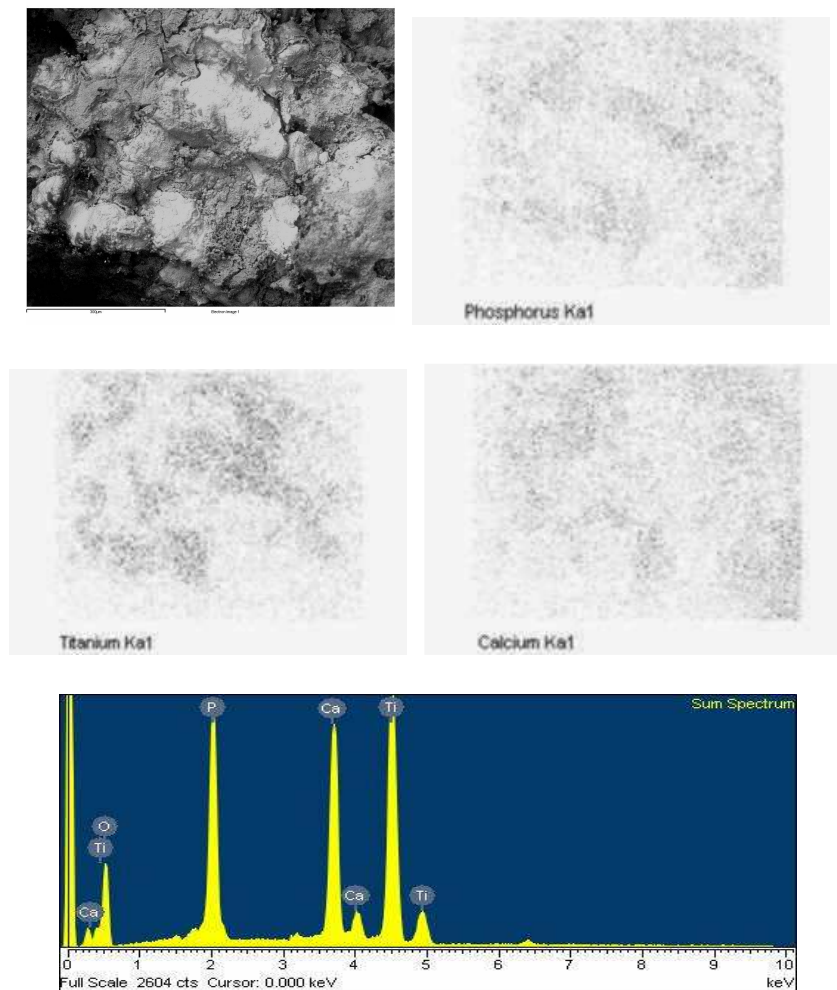


Fig.3. EDX spectre (the zone with 50% HAP)

Initial HAP grains decomposed partly and formed solid solutions inside the titanium matrix. This led to the formation of an adherence layer between the ceramic phase and the matrix.

4. Conclusions

Single composition, as well as gradual titanium-hydroxyapatite samples were produced via a PM method (mixing, pressing, vacuum sintering).

Experimental results show that a high percentage of hydroxyapatite leads to poor mechanical properties and a sharp increase of the hydroxyapatite amount from one layer to another produces cracks.

It is necessary to have a small transition of the hydroxyapatite concentrations between the layers to obtain implants with compositional gradient and good mechanical properties.

The microstructures show that some reactions occur at the hydroxyapatite/titanium interface, leading to the formation of binary or complex solid solutions, as well as to the shifting to new compounds.

A diffusion layer is formed between the matrix and the reinforcement phase. It is useful for the mechanical stability while the titanium matrix remains prevalent in volume (for concentrations up to 20%).

Received

Technical University of Cluj-Napoca

REFERENCES

1. Aho, A.J., Hautamäki, M., Mattila, R., Alander, P., Strandberg, N., Rekola, J., Gunn, J., Lassila L.V.J. and Vallittu, P.K. – *Surface porous fibre-reinforced composite bulk bone substitute, In vitro studies and vivo evaluation in segment defect*, **Cell and Tissue Banking**, **5**, 2004, **213-221**
2. Babini, G.N. and Tampieri, A. – Towards biologically inspired materials, **British Ceramic Transactions**, **Vol. 103, No. 3**, 2004, **101-109**
3. Fumio Watari, Atsuro Yokoyama, Mamoru Omori, Toshio Hirai, Hideomi Kondo, Motohiro Uo and Takao Kawasaki - Biocompatibility of materials and development to functionally graded implant for bio-medical application, **Composites Science and Technology**, **64**, 2004, **893-908**
4. Kutty, M.G., Bhaduri, S., and Bhaduri S.B. – Gradient surface porosity in titanium dental implants: relation between processing parameters and microstructure, **Journal of Materials Science: Materials in Medicine**, **15**, 2004, **145-150**
5. Sadeghian, Z., Heinrich, J. G., and Moztarzadeh, F. - Direct Laser Sintering of Hydroxyapatite Implants by Laser-wise Slurry Deposition (LSD), **cfi/Ber. DKG 81, No. 12**, 2004, **E39-E43**
6. Thian, E.S., Loh, N.H., Khor, K.A. and Tor, S.B. - Processing of biocomposite Ti-6Al-4V/HA powder, **Journal of Materials Science Letters**, **22**, 2003, **775-778**
7. Salgado, A.J., Coutinho, O.P. and Reis, R.L. - Bone Tissue Engineering: State of the Art and Future Trends, **Macromolecular Bioscience**, **4**, 2004, **743-765**

MATERIALE CU GRADIENT PE BAZA DE TITAN SI HIDROXIAPATITA PENTRU IMPLANTE ENDOOSOASE

Rezumat: Un material care să poată substitui osul natural, sub forma produsului final, ar trebui să fie biocompatibil și osteoconductiv, permițând legarea și creșterea osului nou pe suprafața sa poroasă precum și în pori. Mai mult, proprietățile sale mecanice ar trebui să corespundă cu cele ale osului natural. Probele au fost realizate din pulbere de titan dehidratată și pulbere de hidroxiapatită obținută prin procedee sol-gel. După presare în matrită, probele au fost sinterizate în matrită la 1600 °C, în vid. Au fost studiate probe cu diferite concentrații masice de hidroxiapatită: 5, 10, 20, 50 %. O concentrație mare de hidroxiapatită conduce la proprietăți mecanice scăzute, iar o diefernță mare de concentrație de hidroxiapatită de la un strat la altul produce fisuri, așa cum arată rezultatele experimentale. Unele reacții au loc la interfața titan/hidroxiapatită ducând la formarea unor soluții solide și a altor compuși așa cum se poate observa din microstructuri.

Tipar Digital realizat la **Tipografia pim**
Șoseaua Ștefan cel Mare nr. 11
Iași - 700498
Tel. / fax: **0232-212740**
e-mail: editurapim@pimcopy.ro
www.pimcopy.ro